SECTION 5.9: OCEANOGRAPHY AND COASTAL ENGINEERING	
File name: S2052-05-RP-CE-001-Rev1 DSSR Section 5.9	
Author declaration:	I declare that appropriate diligence and quality assurance was applied in the compilation of this report. As such I am confident in the results here described and the conclusions drawn. ..... Name: Stephen Luger Date: 31/03/2022
Peer Reviewer:	I declare that this report has undergone independent peer review by myself, that comments were addressed to my satisfaction, and that as such, it is considered fit for publication. ..... Name: Chris Fleming Date: 31/3/22
Project Manager Authorisation:	..... Name: Andy McClarty Date: 31/03/2022
Eskom Acceptance:	..... Name: FA Vaas Mosserveld Date: 2022-03-31

CONTROLLED DISCLOSURE

When downloaded from the EDS database, this document is uncontrolled and the responsibility rests with the user to ensure it is in line with the authorised version on the database.

AMENDMENT RECORD			
Rev	**Draft**	**Date**	**Description**
0		16 March 2016	Section 5.9 (Oceanography and Coastal Engineering) of the Site Safety Report submitted in 2016.
1		31 March 2022	Section 5.9 updated to reflect the latest regulations, requirements and guidelines. Includes an updated Tsunami Hazard Analysis, additional oceanographic data, updated climate change and improved methodologies.

CONTROLLED DISCLOSURE

When downloaded from the EDS database, this document is uncontrolled and the responsibility rests with the user to ensure it is in line with the authorised version on the database.

EXECUTIVE SUMMARY

Purpose and Scope

Oceanography and coastal engineering studies have been undertaken for the existing Koeberg Nuclear Power Station (KNPS) and the planned development of new nuclear installation(s) (NIs) at the Duynefontyn site. The purpose of this section of this SSR is to identify the requirements and to demonstrate the technical acceptability of the site with regard to coastline stability, flooding from the sea, integrity of cooling water supply and thermal plume dispersion. Design considerations for seawater cooling water intake and outfall layouts are provided.

Climate Change

The effect of climate change on all relevant oceanographic and coastal engineering parameters has been included. For sea level rise (SLR) values of 0.20 m, 0.44 m, 1.36 m and 1.80 m have been applied for the key dates of 2044, 2064, 2110 and 2130, respectively. The applied changes for the other parameters besides SLR are provided in the main report.

Note that the assessment of coastline stability and flooding from the sea are based on the SLR corresponding to the RCP8.5 upper end of likely range (0.44 m in 2064 and 1.80 m in 2130), rather than the maximum plausible SLR (0.79 m in 2064 and 3.26 m in 2130). This additional 0.35 m at the end of decommissioning of the KNPS in 2064, and 1.5 m at the end of decommissioning of the new NIs in 2130, should be considered during the SAR and engineering design phase, either as safety buffer or as part of an adaptive design strategy.

Nearshore Waves

The results indicate a rough wave climate with significant wave heights (the mean of the highest one-third of waves) up to 19.7 m in a depth of 31 m directly offshore of the site. These waves will need to be accounted for in the design of all coastal structures at the site during the SAR and engineering design phases, e.g., intake structures, outfall structures and revetments.

Coastline Erosion

The results show significant erosion of the coastline (up to 358 m), which increases over time due to long-term coastline trends, sea level rise and larger waves.

Further engineering studies should be undertaken to ensure that the breakwater and outfall structures at KNPS can withstand the predicted erosion over the operating life of the plant.

The predicted erosion does not reach the estimated position of the new NIs for 2021 and 2064. For 2130 the southern section the new NIs are eroded for all exceedance

CONTROLLED DISCLOSURE

When downloaded from the EDS database, this document is uncontrolled and the responsibility rests with the user to ensure it is in line with the authorised version on the database.

probabilities modelled. It will thus be necessary to move the position of the new NIs landward, or to design appropriate coastal protection such as revetments.

Flooding from the Sea

Flooding from the sea was assessed due to:

- Storm wave run-up combined with sea level rise, high tides, positive storm surge, wave set-up and basin seiche; and
- Maximum Probable Tsunami (PMT) run-up combined with sea level rise, high tides and positive storm surge.

The results show the following:

- At KNPS, the PMT run-up and inundation are governed by the volcanic flank collapse tsunamis which result in extensive flooding of the KNPS nuclear terrace level located at approximately +8 m msl. No other tsunamigenic sources, including distant earthquakes and local submarine landslide sources, result in run-up above the KNPS nuclear terrace level, even including climate change to 2064.
- The run-up at the KNPS due to storm waves reaches +8 m msl at exceedance probabilities between 10^{-4} y^{-1} and 10^{-6} y^{-1}, however these locations are north and south of the nuclear terrace. Only at 10^{-8} y^{-1} does the wave run-up flood the terrace adjacent to the reactor buildings.
- The predicted flooding at KNPS will require further assessment, i.e., through further analysis of the probability of these events occurring in the remaining 42 y until the end of decommissioning (assumed in 2064), by analysing the impact of the predicted flood water depths and currents on the KNPS structures, systems and components (SSCs), and consideration of protective structures such as wave walls.
- At the new NIs the maximum flood level is +16.7 m msl, due to an extreme 10^{-8} y^{-1} wave storm in 2130. The maximum horizontal inundation is 553 m due to the PMT in 2130. The inundation extends into the estimated position of the new NIs for the PMT in all years.
- For wave storms the inundation does not reach the position of the new NIs in 2021 and 2064, however in 2130 the position of the new NIs is reached for exceedances of 10^{-2} y^{-1} and lower.
- For the new NIs the SSCs will need to be placed above these maximum flood levels and landward of the maximum inundation, or alternatively protective structures such as revetments and wave walls will need to be placed in front of the SSCs.

CONTROLLED DISCLOSURE

When downloaded from the EDS database, this document is uncontrolled and the responsibility rests with the user to ensure it is in line with the authorised version on the database.

Extreme Low Water Levels

The results show the following regarding extreme low water levels at the cooling water intakes:

- At KNPS, the results show that the lowest water level is -2.3 m msl, which is driven by the PMT. The KNPS pumps can accommodate a minimum water level of -3.5 m msl and will thus continue to operate for all events assessed.
- If a basin intake with similar geometry to KNPS is selected for the new NIs, then the intake should accommodate a minimum water level of -2.3 m msl.
- If a tunnel intake in a depth of -20 m msl is selected for the new NIs, then the intake should accommodate a minimum water level of -7.2 m msl, which is driven by the PMT.
- If a tunnel intake in a depth of -30 m msl is selected for the new NIs, then the intake should accommodate a minimum water level of -6.8 m msl, which is driven by the 10^{-8} y^{-1} storm event.

Thermal Plume Dispersion and Recirculation

It is proposed that the new NIs will be cooled using a once-through seawater cooling system. Four different conceptual layouts for the seawater cooling intake and outfall system have been developed and modelled to demonstrate the technical feasibility of the site:

- Layout 0: Existing KNPS intake basin and outfall channel;
- Layout 1: Short tunnel intakes and outfalls;
- Layout 2: Long tunnel intakes and outfalls;
- Layout 3: Basin intake and tunnel outfalls;
- Layout 4: Basin intake and rubble-mound outfall structure.

The PPE for the new NIs specifies that the maximum increase in seawater temperature (ΔT) of the re-circulated cooling water between the discharge and the intake should be less than 1.5°C. The maximum ΔT of the re-circulated water at the KNPS is not specified.

The results show the following:

- The 99th percentile ΔT at the existing KNPS intake is 2.4°C. The new NIs generally increase the ΔT at the existing KNPS intake, with Layout 4 resulting in the largest increase (+0.6°C for the 99th percentile), while Layout 3 had the least impact.
- At the new NIs intake, Layouts 1 to 3 meet the ΔT of 1.5°C for the 99th percentile. Layout 4 has a 99th percentile ΔT of 2.7 and 3.2°C for power outputs of 2500 and 4000 MWe, respectively.

CONTROLLED DISCLOSURE

When downloaded from the EDS database, this document is uncontrolled and the responsibility rests with the user to ensure it is in line with the authorised version on the database.

Extreme Seawater Temperatures

The PPE also specifies a maximum cooling water intake temperature for the new NIs of 30°C. For the existing KNPS a shut-down of the reactor will be necessary if the intake temperature exceeds 23°C. The results show the following:

- Without the new NIs, the best estimate return period to exceed 23°C at the KNPS intake is 98 y for the year 2021 and 35 y for the year 2064.
- In all cases the addition of the new NIs reduces the return period to exceed 23°C at the KNPS intake. Layout 4 with a 4000 MWe power station has the largest impact on the KNPS, with the 23°C threshold reducing to a 29 y return period for the year 2021 and a 10 y return period for the year 2064. Layout 4 will thus increase the probability of a shut-down of the KNPS reactor due to high seawater temperatures.
- At the new NIs intakes, the higher maximum specified intake temperature of 30°C, combined with lower recirculation ΔT's results in significantly lower exceedance probabilities of between 3.4×10^{-6} and 3.8×10^{-4} y^{-1}, with the latter for Layout 4 with the 4000 MWe power station in 2130. These exceedance probabilities indicate that the intake seawater temperatures will need to be considered in the design of the cooling system for the new NIs.

Sedimentation and Scour

The results show the following for the existing and proposed intake basins:

- Under extreme storm conditions scour exceeding -5 m is predicted at the roundhead and along the outside of the southern trunk of the KNPS breakwater. The effect of this on the stability of the breakwater requires additional investigation. The design of any similar coastal structures for the new NIs should account for similar levels of scour.
- Storm-induced sedimentation is not predicted to close off the KNPS intake basin and seawater will be able to enter the intake basin.
- Less than 0.3 m of tsunami-induced sedimentation is predicted in front of the KNPS pumphouses and the intake basin is not closed off by sedimentation during the modelled extreme tsunami event.
- These results would also apply should an intake basin with the same geometry be selected for the new NIs.

The results show the following for the proposed tunnel intakes:

- For operational conditions the volume of sand drawn into the tunnel intakes which will have to be removed from the proposed landside intake basins is less than 2 200 m^3/y. This is significantly less than the average maintenance dredging volume of the existing KNPS intake basin of approximately 132 000 m^3/y.

CONTROLLED DISCLOSURE

When downloaded from the EDS database, this document is uncontrolled and the responsibility rests with the user to ensure it is in line with the authorised version on the database.

- A maintenance dredging programme will be required to prevent excessive sedimentation in the basin and to keep a sufficient buffer for storm events.
- For extreme storm events the sand volume increases significantly and the 10^{-6} storm event results in similar sand volumes over the 4.1-day storm event as the annual maintenance dredging at KNPS. The intake basin will need to be designed to accommodate these sediment volumes without blocking the pumps.

Blockage of Intakes and Biofouling

Based on the KNPS and worldwide experience and it can be concluded that the new NIs intakes could be designed to cope with the marine species found at the site and to minimise the risk of complete blockage of the intake.

Future Work

The estimation of the influence of climate change has been based on the most reliable scientific information available at the time that this study was undertaken, but must be continually reassessed as new data and research results become available (at least every five years). This shall include the IPCC 6th Assessment Report (AR6) which has recently been published in draft format. The SSR would only need to be updated should one of the relevant climate change parameters change significantly.

Marine geotechnical surveys and additional numerical modelling will be required as part of future engineering design studies of the intake and outfall structures.

Based on available information, meteorite impact tsunamis cannot be screened out at the 10^{-8} y^{-1} exceedance probability. Although there are many factors which mitigate the risk (e.g., no currently identified asteroids are predicted to have any consequences in the next 100 years, impact from NEOs can be predicted up to several years in advance for tracked NEOs and a few days or more in advance for previously unidentified NEOs, and ongoing development is expected to greatly increase NEO identification capability), it is recommended that further investigation is carried out to quantify this and update previous assessments.

The tsunami sources due to local earthquakes should be reviewed once the results of the Duynefontyn Probabilistic Seismic Hazard Analysis (PSHA) study currently being undertaken by CGS are available.

CONTROLLED DISCLOSURE

When downloaded from the EDS database, this document is uncontrolled and the responsibility rests with the user to ensure it is in line with the authorised version on the database.

CONTENTS

EXECUTIVE SUMMARY 5.9-3
5.9 OCEANOGRAPHY AND COASTAL ENGINEERING 5.9-23
5.9.1 Introduction 5.9-23
5.9.2 Definitions and Abbreviations 5.9-23
5.9.3 Purpose and Scope 5.9-29
5.9.4 Regulatory Framework 5.9-33
5.9.5 Requirements Documents and Guides 5.9-33
5.9.6 Approach to Evaluation 5.9-34
5.9.6.1 Oceanographic Monitoring 5.9-34
5.9.6.2 Extreme Value Analysis 5.9-39
5.9.6.3 Numerical Modelling 5.9-40
5.9.6.4 Conceptual Design for New NIs 5.9-42
5.9.7 Climate Change 5.9-42
5.9.8 Physical Description of the Site 5.9-49
5.9.9 Hydrographic Conditions 5.9-56
5.9.9.1 Tidal Levels 5.9-57
5.9.9.2 Storm Surge 5.9-60
5.9.9.3 Long Waves 5.9-66
5.9.9.4 Currents 5.9-72
5.9.9.5 Seawater Temperature 5.9-79
5.9.9.6 Salinity 5.9-85
5.9.9.7 Suspended Sediment 5.9-85
5.9.9.8 Waves 5.9-87
5.9.9.9 Joint Probability 5.9-117
5.9.10 Coastline Stability 5.9-126
5.9.10.1 Long-Term Coastline Trends 5.9-126
5.9.10.2 Recession due to Sea Level Rise 5.9-132
5.9.10.3 Longshore Sediment Transport 5.9-136
5.9.10.4 Coastline Changes due to Wave Rotation 5.9-144
5.9.10.5 Cross-Shore Erosion 5.9-146
5.9.10.6 Resultant Coastline Stability 5.9-155
5.9.11 Storm Wave Run-Up and Drawdown 5.9-165

CONTROLLED DISCLOSURE

When downloaded from the EDS database, this document is uncontrolled and the responsibility rests with the user to ensure it is in line with the authorised version on the database.

5.9.11.1 Introduction 5.9-165
5.9.11.2 Model Description 5.9-165
5.9.11.3 Model Setup 5.9-166
5.9.11.4 Model Calibration 5.9-173
5.9.11.5 Cases Modelled 5.9-176
5.9.11.6 Results 5.9-177
5.9.12 Tsunamis 5.9-188
5.9.12.1 Introduction 5.9-188
5.9.12.2 Scope of Work 5.9-188
5.9.12.3 Approach 5.9-189
5.9.12.4 Historical Tsunamis 5.9-190
5.9.12.5 Numerical Modelling 5.9-192
5.9.12.6 Screening of Tsunami Sources 5.9-200
5.9.12.7 Distant Earthquakes 5.9-204
5.9.12.8 Volcanic Flank Collapse 5.9-207
5.9.12.9 Local Submarine Landslides 5.9-213
5.9.12.10 Regional Model Results 5.9-219
5.9.12.11 Tsunami Inundation Model 5.9-220
5.9.12.12 Tsunami Results 5.9-227
5.9.13 Flooding from the Sea 5.9-229
5.9.14 Extreme Low Water Levels 5.9-234
5.9.15 Thermal Plume Dispersion 5.9-238
5.9.15.1 Introduction 5.9-238
5.9.15.2 Discharge Characteristics 5.9-239
5.9.15.3 Engineering Concepts for Intake and Outfall Structures 5.9-240
5.9.15.4 Damage to Cooling Water Intake and Outfall Structures 5.9-249
5.9.15.5 Dispersion Modelling 5.9-249
5.9.15.6 Thermal Recirculation 5.9-274
5.9.15.7 Extreme Seawater Temperatures at Intakes 5.9-276
5.9.16 Sediment Transport 5.9-278
5.9.16.1 Sedimentation and Scour Due to Storms 5.9-278
5.9.16.2 Sedimentation and Scour Due to Tsunamis 5.9-287
5.9.16.3 Suspended Sand at Intakes 5.9-293

CONTROLLED DISCLOSURE

When downloaded from the EDS database, this document is uncontrolled and the responsibility rests with the user to ensure it is in line with the authorised version on the database.

5.9.17 Blockage of Intakes and Biofouling 5.9-298
5.9.18 Uncertainties and Future Work 5.9-302
5.9.19 Monitoring Programme 5.9-303
5.9.20 Management System 5.9-304
5.9.21 Conclusions 5.9-311
5.9.21.1 Climate Change 5.9-311
5.9.21.2 Nearshore Waves 5.9-313
5.9.21.3 Coastline Erosion 5.9-313
5.9.21.4 Flooding from the Sea 5.9-314
5.9.21.5 Extreme Low Water Levels 5.9-316
5.9.21.6 Thermal Plume Dispersion and Recirculation 5.9-318
5.9.21.7 Extreme Seawater Temperatures 5.9-319
5.9.21.8 Sedimentation and Scour 5.9-320
5.9.21.9 Blockage of Intakes and Biofouling 5.9-322
5.9.22 References 5.9-323
APPENDIX A: STORM WAVE RUN-UP RESULTS 5.9-332
APPENDIX B: TSUNAMI RESULTS 5.9-373
APPENDIX C: THERMAL PLUME DISPERSION FIGURES 5.9-384

CONTROLLED DISCLOSURE

When downloaded from the EDS database, this document is uncontrolled and the responsibility rests with the user to ensure it is in line with the authorised version on the database.

TABLES

Table 5.9.1: Definitions.....5.9-23

Table 5.9.2: Abbreviations.....5.9-28

Table 5.9.3: PPE Parameters for new NIs Relevant to Oceanography and Coastal Engineering 5.9-32

Table 5.9.4: Coordinates of Oceanographic Instruments. 5.9-36

Table 5.9.5: Coordinates of Beach Profile Measurements. 5.9-37

Table 5.9.6: Summary of Oceanographic Monitoring Programme.....5.9-38

Table 5.9.7: Overview of Numerical Models Used.....5.9-41

Table 5.9.8: Climate Change Applied for Each Oceanographic Parameter and Date. 5.9-47

Table 5.9.9: Ongoing and Near-Future Projects at KNPS. 5.9-53

Table 5.9.10: Tidal Constituents at Duynefontyn (Baseline Date is 2019).....5.9-59

Table 5.9.11: Predicted Tidal Levels at Duynefontyn (Baseline Date is 2019). ...5.9-60

Table 5.9.12: Extreme Positive Storm Surge and Maximum Still Water Levels. .5.9-64

Table 5.9.13: Extreme Negative Storm Surge and Minimum Still Water Levels. .5.9-65

Table 5.9.14: Extreme Long Wave Amplitudes. 5.9-71

Table 5.9.15: Summary of Measured Current Speeds. 5.9-76

Table 5.9.16: Extreme Depth-Averaged Hourly-Averaged Current Speed at Site B (Water Depth -29 m msl). 5.9-78

Table 5.9.17: Statistics of Measured Hourly Seawater Temperature. 5.9-81

Table 5.9.18: Seasonal Percentiles of Measured Seawater Temperature Stratification. 5.9-81

Table 5.9.19: Extreme Maximum Seawater Temperatures. 5.9-84

Table 5.9.20: Summary of Measured Total Suspended Solids.....5.9-86

Table 5.9.21: Summary of Measured Waves. 5.9-91

Table 5.9.22: Summary of Available Offshore Hindcast Data.....5.9-92

Table 5.9.23: Available Offshore Measured Wave Data.....5.9-93

Table 5.9.24: Comparison of Modelled and Measured Best Estimate Extreme Wave Heights at Cape Point Location (Water Depth -70 m msl).....5.9-97

Table 5.9.25: Extreme Wave Parameters at Point 1 in a Depth of -31 m msl. ..5.9-116

Table 5.9.26: Categories of Dependence (Petroliagkis, et al., 2016). 5.9-119

Table 5.9.27: Joint Exceedance Probability of Positive Storm Surge and Wave Height for χ = 0.316. .....5.9-122

CONTROLLED DISCLOSURE

When downloaded from the EDS database, this document is uncontrolled and the responsibility rests with the user to ensure it is in line with the authorised version on the database.

Table 5.9.28: Joint Exceedance Probability of Negative Storm Surge and Wave Height for Zero Dependence and n = 365 .....5.9-124
Table 5.9.29: Sediment Parameters Used in Longshore Transport Model 5.9-139
Table 5.9.30: Longshore Sediment Transport Results. 5.9-142
Table 5.9.31: Equilibrium Angles and Coastline Rotation. 5.9-145
Table 5.9.32: SBEACH Model Setup Parameters. 5.9-151
Table 5.9.33: Truncation of Dune Crest Levels. 5.9-155
Table 5.9.34: Coastline Stability Adjacent to KNPS. 5.9-156
Table 5.9.35: Coastline Stability in Front of New NIs. 5.9-157
Table 5.9.36: Maximum Coastline Erosion Adjacent to KNPS and in Front of New NIs. 5.9-164
Table 5.9.37: Bottom Roughness Applied in Wave Model. 5.9-173
Table 5.9.38: Extreme Flooding Due to Storm Waves. 5.9-187
Table 5.9.39: Extreme Low Water Levels Due to Storm Waves. 5.9-187
Table 5.9.40: Comparison of Measured and Modelled Amplitudes. 5.9-197
Table 5.9.41: Unit Sources Used in the Refined Source Model SCO3 for the Scotia Subduction Zone (PRDW, 2022a). 5.9-205
Table 5.9.42: Refined Volcanogenic Flank Collapse Sources (PRDW, 2022a).5.9-208
Table 5.9.43: Refined Volcanogenic Deposit Geometries. 5.9-208
Table 5.9.44: Refined Local Submarine Landslide Sources (PRDW, 2022a)....5.9-214
Table 5.9.45: Flooding Due to Tsunamis. 5.9-228
Table 5.9.46: Extreme Low Water Levels due to Tsunamis. 5.9-228
Table 5.9.47: Flooding from the Sea. 5.9-230
Table 5.9.48: Extreme Low Water Levels. 5.9-235
Table 5.9.49: Discharge characteristics for KNPS including SGR and TPU. 5.9-239
Table 5.9.50: Discharge Characteristics for New NIs 5.9-240
Table 5.9.51: Layout 1 Intake and Outfall Configurations. 5.9-243
Table 5.9.52: Layout 2 Intake and Outfall Configurations. 5.9-245
Table 5.9.53: Layout 3 Outfall Configuration. 5.9-247
Table 5.9.54: Layout 4 Outfall Configuration. 5.9-249
Table 5.9.55: Recirculation at KNPS Intake and New NIs Intake. 5.9-275
Table 5.9.56: Extreme Maximum Seawater Temperatures at the Intakes (Including Recirculation). 5.9-277

CONTROLLED DISCLOSURE

When downloaded from the EDS database, this document is uncontrolled and the responsibility rests with the user to ensure it is in line with the authorised version on the database.

Table 5.9.57: Sedimentation and Scour at the KNPS Intake Basin due to Storms. .5.9-286

Table 5.9.58: Sedimentation and Scour at the KNPS Intake Basin due to Tsunamis. 5.9-292

Table 5.9.59: Sand Volume Drawn into Cooling Water Intake Tunnels for 2 500 MWe Power Station. 5.9-297

Table 5.9.60: Sand Volume Drawn into Cooling Water Intake Tunnels for 4 000 MWe Power Station. 5.9-297

Table 5.9.61: Marine Species Found at the Site.....5.9-299

Table 5.9.62: Summary of Major Debris Events at KNPS Since 1997 (EPRI, 2021). 5.9-299

Table 5.9.63: Summary of Measured Biofouling Thickness.....5.9-302

Table 5.9.64: Summary of Activities, Links and Quality Requirements. 5.9-306

Table 5.9.65: Regulatory Compliance Matrix.....5.9-308

Table 5.9.66: Climate Change Applied for Each Oceanographic Parameter and Date. 5.9-312

Table 5.9.67: Extreme Wave Parameters at a Depth of -31 m msl in Front of the Site. 5.9-313

Table 5.9.68: Maximum Coastline Erosion Adjacent to KNPS and in Front of New NIs. 5.9-314

Table 5.9.69: Flooding from the Sea. 5.9-315

Table 5.9.70: Extreme Low Water Levels.....5.9-317

Table 5.9.71: Recirculation at KNPS Intake and New NIs Intake. 5.9-318

Table 5.9.72: Extreme Maximum Seawater Temperatures at the Intakes (Including Recirculation). 5.9-319

Table 5.9.73: Sedimentation and Scour at the KNPS Intake Basin due to Storms. .5.9-320

Table 5.9.74: Sand Volume Drawn into Cooling Water Intake Tunnels. 5.9-321

CONTROLLED DISCLOSURE

When downloaded from the EDS database, this document is uncontrolled and the responsibility rests with the user to ensure it is in line with the authorised version on the database.

FIGURES

Figure 5.9.1: Location of Oceanographic Instruments. 5.9-35

Figure 5.9.2: Location of Beach Profile Measurements. 5.9-36

Figure 5.9.3: Global Mean Sea Level (GMSL) and Regional Mean Sea Level (RMSL) Projections for the Upper End of the Likely Range of RCP8.5 and the Maximum Plausible Scenarios. 5.9-44

Figure 5.9.4: Site Location Including Multi-Beam Bathymetry Offshore of the Site. 5.9-51

Figure 5.9.5: Bathymetry and Topography at the Site Showing the Location of KNPS and the Estimated Location of New NIs. 5.9-52

Figure 5.9.6: Bathymetry: Detail Showing Ongoing or Near-Future Projects at KNPS Included in the Models. 5.9-54

Figure 5.9.7: Measured Sediment Grain Size Offshore and Along the Beach. 5.9-56

Figure 5.9.8: Measured Hourly Water Levels at Site C2 Inside the KNPS Intake Basin. 5.9-57

Figure 5.9.9: Measured Hourly Water Levels at Cape Town. 5.9-58

Figure 5.9.10: Measured Water Level, Predicted Tide and Storm Surge at Cape Town for the Entire Dataset (Top), Detail for 2020 (Top Middle), the May 1984 Storm (Bottom Middle) and the June 2017 Storm (Bottom). 5.9-61

Figure 5.9.11: Extreme Value Analysis of Positive Storm Surge Residuals at Cape Town (Baseline Date is 1993.5). 5.9-62

Figure 5.9.12: Extreme Value Analysis of Negative Storm Surge Residuals at Cape Town (Baseline Date is 1993.5). 5.9-63

Figure 5.9.13: Locations of Tide Gauges 5.9-66

Figure 5.9.14: Propagation of a Meteo-tsunami Event Measured Along the South African Coast 5.9-67

Figure 5.9.15: Extreme Value Analysis of Positive Long Wave Amplitude (Baseline Date is 2013). 5.9-69

Figure 5.9.16: Extreme Value Analysis of Negative Long Wave Amplitude (Baseline Date is 2013). 5.9-70

Figure 5.9.17: Time-Series of Measured Currents at Site A (Water Depth -10 m msl). 5.9-73

Figure 5.9.18: Time-Series of Measured Currents at Site B (Water Depth -29 m msl). 5.9-74

Figure 5.9.19: Measured Current Roses at Sites A and B. 5.9-75

Figure 5.9.20: Extreme Value Analysis of Depth-Averaged Hourly-Averaged Current Speed at Site B (Depth -29 m msl) (Baseline Date is 2015). 5.9-77

CONTROLLED DISCLOSURE

When downloaded from the EDS database, this document is uncontrolled and the responsibility rests with the user to ensure it is in line with the authorised version on the database.

Figure 5.9.21: Time-series of Measured Seawater Temperatures and Stratification at all Sites. Bottom plots show the results for 2020 in more detail.....5.9-80

Figure 5.9.22: Time-series of Seawater Temperatures at Site C (Water Depth -3 m msl) used for the EVA. The blue dots show the events selected for the EVA, i.e., the extreme value series. 5.9-82

Figure 5.9.23: Extreme Value Analysis of Seawater Temperature at Site C (Water Depth -3 m msl) (Baseline Date is 2012).....5.9-83

Figure 5.9.24: Total Suspended Solids Sampling Locations. 5.9-85

Figure 5.9.25: Total Suspended Solids Distribution in Water Column. 5.9-86

Figure 5.9.26: Time-series of Measured Wave Parameters at Site A (Water Depth -10 m msl).....5.9-88

Figure 5.9.27: Time-series of Measured Wave Parameters at Site B (Water Depth -29 m msl).....5.9-89

Figure 5.9.28: Wave Roses at Site A and Site B.....5.9-90

Figure 5.9.29: Locations of Available Offshore Hindcast Data. 5.9-93

Figure 5.9.30: Scatterplot Comparison of Modelled and Measured Operational Wave Heights at Cape Point Location (Water Depth -70 m msl).....5.9-95

Figure 5.9.31: Comparison of Modelled and Measured Best Estimate Extreme Wave Heights at Cape Point Location (Water Depth -70 m msl).....5.9-97

Figure 5.9.32: Mesh Used for the Reanalysis Wave Modelling. 5.9-99

Figure 5.9.33: Bathymetry Used for the Reanalysis Wave Modelling.....5.9-100

Figure 5.9.34: Example Instantaneous Wave Refraction. 5.9-102

Figure 5.9.35: Time-Series Comparison of Modelled and Measured Spectral Wave Parameters at Site A. 5.9-103

Figure 5.9.36: Time-Series Comparison of Modelled and Measured Spectral Wave Parameters at Site B. 5.9-104

Figure 5.9.37: Wave Rose Comparison of Modelled and Measured Waves at Site A (12 March 2008 to 31 December 2009) and Site B (11 July 2008 to 31 December 2009).....5.9-105

Figure 5.9.38: Scatterplot Comparison of Measured and Modelled Wave Height at Site A for 360 Days of Valid Data Overlap (12 March 2008 to 31 December 2009). 5.9-106

Figure 5.9.39: Scatterplot Comparison of Measured and Modelled Wave Height at Site B for 270 Days of Valid Data Overlap (11 July 2008 to 31 December 2009)....5.9-107

Figure 5.9.40: Time-series of 10 Years (2000-2009) of Modelled Operational Wave Parameters at Point 1 (-31 m msl).....5.9-108

CONTROLLED DISCLOSURE

When downloaded from the EDS database, this document is uncontrolled and the responsibility rests with the user to ensure it is in line with the authorised version on the database.

Figure 5.9.41: 3D Scatterplot of 10 Years (2000-2009) of Modelled Operational Wave Parameters at Point 1 (-31 m msl).....5.9-109

Figure 5.9.42: Scatterplot Comparison of Measured and Modelled Wave Height Peaks at Site B for 54 events of Valid Data Overlap between September 2009 and August 2020. .....5.9-110

Figure 5.9.43: Scatterplot Showing Relationship between Wave Height and Period at Point 1 from Modelled Storms Between 1979 and 2020. .....5.9-112

Figure 5.9.44: Scatterplot Showing Relationship between Wave Height and Direction at Point 1 from Modelled Storms between 1979 and 2020. The 5th, 50th, and 95th Percentiles of MWD were Determined from the H_{m0}-MWD Distribution for Waves Exceeding the 1 y^{-1} Exceedance Probability H_{m0}. 5.9-113

Figure 5.9.45: Scatterplot Showing Relationship between Wave Height and Directional Spreading at Point 1 from Modelled Storms between 1979 and 2020. The 50th Percentile of DSD was Determined from the H_{m0}-DSD Distribution for Waves Exceeding the 1 y^{-1} Exceedance Probability H_{m0}. 5.9-114

Figure 5.9.46: Extreme Value Analysis of Wave Height at Point 1 in a Depth of -31 m msl (Baseline Date is 2000). 5.9-115

Figure 5.9.47: Scatterplot of Storm Surge Measured at Cape Town and Offshore Hindcast Wave Height. 5.9-120

Figure 5.9.48: Dependence Parameter χ of Positive Storm Surge and Wave Height at Cape Town. 5.9-121

Figure 5.9.49: Dependence Parameter χ of Negative Storm Surge and Wave Height at Cape Town. 5.9-123

Figure 5.9.50: Scatterplot of Measured Wave Height and Depth-Averaged Current Speed at Site B. 5.9-125

Figure 5.9.51: Dependence Parameter χ of Wave Height and Current Speed at Site B. 5.9-125

Figure 5.9.52: Measured Beach Profiles at Profile 08 located south of KNPS. .5.9-127

Figure 5.9.53: Measured Beach Profiles at Profile 14 located north of KNPS in front of the new NIs. 5.9-127

Figure 5.9.54: Horizontal Movement of the +1 m msl Level Over Time (Profiles 1 to 10 are South of KNPS and Profiles 11 to 21 are North of KNPS).....5.9-128

Figure 5.9.55: Horizontal Movement of the +3 m msl Level Over Time (Profiles 1 to 10 are South of KNPS and Profiles 11 to 21 are North of KNPS).....5.9-129

Figure 5.9.56: Horizontal Movement of the +5 m msl Level Over Time (Profiles 1 to 10 are South of KNPS and Profiles 11 to 21 are North of KNPS).....5.9-130

Figure 5.9.57: Long-term Coastline Trends from Measured Beach Profiles. 5.9-131

CONTROLLED DISCLOSURE

When downloaded from the EDS database, this document is uncontrolled and the responsibility rests with the user to ensure it is in line with the authorised version on the database.

Figure 5.9.58: Plan View of Cross-Shore Profiles Used for Coastline Stability Analysis. 5.9-135

Figure 5.9.59: Example of Profile Recession due to Sea Level Rise for Profile P506 for the year 2130. Also Shown are the Cumulative Coastline Changes due to Wave Rotation and Long-term Trends.....5.9-136

Figure 5.9.60: Location of Profiles A to E Used in the Longshore Sediment Transport Model. 5.9-138

Figure 5.9.61: Time-series of Waves (at the Offshore End of the Profile), Instantaneous Sand Transport (Integrated Across the Profile) and Accumulated Sand Transport at Profile C (Positive is Northward and Negative is Southward). 5.9-141

Figure 5.9.62: Sediment Budget.....5.9-144

Figure 5.9.63: Coastline changes due to Wave Rotation. Positive Values Indicate Accretion and Negative Values Indicate Erosion. 5.9-146

Figure 5.9.64: Comparison of Measured and Modelled Eroded Profiles for the SUPERTANK and Delta Flume Tests. 5.9-148

Figure 5.9.65: Storm Duration Analysis Based on 43 Offshore Storms. The Synthetic Tide For 2021 (Excluding Storm Surge and Sea Level Rise) is Shown for Reference. 5.9-150

Figure 5.9.66: Profile P506 Cross-Shore Erosion Results for Storm Surge Dominant Return Periods. 5.9-152

Figure 5.9.67: Vertical Erosion Analysis of Dune Crest Levels. For Each Return Period the Worst Combination of Storm Surge and Wave Height is Shown. 5.9-154

Figure 5.9.68: Pre-storm Topography and Erosion Lines for 2021 for the 10^{-2}, 10^{-4}, 10^{-6} and 10^{-8} y^{-1} Storms in Front of the KNPS. 5.9-159

Figure 5.9.69: Adjusted Pre-storm Topography and Erosion Lines for 2064 for the 10^{-2}, 10^{-4}, 10^{-6} and 10^{-8} y^{-1} Storms in Front of the KNPS. 5.9-160

Figure 5.9.70: Pre-storm Topography and Erosion Lines for 2021 for the 10^{-2}, 10^{-4}, 10^{-6} and 10^{-8} y^{-1} Storms in Front of the New NIs. 5.9-161

Figure 5.9.71: Adjusted Pre-storm Topography and Erosion Lines for 2064 for the 10^{-2}, 10^{-4}, 10^{-6} and 10^{-8} y^{-1} Storms in Front of the New NIs. 5.9-162

Figure 5.9.72: Adjusted Pre-storm Topography and Erosion Lines for 2130 for the 10^{-2}, 10^{-4}, 10^{-6} and 10^{-8} y^{-1} Storms in Front of the New NIs. 5.9-163

Figure 5.9.73: MIKE 3 Wave Model Domain and Bathymetry 5.9-167

Figure 5.9.74: Detail of MIKE 3 Wave Model Mesh. 5.9-168

Figure 5.9.75: Detail of Model Bathymetry for 2021 for Storm Exceedance Probabilities of 10^{-2} and 10^{-4} y^{-1} (Excluding Dune Erosion). 5.9-169

Figure 5.9.76: Detail of Model Bathymetry for 2021 for Storm Exceedance Probability of 10^{-8} y^{-1} (Including Dune Erosion). 5.9-170

CONTROLLED DISCLOSURE

When downloaded from the EDS database, this document is uncontrolled and the responsibility rests with the user to ensure it is in line with the authorised version on the database.

Figure 5.9.77: Detail of Model Bathymetry for 2064 for Storm Exceedance Probabilities of 10^{-8} (Including Dune Erosion). 5.9-171

Figure 5.9.78: Detail of Model Bathymetry for 2130 for Storm Exceedance Probabilities of 10^{-8} (Including Dune Erosion). 5.9-172

Figure 5.9.79: Maximum Modelled Water Surface Elevation During 7 June 2017 Storm and Measured Debris Line. 5.9-174

Figure 5.9.80: Time-series of Measured and Modelled Water Levels Inside the KNPS Basin for Two Hours During the 13 July 2020 Storm. 5.9-175

Figure 5.9.81: Measured and Modelled Frequency Spectra Inside the KNPS Basin During the 13 July 2020 Storm. 5.9-176

Figure 5.9.82: Instantaneous Water Surface Elevation (Top) and Profiles of Water Surface Elevation Through the New NIs (Middle) and KNPS Breakwater (Bottom) for the 10^{-8} y^{-1} Wave-Dominated Case in 2021. ....5.9-178

Figure 5.9.83: Instantaneous Water Surface Elevation (Colours) and Depth-Averaged Currents (Vectors) at KNPS for the 10^{-8} y^{-1} Wave-Dominated Case in 2021. ....5.9-179

Figure 5.9.84: Instantaneous Water Surface Elevation (Colours) and Depth-Averaged Currents (Vectors) at new NIs for the 10^{-8} y^{-1} Wave-Dominated Case in 2021. 5.9-180

Figure 5.9.85: Definition Sketch for Vertical Run-Up Level and Horizontal Inundation Distance. 5.9-181

Figure 5.9.86: Maximum Water Depth Due to Wave Run-Up at KNPS for the 10^{-8} y^{-1} Storm in 2021. ....5.9-182

Figure 5.9.87: Maximum Depth-Averaged Current Speed Due to Wave Run-Up at KNPS for the 10^{-8} y^{-1} Storm in 2021. ....5.9-183

Figure 5.9.88: Maximum Water Depth Due to Wave Run-Up at the New NIs for the 10^{-8} y^{-1} Storm in 2021. ....5.9-184

Figure 5.9.89: Maximum Depth-Averaged Current Speed Due to Wave Run-Up at the New NIs for the 10^{-8} y^{-1} Storm in 2021. ....5.9-185

Figure 5.9.90: Time-series of Modelled Water Surface Elevations at the KNPS Intake and at Depths of -20 and -30 m msl for the 10^{-8} y^{-1} Storm in 2021. ....5.9-186

Figure 5.9.91: Vertical Cross-Section (Left) and Plan View of the Experiment Showing the Locations of the Four Wave Gauges (Right). 5.9-194

Figure 5.9.92: Snapshots in Time Showing the Propagation of the Slide-generated Waves. Note the Plots Have a Vertical Exaggeration Factor of ×2. ....5.9-195

Figure 5.9.93: Time-series Comparison of Measured and Modelled Water Surface Elevation at the Four Wave Gauges. 5.9-196

Figure 5.9.94: Process of the Kinematics Implementation and Coupling to the Hydrodynamic Model. 5.9-199

CONTROLLED DISCLOSURE

When downloaded from the EDS database, this document is uncontrolled and the responsibility rests with the user to ensure it is in line with the authorised version on the database.

Figure 5.9.95: Maximum and Minimum Water Surface Elevations Along the Coastline at the Site Collated from All the Propagation Sensitivity Runs. 5.9-203

Figure 5.9.96: Scotia Model Domain and Bathymetry. 5.9-206

Figure 5.9.97: Maximum Water Surface Elevation for the SCO3c1 Scenario (Default Asperity Location, 0 km Depth). Isolines Show the Bathymetry Contours at 1 000 m Intervals.....5.9-207

Figure 5.9.98: Tristan da Cunha Model Domain and Bathymetry.....5.9-209

Figure 5.9.99: Cross-section of Tristan da Cunha and the Initial Landslide Geometry. Note the Vertical and Horizontal Axes are Not to Scale. 5.9-210

Figure 5.9.100: Tristan da Cunha D_1 Scenario. Snapshots of Instantaneous Water Surface Elevation. Isolines Show the Bathymetry Contours at 1 000 m Intervals. ..5.9-211

Figure 5.9.101: Tristan da Cunha D_1: Maximum Water Surface Elevation (Top), Snapshot of Instantaneous Water Surface Elevation (Middle), Time-series of Water Surface Elevation at KNPS and at the Location of Maximum Nearshore Water Surface Elevation (Bottom).....5.9-212

Figure 5.9.102: Bathymetry Used for the Local Submarine Landslide Models. The Source Centroids of the Landslides are Shown in Red for the Six Local Submarine Landslides Which Resulted in the Largest Water Surface Elevations at the Site and Orange for the Rest.....5.9-215

Figure 5.9.103: LSL9 D_1 scenario. Snapshots of Instantaneous Water Surface Elevation. Isolines Show the Bathymetry Contours at 200 m Intervals.....5.9-217

Figure 5.9.104: LSL9 D_1 scenario. Maximum Water Surface Elevation (Top), Snapshot of Instantaneous Water Surface Elevation (Middle), Time-series of Water Surface Elevation at KNPS and at the Location of Maximum Nearshore Water Surface Elevation.....5.9-218

Figure 5.9.105: Maximum and Minimum Water Surface Elevations Along the Coastline at the Site Collated from All the Refined Runs. The Shaded Grey Bars Show the Range of Minimum and Maximum Values from the Sensitivity Runs. For Reference, the 10^{-8} y^{-1} Exceedance Probability Long Waves Are Also Shown.....5.9-220

Figure 5.9.106: Tsunami Inundation Model Mesh and Bathymetry. 5.9-221

Figure 5.9.107: Detail of Tsunami Inundation Model Mesh. 5.9-222

Figure 5.9.108: Instantaneous Water Surface Elevation (Colours) and Currents (Vectors) for the Tristan da Cunha D_1 Volcanic Flank Collapse Tsunami at the 2021 High Antecedent Water Level, Showing Inundation from the Second Wave Crest. Thick Vectors Show Current Speeds Exceeding 6 m/s.....5.9-224

Figure 5.9.109: Maximum Water Depth at KNPS for the Tristan da Cunha D_1 Volcanic Flank Collapse Tsunami at the 2021 High Antecedent Water Level.....5.9-226

CONTROLLED DISCLOSURE

When downloaded from the EDS database, this document is uncontrolled and the responsibility rests with the user to ensure it is in line with the authorised version on the database.

Figure 5.9.110: Maximum Water Depth at the New NIs for the Tristan da Cunha D_1 Volcanic Flank Collapse Tsunami at the 2021 High Antecedent Water Level. ..5.9-227

Figure 5.9.111: Vertical Run-up Levels at KNPS.....5.9-231

Figure 5.9.112: Horizontal Inundation Distance at KNPS. 5.9-231

Figure 5.9.113: Vertical Run-up Levels at new NIs. 5.9-232

Figure 5.9.114: Horizontal Inundation Distance at new NIs. 5.9-232

Figure 5.9.115: Extreme Low Water Levels at KNPS Pump Intakes. 5.9-236

Figure 5.9.116: Extreme Low Water Levels at New NIs Pump Intakes (Assuming a Basin Intake with Similar Geometry to KNPS). 5.9-236

Figure 5.9.117: Extreme Low Water Levels at a Depth of -20 m msl Opposite the new NIs (Possible Tunnel Intake Location). 5.9-237

Figure 5.9.118: Extreme Low Water Levels at a Depth of -30 m msl Opposite the new NIs (Possible Tunnel Intake Location). 5.9-237

Figure 5.9.119: Layout 0: Existing KNPS Intake Basin and Outfall Channel. 5.9-240

Figure 5.9.120: Schematic Diagram Showing the Main Components for an Offshore Tunnel Intake and Outfall Configuration. 5.9-241

Figure 5.9.121: Layout 1: Short Tunnel Intakes and Outfalls (4000 MWe). For 2500 MWe the Southern Intake and Outfall Tunnels Are Excluded.....5.9-242

Figure 5.9.122: Layout 2: Long Tunnel Intakes and Outfalls (4000 MWe). For 2500 MWe the Southern Intake and Outfall Tunnels Are Excluded.....5.9-244

Figure 5.9.123: Layout 3: Basin Intake and Tunnel Outfalls (4000 MWe). For 2500 MWe the Southern Outfall Tunnel Is Excluded. 5.9-246

Figure 5.9.124: Layout 4: Basin intake and rubble-mound outfall structure.....5.9-248

Figure 5.9.125: Dynamic Coupling of Near-Field and Far-Field Models: Entrainment Sinks Along the Plume Trajectory and Distributed Sources at the Release Location. 5.9-251

Figure 5.9.126: Model Domain and Bathymetry. 5.9-252

Figure 5.9.127: Detail of Model Mesh Used for Layout 1. .....5.9-253

Figure 5.9.128: Time-Series Comparison of Modelled and Measured Current Speed and Direction at Site A (Depth -10 m msl). 5.9-255

Figure 5.9.129: Time-Series Comparison of Modelled and Measured Current Speed and Direction at Site B (Depth -29 m msl). 5.9-256

Figure 5.9.130: Current Rose Comparison of Modelled and Measured Currents at Site A (1 January 2009 to 31 December 2009). 5.9-257

Figure 5.9.131: Current Rose Comparison of Modelled and Measured Currents at Site B (1 January 2009 to 31 December 2009). 5.9-258

CONTROLLED DISCLOSURE

When downloaded from the EDS database, this document is uncontrolled and the responsibility rests with the user to ensure it is in line with the authorised version on the database.

Figure 5.9.132: Percentile Comparisons of Modelled and Measured Current Speeds at Site A and B (1 January 2009 to 31 December 2009). 5.9-259

Figure 5.9.133: Time-Series Comparison of Modelled and Measured Near-Seabed Seawater Temperatures at Site C1, A, B, D and E.....5.9-261

Figure 5.9.134: Percentile Comparisons of Modelled and Measured Seawater Temperatures at Site C1, A, and B, and Temperature Differences Between the Sites (right). 5.9-262

Figure 5.9.135: KNPS + new NIs (4000 MWe) Layout 1: Example of Instantaneous Seawater Temperature and Currents at Surface. 5.9-265

Figure 5.9.136: KNPS + new NIs (4000 MWe) Layout 4: Example of Instantaneous Seawater Temperature and Currents at Surface. 5.9-266

Figure 5.9.137: KNPS + new NIs (4000 MWe) Layout 1: 99th Percentile ΔT at Surface (top) and Seabed (bottom). 5.9-267

Figure 5.9.138: KNPS (2108 MWe): 99th Percentile ΔT at Worst Water Depth. 5.9-269

Figure 5.9.139: KNPS + new NIs (4000 MWe) Layout 1: 99th Percentile ΔT at Worst Water Depth. 5.9-270

Figure 5.9.140: KNPS + new NIs (4000 MWe) Layout 2: 99th Percentile ΔT at Worst Water Depth. 5.9-271

Figure 5.9.141: KNPS + new NIs (4000 MWe) Layout 3: 99th Percentile ΔT at Worst Water Depth. 5.9-272

Figure 5.9.142: KNPS + new NIs (4000 MWe) Layout 4: 99th Percentile ΔT at Worst Water Depth. 5.9-273

Figure 5.9.143: Recirculation at KNPS Intake and New NIs Intake for the Nine Modelled Cases.....5.9-275

Figure 5.9.144: Storm Sedimentation and Scour Model Bathymetry and Mesh. 5.9-279

Figure 5.9.145: Example Results of 10^{-2} y^{-1} Storm, 50^{th} Percentile Wave Direction, High Water Level, with Waves Dominant, Showing Instantaneous Waves (Top Left), Currents (Top Right) and Sediment Transport (Bottom Left) at the Peak of the Storm, and Bed Level Change at the End of the Storm (Bottom Right). 5.9-283

Figure 5.9.146: Maximum Scour Depth: 10^{-2} y^{-1} Storm, 50^{th} Percentile Wave Direction. 5.9-284

Figure 5.9.147: Maximum Scour Depth: 10^{-8} y^{-1} Storm, 50^{th} Percentile Wave Direction. 5.9-284

Figure 5.9.148: Maximum Scour Depth: 10^{-8} y^{-1} Storm, 5^{th} Percentile Wave Direction. 5.9-285

CONTROLLED DISCLOSURE

When downloaded from the EDS database, this document is uncontrolled and the responsibility rests with the user to ensure it is in line with the authorised version on the database.

Figure 5.9.149: Maximum Bed Level: 10^{-8} y^{-1} Storm, 95th Percentile Wave Direction. 5.9-285

Figure 5.9.150: Bed Level at the Start (Top Left) and End (Top Right) of the Simulation, Integrated Net Transport (Bottom Left), and Bed Level Change at the End of the Simulation (Bottom Right).....5.9-290

Figure 5.9.151: Maximum Bed Level During the Simulation.....5.9-291

Figure 5.9.152: Maximum Scour Depth During the Simulation.....5.9-291

Figure 5.9.153: Tsunami Erosion of the Dune Ridges North and South of KNPS During the Tristan da Cunha D_1 Volcanic Flank Collapse Tsunami for 2021 and a High Antecedent Water Level. 5.9-293

Figure 5.9.154: Example of Modelled Vertical Profile of Suspended Sand in Depths of -20 and -30 m msl at the Peak of the 10^{-8} y^{-1} Storm. 5.9-296

Figure 5.9.155: Biofouling after 6 Months at 8 m Depth (Left) and After 14 Months in 10 m Depth (Right). 5.9-302

CONTROLLED DISCLOSURE

When downloaded from the EDS database, this document is uncontrolled and the responsibility rests with the user to ensure it is in line with the authorised version on the database.

5.9 OCEANOGRAPHY AND COASTAL ENGINEERING

5.9.1 Introduction

This section of this Site Safety Report (SSR) presents the results from the oceanography and coastal engineering studies undertaken for the existing Koeberg Nuclear Power Station (KNPS) and the planned development of new nuclear installation(s) (NIs) at the Duynefontyn site, based on the Technical Specification for this section (Eskom, 2021). Details of the studies undertaken in support of this section are contained in the following reports:

- Duynefontyn Tsunami Hazard Analysis (PRDW, 2022a);
- Duynefontyn Tsunami Hazard Analysis: V&V Report (PRDW, 2021);
- Duynefontyn SSR Ch 5.9: V&V Report (PRDW, 2022b);
- Duynefontyn SSR Ch 5.9: 4 Yrs Oceanographic Monitoring Data (PRDW, 2022c).

This section complements the remaining sections of ***Chapter 5*** (Site Characteristics) related to the site characteristics and provides input for the identification of external hazards associated with coastline stability, flooding from the sea and integrity of cooling water supplies in ***Chapter 6*** (Evaluation of External Events). Hazards associated with flooding from the land are addressed in ***Section 5.10*** (Hydrology and Hydraulics).

5.9.2 Definitions and Abbreviations

The definitions and abbreviations used in this section are provided in ***Table 5.9.1*** and ***Table 5.9.2***, respectively.

Table 5.9.1: Definitions

Definition	Explanation
Added mass	In fluid mechanics, added mass or virtual mass is the inertia added to a system because an accelerating or decelerating body must move (or deflect) some volume of surrounding fluid as it moves through it.
Antecedent still water level	The still water level that existed before the arrival of the tsunami.
Astronomical Tide	The periodic rising and falling of the water level that results from gravitational attraction of the moon, sun and other astronomical bodies acting upon the rotating earth.
Asperity	Region of a fault that experiences little aseismic slip and higher slip during earthquake events.
Atmospheric pressure	The force per unit area exerted by an atmospheric column (the entire body of air above the specified area).
Barometer	A device used to measure atmospheric pressure.

CONTROLLED DISCLOSURE

When downloaded from the EDS database, this document is uncontrolled and the responsibility rests with the user to ensure it is in line with the authorised version on the database.

Basal Coulomb friction	The tangential force between a sliding mass and slip surface, proportional to the magnitude of the normal force. Coulomb friction is independent of contact area and speed of slippage.
Bathymetry	Level of the seabed relative to a defined datum.
Beach profile	Intersection of the beach level with a vertical plane perpendicular to the coastline.
Benthic	Organisms living on the bed of the water body.
Best estimate	In the context of Extreme Value Analysis, the best estimate refers to the estimate from the original data, i.e., the most probable estimate.
Biofouling	The undesirable accumulation of micro-organisms, plants, algae, and animals on submerged structures.
Bottom friction	The effect of the roughness of the seabed on currents or wave orbital velocities.
Bulk density	The density of soil accounting for voids between individual particles. Dry bulk density is calculated as the bulk mass divided by the bulk volume, assuming voids are filled with air. Wet bulk density is calculated as the bulk mass divided by the bulk volume, assuming voids are filled with water. Relative dry or wet bulk density is calculated as the dry or wet bulk density divided by the density of water.
Coastline	The line that forms the boundary between the land and the sea.
Coriolis force	A force that as a result of the earth's rotation deflects moving objects.
Cross-shore	Perpendicular to the shoreline or coastline.
Current	Flow of water in a specific direction.
Current direction	The direction towards which the current is flowing, measured clockwise from true north.
Deep water wave	A deep water wave has this ratio less than 2. A shallow water has a wavelength to water depth ratio exceeding 25. A transitional water wave lies in between shallow and deep water waves.
Directional Standard Deviation (DSD)	A measure of the directional spreading of the waves, calculated from the two-dimensional wave spectrum.
Dispersive and non-dispersive waves	Dispersive waves are when the propagation speed depends on the wave frequency, with low-frequency waves having a higher propagation speed than high-frequency waves. Non-dispersive waves are when the propagation speed is independent of wave frequency.
Drawdown	The minimum water level resulting from a storm wave or a tsunami wave.
Eddy viscosity	A model viscosity used to account for unresolved turbulent processes.
Erosion line	The most landward extent where any erosion of the topography occurs.
Exceedance probability	The probability that an event with a certain value will be exceeded in a given time period.
Flather boundary	A Flather boundary is when both the water surface elevation and the current are specified on the boundary of a hydrodynamic model.
Flood depth	The difference between the water level and ground level.

CONTROLLED DISCLOSURE

When downloaded from the EDS database, this document is uncontrolled and the responsibility rests with the user to ensure it is in line with the authorised version on the database.

Grain size	D_N is the diameter for which N% of the sediment, by mass, has a smaller diameter, e.g., D_{50} is the median grain diameter.
Gaussian	Relating to the Gauss distribution (also called the normal distribution).
Helmholtz mode	Also known as the pumping mode, when the water surface of a semi-enclosed water body moves up and down in phase.
Hindcast	Historical modelled data that provides information for the analysis of atmospheric and marine environments at specific sites.
Hydrodynamics	The movement of fluid.
Hydrostatic and non-hydrostatic models	Hydrostatic models assume a static vertical pressure distribution equal to that of water at rest. Non-hydrostatic models consider the effect of dynamic pressure and are thus appropriate for situations with significant vertical acceleration.
Intertidal zone	The area of the shore that lies between the highest normal high tide and the lowest normal low tide.
Inundation	The maximum horizontal inundation distance that the water reached, measured perpendicularly inland from a predefined baseline.
Joint probability	The statistical measure that calculates the likelihood of two parameters (e.g., waves and storm surge) occurring together at the same time. The joint probability depends on the site-specific level of dependence between parameters.
Landslide	The movement downslope of a mass of rock, debris, earth or soil. This includes five modes of slope movement: falls, topples, slides, spreads, and flows. Subaerial landslides are initiated on land, while submarine landslides are initiated under the surface of the ocean. Slide movements can either be translational or rotational. Rotational slides are also referred to as slumps.
Landslide deformation	Landslides can be rigid (no change in geometry during movement) or deforming (after initial failure the slide loses its internal structure and flows, collapses, or breaks up into debris or rubble).
Littoral drift	The term used for the longshore transport of sediments, along the upper shoreface due to the action of breaking waves and longshore currents.
Long waves	Fluctuations in still water level with periods between 8 and 60 min. Long waves typically include: edge waves, bound waves, tsunamis (generated by geophysical phenomena such as earthquakes) and meteo-tsunamis (generated by atmospheric pressure fluctuations).
Longshore	Moving parallel to the shoreline or coastline.
Mean Sea Level (MSL)	Throughout Section 5.9 the vertical datum used is mean sea level (msl), also known as Land Levelling Datum (LLD).
Mean wave direction (MWD)	The mean direction calculated from the full two-dimensional wave spectrum by weighting the energy at each direction and frequency. Wave direction is defined as the direction from which the wave is coming, measured clockwise from true north.
Mean wave period (T_m)	The spectral estimate of the mean wave period, calculated from the ratio between the zeroth and first spectral moments.
Meteo-tsunami	A long-period wave generated by atmospheric pressure fluctuations.
Moment Magnitude (Mw or **M**)	The magnitude derived from the scalar seismic moment, M_0. Mw is given by the relationship log (M_0 in dyne-cm) = 1.5 Mw +16.1. The moment magnitude scale **M** is

CONTROLLED DISCLOSURE

When downloaded from the EDS database, this document is uncontrolled and the responsibility rests with the user to ensure it is in line with the authorised version on the database.

	given by **M**=2/3log (M_0 in dyne-cm)-10.7. The result is a 0.03-magnitude difference between Mw and **M** for the same value of M_0.
Near-Earth Objects (NEO)	Asteroids and comets that come close to or pass across Earth's orbit around the Sun
Nearshore	Close to the shore, e.g., water depths up to approximately 30 m.
Nikuradse roughness	A method for specifying bottom friction in spectral wave models, where the dissipation coefficient depends on the wave hydrodynamic conditions.
Nowcast	Refers to modelled weather data for the present time, rather than in the past or future.
Operational	Operational conditions are those occurring normally, e.g., up to once per year, as opposed to extreme conditions which occur less than once per year.
Peak wave period (T_p)	The wave period with the maximum wave energy density in the wave energy spectrum.
Probable Maximum Tsunami (PMT)	The PMT is that tsunami for which the impact at the site is derived from the use of best available scientific information to arrive at a set of scenarios reasonably expected to affect the nuclear power plant site, taking into account (1) appropriate consideration of the most severe of the natural phenomena that have been historically reported for the site and surrounding area, with sufficient margin for the limited accuracy, quantity, and period of time in which the historical data have been accumulated; (2) appropriate combinations of the effects of normal and accident conditions with the effects of the natural phenomena; and (3) the importance of the safety functions to be performed.
Reanalysis	A process of historical observational meteorological data assimilation and assessment to generate long term global climate models.
RCP	Representative Concentration Pathway used for climate change scenarios.
Run-up	The maximum vertical run-up level, defined as the highest ground or building level flooded by the storm or tsunami wave. Depending on the topography this point may or may not coincide with the maximum inundation.
Salinity	The measure of all the salts dissolved in water.
Sand budget	The analysis of the erosion or accretion rate of sediment at a specific location by considering the factors that affect the transport of sediment along a coast, e.g., longshore and cross-shore transport, dredging, aeolian and alluvial transport.
Sedimentation	The process of transportation and deposition of sediment particles onto the bottom of a body of water.
Seiche	An oscillation of an enclosed or semi-enclosed body of water in response to an atmospheric, oceanographic or seismic disturbing force.
Semi-diurnal	Having a tidal cycle that experiences two high tides and two low tides during a one-day period.
Scour	The removal of sediment around coastal structures during extreme storm events due to fast flowing water and waves.
Shallow water wave	A shallow water has a wavelength to water depth ratio exceeding 25. A deep water wave has this ratio less than 2. A transitional water wave lies in between shallow and deep water waves.

CONTROLLED DISCLOSURE

When downloaded from the EDS database, this document is uncontrolled and the responsibility rests with the user to ensure it is in line with the authorised version on the database.

Sigma coordinates	In 3D numerical grids, sigma coordinates represent vertical coordinates as a function of total water depth, i.e., layer thickness varying from horizontal grid point to grid point.
Significant wave height (H_{m0})	The energy-based significant wave height, defined by $H_{m0} = 4\sqrt{m_0}$, where m_0 is the zeroth moment of the wave energy spectrum. H_{m0} is approximately equal to the mean of the highest one-third of waves in a sea state having a typical duration of 20 minutes.
Slip (earthquakes)	Movement on a fault plane.
Still Water Level (SWL)	The water level in the absence of waves.
Storm surge	The influence of meteorological effects such as winds and barometric pressure that result in the actual sea level being above or below the predicted astronomical tide level.
Stratification	The water column contains water layers with different densities due to the different salinities, temperatures and suspended sediment concentrations. The less dense water layers lay on top of the higher density layers.
Subduction zone	A convergent boundary where two tectonic plates meet and where one of the plates subducts below the other.
Surf-beat	The long period (typically more than 60 s) oscillation of the water line on the beach, related to the infragravity waves in the surf zone.
Water surface elevation	Level of the water surface relative to a defined datum.
Swell (waves)	Waves that are generated far offshore in the deep sea that propagate onshore and make up the low frequency part of the wave spectrum, defined in this study as wave periods in the range 30 s > T > 6 s.
Synthetic tide	In this context a water surface elevation time-series generated using one tidal constituent.
Topography	Level of the land relative to a defined datum.
Tsunami	A long-period wave caused by an underwater disturbance such as a volcano, submarine landslide or earthquake.
Upwelling	Upwelling is when the surface water is displaced offshore by wind blowing alongshore over the ocean and is then replaced by cold water from below.
Wave direction	The direction from which the wave is coming, measured clockwise from true north.
Wave refraction	The process by which the height and direction of a wave moving in shallow water at an angle to the bed contours is changed.
Wave set-up	An increase in water level due to breaking waves.
Wave shoaling	The increase in wave height as waves propagate into shallower depth.
Wind direction	The direction from which the wind is coming, measured clockwise from true north.
Wind set-up	An increase in water level due to onshore winds.

CONTROLLED DISCLOSURE

When downloaded from the EDS database, this document is uncontrolled and the responsibility rests with the user to ensure it is in line with the authorised version on the database.

Table 5.9.2: Abbreviations

Abbreviation	Explanation
2D	Two-dimensional
3D	Three-dimensional
ADCP	Acoustic Doppler Current Profiler
AR6	6th Assessment Report from the IPCC
CGS	Council for Geoscience
COTS	Commercial-Off-The-Shelf software
CRF	Circulating Water System
CSIR	Council for Science and Industrial Research
DGPS	Differential Global Positioning System
DHI	Danish Hydraulics Institute
DSD	Directional Standard Deviation
DTHA	Dynefontyn Tsunami Hazard Analysis
EMCWF	European Center for Medium-Range Weather Forecasts
EPRI	Electric Power Research Institute
EVAs	Extreme Value Analysis
FM	Flexible Mesh
GMSL	Global Mean Sea Level
HAT	Highest Astronomical Tide
HYCOM	HYbrid Coordinate Ocean Model
IAEA	International Atomic Energy Agency
IPCC	Intergovernmental Panel for Climate Change
KNPS	Koeberg Nuclear Power Station
LAT	Lowest Astronomical Tide
LiDAR	Light Detection and Ranging
LLD	Land Levelling Datum
MHWN	Mean High Water Neaps
MHWS	Mean High Water Springs
ML	Mean (Tidal) Level
MLWN	Mean Low Water Neap
MLWS	Mean Low Water Spring
MSL	Mean Sea Level
MWD	Mean Wave Direction
NASA	US National Aeronautics and Space Administration

CONTROLLED DISCLOSURE

When downloaded from the EDS database, this document is uncontrolled and the responsibility rests with the user to ensure it is in line with the authorised version on the database.

NCEP	National Centers for Environmental Prediction
NEO	Near-Earth Objects
NIs	Nuclear Installation(s)
NNR	National Nuclear Regulator
NOAA	(United States) National Oceanic and Atmospheric Administration
NRC	(United States) Nuclear Regulatory Commission
NS	Navier-Stokes
NSWE	Non-Linear Shallow Water Equations
NTHMP	(United States) National Tsunami Hazard Mitigation Program
PMT	Probable Maximum Tsunami
PPE	Plant Parameter Envelope
RCPs	Representative Concentration Pathways
RMS	Root-Mean-Square
RMSL	Regional Mean Sea Level
SAR	Safety Analysis Report
SBEACH	Storm-induced BEAch Change model
SEC	Essential Service Water System
SLR	Sea Level Rise
SMF	Submarine Mass Failure
SOPs	Standard Operating Procedures
SROCC	IPCC's Special Report: The Ocean and Cryosphere in a Changing Climate
SSCs	Structures, Systems and Components
SSR	Site Safety Report
STPQ3D	Quasi Three-Dimensional Sediment Transport Model
SWL	Still Water Level
TSS	Total Suspended Solids
V&V	Verification and Validation
WANO	World Association of Nuclear Operators

5.9.3 Purpose and Scope

The purpose of this section of this SSR is to identify the requirements and to demonstrate the technical acceptability of the site with regard to coastline stability, flooding from the sea, integrity of cooling water supply and thermal plume dispersion. Design considerations for seawater cooling water intake and outfall layouts for the new NIs are also provided.

CONTROLLED DISCLOSURE

When downloaded from the EDS database, this document is uncontrolled and the responsibility rests with the user to ensure it is in line with the authorised version on the database.

The layout and structure of this section is provided below, including a brief description of the contents of the main subsections and the linkages between them:

- 5.9.1 Introduction
- 5.9.2 Definitions and Abbreviations
- 5.9.4 Regulatory Framework
- 5.9.5 Requirements Documents and Guides
- 5.9.6 Approach to Evaluation: The approach combined oceanographic measurements, extreme value analysis, detailed numerical modelling studies and conceptual engineering design.
- 5.9.7 Climate Change: The effect of climate change on all relevant oceanographic and coastal engineering parameters has been estimated and the changes are described in this subsection. These changes have then been applied as described in the subsection relevant to each parameter.
- 5.9.8 Physical Description of the Site: The topography at the site, the bathymetry offshore and the sediment characteristics are described.
- 5.9.9 Hydrographic Conditions: This section characterises the hydrographic conditions at the site based on measurements and numerical modelling. These conditions comprise tides, storm surge, long waves, currents, seawater temperature, salinity, waves and where relevant the joint probabilities between these parameters. These hydrographic conditions are used as inputs to the coastline stability, flooding from the sea, thermal plume dispersion and sediment transport modelling, as described in the subsections that follow.
- 5.9.10 Coastline Stability: In order to assess the potential instability of the coastline near the site, the following physical processes and timescales have been evaluated by analysing measured data and modelling: long-term coastline trends, recession due to sea level rise, longshore sediment transport, coastline changes due to wave rotation and cross-shore erosion.
- 5.9.11: Storm Wave Run-Up and Drawdown: This section describes the wave modelling undertaken to estimate the maximum vertical run-up, maximum horizontal inundation and minimum vertical drawdown due to storms.
- 5.9.12 Tsunamis: This section describes the modelling undertaken to estimate the maximum vertical run-up, maximum horizontal inundation and minimum vertical drawdown due to tsunamis.

CONTROLLED DISCLOSURE

When downloaded from the EDS database, this document is uncontrolled and the responsibility rests with the user to ensure it is in line with the authorised version on the database.

- 5.9.13 Flooding from the Sea: This section describes flooding due to both storm wave run-up as described in Subsection 5.9.11 and tsunami run-up as described in Subsection 5.9.12.
- 5.9.14 Extreme Low Water Levels: This section describes the extreme low water levels at the cooling water intakes due to both storm drawdown as described in Subsection 5.9.11 and tsunami drawdown as described in Subsection 5.9.12.
- 5.9.15 Thermal Plume Dispersion: This section describes engineering concepts for intake and outfall structures for the new NIs, dispersion modelling of the thermal plumes from the new NIs and KNPS, thermal recirculation and extreme seawater temperatures at the intakes.
- 5.9.16 Sediment Transport: Sediment transport modelling was carried out to assess the sedimentation in the KNPS intake basin entrance and scour around coastal structures due to both extreme storm events and tsunamis. Modelling was also performed to estimate the volume of sand drawn into the tunnel intakes, should these be selected for the new NIs.
- 5.9.17 Blockage of Intakes and Biofouling: This section describes potential mechanisms for blockage of the intakes including biofouling.
- 5.9.18: Uncertainties and Future Work
- 5.9.10: Management System
- 5.9.21 Conclusions.

The evaluation of the site took into account the relevant Plant Parameter Envelope (PPE) values for the new NIs (Eskom, 2022a), as given below.

CONTROLLED DISCLOSURE

When downloaded from the EDS database, this document is uncontrolled and the responsibility rests with the user to ensure it is in line with the authorised version on the database.

Table 5.9.3: PPE Parameters for new NIs Relevant to Oceanography and Coastal Engineering

PPE Parameter	Definition	Enveloping Limits(s)
Plant design life	The designed lifetime of the plant, including planned midlife refurbishments	60 y + 20 y life extension
Maximum flood or tsunami (terrace height)	Design assumption regarding the difference in elevation between finished plant grade and the water level due to the probable maximum flood (or tsunami).	The terrace height must be such that the new NIs terrace is elevated above design basis flooding hazards.
Cooling Water Flow Rate	Total cooling water flow rate through the condenser (also the rate of withdrawal from and return to the water source)	76 m^3/s per 1650 MWe unit
Cooling Water Temperature Rise	Temperature rise across the condenser (temperature of water out minus temperature of water in)	12°C
Cooling Water Temperature Range	The range of water temperatures at the intake	-0.5°C to 30°C
Maximum increase in the cooling water source	Design value for the maximum temperature increase in the cooling water source.	The intake and the outfall configuration should not result in a net rise in CW. The maximum increase in the temperature of the recirculated water should be less than 1.5°C. Increases in the water temperature will most likely be limited by environmental issues for each specific site.

The scope includes both the existing KNPS and the planned new NIs at the Duynefontyn site. As stated in ***Chapter 3*** (Overview of Planned Activities at the Site), it is assumed that KNPS will continue to operate until 2044, after which a 20-y decommissioning period will follow (i.e., until 2064), during which spent fuel will be retained on-site. It is further assumed that the new NIs will become operational from 2030, will operate for 60 y, which will be extended to 80 y (i.e., up to 2110), after which a decommissioning period of 20 y will follow (i.e., up to 2130). Therefore, this section assesses the following dates with respect to climate change:

- 2021: present-day;
- 2044: end of operations for KNPS;
- 2064: end of decommissioning period for KNPS;
- 2110: end of operations for the new NIs;
- 2130: end of decommissioning period for the new NIs.

CONTROLLED DISCLOSURE

When downloaded from the EDS database, this document is uncontrolled and the responsibility rests with the user to ensure it is in line with the authorised version on the database.

5.9.4 Regulatory Framework

The legal and regulatory basis for the overall SSR process is outlined in ***Chapter 2*** of this SSR. The current national regulations specifically relevant to an oceanography and coastal engineering investigation to be taken into account for site selection are Regulation R.927: Regulations on Licensing of Sites for New Nuclear Installations (Department of Energy, 2011) which requires that the SSR provides the following:

"4(5) Natural phenomena and potential man-made hazards must be appropriately accounted for in the design of the new nuclear installation(s) …";

"5(3) The characteristics of the site relevant to the design assessment, risk and dose calculations, including inter alia:

(a) external events;

(b) meteorological data;

(f) projections of the above data commensurate with the design life of the nuclear installation(s)".

5.9.5 Requirements Documents and Guides

The following National Nuclear Regulator (NNR) Requirements Documents were taken into account where applicable:

- RD-0034, Quality and Safety Management Requirements for Nuclear Installations (NNR, 2008);
- RG-0011, Interim Guidance on the Siting of Nuclear Facilities (NNR, 2016a);
- RG-0016, Guidance on the Verification and Validation of Evaluation and Calculation Models used in Safety and Design Analyses (NNR, 2016b);
- PP-0014, Consideration of External Events for Nuclear Installations (NNR, 2014).

The following international guides were consulted to ensure that the work follows international best practice:

- IAEA Safety Guide No. SSG-18, Meteorological and Hydrological Hazards in Site Evaluation for Nuclear Installations (IAEA, 2011);
- IAEA Safety Guide No. NS G 1.9, Design of the Reactor Coolant System and Associated Systems in Nuclear Power Plants (IAEA, 2004);

CONTROLLED DISCLOSURE

When downloaded from the EDS database, this document is uncontrolled and the responsibility rests with the user to ensure it is in line with the authorised version on the database.

- US Nuclear Regulatory Commission (US NRC), Regulation 1.27, Ultimate Heat Sink for Nuclear Power Plants (NRC, 2015);
- US NRC, Regulatory Guide 1.59, Design Basis Floods for Nuclear Power Plants (NRC, 1977);
- US NRC, Regulatory Guide 1.70, Standard Format and Content of Safety Analysis Reports for Nuclear Power Plants (NRC, 1978);
- US NRC, Regulatory Guide 1.206, Combined License Applications for Nuclear Power Plants (NRC, 2007a);
- US NRC, Regulatory Guide 1.102, Flood Protection for Nuclear Power Plants (NRC, 1976);
- US NRC, NUREG-0800, Part 2.4.5, Probable Maximum Surge and Seiche Flooding (NRC, 2007b);
- US NRC, NUREG-0800, Part 2.4.6, Probable Maximum Tsunami Hazards (NRC, 2007c);
- US NRC, NUREG-0800, Part 2.4.11, Low Water Considerations (NRC, 2007d);
- US NRC, NUREG/CR-7046 (PNNL-20091), Design-Basis Flood Estimation for Site Characterization at Nuclear Power Plants in the United States of America (NRC, 2011);
- US NRC, NUREG/CR-7223, Tsunami Hazard Assessment: Best Modeling Practices and State-of-the-Art Technology (NRC, 2016).

5.9.6 Approach to Evaluation

The approach to the site evaluation combined oceanographic measurements, extreme value analysis, detailed numerical modelling studies and conceptual engineering design, as detailed below.

5.9.6.1 Oceanographic Monitoring

A comprehensive oceanographic data collection programme has been implemented at the site. The objective of this programme is to provide baseline data for:

- evaluation of the site and NIs safety;
- design of coastal structures at the site, e.g., intakes and outfalls;
- calibration and validation of the numerical models to confirm that models are accurate and can thus be used for estimation of both frequent and rare events.

CONTROLLED DISCLOSURE

When downloaded from the EDS database, this document is uncontrolled and the responsibility rests with the user to ensure it is in line with the authorised version on the database.

The programme was initiated during SSR1 from 2008 to 2013 and has been continued during SSR2 from 2017 and is currently scheduled to end in March 2022. Data measured up to October 2021 is included in this report, with the exception of seawater temperature for which data up to January 2022 has been included, in order to include a high temperature event that occurred during this period. The locations of the instruments deployed at the Duynefontyn site are provided ***Figure 5.9.1*** and ***Table 5.9.4***. The locations of beach profile measurements are provided in ***Figure 5.9.2*** and ***Table 5.9.5***.

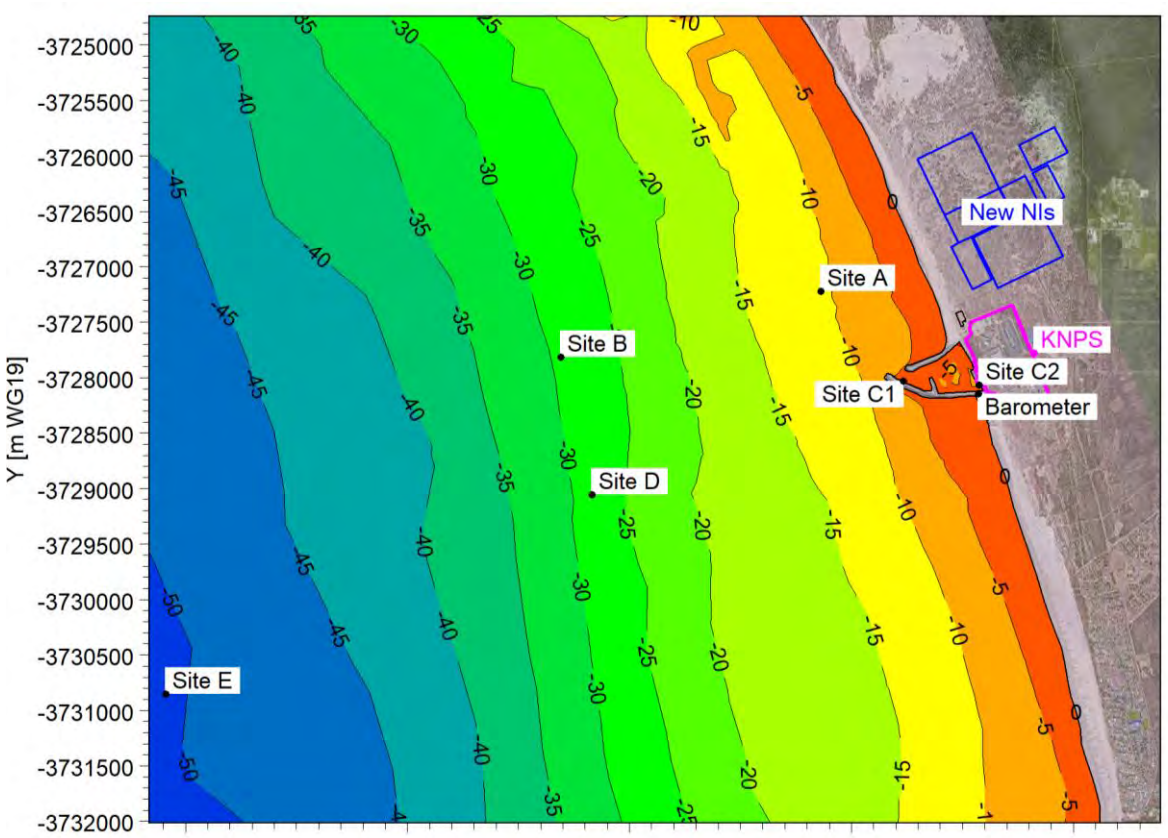


Figure 5.9.1: Location of Oceanographic Instruments.

CONTROLLED DISCLOSURE

When downloaded from the EDS database, this document is uncontrolled and the responsibility rests with the user to ensure it is in line with the authorised version on the database.

Table 5.9.4: Coordinates of Oceanographic Instruments.

Location	Position	Water Depth (m msl)
Site A	18.4148°E, 33.6701°S	-10.0
Site B	18.3895°E, 33.6753°S	-29.0
Site C1	18.4227°E, 33.6774°S	-3.0
Site C2	18.4301°E, 33.6778°S	-3.9
Site D	18.3924°E, 33.6865°S	-27.0
Site E	18.3509°E, 33.7025°S	-50.0
Land-based barometer	18.4300°E, 33.6785°S	+4.7

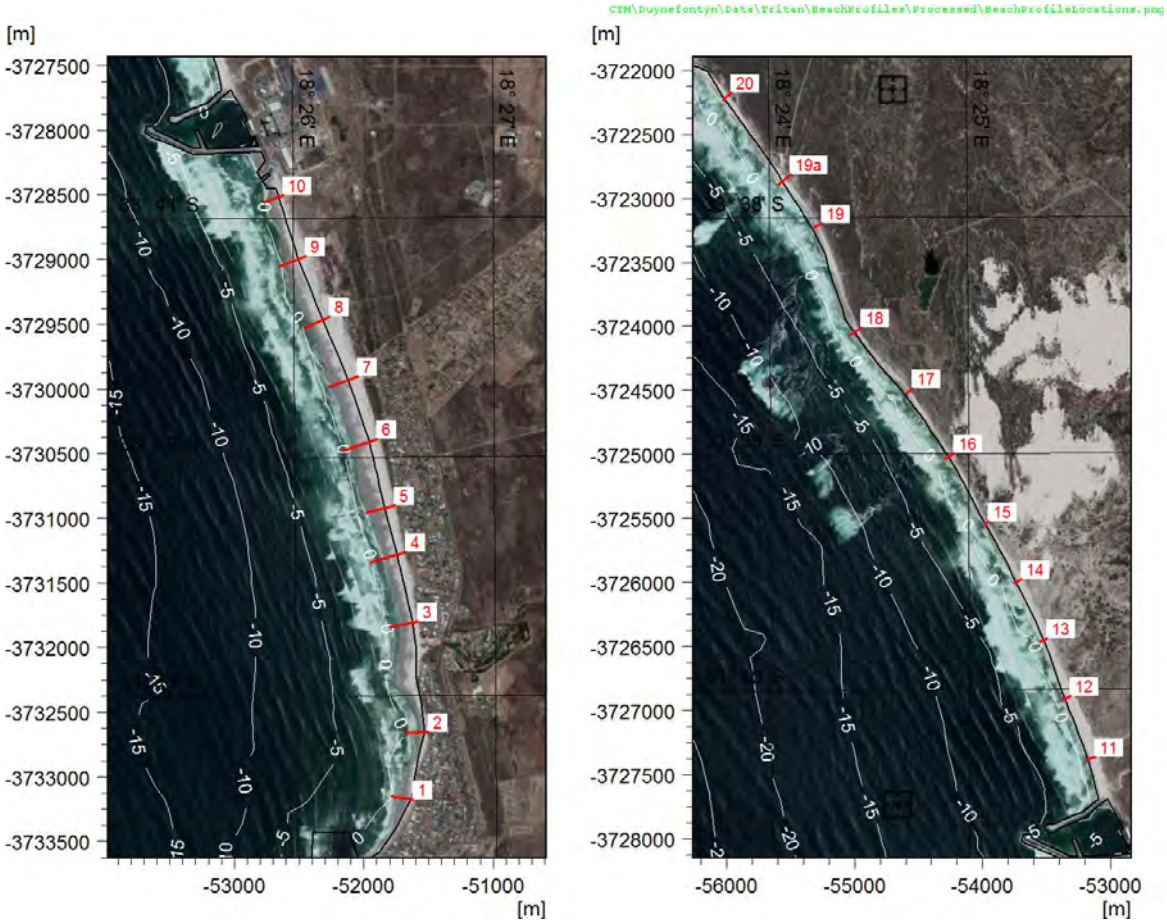


Figure 5.9.2: Location of Beach Profile Measurements.

CONTROLLED DISCLOSURE

When downloaded from the EDS database, this document is uncontrolled and the responsibility rests with the user to ensure it is in line with the authorised version on the database.

Table 5.9.5: Coordinates of Beach Profile Measurements.

Profile	Position	Profile	Position
1	18.4431°E, -33.7239°S	11	18.4272°E, -33.6714°S
2	18.4444°E, -33.7192°S	12	18.4251°E, -33.6671°S
3	18.4436°E, -33.7115°S	13	18.4232°E, -33.6631°S
4	18.4426°E, -33.7067°S	14	18.4211°E, -33.6589°S
5	18.4417°E, -33.7034°S	15	18.4184°E, -33.6548°S
6	18.4402°E, -33.6988°S	16	18.4155°E, -33.6500°S
7	18.4386°E, -33.6944°S	17	18.4120°E, -33.6454°S
8	18.4363°E, -33.6902°S	18	18.4077°E, -33.6411°S
9	18.4344°E, -33.6860°S	19	18.4045°E, -33.6337°S
10	18.4325°E, -33.6817°S	19a	18.4019°E, -33.6303°S
		20	18.3970°E, -33.6245°S

The oceanographic monitoring programme is summarised in ***Table 5.9.6***. The programme has been reviewed and updated over time, e.g., the Acoustic Doppler Current Profiler (ADCP) at Site A was replaced with a temperature sensor during SSR1 and the pressure sensor at Site C2 was added for SSR2.

CONTROLLED DISCLOSURE

When downloaded from the EDS database, this document is uncontrolled and the responsibility rests with the user to ensure it is in line with the authorised version on the database.

Table 5.9.6: Summary of Oceanographic Monitoring Programme

Location	Instrument	Parameters	Sampling Interval	Start Date	End Date	Valid Data
Site A	Acoustic Doppler Current Profiler (ADCP)	Current speed and direction at 0.5 m depth intervals	10 min	Jan 2008	Jul 2010	1.22 y
		Waves: 2D spectrum, significant wave height (H_{m0}), peak wave period (T_p), mean wave direction (MWD)	1 h	Jan 2008	Jul 2010	1.53 y
	Temperature sensor	Water temperature	10 min	Jan 2008	Oct 2021	8.55 y
	Conductivity sensor	Salinity	10 min	Jan 2008	Oct 2010	0.96 y
	Asbestos plate	Biofouling thickness	6 months	May 2008	Nov 2009	4 plates
Site B	Acoustic Doppler Current Profiler (ADCP)	Current speed and direction at 1.0 m depth intervals	10 min	Jul 2008	Oct 2021	7.08 y
		Waves: 2D spectrum, H_{m0}, T_p, MWD	1 h	Jul 2008	Oct 2021	7.00 y
	Temperature sensor	Water temperature	10 min	Jul 2008	Oct 2021	8.57 y
	Conductivity sensor	Salinity	10 min	Oct 2008	Nov 2009	0.54 y
	Asbestos plate	Biofouling thickness	14 months	May 2009	Jul 2010	1 plate
Site C1	Temperature sensor	Water temperature (data provided by C Maxwell)	Daily at 08:00	Jan 1995	Dec 2002	7.21 y
			1 h	Jan 2003	Aug 2011	7.25 y
Site C2	Temperature and pressure sensor	Water temperature	10 min	Jul 2017	Jan 2022	4.11 y
		Water level	1 s	Jul 2017	Oct 2021	3.82 y
	Barometer	Atmospheric pressure (for water level correction)	1 min	Jul 2017	Oct 2021	3.58 y
Site D	Temperature sensor	Water temperature (data provided by Bayworld)	1 h	Jun 2008	Jan 2009	0.55 y
Site E	Temperature sensor	Water temperature (data provided by Bayworld)	1 h	Feb 2008	Jan 2009	0.90 y
Beach Profiles 1 to 20	Survey using Differential Global Positioning System (DGPS)	Beach level	Quarterly for first 2 y, then annually	Apr 2008	Jan 2021	13 surveys
Depths between -5 and -20 m and beach	Grab samples and sieve analysis	Sediment grain size distribution	Once off	Mar 2008	Mar 2008	61 samples
Depths between -5 and -30 m	Niskin bottle and laboratory analysis	Total suspended solids (TSS)	2 monthly	Jun 2008	Jul 2010	142 samples

CONTROLLED DISCLOSURE

When downloaded from the EDS database, this document is uncontrolled and the responsibility rests with the user to ensure it is in line with the authorised version on the database.

The results of these measurements are described in ***Subsections 5.9.9*** and ***5.9.10.1*** below. Further details of the monitoring programme are provided in the Oceanographic Monitoring Report (PRDW, 2022c).

5.9.6.2 Extreme Value Analysis

In line with Eskom's external hazards requirements (Eskom, 2011) and the NNR defined risk categories (NNR, 2014), the external hazards have been quantified for the following annual exceedance probabilities: 10^{-2}, 10^{-4}, 10^{-5}, 10^{-6}, 10^{-7} and 10^{-8} y^{-1}.

The exceedance probability is related to return period as follows:

$$Exceedance\ probability = \frac{1}{return\ period} \qquad \text{Equation 5.9.1}$$

An event with an annual exceedance probability of 10^{-2} y^{-1} means that, on average, the probability of this event being exceeded in one year is 10^{-2}. Equivalently, the event will have a return period of 100 y and will, on average, be exceeded once every 100 y.

The extreme value analyses (EVAs) were undertaken using the MIKE Extreme Value Analysis software (DHI, 2021a) and (DHI, 2021b). The theorical basis and the V&V of the EVA software is described in the supporting V&V Report (PRDW, 2022b).

The analysis was performed by fitting a 3-parameter Weibull distribution using either the method of moments or the method of L-moments to an extreme value series extracted from the input time-series. The extreme value series was selected using the 'peaks over threshold' method (also called the 'partial duration series'), with the threshold defined as the value that is exceeded 4 times per year on average. To ensure independence, two successive events were extracted only if the time between the events exceeded 48 hours.

The uncertainty was calculated using the Jackknife method (DHI, 2021b), in which the analysis is repeated n times, where n is the number of data points in the extreme values series, with one data point excluded at a time. The output of the uncertainty analysis is the mean and standard deviation of the estimate for each probability of exceedance. The estimate is assumed to be normally distributed which allows the 5^{th} and 95^{th} percentile estimates to be calculated. Note that it is only the estimate for each probability of exceedance that is assumed to be normally distributed, whilst the data is assumed to follow the Weibull distribution.

For each annual probability of exceedance the following four estimates are provided:

CONTROLLED DISCLOSURE

When downloaded from the EDS database, this document is uncontrolled and the responsibility rests with the user to ensure it is in line with the authorised version on the database.

- Best estimate = the estimate from the original data set, i.e., the most probable estimate which should be used in preference to the mean estimate;
- Mean estimate = the mean estimate from the Jackknife resampling;
- 5^{th} percentile = mean - 1.645 × standard deviation;
- 95^{th} percentile = mean + 1.645 × standard deviation.

Should the most probable estimate be required, then the best estimate should be used rather than the mean estimate.

The probabilities of exceedance were estimated by performing an extreme value analysis on long-term time-series of the following datasets:

- Storm surge (***Subsection 5.9.9.2***);
- Long waves (***Subsection 5.9.9.3***);
- Currents (***Subsection 5.9.9.4***);
- Seawater temperature (***Subsection 5.9.9.5***);
- Waves (***Subsection 5.9.9.8***).

The results of the extreme value analyses are presented in the relevant subsections below. As discussed in ***Subsection 5.9.18***, the extreme value estimates for probabilities less than 10^{-2} y^{-1} need to be interpreted with caution due to the limited duration of the available datasets.

5.9.6.3 Numerical Modelling

Numerical modelling has been undertaken to extend the duration of the measured oceanographic parameters and to simulate the coastal processes required to quantify the hazards at the site.

The modelling was undertaken using the MIKE suite of software developed by DHI A/S in Denmark. This is Commercial-Off-The-Shelf (COTS) software and was selected for its large international user base, large number of integrated models suitable for analysis of the required physical processes, high quality of available Verification and Validation (V&V) documentation, dedicated user support, and the experience of the PRDW staff in the use of the software. The MIKE software was first released commercially in 1985 and has been under constant development since then.

The models have undergone V&V as per the requirements contained in NSIP02761 (Eskom, 2020a) and RG-0016 (NNR, 2016b). The V&V of models is described in two supporting reports (PRDW, 2021) and (PRDW,

CONTROLLED DISCLOSURE

When downloaded from the EDS database, this document is uncontrolled and the responsibility rests with the user to ensure it is in line with the authorised version on the database.

2022b). As part of the V&V the models have been calibrated against site-specific data measured as part of the monitoring programme.

Table 5.9.7 provides an overview of the numerical models used. The application of the model is described in the User Guide, whilst detailed descriptions of the application areas, governing mathematical equations, numerical space and time discretisation, solution methods, and references are provided in the Scientific Documentation. Hyperlinks to these documents are included in the references. The subsections provide an overview of the modelling undertaken with an emphasis on the model results. Further details of the modelling methodology are included in the V&V reports (PRDW, 2021) and (PRDW, 2022b).

Table 5.9.7: Overview of Numerical Models Used.

Model Name	User Guide	Scientific Documentation	Physical Processes Simulated	Subsection
MIKE Spectral Waves	(DHI, 2021c)	(DHI, 2021d)	Wave refraction, shoaling and breaking	5.9.9.8
MIKE Littoral Processes	(DHI, 2021e)	(DHI, 2021f)	Longshore sediment transport Suspended sand concentration	5.9.10.3 5.9.16.3
SBEACH	(USACE, 1996)	(USACE, 1989) (USACE, 1990)	Cross-shore beach erosion	5.9.10.5
MIKE 3 Wave	(DHI, 2021g)	(DHI, 2021h)	Storm wave run-up and drawdown	5.9.11.2
MIKE 21 Flow	(DHI, 2021i)	(DHI, 2021j)	Tsunami generation and propagation (earthquakes) Tsunami run-up, drawdown and velocity	5.9.12.5
MIKE 3 Flow	(DHI, 2021k)	(DHI, 2021l)	Tsunami generation and propagation (volcanic flank collapse and submarine landslides) Three-dimensional hydrodynamics and thermal plume dispersion	5.9.12.5 5.9.15.5
MIKE 21 Sand Transport	(DHI, 2021m)	(DHI, 2021n)	Sedimentation and scour due to storms Sedimentation and scour due to tsunamis	5.9.16.1 5.9.16.2

To rationalise the number of cases whilst still resolving the impact of climate change, the models were run for the three key dates shown in bold below (the remaining two dates were assessed for climate change but were not simulated in the models):

- **2021: present-day;**
- 2044: end of operations for KNPS;
- **2064: end of decommissioning period for KNPS;**

CONTROLLED DISCLOSURE

When downloaded from the EDS database, this document is uncontrolled and the responsibility rests with the user to ensure it is in line with the authorised version on the database.

- 2110: end of operations for the new NIs;
- **2130: end of decommissioning period for the new NIs.**

Siting requires consideration of site suitability to the end of decommissioning, not just the end of operations. Since climate change results in all key parameters becoming progressively worse over time (refer to ***Subsection 5.9.7***), the model results for 2064 will conservatively envelope those for 2044, and similarly the model results for 2130 will conservatively envelope those for 2110.

The models were run for the following four exceedance probabilities: 10^{-2}, 10^{-4}, 10^{-6} and 10^{-8} y^{-1}. These exceedance probabilities accounted for the joint probability of the relevant input parameters applied in the model, as described in ***Subsection 5.9.9.9***. The best estimate values were used as the model inputs.

The results for all modelled cases are available as spatial plots. The results for the intermediate exceedance probabilities of 10^{-5} and 10^{-7} y^{-1} were obtained by interpolation of the model results and these results are included in the tables of key output parameters, e.g., wave run-up.

5.9.6.4 Conceptual Design for New NIs

The conceptual engineering design was limited to developing various conceptual layouts for the seawater cooling intake and outfall system for the new NIs. No engineering feasibility studies were performed for the SSR and these conceptual layouts thus serve only to demonstrate the technical feasibility of the layouts in terms of:

- thermal plume dispersion;
- recirculation;
- sediment transport around the structures;
- suspended sediments drawn into the intake.

5.9.7 Climate Change

The effect of climate change on all relevant oceanographic and coastal engineering parameters has been estimated. The effect of climate change was evaluated over both the operating life and the decommissioning period of the existing KNPS and the proposed new NIs at the site. The primary guidance is taken from the latest publications from the Intergovernmental Panel for Climate Change (IPCC), along with peer-reviewed journal articles where IPCC projections are outdated or unavailable. The adjustments for climate change had to be finalised before commencing the analyses and modelling studies undertaken for ***Section 5.9***. Therefore, the IPCC

When downloaded from the EDS database, this document is uncontrolled and the responsibility rests with the user to ensure it is in line with the authorised version on the database.

publications up to the IPCC's Special Report: The Ocean and Cryosphere in a Changing Climate (SROCC) (Oppenheimer, et al., 2019) were considered.

The IPCC presents climate change projections for a range of Representative Concentration Pathways (RCPs). The RCPs are based on different greenhouse gas concentration trajectories over the 21st century and are all plausible and illustrative with no probabilities attached. The most conservative pathway based on no change in climate change strategies (RCP8.5) was adopted for climate change projections. For conservatism the upper end of the confidence intervals was applied where these are provided in the projections.

Projections are given relative to a baseline period, which for SROCC is typically 1986-2005. The oceanographic and coastal engineering parameters used in ***Section 5.9*** are based on different datasets available over different periods. For each parameter the baseline date was taken as the middle of the period of available data. Projections derived from literature were converted relative to the baseline date for each parameter.

Projections for sea level rise (SLR) were based on the SROCC, which provides an update of the projections presented in the IPCC 5th Assessment Report with newly derived contributions from Antarctica. The SROCC provides projections of the global mean sea level (GMSL) and regional mean sea level (RMSL) rise to 2100 relative to 1995.5 (1986-2005).

The regional projections at Duynefontyn are above the global mean. Since long-term projections beyond 2100 are only provided for GMSL rise, the long-term projected RMSL rise beyond 2100 was estimated by extrapolating the trend in RMSL vs GMSL observed in projections up to 2100 and applying it to the long-term GMSL projections.

The upper end of the likely range is assessed to have a 17% chance of being exceeded. While the models on which these projections are based cannot provide projections above the likely range, the SROCC suggests from expert elicitation studies that a GMSL rise of 2 m by 2100 cannot be ruled out. The projection above the upper end of the likely range has been assessed here as a maximum plausible scenario. To obtain estimates of the maximum plausible scenario for all required time horizons, the GMSL and RMSL from RCP8.5 were scaled by the ratio of the maximum plausible GMSL to the RCP8.5 GMSL at 2100.

The projections were converted from the 1995.5 baseline date to the baseline date for mean level at KNPS of 2019 (see ***Subsection 5.9.9.1***). The resulting curves of GMSL and RMSL for the upper end of the likely range for RCP8.5 and the maximum plausible scenario are presented in

CONTROLLED DISCLOSURE

When downloaded from the EDS database, this document is uncontrolled and the responsibility rests with the user to ensure it is in line with the authorised version on the database.

Figure 5.9.3, relative to the 2019 mean level. The RMSL projections were used and are presented in ***Table 5.9.8***.

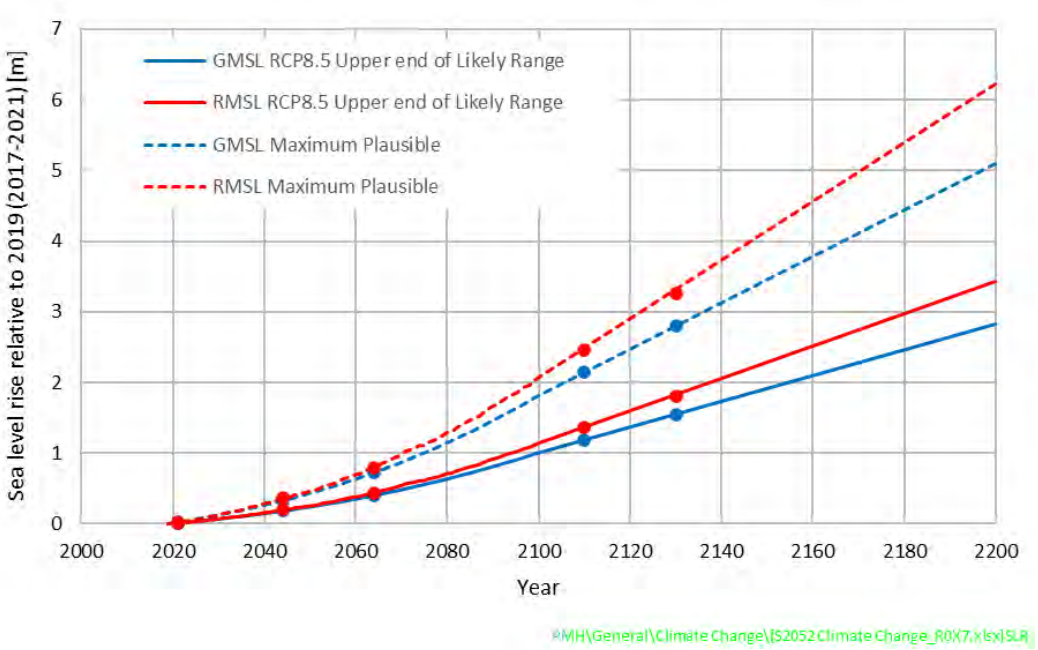


Figure 5.9.3: Global Mean Sea Level (GMSL) and Regional Mean Sea Level (RMSL) Projections for the Upper End of the Likely Range of RCP8.5 and the Maximum Plausible Scenarios.

The SROCC presents basin-averaged trends in seawater temperature derived from an ensemble of earth system models. For the Atlantic basin at a latitude of 35°S, a trend of approximately 2.3°C per century is projected for near-surface seawater temperature. The projected changes relative to the baseline date for measurements at KNPS (2012, see ***Subsection 5.9.9.5***) are presented in ***Table 5.9.8***.

Projections for wind speed and mean sea level (MSL) pressure were obtained from the Methodology for Including Climate Change Forecasts into the Duynefontyn Site Safety Report (Airshed, 2021), in which meteorological projections were derived from data extracted from a 50 km resolution downscaled model ensemble run by the Council for Scientific and Industrial Research. The time-series data covered the period of 1960-2099 for the RCP8.5 scenario and was spatially averaged over a 100 km by 100 km area with Duynefontyn at the centre. Among other parameters, the data included the annual average and annual maximum hourly wind speed, and the annual mean MSL pressure. Projections for dates within the available time span were determined as a 20-year average, while projections for 2110 and 2130 were obtained through extrapolation of the data using a second order polynomial fit. In lieu of data on extreme MSL pressure, the projections for extreme low pressure were assumed the same

CONTROLLED DISCLOSURE

When downloaded from the EDS database, this document is uncontrolled and the responsibility rests with the user to ensure it is in line with the authorised version on the database.

as the annual mean. The projections for extreme high pressure were assumed to be zero, a conservative assumption given the negative trend predicted for the annual mean pressure.

The projections for the annual maximum hourly wind speed and extreme low and high MSL pressure are presented in ***Table 5.9.8***. While the original data was presented relative to 2008 (1997-2019) by Airshed (2021), this was converted to a baseline date of 1993.5 for further use.

Storm surge is mainly composed of an atmospheric pressure component (low pressure for positive storm surge and high pressure for a negative storm surge) and a wind-induced component. The atmospheric pressure component of storm surge is proportional to the gradient in atmospheric pressure through the inverse barometer effect, while the wind set-up component of storm surge is proportional to the square of the wind speed. In lieu of detailed projections available in literature, the projections for storm surge used here were based on the conservative assumption that the wind-setup component is dominant and were thus determined as the square of the projected extreme wind speed increase. The resulting storm surge projections are given in ***Table 5.9.8***, relative to a baseline date of 1993.5 (see ***Subsection 5.9.9.2***).

Considering that long waves such as meteo-tsunamis are generated by the same physical processes as storm surge, i.e., wind and atmospheric pressure, the same approach was used for these events. The projections are given in ***Table 5.9.8*** relative to a baseline date of 2013, appropriate for long wave events (see ***Subsection 5.9.9.3***).

A global ensemble of wave climate projections has recently been published (Morim, et al., 2020) (Morim, et al., 2019) under the Coordinated Wave Climate Experiment Phase 2 (COWCLIP 2.0). The ensemble archive comprises 148 global wave climate simulations from 10 state-of-the-art studies from different international climate research groups, including both dynamical and statistical wind-wave modelling methods. The ensemble includes mean and exceedance statistics of significant wave height (H_{m0}), mean wave period (T_m) and mean wave direction (MWD) for present (1979-2004) and future (2081-2100) time slices.

Ensemble-mean projections for RCP8.5 at the future time slice were extracted offshore of Cape Town for the annual mean H_{m0}, annual mean T_m, and annual mean MWD. Projections at the required dates were linearly interpolated or extrapolated from the available data and converted to the baseline date of 2004.5, appropriate for the operational wave climate (see ***Subsection 5.9.9.8***). The projections for H_{m0} and T_m indicated a small negative trend, which was conservatively set to zero.

CONTROLLED DISCLOSURE

When downloaded from the EDS database, this document is uncontrolled and the responsibility rests with the user to ensure it is in line with the authorised version on the database.

Projections for global changes in extreme wave heights have been determined from a seven-member subset of the wave model ensemble described above (Meucci, et al., 2020). For each of a present-day (1979-2005) and future time slice (2081-2100), extreme wave heights were determined by fitting an exponential distribution to the 1 000 highest wave heights pooled from the seven models (after bias-correction). The projected changes for the $10^{-2}y^{-1}$ exceedance probability significant wave height (H_{m0}) were linearly interpolated or extrapolated to the required dates, and converted to a baseline date of 2000, as appropriate for the extreme wave climate (see ***Subsection 5.9.9.8***). The associated increase in wave period was determined based on wave period being proportional to the square root of the wave height (see ***Figure 5.9.43***).

Coastal hydrodynamics are highly variable and site-specific and are challenging to model at sufficient resolution over long timescales. The currents measured at Duynefontyn were found to be predominantly wind driven (see ***Subsection 5.9.9.4***). In lieu of available projections, the projected increase in current speed was derived from the wind speed projections. This was based on a linear relationship between current speed and wind speed for fully developed depth-averaged currents, which are governed by the balance of bottom friction and shear stress at the water surface due to wind friction. The projections are given in ***Table 5.9.8*** relative to the baseline date of 2015, appropriate for the current measurements at KNPS (see ***Subsection 5.9.9.4***).

Based on the discussion above, ***Table 5.9.8*** shows the climate change applied in ***Section 5.9***.

CONTROLLED DISCLOSURE

When downloaded from the EDS database, this document is uncontrolled and the responsibility rests with the user to ensure it is in line with the authorised version on the database.

Table 5.9.8: Climate Change Applied for Each Oceanographic Parameter and Date.

Parameter	Description	Scenario	Units	Baseline date	2021	2044	2064	2110	2130
Sea level rise (SLR)	Regional mean sea level rise	RCP8.5 Upper end of likely range	m	2019	0.01	0.20	0.44	1.36	1.80
		Maximum plausible	m	2019	0.02	0.36	0.79	2.46	3.26
Seawater temperature	Near-surface	RCP8.5, no uncertainty ranges available	°C	2012	0.2	0.7	1.2	2.3	2.7
Wind speed	Annual average	RCP8.5, mean estimate	%	1993.5	1.4%	3.0%	4.5%	8.7%	11.0%
	Annual maximum		%	1993.5	0.5%	1.2%	1.7%	3.3%	4.2%
Atmospheric pressure	Extreme low pressure	RCP8.5, mean estimate	%	1993.5	-0.01%	-0.03%	-0.05%	-0.09%	-0.12%
	Extreme high pressure		%	1993.5	0%	0%	0%	0%	0%
Storm surge	Extreme positive	RCP8.5, mean estimate	%	1993.5	1.0%	2.3%	3.4%	6.8%	8.6%
	Extreme negative		%	1993.5	1.0%	2.3%	3.4%	6.8%	8.6%
Meteo-tsunami	Positive	RCP8.5, mean estimate	%	2013	0.3%	1.6%	2.7%	6.0%	7.9%
	Negative		%	2013	0.3%	1.6%	2.7%	6.0%	7.9%
Wave height	Extreme in deep water offshore	RCP8.5, no uncertainty ranges available	%	2000	0.8%	1.7%	2.5%	4.2%	5.0%
	Mean in deep water offshore		%	2004.5	0.0%	0.0%	0.0%	0.0%	0.0%
Wave period	Extreme in deep water offshore	RCP8.5, no uncertainty ranges available	%	2000	0.4%	0.8%	1.2%	2.1%	2.5%
	Mean in deep water offshore		%	2004.5	0.0%	0.0%	0.0%	0.0%	0.0%
Wave direction	Extreme in deep water offshore	RCP8.5, no uncertainty ranges available	Degrees, positive clockwise	Not available					
	Mean in deep water offshore			2004.5	-0.7	-1.8	-2.7	-4.8	-5.7
Current speed	Extreme depth-averaged wind-driven current	RCP8.5, mean estimate	%	2015	0.1%	0.8%	1.3%	2.9%	3.8%

Note that the assessment of coastline stability and flooding from the sea are based on the sea level rise (SLR) corresponding to the RCP8.5 upper end of likely range (0.44 m in 2064 and 1.80 m in 2130), rather than the maximum plausible SLR (0.79 m in 2064 and 3.26 m in 2130). This additional 0.35 m in the case of KNPS and 1.5 m in the case of the new NIs should be considered during the SAR and engineering design phase, either as safety buffer or as part of an adaptive design strategy.

It is noted that the IPCC has since published the 6th Assessment Report (AR6) Physical Science Basis (IPCC, In press) in draft format, which remains subject to revisions. A review of the draft version with a view to compare the updated projections to those for parameters based on SROCC indicated the following:

CONTROLLED DISCLOSURE

When downloaded from the EDS database, this document is uncontrolled and the responsibility rests with the user to ensure it is in line with the authorised version on the database.

- Projections are based on a new set of scenarios (Shared Socioeconomic Pathways, SSP) which cover a broader range than the RCPs.
- A new set of climate and earth system models with improved representation of physical processes and biogeochemical cycles, run at higher resolutions that better capture smaller-scale processes, have improved the simulation of most large-scale indicators of climate change.
- While derived using substantially updated methods, the AR6 sea level projections are broadly consistent with those of the SROCC. For a standardised baseline date, at the upper end of the likely range for the most conservative scenario, the AR6 projects GMSL rise of 1.02 m by 2100 compared to 1.07 m from SROCC.
- The likely range only includes processes in whose projections there is at least medium confidence. Low confidence projections are also provided, which include ice-sheet related processes whose quantification is highly uncertain or that are characterised by deep uncertainty. For this scenario, the AR6 projects GMSL rise of 1.6 m (83rd percentile) and 2.3 m (95th percentile) by 2100 relative to 1995-2014, increasing to 4.8 m and 5.4 m, respectively, by 2150. These projections are higher than the maximum plausible scenario used in this study, which for the same baseline date, projects GMSL rise of 1.9 m in 2100 and 3.6 m in 2150.
- The AR6 projects a regional sea surface temperature increase near Cape Town of approximately 2.2°C per century, which is consistent with the projections used here.
- The AR6 does not present wave projections but reports medium confidence in the projections of mean wave climate and low confidence in projections of extreme wave climate due to limited evidence. In both cases, the studies used to derive the projections in ***Table 5.9.6*** are mentioned.

The projections above do not deviate substantially from those used in this study, except for the maximum plausible sea level rise scenario. Updated maximum plausible regional sea level rise projections should be determined for consideration in the SAR and engineering design phase. In general, climate change projections must be continually reassessed as new data and research results become available (at least every five years). The SSR would only need to be updated should one of the relevant climate change parameters change significantly.

CONTROLLED DISCLOSURE

When downloaded from the EDS database, this document is uncontrolled and the responsibility rests with the user to ensure it is in line with the authorised version on the database.

5.9.8 Physical Description of the Site

The topography at the site and the bathymetry offshore of the site were obtained from the following sources:

- Global gridded data available from General Bathymetric Charts of the Oceans (GEBCO Compilation Group, 2020);
- Gridded topography data available from the City of Cape Town (2015);
- C-MAP Electronic Charts and available local surveys in areas surrounding Cape Town (DHI, 2021q);
- Multi-beam bathymetric surveys offshore of Duynefontyn by CGS (2006);
- Multi-beam bathymetric surveys of Table Bay by Fugro (2007);
- Single-beam bathymetric surveys of the KNPS intake basin and adjacent seabed by Tritan Survey (2007);
- Beach profiles by Tritan Survey (2021); and
- Light Detection and Ranging (LiDAR) survey of the Duynefontyn site and upper beach by Southern Mapping Geospatial (SRK, 2021).

The last-mentioned LiDAR survey levels were compared to benchmarks available from a KNPS construction drawing (Eskom, 2020c). The comparison indicated that the LiDAR levels are on average 0.29 m lower than the benchmarks. Based on this comparison the LiDAR levels were raised by 0.29 m.

Throughout ***Section 5.9*** the vertical datum used is mean sea level (msl) also known as Land Levelling Datum (LLD).

The horizontal coordinate system is WG19 defined as follows:

- Map projection: Gauss Conformal
- Datum: Hartebeesthoek 94
- Spheroid: WGS84
- Scale factor: 1
- Central meridian: 19° E
- Reference system: WG19
- Co-ordinates: Eastings (X, increasing eastwards)
- Northings (Y, increasing northwards)
- Distance units: metres.

CONTROLLED DISCLOSURE

When downloaded from the EDS database, this document is uncontrolled and the responsibility rests with the user to ensure it is in line with the authorised version on the database.

Figure 5.9.4 shows the site location including multi-beam bathymetry (CGS, 2006) offshore of the site. ***Figure 5.9.5*** shows the bathymetry offshore of the site and the topography at the site. The Security Protected Area of the KNPS is indicated in magenta. The estimated position of the new NIs and associated permanent facilities are shown in blue. These correspond to the solid red areas shown in ***Drawing 3.3*** in ***Chapter 3*** (Overview of Planned Activities at the Site).

CONTROLLED DISCLOSURE

When downloaded from the EDS database, this document is uncontrolled and the responsibility rests with the user to ensure it is in line with the authorised version on the database.

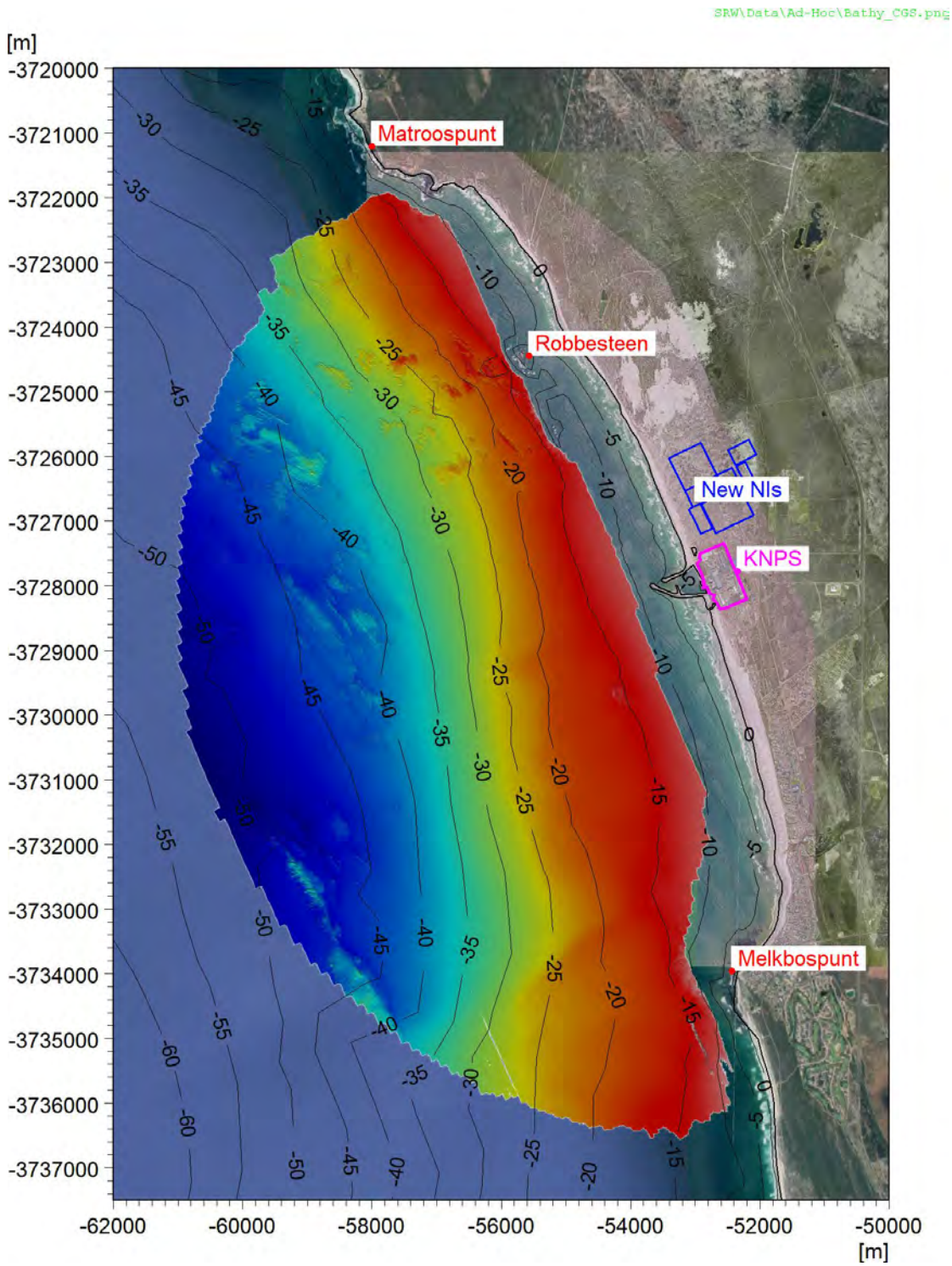


Figure 5.9.4: Site Location Including Multi-Beam Bathymetry Offshore of the Site.

CONTROLLED DISCLOSURE

When downloaded from the EDS database, this document is uncontrolled and the responsibility rests with the user to ensure it is in line with the authorised version on the database.

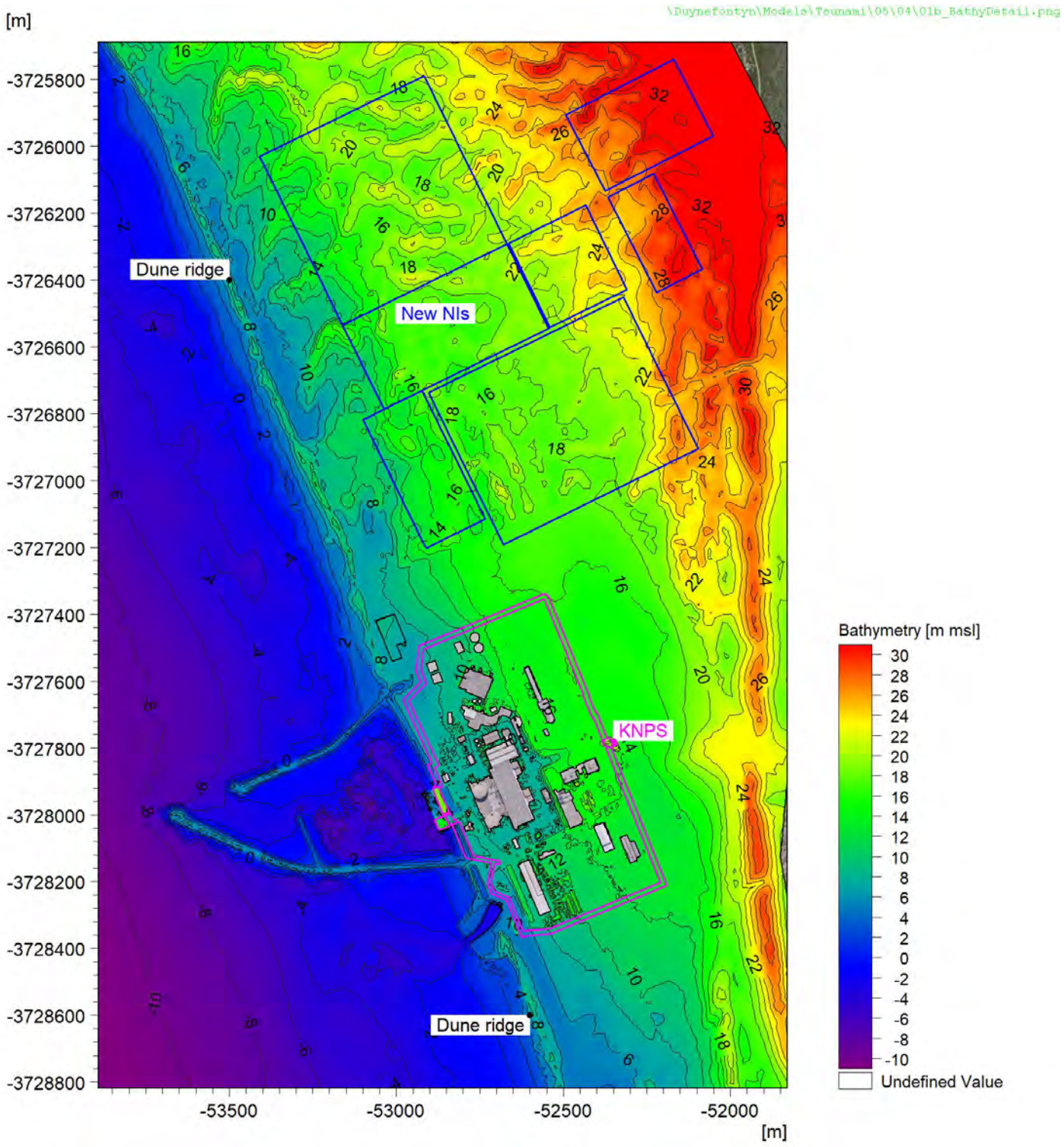


Figure 5.9.5: Bathymetry and Topography at the Site Showing the Location of KNPS and the Estimated Location of New NIs.

In addition to the topography and bathymetry datasets described above, there are several ongoing or near-future projects at KNPS within the area of

CONTROLLED DISCLOSURE

When downloaded from the EDS database, this document is uncontrolled and the responsibility rests with the user to ensure it is in line with the authorised version on the database.

interest. These are summarised in ***Table 5.9.9***, which also indicates which projects were built into the models used in this section, based on information provided by Eskom. The KNPS projects included in the model are shown in ***Figure 5.9.6***.

Table 5.9.9: Ongoing and Near-Future Projects at KNPS.

Project	Description	Included in models?
Koeberg Insulator Pollution Testing Station (KIPTS)	Pad with containerised offices.	Yes. Presently under construction.
Weskusfleur HV Yard	Terrace with low point at +16.6 m msl. Two storey building.	No. Terrace at high level and far landward.
Original Steam Generator Interim Storage Facility (OSGISF)	Two rectangular reinforced concrete buildings (26 m x 26 m x 9 m high), each to store 3 OSGs (3 per unit).	Yes. Already under construction.
Containment Wall Mock-up	10 m long x 3 m high x 1 m thick wall, east-west alignment, permanent structure.	No. Small structure, unlikely to affect run-up. Location and orientation not finalised.
External Events Response Initiative (EERI)	Hardened water storage tanks north of Low-Level Waste (LLW): 2 tanks, diameter = 27 m, height = 10.5 m. Hardened storage facility at Bulk Stores.	Hardened water storage tanks included. Hardened storage facility not included (outside area of interest).
LP Turbine Rotors Temporary Storage	Pad with three rotors under rigid canopies (12 m x 6 m x 6 m high), plus spare LP Gen Rotor, gas cylinder cages, and other spares.	No. Small structures, unlikely to affect run-up.
Spent Fuel Cask Temporary Interim Storage Facility (TISF)	Five pads, one of which is for an office building, ancillary building, and a laydown area.	Yes.

CONTROLLED DISCLOSURE

When downloaded from the EDS database, this document is uncontrolled and the responsibility rests with the user to ensure it is in line with the authorised version on the database.

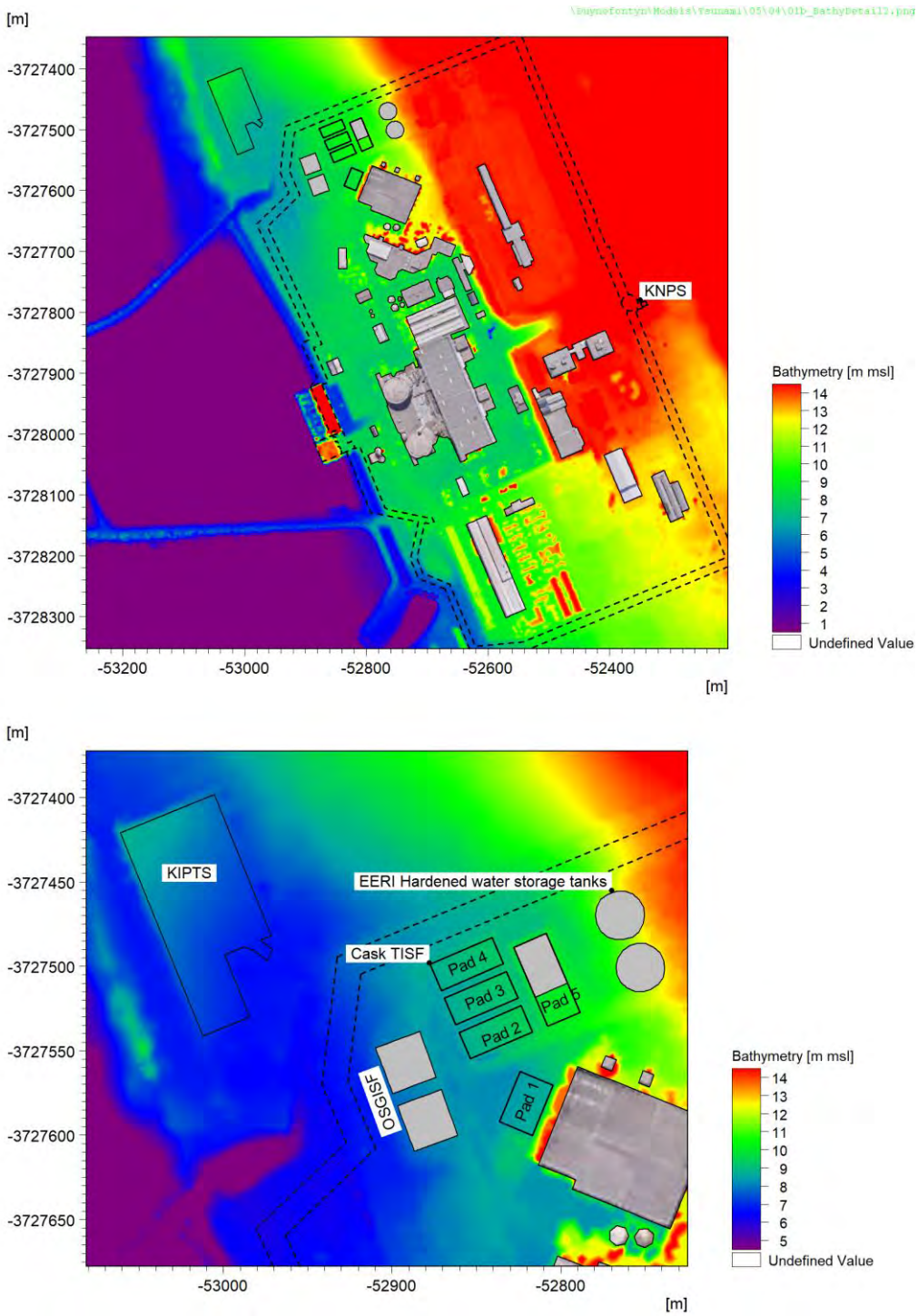


Figure 5.9.6: Bathymetry: Detail Showing Ongoing or Near-Future Projects at KNPS Included in the Models.

Notable physical features of the site shown in the figures above include:

- The site is located in the centre of a 14 km long sandy beach between Melkbospunt and Matroospunt.

CONTROLLED DISCLOSURE

When downloaded from the EDS database, this document is uncontrolled and the responsibility rests with the user to ensure it is in line with the authorised version on the database.

- A shore-parallel dune ridge exists along the coastline from approximately 3 km south of KNPS to approximately 2 km north of KNPS. Further north, the coastline is characterised by a cliff.
- The inshore seabed is predominantly sandy but there are rock outcrops further offshore and to the north, the most prominent being Robbesteen.
- In the breaker zone between -5 m msl and +2 m msl the average seabed slope ranges from 1:42 in the north to 1:60 in the south. Further offshore, between -30 m msl and -5 m msl the average seabed slope ranges from 1:100 in the north to 1:145 in the south.
- Previous geotechnical investigations indicated that rocks of the Malmesbury Group of Precambrian age occur at the site between -6 and -13 m msl. Additional geological information is presented in ***Section 5.13*** (Geology) and ***Section 5.15*** (Geotechnical Characterisation).
- The KNPS nuclear terrace level varies between approximately +7.5 and +8.2 m msl.
- The KNPS cooling water system comprises an intake basin and an outfall channel discharging into the surf-zone.
- At the new NIs, the terrain landward of the dune ridge is characterised by a series of lightly vegetated dunes and valleys. The natural ground level at the estimated locations of the new NIs ranges from +9.5 to +37 m msl.
- Directly north of the proposed new NIs is a mobile dune system.

Sediment samples have been collected from the nearshore (depths between -10 and -20 m msl) and from the beach at the high and low water marks (see ***Figure 5.9.7***). The sand on the beach south of the KNPS has a D_{50} of approximately 0.2 mm and a grading of approximately 1.2. The sand on the beach north of the KNPS has a D_{50} of approximately 0.4 mm and a grading of approximately 1.4, reflecting the steeper beach slope north of the KNPS. The sand offshore has a D_{50} of approximately 0.15 mm and a grading of approximately 1.2, reflecting the deposition of finer sediments in deeper water. The sand in the KNPS intake basin typically has a D_{50} of 0.24 mm with a grading of 1.4 (PRDW, 2005).

CONTROLLED DISCLOSURE

When downloaded from the EDS database, this document is uncontrolled and the responsibility rests with the user to ensure it is in line with the authorised version on the database.

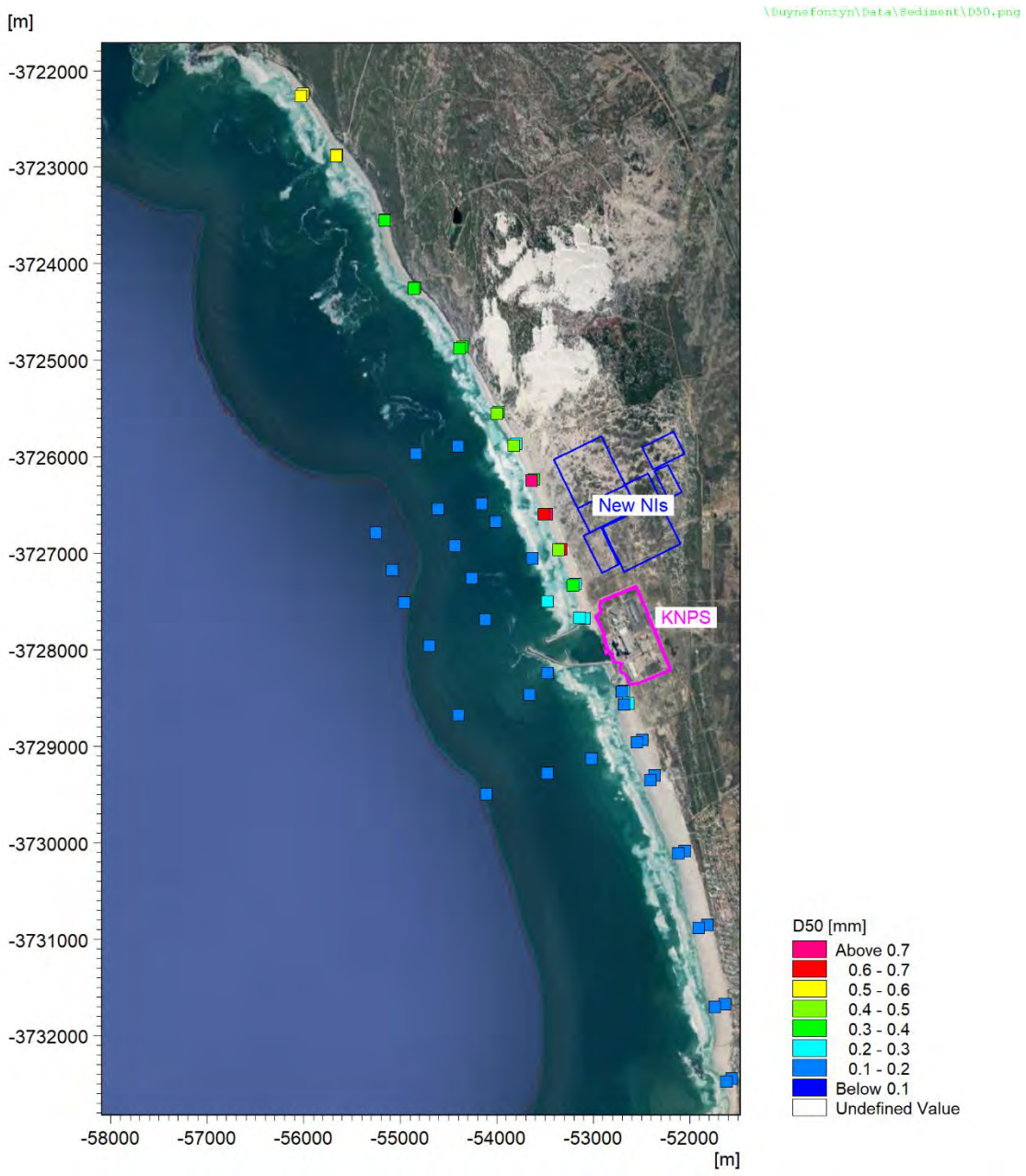


Figure 5.9.7: Measured Sediment Grain Size Offshore and Along the Beach.

5.9.9 Hydrographic Conditions

This section characterises the hydrographic conditions at the site based on measurements and numerical modelling. These hydrographic conditions are used as inputs to the coastline stability, flooding from the sea, thermal plume dispersion and sediment transport modelling, as described in the subsections that follow.

CONTROLLED DISCLOSURE

When downloaded from the EDS database, this document is uncontrolled and the responsibility rests with the user to ensure it is in line with the authorised version on the database.

5.9.9.1 Tidal Levels

Water levels have been measured at Site C2 inside the KNPS intake basin using a levelled pressure sensor corrected for atmospheric pressure. Details of the locations, instruments, sampling intervals, dates and length of valid data are provided in ***Subsection 5.9.6.1***. The data from August 2017 to June 2021 (3.3 y) was used in the tidal analysis. The hourly measured water level is plotted in ***Figure 5.9.8***.

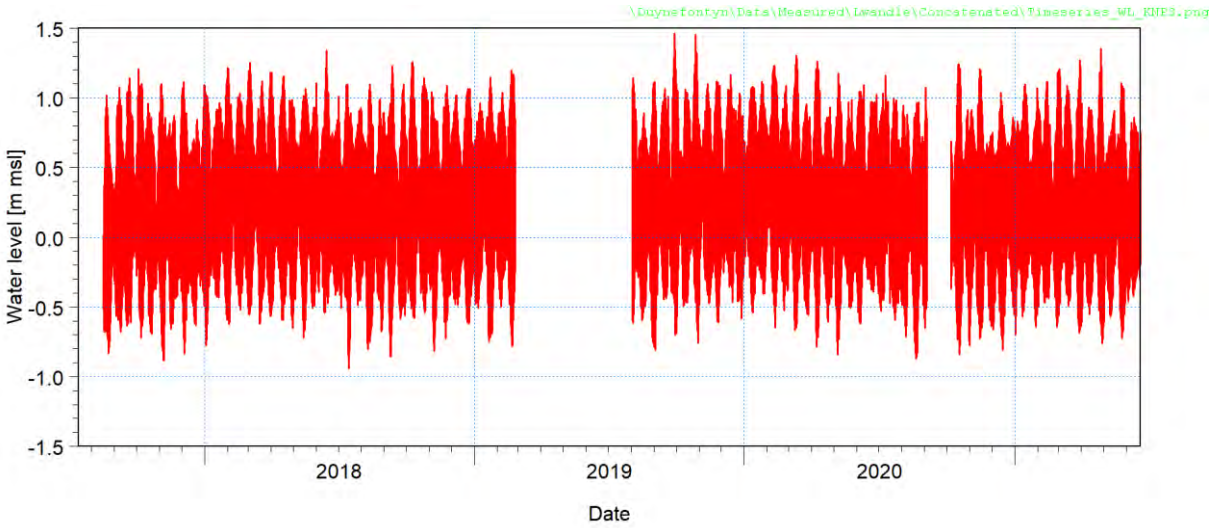


Figure 5.9.8: Measured Hourly Water Levels at Site C2 Inside the KNPS Intake Basin.

In addition, the hourly measured tide for Cape Town for the period 1967 to 2020 was kindly provided by the Hydrographer of the South African Navy (who is not responsible for any transcription errors or errors due to calculations using the data). The tide gauge was initially located in Granger Bay and was later moved to the North Spur within the Port of Cape Town. Both these locations are 25 km from the site. The hourly measured data are plotted in ***Figure 5.9.9***.

CONTROLLED DISCLOSURE

When downloaded from the EDS database, this document is uncontrolled and the responsibility rests with the user to ensure it is in line with the authorised version on the database.

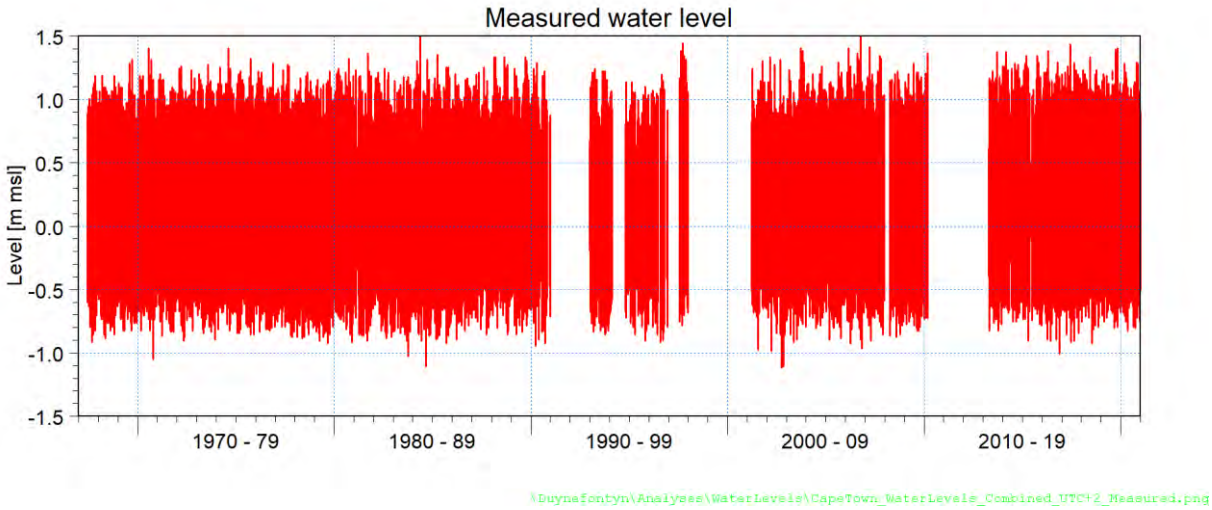


Figure 5.9.9: Measured Hourly Water Levels at Cape Town.

A linear regression fitted to the annual average water level over the measured period indicated a trend of +0.94 mm/year, which was removed prior to further analysis. Tidal harmonic analyses were carried out using the MIKE 21 tidal analysis and prediction toolbox (DHI, 2021a) and (DHI, 2021b) to obtain the tidal constituents for both the Site C2 and detrended Cape Town datasets. To characterise the astronomical tide at Duynefontyn, the constituents from Site C2 were used, except for the Solar Annual (SA) and Solar Semi-Annual (SSA) constituents, which are best determined from long-term datasets. The SA and SSA constituents from the Cape Town dataset were used. The Mean Level (ML) at Duynefontyn was calculated as the arithmetic average of the monthly mean levels over the measurement period. The level is representative of a baseline date of 2019, the approximate mid-point of the dataset.

The resulting main tidal constituents and predicted tidal levels are provided in ***Table 5.9.10*** and ***Table 5.9.11***. Tides along the entire South African coastline are semi-diurnal and microtidal.

CONTROLLED DISCLOSURE

When downloaded from the EDS database, this document is uncontrolled and the responsibility rests with the user to ensure it is in line with the authorised version on the database.

Table 5.9.10: Tidal Constituents at Duynefontyn (Baseline Date is 2019).

Constituent Symbol	Constituent Name	Amplitude	Phase
		(m)	(º)
Z0	Elevation of ML above msl	0.216	0.0
M2	Principal lunar semi-diurnal	0.502	91.3
S2	Principal solar semi-diurnal	0.222	113.5
N2	Larger lunar elliptic semi-diurnal	0.112	82.9
K2	Luni-solar semi-diurnal	0.064	108.6
K1	Luni-solar diurnal	0.058	137.9
SA	Solar annual long-period	0.023	25.9
NU2	Larger lunar evectional constituent	0.021	83.9
MU2	Variational semi-diurnal	0.021	66.0
2N2	Lunar elliptical semidiurnal second-order	0.018	67.8
P1	Principal solar diurnal	0.016	138.9
O1	Principal lunar diurnal	0.014	261.6
T2	Larger solar elliptic semi-diurnal	0.012	119.4
L2	Smaller lunar elliptic semi-diurnal	0.011	98.9
SSA	Solar semi-annual long-period	0.008	308.7
Q1	Larger lunar elliptic diurnal	0.008	236.5
MM	Lunar monthly long-period	0.008	315.2
S1	Solar diurnal	0.006	214.3
M3	Lunar terdiurnal	0.005	19.4
J1	Smaller lunar elliptic diurnal	0.005	151.1
M4	Shallow water overtides of principal lunar	0.005	158.7
EPS2	Not available	0.005	47.9
OO1	Lunar diurnal	0.005	196.6
MKS2	Not available	0.005	47.4
MSF	Lunisolar synodic fortnightly	0.004	119.6
H2	Not available	0.004	68.4
ETA2	Not available	0.004	123.4
MSM	Not available	0.004	244.7
MF	Lunar fortnightly long-period	0.003	112.1
LDA2	Smaller lunar evectional	0.003	85.0
MN4	Shallow water quarter diurnal	0.003	103.0

CONTROLLED DISCLOSURE

When downloaded from the EDS database, this document is uncontrolled and the responsibility rests with the user to ensure it is in line with the authorised version on the database.

Table 5.9.11: Predicted Tidal Levels at Duynefontyn (Baseline Date is 2019).

Parameter	Level (m msl)
Highest Astronomical Tide (HAT)	1.286
Mean High Water Springs (MHWS)	0.979
Mean High Water Neaps (MHWN)	0.491
Mean Level (ML)	0.216
Mean Low Water Neaps (MLWN)	-0.053
Mean Low Water Springs (MLWS)	-0.531
Lowest Astronomical Tide (LAT)	-0.770

The US NRC's recommended initial tidal water level to apply for storm surge and tsunami run-up calculations is the 90th percentile high tide (NRC, 2009). This is defined as the high tide level that is exceeded by 10 per cent of the high tides over a continuous 19 y period. For low water calculations the 10th percentile low tide is the recommended initial level. The predicted tides at the site were used to calculate the following initial tidal levels:

- 90th percentile high tide = +1.00 m msl;
- 10th percentile low tide = -0.55 m msl.

5.9.9.2 Storm Surge

Storm surge is for the purpose of this report defined as the influence of meteorological effects such as winds and barometric pressure that result in the actual sea level being above or below the predicted astronomical tide level. The storm surge events have durations of hours to days and can thus be extracted from hourly tidal measurements. In this report water level fluctuations with shorter periods between 8 and 60 minutes that can be extracted from 1 to 3-minute tidal measurements are referred to as long waves and are described in ***Subsection 5.9.9.3***.

The measured hourly water level in the Port of Cape Town from 1967 to 2020 was used for the storm surge analysis. These data were preferred over the water levels measured at Site C2 inside the KNPS basin due to the longer duration of the data (39 y vs 3.3 y) and because the water levels measured inside the basin included wave setup in addition to storm surge. The detrended measured water level in the Port of Cape Town (***Subsection 5.9.9.1***) was subtracted from the predicted tide in the Port of Cape Town to obtain the storm surge. The measured water level, predicted tide and storm surge are plotted in ***Figure 5.9.10***.

CONTROLLED DISCLOSURE

When downloaded from the EDS database, this document is uncontrolled and the responsibility rests with the user to ensure it is in line with the authorised version on the database.

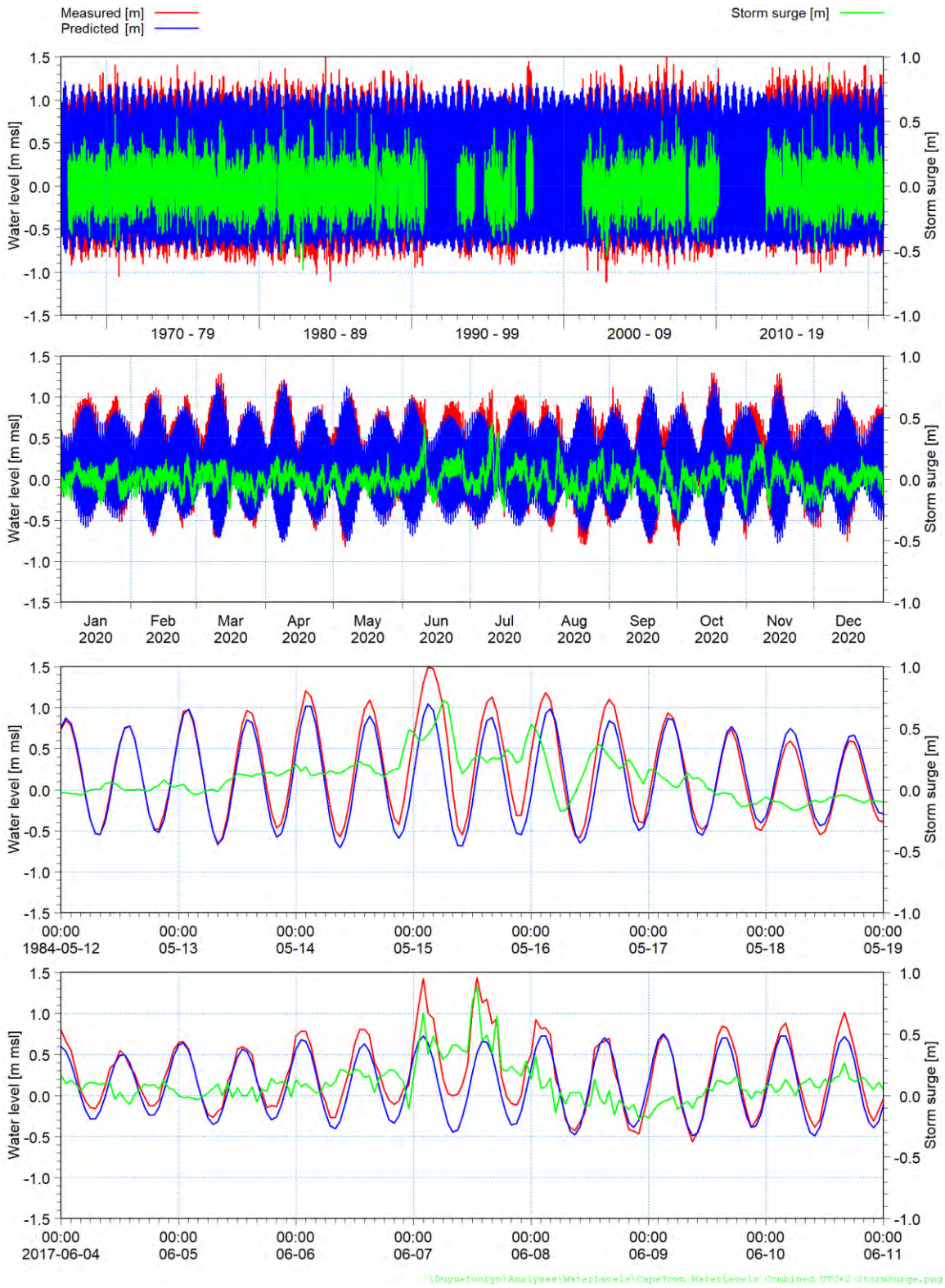


Figure 5.9.10: Measured Water Level, Predicted Tide and Storm Surge at Cape Town for the Entire Dataset (Top), Detail for 2020 (Top Middle), the May 1984 Storm (Bottom Middle) and the June 2017 Storm (Bottom).

CONTROLLED DISCLOSURE

When downloaded from the EDS database, this document is uncontrolled and the responsibility rests with the user to ensure it is in line with the authorised version on the database.

An extreme value analysis (refer to ***Subsection 5.9.6.2*** for the methodology) was performed on the positive storm surge (measured water level higher than predicted tide) and negative storm surge (measured water level lower than the predicted tide). The extreme value analysis results for positive and negative storm surges are plotted in ***Figure 5.9.11*** and ***Figure 5.9.12***, respectively. The baseline date is 1993.5 which is the middle of the measurement period.

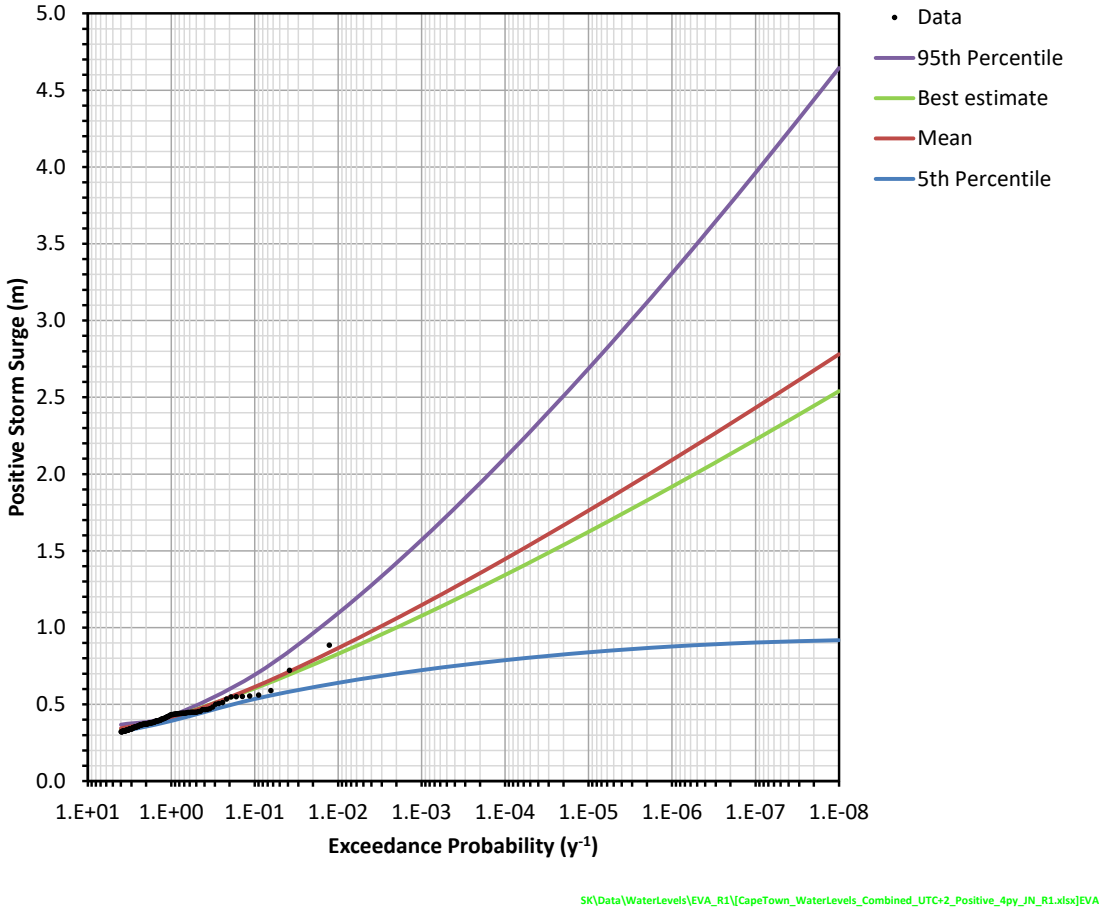
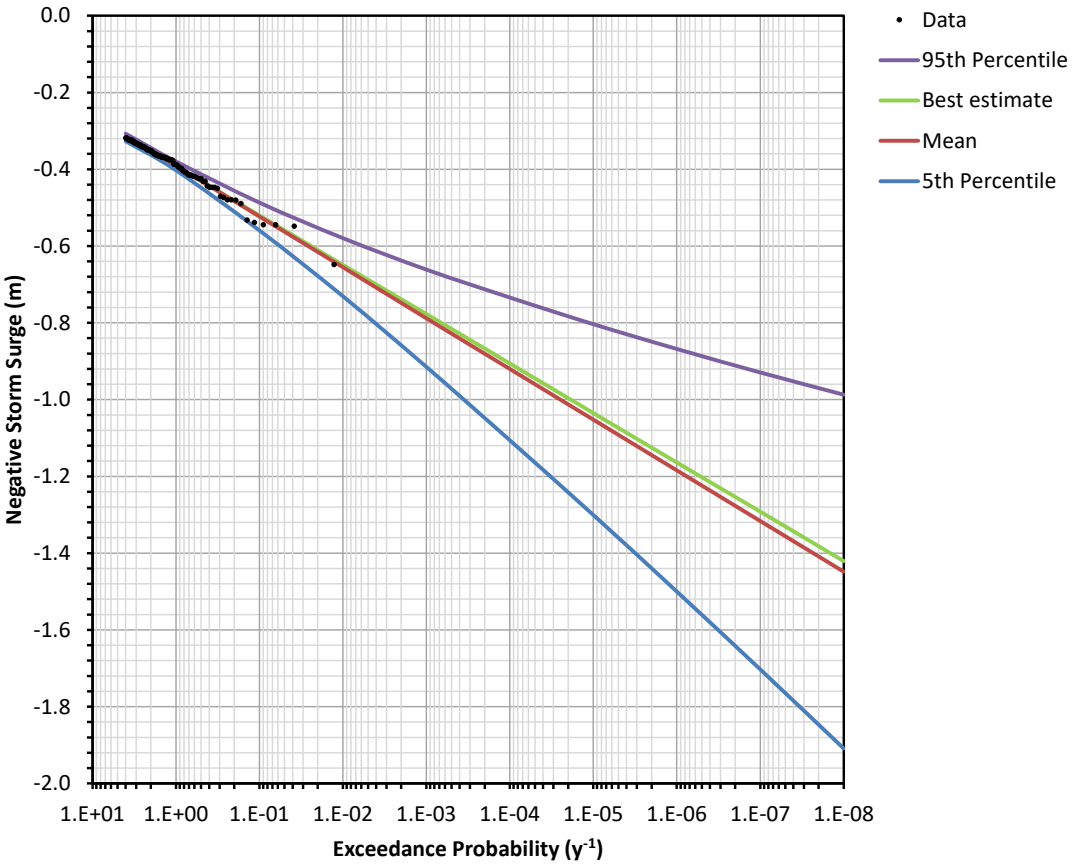


Figure 5.9.11: Extreme Value Analysis of Positive Storm Surge Residuals at Cape Town (Baseline Date is 1993.5).

CONTROLLED DISCLOSURE

When downloaded from the EDS database, this document is uncontrolled and the responsibility rests with the user to ensure it is in line with the authorised version on the database.



SK\Data\WaterLevels\EVA_R1\[CapeTown_WaterLevels_Combined_UTC+2_Negative_4py_JN_R1.xlsx]EVA_Reordered

Figure 5.9.12: Extreme Value Analysis of Negative Storm Surge Residuals at Cape Town (Baseline Date is 1993.5).

The positive storm surge was then adjusted for climate change (***Subsection 5.9.7***) and added to the 90% high tide (***Subsection 5.9.9.1***) and the sea level rise (***Subsection 5.9.7***) to obtain the maximum still water level at the five dates of interest, as shown in ***Table 5.9.3***. The minimum still water level was calculated in the same way except that the 10% low tide was used (***Subsection 5.9.9.1***) and sea level rise was conservatively set to zero, with the results shown in ***Table 5.9.13***.

CONTROLLED DISCLOSURE

When downloaded from the EDS database, this document is uncontrolled and the responsibility rests with the user to ensure it is in line with the authorised version on the database.

Table 5.9.12: Extreme Positive Storm Surge and Maximum Still Water Levels.

Exceedance Probability	Uncertainty	Tide [a]	Sea Level Rise [b]					Positive Storm Surge [c]					Maximum Still Water Level				
(y^{-1})		(m msl)	(m)					(m)					(m msl)				
			2021	2044	2064	2110	2130	2021	2044	2064	2110	2130	2021	2044	2064	2110	2130
1	5th Percentile	1.00	0.01	0.20	0.44	1.36	1.80	0.40	0.40	0.41	0.42	0.43	1.41	1.60	1.85	2.78	3.23
	Mean	1.00	0.01	0.20	0.44	1.36	1.80	0.41	0.42	0.42	0.44	0.44	1.42	1.62	1.86	2.80	3.25
	Best Estimate[d]	1.00	0.01	0.20	0.44	1.36	1.80	0.42	0.42	0.43	0.44	0.45	1.43	1.63	1.87	2.80	3.25
	95th Percentile	1.00	0.01	0.20	0.44	1.36	1.80	0.43	0.44	0.44	0.45	0.46	1.44	1.64	1.88	2.81	3.26
10^{-1}	5th Percentile	1.00	0.01	0.20	0.44	1.36	1.80	0.54	0.55	0.55	0.57	0.58	1.55	1.75	1.99	2.93	3.38
	Mean	1.00	0.01	0.20	0.44	1.36	1.80	0.62	0.63	0.63	0.66	0.67	1.63	1.83	2.07	3.02	3.47
	Best Estimate[d]	1.00	0.01	0.20	0.44	1.36	1.80	0.61	0.62	0.62	0.65	0.66	1.62	1.82	2.06	3.00	3.46
	95th Percentile	1.00	0.01	0.20	0.44	1.36	1.80	0.70	0.71	0.72	0.74	0.75	1.71	1.91	2.16	3.10	3.55
10^{-2}	5th Percentile	1.00	0.01	0.20	0.44	1.36	1.80	0.65	0.65	0.66	0.68	0.70	1.66	1.86	2.10	3.04	3.50
	Mean	1.00	0.01	0.20	0.44	1.36	1.80	0.88	0.89	0.90	0.93	0.94	1.89	2.09	2.34	3.29	3.74
	Best Estimate[d]	1.00	0.01	0.20	0.44	1.36	1.80	0.84	0.85	0.86	0.89	0.90	1.85	2.05	2.30	3.25	3.70
	95th Percentile	1.00	0.01	0.20	0.44	1.36	1.80	1.11	1.12	1.13	1.17	1.19	2.12	2.32	2.57	3.53	3.99
10^{-3}	5th Percentile	1.00	0.01	0.20	0.44	1.36	1.80	0.73	0.74	0.75	0.77	0.78	1.74	1.94	2.19	3.13	3.59
	Mean	1.00	0.01	0.20	0.44	1.36	1.80	1.16	1.17	1.19	1.22	1.25	2.17	2.38	2.62	3.58	4.05
	Best Estimate[d]	1.00	0.01	0.20	0.44	1.36	1.80	1.09	1.10	1.11	1.15	1.17	2.10	2.30	2.55	3.51	3.97
	95th Percentile	1.00	0.01	0.20	0.44	1.36	1.80	1.59	1.61	1.62	1.68	1.71	2.60	2.81	3.06	4.04	4.51
10^{-4}	5th Percentile	1.00	0.01	0.20	0.44	1.36	1.80	0.80	0.81	0.81	0.84	0.86	1.81	2.01	2.25	3.20	3.66
	Mean	1.00	0.01	0.20	0.44	1.36	1.80	1.46	1.48	1.50	1.55	1.57	2.47	2.68	2.94	3.91	4.37
	Best Estimate[d]	1.00	0.01	0.20	0.44	1.36	1.80	1.36	1.37	1.39	1.43	1.46	2.37	2.58	2.83	3.79	4.26
	95th Percentile	1.00	0.01	0.20	0.44	1.36	1.80	2.13	2.16	2.18	2.25	2.29	3.14	3.36	3.62	4.61	5.09
10^{-5}	5th Percentile	1.00	0.01	0.20	0.44	1.36	1.80	0.85	0.86	0.87	0.90	0.91	1.86	2.06	2.31	3.26	3.71
	Mean	1.00	0.01	0.20	0.44	1.36	1.80	1.78	1.80	1.82	1.88	1.91	2.79	3.01	3.26	4.24	4.72
	Best Estimate[d]	1.00	0.01	0.20	0.44	1.36	1.80	1.64	1.66	1.68	1.73	1.76	2.65	2.86	3.12	4.09	4.57
	95th Percentile	1.00	0.01	0.20	0.44	1.36	1.80	2.72	2.75	2.78	2.87	2.92	3.73	3.95	4.22	5.23	5.72
10^{-6}	5th Percentile	1.00	0.01	0.20	0.44	1.36	1.80	0.89	0.90	0.91	0.94	0.95	1.90	2.10	2.35	3.30	3.75
	Mean	1.00	0.01	0.20	0.44	1.36	1.80	2.11	2.14	2.16	2.23	2.27	3.13	3.34	3.60	4.59	5.07
	Best Estimate[d]	1.00	0.01	0.20	0.44	1.36	1.80	1.94	1.96	1.98	2.05	2.08	2.95	3.16	3.42	4.41	4.88
	95th Percentile	1.00	0.01	0.20	0.44	1.36	1.80	3.34	3.38	3.42	3.53	3.59	4.35	4.59	4.86	5.89	6.39
10^{-7}	5th Percentile	1.00	0.01	0.20	0.44	1.36	1.80	0.91	0.92	0.93	0.96	0.98	1.92	2.13	2.37	3.32	3.78
	Mean	1.00	0.01	0.20	0.44	1.36	1.80	2.46	2.49	2.51	2.60	2.64	3.47	3.69	3.95	4.96	5.44
	Best Estimate[d]	1.00	0.01	0.20	0.44	1.36	1.80	2.25	2.28	2.30	2.38	2.42	3.26	3.48	3.74	4.73	5.22
	95th Percentile	1.00	0.01	0.20	0.44	1.36	1.80	4.00	4.05	4.10	4.23	4.30	5.01	5.26	5.53	6.59	7.10
10^{-8}	5th Percentile	1.00	0.01	0.20	0.44	1.36	1.80	0.93	0.94	0.95	0.98	1.00	1.94	2.14	2.39	3.34	3.80
	Mean	1.00	0.01	0.20	0.44	1.36	1.80	2.81	2.85	2.87	2.97	3.02	3.82	4.05	4.31	5.33	5.82
	Best Estimate[d]	1.00	0.01	0.20	0.44	1.36	1.80	2.57	2.60	2.63	2.71	2.76	3.58	3.80	4.07	5.07	5.56
	95th Percentile	1.00	0.01	0.20	0.44	1.36	1.80	4.69	4.75	4.80	4.96	5.05	5.70	5.96	6.24	7.32	7.85

Notes:

(a) 90th percentile high tide, baseline date is 2019.
(b) Baseline date is 2019.
(c) Baseline date is 1993.5.
(d) Should the most probable estimate be required, then the best estimate should be used rather than the mean estimate.

CONTROLLED DISCLOSURE

When downloaded from the EDS database, this document is uncontrolled and the responsibility rests with the user to ensure it is in line with the authorised version on the database.

Table 5.9.13: Extreme Negative Storm Surge and Minimum Still Water Levels.

Exceedance Probability	Uncertainty	Tide [a]	Sea Level Rise [b]					Negative Storm Surge [c]					Minimum Still Water Level				
(y^{-1})		(m msl)	(m)					(m)					(m msl)				
			2021	2044	2064	2110	2130	2021	2044	2064	2110	2130	2021	2044	2064	2110	2130
1	5th Percentile	-0.55	0.00	0.00	0.00	0.00	0.00	-0.41	-0.41	-0.42	-0.43	-0.44	-0.96	-0.96	-0.97	-0.98	-0.99
	Mean	-0.55	0.00	0.00	0.00	0.00	0.00	-0.40	-0.40	-0.40	-0.42	-0.42	-0.95	-0.95	-0.96	-0.97	-0.98
	Best Estimate[d]	-0.55	0.00	0.00	0.00	0.00	0.00	-0.40	-0.40	-0.41	-0.42	-0.43	-0.95	-0.95	-0.96	-0.97	-0.98
	95th Percentile	-0.55	0.00	0.00	0.00	0.00	0.00	-0.38	-0.39	-0.39	-0.41	-0.41	-0.94	-0.94	-0.95	-0.96	-0.97
10^{-1}	5th Percentile	-0.55	0.00	0.00	0.00	0.00	0.00	-0.56	-0.57	-0.58	-0.60	-0.61	-1.12	-1.13	-1.13	-1.15	-1.16
	Mean	-0.55	0.00	0.00	0.00	0.00	0.00	-0.53	-0.54	-0.54	-0.56	-0.57	-1.08	-1.09	-1.09	-1.11	-1.12
	Best Estimate[d]	-0.55	0.00	0.00	0.00	0.00	0.00	-0.53	-0.53	-0.54	-0.56	-0.56	-1.08	-1.09	-1.09	-1.11	-1.12
	95th Percentile	-0.55	0.00	0.00	0.00	0.00	0.00	-0.49	-0.50	-0.50	-0.52	-0.53	-1.04	-1.05	-1.06	-1.07	-1.08
10^{-2}	5th Percentile	-0.55	0.00	0.00	0.00	0.00	0.00	-0.74	-0.75	-0.76	-0.78	-0.79	-1.29	-1.30	-1.31	-1.33	-1.35
	Mean	-0.55	0.00	0.00	0.00	0.00	0.00	-0.66	-0.67	-0.68	-0.70	-0.71	-1.21	-1.22	-1.23	-1.25	-1.26
	Best Estimate[d]	-0.55	0.00	0.00	0.00	0.00	0.00	-0.66	-0.66	-0.67	-0.69	-0.70	-1.21	-1.22	-1.22	-1.25	-1.26
	95th Percentile	-0.55	0.00	0.00	0.00	0.00	0.00	-0.59	-0.59	-0.60	-0.62	-0.63	-1.14	-1.15	-1.15	-1.17	-1.18
10^{-3}	5th Percentile	-0.55	0.00	0.00	0.00	0.00	0.00	-0.92	-0.94	-0.95	-0.98	-0.99	-1.48	-1.49	-1.50	-1.53	-1.55
	Mean	-0.55	0.00	0.00	0.00	0.00	0.00	-0.80	-0.81	-0.81	-0.84	-0.86	-1.35	-1.36	-1.37	-1.39	-1.41
	Best Estimate[d]	-0.55	0.00	0.00	0.00	0.00	0.00	-0.79	-0.80	-0.80	-0.83	-0.84	-1.34	-1.35	-1.36	-1.38	-1.40
	95th Percentile	-0.55	0.00	0.00	0.00	0.00	0.00	-0.67	-0.68	-0.68	-0.71	-0.72	-1.22	-1.23	-1.24	-1.26	-1.27
10^{-4}	5th Percentile	-0.55	0.00	0.00	0.00	0.00	0.00	-1.12	-1.13	-1.14	-1.18	-1.20	-1.67	-1.68	-1.70	-1.73	-1.75
	Mean	-0.55	0.00	0.00	0.00	0.00	0.00	-0.93	-0.94	-0.95	-0.98	-1.00	-1.48	-1.49	-1.50	-1.54	-1.55
	Best Estimate[d]	-0.55	0.00	0.00	0.00	0.00	0.00	-0.92	-0.93	-0.94	-0.97	-0.98	-1.47	-1.48	-1.49	-1.52	-1.54
	95th Percentile	-0.55	0.00	0.00	0.00	0.00	0.00	-0.74	-0.75	-0.76	-0.78	-0.80	-1.29	-1.30	-1.31	-1.34	-1.35
10^{-5}	5th Percentile	-0.55	0.00	0.00	0.00	0.00	0.00	-1.31	-1.33	-1.34	-1.39	-1.41	-1.87	-1.88	-1.90	-1.94	-1.97
	Mean	-0.55	0.00	0.00	0.00	0.00	0.00	-1.06	-1.08	-1.09	-1.12	-1.14	-1.62	-1.63	-1.64	-1.68	-1.70
	Best Estimate[d]	-0.55	0.00	0.00	0.00	0.00	0.00	-1.05	-1.06	-1.07	-1.11	-1.12	-1.60	-1.61	-1.62	-1.66	-1.68
	95th Percentile	-0.55	0.00	0.00	0.00	0.00	0.00	-0.81	-0.82	-0.83	-0.86	-0.87	-1.36	-1.38	-1.38	-1.41	-1.43
10^{-6}	5th Percentile	-0.55	0.00	0.00	0.00	0.00	0.00	-1.52	-1.53	-1.55	-1.60	-1.63	-2.07	-2.09	-2.10	-2.15	-2.18
	Mean	-0.55	0.00	0.00	0.00	0.00	0.00	-1.20	-1.21	-1.22	-1.26	-1.29	-1.75	-1.76	-1.78	-1.82	-1.84
	Best Estimate[d]	-0.55	0.00	0.00	0.00	0.00	0.00	-1.18	-1.19	-1.20	-1.24	-1.26	-1.73	-1.74	-1.76	-1.80	-1.82
	95th Percentile	-0.55	0.00	0.00	0.00	0.00	0.00	-0.88	-0.89	-0.90	-0.93	-0.94	-1.43	-1.44	-1.45	-1.48	-1.50
10^{-7}	5th Percentile	-0.55	0.00	0.00	0.00	0.00	0.00	-1.72	-1.74	-1.76	-1.82	-1.85	-2.27	-2.30	-2.31	-2.37	-2.40
	Mean	-0.55	0.00	0.00	0.00	0.00	0.00	-1.33	-1.35	-1.36	-1.41	-1.43	-1.88	-1.90	-1.91	-1.96	-1.98
	Best Estimate[d]	-0.55	0.00	0.00	0.00	0.00	0.00	-1.31	-1.32	-1.34	-1.38	-1.40	-1.86	-1.88	-1.89	-1.93	-1.96
	95th Percentile	-0.55	0.00	0.00	0.00	0.00	0.00	-0.94	-0.95	-0.96	-0.99	-1.01	-1.49	-1.50	-1.51	-1.55	-1.56
10^{-8}	5th Percentile	-0.55	0.00	0.00	0.00	0.00	0.00	-1.93	-1.95	-1.97	-2.04	-2.07	-2.48	-2.51	-2.53	-2.59	-2.63
	Mean	-0.55	0.00	0.00	0.00	0.00	0.00	-1.46	-1.48	-1.50	-1.55	-1.57	-2.02	-2.03	-2.05	-2.10	-2.13
	Best Estimate[d]	-0.55	0.00	0.00	0.00	0.00	0.00	-1.44	-1.45	-1.47	-1.52	-1.54	-1.99	-2.01	-2.02	-2.07	-2.10
	95th Percentile	-0.55	0.00	0.00	0.00	0.00	0.00	-1.00	-1.01	-1.02	-1.05	-1.07	-1.55	-1.56	-1.57	-1.61	-1.63

Notes:

(a) 10th percentile low tide, baseline date is 2019.
(b) Conservatively set to zero.
(c) Baseline date is 1993.5.
(d) Should the most probable estimate be required, then the best estimate should be used rather than the mean estimate.

CONTROLLED DISCLOSURE

When downloaded from the EDS database, this document is uncontrolled and the responsibility rests with the user to ensure it is in line with the authorised version on the database.

These still water levels (defined as the water level in the absence of waves) were used as inputs to the coastline stability, flooding from the sea and integrity of cooling water supply, as described in the subsections below.

5.9.9.3 Long Waves

Long waves are, for the purpose of this report, defined as fluctuations in still water level with periods between 8 and 60 min. Long waves typically include: edge waves, bound waves, tsunamis (generated by geophysical phenomena such as earthquakes) and meteo-tsunamis (generated by atmospheric pressure fluctuations). The other type of waves described in this report are wind waves with periods between 3 s and 25 s, which are described in ***Subsection 5.9.9.8***.

Meteo-tsunamis can produce similar wave patterns to tsunamis, i.e., a sequence of wave trains with a wave period of 10 to 20 min. On 21 August 2008 a series of water level fluctuations was measured on the west and south coasts of South Africa, with the largest amplitude of approximately 0.7 m measured at Port Nolloth (see ***Figure 5.9.13*** and ***Figure 5.9.14***). The measurement of atmospheric pressure fluctuations at Port Nolloth coinciding with the onset of this event provides compelling evidence that this was a meteo-tsunami (CGS, 2008).

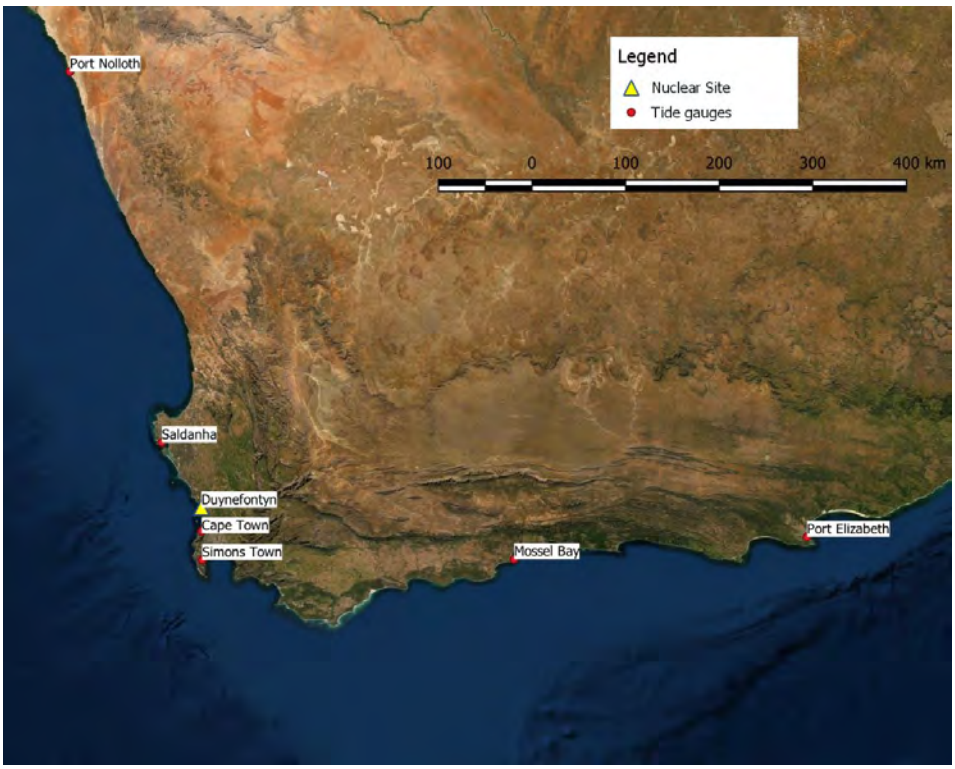


Figure 5.9.13: Locations of Tide Gauges

CONTROLLED DISCLOSURE

When downloaded from the EDS database, this document is uncontrolled and the responsibility rests with the user to ensure it is in line with the authorised version on the database.

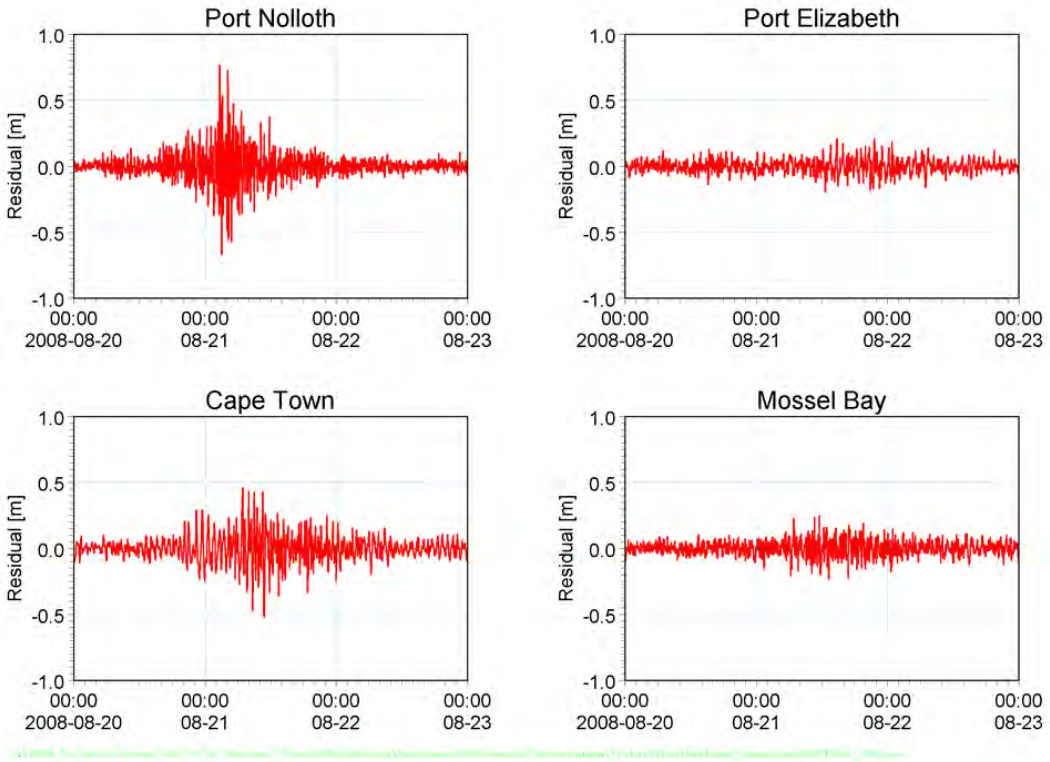


Figure 5.9.14: Propagation of a Meteo-tsunami Event Measured Along the South African Coast

An analysis of available South African analogue tidal records from 1958 to 1986 (Wijnberg, 1993) identified a number long wave events, the largest having an amplitude of 0.6 m measured at Port Nolloth on 1 June 1986.

All the available high frequency (1- or 3-minute) digital data from tide gauges at Port Nolloth, Simon's Town, Cape Town, Mossel Bay and Port Elizabeth have been processed to determine the occurrence and severity of long waves (see ***Figure 5.9.13*** for these locations). The data have been kindly provided by the Hydrographer of the South African Navy (who is not responsible for any transcription errors or errors due to calculations using the data). PRDW undertook the following processing of the measured water surface elevation data to ensure the data quality was fit for purpose:

- comparison of measured water surface elevation to the predicted tide to identify and correct levelling issues;
- removal of spikes, defined as a large water surface elevation change occurring for one time step only;
- intercomparison of data from different measurement sites to confirm extreme events;
- identification of typical signatures of long wave events;

CONTROLLED DISCLOSURE

When downloaded from the EDS database, this document is uncontrolled and the responsibility rests with the user to ensure it is in line with the authorised version on the database.

- identification of known events (reported tsunamis, meteo-tsunamis and storms).

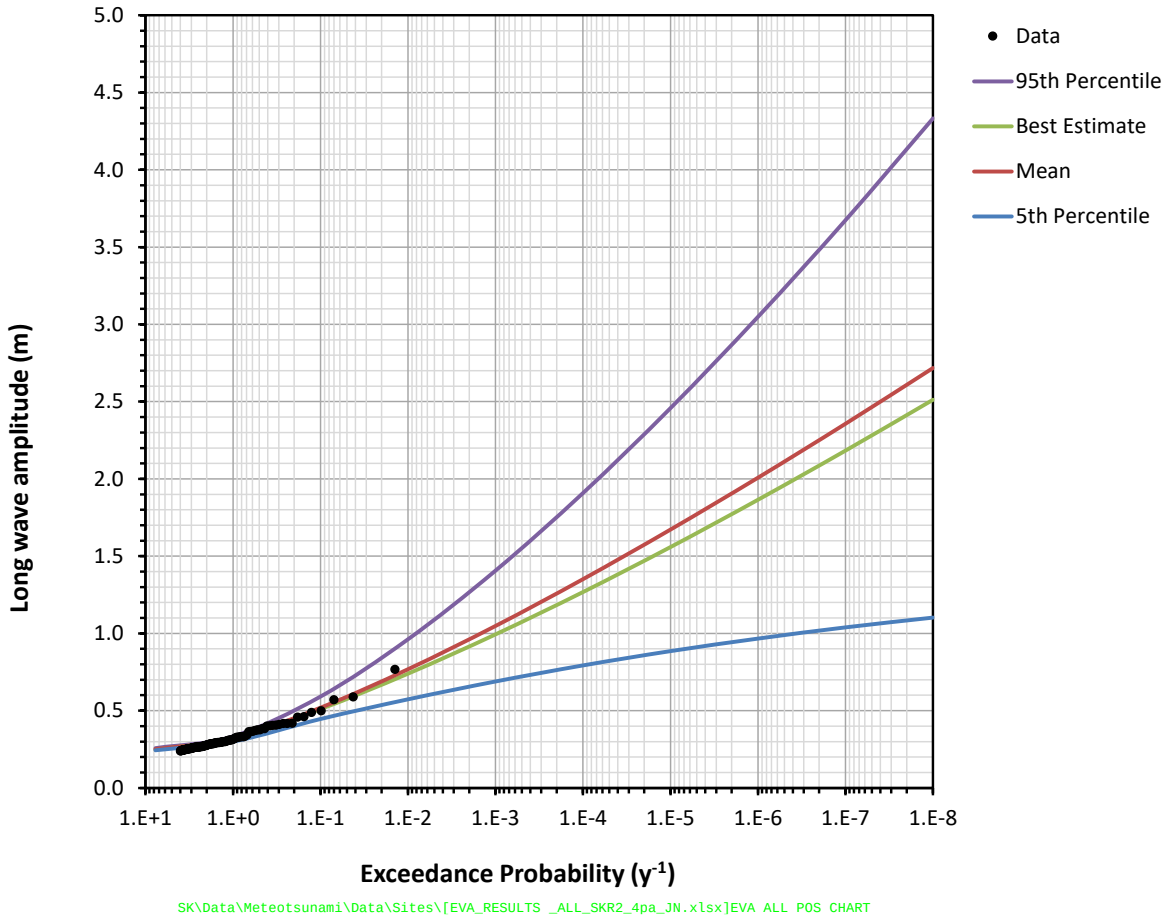
Considering that the long waves have been defined as having periods from 8 to 60 min, and the high frequency tidal data are measured at either 1- or 3-min intervals, this provides either 3 or 8 points per wave period for the shortest wave period of 8 min.

The water level residuals (difference between the measured data and a 60 min running mean) have been extracted at each tide gauge. Since these high frequency digital tidal recordings are available only from 2005, the data for each tide gauge were combined into one longer time-series based on the assumption that the long wave events at each location are independent, thus creating a data set with a duration of 35.58 y. ***Figure 5.9.14*** indicates that although the meteo-tsunami event propagates along the coast, it is significantly larger near the source location (in this case Port Nolloth) compared to the other tide gauge locations, supporting the assumption of independence.

An extreme value analysis (refer to ***Subsection 5.9.6.2*** for the methodology) was then performed on the positive and negative long wave amplitudes. The extreme value analysis results are plotted in ***Figure 5.9.15*** and ***Figure 5.9.16***. The baseline date is 2013 which is the middle of the measurement period.

CONTROLLED DISCLOSURE

When downloaded from the EDS database, this document is uncontrolled and the responsibility rests with the user to ensure it is in line with the authorised version on the database.



SK\Data\Meteotsunami\Data\Sites\[EVA_RESULTS _ALL_SKR2_4pa_JN.xlsx]EVA ALL POS CHART

Figure 5.9.15: Extreme Value Analysis of Positive Long Wave Amplitude (Baseline Date is 2013).

CONTROLLED DISCLOSURE

When downloaded from the EDS database, this document is uncontrolled and the responsibility rests with the user to ensure it is in line with the authorised version on the database.

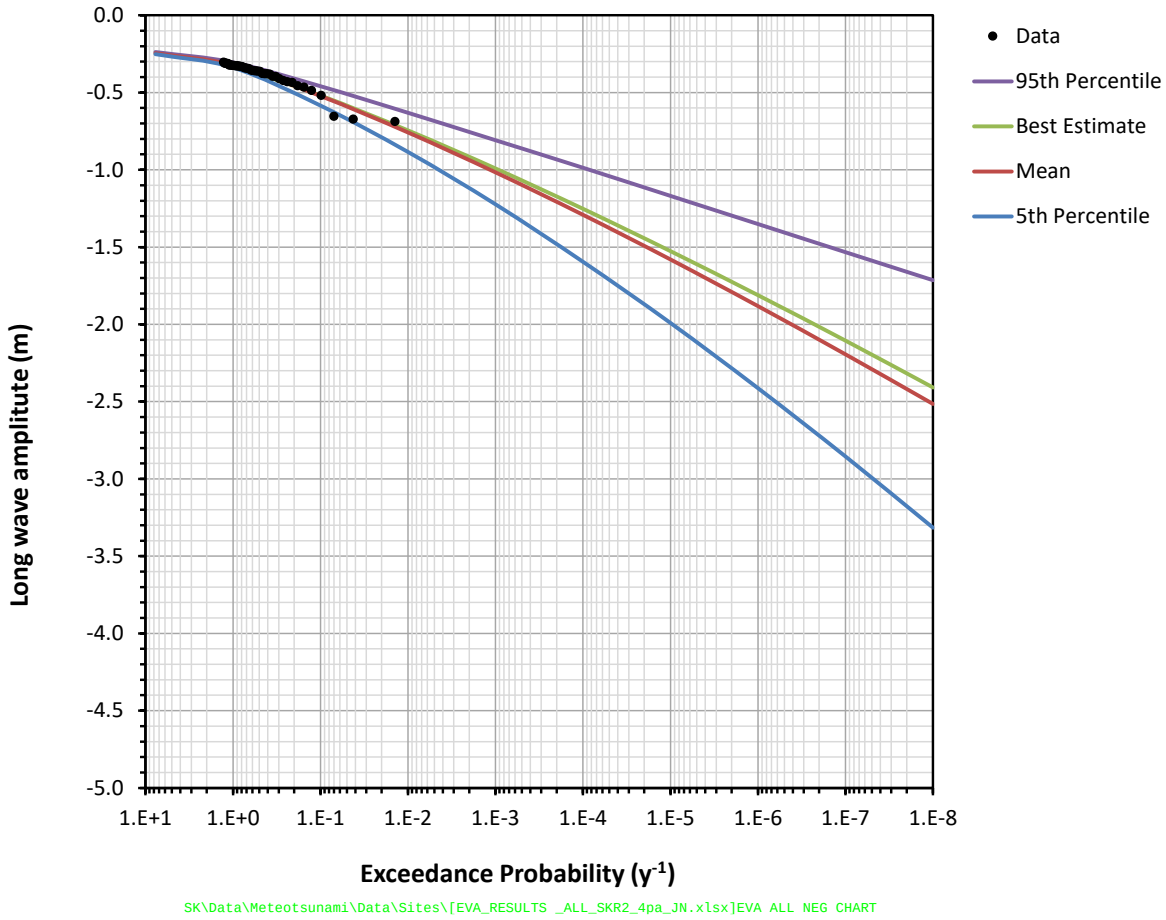


Figure 5.9.16: Extreme Value Analysis of Negative Long Wave Amplitude (Baseline Date is 2013).

The long wave amplitudes were then adjusted for climate change (***Subsection 5.9.7***) and are shown in ***Table 5.9.14***.

CONTROLLED DISCLOSURE

When downloaded from the EDS database, this document is uncontrolled and the responsibility rests with the user to ensure it is in line with the authorised version on the database.

Table 5.9.14: Extreme Long Wave Amplitudes.

Exceedance Probability	Uncertainty	Positive Long Wave Amplitude					Negative Long Wave Amplitude				
(y^{-1})		(m)					(m)				
		2021	2044	2064	2110	2130	2021	2044	2064	2110	2130
1	5th Percentile	0.30	0.31	0.31	0.32	0.32	-0.34	-0.34	-0.35	-0.36	-0.37
	Mean	0.32	0.32	0.33	0.34	0.34	-0.32	-0.33	-0.33	-0.34	-0.35
	Best Estimate[a]	0.32	0.33	0.33	0.34	0.35	-0.32	-0.33	-0.33	-0.34	-0.35
	95th Percentile	0.33	0.34	0.34	0.35	0.36	-0.31	-0.31	-0.31	-0.32	-0.33
10^{-1}	5th Percentile	0.45	0.45	0.46	0.47	0.48	-0.59	-0.59	-0.60	-0.62	-0.63
	Mean	0.52	0.53	0.53	0.55	0.56	-0.52	-0.53	-0.54	-0.55	-0.56
	Best Estimate[a]	0.51	0.52	0.52	0.54	0.55	-0.52	-0.53	-0.53	-0.55	-0.56
	95th Percentile	0.59	0.60	0.61	0.63	0.64	-0.46	-0.47	-0.47	-0.49	-0.50
10^{-2}	5th Percentile	0.58	0.58	0.59	0.61	0.62	-0.89	-0.90	-0.91	-0.94	-0.95
	Mean	0.77	0.78	0.79	0.81	0.83	-0.76	-0.77	-0.78	-0.80	-0.82
	Best Estimate[a]	0.74	0.75	0.76	0.78	0.80	-0.75	-0.76	-0.76	-0.79	-0.80
	95th Percentile	0.97	0.98	0.99	1.02	1.04	-0.63	-0.64	-0.65	-0.67	-0.68
10^{-3}	5th Percentile	0.69	0.70	0.71	0.73	0.74	-1.23	-1.24	-1.26	-1.30	-1.32
	Mean	1.05	1.06	1.08	1.11	1.13	-1.02	-1.03	-1.04	-1.08	-1.10
	Best Estimate[a]	1.00	1.01	1.02	1.05	1.07	-0.99	-1.01	-1.02	-1.05	-1.07
	95th Percentile	1.41	1.43	1.44	1.49	1.52	-0.81	-0.82	-0.83	-0.86	-0.87
10^{-4}	5th Percentile	0.80	0.81	0.81	0.84	0.86	-1.60	-1.62	-1.64	-1.69	-1.72
	Mean	1.36	1.37	1.39	1.43	1.46	-1.30	-1.31	-1.33	-1.37	-1.39
	Best Estimate[a]	1.27	1.29	1.30	1.34	1.37	-1.26	-1.27	-1.29	-1.33	-1.35
	95th Percentile	1.92	1.94	1.96	2.02	2.06	-0.99	-1.00	-1.01	-1.05	-1.06
10^{-5}	5th Percentile	0.89	0.90	0.91	0.94	0.96	-2.00	-2.02	-2.04	-2.11	-2.15
	Mean	1.68	1.70	1.72	1.77	1.80	-1.59	-1.61	-1.62	-1.68	-1.70
	Best Estimate[a]	1.56	1.58	1.60	1.65	1.68	-1.53	-1.55	-1.57	-1.62	-1.65
	95th Percentile	2.47	2.50	2.52	2.61	2.65	-1.17	-1.19	-1.20	-1.24	-1.26
10^{-6}	5th Percentile	0.97	0.98	0.99	1.03	1.04	-2.42	-2.45	-2.48	-2.56	-2.60
	Mean	2.01	2.04	2.06	2.13	2.17	-1.89	-1.91	-1.93	-2.00	-2.03
	Best Estimate[a]	1.87	1.90	1.91	1.98	2.01	-1.82	-1.84	-1.86	-1.92	-1.95
	95th Percentile	3.06	3.10	3.13	3.23	3.29	-1.36	-1.37	-1.39	-1.43	-1.46
10^{-7}	5th Percentile	1.04	1.06	1.07	1.10	1.12	-2.86	-2.90	-2.93	-3.03	-3.08
	Mean	2.36	2.39	2.42	2.50	2.54	-2.20	-2.23	-2.25	-2.33	-2.37
	Best Estimate[a]	2.19	2.22	2.24	2.32	2.35	-2.11	-2.14	-2.16	-2.23	-2.27
	95th Percentile	3.69	3.73	3.77	3.90	3.96	-1.54	-1.56	-1.57	-1.63	-1.65
10^{-8}	5th Percentile	1.11	1.12	1.13	1.17	1.19	-3.33	-3.37	-3.40	-3.52	-3.58
	Mean	2.73	2.76	2.79	2.88	2.93	-2.52	-2.56	-2.58	-2.67	-2.71
	Best Estimate[a]	2.52	2.55	2.58	2.66	2.71	-2.42	-2.45	-2.47	-2.55	-2.60
	95th Percentile	4.35	4.40	4.45	4.60	4.67	-1.72	-1.74	-1.76	-1.82	-1.85

Notes:

(a) Should the most probable estimate be required, then the best estimate should be used rather than the mean estimate.

Since long waves (including meteo-tsunamis) can produce similar wave patterns and associated run-up and drawdown to geological tsunamis, i.e.,

CONTROLLED DISCLOSURE

When downloaded from the EDS database, this document is uncontrolled and the responsibility rests with the user to ensure it is in line with the authorised version on the database.

a sequence of wave trains with a wave period of 10 to 20 min, the extreme positive and negative long wave amplitudes were compared to the geological tsunami results as described in ***Subsection 5.9.12***. The long wave results used were the positive (95th percentile) and negative (5th percentile) 10^{-8} y^{-1} exceedance probability long wave amplitudes (***Table 5.9.14***).

Figure 5.9.105 shows that the minimum and maximum water surface elevations from the long waves are less than those from any of the geological tsunamis, i.e., distant earthquakes, volcanic flank collapse and local submarine landslides. The long waves (including meteo-tsunamis) are thus enveloped by the other tsunami types and are not analysed further.

5.9.9.4 Currents

Currents have been measured at Site A (water depth -10 m msl) and at Site B (water depth -29.0 m msl). Details of the locations, instruments, sampling intervals, dates and length of valid data are provided in ***Subsection 5.9.6.1***.

The surface and bottom currents are presented below as time-series (***Figure 5.9.17*** and ***Figure 5.9.18***), current roses (***Figure 5.9.19***) and statistics (***Table 5.9.15***). Note that current direction is the direction towards which the current is flowing, measured clockwise from true north.

CONTROLLED DISCLOSURE

When downloaded from the EDS database, this document is uncontrolled and the responsibility rests with the user to ensure it is in line with the authorised version on the database.

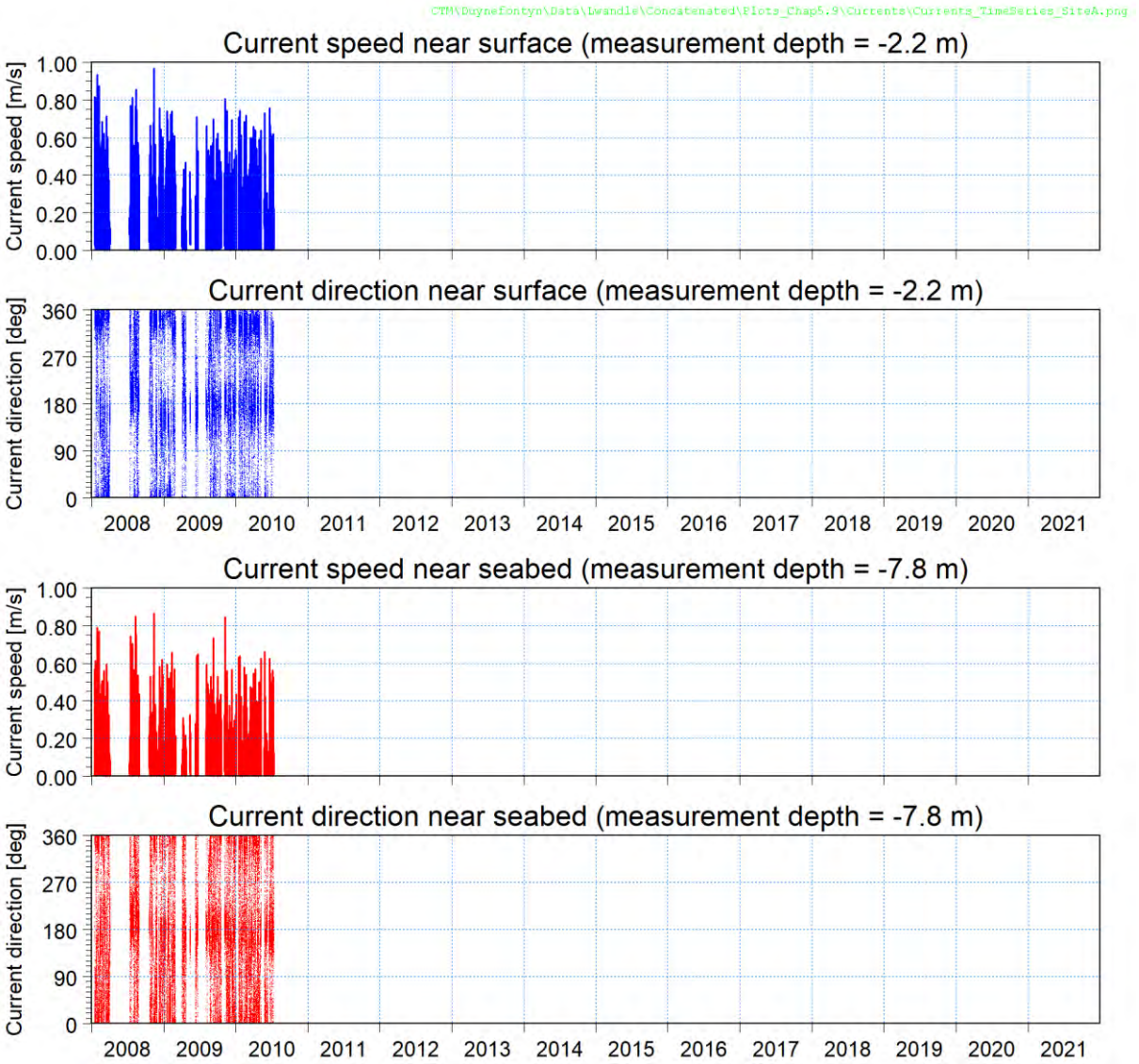


Figure 5.9.17: Time-Series of Measured Currents at Site A (Water Depth -10 m msl).

CONTROLLED DISCLOSURE

When downloaded from the EDS database, this document is uncontrolled and the responsibility rests with the user to ensure it is in line with the authorised version on the database.

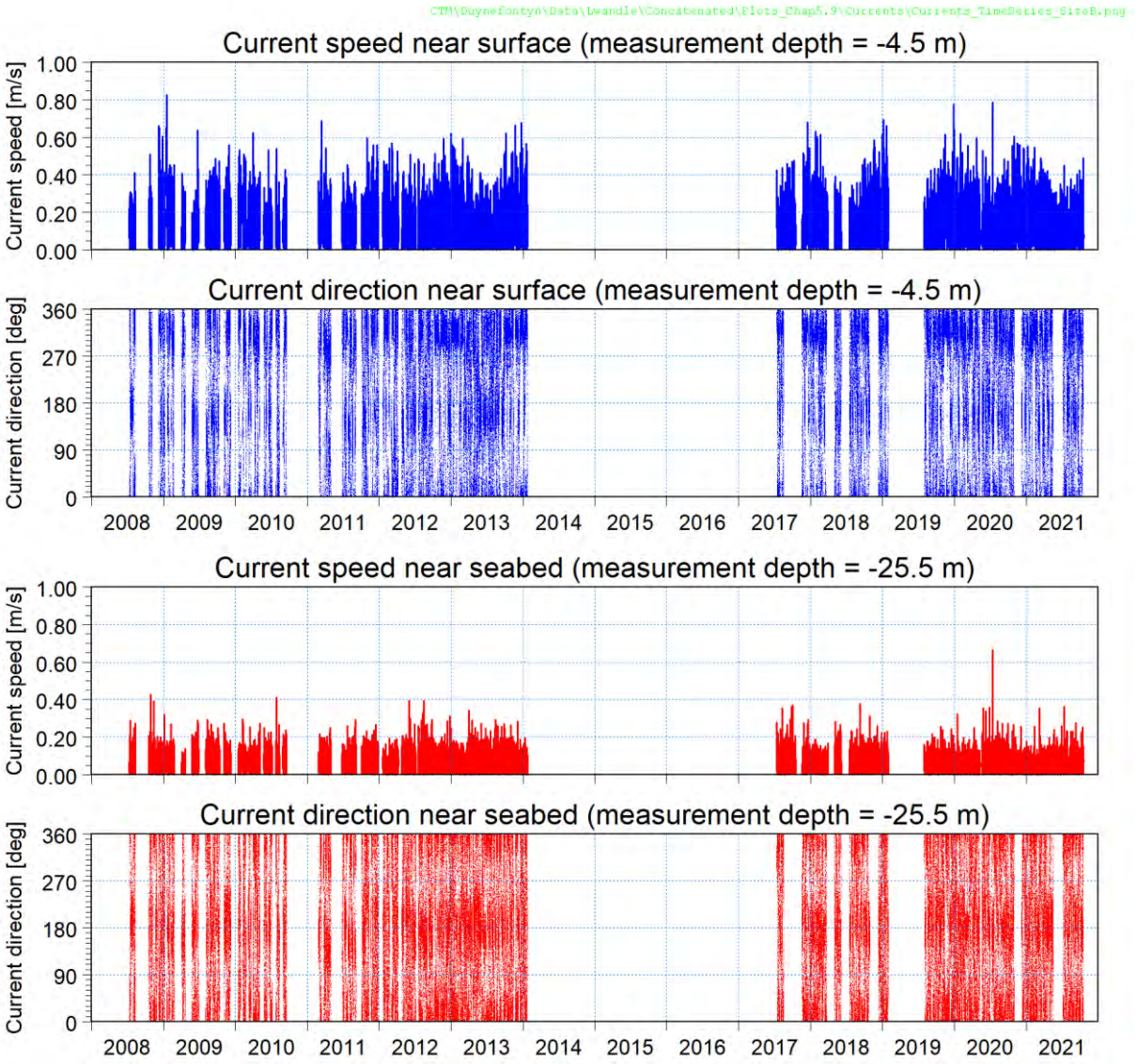


Figure 5.9.18: Time-Series of Measured Currents at Site B (Water Depth -29 m msl).

CONTROLLED DISCLOSURE

When downloaded from the EDS database, this document is uncontrolled and the responsibility rests with the user to ensure it is in line with the authorised version on the database.

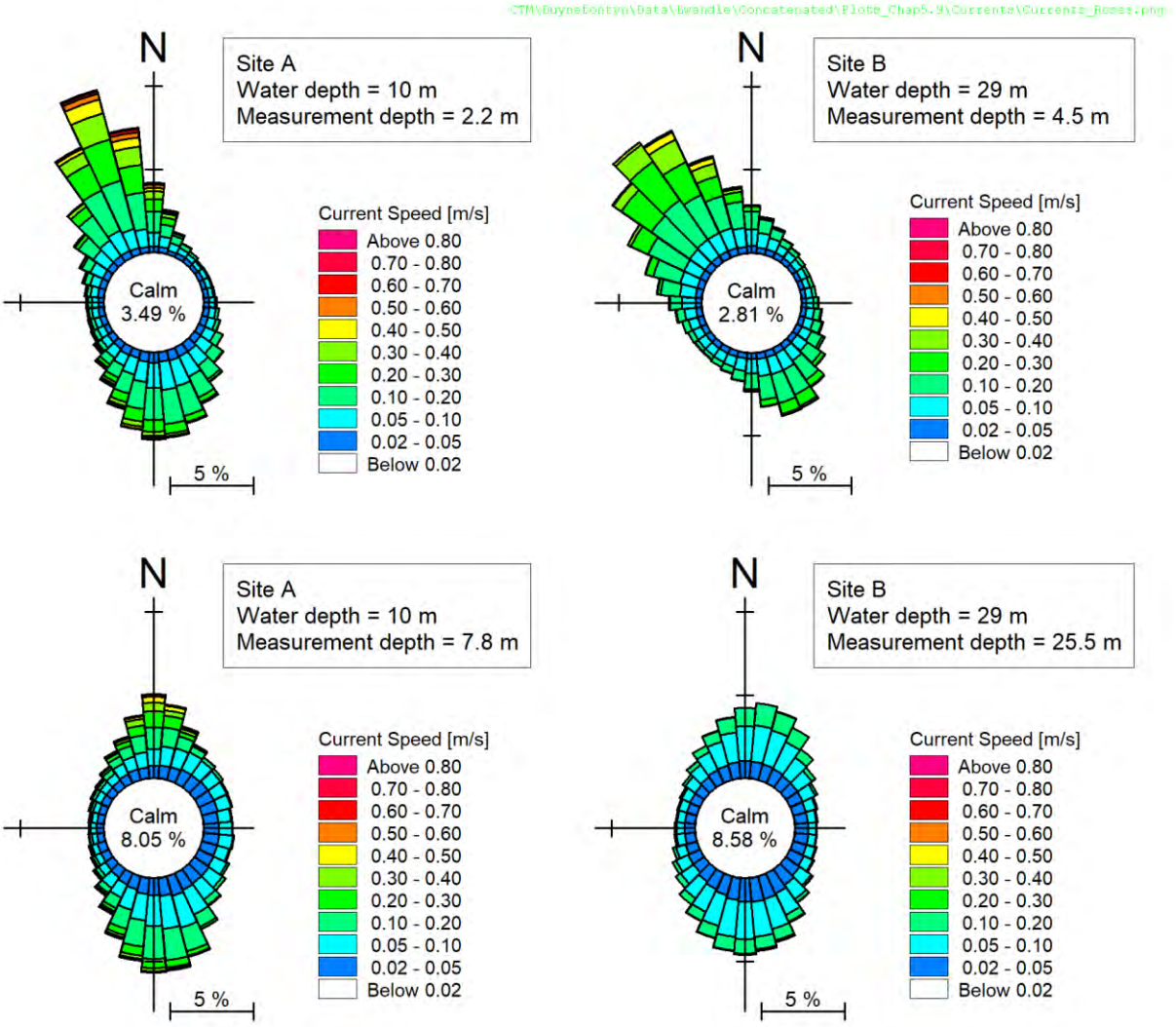


Figure 5.9.19: Measured Current Roses at Sites A and B.

CONTROLLED DISCLOSURE

When downloaded from the EDS database, this document is uncontrolled and the responsibility rests with the user to ensure it is in line with the authorised version on the database.

Table 5.9.15: Summary of Measured Current Speeds.

Percentile	Site A (Water Depth -10 m msl)		Site B (Water Depth -29 m msl)	
	Near Surface (-2.2 m msl)	Near Seabed (-7.8 m msl)	Near Surface (-4.5 m msl)	Near Seabed (-25.5 m msl)
(%)	(m/s)			
0	0.00	0.00	0.00	0.00
1	0.01	0.01	0.01	0.01
5	0.02	0.02	0.03	0.01
10	0.04	0.02	0.04	0.02
20	0.05	0.03	0.06	0.03
30	0.07	0.04	0.07	0.04
40	0.09	0.05	0.09	0.05
50	0.11	0.07	0.11	0.06
60	0.14	0.08	0.14	0.07
70	0.17	0.10	0.17	0.08
80	0.23	0.14	0.21	0.09
90	0.32	0.22	0.27	0.12
95	0.40	0.31	0.32	0.14
99	0.59	0.48	0.42	0.19
100	0.97	0.87	0.82	0.67

The current speeds are moderate (<1 m/s), with higher speeds near the surface. The currents are predominantly wind-driven, with the surface current direction predominantly north-westerly in summer in response to the strong south-easterly winds, and south-easterly in winter in response to the north-westerly winds. The bottom current directions are rotated clockwise relative to the surface currents by Ekman effects, which leads to upwelling of cold water during south-easterly winds.

An extreme value analysis (refer to ***Subsection 5.9.6.2*** for the methodology) was performed on the depth-averaged and hourly-averaged current speeds measured Site B, which has 6.55 y of data and is the longest available current dataset. The currents measured at 1 m intervals in the water column were used to calculate the depth-averaged current using vector averaging, after which the 10-minute data was used to calculate the hourly-averaged data using vector averaging. The results are plotted in ***Figure 5.9.20***. The baseline date is 2015 which is the middle of the measurement period. As expected, when extrapolating this short-duration 6.55 y dataset to an exceedance probability of 10^{-8} y^{-1}, the percentiles indicate a high level of uncertainty. It is noted that only the best estimate and not the percentiles has been to calculate the suspended sand concentrations in ***Subsection 5.9.16.3***.

The extreme current speeds were then adjusted for climate change (***Subsection 5.9.7***) and are presented in ***Table 5.9.16***.

CONTROLLED DISCLOSURE

When downloaded from the EDS database, this document is uncontrolled and the responsibility rests with the user to ensure it is in line with the authorised version on the database.

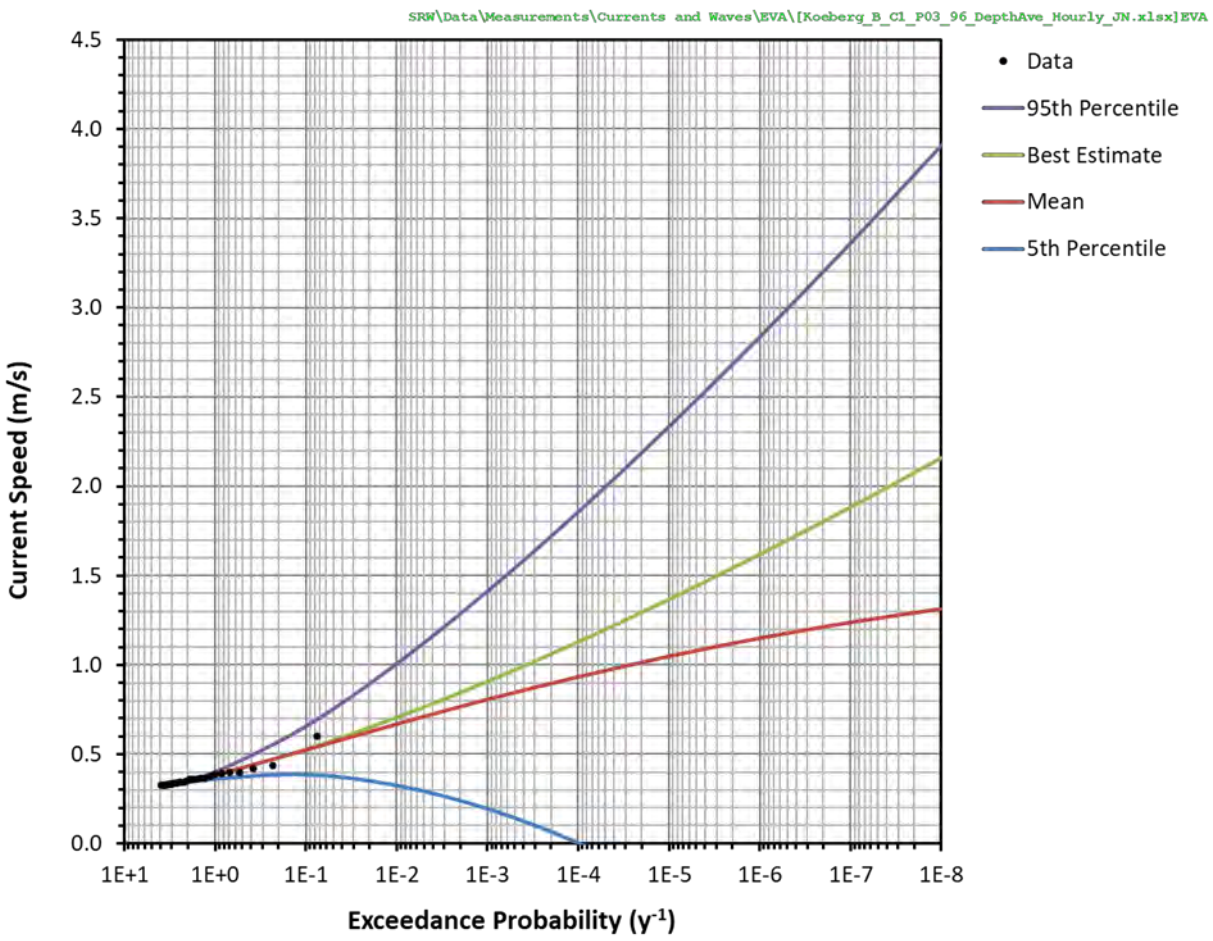


Figure 5.9.20: Extreme Value Analysis of Depth-Averaged Hourly-Averaged Current Speed at Site B (Depth -29 m msl) (Baseline Date is 2015).

CONTROLLED DISCLOSURE

When downloaded from the EDS database, this document is uncontrolled and the responsibility rests with the user to ensure it is in line with the authorised version on the database.

Table 5.9.16: Extreme Depth-Averaged Hourly-Averaged Current Speed at Site B (Water Depth -29 m msl).

Exceedance Probability	Uncertainty	Current Speed				
(y^{-1})		(m/s)				
		2021	2044	2064	2110	2130
1	5th Percentile	0.36	0.36	0.37	0.37	0.38
	Mean	0.38	0.39	0.39	0.39	0.40
	Best Estimate(a)	0.38	0.38	0.39	0.39	0.40
	95th Percentile	0.40	0.41	0.41	0.42	0.42
10^{-1}	5th Percentile	0.39	0.39	0.39	0.40	0.40
	Mean	0.52	0.53	0.53	0.54	0.54
	Best Estimate(a)	0.53	0.53	0.53	0.54	0.55
	95th Percentile	0.66	0.66	0.67	0.68	0.68
10^{-2}	5th Percentile	0.33	0.33	0.33	0.33	0.34
	Mean	0.67	0.67	0.68	0.69	0.69
	Best Estimate(a)	0.70	0.71	0.71	0.72	0.73
	95th Percentile	1.01	1.02	1.02	1.04	1.05
10^{-3}	5th Percentile	0.19	0.20	0.20	0.20	0.20
	Mean	0.81	0.81	0.82	0.83	0.84
	Best Estimate(a)	0.91	0.91	0.92	0.93	0.94
	95th Percentile	1.42	1.43	1.43	1.46	1.47
10^{-4}	5th Percentile	0.00	0.00	0.00	0.00	0.00
	Mean	0.93	0.94	0.94	0.96	0.97
	Best Estimate(a)	1.13	1.14	1.14	1.16	1.17
	95th Percentile	1.86	1.87	1.88	1.91	1.93
10^{-5}	5th Percentile	0.00	0.00	0.00	0.00	0.00
	Mean	1.05	1.05	1.06	1.08	1.09
	Best Estimate(a)	1.37	1.38	1.38	1.41	1.42
	95th Percentile	2.34	2.35	2.37	2.40	2.42
10^{-6}	5th Percentile	0.00	0.00	0.00	0.00	0.00
	Mean	1.15	1.16	1.16	1.18	1.19
	Best Estimate(a)	1.62	1.63	1.64	1.67	1.68
	95th Percentile	2.84	2.86	2.87	2.92	2.95
10^{-7}	5th Percentile	0.00	0.00	0.00	0.00	0.00
	Mean	1.24	1.25	1.25	1.27	1.28
	Best Estimate(a)	1.88	1.90	1.91	1.94	1.95
	95th Percentile	3.37	3.39	3.40	3.46	3.49
10^{-8}	5th Percentile	0.00	0.00	0.00	0.00	0.00
	Mean	1.31	1.32	1.33	1.35	1.36
	Best Estimate(a)	2.16	2.17	2.19	2.22	2.24
	95th Percentile	3.91	3.94	3.96	4.02	4.06

Notes:

(a) Should the most probable estimate be required, then the best estimate should be used rather than the mean estimate.

CONTROLLED DISCLOSURE

When downloaded from the EDS database, this document is uncontrolled and the responsibility rests with the user to ensure it is in line with the authorised version on the database.

The measured currents were used to calibrate the 3D hydrodynamic model as described in ***Subsection 5.9.15.4***. The best estimate extreme currents were used to calculate the suspended sand concentrations in ***Subsection 5.9.16.3***.

5.9.9.5 Seawater Temperature

Seawater temperatures have been measured at Sites A, B, C1, C2, D and E. Details of the locations, instruments, sampling intervals, dates and length of valid data are provided in ***Subsection 5.9.6.1***. A comparison between the temperatures measured at C1 in the intake basin and the temperatures measured at the pump intakes showed that the temperatures at C1 are representative of the intake temperatures. Due to their proximity, Sites C1 and C2 are combined and referred to as Site C.

The temperatures are presented below as time-series (***Figure 5.9.21)*** and for sites with sufficiently long durations as seasonal statistics (***Table 5.9.17*** and ***Table 5.9.18***).

CONTROLLED DISCLOSURE

When downloaded from the EDS database, this document is uncontrolled and the responsibility rests with the user to ensure it is in line with the authorised version on the database.

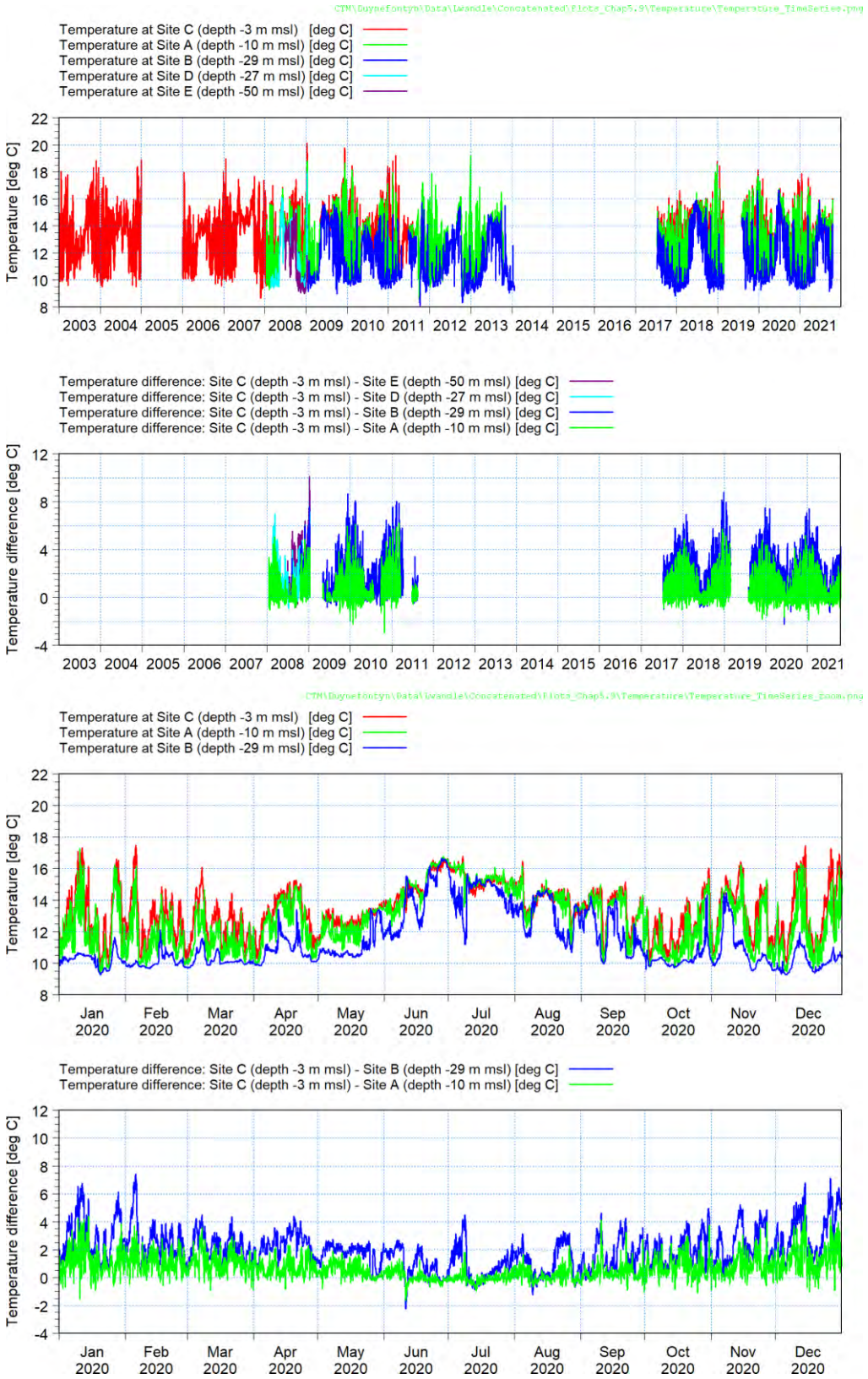


Figure 5.9.21: Time-series of Measured Seawater Temperatures and Stratification at all Sites. Bottom plots show the results for 2020 in more detail.

CONTROLLED DISCLOSURE

When downloaded from the EDS database, this document is uncontrolled and the responsibility rests with the user to ensure it is in line with the authorised version on the database.

Table 5.9.17: Statistics of Measured Hourly Seawater Temperature.

Percentile	Site C (Water Depth -3 m msl)	Site A (Water Depth -10 m msl)	Site B (Water Depth -29 m msl)
(%)	(°C)		
0	8.67	8.17	8.12
1	10.15	9.48	9.11
5	10.79	9.87	9.41
10	11.21	10.17	9.56
20	11.85	10.72	9.80
30	12.47	11.29	10.01
40	13.06	11.93	10.30
50	13.57	12.64	10.76
60	14.00	13.28	11.39
70	14.41	13.86	12.32
80	14.84	14.36	13.23
90	15.43	15.01	14.15
95	15.94	15.43	14.66
99	17.13	16.46	15.46
100	20.14[(a)]	19.22	17.94

Notes:

(a) These statistics apply to hourly data measured from January 2003 to October 2021. A higher maximum temperature of 22.3°C is included in the extended dataset used for the extreme value analysis of the temperatures, as described lower down in this subsection.

Table 5.9.18: Seasonal Percentiles of Measured Seawater Temperature Stratification.

Location	Summer			Autumn			Winter			Spring		
	5%	50%	95%	5%	50%	95%	5%	50%	95%	5%	50%	95%
	(°C)											
Temperature difference: Site C (-3 m msl) - Site A (-10 m msl)	-0.02	1.07	3.08	0.04	1.00	2.48	-0.32	0.04	1.00	-0.23	0.36	1.68
Temperature difference: Site C (-3 m msl) - Site B (-29 m msl)	0.97	2.75	5.97	0.72	2.33	4.61	-0.36	0.75	2.60	-0.07	1.64	3.76

The temperatures in the vicinity of Duynefontyn display a distinct seasonality. Temperatures in summer are significantly more variable than in winter, with solar heating (resulting in higher temperatures) and upwelling events (resulting in lower temperatures) occurring most frequently during summer. There is a decrease in temperature with increasing depth below the water surface. The stratification between the different water depths shows a seasonal trend, with the sea being stratified during summer and being more isothermal during winter.

In order to include as many extreme events as possible, an extended dataset from January 1995 to January 2022 has been used for the extreme value analysis of seawater temperature. The data at Site C1 for the period January 1995 to December 2002 was only available daily at 08:00. Due to

CONTROLLED DISCLOSURE

When downloaded from the EDS database, this document is uncontrolled and the responsibility rests with the user to ensure it is in line with the authorised version on the database.

solar heating and other processes, the maximum temperature during the day generally exceeds the temperature at 08:00. An analysis of the 11.36 y of hourly data at Sites C1 and C2 showed that the maximum daily temperature exceeds the temperature at 08:00 as follows: median = 0.8°C, 80th percentile = 1.5°C and 95th percentile = 2.4°C. Adding the 80th percentile value of 1.5°C to the temperature value at 08:00 was considered a sufficiently conservative approach to estimate the maximum daily temperature. Applying this adjustment at Site C1 for the period 1995 to 2002 resulted in a maximum temperature over this period of 22.3°C in December 1999.

Figure 5.9.22 shows the time-series of the seawater temperatures at Site C used for the extreme value analysis. Note that the data from January 1995 to December 2002 is the daily maximum, whilst the data from January 2003 to January 2022 is hourly data.

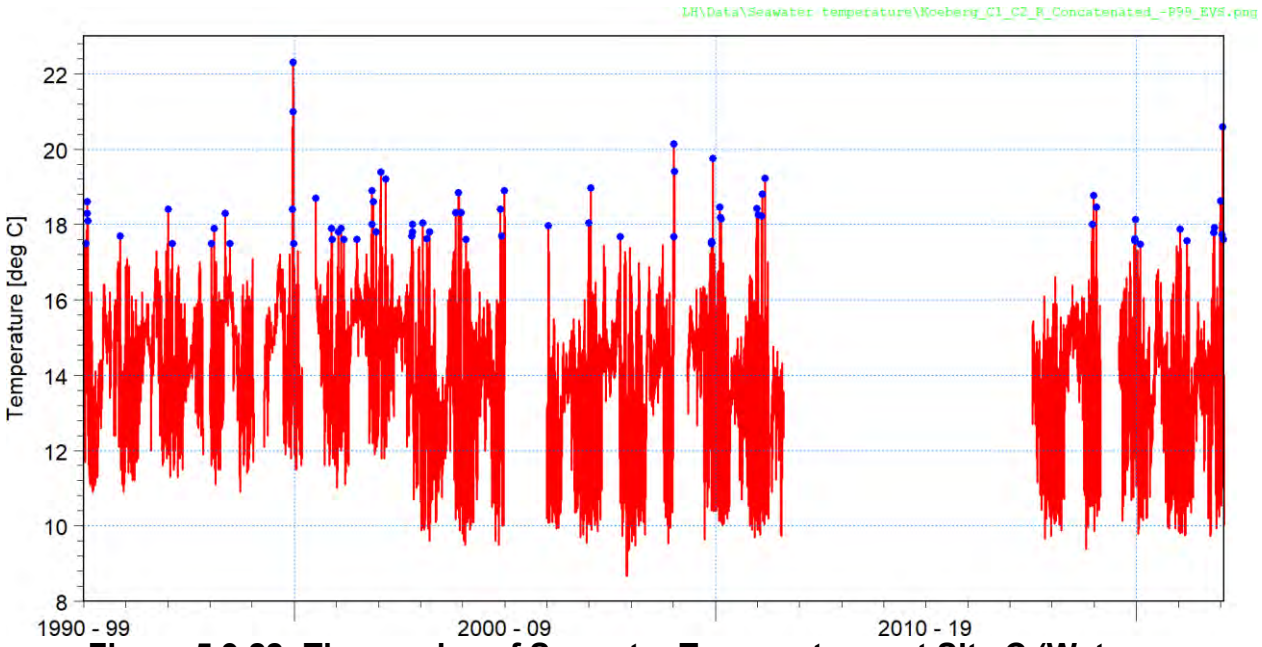


Figure 5.9.22: Time-series of Seawater Temperatures at Site C (Water Depth -3 m msl) used for the EVA. The blue dots show the events selected for the EVA, i.e., the extreme value series.

An extreme value analysis (refer to ***Subsection 5.9.6.2*** for the methodology) was performed on the measured seawater temperatures at Site C, which has 18.57 y of data. The results are plotted in ***Figure 5.9.11***. The baseline date is 2012 which is approximately the middle of the measurement period.

CONTROLLED DISCLOSURE

When downloaded from the EDS database, this document is uncontrolled and the responsibility rests with the user to ensure it is in line with the authorised version on the database.

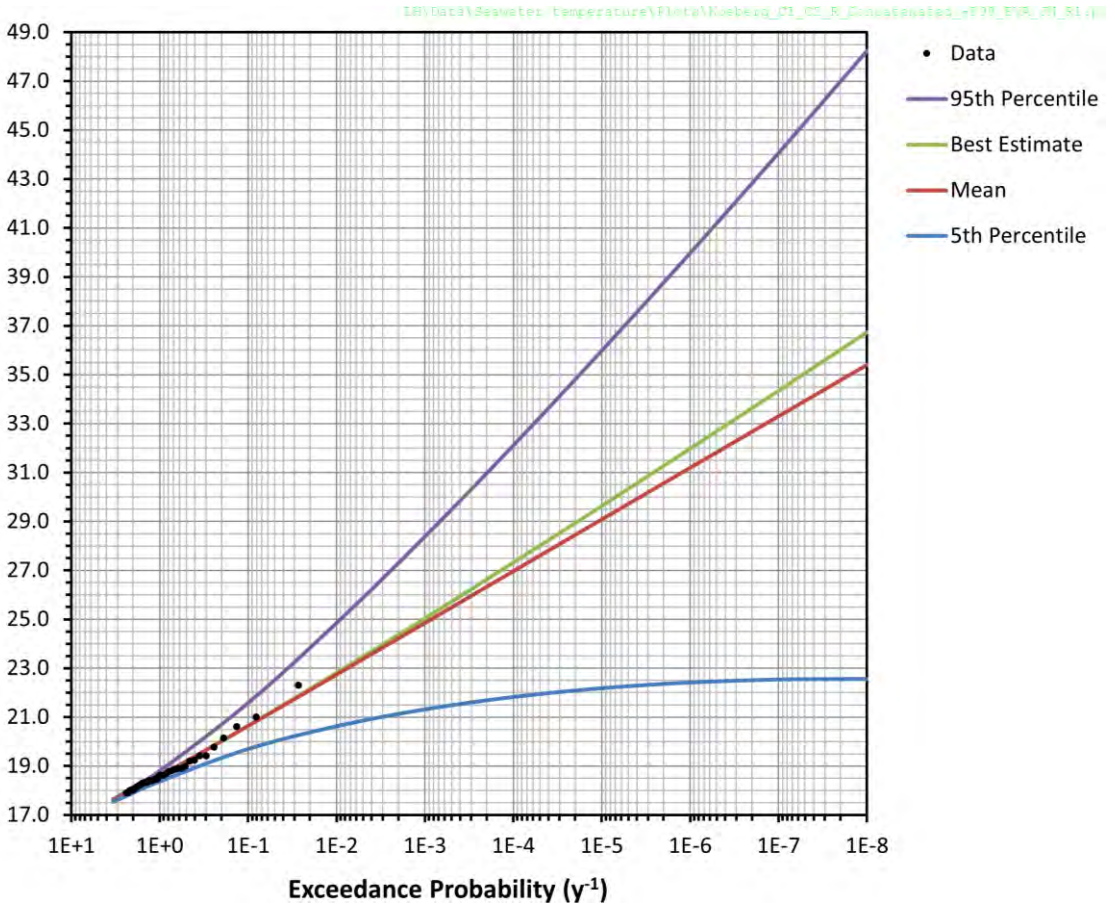


Figure 5.9.23: Extreme Value Analysis of Seawater Temperature at Site C (Water Depth -3 m msl) (Baseline Date is 2012).

Site C in a water depth of -3 m msl is representative of near-surface seawater intakes such as the existing KNPS basin intake and future similar intakes. Tunnel intakes in water depths of -20 m msl and -30 m msl have also been considered for the new NIs, with the intakes located 4 m above the seabed resulting in intake depths of -16 m msl and -26 m msl (see ***Subsection 5.9.15.3***). The extreme seawater temperatures at these intake depths have been estimated based on the measured temperatures at the site as shown in ***Table 5.9.17***. Calculating the difference between the 95th percentile temperatures at Sites A, B and C, and applying a linear trend over depth results in a temperature reduction of 0.8°C between -3 m msl and -16 m msl, and a reduction of 1.2°C between -3 m msl and -26 m msl.

The extreme maximum seawater temperatures were then adjusted for climate change (***Subsection 5.9.7***) and are presented in ***Table 5.9.19***. These extreme temperatures will be combined with the thermal plume recirculation temperatures (***Subsection 5.9.14***) to obtain the maximum temperatures at the cooling water intake (see ***Subsection 5.9.15.6***).

CONTROLLED DISCLOSURE

When downloaded from the EDS database, this document is uncontrolled and the responsibility rests with the user to ensure it is in line with the authorised version on the database.

Table 5.9.19: Extreme Maximum Seawater Temperatures.

Exceedance Probability	Uncertainty	Water Depth -3 m msl					Water Depth -20 m msl (Intake Depth -16 m msl)					Water Depth -30 m msl (Intake Depth -26 m msl)				
(y^{-1})		(°C)					(°C)					(°C)				
		2021	2044	2064	2110	2130	2021	2044	2064	2110	2130	2021	2044	2064	2110	2130
1	5th Percentile	18.6	19.1	19.6	20.6	21.1	17.8	18.3	18.8	19.8	20.3	17.4	17.9	18.4	19.4	19.9
	Mean	18.8	19.3	19.8	20.8	21.3	18.0	18.5	19.0	20.1	20.5	17.6	18.1	18.6	19.6	20.1
	Best Estimate[a]	18.8	19.3	19.8	20.8	21.3	18.0	18.5	19.0	20.1	20.5	17.6	18.1	18.6	19.6	20.1
	95th Percentile	19.0	19.5	20.0	21.1	21.5	18.2	18.8	19.2	20.3	20.7	17.8	18.3	18.8	19.9	20.3
10^{-1}	5th Percentile	19.9	20.4	20.9	21.9	22.4	19.1	19.6	20.1	21.2	21.6	18.7	19.2	19.7	20.7	21.2
	Mean	20.8	21.4	21.8	22.9	23.4	20.1	20.6	21.1	22.1	22.6	19.7	20.2	20.6	21.7	22.2
	Best Estimate[a]	20.8	21.4	21.8	22.9	23.4	20.1	20.6	21.1	22.1	22.6	19.7	20.2	20.6	21.7	22.2
	95th Percentile	21.8	22.3	22.8	23.8	24.3	21.0	21.5	22.0	23.1	23.5	20.6	21.1	21.6	22.6	23.1
10^{-2}	5th Percentile	20.8	21.4	21.8	22.9	23.3	20.0	20.6	21.0	22.1	22.6	19.6	20.2	20.6	21.7	22.1
	Mean	22.9	23.5	23.9	25.0	25.5	22.2	22.7	23.2	24.2	24.7	21.8	22.3	22.7	23.8	24.3
	Best Estimate[a]	23.0	23.5	24.0	25.1	25.5	22.2	22.8	23.2	24.3	24.7	21.8	22.3	22.8	23.9	24.3
	95th Percentile	25.1	25.6	26.0	27.1	27.6	24.3	24.8	25.3	26.3	26.8	23.9	24.4	24.8	25.9	26.4
10^{-3}	5th Percentile	21.5	22.0	22.5	23.6	24.0	20.7	21.3	21.7	22.8	23.2	20.3	20.8	21.3	22.4	22.8
	Mean	25.1	25.6	26.0	27.1	27.6	24.3	24.8	25.3	26.3	26.8	23.9	24.4	24.8	25.9	26.4
	Best Estimate[a]	25.2	25.8	26.2	27.3	27.8	24.5	25.0	25.5	26.5	27.0	24.1	24.6	25.0	26.1	26.6
	95th Percentile	28.6	29.1	29.6	30.6	31.1	27.8	28.3	28.8	29.9	30.3	27.4	27.9	28.4	29.4	29.9
10^{-4}	5th Percentile	22.0	22.6	23.0	24.1	24.5	21.2	21.8	22.2	23.3	23.8	20.8	21.4	21.8	22.9	23.3
	Mean	27.2	27.7	28.2	29.2	29.7	26.4	26.9	27.4	28.4	28.9	26.0	26.5	27.0	28.0	28.5
	Best Estimate[a]	27.5	28.1	28.5	29.6	30.0	26.7	27.3	27.7	28.8	29.3	26.3	26.9	27.3	28.4	28.8
	95th Percentile	32.3	32.8	33.3	34.4	34.8	31.5	32.1	32.5	33.6	34.0	31.1	31.6	32.1	33.2	33.6
10^{-5}	5th Percentile	22.4	22.9	23.4	24.4	24.9	21.6	22.1	22.6	23.7	24.1	21.2	21.7	22.2	23.2	23.7
	Mean	29.3	29.8	30.3	31.3	31.8	28.5	29.0	29.5	30.6	31.0	28.1	28.6	29.1	30.1	30.6
	Best Estimate[a]	29.8	30.4	30.8	31.9	32.3	29.1	29.6	30.0	31.1	31.6	28.6	29.2	29.6	30.7	31.1
	95th Percentile	36.2	36.7	37.2	38.2	38.7	35.4	35.9	36.4	37.5	37.9	35.0	35.5	36.0	37.0	37.5
10^{-6}	5th Percentile	22.6	23.1	23.6	24.7	25.1	21.8	22.4	22.8	23.9	24.3	21.4	21.9	22.4	23.5	23.9
	Mean	31.4	31.9	32.4	33.4	33.9	30.6	31.1	31.6	32.7	33.1	30.2	30.7	31.2	32.2	32.7
	Best Estimate[a]	32.2	32.7	33.2	34.2	34.7	31.4	31.9	32.4	33.4	33.9	31.0	31.5	32.0	33.0	33.5
	95th Percentile	40.2	40.7	41.2	42.2	42.7	39.4	39.9	40.4	41.5	41.9	39.0	39.5	40.0	41.0	41.5
10^{-7}	5th Percentile	22.7	23.3	23.7	24.8	25.2	22.0	22.5	22.9	24.0	24.5	21.5	22.1	22.5	23.6	24.0
	Mean	33.5	34.0	34.5	35.6	36.0	32.7	33.3	33.7	34.8	35.2	32.3	32.8	33.3	34.4	34.8
	Best Estimate[a]	34.5	35.1	35.5	36.6	37.1	33.8	34.3	34.8	35.8	36.3	33.4	33.9	34.3	35.4	35.9
	95th Percentile	44.3	44.8	45.3	46.3	46.8	43.5	44.0	44.5	45.5	46.0	43.1	43.6	44.1	45.1	45.6
10^{-8}	5th Percentile	22.8	23.3	23.8	24.8	25.3	22.0	22.5	23.0	24.0	24.5	21.6	22.1	22.6	23.6	24.1
	Mean	35.6	36.1	36.6	37.7	38.1	34.8	35.4	35.8	36.9	37.3	34.4	34.9	35.4	36.5	36.9
	Best Estimate[a]	36.9	37.5	37.9	39.0	39.4	36.2	36.7	37.1	38.2	38.7	35.7	36.3	36.7	37.8	38.2
	95th Percentile	48.5	49.0	49.4	50.5	51.0	47.7	48.2	48.7	49.7	50.2	47.3	47.8	48.2	49.3	49.8

Notes:

(a) Should the most probable estimate be required, then the best estimate should be used rather than the mean estimate.

Regarding the possibility of ice occurring in the sea surrounding the site, the lowest seawater temperature measured in all the data sets described in this

CONTROLLED DISCLOSURE

When downloaded from the EDS database, this document is uncontrolled and the responsibility rests with the user to ensure it is in line with the authorised version on the database.

section is 8.12°C, and an extreme value analysis of the minimum measured temperatures at Site C was above 0°C at an exceedance of 10^{-8} y^{-1}. On this basis ice is not anticipated to form in the sea at the site and the minimum cooling water intake temperature of -0.5°C will be met.

5.9.9.6 Salinity

Salinity has been measured at Sites A and B. The salinity averages 35.0 psu which is in line with the global average sea surface salinity, and shows little variation (<1 psu) which is due to the lack of any significant river discharges within a 100 km radius of the site. Salinity is thus a minor safety and design parameter, in contrast to the sea temperature which is an important determinant of the efficiency of the seawater cooling system.

5.9.9.7 Suspended Sediment

One hundred and forty-two water samples have been collected at the site and analysed for Total Suspended Solids (TSS), which comprise organic (e.g., algae) and inorganic (e.g., silt and clay) particles suspended in the water column. The sampling locations and the results are provided in ***Figure 5.9.24***, ***Figure 5.9.25*** and ***Table 5.9.20***.

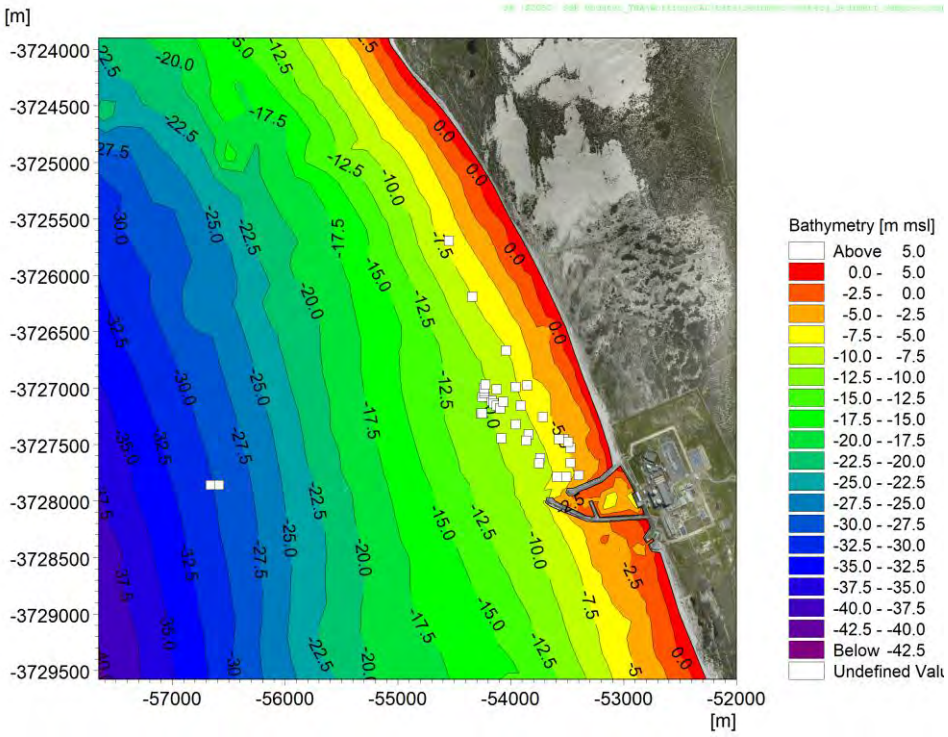


Figure 5.9.24: Total Suspended Solids Sampling Locations.

CONTROLLED DISCLOSURE

When downloaded from the EDS database, this document is uncontrolled and the responsibility rests with the user to ensure it is in line with the authorised version on the database.

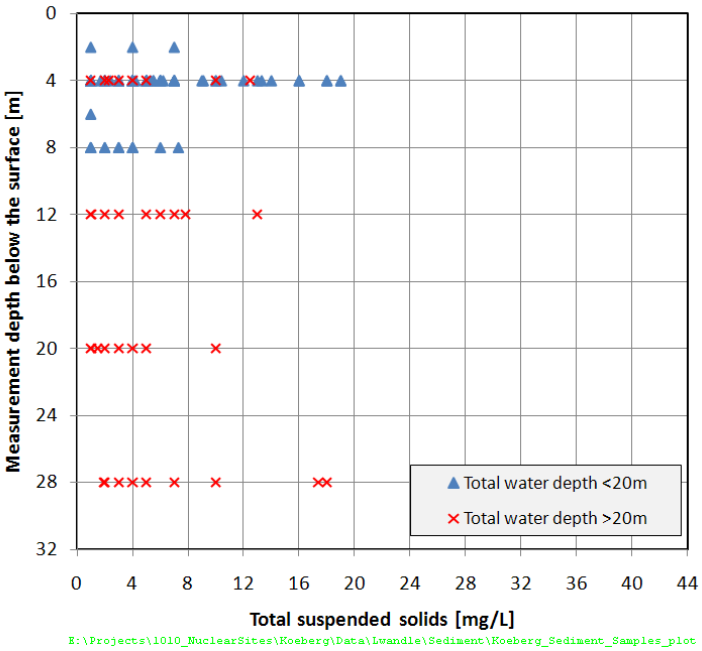


Figure 5.9.25: Total Suspended Solids Distribution in Water Column.

Table 5.9.20: Summary of Measured Total Suspended Solids.

Percentile (%)	TSS (mg/L)
0	1
1	1
5	1
10	1
20	2
30	2
40	3
50	4
60	5
70	6
80	7
90	12
95	16
99	19
100	75

The measured TSS concentrations are generally low, although these are expected to increase during storms, large rainfall events and algal blooms. The results show little difference in TSS concentrations between shallower inshore sampling sites and the deeper offshore sites. The TSS concentration is relatively uniform over the water column implying that these are finer cohesive sediment particles (D_{50} < 0.063 mm) rather than larger

CONTROLLED DISCLOSURE

When downloaded from the EDS database, this document is uncontrolled and the responsibility rests with the user to ensure it is in line with the authorised version on the database.

sand particles (which would show significantly higher concentrations near the seabed due to settling).

These finer particles are likely to remain in suspension and pass through the cooling system, rather than deposit in the intake basin. The impact of larger sand-sized particles (D_{50} > 0.063 mm) on the intake basins is addressed using modelling (see ***Subsection 5.9.16.3***).

5.9.9.8 Waves

Measured waves

Waves have been measured at Site A (water depth -10 m msl) and at Site B (water depth -29.0 m msl). Details of the locations, instruments, sampling intervals, dates and length of valid data are provided in ***Subsection 5.9.6.1***.

The measured wave parameters are presented below as time-series (***Figure 5.9.17*** and ***Figure 5.9.18***), wave roses (***Figure 5.9.19***) and statistics (***Table 5.9.15***). H_{m0} is the significant wave height, T_p is the peak wave direction, and MWD is the wave energy weighted mean wave direction. Note that wave direction is the direction from which the waves are coming, measured clockwise from true north.

CONTROLLED DISCLOSURE

When downloaded from the EDS database, this document is uncontrolled and the responsibility rests with the user to ensure it is in line with the authorised version on the database.

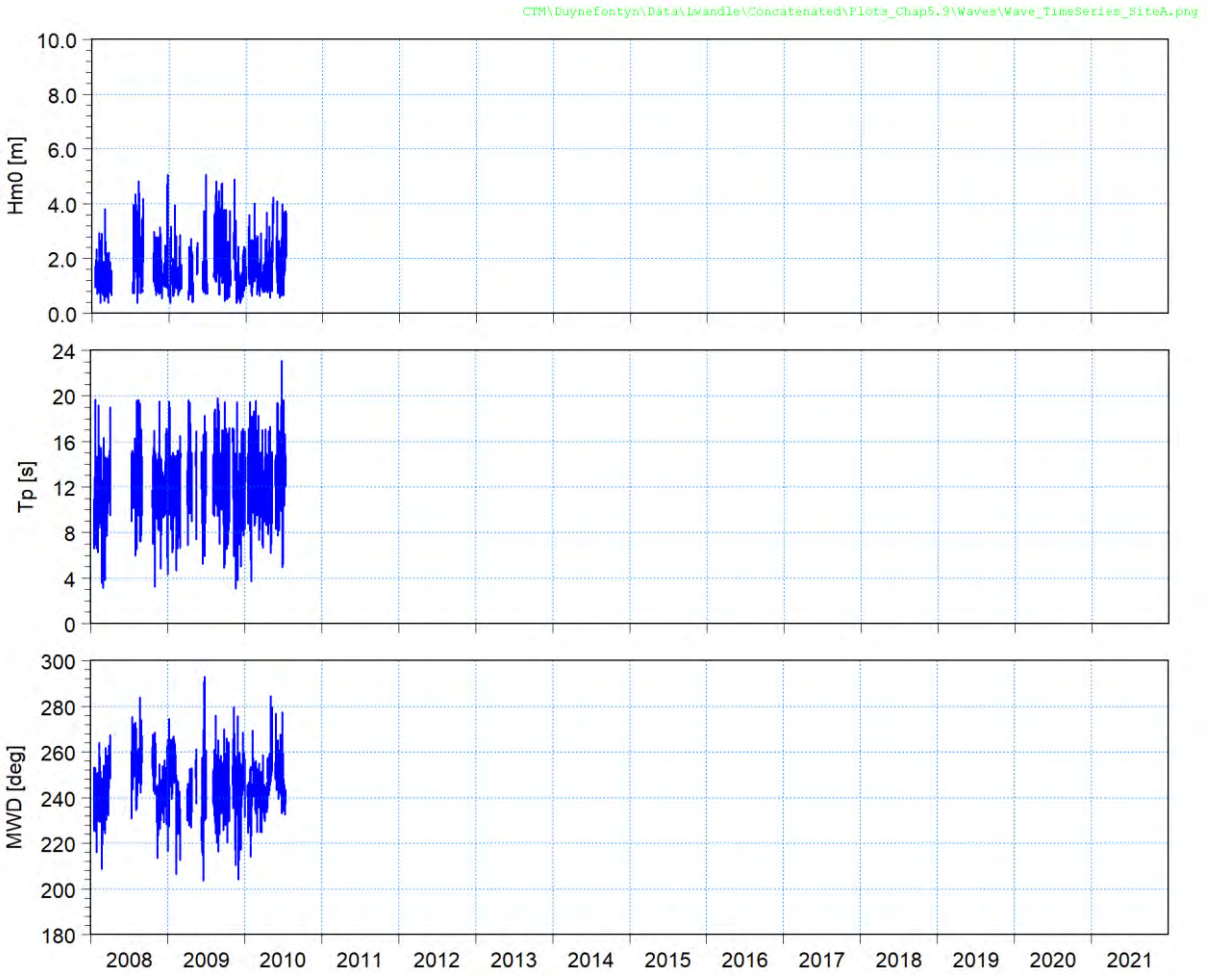


Figure 5.9.26: Time-series of Measured Wave Parameters at Site A (Water Depth -10 m msl).

CONTROLLED DISCLOSURE

When downloaded from the EDS database, this document is uncontrolled and the responsibility rests with the user to ensure it is in line with the authorised version on the database.

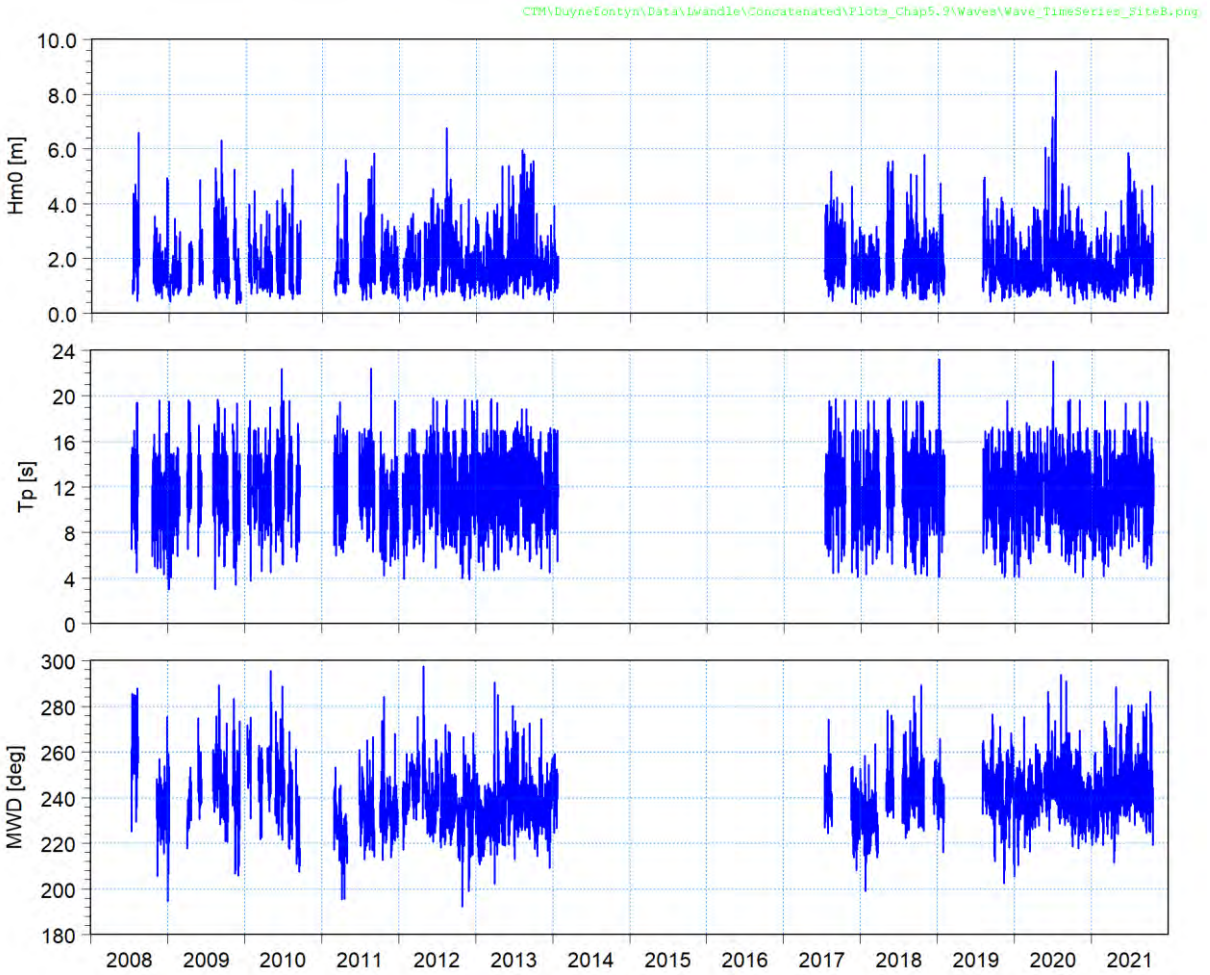


Figure 5.9.27: Time-series of Measured Wave Parameters at Site B (Water Depth -29 m msl).

CONTROLLED DISCLOSURE

When downloaded from the EDS database, this document is uncontrolled and the responsibility rests with the user to ensure it is in line with the authorised version on the database.

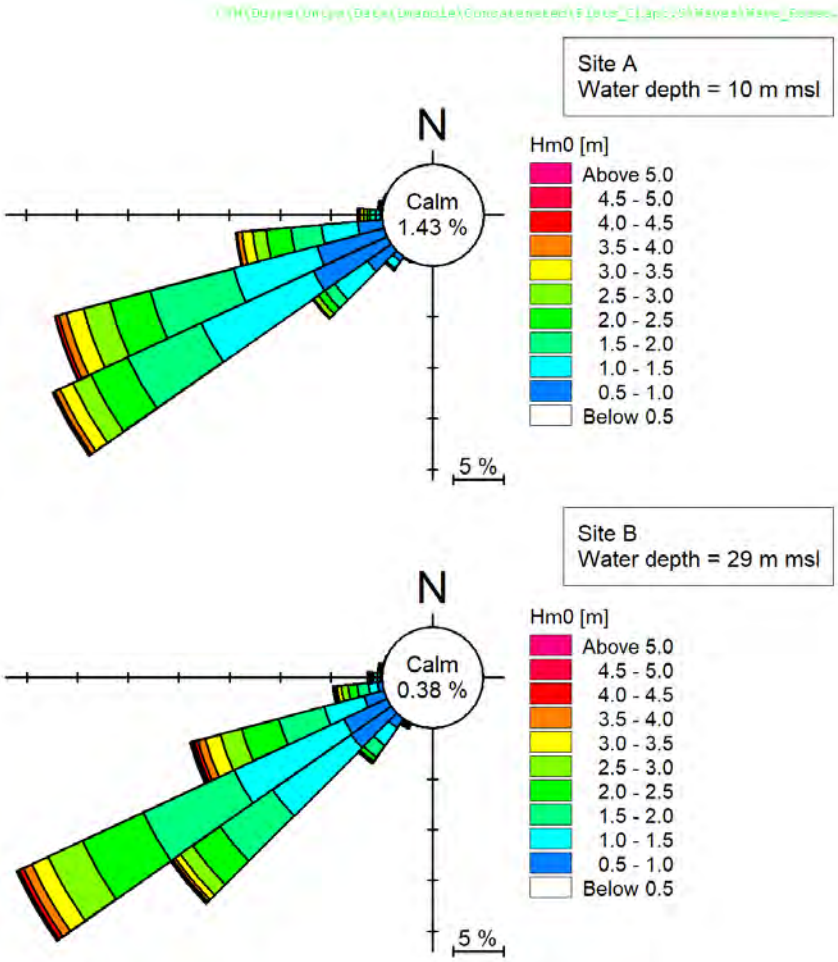


Figure 5.9.28: Wave Roses at Site A and Site B.

CONTROLLED DISCLOSURE

When downloaded from the EDS database, this document is uncontrolled and the responsibility rests with the user to ensure it is in line with the authorised version on the database.

Table 5.9.21: Summary of Measured Waves.

Percentile	Significant Wave Height (H_{m0})	
	Site A (Water Depth -10 m msl)	Site B (Water Depth -29 m msl)
(%)	(m)	(m)
0	0.37	0.33
1	0.48	0.57
5	0.65	0.77
10	0.78	0.92
20	0.96	1.12
30	1.13	1.29
40	1.30	1.45
50	1.46	1.63
60	1.65	1.83
70	1.91	2.07
80	2.24	2.39
90	2.81	2.90
95	3.27	3.37
99	3.99	4.43
100	5.06	8.85

The measured wave data indicates a rough wave climate with a median H_{m0} of 1.63 m at Site B. The maximum H_{m0} of 8.85 m was measured during a storm event on 13 July 2020.There is a significant seasonal variation in wave height, with the smallest waves occurring during summer (Dec to Feb) and the largest waves occurring during winter (Jun to Aug). The dominant wave direction at the site is 240° and shifts slightly westward in winter and southward in summer. These wave measurements were used to calibrate the wave refraction model, as described below.

Offshore hindcast data

Due to the limited duration (7.0 y) of the measured wave data at the site, offshore wave data from a global hindcast model has been transformed to the site using a spectral wave model. The validation of the offshore hindcast data is described in this subsection.

Global hindcast wave data is freely available from the US National Oceanic and Atmospheric Administration's (NOAA) National Centers for Environmental Prediction (NCEP). The NCEP data is produced using the WAVEWATCH III multi-grid spectral wave model. Three datasets are currently available (NCEP, 2021):

- Reanalysis (1979-2009): A 31 year hindcast generated from the NCEP Climate Forecast System Reanalysis and Reforecast (CFSRR) homogeneous dataset of hourly high-resolution winds.

CONTROLLED DISCLOSURE

When downloaded from the EDS database, this document is uncontrolled and the responsibility rests with the user to ensure it is in line with the authorised version on the database.

- Production (2005 to 2019): An hindcast dataset produced by rerunning the model from the operational wind fields to produce best-estimate nowcast datasets.
- Forecast (2007 to 2021): Archived dataset of ocean wave nowcasts and predictions using operational and assimilated NCEP atmospheric products as input.

The Reanalysis and Production datasets comprise wave partition data on a 1 degree geographical grid at hourly intervals, while the Forecast dataset is available on a 0.5 degree geographical grid at 3-hourly intervals. The wave partition data characterises the sea state by identifying wave parameters (H_{m0}, T_p, MWD, and directional standard deviation (DSD)) for each of a variable number of peaks in the 2D wave spectrum. The wave partition data has been used to reconstitute the full 2D spectrum at each node and time step. In addition, the NCEP datasets also include space and time varying 10-m wind fields.

Table 5.9.22 summarises the available offshore hindcast data as used for the operational and extreme wave refraction. ***Figure 5.9.29*** shows the closest nodes available to the site from the three datasets. Note that latitudes of the NCEP Production dataset are offset by 0.5°.

Table 5.9.22: Summary of Available Offshore Hindcast Data

Dataset	Resolution		Dates Available	Dates Used in Models	
	Spatial (°)	Temporal (h)		Operational	Extremes
Reanalysis	1	1	1979 - 2009	2000 – 2009	1979 - 2009
Production	1	1	2005 – 2019	N/A	2010 - March 2019
Forecast	0.5	3	2007 - 2021	N/A	April 2019 - 2021

CONTROLLED DISCLOSURE

When downloaded from the EDS database, this document is uncontrolled and the responsibility rests with the user to ensure it is in line with the authorised version on the database.

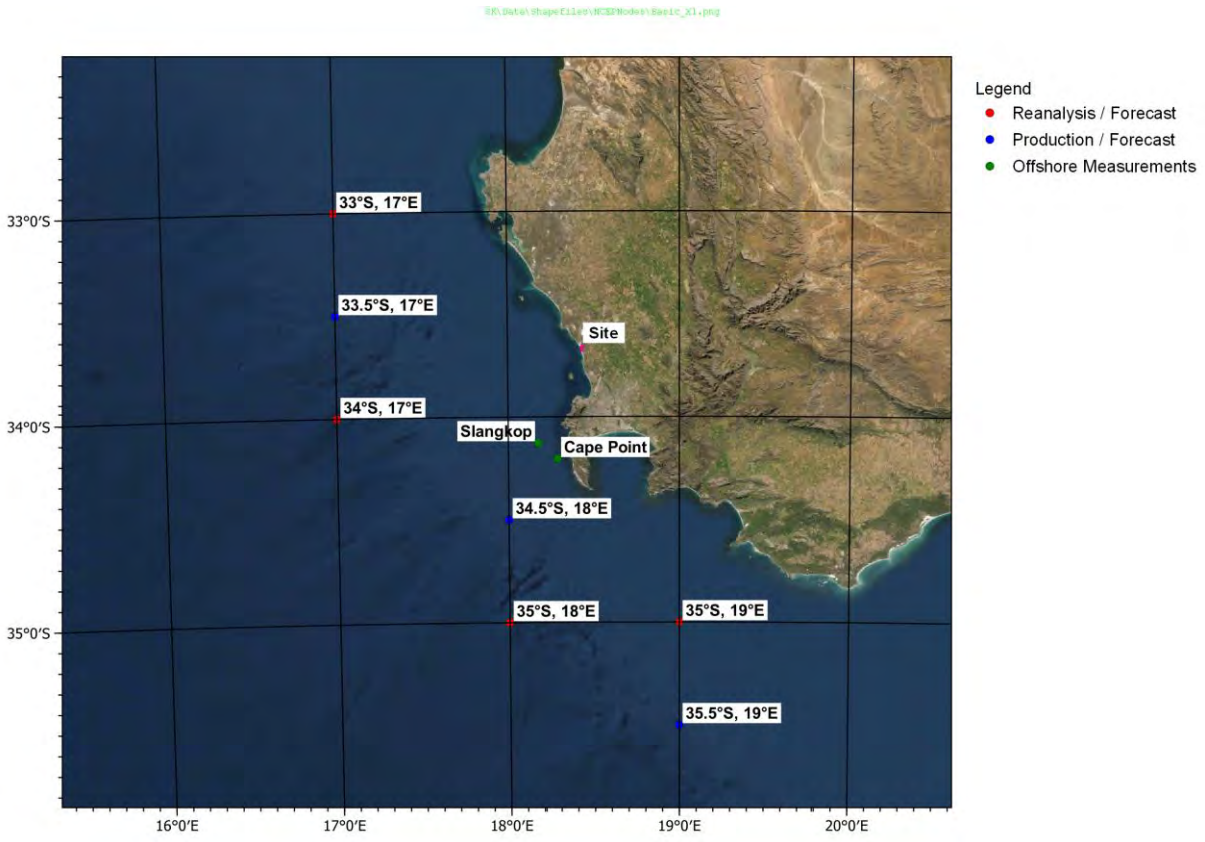


Figure 5.9.29: Locations of Available Offshore Hindcast Data.

Long-term wave measurements in deep water are available off Kommetjie on the Cape Peninsula. The data is measured by Council for Science and Industrial Research (CSIR) on behalf of Transnet National Ports Authority (TNPA), who have kindly given permission for PRDW to use these data for this project. A summary of the available datasets is given in ***Table 5.9.23*** and the locations are shown in ***Figure 5.9.29***.

Table 5.9.23: Available Offshore Measured Wave Data

Location	Longitude (°)	Latitude (°)	Water Depth (m msl)	Date Range	Measuring Interval	Instrument and Setup
Slangkop	18.17666	-34.12666	-170	Oct 1978 to Sep 1989	6 hours	Waverider buoy, 17-minute bursts
				Oct 1989 to May 1993	3 hours	
Cape Point	18.28667	-34.20400	-70	Jun 1994 to Dec 2002	3 hours	
				Jan 2003 to Apr 2021	30 minutes	

CONTROLLED DISCLOSURE

When downloaded from the EDS database, this document is uncontrolled and the responsibility rests with the user to ensure it is in line with the authorised version on the database.

The deep water Waverider buoy was originally located at Slangkop in a depth of 170 m, but was later moved to the Cape Point location with a shallower depth of 70 m. As can be inferred from the table, technological advances allowed a gradual increase in the frequency of the Waverider measurements over time. The Slangkop and Cape Point datasets were combined. The wave heights measured at Slangkop were scaled using a spectral wave-derived refraction coefficient, and were then concatenated to the Cape Point data, extending the dataset to span the 42.5-year period of 1978-2021. Accounting for gaps in the data, the total record length of the combined dataset is 36.5 years.

The hindcast datasets were compared to the measurements by back-refracting the measured waves from Cape Point to the boundaries using refraction coefficients obtained from preliminary wave modelling. For the operational wave climate the NCEP Reanalysis dataset was scaled using a two-part linear function, fitted to the quantile-quantile (Q-Q) distributions, to produce a better fit of modelled and measured wave heights:

$$y = 1.00 \cdot x - 0.23, \quad x \leq 6.30 \text{ m}$$
$$y = 1.48 \cdot x - 3.24, \quad x > 6.30 \text{ m}$$

Equation 5.9.2

where:

x = Unscaled NCEP offshore wave height (m)

y = Scaled NCEP offshore wave height (m)

Subsequent to the boundary scaling, the model was run for the period of 2000 to 2009 (10 years) to obtain wave heights at Cape Point for comparison to the measurements. ***Figure 5.9.30*** presents a scatterplot comparison of modelled and measured operational wave heights at Cape Point.

CONTROLLED DISCLOSURE

When downloaded from the EDS database, this document is uncontrolled and the responsibility rests with the user to ensure it is in line with the authorised version on the database.

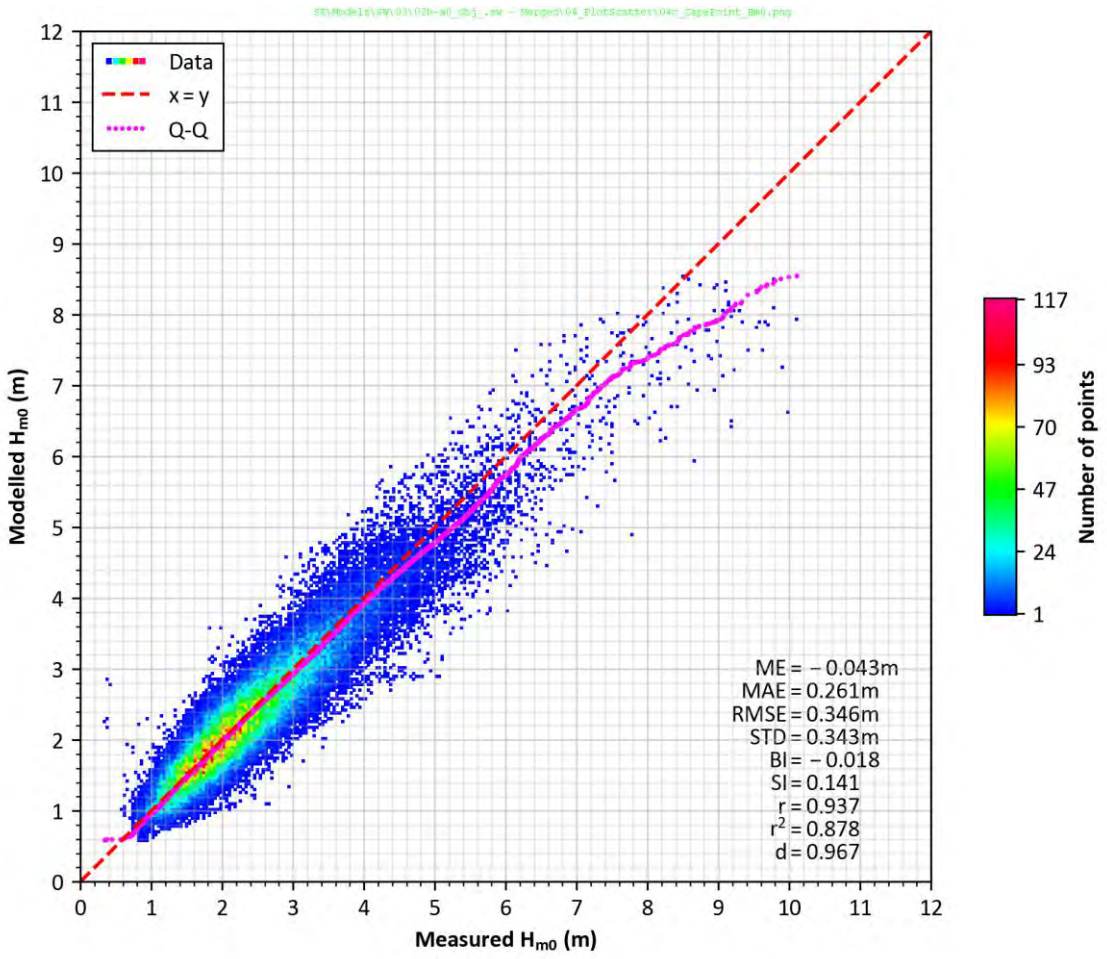


Figure 5.9.30: Scatterplot Comparison of Modelled and Measured Operational Wave Heights at Cape Point Location (Water Depth -70 m msl)

The modelled H_{m0} underestimates some of the larger wave events but correlates well to operational wave heights of the measurements. The scaled NCEP Reanalysis hindcast wave data is therefore considered to provide a sufficiently accurate characterisation of the operational wave climate offshore of Cape Town. The extreme wave climate was calibrated separately as described below.

For the extreme wave climate new scaling factors which are more biased towards storm peaks were applied to the Reanalysis dataset:

$$y = 1.10 \cdot x - 1.19, \quad x \leq 6.80 \text{ m}$$
$$y = 1.77 \cdot x - 5.66, \quad x > 6.80 \text{ m}$$

Equation 5.9.3

The Production and Forecast datasets were left unscaled.

CONTROLLED DISCLOSURE

When downloaded from the EDS database, this document is uncontrolled and the responsibility rests with the user to ensure it is in line with the authorised version on the database.

The storm events between 1979 and 2021 were modelled and validated against the measured wave heights at Cape Point by comparing EVA analyses (refer to ***Subsection 5.9.6.2***) of the two datasets.

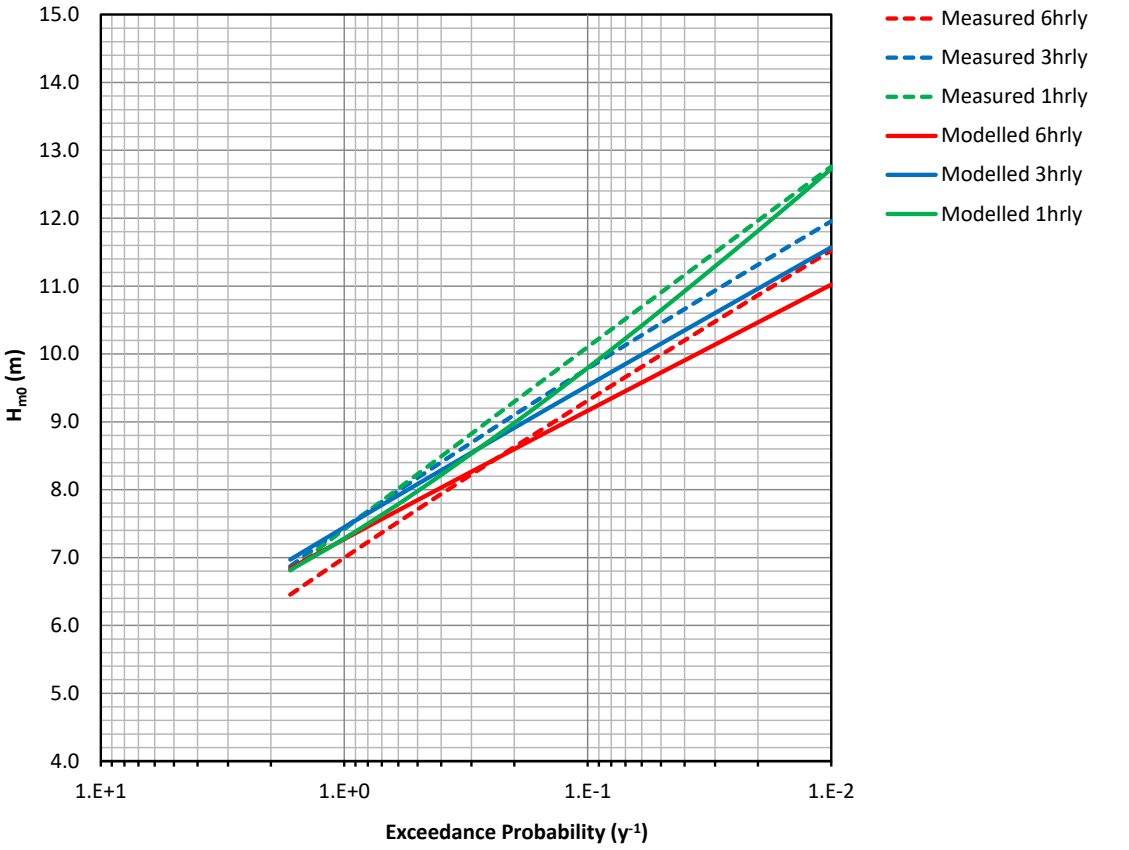
It is preferable for the EVA to be carried out on a homogeneous dataset. From the combined measured wave data, the following homogeneous subsets are available:

- 6-hourly data for the period of 1978-2021 (36.5 years accounting for gaps);
- 3-hourly data for the period of 1990-2021 (28.1 years accounting for gaps); and
- 1-hour averaged data for the period of 2003-2021 (17.3 years accounting for gaps).

A comparison of modelled and measured best estimate extreme wave heights at Cape Point is shown in ***Figure 5.9.31*** and summarised in ***Table 5.9.24***.

CONTROLLED DISCLOSURE

When downloaded from the EDS database, this document is uncontrolled and the responsibility rests with the user to ensure it is in line with the authorised version on the database.



SK\Models\SW\02_PostProcess_X3\03_EVA_4pa\[EVA_CompareAll.xlsx]Table

Figure 5.9.31: Comparison of Modelled and Measured Best Estimate Extreme Wave Heights at Cape Point Location (Water Depth -70 m msl)

Table 5.9.24: Comparison of Modelled and Measured Best Estimate Extreme Wave Heights at Cape Point Location (Water Depth -70 m msl)

Exceedance Probability	Modelled H_{m0}			Measured H_{m0}			Percentage error		
	6 hr	3 hr	1 hr	6 hr	3 hr	1 hr	6 hr	3 hr	1 hr
(y^{-1})	(m)			(m)			(%)		
$2x10^{-1}$	8.6	8.9	9.0	8.6	9.1	9.3	-0.4%	-2.1%	-3.4%
$1x10^{-1}$	9.2	9.5	9.8	9.3	9.8	10.1	-1.6%	-2.6%	-3.0%
$2x10^{-2}$	10.5	11.0	11.8	10.9	11.3	12.0	-3.7%	-3.1%	-1.3%
$1x10^{-2}$	11.0	11.6	12.7	11.5	12.0	12.8	-4.4%	-3.2%	-0.3%

The extreme values for both the measured and modelled data increase as the sampling interval decreases; this trend is due both to the higher frequency data giving a higher storm peak and a reduction in the record length containing the largest storm on record (June 2017). Discrepancies can be expected in the EVA curves for the lower sampling frequencies due

CONTROLLED DISCLOSURE

When downloaded from the EDS database, this document is uncontrolled and the responsibility rests with the user to ensure it is in line with the authorised version on the database.

to the storm peaks occurring between 1 and 6 hours earlier or later between the modelled and measured datasets. The EVA curves for the 1 hourly datasets present the most favourable comparison with a narrow error range of -3.4 % (0.3 m, $2x10^{-1}$ y^{-1} exceedance probability) to -0.3% (0.1 m, $1x10^{-2}$ y^{-1} exceedance probability). The most accurate 1 hourly dataset will be used for the wave modelling described below.

These results show that the extreme offshore hindcast data is sufficiently calibrated for this study. Full details of the offshore wave hindcast V&V are provided in the V&V Report (PRDW, 2022b).

Spectral wave modelling

The MIKE 21 Spectral Waves (SW) Flexible Mesh model was used for the wave transformation modelling. The details of the physical processes and numerical implementation are provided in the model documentation (see ***Table 5.9.7***), while details of the model setup, sensitivity testing, and V&V are provided in the V&V Report (PRDW, 2022b).

The model simulates the growth, decay and transformation of wind-generated waves and swells in offshore and coastal areas using unstructured meshes. The model includes the following physical phenomena:

- Wind-wave generation;
- Non-linear wave-wave interaction;
- Dissipation due to whitecapping;
- Dissipation due to bottom friction;
- Dissipation due to depth-induced wave breaking;
- Refraction and shoaling due to depth variations;
- The effect of time-varying water depth.

Figure 5.9.32 and ***Figure 5.9.33*** show the mesh and bathymetry used for the Reanalysis wave refraction modelling. Note that the Production hindcast data necessitated a different mesh to align the offshore boundaries with the NCEP nodes. The Forecast dataset used the same mesh as the Production hindcast mesh.

CONTROLLED DISCLOSURE

When downloaded from the EDS database, this document is uncontrolled and the responsibility rests with the user to ensure it is in line with the authorised version on the database.

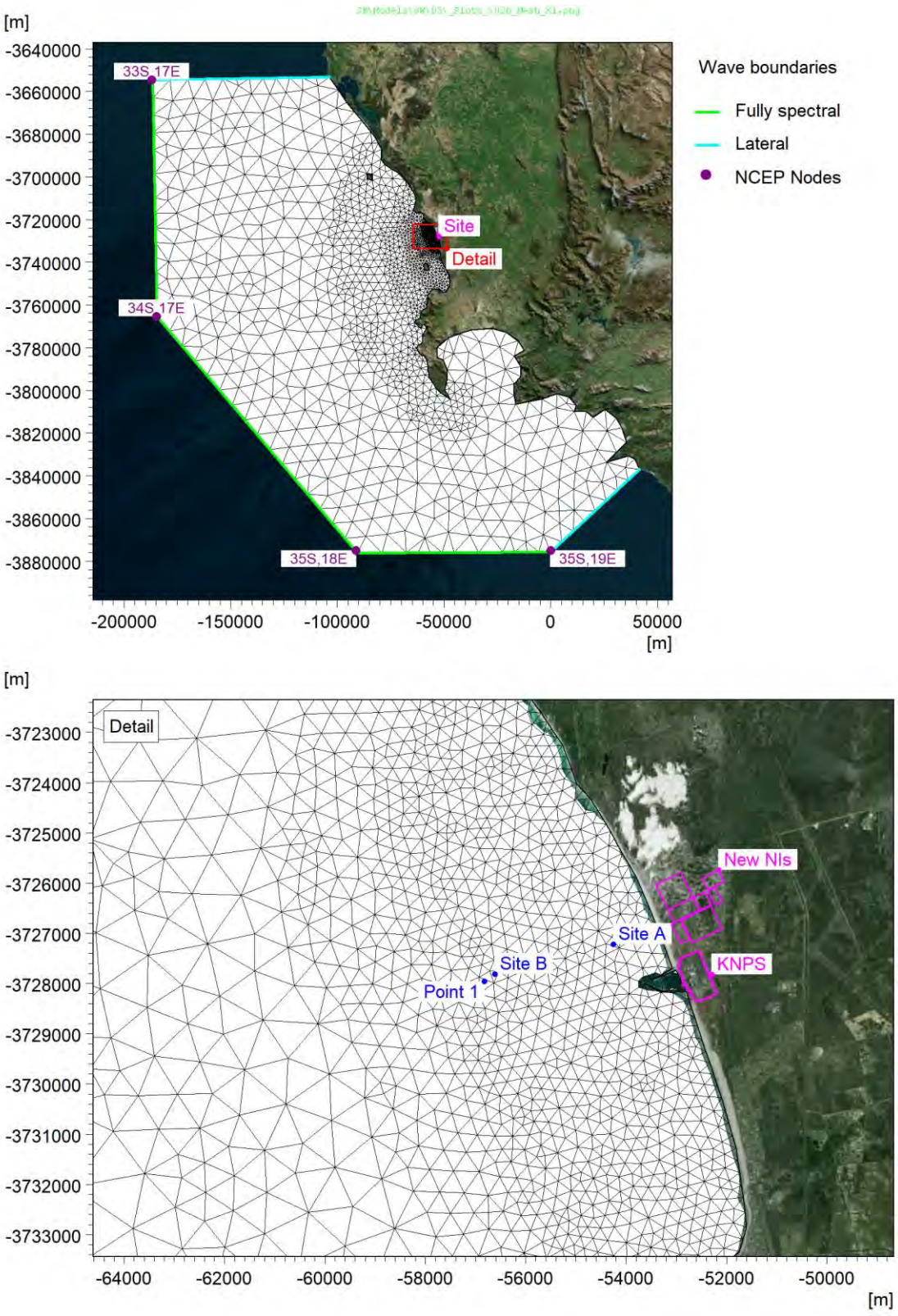


Figure 5.9.32: Mesh Used for the Reanalysis Wave Modelling.

CONTROLLED DISCLOSURE

When downloaded from the EDS database, this document is uncontrolled and the responsibility rests with the user to ensure it is in line with the authorised version on the database.

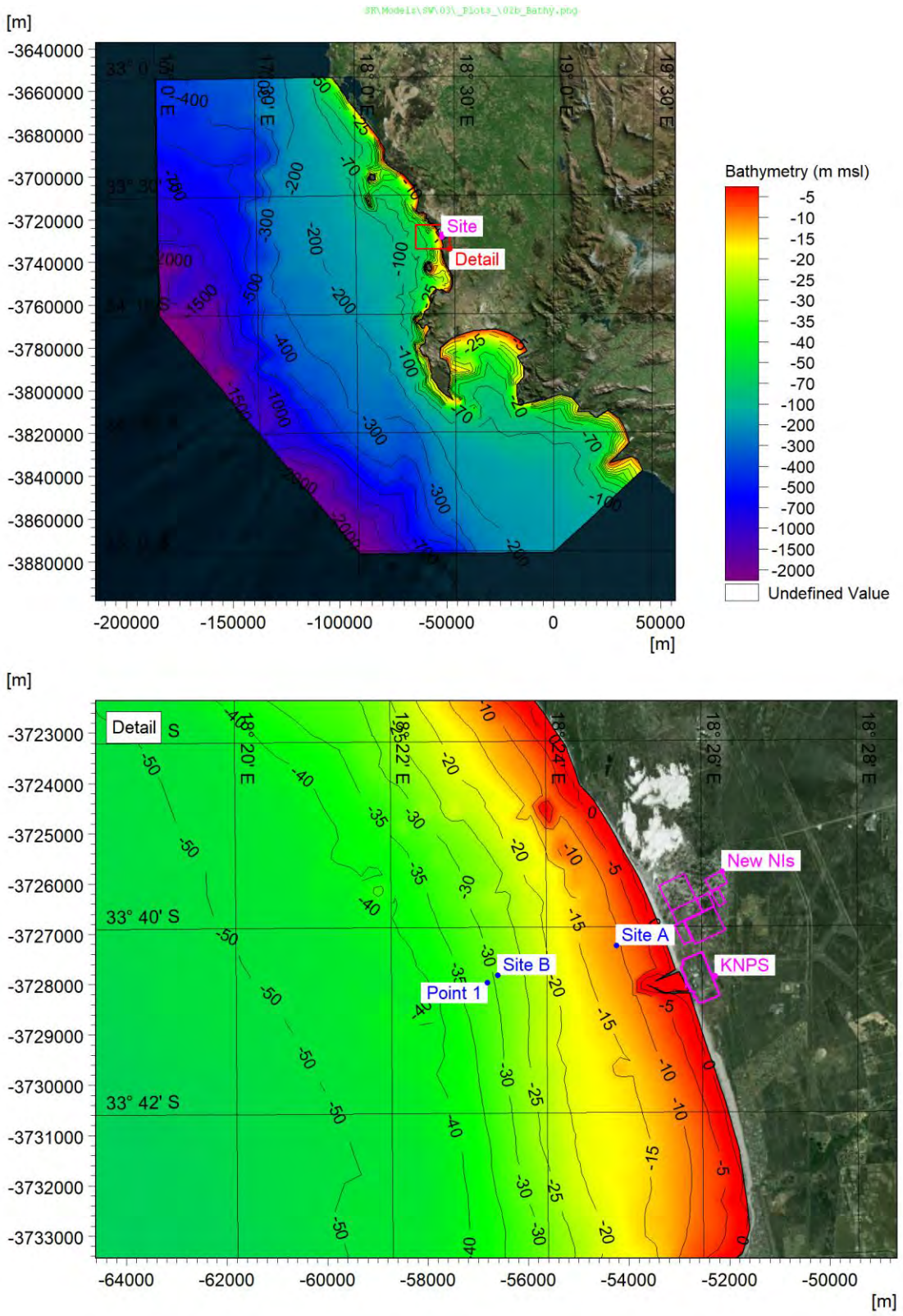


Figure 5.9.33: Bathymetry Used for the Reanalysis Wave Modelling.

CONTROLLED DISCLOSURE

When downloaded from the EDS database, this document is uncontrolled and the responsibility rests with the user to ensure it is in line with the authorised version on the database.

The hindcast spectral wave data was applied along the offshore boundaries with lateral wave boundaries connecting the land and spectral boundaries at the northern and south-eastern extents (see ***Figure 5.9.32***).

The NCEP wind data was applied as a space and time varying wind field over the model domain. The uncoupled formulation of air-sea interaction was used for the wind-wave generation.

Bottom friction was modelled using a spatially varying Nikuradse roughness ranging between k_N = 0.02 m and 0.10 m. The predicted tidal levels at Duynefontyn (***Subsection 5.9.9.1***) was applied as a time-varying water level over the model domain. The model was run in the fully spectral, instationary formulation.

Figure 5.9.34 shows an example instantaneous wave refraction plot.

CONTROLLED DISCLOSURE

When downloaded from the EDS database, this document is uncontrolled and the responsibility rests with the user to ensure it is in line with the authorised version on the database.

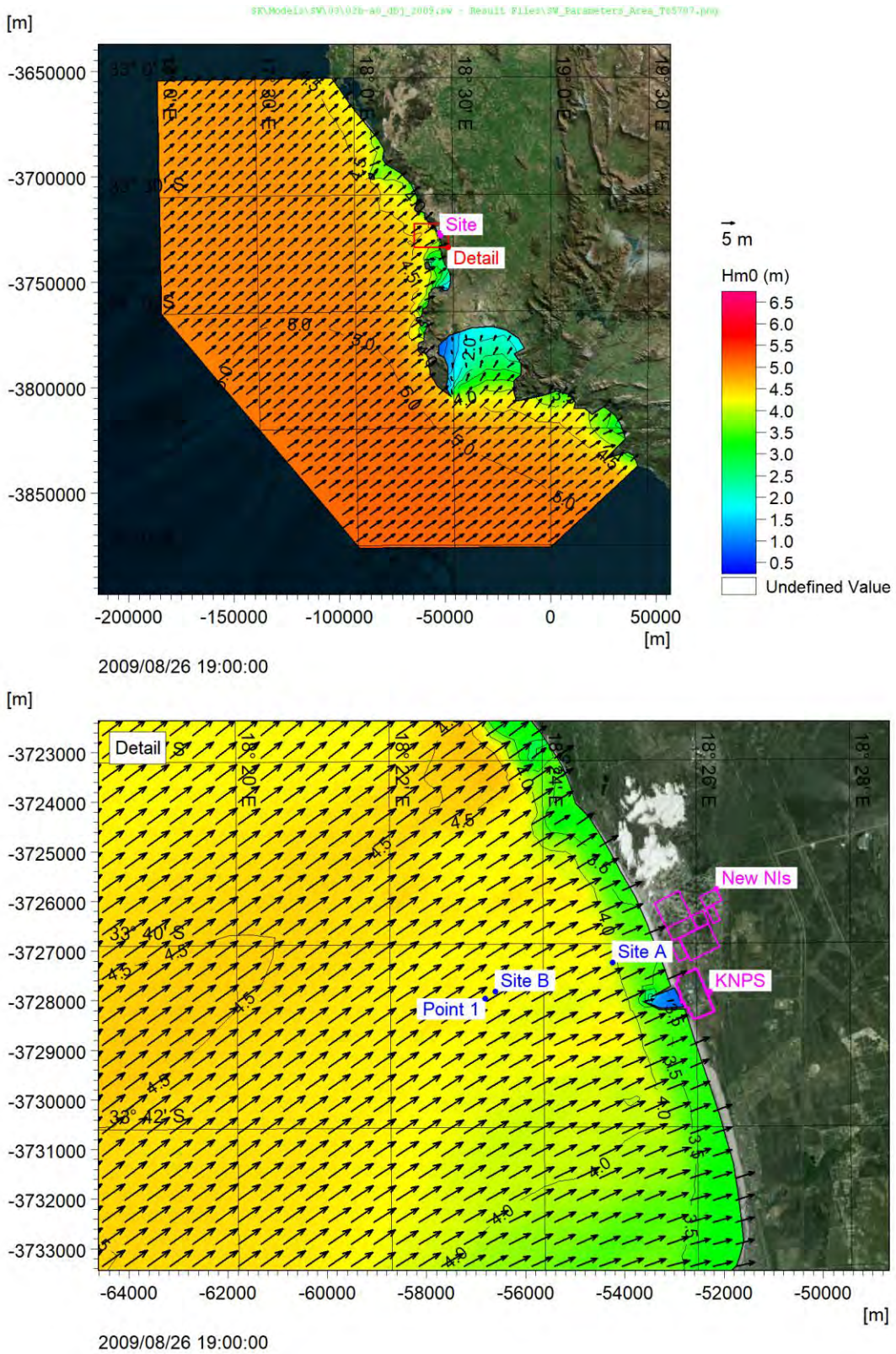


Figure 5.9.34: Example Instantaneous Wave Refraction.

CONTROLLED DISCLOSURE

When downloaded from the EDS database, this document is uncontrolled and the responsibility rests with the user to ensure it is in line with the authorised version on the database.

The nearshore operational waves were validated against measurements available at Site A and Site B (the measurement programme is detailed in ***Subsection 5.9.6.1***). The measured and modelled data had 360 days of valid data overlap (12 March 2008 to 31 December 2009) at Site A and 270 days of valid data overlap (11 July 2008 to 31 December 2009) at Site B.

Figure 5.9.35 and ***Figure 5.9.36*** show time-series comparisons of modelled and measured spectral wave parameters at Site A and Site B respectively. Wave roses are presented in ***Figure 5.9.37*** and scatterplot comparisons in ***Figure 5.9.38*** (Site A) and ***Figure 5.9.39*** (Site B) where the data overlap.

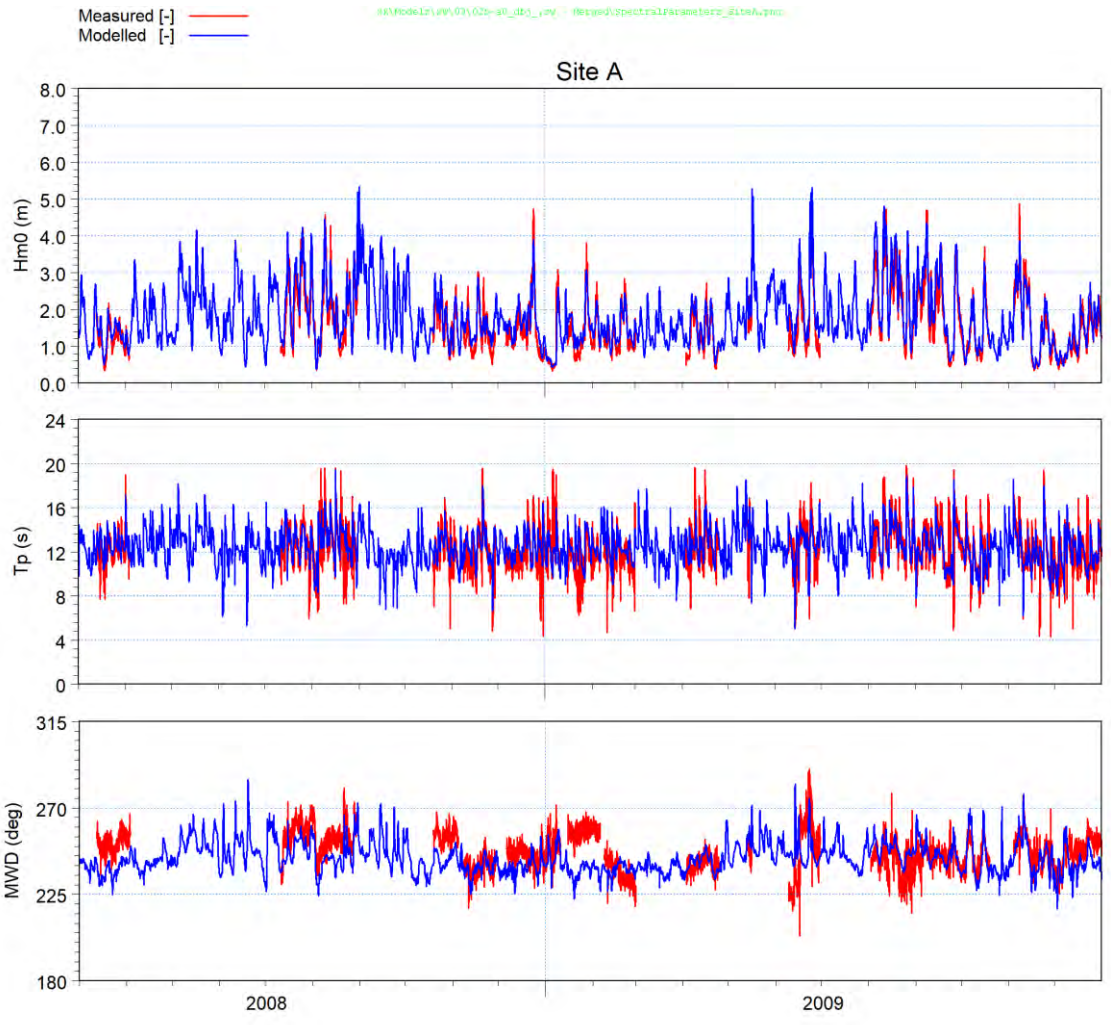


Figure 5.9.35: Time-Series Comparison of Modelled and Measured Spectral Wave Parameters at Site A.

CONTROLLED DISCLOSURE

When downloaded from the EDS database, this document is uncontrolled and the responsibility rests with the user to ensure it is in line with the authorised version on the database.

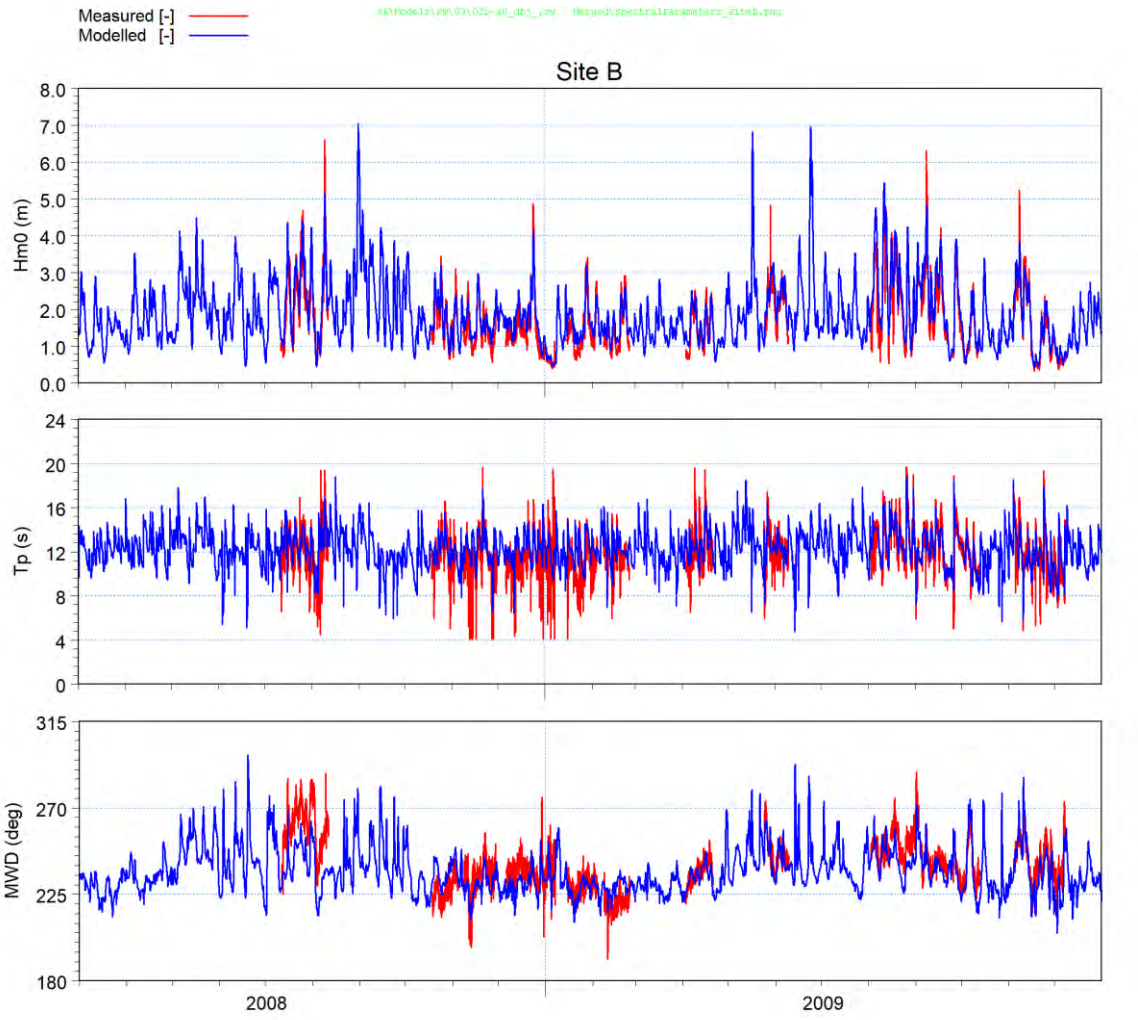


Figure 5.9.36: Time-Series Comparison of Modelled and Measured Spectral Wave Parameters at Site B.

CONTROLLED DISCLOSURE

When downloaded from the EDS database, this document is uncontrolled and the responsibility rests with the user to ensure it is in line with the authorised version on the database.

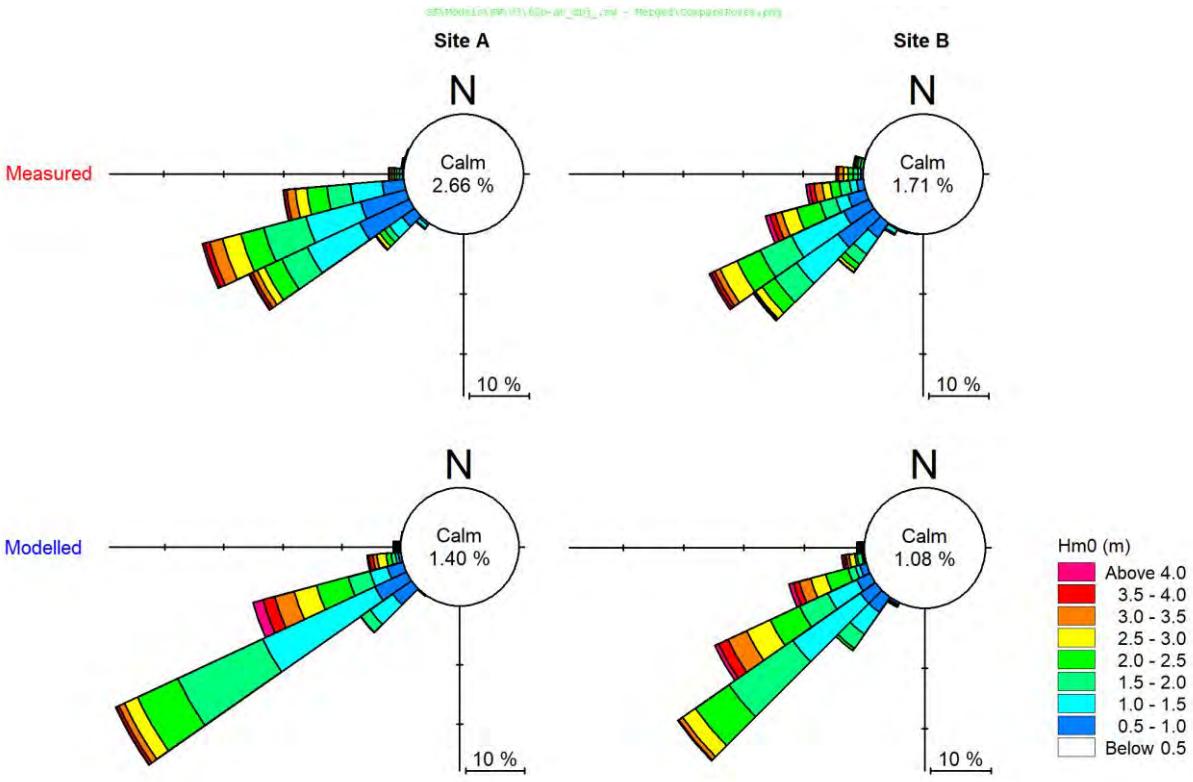


Figure 5.9.37: Wave Rose Comparison of Modelled and Measured Waves at Site A (12 March 2008 to 31 December 2009) and Site B (11 July 2008 to 31 December 2009).

CONTROLLED DISCLOSURE

When downloaded from the EDS database, this document is uncontrolled and the responsibility rests with the user to ensure it is in line with the authorised version on the database.

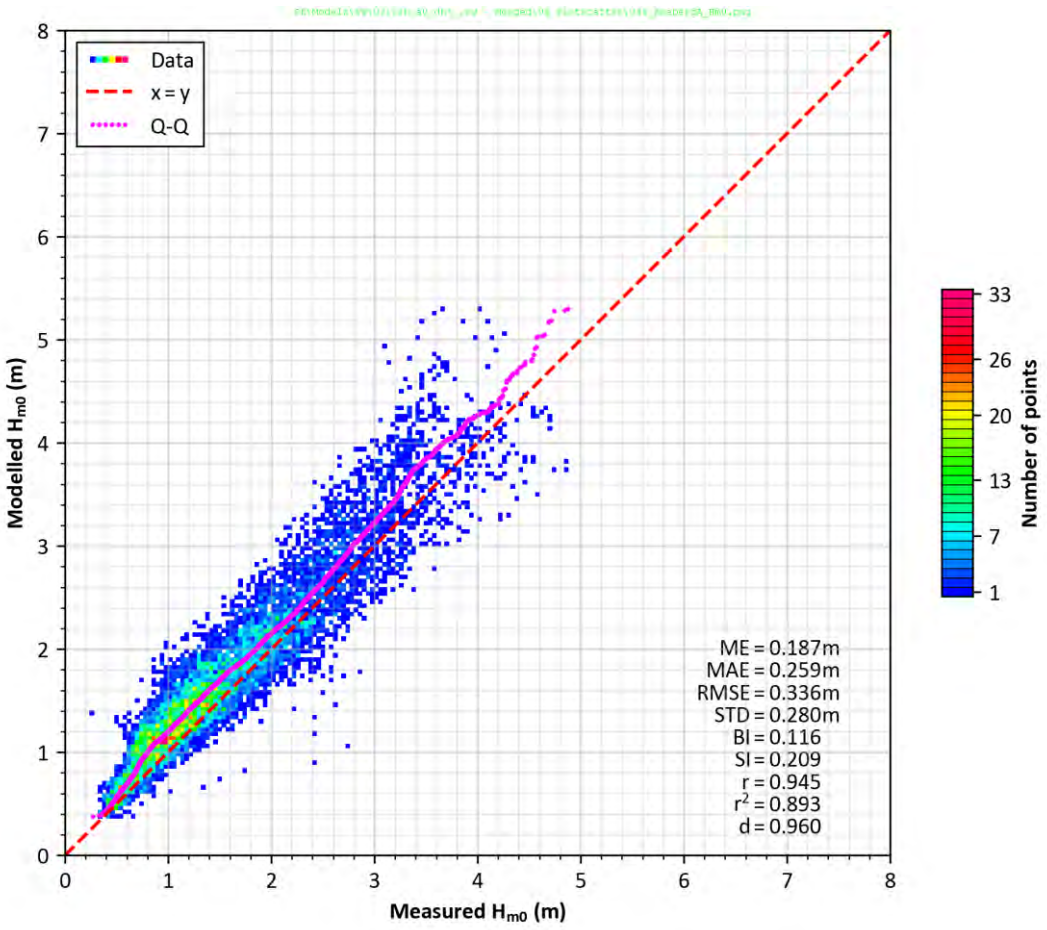


Figure 5.9.38: Scatterplot Comparison of Measured and Modelled Wave Height at Site A for 360 Days of Valid Data Overlap (12 March 2008 to 31 December 2009).

CONTROLLED DISCLOSURE

When downloaded from the EDS database, this document is uncontrolled and the responsibility rests with the user to ensure it is in line with the authorised version on the database.

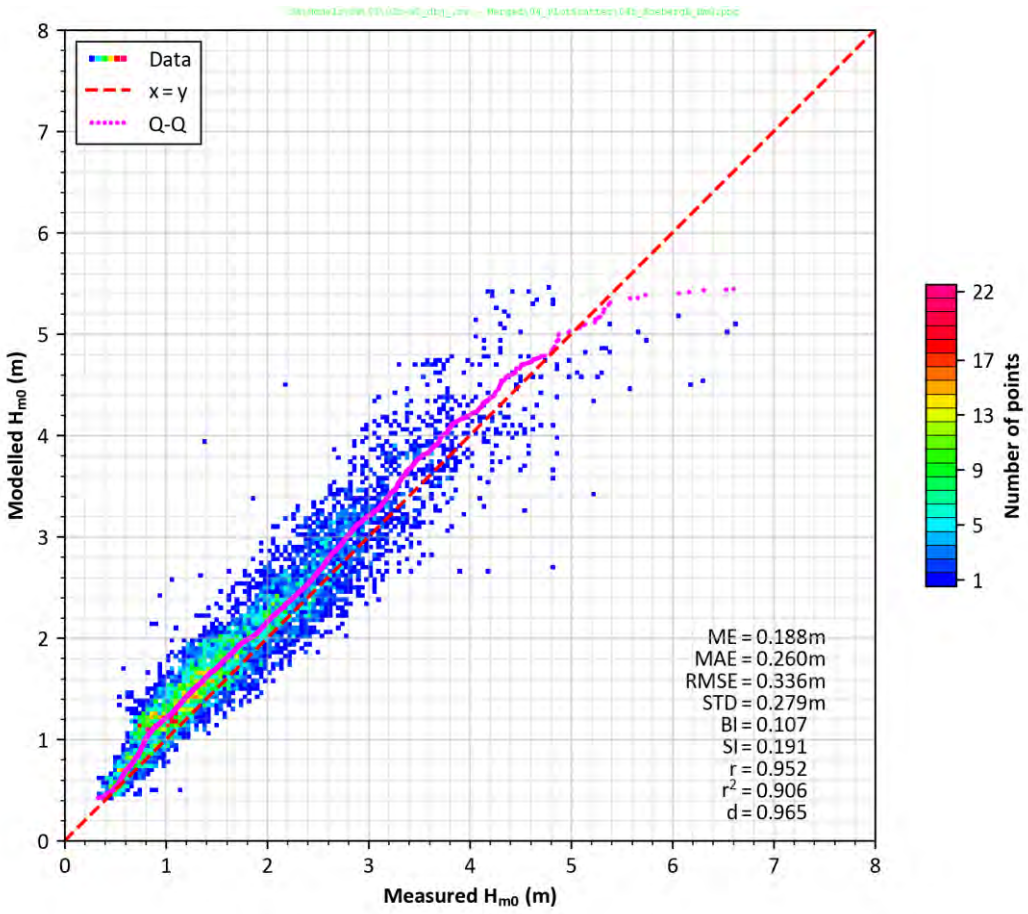


Figure 5.9.39: Scatterplot Comparison of Measured and Modelled Wave Height at Site B for 270 Days of Valid Data Overlap (11 July 2008 to 31 December 2009).

The results above show that the wave model accurately reproduces the spectral wave parameters at both sites with a slight bias of overprediction of the nearshore wave heights. The comparison shows that the wave model is calibrated for determining nearshore wave conditions at the Duynefontyn site.

Nearshore operational wave climate

Ten years of hourly operational waves were required as input to the longshore sediment transport modelling described in ***Subsection 5.9.10.3***. Ten years of offshore hindcast data were thus transformed to Point 1 (X = -56820, Y = -3727958, depth = -31 m msl, refer ***Figure 5.9.34***) offshore of the Duynefontyn site using the calibrated spectral wave model using the Reanalysis hindcast dataset described above.

Figure 5.9.40 and ***Figure 5.9.41*** present the time-series and a 3D scatterplot of 10 years of modelled spectral wave parameters at Point 1.

CONTROLLED DISCLOSURE

When downloaded from the EDS database, this document is uncontrolled and the responsibility rests with the user to ensure it is in line with the authorised version on the database.

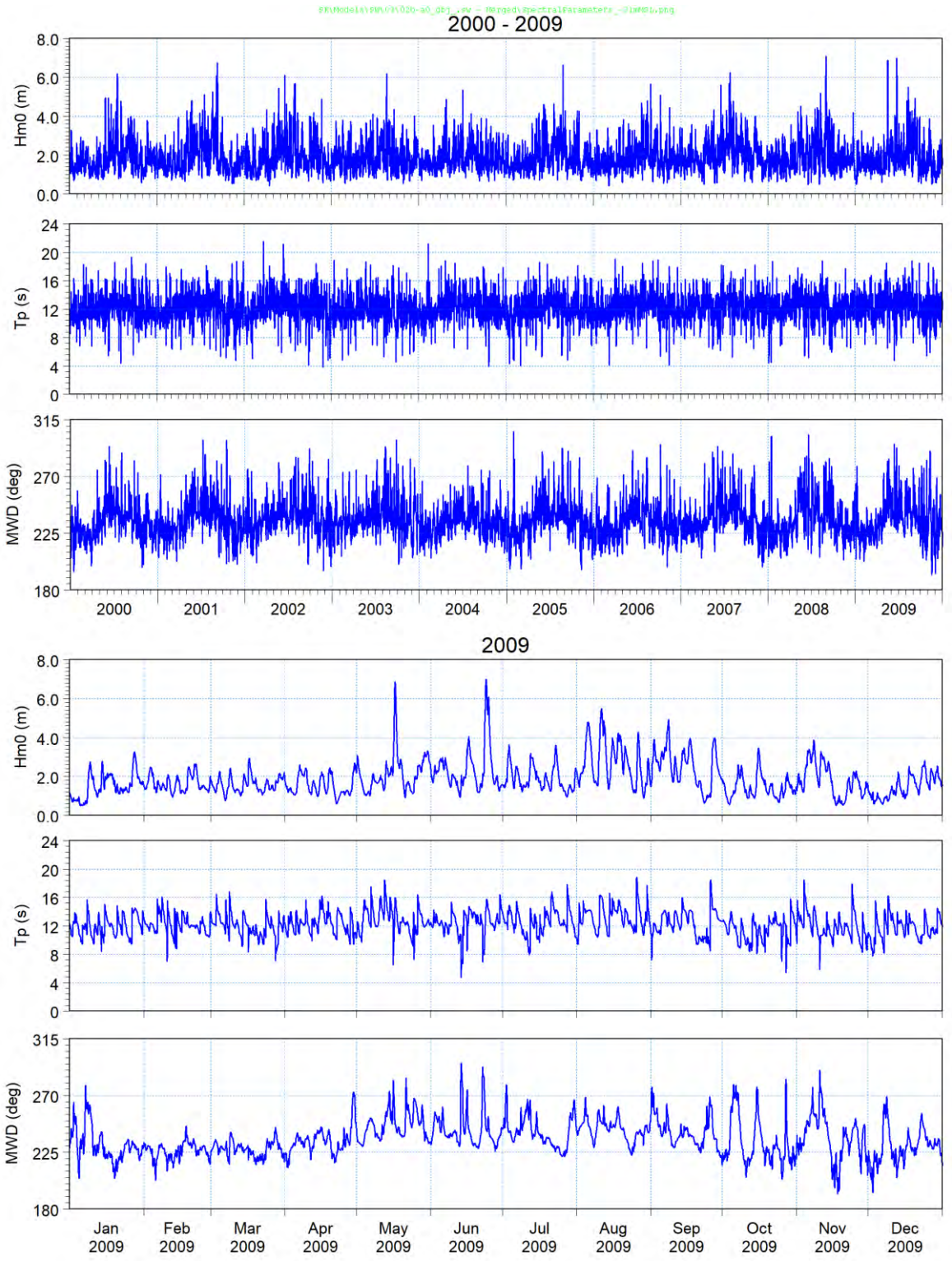


Figure 5.9.40: Time-series of 10 Years (2000-2009) of Modelled Operational Wave Parameters at Point 1 (-31 m msl).

CONTROLLED DISCLOSURE

When downloaded from the EDS database, this document is uncontrolled and the responsibility rests with the user to ensure it is in line with the authorised version on the database.

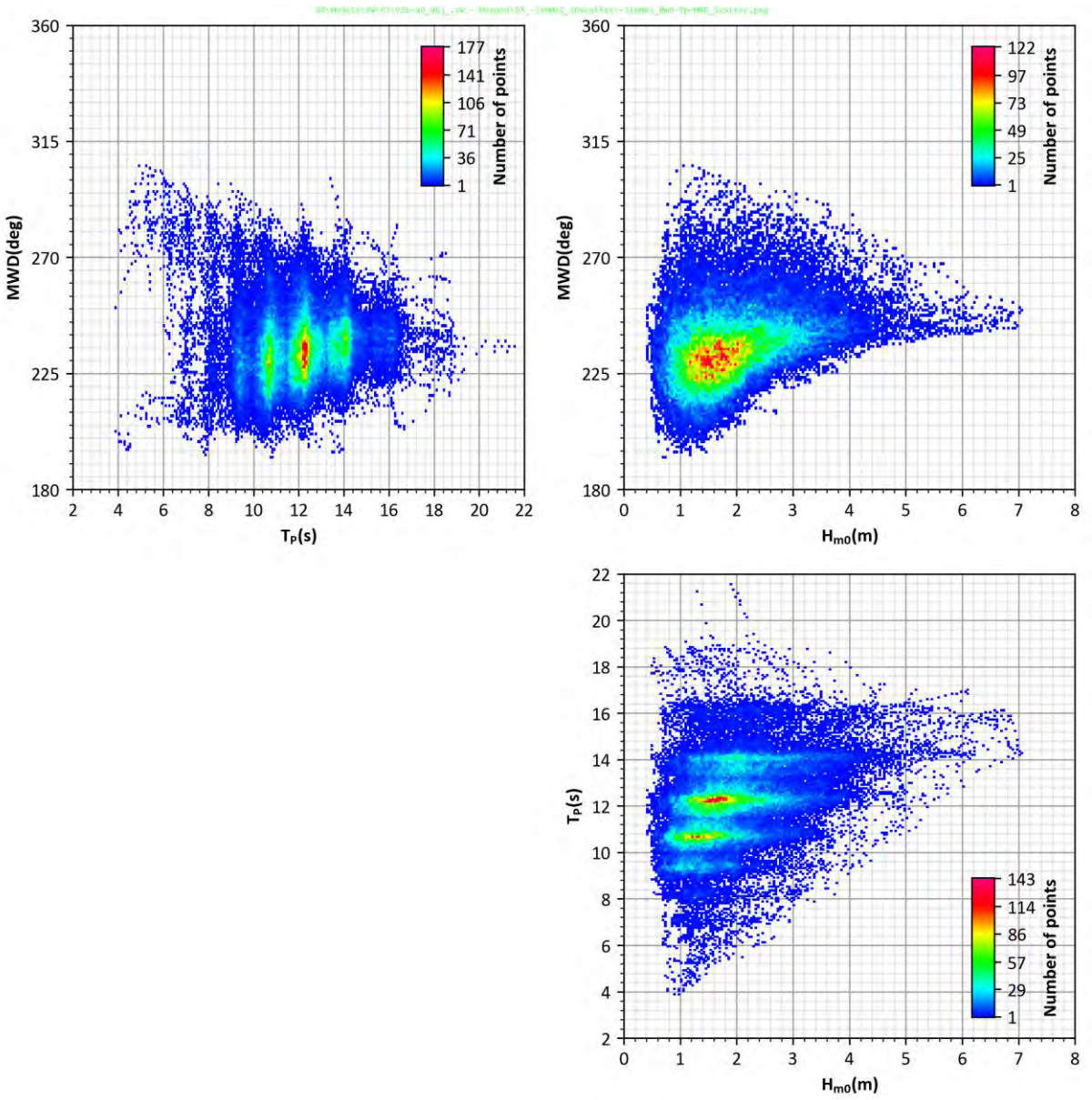


Figure 5.9.41: 3D Scatterplot of 10 Years (2000-2009) of Modelled Operational Wave Parameters at Point 1 (-31 m msl).

Two additional 10-year sets were modelled for the 2064 (end of decommissioning period for KNPS) and 2130 (end of decommissioning period for the new NIs) dates. To account for the effect of climate change the model boundary conditions were adjusted to include the rotation of wave direction and increase in water elevation as per ***Table 5.9.8***. The wave height and period were not adjusted.

CONTROLLED DISCLOSURE

When downloaded from the EDS database, this document is uncontrolled and the responsibility rests with the user to ensure it is in line with the authorised version on the database.

Nearshore extreme wave climate

The nearshore extreme waves were validated against measurements at Site B. The measured and modelled data had 54 storm events with valid data overlap between September 2009 and August 2020. ***Figure 5.9.42*** presents a scatterplot comparison of measured and modelled wave height peaks at Site B. This result indicates a good calibration for extreme events.

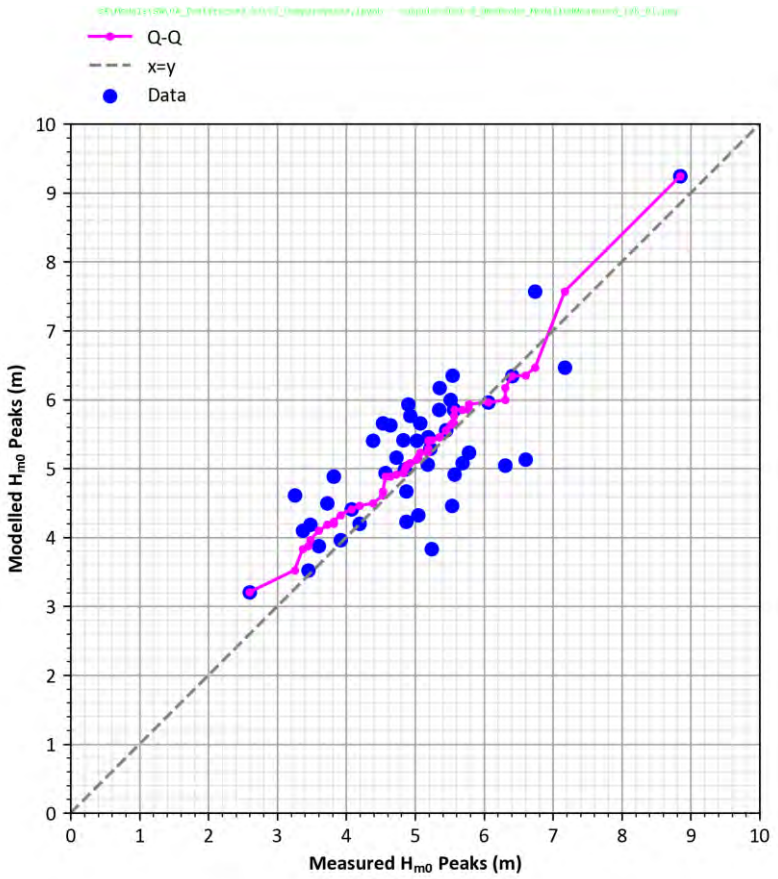


Figure 5.9.42: Scatterplot Comparison of Measured and Modelled Wave Height Peaks at Site B for 54 events of Valid Data Overlap between September 2009 and August 2020.

On average the model is able to reproduce the storms peaks from the measurements. The model results for the largest storm on record (13 July 2020) is only 4.4% (+0.40 m) higher than the measurements.

To determine the nearshore extreme wave climate, all storm events in the 42.1-year offshore hindcast dataset were refracted to Point 1 located directly in front of the site using the calibrated spectral wave model described above.

CONTROLLED DISCLOSURE

When downloaded from the EDS database, this document is uncontrolled and the responsibility rests with the user to ensure it is in line with the authorised version on the database.

Since the current study is focused on the extreme wave climate, modelling the full 42.1 y of available data was not necessary. Rather, a series of storms with large wave heights or strong north-westerly winds were selected from a time-series of hindcast wave data at the offshore node closest to the project site. The storm peaks were identified using the 'peaks over threshold' or 'partial duration series' method, with the threshold defined as the value that was exceeded five times per year on average, resulting in a total selection of 211 storm events. To ensure independence, two successive events were selected only if the time between the events exceeded 48 hours. Each of the 211 storm events were then modelled for a duration of 24 hours before and 24 hours after the offshore storm peak.

Scatterplots over the duration of each storm event of H_{m0} compared to T_p, MWD and DSD are presented in the following figures:

- ***Figure 5.9.43***: scatterplot comparison of H_{m0} and T_p at Point 1, as well as the H_{m0}-T_p relationship (where the $H_{m0}^{0.5}$ factor is based on limiting the wave steepness and the 5.4 factor is a site-specific fit to the data) used to determine the extreme wave periods associated with the extreme wave heights.
- ***Figure 5.9.44***: scatterplot comparison of H_{m0} and MWD used to determine the extreme wave directions associated with the extreme wave heights. The 5^{th}, 50^{th}, and 95^{th} percentiles of MWD were determined from the H_{m0}-MWD distribution for waves exceeding the 1 y^{-1} exceedance probability H_{m0}. ($H_{m0} \geq 6.1$ m, ***Table 5.9.25***).
- ***Figure 5.9.45***: scatterplot comparison of H_{m0} and DSD used to determine the extreme wave directional distributions associated with the extreme wave heights. The 50^{th} percentile of DSD was determined from the H_{m0}-DSD distribution for waves exceeding the 1 y^{-1} exceedance probability H_{m0}.

CONTROLLED DISCLOSURE

When downloaded from the EDS database, this document is uncontrolled and the responsibility rests with the user to ensure it is in line with the authorised version on the database.

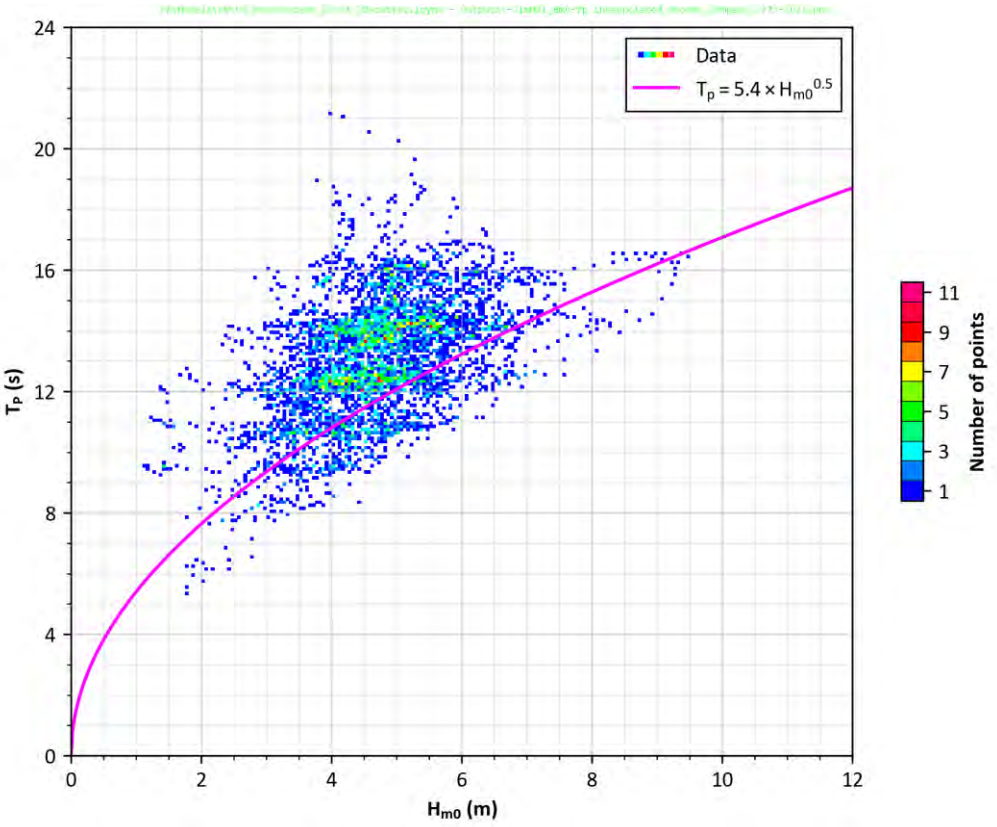


Figure 5.9.43: Scatterplot Showing Relationship between Wave Height and Period at Point 1 from Modelled Storms Between 1979 and 2020.

CONTROLLED DISCLOSURE

When downloaded from the EDS database, this document is uncontrolled and the responsibility rests with the user to ensure it is in line with the authorised version on the database.

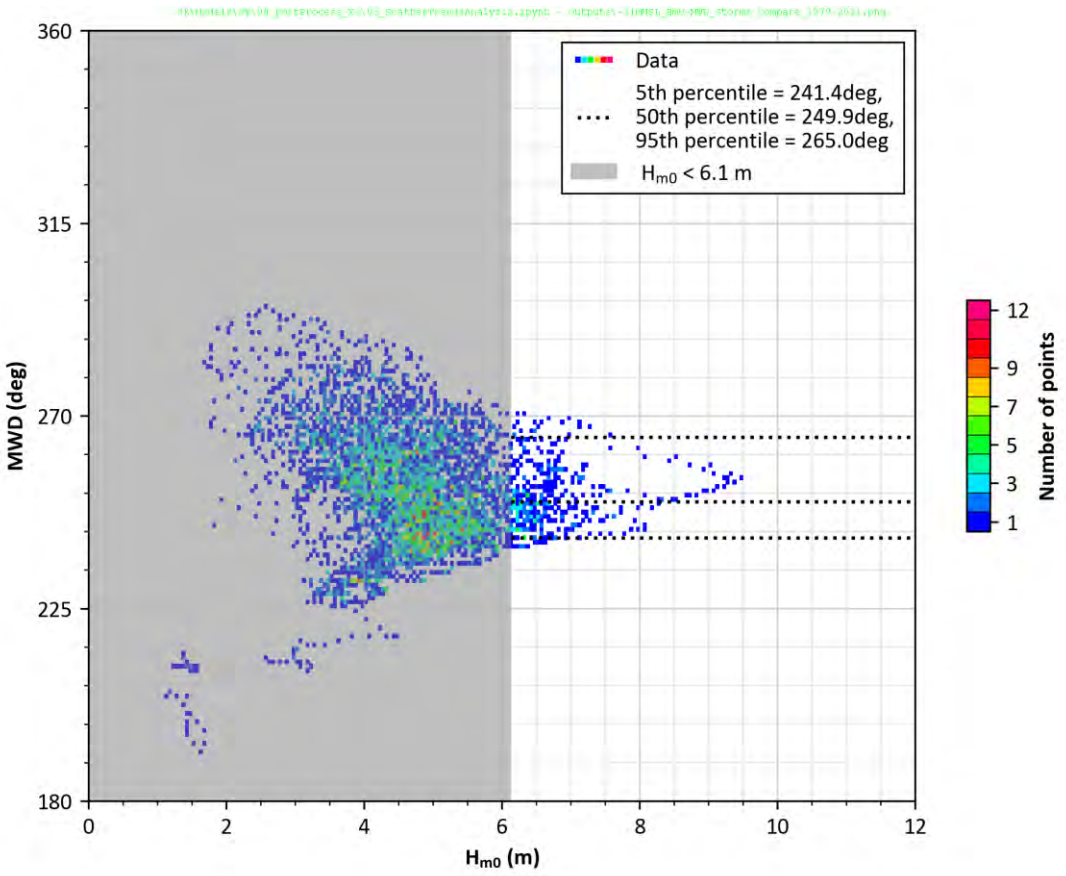


Figure 5.9.44: Scatterplot Showing Relationship between Wave Height and Direction at Point 1 from Modelled Storms between 1979 and 2020. The 5th, 50th, and 95th Percentiles of MWD were Determined from the H_{m0}-MWD Distribution for Waves Exceeding the 1 y^{-1} Exceedance Probability H_{m0}.

CONTROLLED DISCLOSURE

When downloaded from the EDS database, this document is uncontrolled and the responsibility rests with the user to ensure it is in line with the authorised version on the database.

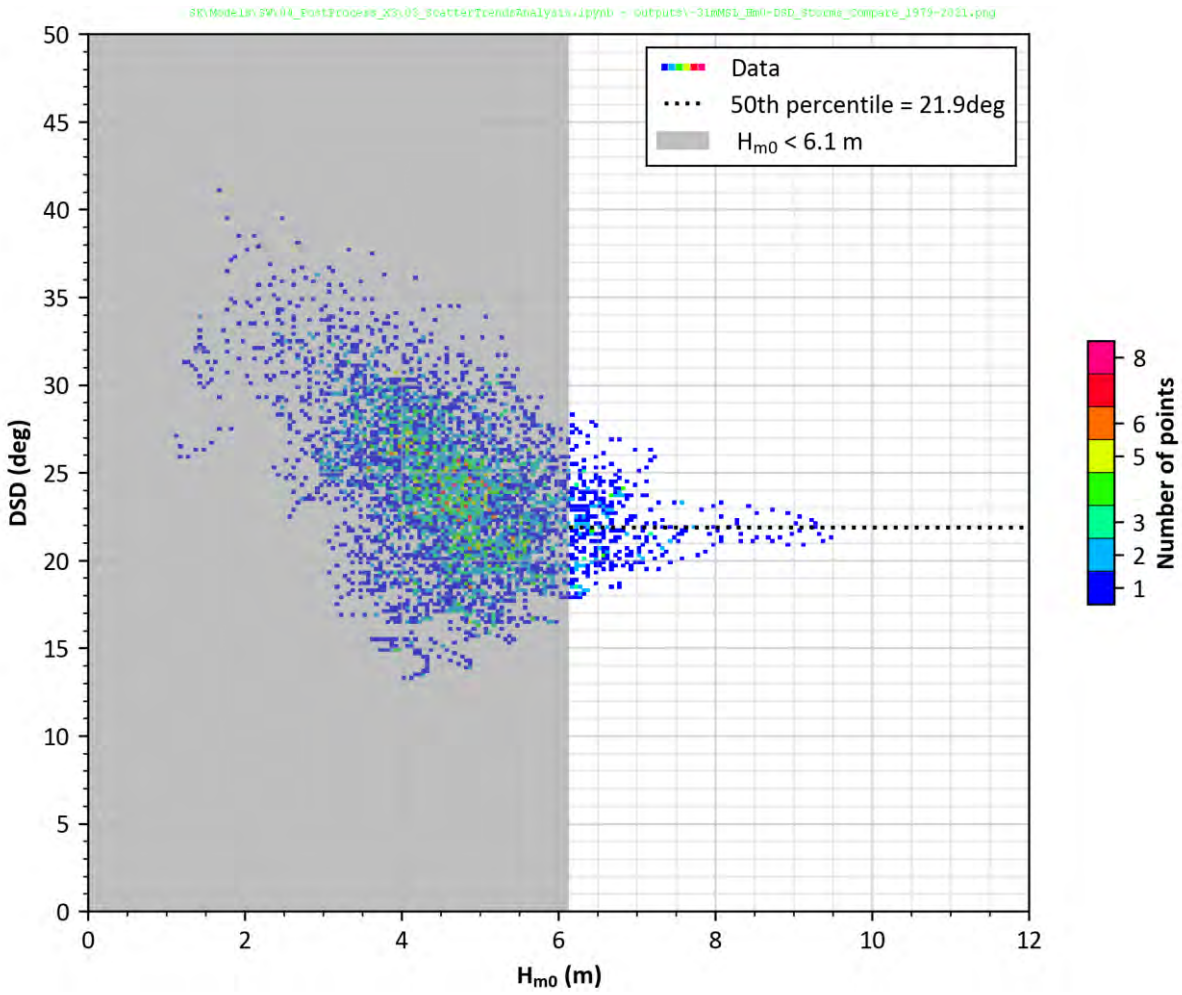


Figure 5.9.45: Scatterplot Showing Relationship between Wave Height and Directional Spreading at Point 1 from Modelled Storms between 1979 and 2020. The 50th Percentile of DSD was Determined from the H_{m0}-DSD Distribution for Waves Exceeding the 1 y^{-1} Exceedance Probability H_{m0}.

An extreme value analysis (refer to ***Subsection 5.9.6.2*** for the methodology) was then performed on the modelled nearshore wave heights during the 211 storm events, with the threshold defined as the value that was exceeded four times per year on average. The EVA results are presented in ***Figure 5.9.46***. The baseline date is 2000 which is the middle of the modelled period.

CONTROLLED DISCLOSURE

When downloaded from the EDS database, this document is uncontrolled and the responsibility rests with the user to ensure it is in line with the authorised version on the database.

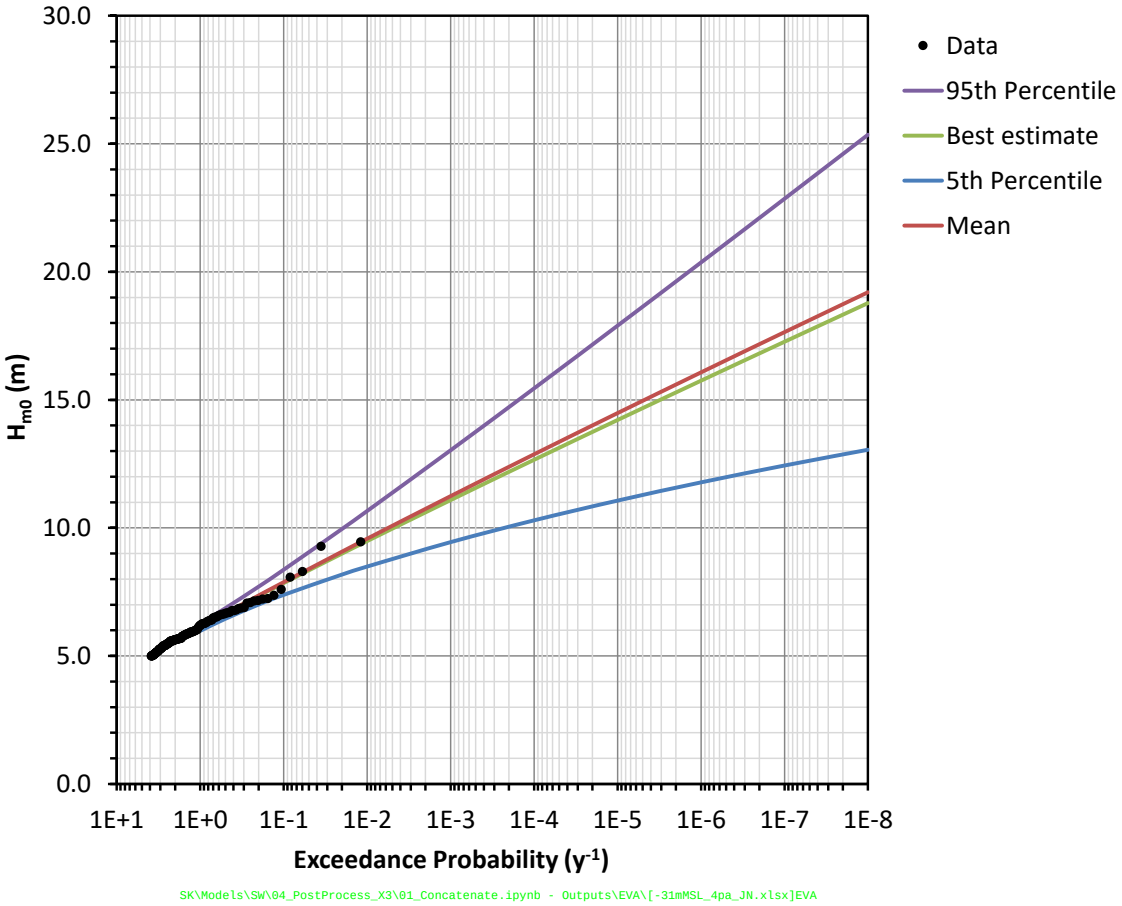


Figure 5.9.46: Extreme Value Analysis of Wave Height at Point 1 in a Depth of -31 m msl (Baseline Date is 2000).

The extreme wave heights were then adjusted for climate change (***Subsection 5.9.7***) and are presented in ***Table 5.9.25***. The associated T_p, MWD and DSD are also shown.

CONTROLLED DISCLOSURE

When downloaded from the EDS database, this document is uncontrolled and the responsibility rests with the user to ensure it is in line with the authorised version on the database.

Table 5.9.25: Extreme Wave Parameters at Point 1 in a Depth of -31 m msl.

Exceedance Probability	Uncertainty	Hm0					Tp					MWD[a]			DSD[b]
												5%	50%	95%	
(y^{-1})		(m)					(m)					(°)			(°)
		2021	2044	2064	2110	2130	2021	2044	2064	2110	2130	All	All	All	All
1	5th Percentile	6.0	6.1	6.1	6.2	6.3	13.3	13.3	13.4	13.5	13.5	241	250	265	21.9
	Mean	6.2	6.2	6.3	6.4	6.4	13.4	13.5	13.5	13.6	13.7	241	250	265	21.9
	Best Estimate[c]	6.2	6.2	6.3	6.4	6.4	13.4	13.5	13.5	13.7	13.7	241	250	265	21.9
	95th Percentile	6.3	6.4	6.4	6.5	6.6	13.6	13.6	13.7	13.8	13.9	241	250	265	21.9
10^{-1}	5th Percentile	7.4	7.5	7.6	7.7	7.8	14.7	14.8	14.9	15.0	15.0	241	250	265	21.9
	Mean	7.9	8.0	8.1	8.2	8.3	15.2	15.3	15.3	15.5	15.5	241	250	265	21.9
	Best Estimate[c]	7.9	8.0	8.0	8.2	8.2	15.2	15.3	15.3	15.4	15.5	241	250	265	21.9
	95th Percentile	8.4	8.5	8.6	8.7	8.8	15.7	15.8	15.8	16.0	16.0	241	250	265	21.9
10^{-2}	5th Percentile	8.6	8.6	8.7	8.9	8.9	15.8	15.9	15.9	16.1	16.1	241	250	265	21.9
	Mean	9.7	9.7	9.8	10.0	10.1	16.8	16.9	16.9	17.1	17.1	241	250	265	21.9
	Best Estimate[c]	9.6	9.6	9.7	9.9	10.0	16.7	16.8	16.8	17.0	17.0	241	250	265	21.9
	95th Percentile	10.8	10.8	10.9	11.1	11.2	17.7	17.8	17.9	18.0	18.1	241	250	265	21.9
10^{-3}	5th Percentile	9.5	9.6	9.7	9.8	9.9	16.7	16.7	16.8	16.9	17.0	241	250	265	21.9
	Mean	11.3	11.4	11.5	11.7	11.8	18.2	18.3	18.3	18.5	18.6	241	250	265	21.9
	Best Estimate[c]	11.2	11.3	11.4	11.6	11.6	18.1	18.1	18.2	18.4	18.4	241	250	265	21.9
	95th Percentile	13.1	13.3	13.4	13.6	13.7	19.6	19.7	19.7	19.9	20.0	241	250	265	21.9
10^{-4}	5th Percentile	10.4	10.5	10.6	10.7	10.8	17.4	17.5	17.5	17.7	17.8	241	250	265	21.9
	Mean	13.0	13.1	13.2	13.4	13.5	19.5	19.5	19.6	19.8	19.9	241	250	265	21.9
	Best Estimate[c]	12.8	12.9	13.0	13.2	13.3	19.3	19.4	19.4	19.6	19.7	241	250	265	21.9
	95th Percentile	15.6	15.7	15.8	16.1	16.2	21.3	21.4	21.5	21.7	21.8	241	250	265	21.9
10^{-5}	5th Percentile	11.2	11.3	11.3	11.5	11.6	18.0	18.1	18.2	18.3	18.4	241	250	265	21.9
	Mean	14.6	14.7	14.8	15.1	15.2	20.6	20.7	20.8	21.0	21.1	241	250	265	21.9
	Best Estimate[c]	14.3	14.5	14.6	14.8	14.9	20.4	20.5	20.6	20.8	20.9	241	250	265	21.9
	95th Percentile	18.0	18.2	18.3	18.7	18.8	22.9	23.0	23.1	23.3	23.4	241	250	265	21.9
10^{-6}	5th Percentile	11.9	12.0	12.1	12.3	12.4	18.6	18.7	18.8	18.9	19.0	241	250	265	21.9
	Mean	16.2	16.3	16.5	16.8	16.9	21.7	21.8	21.9	22.1	22.2	241	250	265	21.9
	Best Estimate[c]	15.9	16.0	16.1	16.4	16.5	21.5	21.6	21.7	21.9	22.0	241	250	265	21.9
	95th Percentile	20.5	20.7	20.9	21.2	21.4	24.5	24.6	24.7	24.9	25.0	241	250	265	21.9
10^{-7}	5th Percentile	12.5	12.7	12.7	13.0	13.1	19.1	19.2	19.3	19.4	19.5	241	250	265	21.9
	Mean	17.8	17.9	18.1	18.4	18.5	22.8	22.9	23.0	23.2	23.2	241	250	265	21.9
	Best Estimate[c]	17.4	17.6	17.7	18.0	18.1	22.5	22.6	22.7	22.9	23.0	241	250	265	21.9
	95th Percentile	23.0	23.2	23.4	23.8	24.0	25.9	26.0	26.1	26.4	26.5	241	250	265	21.9
10^{-8}	5th Percentile	13.2	13.3	13.4	13.6	13.7	19.6	19.7	19.8	19.9	20.0	241	250	265	21.9
	Mean	19.4	19.5	19.7	20.0	20.2	23.8	23.9	24.0	24.2	24.3	241	250	265	21.9
	Best Estimate[c]	18.9	19.1	19.2	19.6	19.7	23.5	23.6	23.7	23.9	24.0	241	250	265	21.9
	95th Percentile	25.6	25.8	26.0	26.4	26.6	27.3	27.4	27.5	27.8	27.9	241	250	265	21.9

Notes:

(a) The 5%, 50% and 95% refer to the 5th, 50th, and 95th percentiles from the MWD distribution for waves exceeding the 1 y^{-1} exceedance probability H_{m0}.

(b) DSD is the 50th percentile from the DSD distribution for waves exceeding the 1 y^{-1} exceedance probability H_{m0}.

(c) Should the most probable estimate be required, then the best estimate should be used rather than the mean estimate.

CONTROLLED DISCLOSURE

When downloaded from the EDS database, this document is uncontrolled and the responsibility rests with the user to ensure it is in line with the authorised version on the database.

The extreme wave climate above was used as input to the cross-shore erosion modelling (***Subsection 5.9.10.5***), the storm wave run-up and drawdown modelling (***Subsection 5.9.11***) and the sediment transport modelling (***Subsection 5.9.16***). The modelling took into account that the most extreme waves in this table would break in a depth of -31 m msl.

5.9.9.9 Joint Probability

Introduction

The numerical modelling described in ***Subsections 5.9.10*** to ***5.9.16*** requires the joint probability of the hydrographic parameters used as inputs to the models, such as waves and storm surge.

In all cases the US NRC's recommendation (NRC, 2009) is used for the initial tidal water level, i.e., for the high water cases the 90th percentile high tide and for low water cases is the 10th percentile low tide. These levels are analysed and presented in ***Subsection 5.9.9.1***.

The tidal level is then combined with SLR and the storm surge to obtain the still water level, as analysed and presented in ***Table 5.9.12*** and ***Table 5.9.13***.

The joint probabilities between the following parameters are then required:

- Waves and positive storm surge:

  The cross-shore erosion modelling (***Subsection 5.9.10.5***), the storm wave run-up modelling (***Subsection 5.9.11***), and the storm sedimentation and scour modelling (***Subsection 5.9.16.1***) requires the joint probability of waves and positive storm surge.

- Waves and negative storm surge:

  Modelling the extreme wave drawdown (***Subsection 5.9.11***) and extreme scour (***Subsection 5.9.16.1***) requires the joint probability of waves and negative storm surge.

- Waves and currents:

  Modelling the suspended sand at the cooling water intakes (***Subsection 5.9.16.3***) requires the joint probability of waves and currents.

- Tsunamis and storm surge:

  Modelling the tsunami run-up and drawdown (***Subsection 5.9.12.11***) requires the joint probability of tsunamis and positive and negative storm surge.

CONTROLLED DISCLOSURE

When downloaded from the EDS database, this document is uncontrolled and the responsibility rests with the user to ensure it is in line with the authorised version on the database.

The joint probability depends on the site-specific level of dependence between the parameters. The methodology applied for estimating the joint probabilities is described below, followed by the estimation of the joint probabilities for each of the combinations in the bullet list above.

Methodology

A methodology for calculating the joint probability and resultant impact on coastal flooding of storm surge vs wave height, storm surge vs river discharge and wave height vs river discharge is described by (Petroliagkis, et al., 2016). This methodology has been applied in this section, based on the similarity of the application and the solid theoretical basis presented in (Petroliagkis, et al., 2016). The joint (combined) exceedance probability of two variables (e.g., storm surge and wave height) is given by:

$$P_{X,Y} = \chi \sqrt{P_X \cdot P_Y} \qquad \text{Equation 5.9.4}$$

where:

$P_{X,Y}$ = joint exceedance probability of two variables occurring together (y^{-1})

P_X = exceedance probability of first variable X (y^{-1})

P_Y = exceedance probability of second variable Y (y^{-1})

χ = dependence between the first and second variables ranging between 1 when fully dependent and 0 when independent.

The dependence parameter χ is calculated from a site-specific dataset containing simultaneous values of the first (X) and second (Y) variables. The methodology requires counting the number of events where both variables simultaneously exceed a common percentile threshold (x*, y*), which enables χ to be calculated for each percentile as shown in Equation 5.9.5.

$$\chi = 2 - \frac{ln\left[\frac{\text{Number of (X,Y) such that } X \le x^* \text{ and } Y \le y^*}{\text{Total number of (X,Y)}}\right]}{\frac{1}{2} ln\left[\frac{\text{Number of } X \le x^*}{\text{Total number of X}} * \frac{\text{Number of } Y \le y^*}{\text{Total number of Y}}\right]} \qquad \text{Equation 5.9.5}$$

The largest χ is then selected from the range of percentiles representing the more extreme events, e.g., events above the 85th percentile, since only the extreme events are of interest. The applicable formulas and the full details of the methodology are provided in (Petroliagkis, et al., 2016). The following categories of dependence are defined:

CONTROLLED DISCLOSURE

When downloaded from the EDS database, this document is uncontrolled and the responsibility rests with the user to ensure it is in line with the authorised version on the database.

Table 5.9.26: Categories of Dependence (Petroliagkis, et al., 2016).

Dependence Parameter χ	Category
X ≤ -0.06	Negative
-0.05 ≤ X ≤ 0.05	Zero
0.06 ≤ X ≤ 0.14	Low
0.15 ≤ X ≤ 0.24	Modest
0.25 ≤ X ≤ 0.34	Well
0.35 ≤ X ≤ 0.44	Strong
X ≥ 0.45	Very Strong

In the case of zero dependence (X = 0) ***Equation 5.9.6*** is applied:

$$P_{X,Y} = \frac{P_X \cdot P_Y}{n}$$ Equation 5.9.6

where:

$P_{X,Y}$ = joint exceedance probability of two variables occurring together (y^{-1})

P_X = exceedance probability of first variable (y^{-1})

P_Y = exceedance probability of second variable (y^{-1})

n = number of sampling intervals per year, e.g., for daily data n = 365.

The reason for the “n” in ***Equation 5.9.6*** is that the probabilities are given in years whilst the data is being sampled at a different frequency, e.g., daily. If the data is also sampled yearly, then n =1.

Waves and positive storm surge

The site-specific dataset used was the hourly measured storm surge at Cape Town (refer ***Subsection 5.9.9.2***) and the hourly offshore wave hindcast at nodes 35.0°S, 18.0 E (1979-2009) and 34.5°S, 18.0 E (2010-2021) (refer ***Subsection 5.9.9.8***). ***Figure 5.9.47*** shows a scatterplot of these data using 230 430 hourly data pairs, equivalent to 26.3 years.

CONTROLLED DISCLOSURE

When downloaded from the EDS database, this document is uncontrolled and the responsibility rests with the user to ensure it is in line with the authorised version on the database.

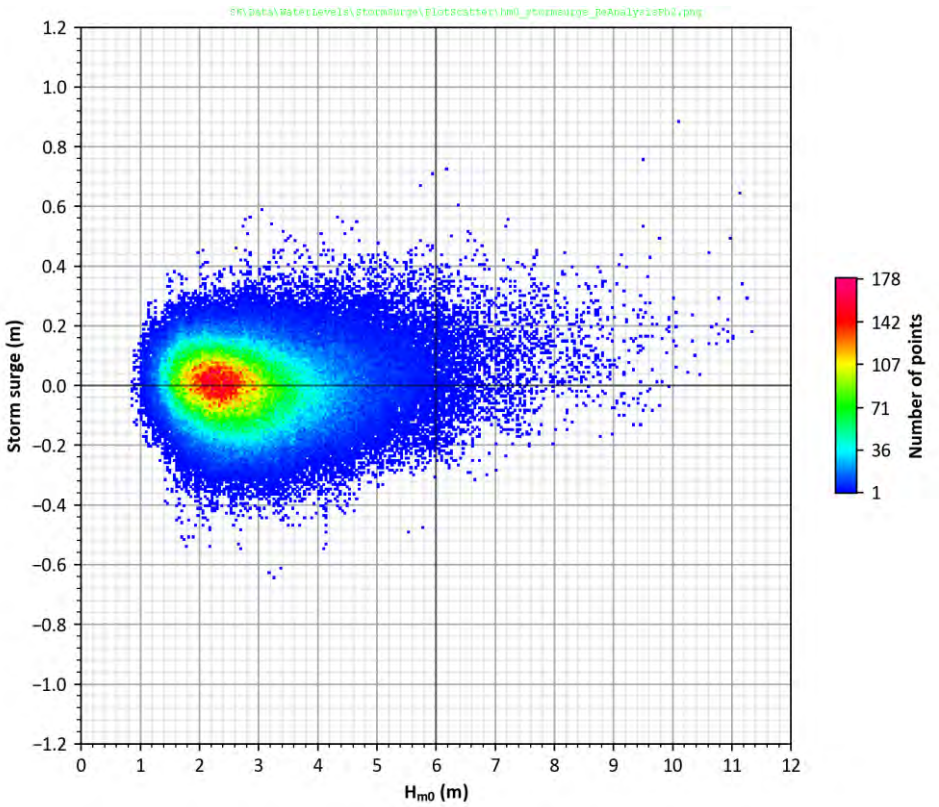


Figure 5.9.47: Scatterplot of Storm Surge Measured at Cape Town and Offshore Hindcast Wave Height.

As shown in ***Figure 5.9.47***, storm surge and wave height are only moderately correlated at Cape Town, since the frontal weather systems generating the waves hundreds to thousands of kilometres offshore do not arrive at the same time as the waves.

CONTROLLED DISCLOSURE

When downloaded from the EDS database, this document is uncontrolled and the responsibility rests with the user to ensure it is in line with the authorised version on the database.

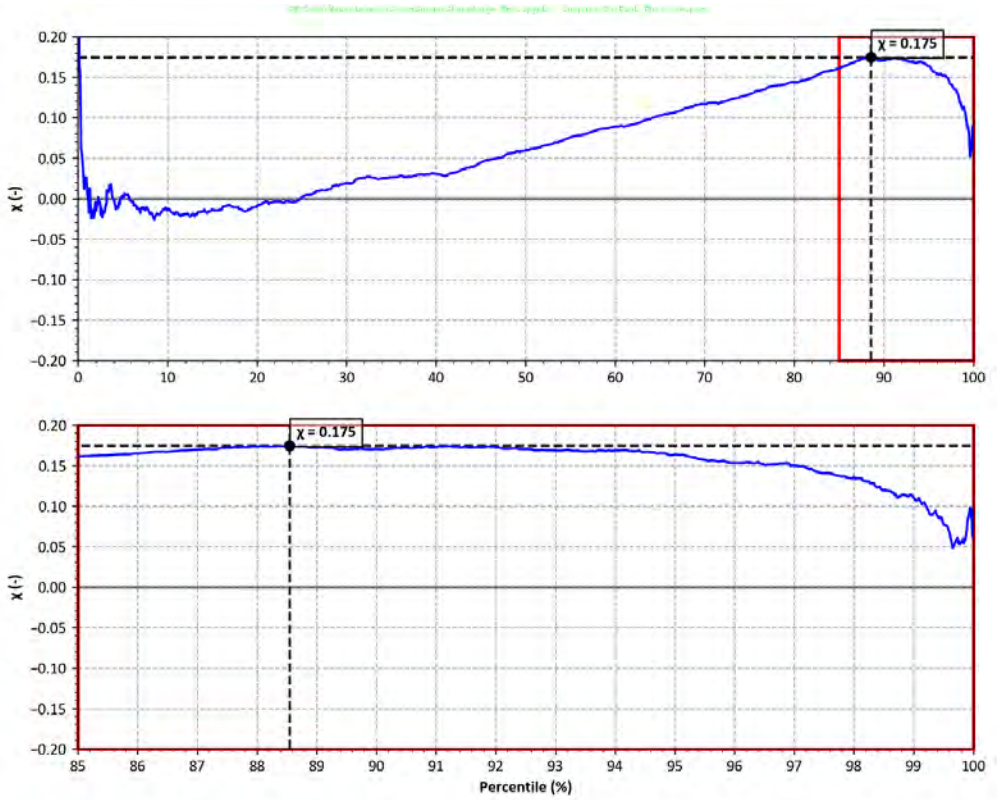


Figure 5.9.48: Dependence Parameter *χ* of Positive Storm Surge and Wave Height at Cape Town.

Figure 5.9.48 shows the calculated dependence parameter χ of positive storm surge and wave height. The results show that χ has a maximum value of 0.175 which is categorised in ***Table 5.9.26*** as a "modest" dependence. Considering the limited number of extreme storms in the dataset used to calculate χ, the next highest level of dependence has been conservatively applied which is the "well" level of dependence with χ between 0.25 to 0.34 (see ***Table 5.9.26***).

Selecting $\chi = \frac{1}{\sqrt{10}} = 0.316$ provides a value in the middle the "well" level of dependence, which when applied in ***Equation 5.9.4*** has the convenient property that the joint exceedance probability will have the same exceedance probability as variable 1 when combined with a factor 10 higher exceedance probability for variable 2, and vice versa, as shown in ***Table 5.9.27***. For each joint exceedance probability both combinations of storm surge and wave height have been modelled and the most conservative result has been selected.

CONTROLLED DISCLOSURE

When downloaded from the EDS database, this document is uncontrolled and the responsibility rests with the user to ensure it is in line with the authorised version on the database.

Table 5.9.27: Joint Exceedance Probability of Positive Storm Surge and Wave Height for χ = 0.316.

Joint Exceedance Probability of Positive Storm Surge and Wave Height	Exceedance Probability of Positive Storm Surge	Exceedance Probability of Wave Height
(y^{-1})	(y^{-1})	(y^{-1})
10^{-2}	10^{-2}	10^{-1}
	10^{-1}	10^{-2}
10^{-4}	10^{-4}	10^{-3}
	10^{-3}	10^{-4}
10^{-6}	10^{-6}	10^{-5}
	10^{-5}	10^{-6}
10^{-8}	10^{-8}	10^{-7}
	10^{-7}	10^{-8}

Waves and negative storm surge

Figure 5.9.49 shows the calculated dependence parameter χ of negative storm surge and wave height.

CONTROLLED DISCLOSURE

When downloaded from the EDS database, this document is uncontrolled and the responsibility rests with the user to ensure it is in line with the authorised version on the database.

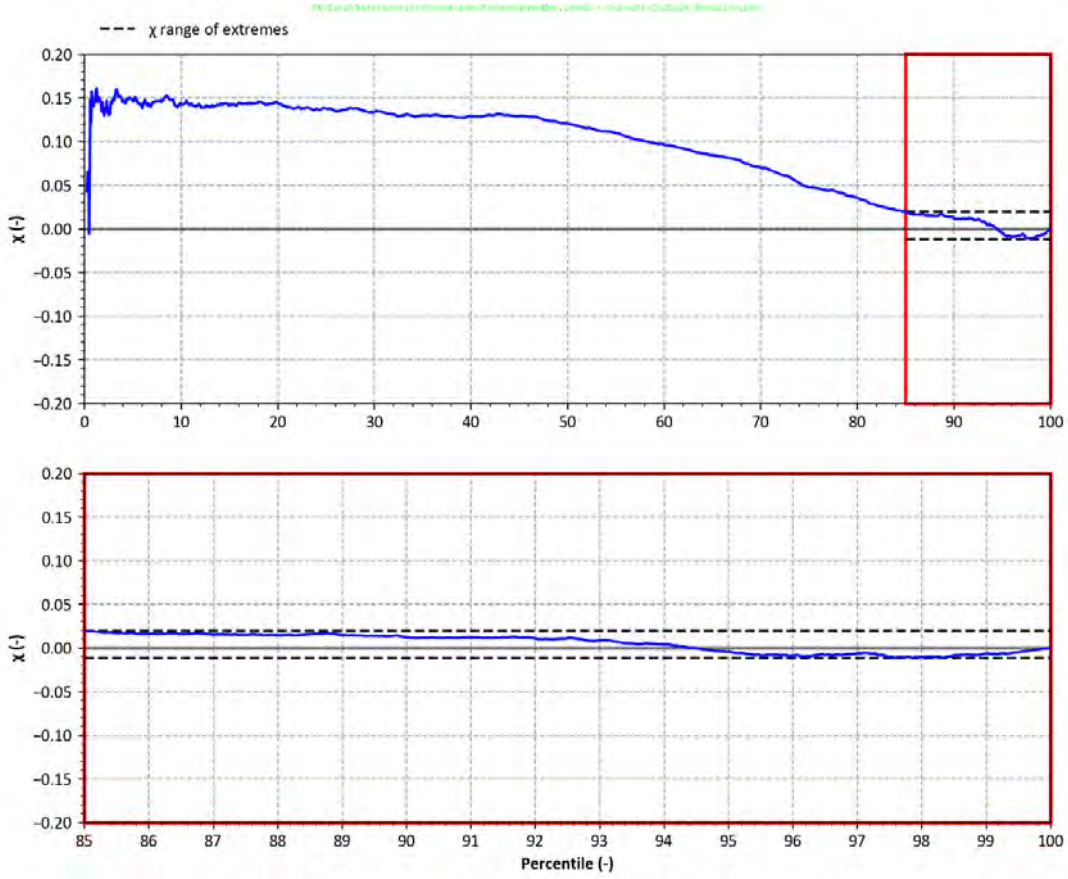


Figure 5.9.49: Dependence Parameter *χ* of Negative Storm Surge and Wave Height at Cape Town.

The results show that χ has ranges between -0.012 and 0.020, which is categorised in ***Table 5.9.26*** as a "zero" dependence and thus the joint probability of negative storm surge and wave height can be calculated using ***Equation 5.9.6***.

When combining negative storm surge and wave height for the model inputs, all exceedance probabilities for variable 1 were combined with an exceedance probability of 1 y^{-1} for variable 2, and vice versa. The results in ***Table 5.9.28*** show that this approach is conservative, i.e., the modelled joint exceedance probabilities using this approach are significantly higher than the theoretical joint exceedance probabilities calculated using ***Equation 5.9.6***. For each joint exceedance probability both combinations of storm surge and wave height have been modelled and the most conservative result has been selected.

CONTROLLED DISCLOSURE

When downloaded from the EDS database, this document is uncontrolled and the responsibility rests with the user to ensure it is in line with the authorised version on the database.

Table 5.9.28: Joint Exceedance Probability of Negative Storm Surge and Wave Height for Zero Dependence and n = 365

Modelled Joint Exceedance Probability of Negative Storm Surge and Wave Height	Exceedance Probability of Negative Storm Surge	Exceedance Probability of Wave Height	Theoretical Joint Probability of Negative Storm Surge and Wave Height
(y^{-1})	(y^{-1})	(y^{-1})	(y^{-1})
10^{-2}	10^{-2}	1	$2.74x10^{-5}$
	1	10^{-2}	
10^{-4}	10^{-4}	1	$2.74x10^{-7}$
	1	10^{-4}	
10^{-6}	10^{-6}	1	$2.74x10^{-9}$
	1	10^{-6}	
10^{-8}	10^{-8}	1	$2.74x10^{-11}$
	1	10^{-8}	

Waves and currents

The dataset used was the hourly-averaged depth-averaged currents measured at Site B (see ***Subsection 5.9.9.4***) and the wave height measured at the same location (see ***Subsection 5.9.9.8***). ***Figure 5.9.50*** shows a scatterplot of these data using 54 321 hourly data pairs, equivalent to 6.2 y.

CONTROLLED DISCLOSURE

When downloaded from the EDS database, this document is uncontrolled and the responsibility rests with the user to ensure it is in line with the authorised version on the database.

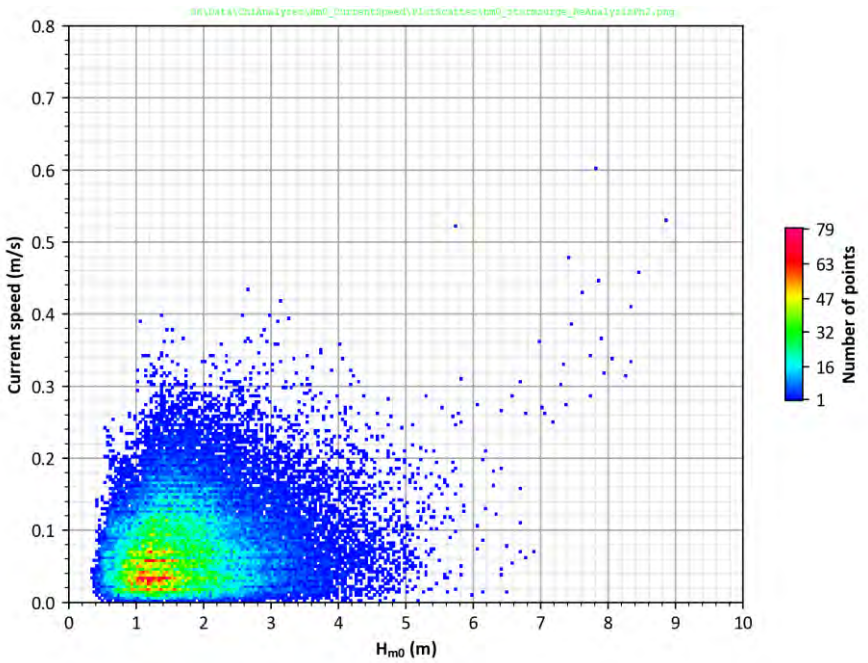


Figure 5.9.50: Scatterplot of Measured Wave Height and Depth-Averaged Current Speed at Site B.

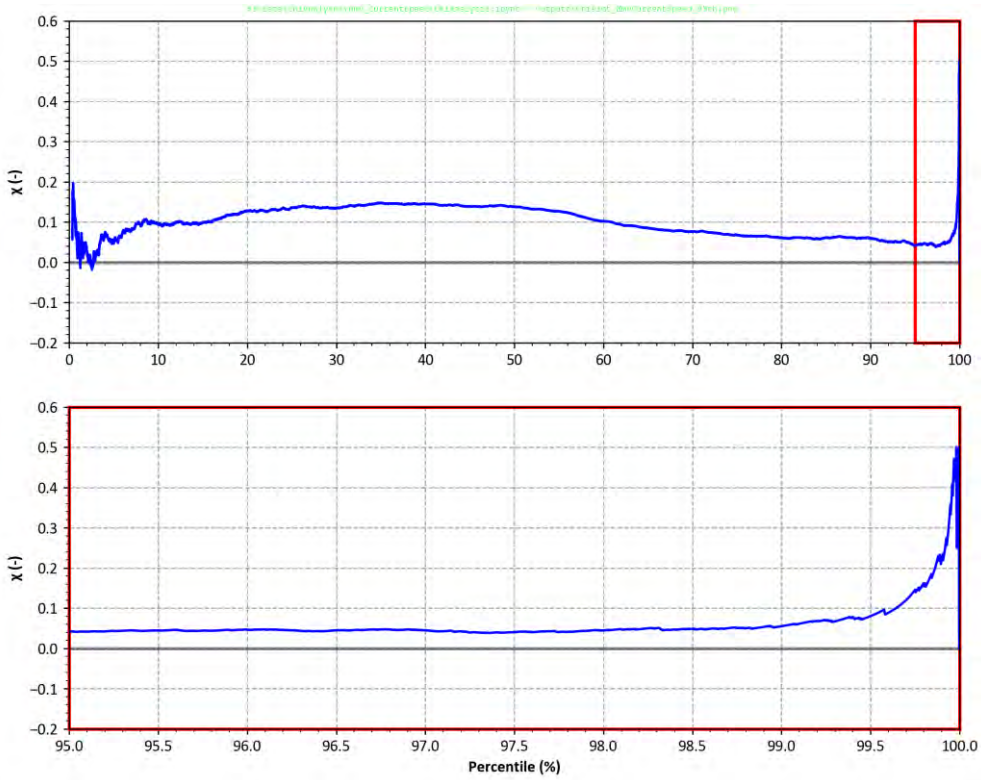


Figure 5.9.51: Dependence Parameter χ of Wave Height and Current Speed at Site B.

CONTROLLED DISCLOSURE

When downloaded from the EDS database, this document is uncontrolled and the responsibility rests with the user to ensure it is in line with the authorised version on the database.

Figure 5.9.48 shows the calculated dependence parameter χ of wave height and current speed. The results show that χ has a maximum value of 0.5 but is less than 0.316 for 99.9% of the time. Based on these results a χ of 0.316 corresponding to a "well" level of dependence has been applied, which is the same as the for positive storm surge and waves. Thus the same joint exceedance probabilities apply as shown in ***Table 5.9.27***, with positive storm surge replaced by current speed in this case.

Tsunamis and storm surge

Geological tsunamis and storm surge are considered to be independent and the tsunamis were thus conservatively combined with the 10^{-1} y^{-1} exceedance probability positive storm surge (***Table 5.9.12***) and the 10^{-1} y^{-1} exceedance probability negative storm surge (***Table 5.9.13***).

The dependence between meteo-tsunamis and storm surge is not as clear cut, however the meteo-tsunamis are enveloped by the geological tsunamis to such a magnitude (***Figure 5.9.105***) that a meteo-tsunami combined with a significantly lower probability storm surge than 10^{-1} y^{-1} would still be enveloped by the geological tsunamis.

5.9.10 Coastline Stability

In order to assess the potential instability of the coastline near the site, the following physical processes and timescales have been evaluated:

- Long-term coastline trends;
- Recession due to sea level rise;
- Longshore sediment transport;
- Coastline changes due to wave rotation;
- Cross-shore erosion.

5.9.10.1 Long-Term Coastline Trends

Beach profiles have been measured since 2008 at 20 locations as part of the oceanographic monitoring programme for this SSR. Details of the profile locations, instruments, sampling intervals, dates and number of surveys are provided in ***Subsection 5.9.6.1***. Profile measurements are also available for the period 1977 to 1980 as part of the oceanographic investigations for the KNPS.

Examples of the measured beach profiles for Profiles 08 and 14 are shown in ***Figure 5.9.52*** and ***Figure 5.9.53***, respectively (see ***Figure 5.9.2*** for the locations of these beach profiles). The full set of profiles is presented in the Oceanographic Monitoring Report (PRDW, 2022c).

CONTROLLED DISCLOSURE

When downloaded from the EDS database, this document is uncontrolled and the responsibility rests with the user to ensure it is in line with the authorised version on the database.

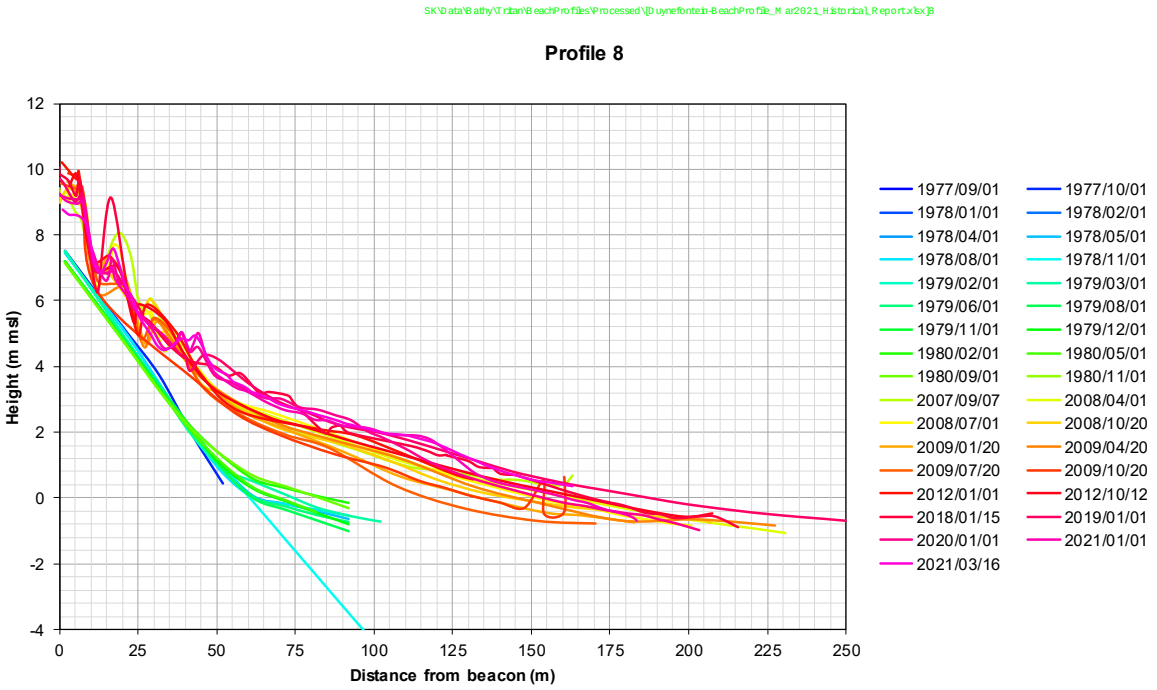


Figure 5.9.52: Measured Beach Profiles at Profile 08 located south of KNPS.

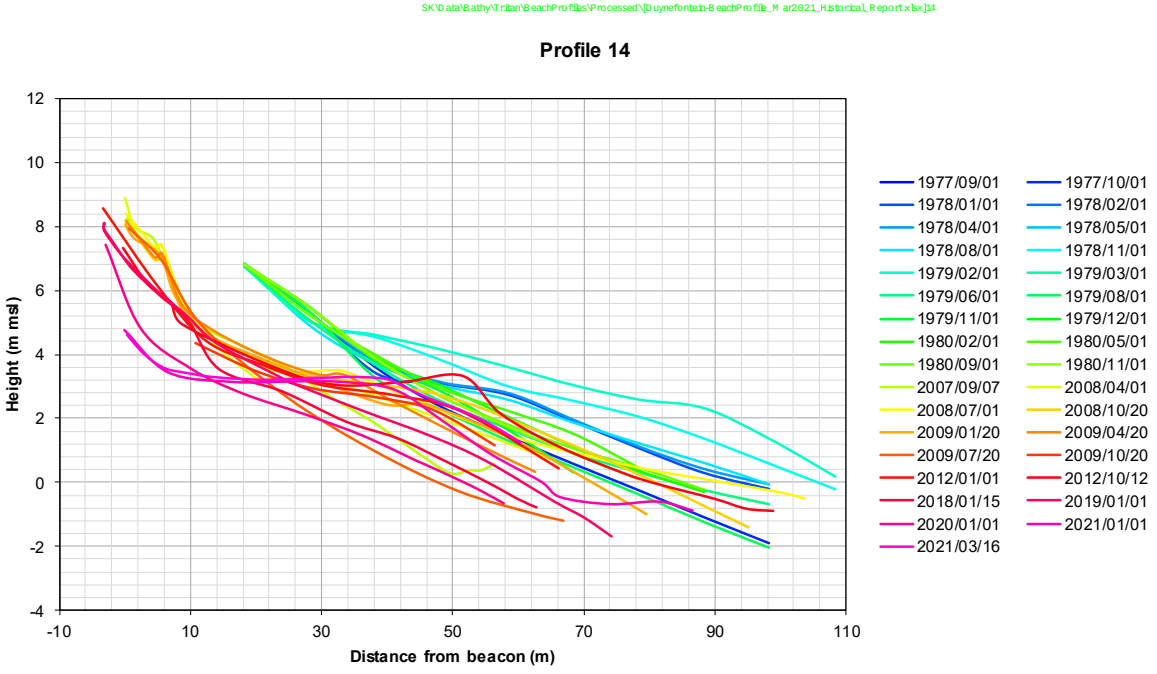


Figure 5.9.53: Measured Beach Profiles at Profile 14 located north of KNPS in front of the new NIs.

To determine the long-term trends, the horizontal distance from the start of the beach profile to the 0, +1, +2, +3, +4, +5 and +6 m msl levels on the profiles have been extracted for each of the profiles. A trend line has been

CONTROLLED DISCLOSURE

When downloaded from the EDS database, this document is uncontrolled and the responsibility rests with the user to ensure it is in line with the authorised version on the database.

fitted to the relevant data and the slope of the trend lines have been used to estimate erosion/accretion rates for each profile based on the horizontal changes at these elevations, as shown in ***Figure 5.9.54*** to ***Figure 5.9.57***.

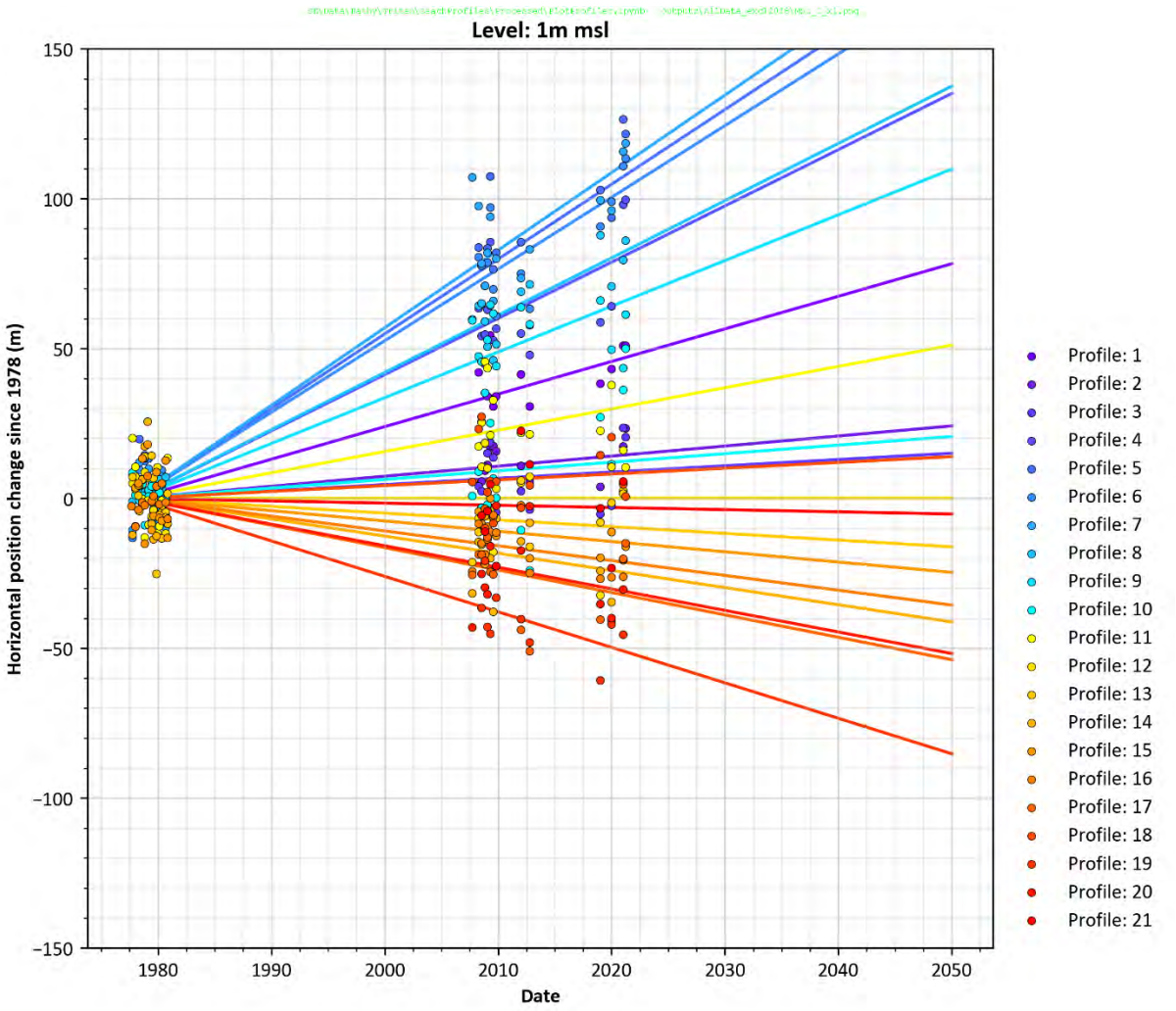


Figure 5.9.54: Horizontal Movement of the +1 m msl Level Over Time (Profiles 1 to 10 are South of KNPS and Profiles 11 to 21 are North of KNPS).

CONTROLLED DISCLOSURE

When downloaded from the EDS database, this document is uncontrolled and the responsibility rests with the user to ensure it is in line with the authorised version on the database.

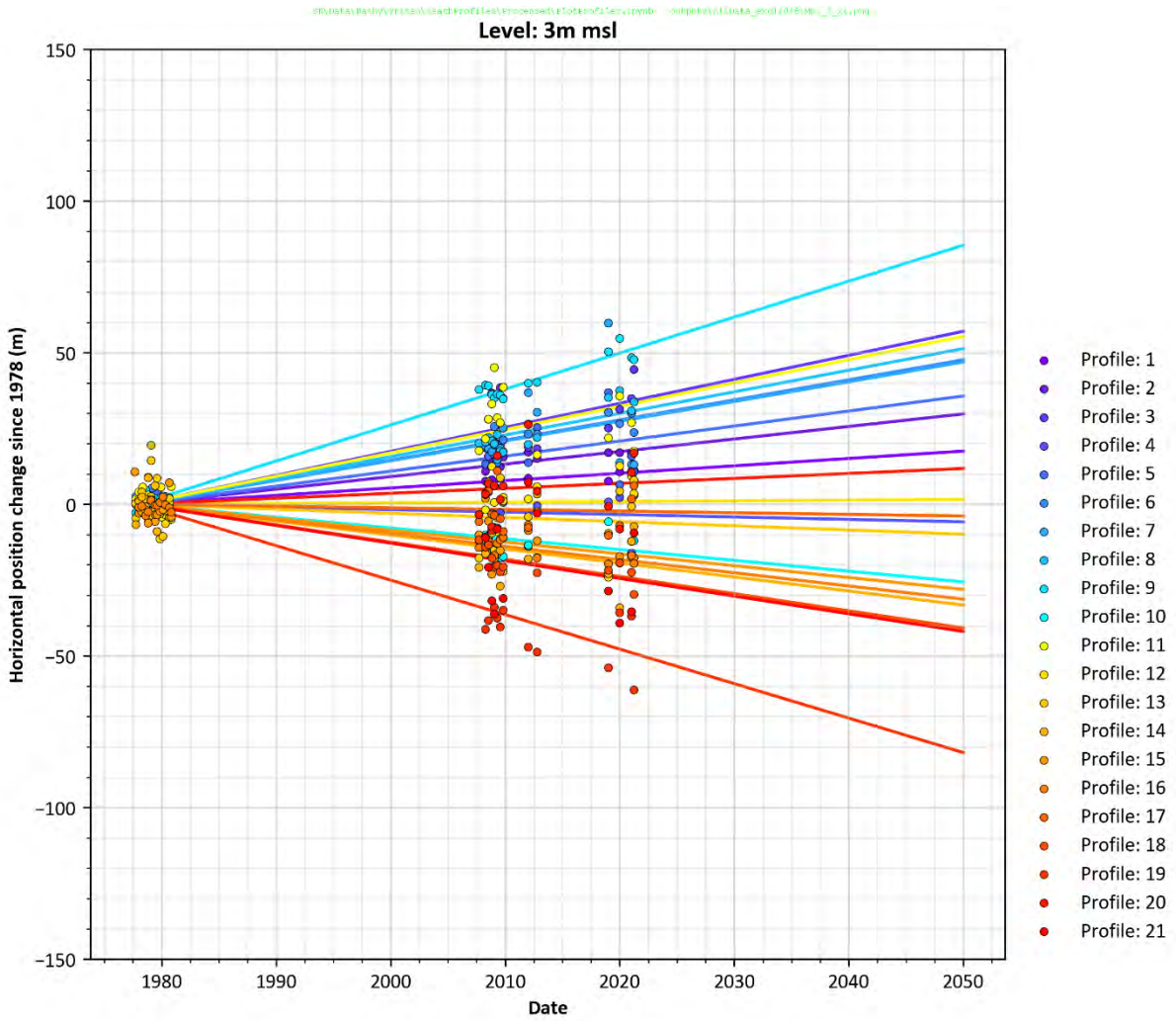


Figure 5.9.55: Horizontal Movement of the +3 m msl Level Over Time (Profiles 1 to 10 are South of KNPS and Profiles 11 to 21 are North of KNPS).

CONTROLLED DISCLOSURE

When downloaded from the EDS database, this document is uncontrolled and the responsibility rests with the user to ensure it is in line with the authorised version on the database.

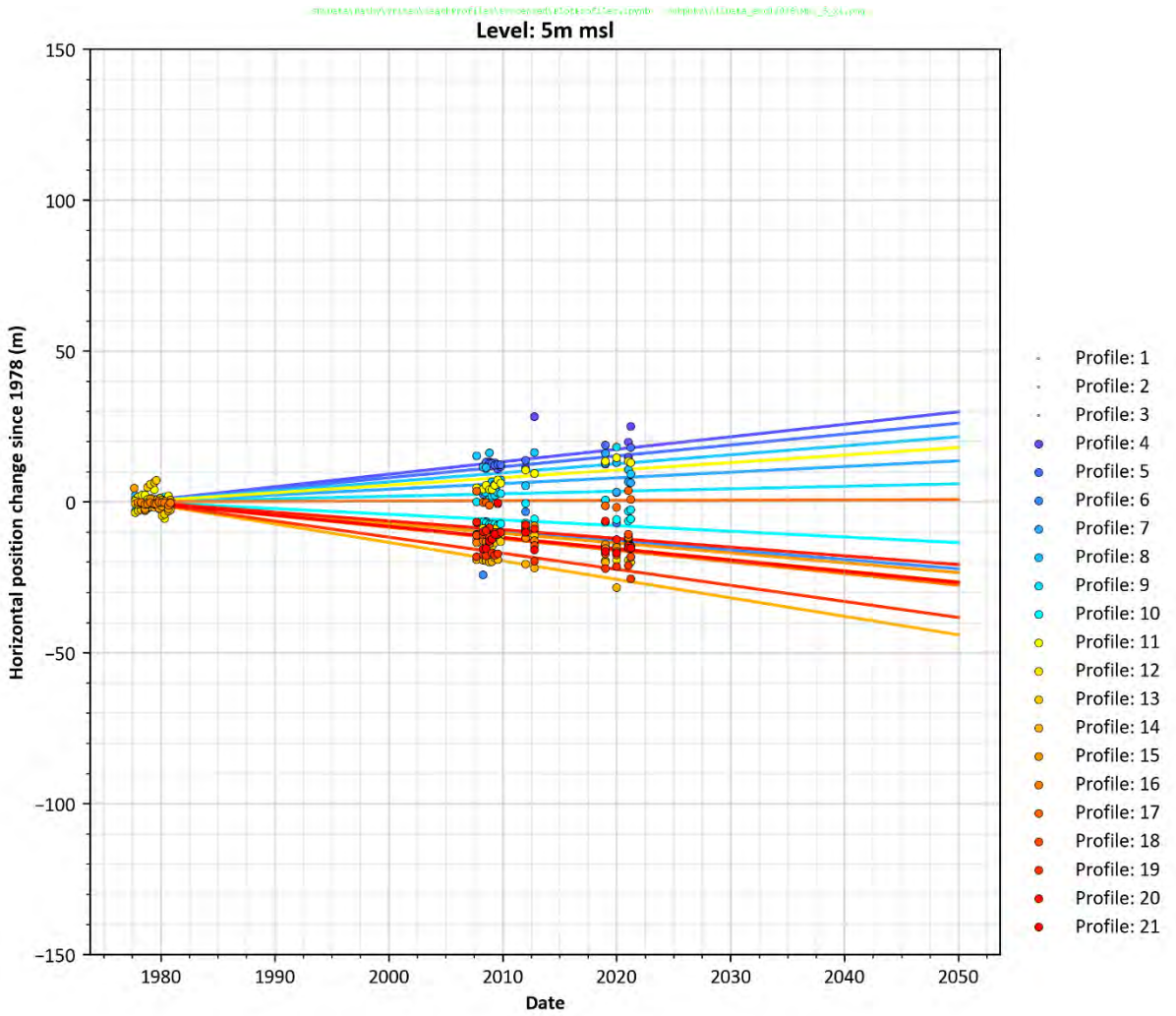


Figure 5.9.56: Horizontal Movement of the +5 m msl Level Over Time (Profiles 1 to 10 are South of KNPS and Profiles 11 to 21 are North of KNPS).

CONTROLLED DISCLOSURE

When downloaded from the EDS database, this document is uncontrolled and the responsibility rests with the user to ensure it is in line with the authorised version on the database.

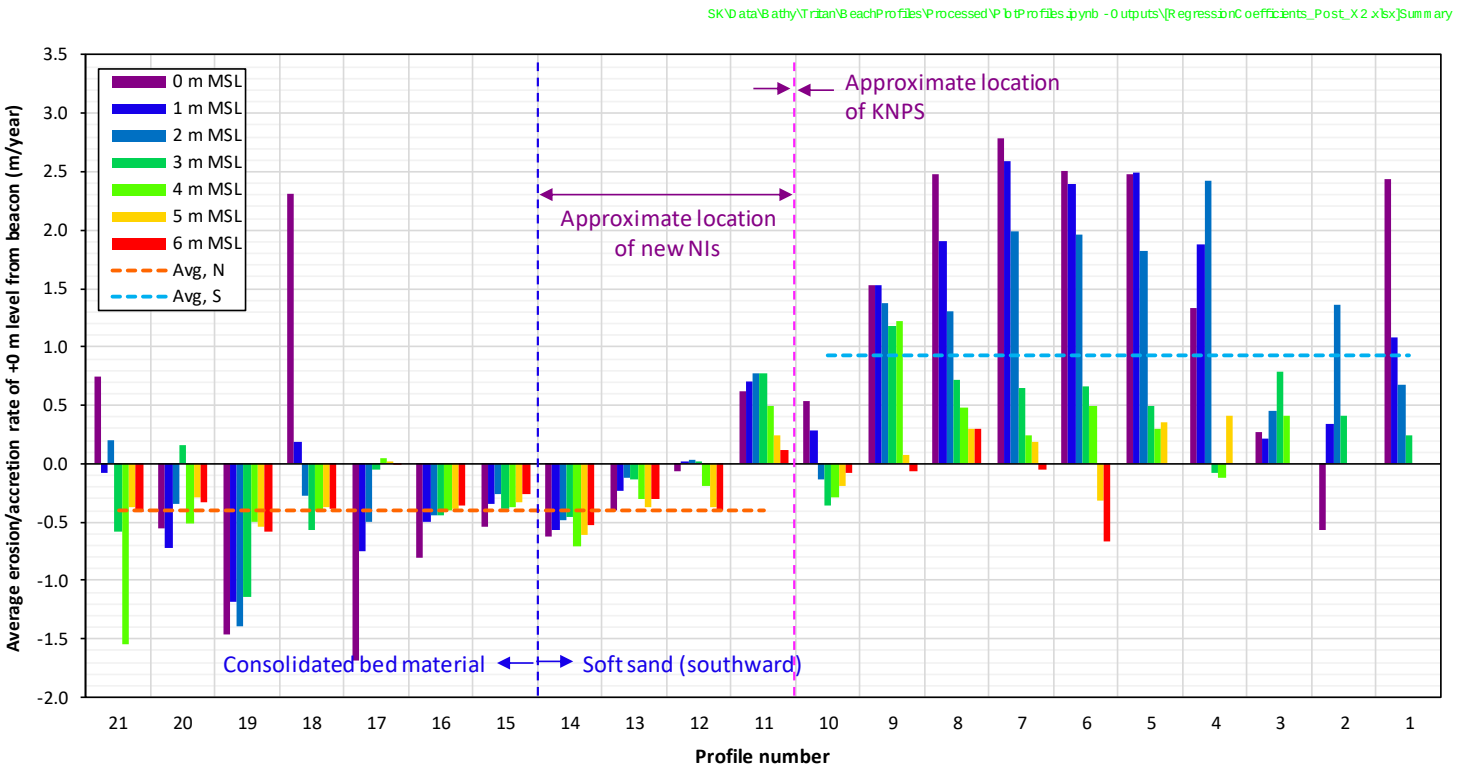


Figure 5.9.57: Long-term Coastline Trends from Measured Beach Profiles.

These results show the following:

- The profiles south of the KNPS are generally accreting, particularly on the lower parts of the profiles, i.e., beach flattening. Profile 10 located directly south of the KNPS outfall channel is stabilised by the outfall structure.
- Profile 11 located directly north of the KNPS also shows accretion, whilst the remaining profiles north of KNPS show erosion.
- The coastline trends appear to be linear over the last 44 years, with little evidence of acceleration or stabilisation.
- For the calculation of the long-term coastline changes the following average changes have been applied:
    - South of KNPS (average of all levels for Profiles 1 to 9): accretion of 0.93 m/y;
    - North of KNPS (average of all levels for Profiles 12 to 21): erosion of -0.40 m/y.

The resultant coastline changes are provided in ***Table 5.9.34*** and ***Table 5.9.35***.

CONTROLLED DISCLOSURE

When downloaded from the EDS database, this document is uncontrolled and the responsibility rests with the user to ensure it is in line with the authorised version on the database.

5.9.10.2 Recession due to Sea Level Rise

The shore response model proposed by Bruun (1962) has been applied to estimate coastline recession to long-term sea level rise at the site. The basic assumption behind the Bruun Rule is that with a rise in sea level, the equilibrium profile of the beach and the nearshore moves upward and landward conserving both mass and the original profile according to the following assumptions:

- The upper beach erodes because of a landward translation of the profile.
- Sediment eroded from the upper beach is deposited immediately offshore, with the eroded and deposited volumes being equal.
- The rise in the nearshore seafloor is equal to the rise in sea level.

The Bruun Rule is considered as a standard approach to coastline recession in coastal engineering applications, e.g., The Coastal Engineering Manual (USACE, 2002). There are several limitations which have been discussed in literature, e.g., Ranasinghe and Stive (2009), Shand, et al., (2013), however most of these limitations are not applicable for the application of the Bruun Rule at this site, as discussed below:

- Time is required for the equilibrium profile to be established, however, for this application the timescale of SLR at the site (see ***Table 5.9.8***) is large compared to the timescale of the beach profile reshaping processes.
- The Bruun Rule does not accommodate erosion/accretion due to gradients in alongshore sediment transport. However, for this application the erosion/accretion due to gradients in alongshore sediment transport are calculated separately (see ***Subsections 5.9.10.1*** and ***5.9.10.3***).
- The Bruun Rule assumes uniform sediment size along profile and does not account for control by hard structures such as substrate geology or adjacent headlands. For this SSR the effect of headlands on shoreline erosion/accretion is calculated separately in ***Subsection 5.9.10.4***.
- The preservation of an equilibrium profile shape assumes a stationary wave climate. For this SSR the mean wave height at the site is not predicted to change over time due to climate change (see ***Table 5.9.8***).
- There is some uncertainly associated with the estimation of the slope of the active profile, which is governed by the depth of closure using empirical formulations. In this SSR the inner Hallermeier equation has been used (USACE, 2002). The Hallermeier analytical equation is one of the most widely accepted for defining closure depths as it is based

CONTROLLED DISCLOSURE

When downloaded from the EDS database, this document is uncontrolled and the responsibility rests with the user to ensure it is in line with the authorised version on the database.

on site-specific physical characteristics and processes (Shand, et al., 2013).

D'Anna, et al., (2021) analysed the integration of SLR-driven recession into equilibrium shoreline models for a cross-shore-transport dominated coast. They demonstrated that, when Bruun's assumptions are satisfied, that the model can explicitly calculate the wave-erosion component of the SLR recession with a trend similar to the Bruun Rule.

Ranashinge, et al., (2011) developed a process-based model which provides probabilistic estimates of SLR-driven coastal recession based on the governing physical processes. Comparison of this model and the Bruun Rule for a case study at Narrabeen beach (Sydney, Australia) showed the Bruun Rule, when using the inner depth of closure method from Hallermeier, provided a conservative result, where the erosion predicted by the Bruun Rule was only exceeded by 8% of the probabilistic results.

Based on the discussion above the Bruun Rule is considered to be an appropriate and conservative method for estimating the coastline recession due to long-term sea level rise at the site.

Bruun's Rule has been applied in the following form (USACE, 2002) and (Hands, 1983):

$$\mathrm{x} = \frac{\mathrm{z\,X}}{\mathrm{Z}} \qquad \text{Equation 5.9.7}$$

where:

x = profile recession due to sea level rise

z = sea level rise

Z = vertical distance from the depth of closure (the depth at which no significant changes in seabed level occurs) to the upper point of profile adjustment (the maximum wave run-up level)

X = the corresponding horizontal distance from the depth of closure to the upper point of profile adjustment

The depth of closure was approximated using the inner Hallermeier analytical equation (USACE, 2002):

$$d_\ell = 2.28H_e - 68.5\left(\frac{H_e^2}{gT_e^2}\right) \qquad \text{Equation 5.9.8}$$

where:

d_ℓ = is the annual depth of closure below the mean water level

CONTROLLED DISCLOSURE

When downloaded from the EDS database, this document is uncontrolled and the responsibility rests with the user to ensure it is in line with the authorised version on the database.

H_e = the non-breaking significant wave height that is exceeded 12 hours per year (0.137%)

T_e = the wave period associated with H_e

g = gravitational acceleration (9.81 m/s^2)

The depth of closure was calculated from 10 years of modelled wave data at Site B (***Subsection 5.9.8.7***) with H_e = 5.90 m and T_e = 14.4 s, which yielded d_ℓ = -12.3 m msl.

Fourteen cross-shore profiles were interpolated from the available bathymetry and topography datasets (***Section 5.9.8***). ***Figure 5.9.58*** presents a plan view of the 14 cross-shore profiles used for coastline stability analysis. Note that these profiles are different to the measured profiles described in ***Subsection 5.9.10.1***.

For each profile the upper point of profile adjustment was assumed to be at the crest level of the foredune. With the known sea level rise (***Table 5.9.8***) the profile recession was calculated per profile using ***Equation 5.9.7***. Landward migration of the foredune due to overwash and aeolian transport is included, similar to Cowell, et al., (1992) and McCarrol, et al., (2021).

Figure 5.9.59 illustrates an example of profile recession due to sea level rise using ***Equation 5.9.7*** for profile P506 for the year 2130. Also shown are the cumulative coastline changes due to wave rotation (***Subsection 5.9.10.4***) and long-term trends (***Subsection 5.9.10.1***).

The resultant coastline changes for all profiles are provided in ***Table 5.9.34*** (KNPS) and ***Table 5.9.35*** (New NIs).

CONTROLLED DISCLOSURE

When downloaded from the EDS database, this document is uncontrolled and the responsibility rests with the user to ensure it is in line with the authorised version on the database.

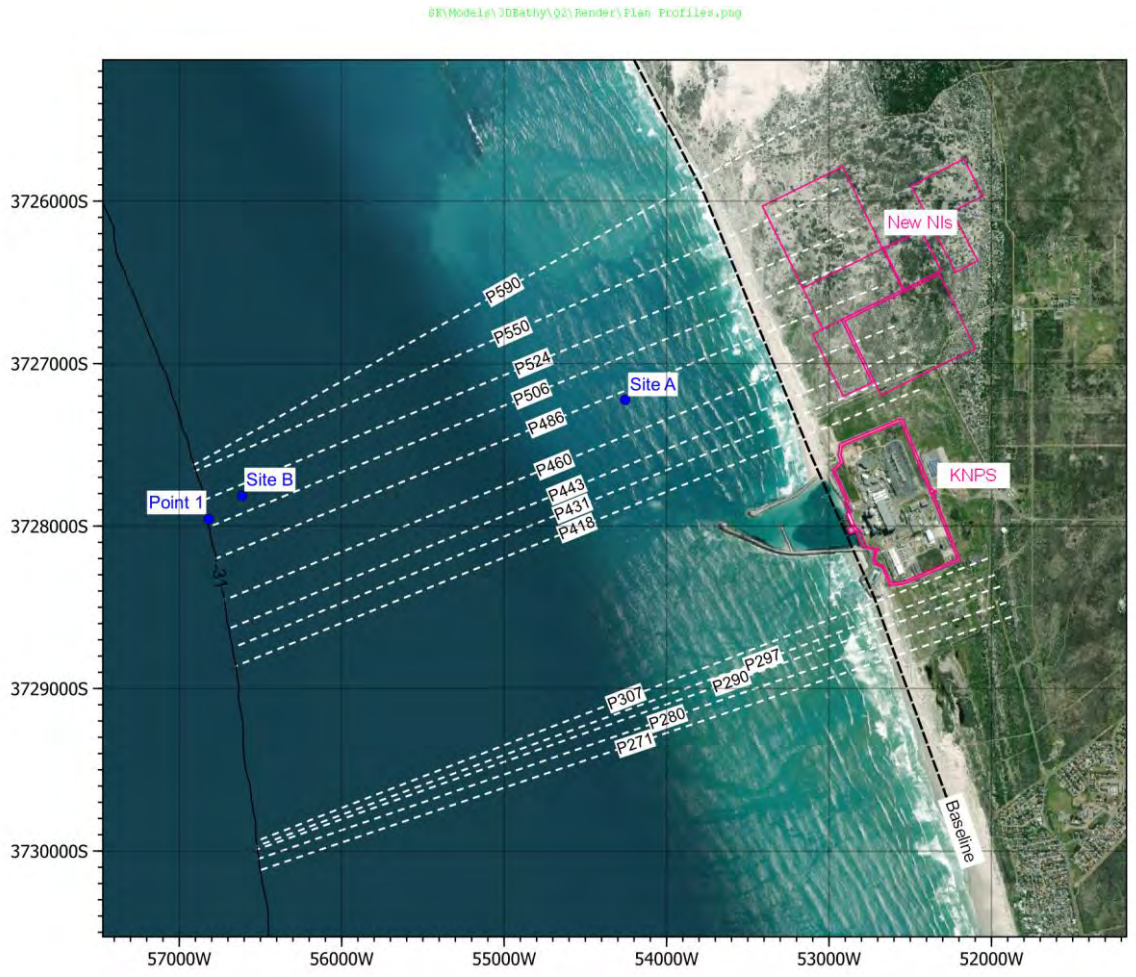


Figure 5.9.58: Plan View of Cross-Shore Profiles Used for Coastline Stability Analysis.

CONTROLLED DISCLOSURE

When downloaded from the EDS database, this document is uncontrolled and the responsibility rests with the user to ensure it is in line with the authorised version on the database.

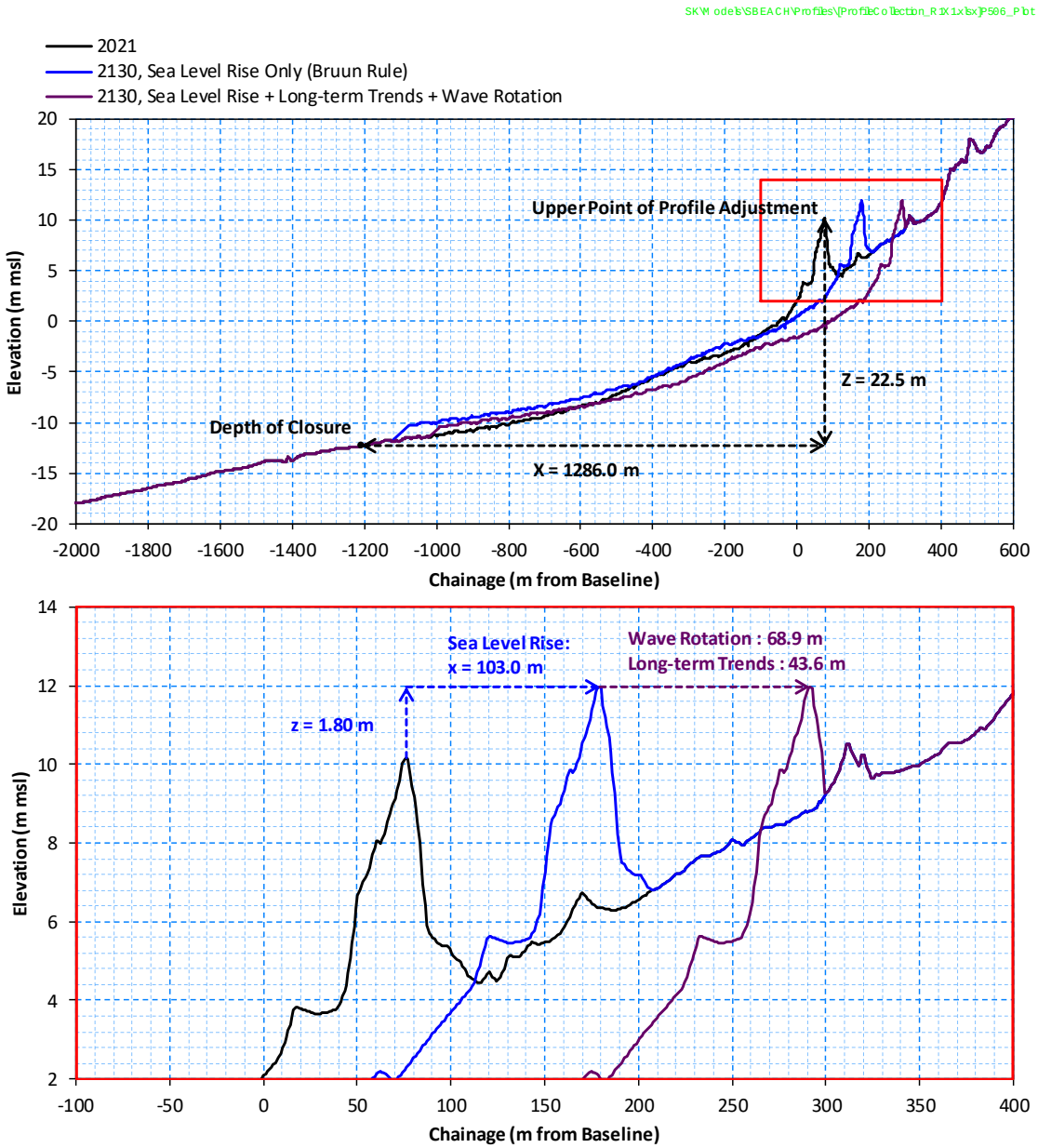


Figure 5.9.59: Example of Profile Recession due to Sea Level Rise for Profile P506 for the year 2130. Also Shown are the Cumulative Coastline Changes due to Wave Rotation and Long-term Trends.

5.9.10.3 Longshore Sediment Transport

Littoral drift modelling

The MIKE Littoral Processes model was used to calculate the longshore sediment transport potential along the coastline at the site. The details of the physical processes and numerical implementation are provided in the model documentation (see ***Table 5.9.7***), while details of the model setup, sensitivity testing, and V&V are provided in the V&V Report (PRDW, 2022b).

CONTROLLED DISCLOSURE

When downloaded from the EDS database, this document is uncontrolled and the responsibility rests with the user to ensure it is in line with the authorised version on the database.

The calculation of littoral transport consists of three calculation parts:

- Wave transformation;
- Longshore current calculation;
- Sediment transport calculation.

The cross-shore distributions of wave height and direction are found by solving the wave energy balance equation for an arbitrary coastal profile. The longshore current and setup are found by solving the long and cross-shore momentum balance equations. The model includes a description for regular and irregular waves, the influence of tidal current and non-uniform bottom friction, as well as wave refraction, shoaling and breaking.

The non-cohesive sediment transport rates are found directly by calls to the quasi three-dimensional sediment transport model (STPQ3D). The transport rates are integrated based on the local wave, current and sediment conditions. As a result, the littoral drift calculation is able to give a deterministic description of the cross-shore distribution of longshore sediment transport for an arbitrary, non-uniform bathymetry and sediment profile. By applying a time varying wave climate, one can obtain a detailed description of the sand budget.

Longshore transport was calculated at five cross-shore profiles, labelled “A” to “E” in ***Figure 5.9.60***. The profiles were extracted from the bathymetry dataset described in ***Subsection 5.9.8***, and extend from a depth of -12 m msl to the shoreline, at a constant 5 m horizontal resolution.

CONTROLLED DISCLOSURE

When downloaded from the EDS database, this document is uncontrolled and the responsibility rests with the user to ensure it is in line with the authorised version on the database.



Figure 5.9.60: Location of Profiles A to E Used in the Longshore Sediment Transport Model.

CONTROLLED DISCLOSURE

When downloaded from the EDS database, this document is uncontrolled and the responsibility rests with the user to ensure it is in line with the authorised version on the database.

The sediment parameters used are presented in ***Table 5.9.29***. These were based on the sediment data described in ***Subsection 5.9.8***.

Table 5.9.29: Sediment Parameters Used in Longshore Transport Model

Profile	Median Grain Diameter (D_{50})	Sediment Grading $(D_{84}/D_{16})^{0.5}$
	(mm)	(-)
A	0.20	1.2
B	0.20	1.2
C	0.35	1.6
D	0.35	1.6
E	0.54	1.4

The predicted tide at Duynefontyn described in ***Subsection 5.9.9.1*** was applied as a time-varying boundary condition. Wave boundary conditions for the period of 2000 to 2009 were extracted from the operational wave model (see ***Subsection 5.9.9.8***) at the offshore end of each profile, to be applied as time-varying boundary conditions. These include the Root-Mean-Square (RMS) wave height ($H_{rms} = H_{m0} / 1.41$), T_p, and MWD.

The model settings were as follows: the critical Shields parameter was set to 0.045, ripples were excluded, the deterministic formulation for bed concentration was used, the wave theory was Stokes' 1st Order, the wave breaker index was 0.8, the roughness height for bed resistance was 0.004 m, and the reduction factor for wave spreading was 0.7.

Cases modelled

Ten years (2000 to 2009) of operational conditions were modelled at each cross-shore profile. The simulations were run for present-day conditions (2021) and were repeated for future dates of 2064 and 2130, accounting for climate change as follows:

- For each date, the wave conditions were extracted from the relevant spectral wave model simulation (see ***Subsection 5.9.9.8***), which included the effects of climate change-induced sea level rise and rotation of the offshore wave climate.
- The water level boundary conditions were adjusted for sea level rise by adding a fixed offset for each date.
- As described in ***Subsection 5.9.10.2***, the cross-shore profile moves upward and backward with long-term sea level rise. Vertical adjustments were therefore applied to the cross-shore profiles in line with the sea level rise allowances presented in ***Table 5.9.8***. A transitional area of 100 m was used to ensure the depth of the offshore end of the profile was consistent with the wave model. The height of the

CONTROLLED DISCLOSURE

When downloaded from the EDS database, this document is uncontrolled and the responsibility rests with the user to ensure it is in line with the authorised version on the database.

steep cliff at Profile E was not increased as there is no physical mechanism for growth of the cliff due to sea level rise.

Results

Time-series of the wave conditions at the offshore end of the profile, instantaneous sediment transport (integrated across the profile), and accumulated sediment transport are shown in ***Figure 5.9.61*** for the full 10-year period at Profile C for 2021. The modelled longshore sediment transport rates for 2021, 2064, and 2130 are summarised in ***Table 5.9.30***.

CONTROLLED DISCLOSURE

When downloaded from the EDS database, this document is uncontrolled and the responsibility rests with the user to ensure it is in line with the authorised version on the database.

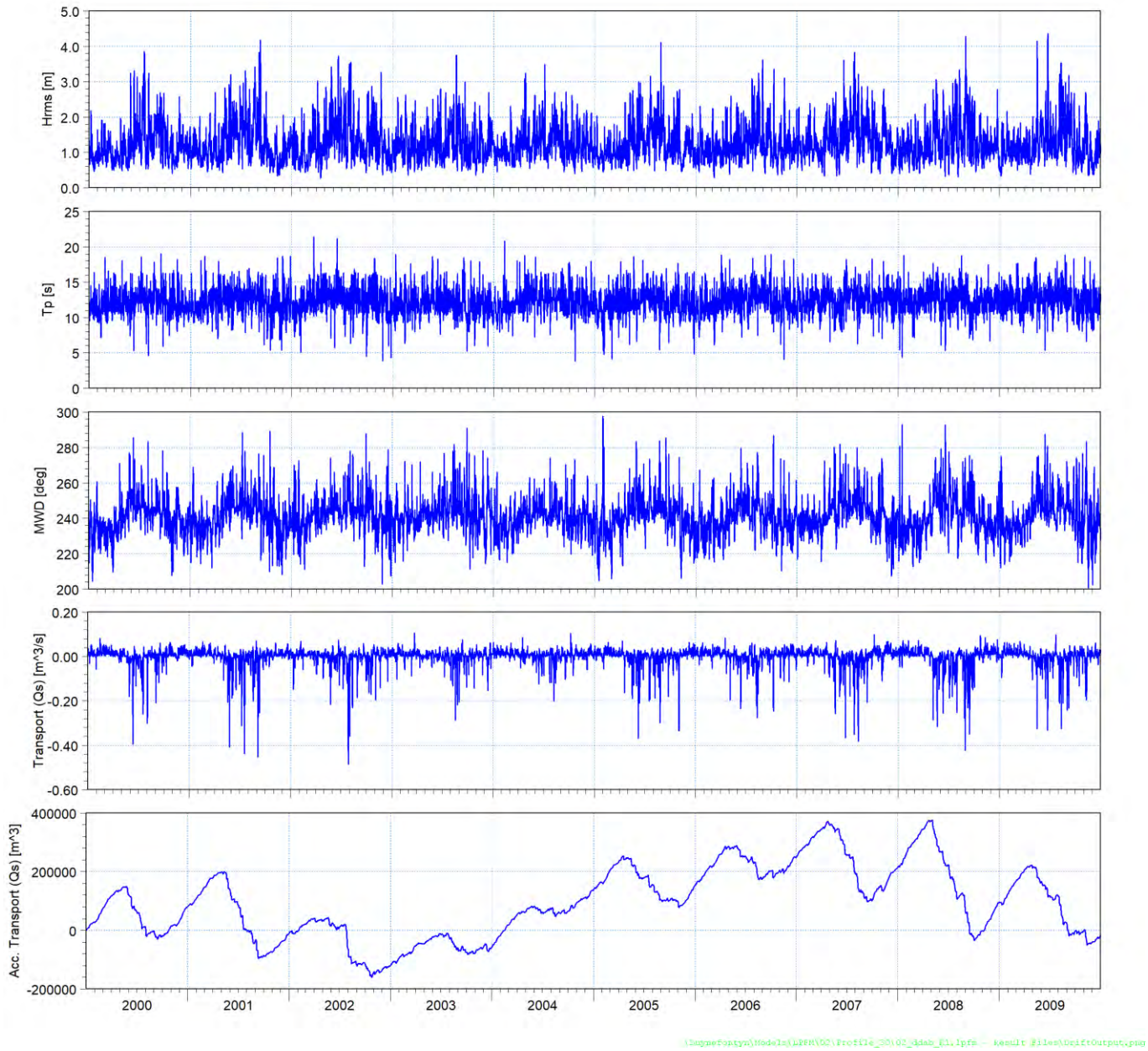


Figure 5.9.61: Time-series of Waves (at the Offshore End of the Profile), Instantaneous Sand Transport (Integrated Across the Profile) and Accumulated Sand Transport at Profile C (Positive is Northward and Negative is Southward).

CONTROLLED DISCLOSURE

When downloaded from the EDS database, this document is uncontrolled and the responsibility rests with the user to ensure it is in line with the authorised version on the database.

Table 5.9.30: Longshore Sediment Transport Results.

Profile	Net Transport			Gross Transport			Southward Transport			Northward Transport			Depth Above Which 95% of the Gross Transport Occurs		
	($x10^3$ m^3/y)			($x10^3$ m^3/y)			($x10^3$ m^3/y)			($x10^3$ m^3/y)			(m msl)		
	2021	2064	2130	2021	2064	2130	2021	2064	2130	2021	2064	2130	2021	2064	2130
A	0	0	0	1380	1380	1420	690	690	710	690	690	710	-6.5	-6.1	-5.1
B	0	0	0	1260	1260	1310	630	630	650	630	630	650	-6.8	-6.5	-5.4
C	0	0	0	620	630	640	310	320	320	310	320	320	-6.9	-6.5	-5.4
D	0	0	0	540	540	570	270	270	280	270	270	280	-6.5	-6.1	-4.9
E	0	0	0	530	530	550	270	270	270	270	270	280	-6.8	-6.5	-5.3

The results for 2021 indicate the following:

- During the summer months when the waves are more southerly, the transport is mostly northward. During winter months when the waves are more westerly, the transport is mostly southward.
- Due to interannual variability, some years have a net northward transport while some years have a net southward transport.
- At all profiles the net transport accumulated over the ten modelled years is very low, suggesting little sediment exchange with adjacent beach cells. The lack of a gradient in the net transport indicates that the coastline is in a state of dynamic equilibrium.
- The gross transport is approximately 1.3 million m^3/y south of KNPS and approximately 560 000 m^3/y north of KNPS, which is due to the finer grain size south of KNPS (see ***Table 5.9.29***).

For the future dates of 2064 and 2130, the coastline orientation was chosen to match the existing net transport of approximately zero. This assumes that climate change occurs at a slow enough rate that the future coastlines reach dynamic equilibrium. This is a reasonable assumption given the time scales involved (decades to centuries) and the relatively high gross transport rates which facilitate the redistribution of sediment along the coast.

An analysis of the long-term profile data (see ***Subsection 5.9.10.1***) was conducted to estimate the associated volume changes to provide insight to the local sediment budget. Beach cells were defined between each of the 21 measured profiles (shown in ***Figure 5.9.2***). For each cell, the average trend was calculated as the average over all levels (+1 m msl to +6 m msl) over the two profiles defining the edges of the cell. The active height was estimated as the difference between the height of the primary dune crest and the depth above which 95% of the gross longshore transport occurs (see ***Table 5.9.30***). For these depths, average values were calculated for the beaches to the south (Profiles A and B) and north (Profiles C to E) of

CONTROLLED DISCLOSURE

When downloaded from the EDS database, this document is uncontrolled and the responsibility rests with the user to ensure it is in line with the authorised version on the database.

KNPS. The volume in each cell was calculated as the product of the average trend, the cell length, and the active height.

The beach south of KNPS was found to gain approximately 50 000 m^3/y, while the beach north of KNPS loses approximately 50 000 m^3/y. Historical dredging records indicate an average of approximately 130 000 m^3/y is dredged from the KNPS intake basin and deposited on the beach to the south (PRDW, 2005). This information was interpreted together with the longshore transport modelling results for 2021 to arrive at the following sediment budget (illustrated in ***Figure 5.9.62***):

- The local coastline is in dynamic equilibrium with a net zero exchange of sediment with adjacent cell boundaries at Melkbospunt and Matroospunt.
- While there is significant gross transport, there is a net zero sediment transport between the beaches south and north of KNPS due longshore transport.
- The southern beach with a high gross transport (approximately 1.3 million m^3/y) supplies approximately 80 000 m^3/y to the KNPS intake basin.
- The northern beach with a lower gross transport supplies approximately 50 000 m^3/y to the KNPS intake basin.
- Approximately 130 000 m^3/y is dredged from the intake basin and deposited on the southern beach.
- This results in a deficit of 50 000 m^3/y on the northern beach and a surplus of 50 000 m^3/y on the southern beach, in line with long-term coastline trends described in ***Subsection 5.9.10.1***.

CONTROLLED DISCLOSURE

When downloaded from the EDS database, this document is uncontrolled and the responsibility rests with the user to ensure it is in line with the authorised version on the database.



Figure 5.9.62: Sediment Budget

5.9.10.4 Coastline Changes due to Wave Rotation

The equilibrium coastline angles obtained from the longshore sediment transport modelling (***Subsection 5.9.10.3***) are presented in ***Table 5.9.31***, which also presents the rotation relative to the 2021 equilibrium orientation.

CONTROLLED DISCLOSURE

When downloaded from the EDS database, this document is uncontrolled and the responsibility rests with the user to ensure it is in line with the authorised version on the database.

Table 5.9.31: Equilibrium Angles and Coastline Rotation.

Profile	Equilibrium Coastline Angle (°N)			Coastline Rotation Relative to 2021 (°)	
	2021	2064	2130	2064	2130
A	249.59	248.95	248.13	-0.64	-1.46
B	247.36	246.70	245.93	-0.66	-1.43
C	245.30	244.57	243.49	-0.73	-1.81
D	243.98	243.21	242.14	-0.77	-1.84
E	234.70	233.92	233.07	-0.78	-1.63
Average for coastline south of KNPS (Profile A to B)				-0.65	-1.44
Average for coastline north of KNPS (Profile C to E)				-0.76	-1.76

The average rotations for the southern and northern coastlines were used to derive the associated changes to the coastline position. The northern coastline was assumed to pivot about a point midway between the hard points of KNPS in the south and Matroospunt in the north. The southern coastline was assumed to pivot about a point midway between the hard points of KNPS in the north and Melkbospunt in the south. The resulting rotations are shown in ***Figure 5.9.63***, which presents the changes in the position of the 0 m msl contour due to wave rotation. The resultant coastline changes are provided in ***Table 5.9.34*** and ***Table 5.9.35***.

CONTROLLED DISCLOSURE

When downloaded from the EDS database, this document is uncontrolled and the responsibility rests with the user to ensure it is in line with the authorised version on the database.

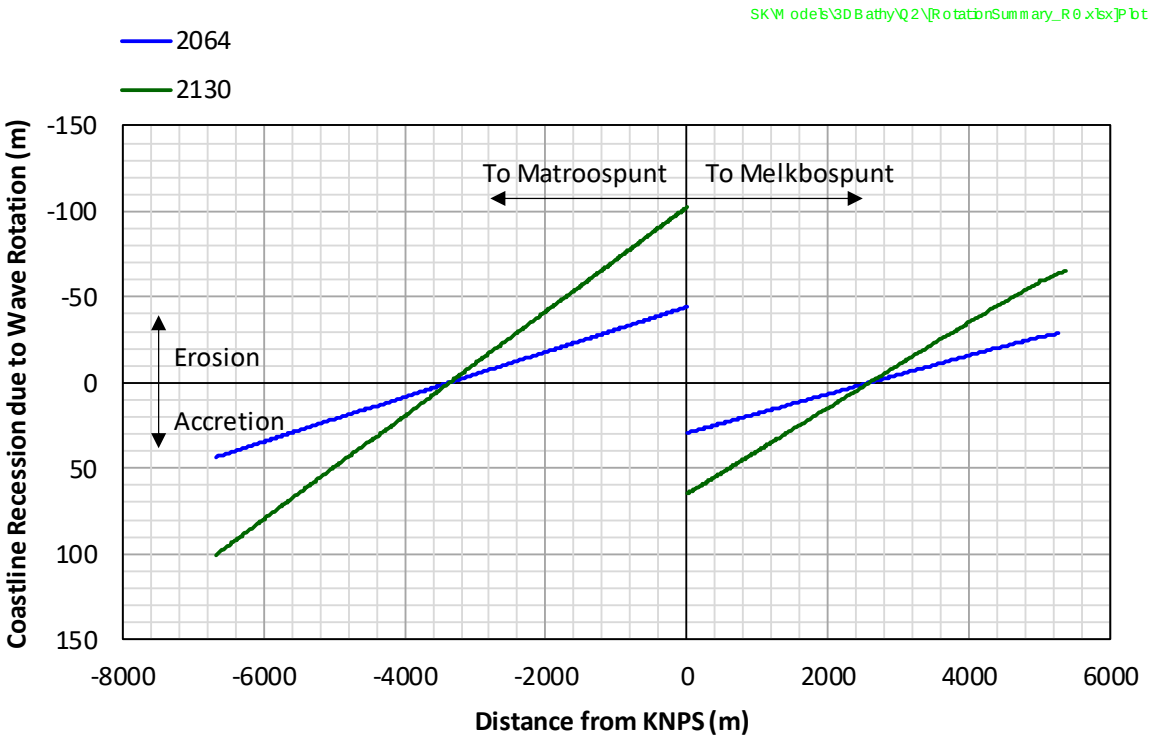


Figure 5.9.63: Coastline changes due to Wave Rotation. Positive Values Indicate Accretion and Negative Values Indicate Erosion.

5.9.10.5 Cross-Shore Erosion

Introduction

This section assesses the cross-shore erosion of the beach during storms. This erosion contributes to the total coastline erosion, whilst erosion of the dune crests increases the flooding risk.

Cross-shore erosion modelling

The SBEACH (Storm-induced BEAch CHange) storm erosion model was used to simulate the erosion of the beach in front of KNPS and new NIs during storm events.

The details of the physical processes and numerical implementation are provided in the model documentation (see ***Table 5.9.7***), while details of the model setup, sensitivity testing, and V&V are provided in the V&V Report (PRDW, 2022b).

The model consists of a wave model and a beach response model. The wave model calculates the transformation of wave height and direction at user specified grid points along the beach profile, taking into account the

CONTROLLED DISCLOSURE

When downloaded from the EDS database, this document is uncontrolled and the responsibility rests with the user to ensure it is in line with the authorised version on the database.

effects of wave refraction, shoaling and dissipation due to depth-induced breaking. Water level variations due to wave- and wind-induced setup are also included in the wave model. The formulation of the wave model is based on the solution of best practice deterministic equations.

The beach response model is empirically based, with the underlying assumptions and relationships derived from observations made from prototype-scale laboratory experiments. The model assumes the conservation of sediment across the profile (longshore processes are considered to be uniform and neglected in calculating profile change). The direction and rate of cross-shore transport is determined from the local wave, water level, beach profile and sediment properties, and the equation describing the conservation of beach material is solved to compute profile change as a function of time.

Model validation

The model was validated against four physical model tests. Two cases were selected from the SUPERTANK experiments, as tested in the SBEACH Model Validation Report (USACE, 1996b), and two cases from physical model tests performed in the Delta Flume by Van Gent, et al. (2008). The objective was to predict the measured erosion of the dunes.

Figure 5.9.64 presents a comparison of measured and modelled eroded profiles for the SUPERTANK and Delta Flume tests.

CONTROLLED DISCLOSURE

When downloaded from the EDS database, this document is uncontrolled and the responsibility rests with the user to ensure it is in line with the authorised version on the database.

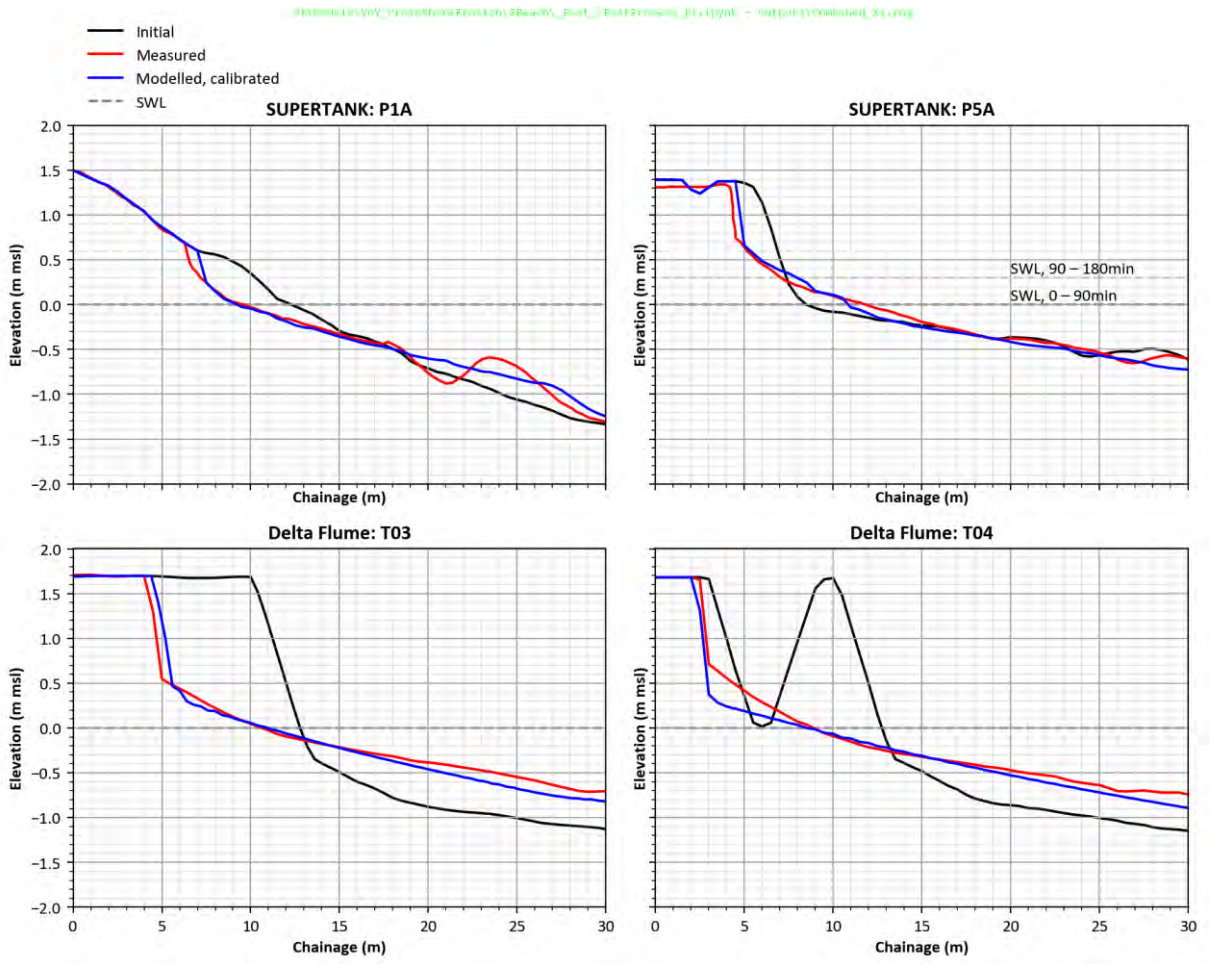


Figure 5.9.64: Comparison of Measured and Modelled Eroded Profiles for the SUPERTANK and Delta Flume Tests.

The model generally showed a good agreement to the measured profiles above the SWL which is important in the context of flooding and erosion. Further details of the model V&V are provided in the V&V Report (PRDW, 2022b).

Cases modelled

The model was run for extreme storms with exceedance probabilities of 10^{-2}, 10^{-4}, 10^{-6} and 10^{-8} y^{-1}. The model was run for the following dates to include the effect of climate change on waves, water levels and coastline stability:

- 2021: present-day;
- 2064: end of decommissioning period for KNPS;
- 2130: end of decommissioning period for the new NIs.

CONTROLLED DISCLOSURE

When downloaded from the EDS database, this document is uncontrolled and the responsibility rests with the user to ensure it is in line with the authorised version on the database.

The model boundary conditions are the extreme wave parameters (H_{m0} and T_p) as shown in ***Table 5.9.25***, combined with the extreme maximum still water levels (comprising a synthetic tide, sea level rise and storm surge) as shown in ***Table 5.9.12***. The wave direction was conservatively assumed to be shore normal. The synthetic tide was generated using a semi-diurnal signal with a fixed tidal range of 1.55 m (10^{th} percentile low tide to 90^{th} percentile high tide) and a maximum elevation equal to the extreme maximum still water level. The peak of the synthetic tide time-series was aligned with the peak of the wave height. The best estimate values were used in the modelling.

The storm duration was predicted by fitting a schematized storm time-series to 43 hindcast storms, from the NCEP nodes 35.0°S, 18.0 E (1979-2009) and 34.5°S, 18.0 E (2010-2021), offshore of Cape Town (refer to ***Subsection 5.9.9.8***). Since no correlation was observed between the wave height peak and duration of the storm a constant duration was used for all storms. The storm duration was based on the 95^{th} percentile time required for the wave height to increase from the average wave height to the storm peak and then to reduce back to the average height. The resulting storm has a duration of 98 hours (4.1 days). ***Figure 5.9.65*** compares the schematized wave height time-series of 4 example storms to the 43 storms. Also shown is an example synthetic tide signal. The storm duration is assumed to be independent of depth, and therefore applicable to nearshore extremes.

CONTROLLED DISCLOSURE

When downloaded from the EDS database, this document is uncontrolled and the responsibility rests with the user to ensure it is in line with the authorised version on the database.

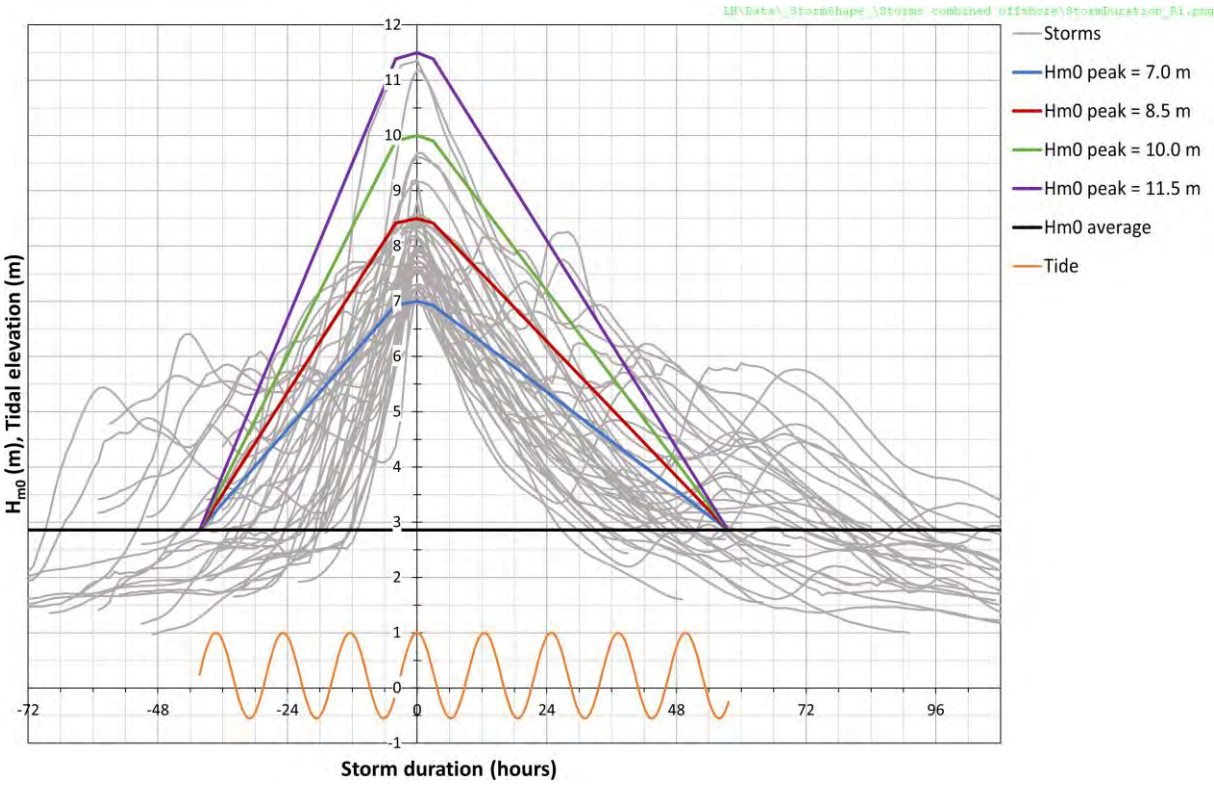


Figure 5.9.65: Storm Duration Analysis Based on 43 Offshore Storms. The Synthetic Tide For 2021 (Excluding Storm Surge and Sea Level Rise) is Shown for Reference.

The joint exceedance probability between the waves and storm surge was accounted for as described in ***Subsection 5.9.9.9***. The waves were combined with the positive storm surge as shown in ***Table 5.9.27***, where for example the 10^{-4} y^{-1} wave is combined with the 10^{-3} y^{-1} storm surge and vice versa.

For each joint probability both combinations of storm surge and wave height were modelled. The total number of cases modelled was thus 3 dates × 4 exceedance probabilities × 2 joint probability combinations = 24 cases per profile. The same fourteen cross-shore profiles used for the sea level rise recession (***Figure 5.9.58***) were modelled, with the seaward end of the profile at the -31 m msl depth contour. A variable grid size was used for each profile, varying between 16 m in deep water to 2 m in the erosion zone.

The model setup parameters were based on calibrated parameters from the V&V and site-specific data (median grain size, avalanching slope, seawater temperature) and are summarised in ***Table 5.9.32***. Details of the model calibration parameters are provided in the V&V Report (PRDW, 2022b).

CONTROLLED DISCLOSURE

When downloaded from the EDS database, this document is uncontrolled and the responsibility rests with the user to ensure it is in line with the authorised version on the database.

Table 5.9.32: SBEACH Model Setup Parameters.

Setup Parameter	Input
Land surf zone depth	0.1 m
Median grain size (representative of upper beach and dune)	0.17 mm
Maximum slope prior to avalanching	30^{o}
Transport rate coefficient	2E-6 m^{4}/N
Overwash transport parameter	0.005
Coefficient for slope-dependent term	0.003 m^{2}/s
Transport rate decay coefficient	0.5
Seawater temperature	13^{o}C

Results

Figure 5.9.66 presents an example of the erosion results for the three dates and four storm exceedances at profile P506.

CONTROLLED DISCLOSURE

When downloaded from the EDS database, this document is uncontrolled and the responsibility rests with the user to ensure it is in line with the authorised version on the database.

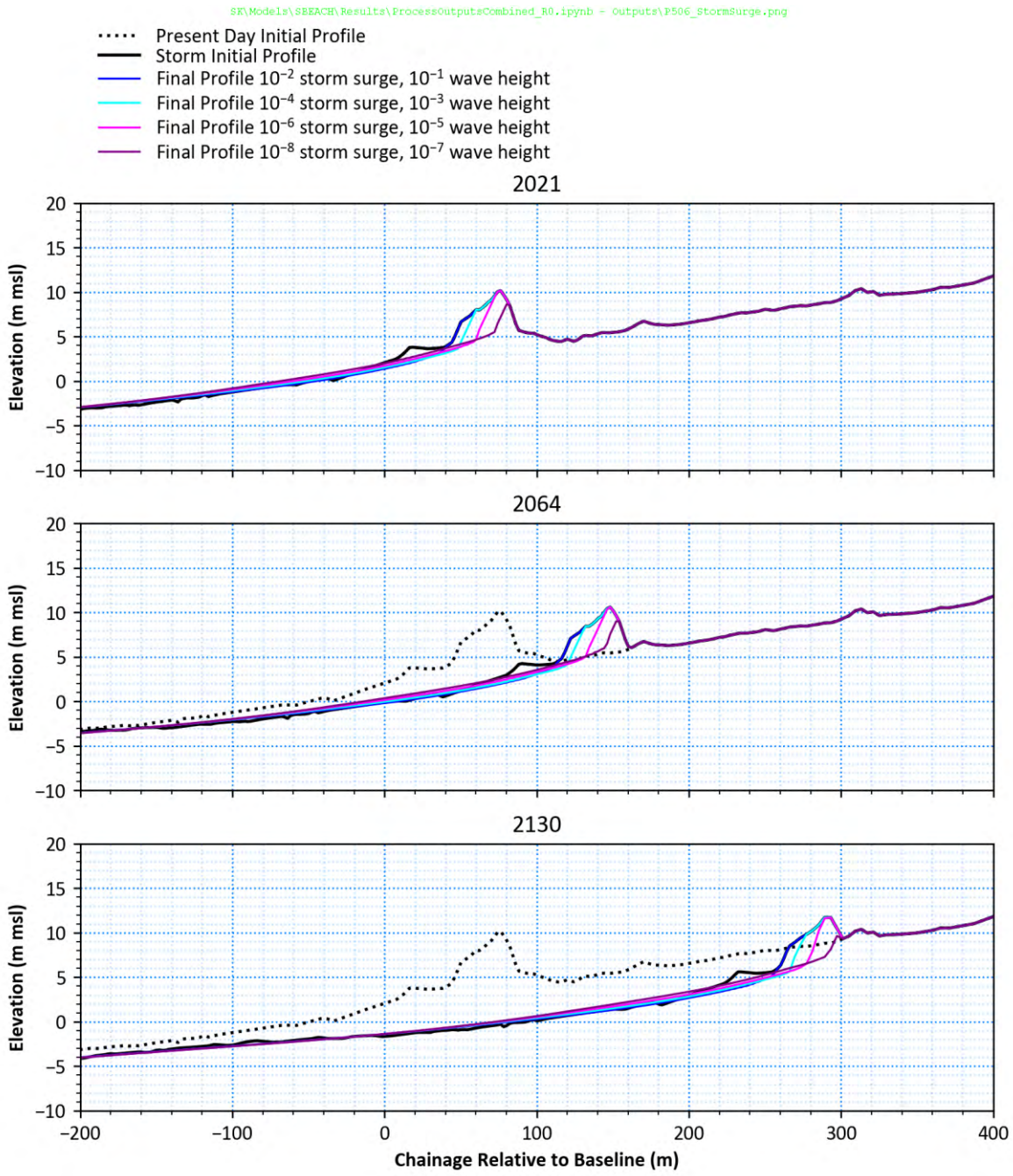


Figure 5.9.66: Profile P506 Cross-Shore Erosion Results for Storm Surge Dominant Return Periods.

In ***Figure 5.9.66*** the following results are shown:

- "Present Day Initial Profile" is the beach and dune profile as measured in 2021.

CONTROLLED DISCLOSURE

When downloaded from the EDS database, this document is uncontrolled and the responsibility rests with the user to ensure it is in line with the authorised version on the database.

- "Storm Initial Profile" is the profile prior to the storm and is the sum of the following:
    - Long-term coastline trends (***Subsection 5.9.10.1***);
    - Recession due to sea level rise (***Subsection 5.9.10.2***); and
    - Coastline changes due to wave rotation (***Subsection 5.9.10.4***).
- "Final Profile" is the profile including cross-shore erosion due to the storm with the mentioned exceedance probability.

The coastline stability was evaluated by measuring the horizontal distance from the baseline to the most-landward extent where any erosion or accretion were observed on the profiles. The resultant coastline changes are provided in ***Table 5.9.34*** and ***Table 5.9.35***.

The erosion of the dune crests is expected to increase the flooding potential at KNPS and the new NIs. Each profile was analysed per storm combination to determine the post-storm vertical elevation of the foredune ridges. ***Figure 5.9.67*** presents the vertical erosion analysis of dune crest levels and the schematised truncation level of dune crest levels north and south of the KNPS are summarised in ***Table 5.9.33***.

CONTROLLED DISCLOSURE

When downloaded from the EDS database, this document is uncontrolled and the responsibility rests with the user to ensure it is in line with the authorised version on the database.

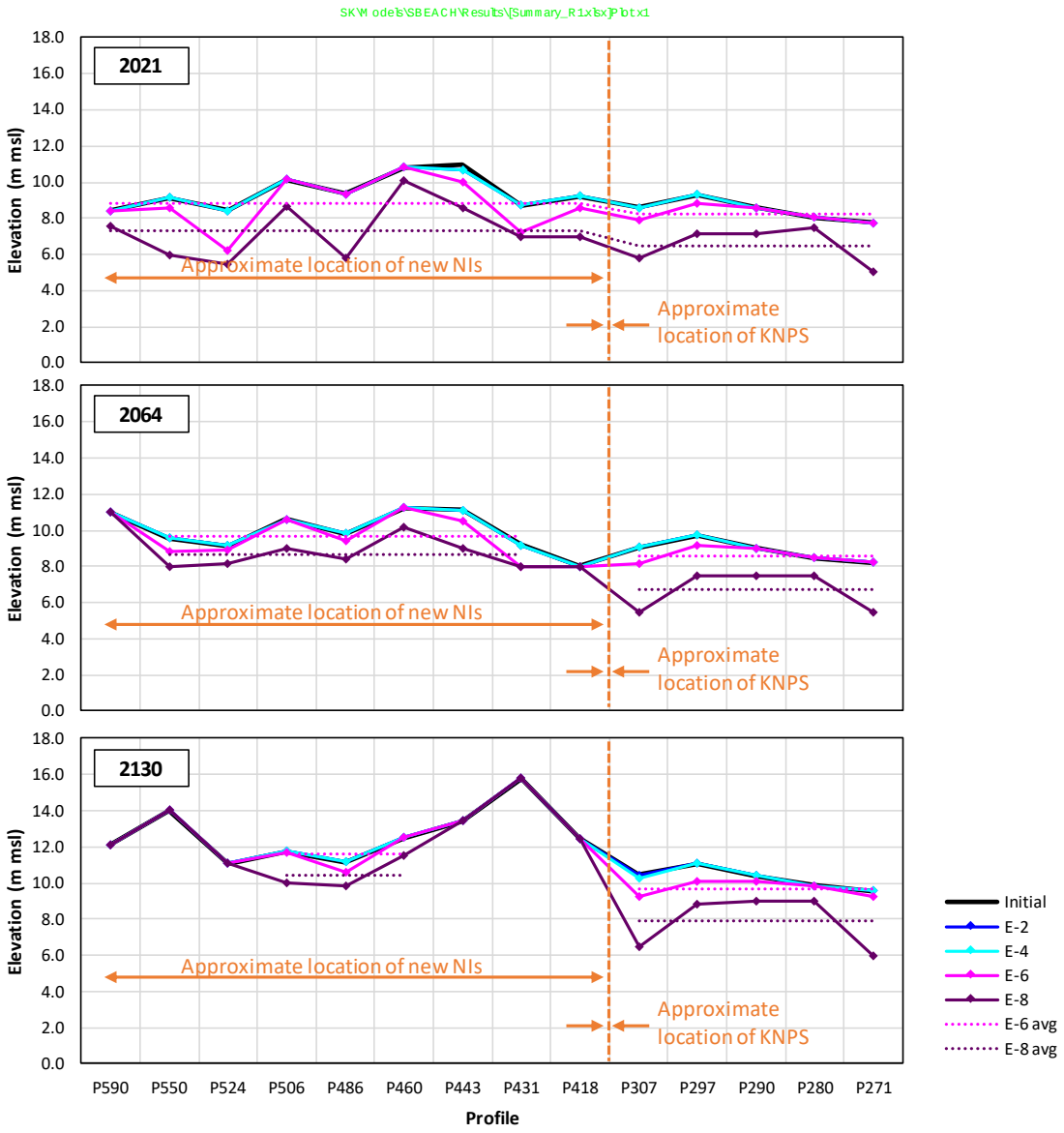


Figure 5.9.67: Vertical Erosion Analysis of Dune Crest Levels. For Each Return Period the Worst Combination of Storm Surge and Wave Height is Shown.

CONTROLLED DISCLOSURE

When downloaded from the EDS database, this document is uncontrolled and the responsibility rests with the user to ensure it is in line with the authorised version on the database.

Table 5.9.33: Truncation of Dune Crest Levels.

Date	Storm Exceedance Probability	Truncation Level	
		North of KNPS	South of KNPS
	(y^{-1})	(m msl)	(m msl)
2021	10^{-2}	-	-
	10^{-4}	-	-
	10^{-6}	8.8	8.2
	10^{-8}	7.4	6.5
2064	10^{-2}	-	-
	10^{-4}	-	-
	10^{-6}	9.6	8.6
	10^{-8}	8.7	6.7
2130	10^{-2}	-	-
	10^{-4}	-	-
	10^{-6}	11.6	9.7
	10^{-8}	10.4	7.9

From ***Figure 5.9.67*** the vertical dune erosion for the 10^{-2} and 10^{-4} exceedance probabilities (blue and cyan curves) were negligible for all of the dates and storm combinations modelled. For the 10^{-6} and 10^{-8} exceedance probabilities (magenta and purple curves) the average dune crests (dotted lines) were determined from the profiles north and south of the KNPS where notable erosion occurred.

These levels, as summarised in ***Table 5.9.33***, were used to schematically truncate the dune ridges to the average level after the cross-shore erosion by adjusting the bathymetries used for the storm wave run-up and drawdown modelling (***Subsection 5.9.11***). For example, ***Figure 5.9.75*** (excluding dune erosion) and ***Figure 5.9.76*** (including dune erosion) show the effect of the dune erosion due to the 10^{-8} erosion event for 2021. In this example the dune ridges are truncated to 7.4 and 6.5 m msl north and south of the KNPS respectively.

5.9.10.6 Resultant Coastline Stability

The total coastline change is the sum of the following components assessed in the subsections above:

- Long-term coastline trends (***Subsection 5.9.10.1***);
- Recession due to sea level rise (***Subsection 5.9.10.2***);
- Coastline changes due to wave rotation (***Subsection 5.9.10.4***);
- Cross-shore erosion (***Subsection 5.9.10.5***).

The resulting coastline stability for all exceedance probabilities is shown in ***Table 5.9.34*** and ***Table 5.9.35***, and the corresponding erosion lines for all modelled probabilities are plotted in ***Figure 5.9.68*** to ***Figure 5.9.72*** below.

CONTROLLED DISCLOSURE

When downloaded from the EDS database, this document is uncontrolled and the responsibility rests with the user to ensure it is in line with the authorised version on the database.

Table 5.9.34: Coastline Stability Adjacent to KNPS.

Exceedance Probability	Profile No.[a]	Long-term Trends		Sea Level Rise		Wave Rotation		Cross-Shore Erosion		Total Coastline Change[b]	
		(m)		(m)		(m)		(m)		(m from Baseline[c])	
(y^{-1})		2021	2064	2021	2064	2021	2064	2021	2064	2021	2064
10^{-2}	P271	0	40	0	-29	0	26	-35	-36	-35	1
	P280	0	40	0	-29	0	27	-34	-36	-34	2
	P290	0	40	0	-28	0	28	-42	-42	-42	-2
	P297	0	40	0	-27	0	29	-52	-52	-52	-10
	P307	0	40	0	-26	0	25	-54	-55	-54	-16
	P418	0	-17	0	-26	0	-41	-32	-32	-32	-116
	P431	0	-17	0	-29	0	-40	-59	-60	-59	-145
10^{-4}	P271	0	40	0	-29	0	26	-55	-56	-55	-19
	P280	0	40	0	-29	0	27	-52	-52	-52	-14
	P290	0	40	0	-28	0	28	-56	-56	-56	-16
	P297	0	40	0	-27	0	29	-68	-70	-68	-28
	P307	0	40	0	-26	0	25	-74	-73	-74	-34
	P418	0	-17	0	-26	0	-41	-56	-54	-56	-138
	P431	0	-17	0	-29	0	-40	-73	-74	-73	-159
10^{-5}	P271	0	40	0	-29	0	26	-66	-66	-66	-29
	P280	0	40	0	-29	0	27	-59	-60	-59	-22
	P290	0	40	0	-28	0	28	-65	-66	-65	-26
	P297	0	40	0	-27	0	29	-73	-74	-73	-32
	P307	0	40	0	-26	0	25	-77	-76	-77	-37
	P418	0	-17	0	-26	0	-41	-64	-62	-64	-146
	P431	0	-17	0	-29	0	-40	-80	-82	-80	-167
10^{-6}	P271	0	40	0	-29	0	26	-77	-76	-77	-39
	P280	0	40	0	-29	0	27	-66	-68	-66	-30
	P290	0	40	0	-28	0	28	-74	-76	-74	-36
	P297	0	40	0	-27	0	29	-78	-78	-78	-36
	P307	0	40	0	-26	0	25	-80	-79	-80	-40
	P418	0	-17	0	-26	0	-41	-72	-70	-72	-154
	P431	0	-17	0	-29	0	-40	-87	-90	-87	-175
10^{-7}	P271	0	40	0	-29	0	26	-181	-209	-181	-172
	P280	0	40	0	-29	0	27	-74	-75	-74	-37
	P290	0	40	0	-28	0	28	-80	-82	-80	-42
	P297	0	40	0	-27	0	29	-82	-83	-82	-41
	P307	0	40	0	-26	0	25	-120	-141	-120	-102
	P418	0	-17	0	-26	0	-41	-94	-79	-94	-163
	P431	0	-17	0	-29	0	-40	-98	-97	-98	-182
10^{-8}	P271	0	40	0	-29	0	26	-286	-343	-286	-306
	P280	0	40	0	-29	0	27	-82	-82	-82	-44
	P290	0	40	0	-28	0	28	-86	-88	-86	-48
	P297	0	40	0	-27	0	29	-86	-88	-86	-46
	P307	0	40	0	-26	0	25	-160	-203	-160	-164
	P418	0	-17	0	-26	0	-41	-116	-88	-116	-172
	P431	0	-17	0	-29	0	-40	-109	-104	-109	-189

Notes

(a) Refer to ***Figure 5.9.68*** to ***Figure 5.9.72*** below for locations of profiles.

(b) Defined as the most landward extent where any erosion (-ve) or accretion (+ve) occurs on the profile.

(c) At KNPS the baseline is parallel to the terrace and seaward of the intakes, as shown in ***Figure 5.9.68***.

CONTROLLED DISCLOSURE

When downloaded from the EDS database, this document is uncontrolled and the responsibility rests with the user to ensure it is in line with the authorised version on the database.

Table 5.9.35: Coastline Stability in Front of New NIs.

Exceedance Probability	Profile No.[a]	Long-term Trends (m)			Sea Level Rise (m)			Wave Rotation (m)			Cross-Shore Erosion (m)			Total Coastline Change[b] (m from Baseline[c])		
(y^{-1})		2021	2064	2130	2021	2064	2130	2021	2064	2130	2021	2064	2130	2021	2064	2130
10^{-2}	P418	0	-17	-44	0	-26	-107	0	-41	-96	-32	-32	-35	-32	-116	-281
	P431	0	-17	-44	0	-29	-117	0	-40	-92	-59	-60	-93	-59	-145	-346
	P443	0	-17	-44	0	-28	-113	0	-38	-88	-96	-95	-58	-96	-178	-303
	P460	0	-17	-44	0	-26	-107	0	-36	-83	-57	-55	-58	-57	-135	-292
	P486	0	-17	-44	0	-28	-113	0	-32	-75	-46	-49	-53	-46	-126	-285
	P506	0	-17	-44	0	-25	-103	0	-30	-69	-41	-43	-42	-41	-115	-257
	P524	0	-17	-44	0	-25	-102	0	-27	-63	-65	-63	-60	-65	-133	-269
	P550	0	-17	-44	0	-24	-97	0	-24	-56	-37	-36	-39	-37	-101	-235
	P590	0	-17	-44	0	-22	-92	0	-19	-44	-48	-47	-65	-48	-106	-244
10^{-4}	P418	0	-17	-44	0	-26	-107	0	-41	-96	-56	-54	-55	-56	-138	-301
	P431	0	-17	-44	0	-29	-117	0	-40	-92	-73	-74	-93	-73	-159	-346
	P443	0	-17	-44	0	-28	-113	0	-38	-88	-96	-95	-82	-96	-178	-327
	P460	0	-17	-44	0	-26	-107	0	-36	-83	-75	-75	-70	-75	-155	-304
	P486	0	-17	-44	0	-28	-113	0	-32	-75	-66	-69	-65	-66	-146	-297
	P506	0	-17	-44	0	-25	-103	0	-30	-69	-59	-59	-61	-59	-131	-276
	P524	0	-17	-44	0	-25	-102	0	-27	-63	-71	-71	-73	-71	-141	-282
	P550	0	-17	-44	0	-24	-97	0	-24	-56	-63	-62	-67	-63	-127	-263
	P590	0	-17	-44	0	-22	-92	0	-19	-44	-64	-65	-69	-64	-124	-248
10^{-5}	P418	0	-17	-44	0	-26	-107	0	-41	-96	-64	-62	-67	-64	-146	-313
	P431	0	-17	-44	0	-29	-117	0	-40	-92	-80	-82	-97	-80	-167	-350
	P443	0	-17	-44	0	-28	-113	0	-38	-88	-97	-97	-90	-97	-180	-335
	P460	0	-17	-44	0	-26	-107	0	-36	-83	-82	-82	-80	-82	-162	-314
	P486	0	-17	-44	0	-28	-113	0	-32	-75	-73	-75	-73	-73	-152	-305
	P506	0	-17	-44	0	-25	-103	0	-30	-69	-66	-67	-69	-66	-139	-284
	P524	0	-17	-44	0	-25	-102	0	-27	-63	-107	-77	-77	-107	-147	-286
	P550	0	-17	-44	0	-24	-97	0	-24	-56	-68	-67	-70	-68	-132	-266
	P590	0	-17	-44	0	-22	-92	0	-19	-44	-69	-71	-74	-69	-130	-253
10^{-6}	P418	0	-17	-44	0	-26	-107	0	-41	-96	-72	-70	-79	-72	-154	-325
	P431	0	-17	-44	0	-29	-117	0	-40	-92	-87	-90	-101	-87	-175	-354
	P443	0	-17	-44	0	-28	-113	0	-38	-88	-98	-99	-98	-98	-182	-343
	P460	0	-17	-44	0	-26	-107	0	-36	-83	-89	-89	-90	-89	-169	-324
	P486	0	-17	-44	0	-28	-113	0	-32	-75	-80	-81	-81	-80	-158	-313
	P506	0	-17	-44	0	-25	-103	0	-30	-69	-73	-75	-77	-73	-147	-292
	P524	0	-17	-44	0	-25	-102	0	-27	-63	-143	-83	-81	-143	-153	-290
	P550	0	-17	-44	0	-24	-97	0	-24	-56	-73	-72	-73	-73	-137	-269
	P590	0	-17	-44	0	-22	-92	0	-19	-44	-74	-77	-79	-74	-136	-258
10^{-7}	P418	0	-17	-44	0	-26	-107	0	-41	-96	-94	-79	-83	-94	-163	-329
	P431	0	-17	-44	0	-29	-117	0	-40	-92	-98	-97	-103	-98	-182	-356
	P443	0	-17	-44	0	-28	-113	0	-38	-88	-101	-102	-104	-101	-185	-349
	P460	0	-17	-44	0	-26	-107	0	-36	-83	-92	-92	-94	-92	-172	-328
	P486	0	-17	-44	0	-28	-113	0	-32	-75	-114	-86	-87	-114	-163	-319
	P506	0	-17	-44	0	-25	-103	0	-30	-69	-77	-78	-81	-77	-150	-296
	P524	0	-17	-44	0	-25	-102	0	-27	-63	-143	-104	-93	-143	-174	-302
	P550	0	-17	-44	0	-24	-97	0	-24	-56	-115	-84	-85	-115	-149	-281
	P590	0	-17	-44	0	-22	-92	0	-19	-44	-82	-84	-84	-82	-143	-263

CONTROLLED DISCLOSURE

When downloaded from the EDS database, this document is uncontrolled and the responsibility rests with the user to ensure it is in line with the authorised version on the database.

10^{-8}	P418	0	-17	-44	0	-26	-107	0	-41	-96	-116	-88	-87	-116	-172	-333
	P431	0	-17	-44	0	-29	-117	0	-40	-92	-109	-104	-105	-109	-189	-358
	P443	0	-17	-44	0	-28	-113	0	-38	-88	-104	-105	-110	-104	-188	-355
	P460	0	-17	-44	0	-26	-107	0	-36	-83	-95	-95	-98	-95	-175	-332
	P486	0	-17	-44	0	-28	-113	0	-32	-75	-148	-91	-93	-148	-168	-325
	P506	0	-17	-44	0	-25	-103	0	-30	-69	-81	-81	-85	-81	-153	-300
	P524	0	-17	-44	0	-25	-102	0	-27	-63	-143	-125	-105	-143	-195	-314
	P550	0	-17	-44	0	-24	-97	0	-24	-56	-157	-96	-96	-157	-161	-292
	P590	0	-17	-44	0	-22	-92	0	-19	-44	-90	-91	-89	-90	-150	-268

Notes

(a) Refer to ***Figure 5.9.68*** to ***Figure 5.9.72*** below for locations of profiles.

(b) Defined as the most landward extent where any erosion (-ve) or accretion (+ve) occurs on the profile.

(c) At the new NIs the baseline corresponds to the present-day +2 m msl contour, as shown in ***Figure 5.9.70***.

The pre-storm topography and the erosion lines in front of KNPS and the new NIs for the 10^{-2}, 10^{-4}, 10^{-6} and 10^{-8} y^{-1} storms for all modelled years are plotted in ***Figure 5.9.68*** to ***Figure 5.9.72***. The erosion lines are defined as the line drawn in horizontal (x,y) space demarcating the most landward extent where any erosion or accretion of the topography occurs. For each return period the worst combination of storm surge and wave height is shown, i.e., the most landward extent of erosion.

CONTROLLED DISCLOSURE

When downloaded from the EDS database, this document is uncontrolled and the responsibility rests with the user to ensure it is in line with the authorised version on the database.

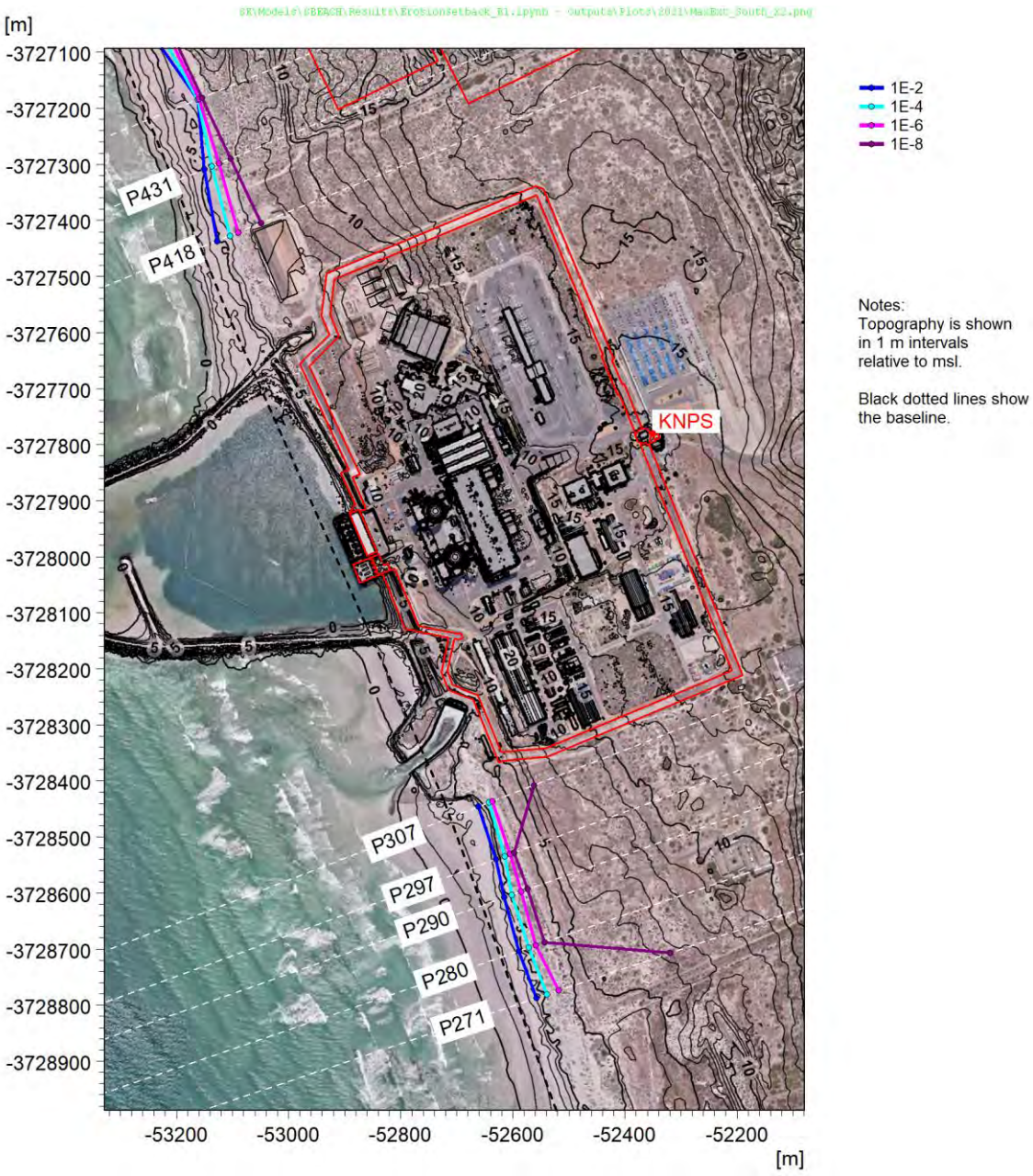


Figure 5.9.68: Pre-storm Topography and Erosion Lines for 2021 for the 10^{-2}, 10^{-4}, 10^{-6} and 10^{-8} y^{-1} Storms in Front of the KNPS.

CONTROLLED DISCLOSURE

When downloaded from the EDS database, this document is uncontrolled and the responsibility rests with the user to ensure it is in line with the authorised version on the database.

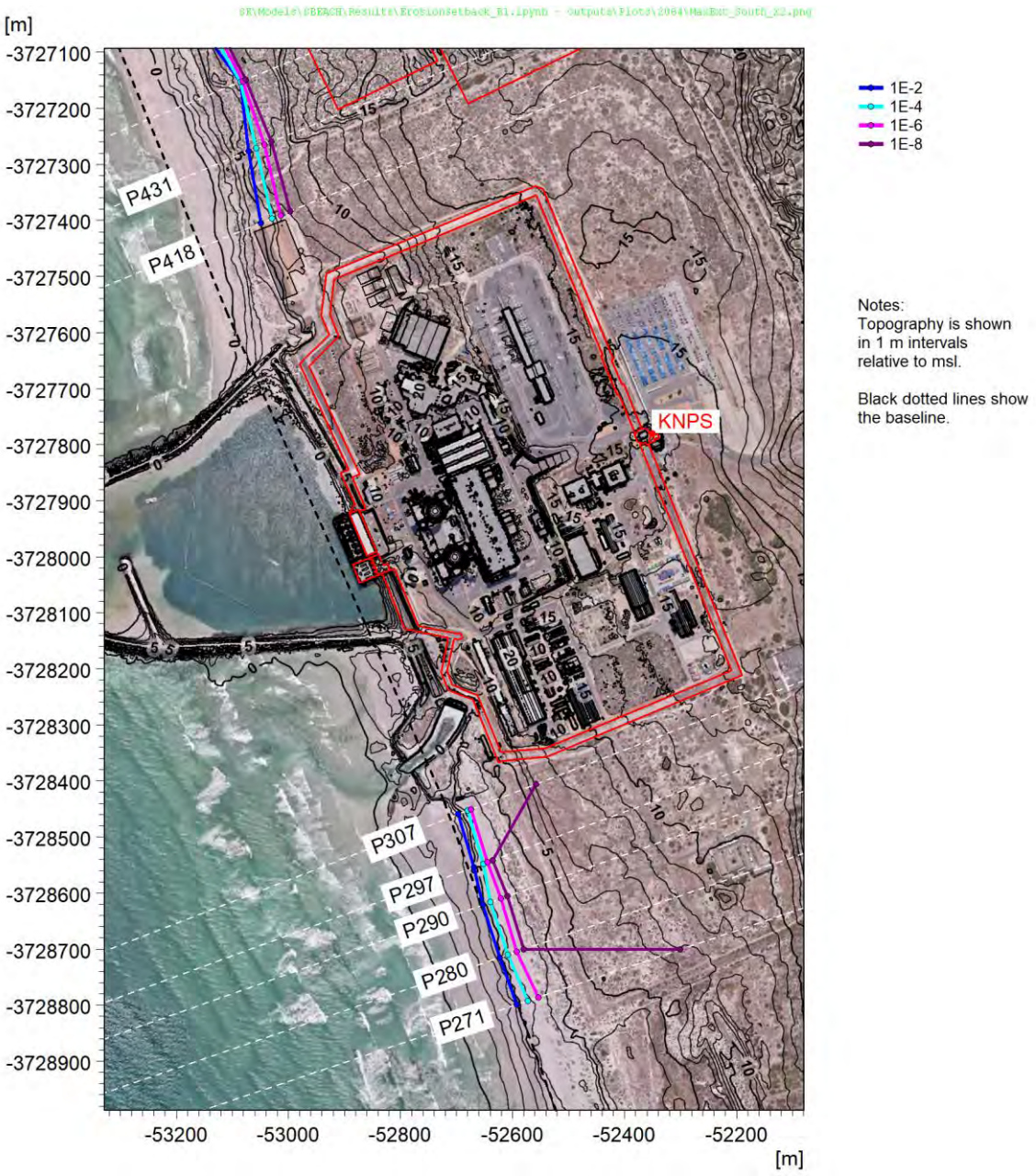


Figure 5.9.69: Adjusted Pre-storm Topography and Erosion Lines for 2064 for the 10^{-2}, 10^{-4}, 10^{-6} and 10^{-8} y^{-1} Storms in Front of the KNPS.

CONTROLLED DISCLOSURE

When downloaded from the EDS database, this document is uncontrolled and the responsibility rests with the user to ensure it is in line with the authorised version on the database.

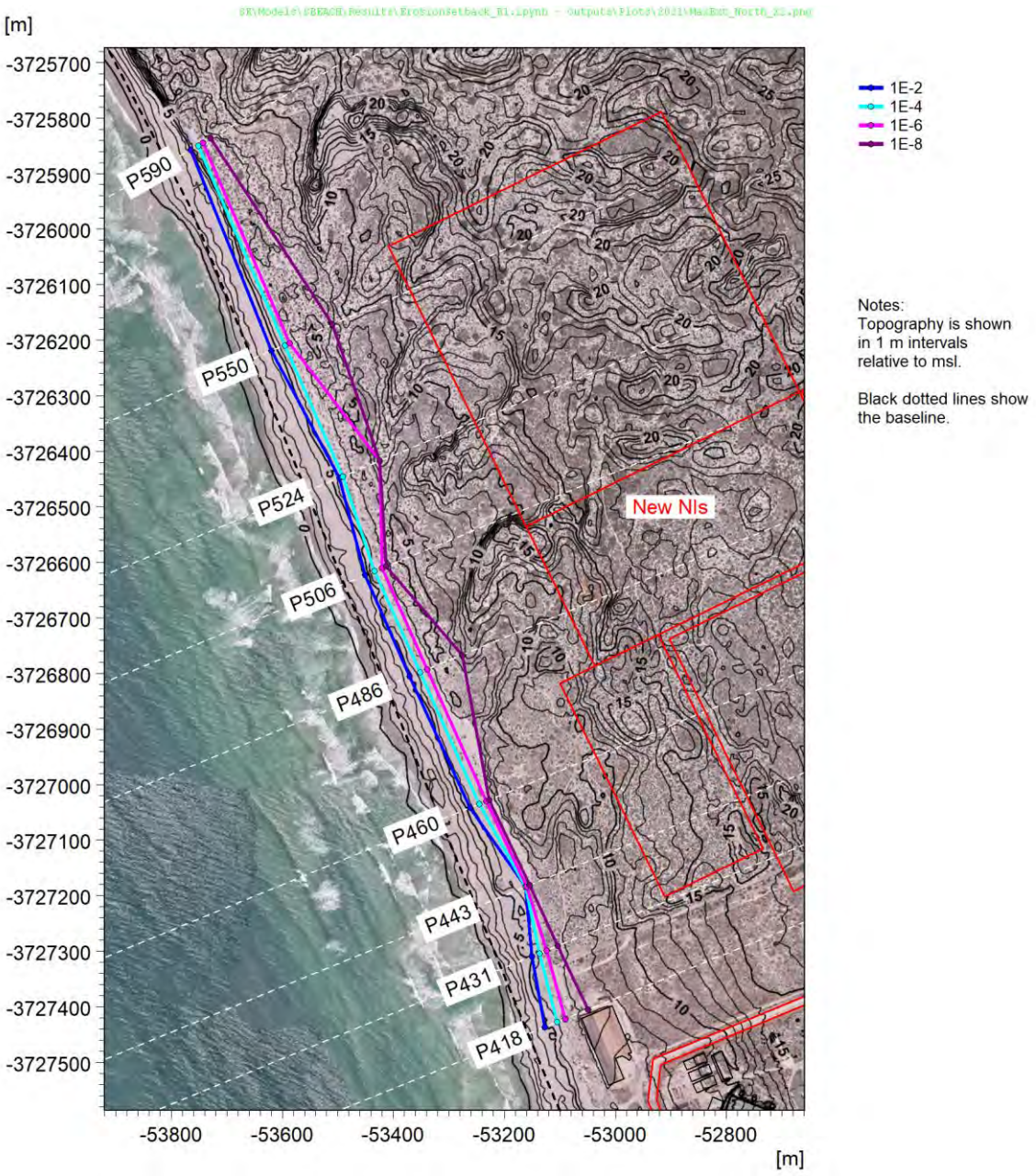


Figure 5.9.70: Pre-storm Topography and Erosion Lines for 2021 for the 10^{-2}, 10^{-4}, 10^{-6} and 10^{-8} y^{-1} Storms in Front of the New NIs.

CONTROLLED DISCLOSURE

When downloaded from the EDS database, this document is uncontrolled and the responsibility rests with the user to ensure it is in line with the authorised version on the database.

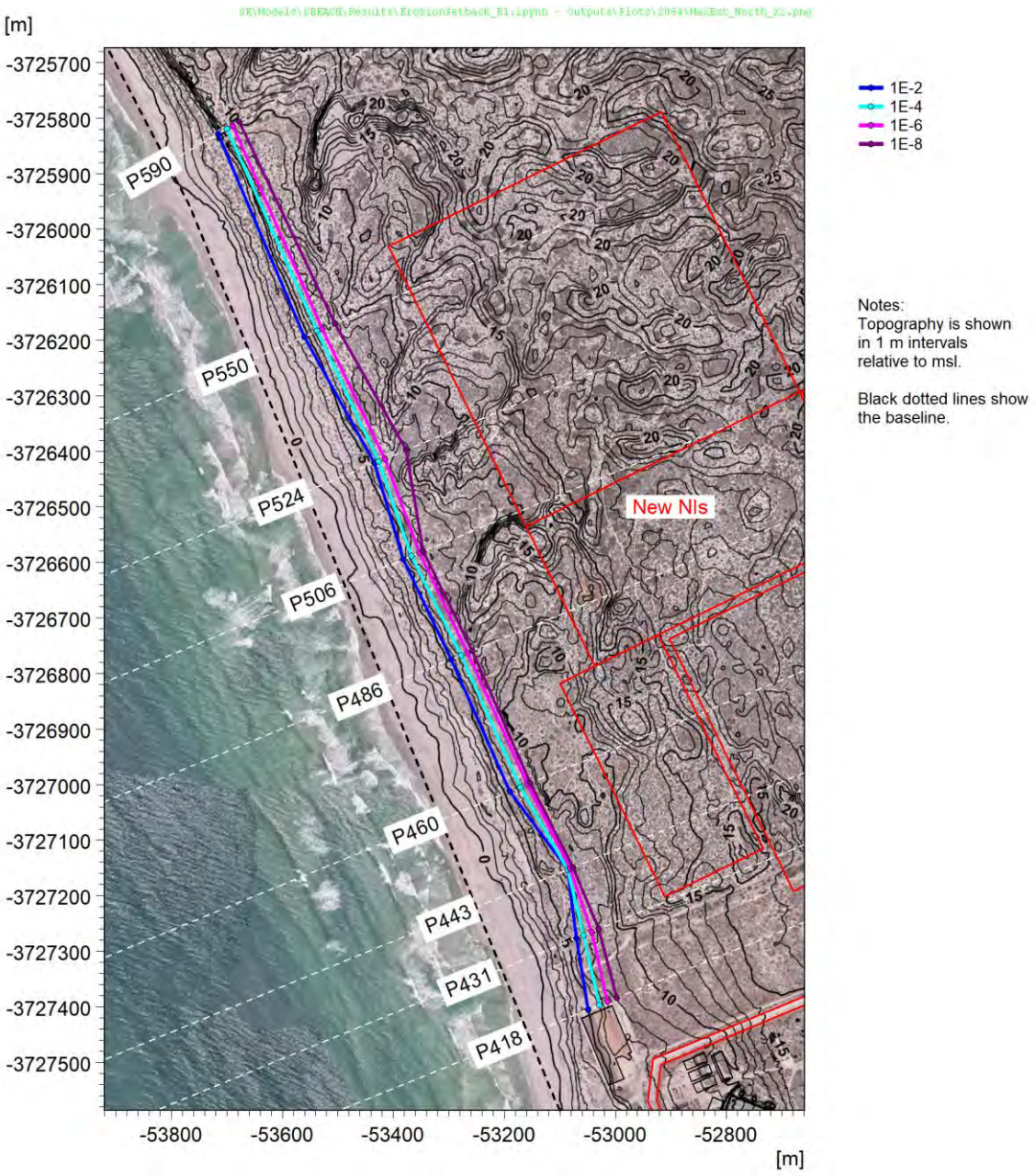


Figure 5.9.71: Adjusted Pre-storm Topography and Erosion Lines for 2064 for the 10^{-2}, 10^{-4}, 10^{-6} and 10^{-8} y^{-1} Storms in Front of the New NIs.

CONTROLLED DISCLOSURE

When downloaded from the EDS database, this document is uncontrolled and the responsibility rests with the user to ensure it is in line with the authorised version on the database.

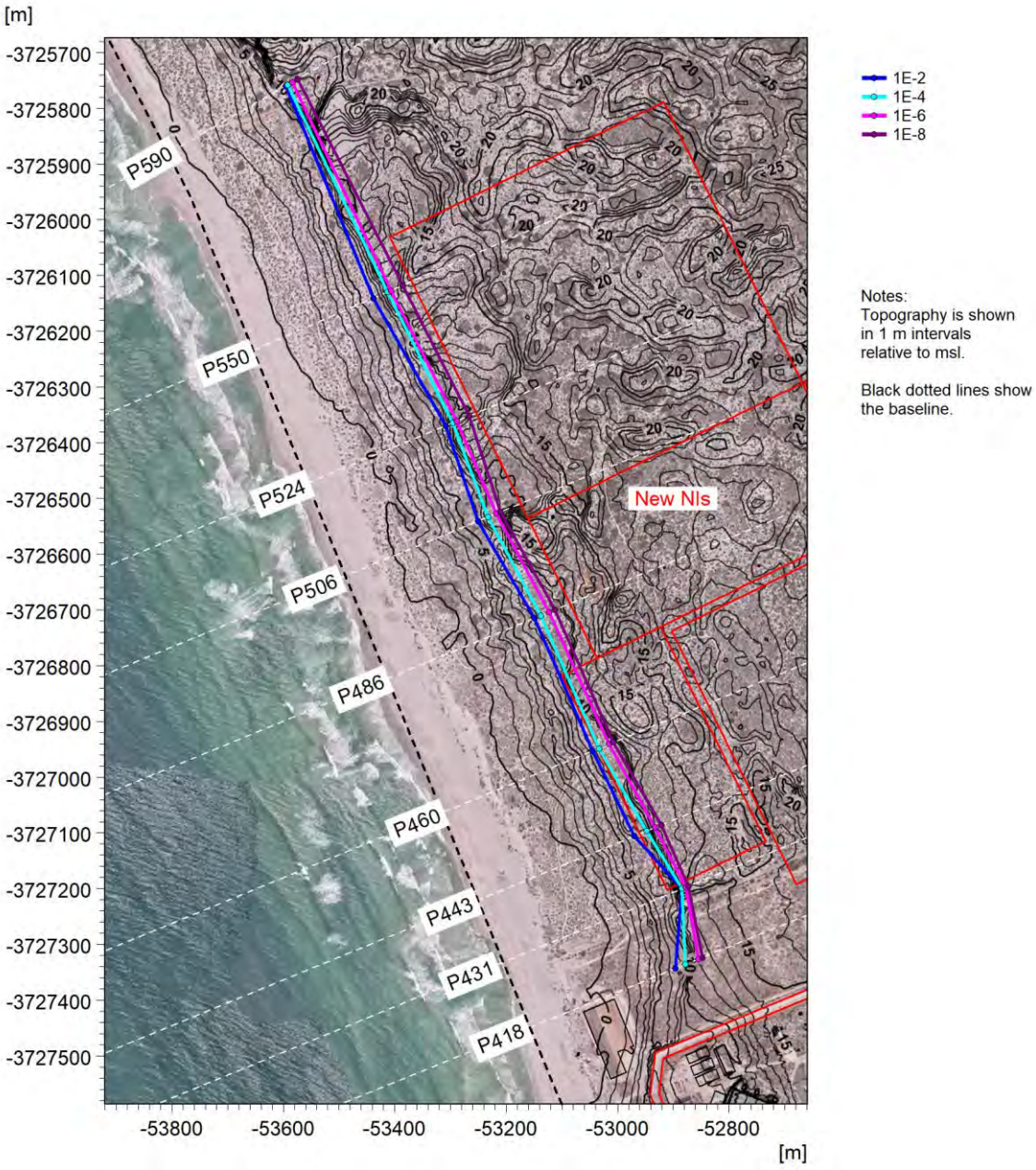


Figure 5.9.72: Adjusted Pre-storm Topography and Erosion Lines for 2130 for the 10^{-2}, 10^{-4}, 10^{-6} and 10^{-8} y^{-1} Storms in Front of the New NIs.

Table 5.9.36 summarises the maximum coastline erosion at KNPS and the new NIs.

CONTROLLED DISCLOSURE

When downloaded from the EDS database, this document is uncontrolled and the responsibility rests with the user to ensure it is in line with the authorised version on the database.

Table 5.9.36: Maximum Coastline Erosion Adjacent to KNPS and in Front of New NIs.

Exceedance Probability	Total Coastline Erosion[(a)] Adjacent to KNPS)		Total Coastline Erosion[(a)] in Front of New NIs		
(y^{-1})	(m from Baseline[(b)])		(m from Baseline[(c)])		
	2021	2064	2021	2064	2130
10^{-2}	-59	-145	-96	-178	-346
10^{-4}	-74	-159	-96	-178	-346
10^{-5}	-80	-167	-107	-180	-350
10^{-6}	-87	-175	-143	-182	-354
10^{-7}	-181	-182	-143	-185	-356
10^{-8}	-286	-306	-157	-195	-358

Note:
(a) Defined as the most landward extent where any erosion occurs.
(b) At KNPS the baseline is parallel to the terrace and seaward of the intakes.
(c) At the new NIs the baseline corresponds to the present-day +2 m msl contour.

These results show the following:

- The coastline erosion increases over time due to long-term coastline trends, sea level rise and larger waves.
- At KNPS the maximum coastline erosion occurred on the northern side of the site, except for the 10^{-8} y^{-1} storm where the dune ridge was breached south of KNPS. Further engineering studies should be undertaken to ensure that the breakwater and outfall structures at KNPS can withstand the predicted erosion over the operating life of the plant.
- The coastline erosion is generally larger at the new NIs than KNPS, but does not reach the estimated position of the new NIs for 2021 and 2064. For 2130 the southern section the new NIs are eroded for all exceedance probabilities modelled.
- Note that these erosion lines show the extent of erosion of the topography which will threaten safety related structures, systems and components (SSCs) at these locations. Wave run-up and flooding due to storm waves or tsunamis will extend further inland than these erosion lines. Flooding is assessed in the following sections.
- Note that the assessment of coastline erosion is based on the sea level rise (SLR) corresponding to the RCP8.5 upper end of likely range (0.44 m in 2064 and 1.80 m in 2130), rather than the maximum plausible SLR (0.79 m in 2064 and 3.26 m in 2130). This additional 0.35 m in the case of KNPS and 1.5 m in the case of the new NIs should be considered during the SAR and engineering design phase, either as safety buffer or as part of an adaptive design strategy.

CONTROLLED DISCLOSURE

When downloaded from the EDS database, this document is uncontrolled and the responsibility rests with the user to ensure it is in line with the authorised version on the database.

5.9.11 Storm Wave Run-Up and Drawdown

5.9.11.1 Introduction

This section describes the wave modelling undertaken to estimate the maximum vertical run-up, maximum horizontal inundation and minimum vertical drawdown due to storms at both the existing KNPS and the new NIs. These results are compared to the equivalent tsunami results (see ***Subsection 5.9.12***) to determine the extreme flooding from the sea (see ***Subsections 5.9.13***) and the extreme low water levels at the cooling water intakes (see ***Subsection 5.9.14***).

5.9.11.2 Model Description

The MIKE 3 Wave model was used for the wave run-up and drawdown modelling. The details of the physical processes and numerical implementation are provided in the model documentation (see ***Table 5.9.7***), while details of the model setup, sensitivity testing, and V&V are provided in the V&V Report (PRDW, 2022b).

The MIKE 3 Wave is a phase-resolving wave model based on the 3D Navier-Stokes equations. An unstructured (flexible) mesh is used in the horizontal dimension with sigma layers in the vertical. The model includes the following processes:

- Wave refraction;
- Wave diffraction;
- Bottom friction;
- Non-linear wave transformation;
- Surf and swash zone hydrodynamics;
- Wave breaking and run-up;
- Wave overtopping;
- Coastal flooding;
- Wave transmission (and reflection) through porous structures.

The model is based on the numerical solution of the three-dimensional incompressible Reynolds-averaged Navier-Stokes equations. Thus, the model consists of continuity and momentum equations, and it is closed by a k-ε turbulence closure scheme in the vertical and horizontal. The free surface is taken into account using a sigma coordinate transformation approach. The spatial discretization of the governing equations in conserved form is performed using a cell-centred finite volume method. The time integration is performed using a semi-implicit scheme. The vertical

When downloaded from the EDS database, this document is uncontrolled and the responsibility rests with the user to ensure it is in line with the authorised version on the database.

convective and diffusion terms are discretized using an implicit scheme to remove the stability limitations associated with the vertical resolution. The remaining terms are discretized using a second-order explicit Runge-Kutta scheme. The projection method is employed for the non-hydrostatic pressure. The interface convective fluxes are calculated using a HLLC approximate Riemann solver. This shock-capturing scheme enables robust and stable simulation of flows involving shocks or discontinuities such as bores and hydraulic jumps. This is essential for modelling of waves in the breaking zone or porous structures. The numerical dissipation accounts for the dissipation in the breaking waves.

5.9.11.3 Model Setup

The model domain and bathymetry are shown in ***Figure 5.9.73***. The wave generation line was placed along the -31 m msl contour, with the offshore boundary extending seaward of this for a minimum of 400 m to accommodate the wave relaxation zone for wave generation and absorption. The bathymetry behind the generation line was artificially flattened to -31 m msl to aid in the stability of the wave generation. The model extends landwards to approximately +17 m msl.

The model mesh comprises triangles with a resolution varying between approximately 23 m offshore and approximately 7 m nearshore. This resulted in a resolution of approximately 11 points per wavelength in the surf-zone. The vertical mesh comprises three sigma layers with the bottom layer comprising 50%, the middle layer 30% and the surface layer 20% of the water column. A detailed view of the mesh presented in ***Figure 5.9.74***.

CONTROLLED DISCLOSURE

When downloaded from the EDS database, this document is uncontrolled and the responsibility rests with the user to ensure it is in line with the authorised version on the database.

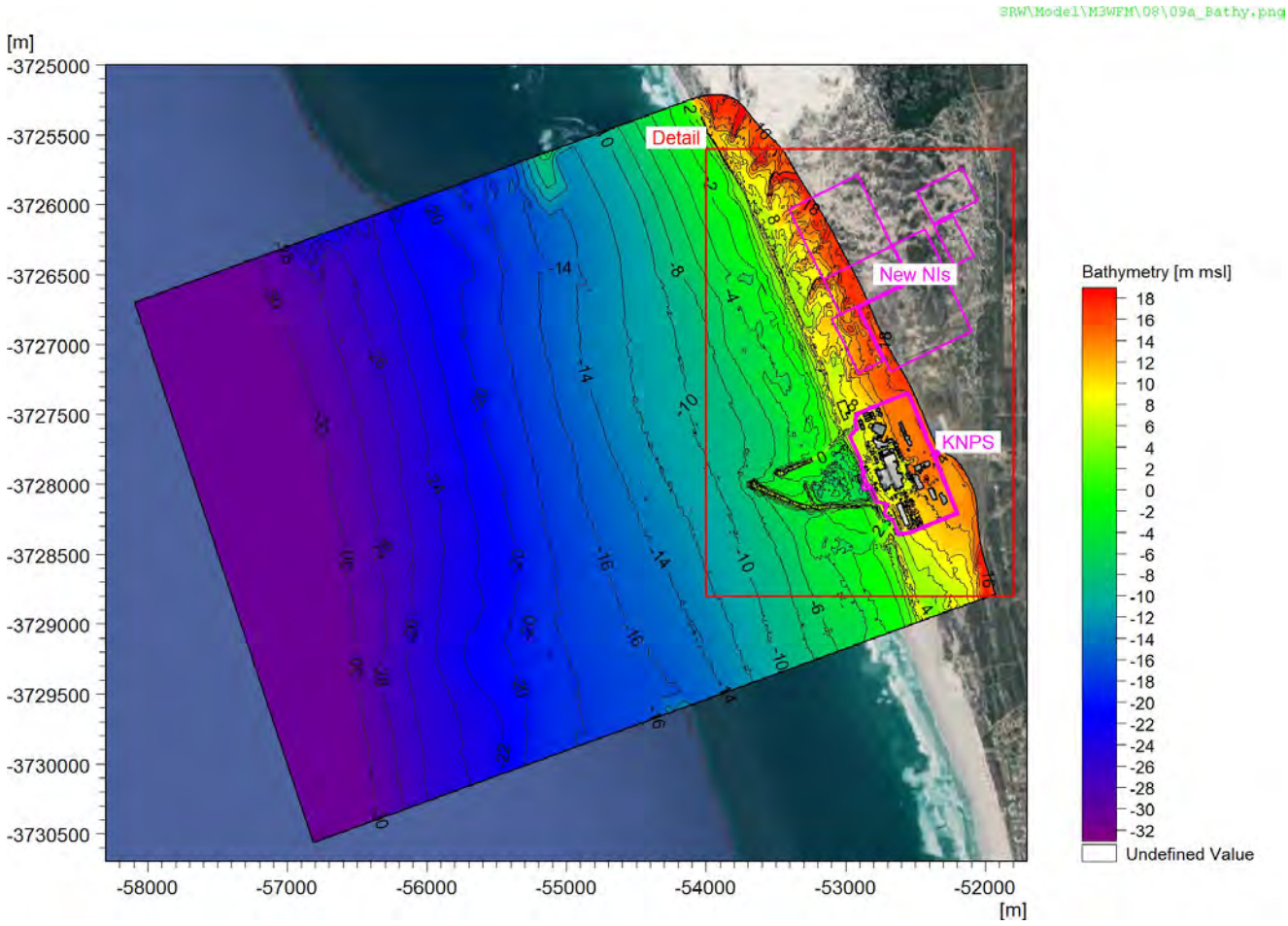


Figure 5.9.73: MIKE 3 Wave Model Domain and Bathymetry

CONTROLLED DISCLOSURE

When downloaded from the EDS database, this document is uncontrolled and the responsibility rests with the user to ensure it is in line with the authorised version on the database.



Figure 5.9.74: Detail of MIKE 3 Wave Model Mesh.

Three base bathymetries were applied for the three years modelled (2021, 2064 and 2130). For 2021 the existing bathymetry was used. For 2064 and 2130, the coastline position was adjusted to account for climate change and long-term trends as described in ***Subsection 5.9.10***. Additionally, based on the cross-shore erosion modelling an eroded dune profile was applied for the 10^{-6} and 10^{-8} y^{-1} storm events (see ***Subsection 5.9.10.5***). This resulted in a total of nine different bathymetries used in the model runs. ***Figure 5.9.75*** to ***Figure 5.9.77*** show four examples of the model bathymetry in front of KNPS and the new NIs.

CONTROLLED DISCLOSURE

When downloaded from the EDS database, this document is uncontrolled and the responsibility rests with the user to ensure it is in line with the authorised version on the database.

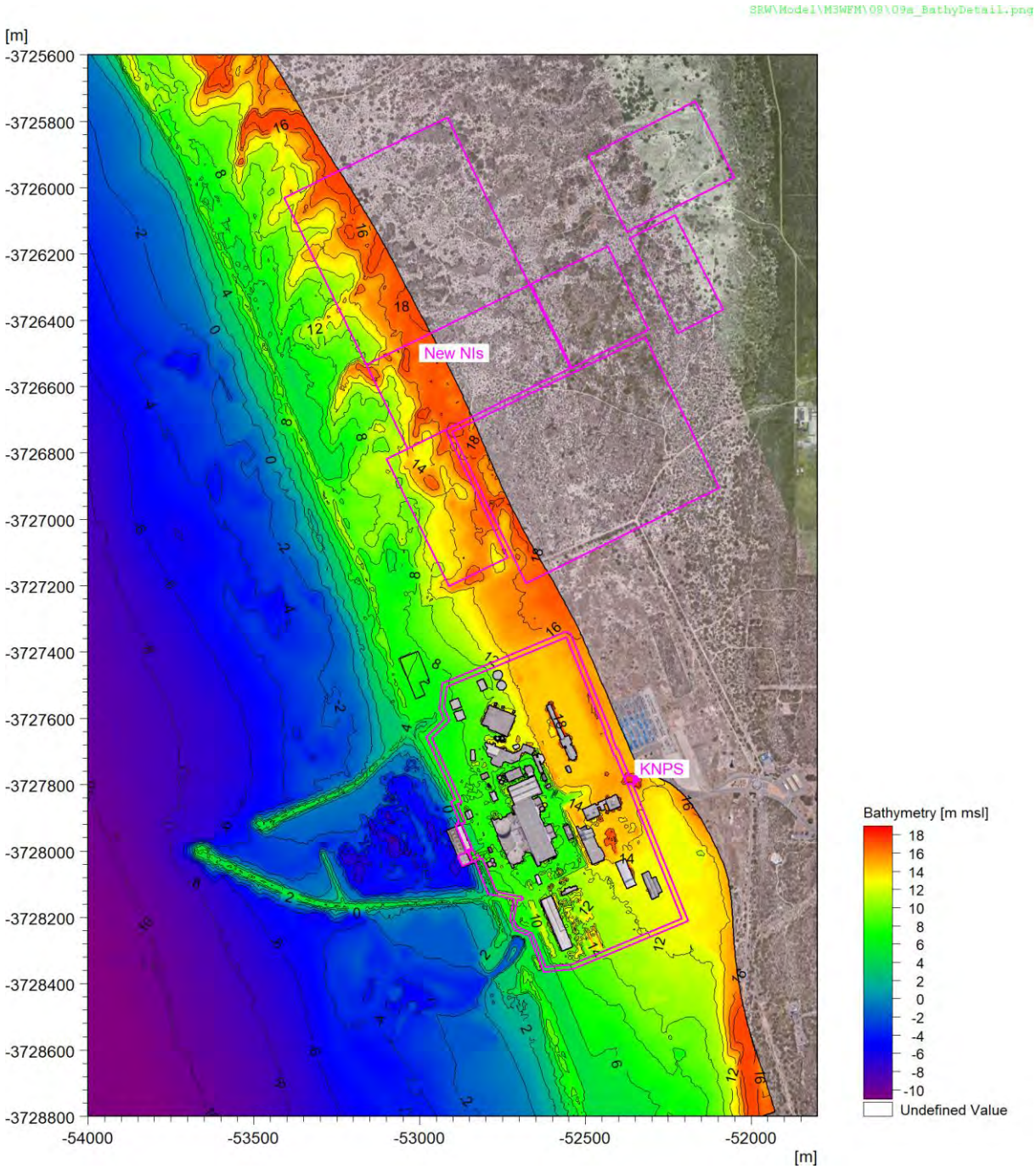


Figure 5.9.75: Detail of Model Bathymetry for 2021 for Storm Exceedance Probabilities of 10^{-2} and 10^{-4} y^{-1} (Excluding Dune Erosion).

CONTROLLED DISCLOSURE

When downloaded from the EDS database, this document is uncontrolled and the responsibility rests with the user to ensure it is in line with the authorised version on the database.

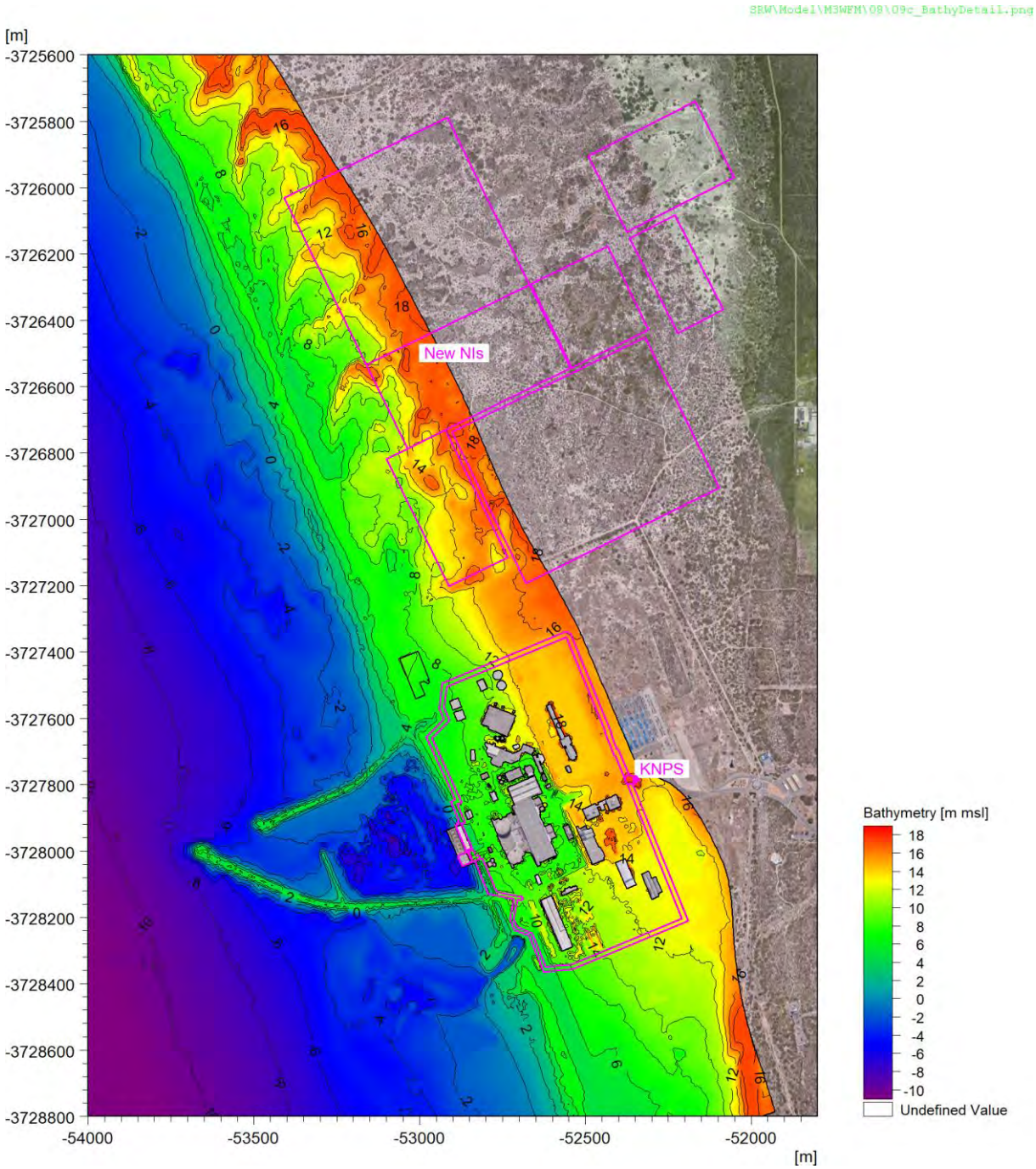


Figure 5.9.76: Detail of Model Bathymetry for 2021 for Storm Exceedance Probability of 10^{-8} y^{-1} (Including Dune Erosion).

CONTROLLED DISCLOSURE

When downloaded from the EDS database, this document is uncontrolled and the responsibility rests with the user to ensure it is in line with the authorised version on the database.

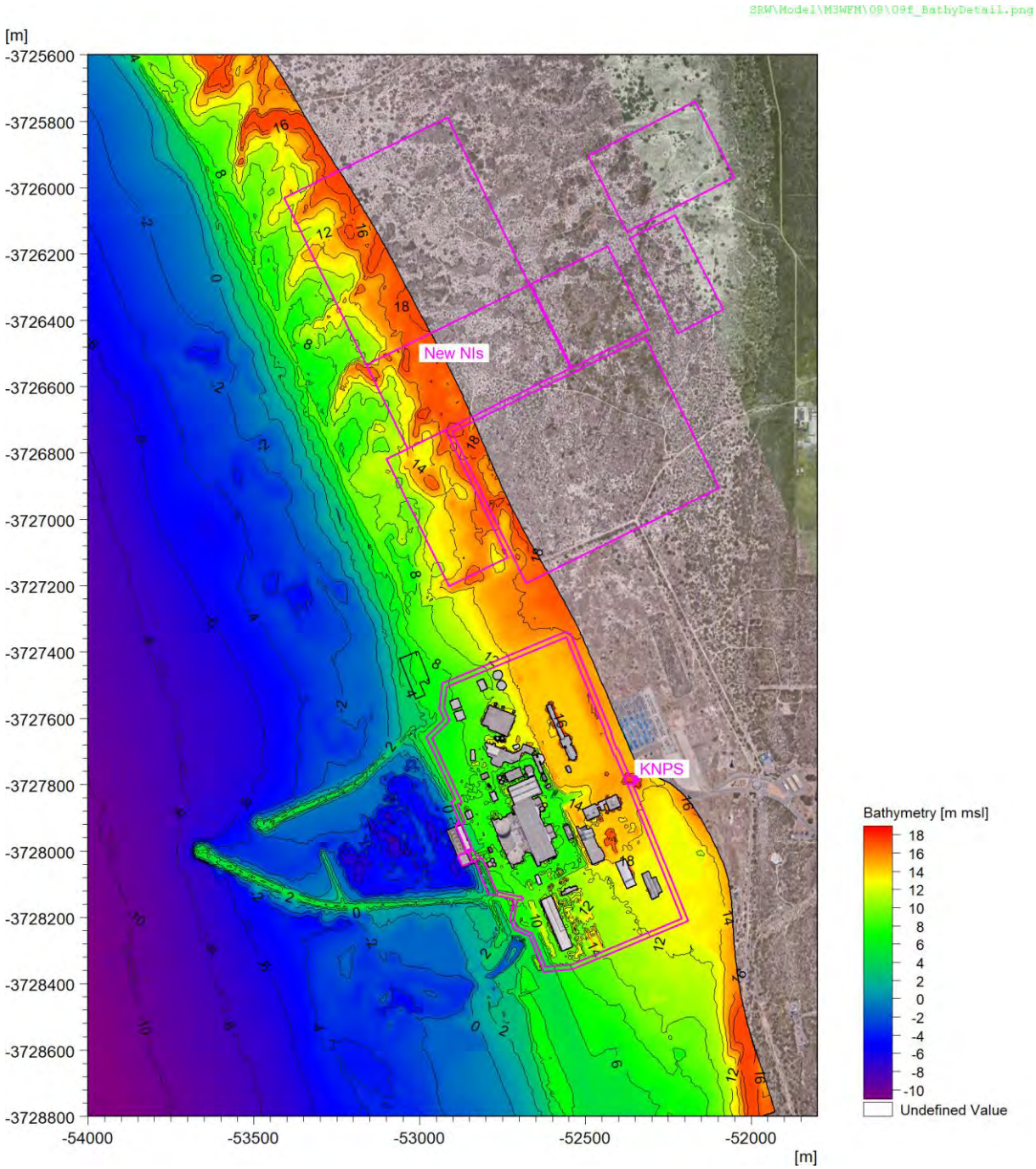


Figure 5.9.77: Detail of Model Bathymetry for 2064 for Storm Exceedance Probabilities of 10^{-8} (Including Dune Erosion).

CONTROLLED DISCLOSURE

When downloaded from the EDS database, this document is uncontrolled and the responsibility rests with the user to ensure it is in line with the authorised version on the database.

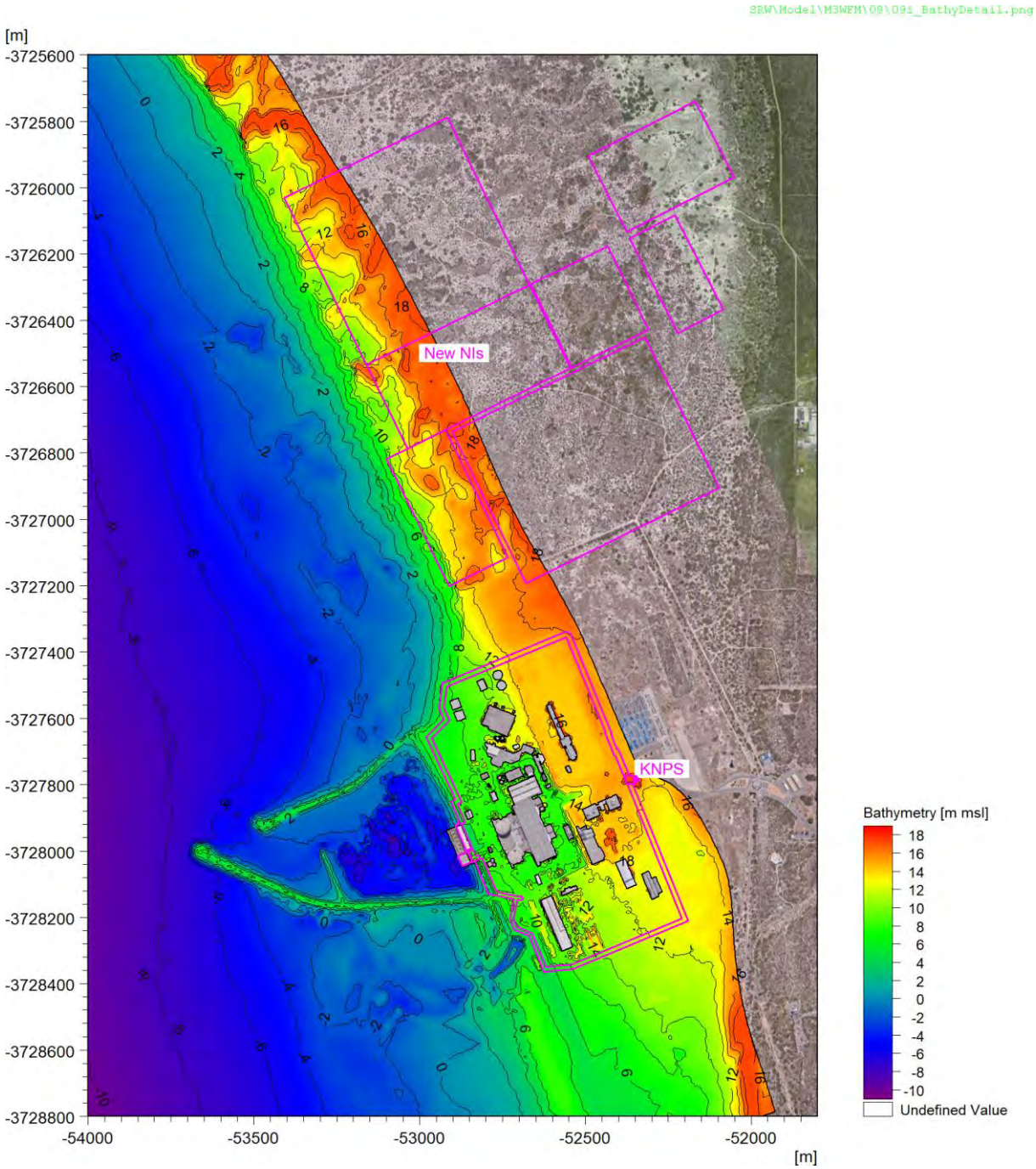


Figure 5.9.78: Detail of Model Bathymetry for 2130 for Storm Exceedance Probabilities of 10^{-8} (Including Dune Erosion).

For each surface type in the model domain the corresponding Manning roughness was estimated from literature as described in detail in (PRDW, 2022a). These were then converted to a roughness height (k_s) for use in the MIKE 3 Wave model, as shown in ***Table 5.9.37***.

CONTROLLED DISCLOSURE

When downloaded from the EDS database, this document is uncontrolled and the responsibility rests with the user to ensure it is in line with the authorised version on the database.

Table 5.9.37: Bottom Roughness Applied in Wave Model.

Surface Cover Type	Manning's M [(a)] ($m^{1/3}/s$)	Roughness Height k_s [(b)] (m)
Sandy seabed	32	0.25
Vegetated areas	26	0.869
Rubble-mound rock structures	20	4.196
Paved surfaces	62.5	0.005

Notes:

(a) Manning's M is the reciprocal of the generally used Manning's n. Larger values of Manning's M correspond to lower bed roughness.

(b) k_s can be related to M through the equation $M = \frac{25.4}{k_s^{1/6}}$ (DHI, 2021k).

5.9.11.4 Model Calibration

The modelled run-up level was calibrated against the debris line measured on the beach in front of the new NIs on 14 April 2021. The model was used to simulate the wave run-up during the storm of 7 June 2017 (H_{m0} = 9.4 m and T_p = 16.5 s at -31 m msl), which is the largest storm in the last five years and thus likely to have defined the debris line. The results are shown in ***Figure 5.9.79***. The maximum level reached by the debris line was approximately +7.2 m msl, while the modelled run-up reached +7.0 m msl. The maximum modelled horizontal inundation ranged between being 28 m seaward of the debris line to 12 m landward of the debris line. Some of these differences can be explained by localised changes in the beach between the 2017 storm and the 2021 LiDAR survey used in the model.

CONTROLLED DISCLOSURE

When downloaded from the EDS database, this document is uncontrolled and the responsibility rests with the user to ensure it is in line with the authorised version on the database.

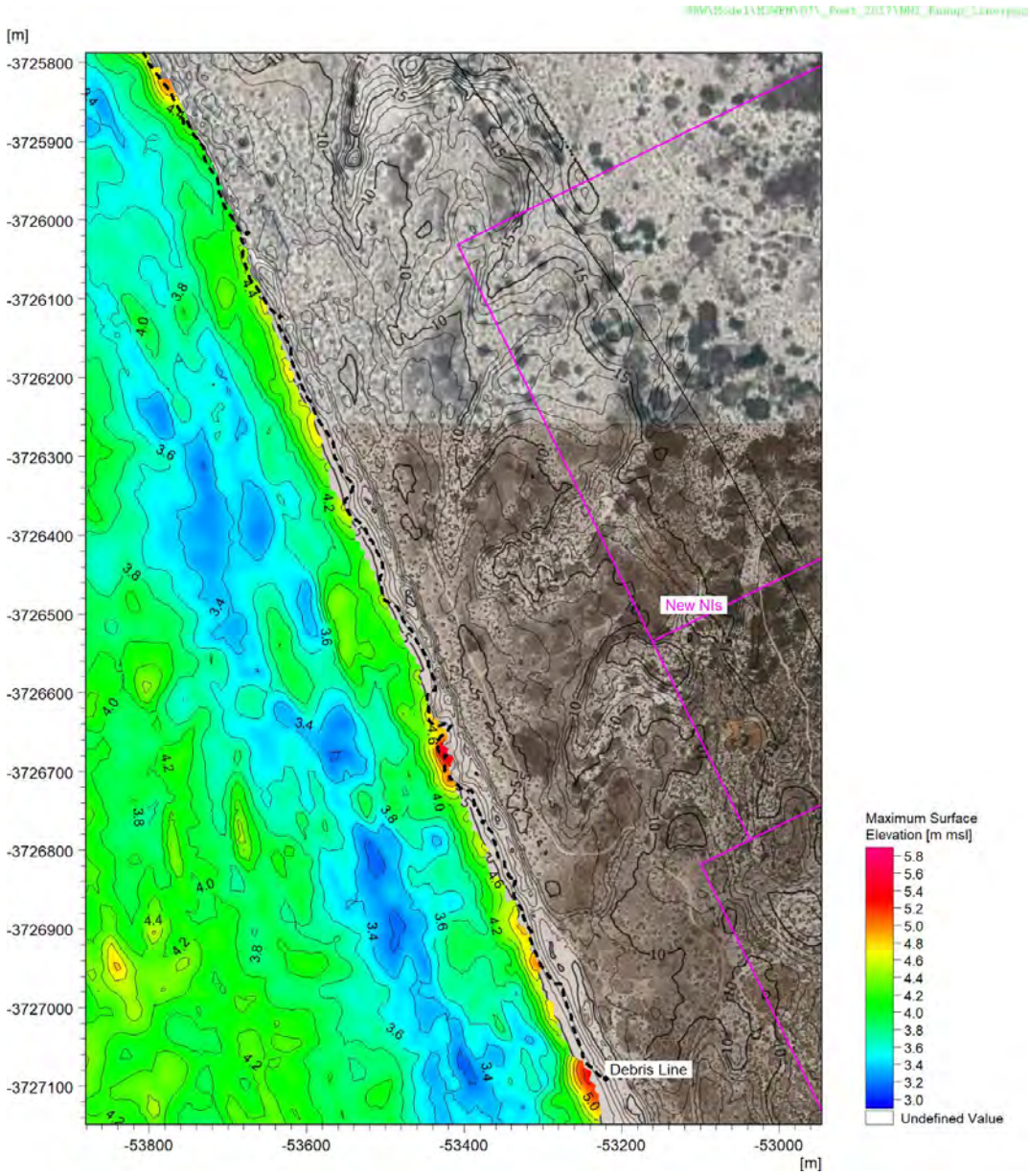


Figure 5.9.79: Maximum Modelled Water Surface Elevation During 7 June 2017 Storm and Measured Debris Line.

The model was also calibrated against measured water levels inside the KNPS intake basin (see ***Subsection 5.9.6.1***) during a storm event on 13 July 2020 (although the storm peaked at H_{m0} = 8.9 m, the waves at the closest high tide were modelled: H_{m0} = 7.6 m and T_p = 17.0 s at -29 m msl).

Figure 5.9.80 shows the time-series of measured and modelled water levels inside the KNPS basin over the 2-hour simulation at the peak of the storm. Note that it is not expected to model the exact measured time-series as the water level time-series applied at the model boundary is generated from the specified wave spectrum using random phasing. The time-series

CONTROLLED DISCLOSURE

When downloaded from the EDS database, this document is uncontrolled and the responsibility rests with the user to ensure it is in line with the authorised version on the database.

shows that the 17 s swell is insignificant inside the basin and the water levels are dominated by longer period bound infragravity waves, surf-beat and basin seiching (resonance). An analysis of the model results (PRDW, 2021) showed that the maximum and minimum water levels were within 10% of the measurements.

Figure 5.9.81 shows measured and modelled frequency spectra inside the KNPS basin during the same storm. The results show that the model generally does well at capturing the basin resonance modes at 85 s (0.0118 Hz), 114 s (0.0088 Hz), and 170 s (0.0059 Hz) as well as capturing the Helmholtz mode at approximately 17 mins (0.00098 Hz).

Further details of the site-specific model calibration and model validation are provided in the V&V report (PRDW, 2021).

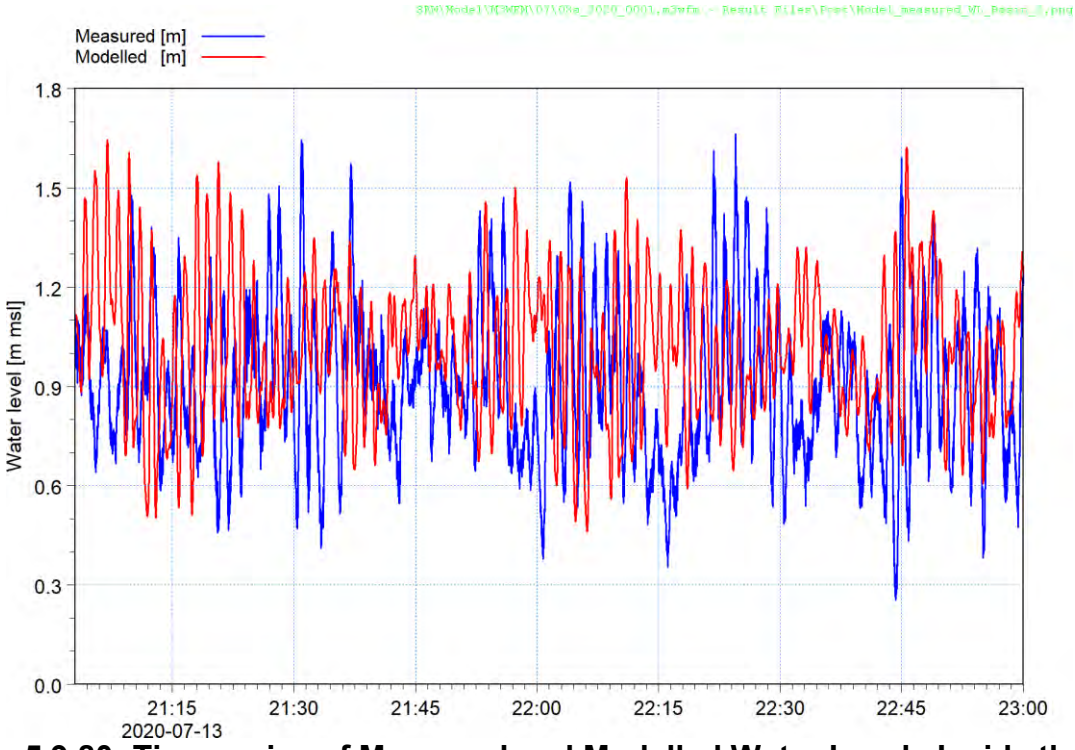


Figure 5.9.80: Time-series of Measured and Modelled Water Levels Inside the KNPS Basin for Two Hours During the 13 July 2020 Storm.

CONTROLLED DISCLOSURE

When downloaded from the EDS database, this document is uncontrolled and the responsibility rests with the user to ensure it is in line with the authorised version on the database.

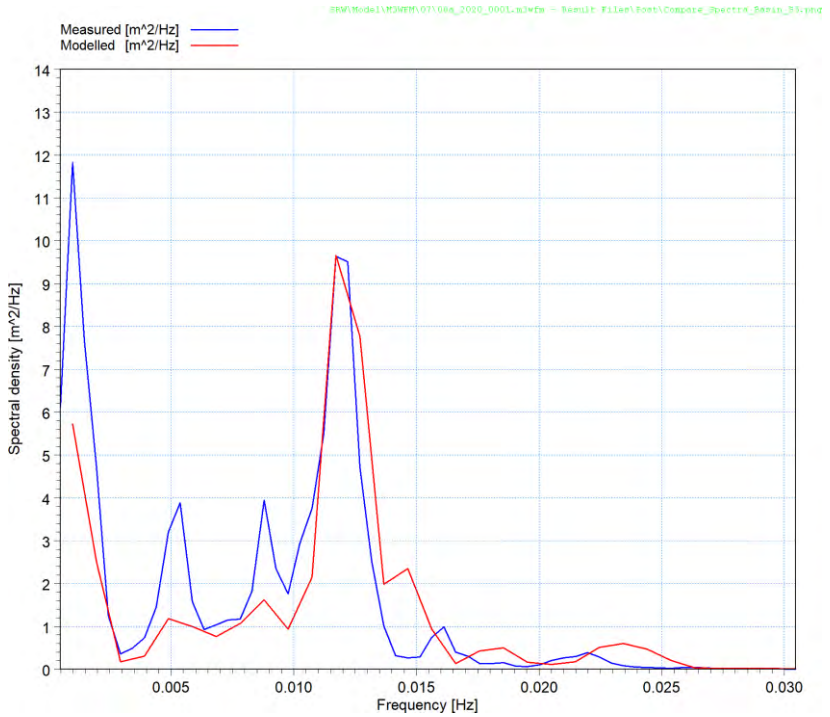


Figure 5.9.81: Measured and Modelled Frequency Spectra Inside the KNPS Basin During the 13 July 2020 Storm.

5.9.11.5 Cases Modelled

The model was run for extreme storms with exceedance probabilities of 10^{-2}, 10^{-4}, 10^{-6} and 10^{-8} y^{-1}. The model was run for the following dates to include the effect of climate change on waves, water levels and coastline stability:

- 2021: present-day;
- 2064: end of decommissioning period for KNPS;
- 2130: end of decommissioning period for the new NIs.

The model boundary conditions are the extreme wave parameters (H_{m0}, T_p, MWD and DSD) as shown in ***Table 5.9.25***, combined with the extreme maximum or minimum still water levels (comprising tide, sea level rise and storm surge) as shown in ***Table 5.9.12*** and ***Table 5.9.13***, respectively. The best estimate values were used in the modelling.

The joint exceedance probability between the waves and storm surge was accounted for as described in ***Subsection 5.9.9.9***. For the extreme wave run-up simulations the waves were combined with the positive storm surge as shown in ***Table 5.9.27***, where for example the 10^{-4} y^{-1} wave is combined with the 10^{-3} y^{-1} storm surge and vice versa. For the extreme wave drawdown simulations, the waves were combined with the negative storm

CONTROLLED DISCLOSURE

When downloaded from the EDS database, this document is uncontrolled and the responsibility rests with the user to ensure it is in line with the authorised version on the database.

surge as shown in ***Table 5.9.28***, where for example the 10^{-4} y^{-1} wave is combined with the 1 y^{-1} storm surge and vice versa.

For each joint probability both combinations of storm surge and wave height were modelled. The total number of cases modelled was thus 3 dates × 4 exceedance probabilities × 2 joint probability combinations = 24 cases for run-up and another 24 cases for drawdown.

The waves in the model were generated at the -31 m msl contour. A JONSWAP spectrum was used with a gamma of 3.3. The specified wave parameters are used by the model to generate a sea state by applying random phases and directions. The duration of each simulation was set to two hours. This allowed at least 390 waves to be simulated including a range of wave groups, as well as allowing overtopping and resultant ponding of water behind the dunes.

5.9.11.6 Results

To illustrate the model outputs and post-processing, selected figures are shown below for the 10^{-8} wave-dominated case in 2021.

Figure 5.9.82 shows an example of the progression of waves across the model domain, including profiles of the water surface elevation and orbital velocities through both the KNPS breakwater and through the dune in front of the new NIs. For this extreme case the KNPS breakwaters are submerged. The following processes can be seen: wave breaking, wave setup, wave run-up and transmission over the dune and breakwater, wave overtopping and ponding landward of the dune crest.

Figure 5.9.83 shows an example of the instantaneous water surface elevation and depth-averaged currents at KNPS. The arriving wave can be seen running up the revetment inside the KNPS basin and starting to flood up towards the terrace. Additionally, some run-up on both the north and south beaches outside the breakwater can be seen flowing in towards the KNPS terrace.

Figure 5.9.84 shows an example of the instantaneous water surface elevation and depth-averaged currents at the new NIs. The arriving wave can be seen overtopping the dune crest, running down the back of the dune, ponding in the valley behind the dune, and the ponded water starting to flow back to sea through the low points in the dune.

CONTROLLED DISCLOSURE

When downloaded from the EDS database, this document is uncontrolled and the responsibility rests with the user to ensure it is in line with the authorised version on the database.

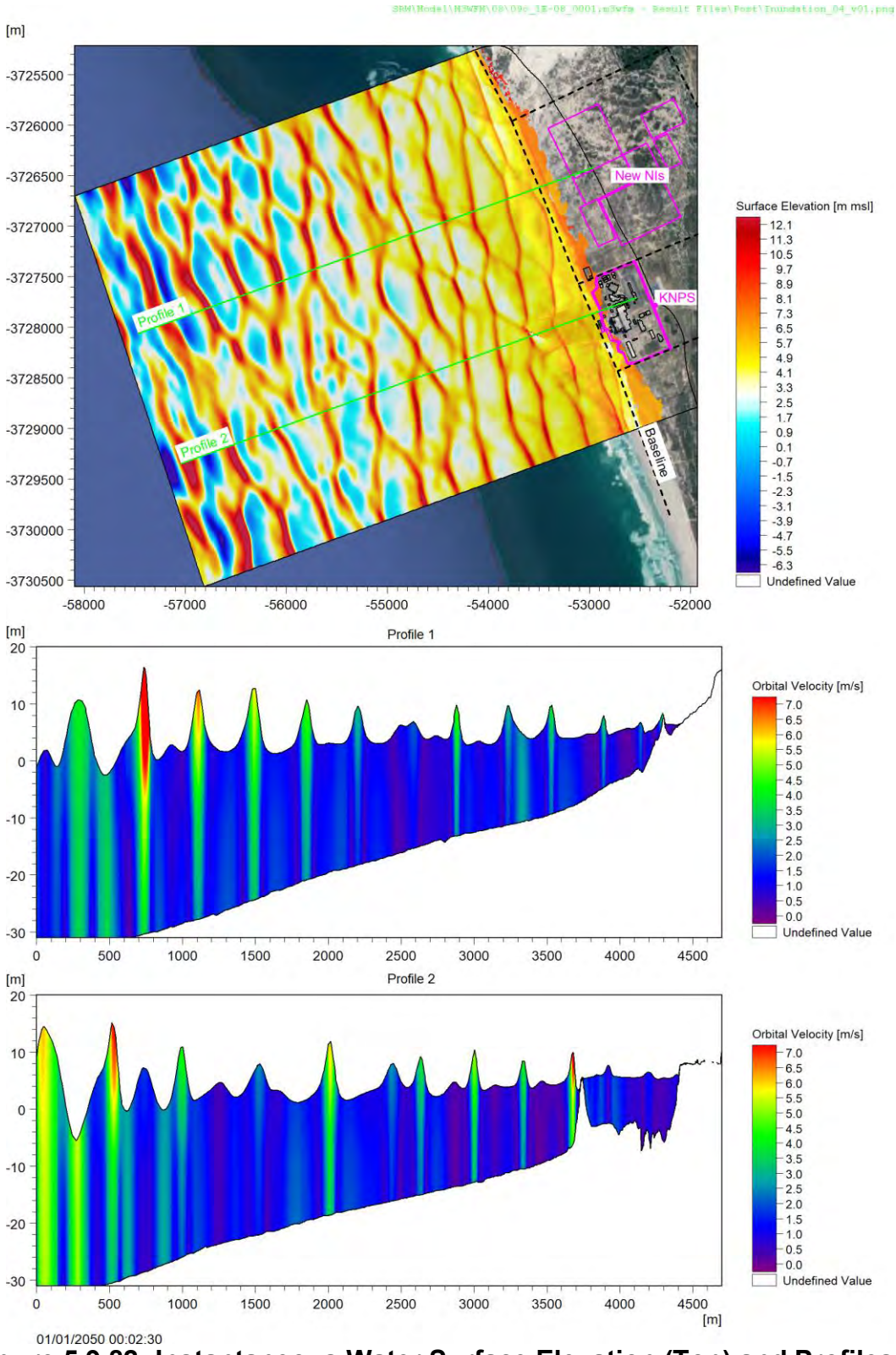


Figure 5.9.82: Instantaneous Water Surface Elevation (Top) and Profiles of Water Surface Elevation Through the New NIs (Middle) and KNPS Breakwater (Bottom) for the 10^{-8} y^{-1} Wave-Dominated Case in 2021.

CONTROLLED DISCLOSURE

When downloaded from the EDS database, this document is uncontrolled and the responsibility rests with the user to ensure it is in line with the authorised version on the database.

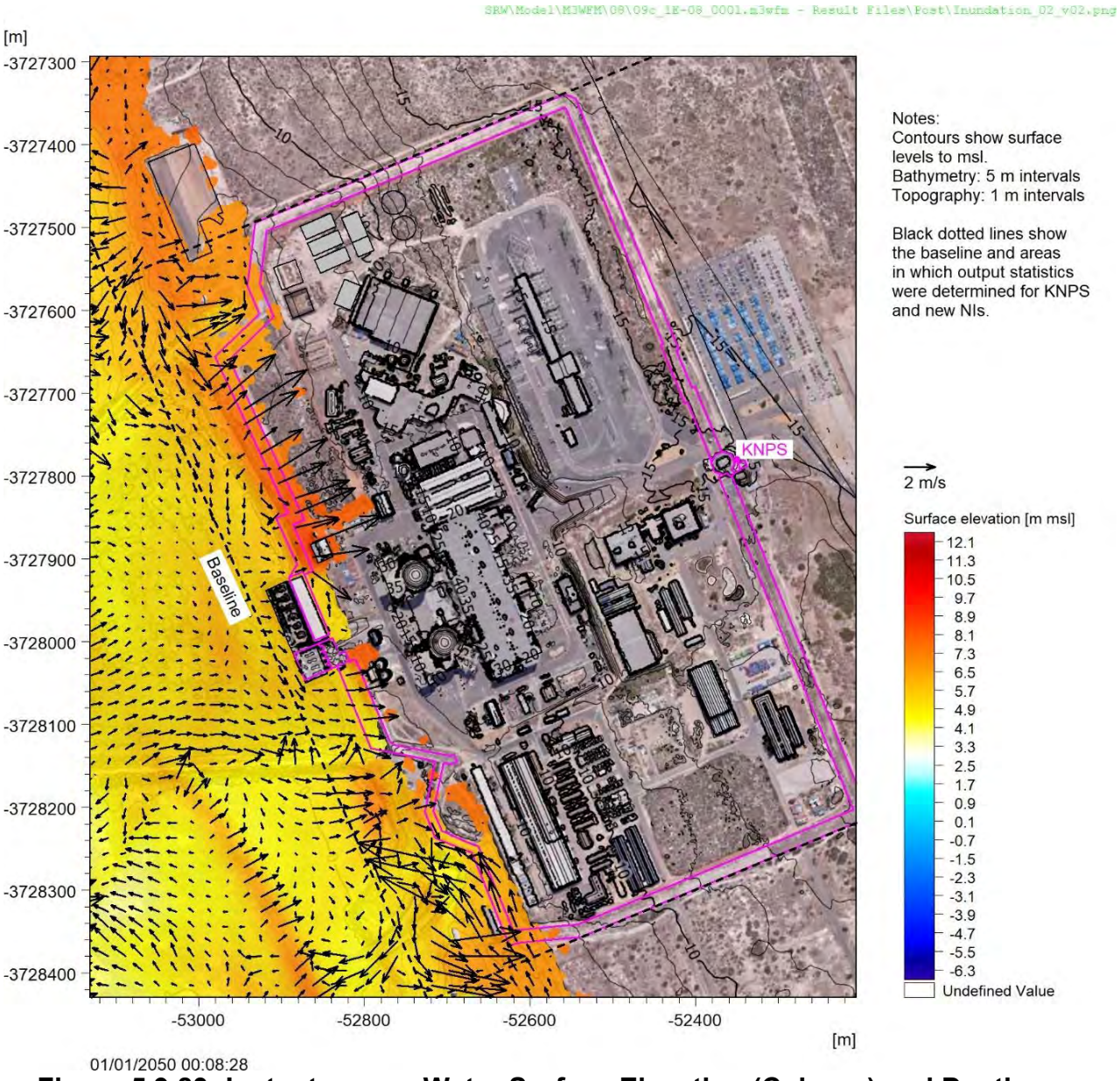


Figure 5.9.83: Instantaneous Water Surface Elevation (Colours) and Depth-Averaged Currents (Vectors) at KNPS for the 10^{-8} y^{-1} Wave-Dominated Case in 2021.

CONTROLLED DISCLOSURE

When downloaded from the EDS database, this document is uncontrolled and the responsibility rests with the user to ensure it is in line with the authorised version on the database.

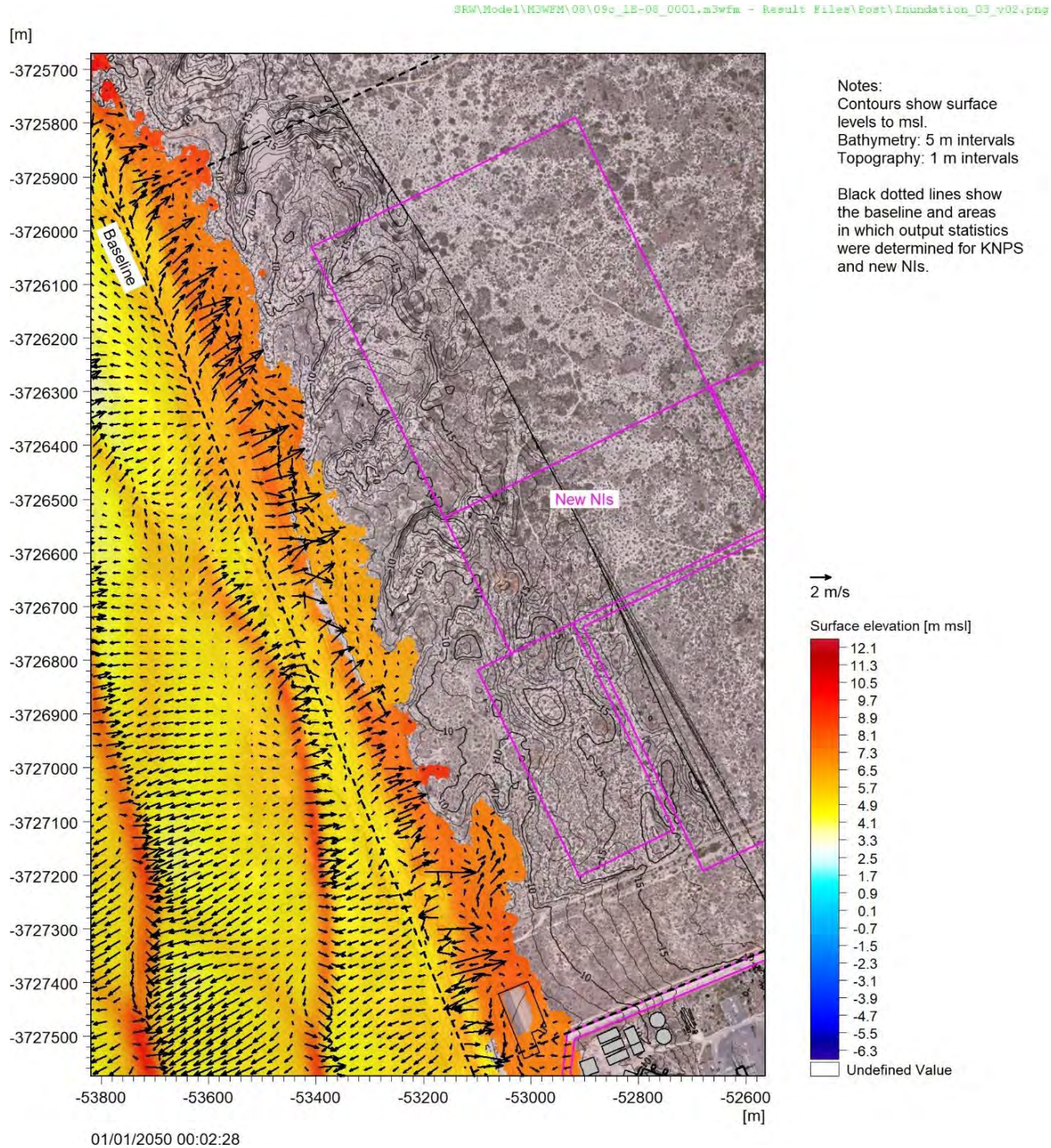


Figure 5.9.84: Instantaneous Water Surface Elevation (Colours) and Depth-Averaged Currents (Vectors) at new NIs for the 10^{-8} y^{-1} Wave-Dominated Case in 2021.

The following key results were extracted from the model outputs for each case:

CONTROLLED DISCLOSURE

When downloaded from the EDS database, this document is uncontrolled and the responsibility rests with the user to ensure it is in line with the authorised version on the database.

- The maximum water depth and maximum current speed over the simulation.
- The maximum horizontal inundation distance that the water reached, measured perpendicularly inland from a predefined baseline (see ***Figure 5.9.85***). Separate domains were used for KNPS and the new NIs. For KNPS, the baseline was chosen to run parallel to the terrace and seaward of the intakes. At the new NIs, the baseline was chosen to approximately correspond to the present-day +2 m msl contour. The baselines and domains are illustrated in ***Figure 5.9.86*** and ***Figure 5.9.88*** for KNPS and the new NIs, respectively.
- The maximum vertical run-up level, defined as the highest ground or building level that was flooded (see ***Figure 5.9.85***). Depending on the topography this point may or may not coincide with the maximum horizontal inundation (in the figure they do not coincide). The same domains as for the horizontal inundation were used.
- The minimum drawdown level at the KNPS cooling water intake pumps, and at the -20 m and -30 m msl depths opposite the new NIs.
- For each exceedance probability, both joint probability combinations of storm surge and wave height were modelled, with only the most conservative result reported here.

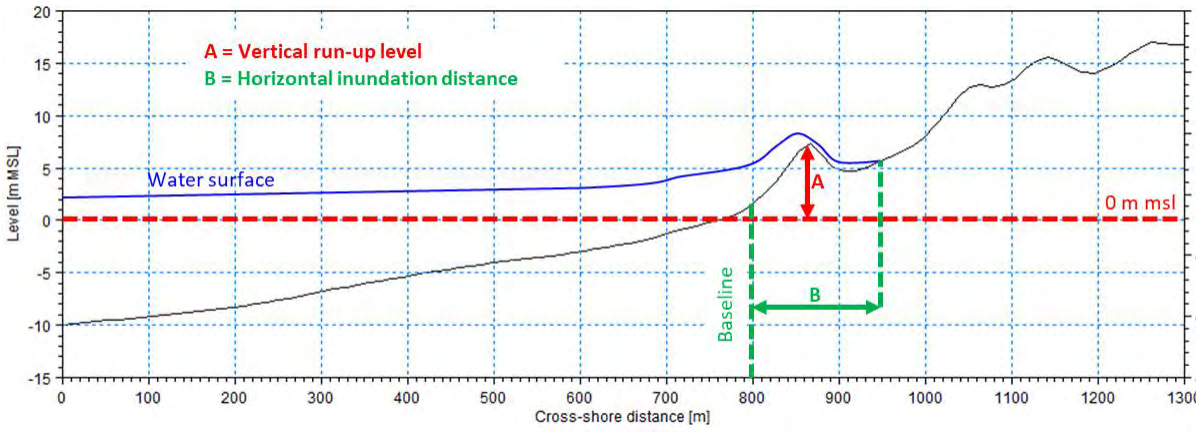


Figure 5.9.85: Definition Sketch for Vertical Run-Up Level and Horizontal Inundation Distance.

It is noted that the maximum vertical run-up level differs from the maximum water surface elevation (the highest level of the water surface). The impact of run-up and inundation on specific SSCs on the nuclear terrace can be assessed using the provided spatial outputs of maximum water depth (equal to the maximum water surface elevation above the natural ground level) and maximum current speed.

CONTROLLED DISCLOSURE

When downloaded from the EDS database, this document is uncontrolled and the responsibility rests with the user to ensure it is in line with the authorised version on the database.

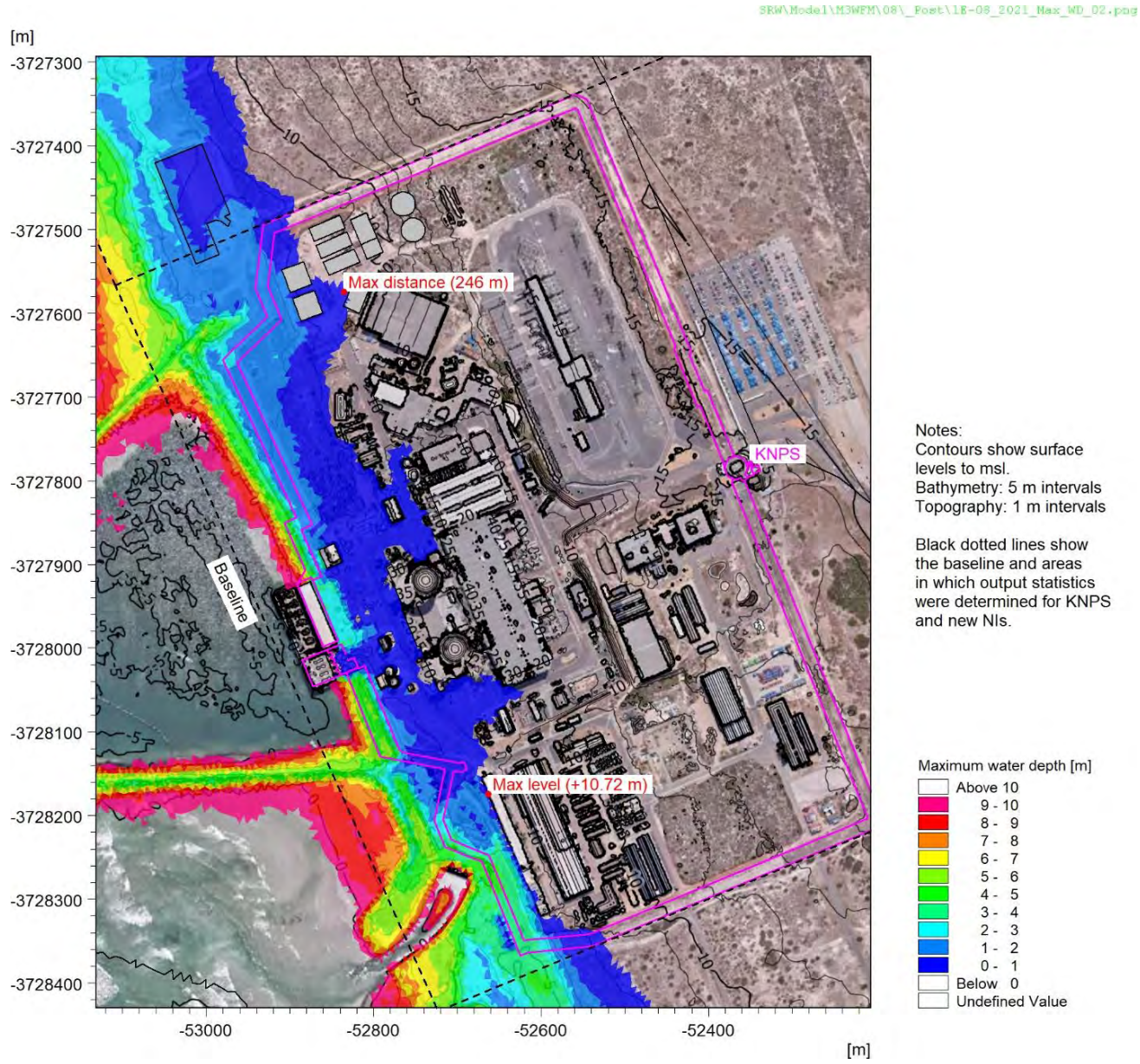


Figure 5.9.86: Maximum Water Depth Due to Wave Run-Up at KNPS for the 10^{-8} y^{-1} Storm in 2021.

Figure 5.9.86 shows the maximum water depth due to wave run-up at KNPS for the 10^{-8} exceedance storm in 2021. The maximum horizontal inundation distance and the maximum vertical run-up level are also indicated. The maximum vertical run-up level of +10.72 m occurs on the wall of a building directly landward of the outfall. The water depth on the terrace near the reactor building reaches up to 1 m. The maximum inundation distance of 246 m occurs on the northern part of the terrace.

CONTROLLED DISCLOSURE

When downloaded from the EDS database, this document is uncontrolled and the responsibility rests with the user to ensure it is in line with the authorised version on the database.

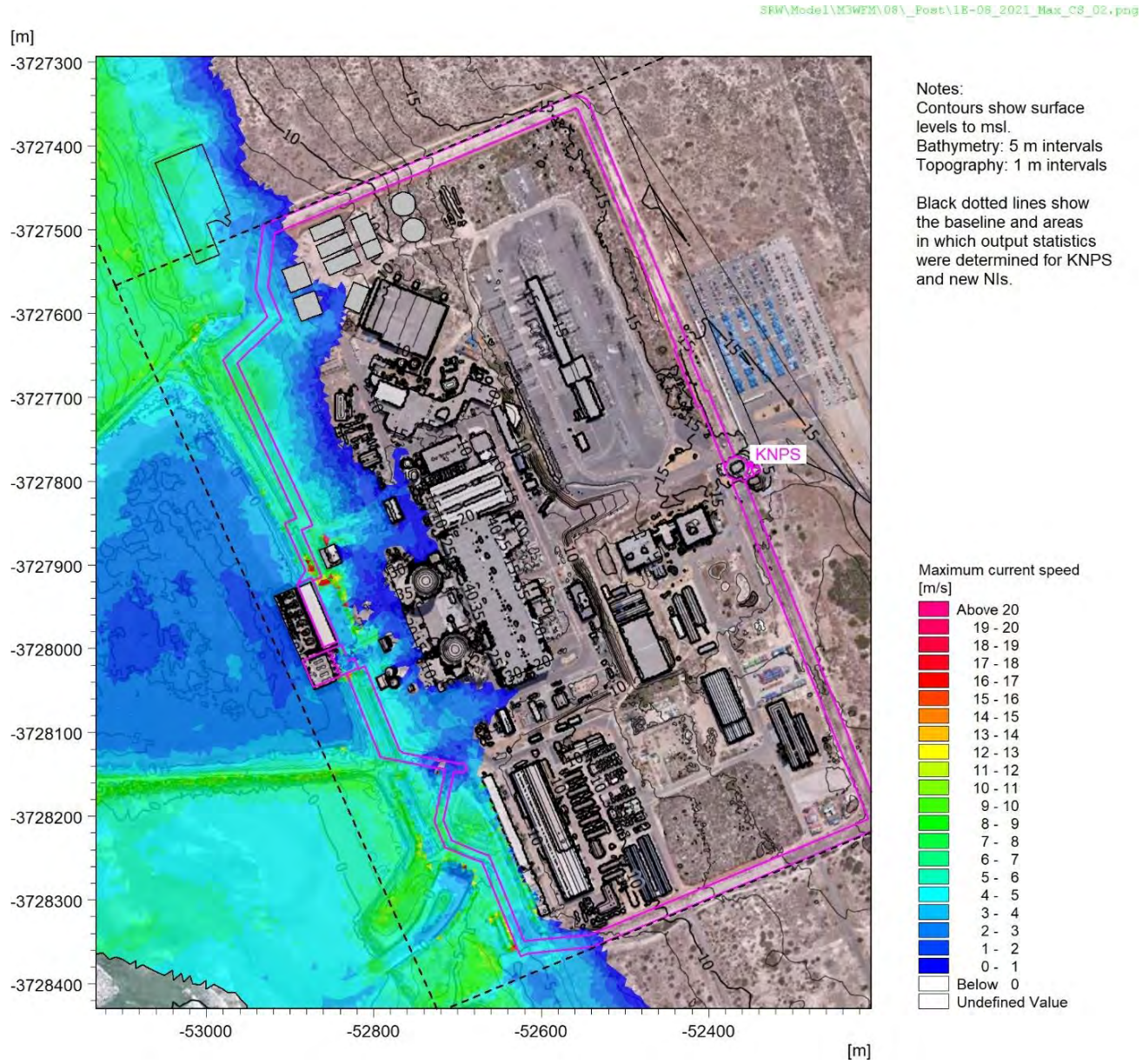


Figure 5.9.87: Maximum Depth-Averaged Current Speed Due to Wave Run-Up at KNPS for the 10^{-8} y^{-1} Storm in 2021.

Figure 5.9.87 shows the corresponding maximum depth-averaged currents. The largest current speeds occur locally at the edges of structures, such as the breakwater crest, outfall channel, walls and building edges where current speeds exceed 12 m/s. Current speeds on the terrace near the reactor building reach approximately 5 m/s.

CONTROLLED DISCLOSURE

When downloaded from the EDS database, this document is uncontrolled and the responsibility rests with the user to ensure it is in line with the authorised version on the database.

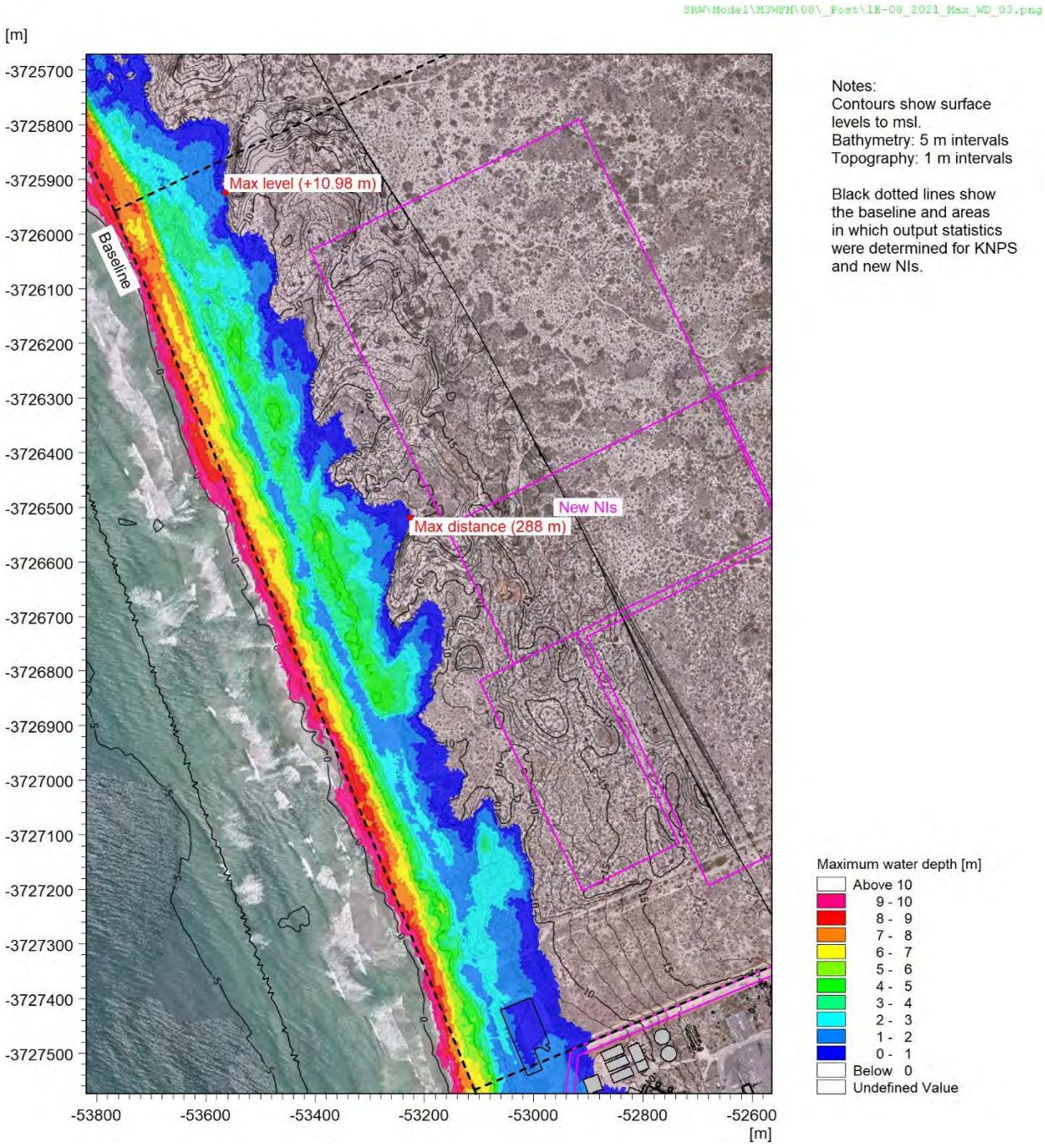


Figure 5.9.88: Maximum Water Depth Due to Wave Run-Up at the New NIs for the 10^{-8} y^{-1} Storm in 2021.

Figure 5.9.88 shows the maximum water depth due to wave run-up at the new NIs for the 10^{-8} exceedance storm in 2021. The maximum vertical run-up level of +10.98 m occurs against a dune in the northern part of the domain. The maximum inundation distance of 288 m occurs in a valley in the centre of the domain. In this case the run-up does not reach the estimated position of the new NIs.

CONTROLLED DISCLOSURE

When downloaded from the EDS database, this document is uncontrolled and the responsibility rests with the user to ensure it is in line with the authorised version on the database.

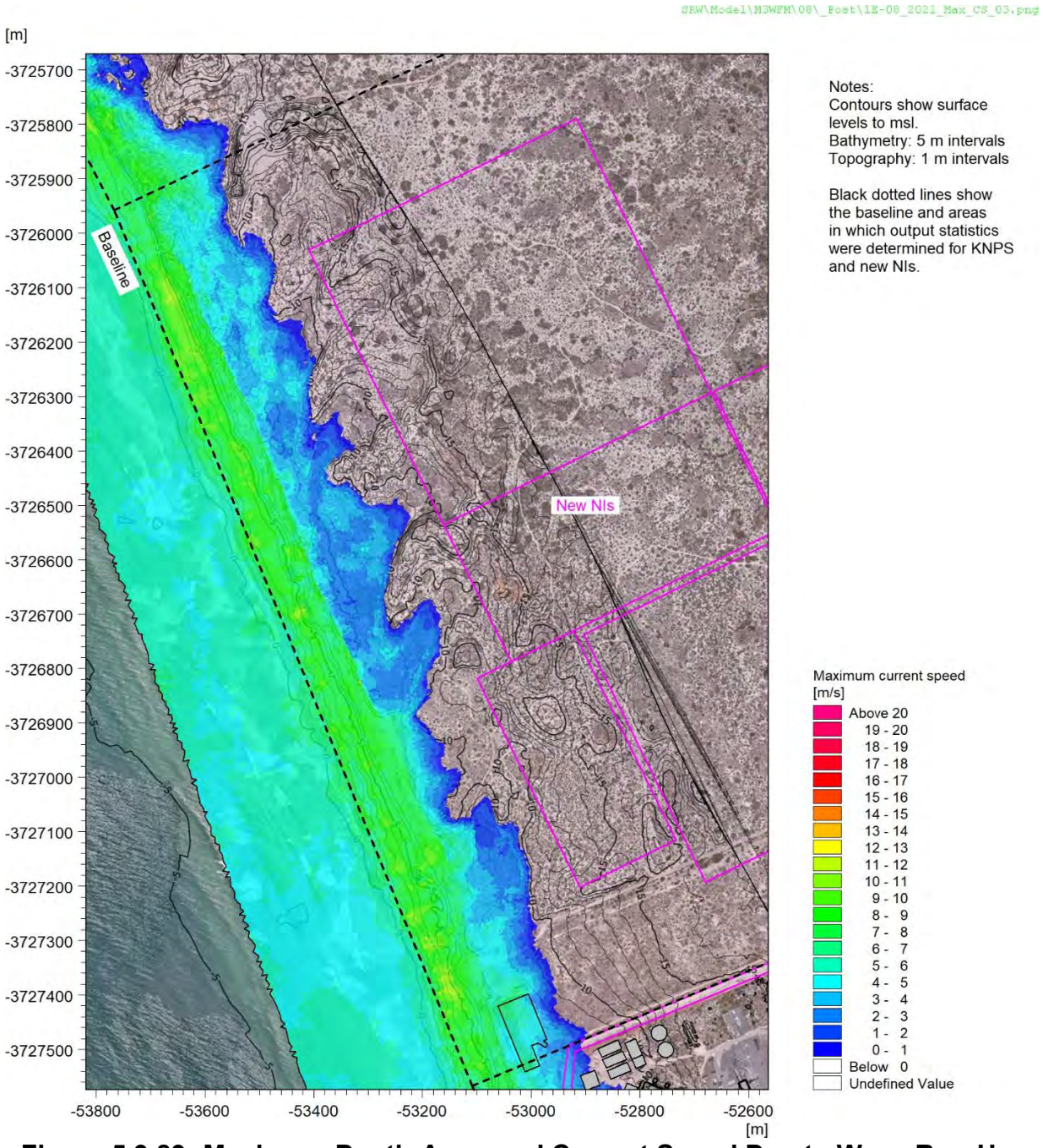


Figure 5.9.89: Maximum Depth-Averaged Current Speed Due to Wave Run-Up at the New NIs for the 10^{-8} y^{-1} Storm in 2021.

Figure 5.9.89 shows the corresponding maximum depth-averaged currents. The largest current speeds of 12 m/s occur on the dune crests, whilst the currents at the maximum inundation line are low.

CONTROLLED DISCLOSURE

When downloaded from the EDS database, this document is uncontrolled and the responsibility rests with the user to ensure it is in line with the authorised version on the database.

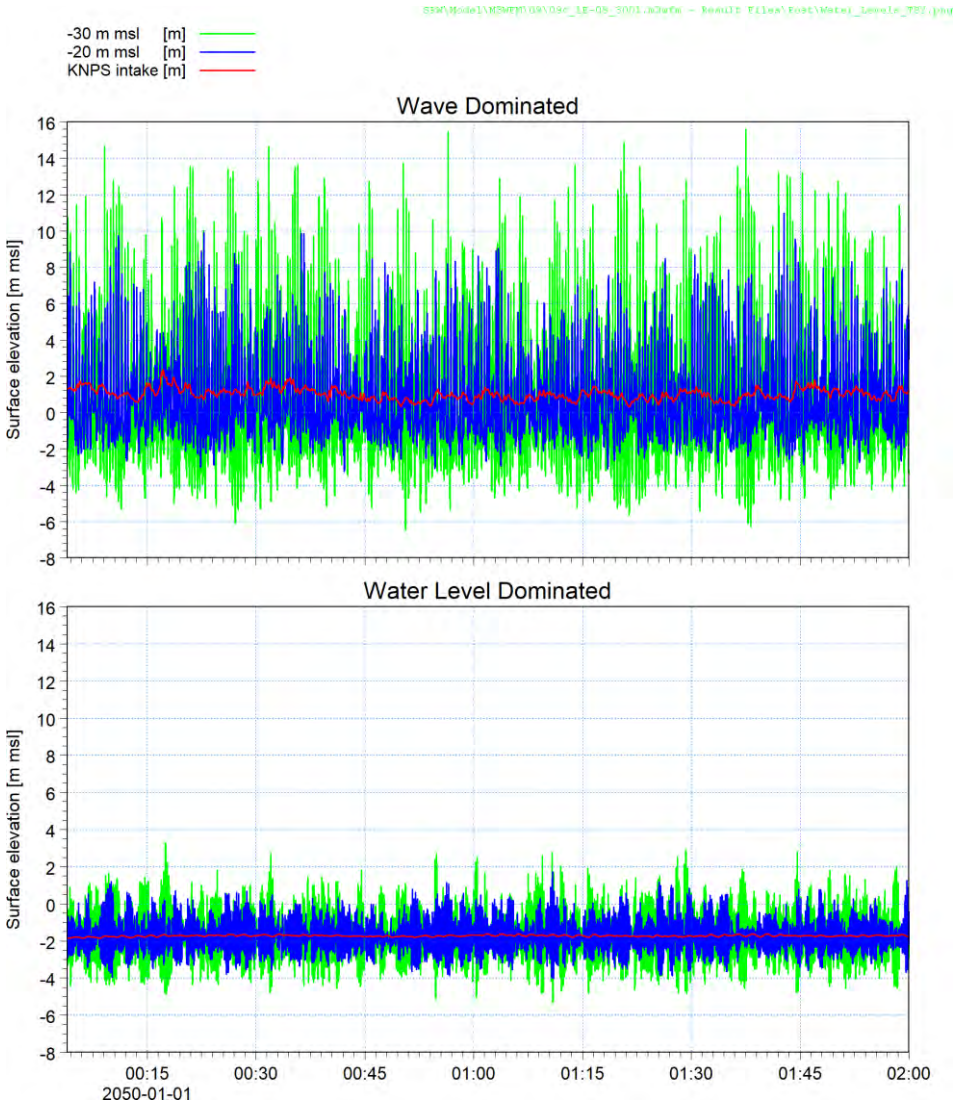


Figure 5.9.90: Time-series of Modelled Water Surface Elevations at the KNPS Intake and at Depths of -20 and -30 m msl for the 10^{-8} y^{-1} Storm in 2021.

Figure 5.9.90 shows the modelled water surface elevations at the KNPS cooling water intake pumps inside the intake basin, and at the -20 m and -30 m msl depths opposite the new NIs, corresponding to possible tunnel intake locations. In this case the water level-dominated case (10^{-8} y^{-1} low water level and 1 y^{-1} wave) generates the lowest water levels at the KNPS intake and at -20 m msl, whilst the wave-dominated case (10^{-8} y^{-1} wave and 1 y^{-1} low water level) generates the lowest water levels at -30 m msl due to less depth-limitation in deeper water.

The results shown above have been for the 10^{-8} exceedance storm in 2021. The full set of results for all modelled probabilities and dates are provided in ***Appendix A***.

CONTROLLED DISCLOSURE

When downloaded from the EDS database, this document is uncontrolled and the responsibility rests with the user to ensure it is in line with the authorised version on the database.

The extreme flooding results for all exceedance probabilities are provided in ***Table 5.9.38***.

Table 5.9.38: Extreme Flooding Due to Storm Waves.

Exceedance Probability	KNPS				New NIs					
	Maximum Vertical Run-up Level		Maximum Horizontal Inundation Distance		Maximum Vertical Run-up Level			Maximum Horizontal Inundation Distance		
(y^{-1})	(m msl)		(m from Baseline[(a)])		(m msl)			(m from Baseline[(b)])		
	2021	2064	2021	2064	2021	2064	2130	2021	2064	2130
10^{-2}	6.55	6.53	104	127	6.38	6.66	9.38	79	160	328
10^{-4}	7.85	7.67	145	186	8.97	9.87	12.41	125	210	345
10^{-5}	8.69	8.33	156	222	9.10	10.35	13.36	177	257	365
10^{-6}	9.54	9.00	168	258	9.23	10.83	14.31	229	305	385
10^{-7}	10.13	10.41	207	321	10.11	12.03	15.52	259	321	406
10^{-8}	10.72	11.83	246	383	10.98	13.24	16.73	288	336	427

Notes:
(a) At KNPS the baseline is parallel to the terrace and seaward of the intakes.
(b) At the new NIs the baseline corresponds to the present-day +2 m msl contour.

The extreme low water levels for all exceedance probabilities are provided in ***Table 5.9.39***. The results of the minimum drawdown levels at the KNPS intake pumps are repeated for the new NIs (with the inclusion of the year 2130) as an estimate of the minimum drawdown in the case that an intake basin with similar geometry is selected for the new NIs.

Table 5.9.39: Extreme Low Water Levels Due to Storm Waves.

Exceedance Probability	KNPS		New NIs								
	Minimum vertical drawdown level at pumps		Minimum vertical drawdown level at pumps[(a)]			Minimum vertical drawdown at -20 m msl			Minimum vertical drawdown at -30 m msl		
(y^{-1})	(m msl)		(m msl)			(m msl)			(m msl)		
	2021	2064	2021	2064	2130	2021	2064	2130	2021	2064	2130
10^{-2}	-1.10	-1.11	-1.10	-1.11	-1.13	-3.55	-3.47	-3.47	-4.87	-4.79	-5.27
10^{-4}	-1.42	-1.39	-1.42	-1.39	-1.45	-3.66	-3.81	-3.85	-5.39	-5.44	-5.55
10^{-5}	-1.53	-1.54	-1.53	-1.54	-1.62	-3.74	-3.86	-3.93	-5.76	-6.04	-6.17
10^{-6}	-1.64	-1.69	-1.64	-1.69	-1.80	-3.83	-3.90	-4.01	-6.14	-6.64	-6.79
10^{-7}	-1.79	-1.83	-1.79	-1.83	-1.95	-3.94	-4.00	-4.03	-6.41	-6.61	-6.80
10^{-8}	-1.94	-1.97	-1.94	-1.97	-2.09	-4.04	-4.10	-4.05	-6.68	-6.58	-6.82

Notes:
(a) Assuming a basin intake with similar geometry to KNPS.

CONTROLLED DISCLOSURE

When downloaded from the EDS database, this document is uncontrolled and the responsibility rests with the user to ensure it is in line with the authorised version on the database.

The warning time for these storm events is related to the wave and storm surge forecasts provided by the South African Weather Service and other forecast agencies. It is likely that an extreme storm event will be identified a number of days in advance.

As described in ***Subsection 5.9.10.5***, the duration of an extreme storm is approximately 4 days, although the maximum run-up and minimum drawdown are likely to occur over a few hours at the peak of the storm and will be associated with a group of large waves.

These results are compared to the equivalent tsunami results (see ***Subsection 5.9.12***) to determine the extreme flooding from the sea (see ***Subsection 5.9.13***) and the extreme low water levels at the cooling water intakes (see ***Subsection 5.9.14***). Further discussion of these results is provided in these sections.

5.9.12 Tsunamis

5.9.12.1 Introduction

This section describes the modelling undertaken to estimate the maximum vertical run-up, maximum horizontal inundation and minimum vertical drawdown at both the existing KNPS and the new NIs due to tsunamis. It presents a summary of the Duynefontyn Tsunami Hazard Analysis (DTHA), which is fully described in the DTHA Report (PRDW, 2022a). These results are compared to the equivalent storm results (see ***Subsection 5.9.11***) to determine the extreme flooding from the sea (see ***Subsection 5.9.13***) and the extreme low water levels at the cooling water intakes (see ***Subsection 5.9.14***).

5.9.12.2 Scope of Work

The scope of work of the DTHA (Eskom, 2021) is to perform a tsunami hazard analysis which emulates international best practice. The hazard due to the following tsunamigenic sources is assessed:

- Distant earthquakes;
- Local earthquakes;
- Submarine slumps;
- Submarine slides;
- Volcanoes;
- Local subaerial landslides; and
- Meteorites: a discussion shall be included on meteorite impact tsunamis and their potential impact on the site.

When downloaded from the EDS database, this document is uncontrolled and the responsibility rests with the user to ensure it is in line with the authorised version on the database.

The output of the analysis is the Probable Maximum Tsunami (PMT) run-up, drawdown and velocity at the site. The PMT is defined by the US NRC (2009) as that tsunami for which the impact at the site is derived from the use of best available scientific information to arrive at a set of scenarios reasonably expected to affect the nuclear power plant site, taking into account (1) appropriate consideration of the most severe of the natural phenomena that have been historically reported for the site and surrounding area, with sufficient margin for the limited accuracy, quantity, and period of time in which the historical data have been accumulated; (2) appropriate combinations of the effects of normal and accident conditions with the effects of the natural phenomena; and (3) the importance of the safety functions to be performed.

The aim of the source characterisation is to characterize tsunami source scenarios that generate the largest tsunami wave flooding events at the Duynefontyn site that are geologically supported. Development of Maximum Probable Event scenarios balances the regulator guidance to characterise the maximum event with the best available scientific data and consensus.

5.9.12.3 Approach

As discussed in the Safety Justification for the DTHA (Eskom, 2020b), the approach is systematic and hierarchal, comprising data gathering, source characterisation, numerical modelling of tsunami propagation and sensitivity testing in order to determine the deterministic PMT at the site. The approach is consistent with the latest guidance from the United States Nuclear Regulatory Commission (NRC, 2016), the International Atomic Energy Agency (IAEA, 2011) and (IAEA, 2012), as well as the National Nuclear Regulator (NNR, 2014) and (NNR, 2016a).

The approach for the DTHA comprises the seven tasks listed below, which are described in detail in the DTHA Report (PRDW, 2022a).

- Data gathering;
- Preliminary source characterisation;
- Numerical model construction;
- Tsunami propagation sensitivity runs;
- Refinement of tsunamigenic sources;
- Tsunami propagation refined runs;
- Review and update SSR (this document).

PRDW has appointed the Council for Geoscience (CGS) to support the DTHA through the identification and characterisation of geological tsunamigenic sources for the Duynefontyn site.

CONTROLLED DISCLOSURE

When downloaded from the EDS database, this document is uncontrolled and the responsibility rests with the user to ensure it is in line with the authorised version on the database.

5.9.12.4 Historical Tsunamis

Historical accounts reporting tsunami events and/or mechanisms leading to tsunamis such as earthquakes or submarine landslides do not extend far back in time along the South African coast when compared with records in some other global areas. A list of known tsunami or tsunami-like events is provided below based primarily on summaries provided in (CGS, 2008) and (CGS, 2022). Earthquake magnitudes (Mw or **M**) are cited as reported, where Mw = 2/3 log(M_0) - 10.73 and **M** = 2/3 log(M_0) - 10.7 (CGS, 2022), also see ***Subsection 5.9.12.5***.

- Although contentious, reports of an earthquake north of the central Cape Town area in 1809 included inference of a tsunami wave. The run-up height and inundation distance inland (if applicable) remain unknown.
- Modelling indicates that the 1833 Mentawai, Indonesia tsunami potentially inundated the Algoa Bay coast, but there is currently no known evidence or records of the event from South Africa.
- The 1883 Krakatau tsunami event, generated by a series of volcanic eruptions in Indonesia, was reportedly observed at Gqeberha (formerly Port Elizabeth) Harbour and the Cape of Good Hope (now known as Cape Town).
- The earliest reported tsunami caused by remote submarine seismicity that affected South Africa was triggered by the Mw 9.5 earthquake off the south-central Chilean coast on 22 May 1960. The Chilean event was recorded globally and in southern Africa tidal irregularities associated with this event were recorded at Mossel Bay and Lüderitz.
- A tsunami was reported in the West Coast village of Dwarskersbos, 170 km northwest of Cape Town, in the early hours of 27 August 1969. Field surveys estimate a maximum run-up height of 2.9 m above sea level and a maximum horizontal inundation distance of 260 m from the shoreline. Numerical modelling suggests the event to be a meteo-tsunami (Okal, et al., 2014).
- The 2004 Indian Ocean Tsunami was recorded by South African tide gauges on the eastern and southeastern seaboard with a maximum trough-to-crest wave height at Gqeberha measuring 2.7 m, although the maximum crest level was truncated due to an instrumentation problem. The maximum positive amplitude has been estimated to be 1.93 m (PRDW, 2022a). Lesser waves were measured at Richards Bay (1.5 m), East London (1.3 m) and Mossel Bay (1.6 m). Maximum recorded wave heights on the Atlantic seaboard were 0.75 m in Cape Town and 0.5 m at Port Nolloth.

CONTROLLED DISCLOSURE

When downloaded from the EDS database, this document is uncontrolled and the responsibility rests with the user to ensure it is in line with the authorised version on the database.

- On 12 September 2007, a Mw 8.4 earthquake occurred 130 km southwest of Bengkulu, Sumatra, Indonesia. Maximum wave amplitudes of approximately 0.4 m were measured at Gqeberha.
- On 21 August 2008 a series of water level fluctuations was measured on the west and south coasts of South Africa, with the largest amplitude of approximately 0.7 m measured at Port Nolloth (see ***Figure 5.9.13*** and ***Figure 5.9.14***). The measurement of atmospheric pressure fluctuations at Port Nolloth coinciding with the onset of this event provides compelling evidence that this was a meteo-tsunami.
- On 12 August 2021 two earthquakes occurred within several minutes of each other near the South Sandwich Islands and Scotia subduction zone. These thrust events, a **M** 7.5 event followed by a **M** 8.1 event, generated a tsunami that was measured on tide gauges around the globe including South Africa. Crest-to-trough wave heights of 1.3 m at Mossel Bay and 0.7 m at Cape Town have been reported based on raw tide gauge measurements (CGS, 2022). Maximum positive and minimum negative amplitudes of 0.55 m and -0.53 m, respectively, were observed in the KNPS intake basin on 13 August 2021 (PRDW, 2022c).
- It has been proposed that a series of large imbricated granite boulders at Clifton and Bantry Bay were laid down by a storm or tsunami event. The estimated mass of these individual boulders ranges from a few tons to 150 tons and it is suggested that minimum wave velocities required to deposit these rocks to have been in the order of $U \geq 18$ m/s to transport a boulder of 10 x 5 x 2 m in saltating mode of transport. It has been hypothesised that it is likely that the megaboulder bed was produced by tsunami waves resulting from meteor impact in the ocean, a process for which there is no upper energy limit. This hypothesis is yet to be formally published or confirmed by supporting field investigations, perhaps from a different part of the Table Bay coast. In the absence of other tsunami deposits to support a tsunami origin, it is quite possible these boulders were emplaced during older middle to late Pleistocene sea level highstands or within a middle Holocene (+2 to 3.5 m) highstand. Based on global studies the boulders are within the range of size and location for movement by storm waves.

Based on the historical records, the maximum recorded tsunami in South Africa was for the 2004 Indian Ocean Tsunami, with an estimated maximum positive amplitude of 1.93 m at Gqeberha. The highest documented run-up estimate is 2.9 m above sea level for the Dwarskersbos tsunami in 1969, postulated to be a meteo-tsunami.

A palaeotsunami field study was completed in February 2022 (PRDW, 2022d). There is no new information from this study that would justify changes to the tsunami source characterisation model used in this THA, as

CONTROLLED DISCLOSURE

When downloaded from the EDS database, this document is uncontrolled and the responsibility rests with the user to ensure it is in line with the authorised version on the database.

described in the DTHA Report (PRDW, 2022a). However, considering (1) the potential for post-depositional processes to obscure or remove fine-grained tsunami deposits, (2) the limited time-period of the geologic record at the studied sites, and (3) the incomplete Pleistocene/Holocene geologic record, the results of palaeotsunami field study do not preclude the possibility of events considered in the tsunami source characterisation model.

5.9.12.5 Numerical Modelling

Model description

The MIKE 21/3 Flow Model Flexible Mesh was used for the tsunami modelling. The details of the physical processes and numerical implementation are provided in the model documentation (see ***Table 5.9.7***), while details of the model setup, sensitivity testing, and V&V are provided in the DTHA V&V Report (PRDW, 2021).

In the 2D formulation the model solves the non-linear, non-dispersive, hydrostatic shallow water equations (NSWE), i.e., the depth-integrated incompressible Reynolds averaged Navier-Stokes equations. The time integration of the shallow water equations is performed using an explicit scheme. Horizontal eddy viscosity is modelled with the Smagorinsky formulation. An unstructured flexible mesh comprising triangles or quadrangles with variable sizes is utilised. The 2D NSWE formulation was used to model the propagation of tsunamis forced by local and distant earthquakes, as well as the local inundation modelling, since in these cases the non-dispersive hydrostatic shallow water assumption is valid, i.e., the tsunami wavelength to water depth ratio exceeds approximately 25.

In the 3D formulation, the model was used to solve the non-linear, dispersive, non-hydrostatic Navier-Stokes (NS) equations. The model consists of the continuity and momentum equations and is closed by a k- ε horizontal and vertical turbulence closure scheme. The time integration is performed using a semi-implicit scheme, where the horizontal terms are treated explicitly, and the vertical terms are treated implicitly. In the vertical direction a structured mesh, based on a sigma-coordinate transformation is used, while the geometrical flexibility of the unstructured flexible mesh comprising triangles or quadrangles with variable sizes is utilised in the horizontal plane. The 3D NS formulation was used to model the propagation of tsunamis forced by volcanic flank collapse and local submarine landslides, since in these cases the tsunami wavelength is shorter requiring the dispersive non-hydrostatic Navier-Stokes equations.

CONTROLLED DISCLOSURE

When downloaded from the EDS database, this document is uncontrolled and the responsibility rests with the user to ensure it is in line with the authorised version on the database.

Verification and Validation

The numerical models used in the THA have undergone V&V as per the requirements contained in NSIP02761 (Eskom, 2020a) and RG-0016 (NNR, 2016b). As part of the model validation process, a set of tsunami benchmark tests available from the United States National Tsunami Hazard Mitigation Program (NTHMP) was simulated. An extract of the DTHA V&V Report (PRDW, 2021) is presented here, showing the simulation of a three-dimensional rigid submarine landslide.

The goal of the benchmark problem (Benchmark no. 2 of the 2017 NTHMP workshop) was to compare model results with laboratory measurements performed by Enet, et al. (2003). The physical modelling experiment investigated tsunami generation by submarine mass failure (SMF) with an idealised three-dimensional quasi-Gaussian mound translating down a plane slope.

The benchmark required reproducing the physical model conditions (experimental set-up, slide shape, density, submergence depth and kinematics) to simulate water surface elevations measured at four wave gauges. Guidance on the numerical model setup and parameters is provided by Enet & Grilli (2007).

The MIKE 3 Flow Model FM solving the non-hydrostatic dispersive Navier-Stokes equations was used for this benchmark problem. The water surface elevation was measured at four wave gauges. The first wave gauge was placed above the centroid of the SMF at its starting position (point of minimum submergence), and the other three gauges were placed offshore of the SMF's starting position.

Figure 5.9.91 presents the vertical cross-section for the tsunami landslide experiments and the plan view of the experiment with locations of the four wave gauges. A flexible mesh comprising triangles with a resolution of 0.04 m was used. Vertically, 10 equidistant sigma layers were used.

CONTROLLED DISCLOSURE

When downloaded from the EDS database, this document is uncontrolled and the responsibility rests with the user to ensure it is in line with the authorised version on the database.

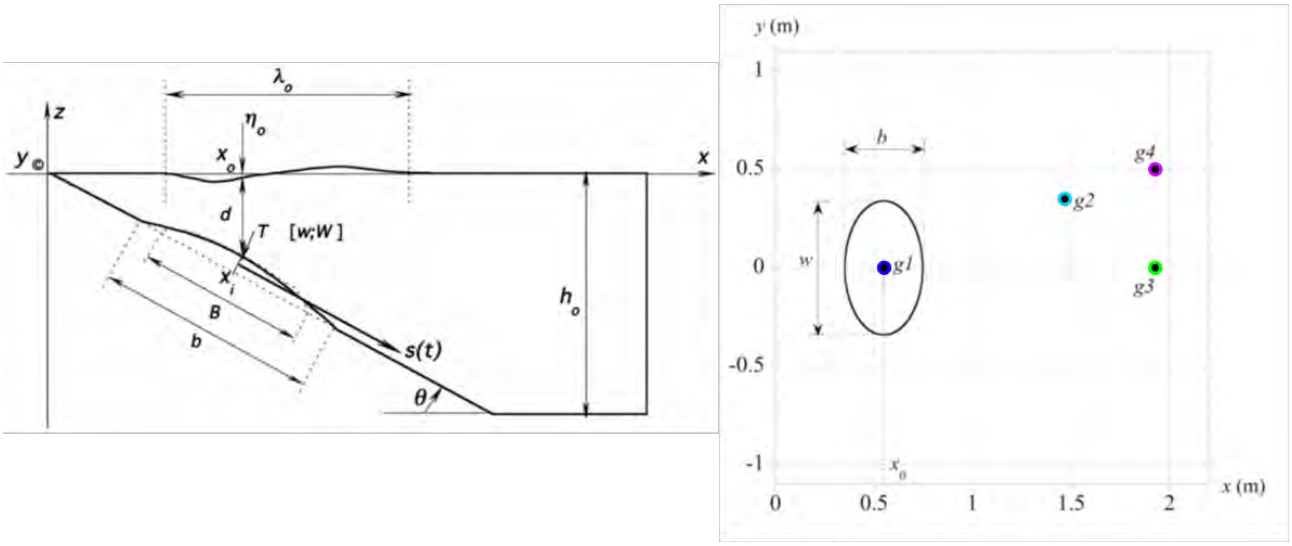


Figure 5.9.91: Vertical Cross-Section (Left) and Plan View of the Experiment Showing the Locations of the Four Wave Gauges (Right).

The shape and kinematics of the landslide were first solved using the numerical routine described further below. The landslide was then coupled to the MIKE 3 Flow Model using a space- and time-varying bathymetry adjustment emulating the shape and kinematics of the rigid SMF. The following parameters were modelled (with reference to ***Figure 5.9.91***):

- T: Thickness of Gaussian-shaped SMF = 0.082 m
- b: Length of Gaussian-shaped SMF = 0.395 m
- w: Width of Gaussian-shaped SMF = 0.680 m
- θ: Plane slope = 15°
- h_0: Water depth = 1.8 m
- d: Submergence depth = 61 mm

Snapshots in time showing the propagation of the slide-generated waves are shown in ***Figure 5.9.92***. ***Figure 5.9.93*** presents a time-series comparison of measured and modelled water surface elevation at the four wave gauges. The measured and modelled amplitudes are compared in ***Table 5.9.40***.

CONTROLLED DISCLOSURE

When downloaded from the EDS database, this document is uncontrolled and the responsibility rests with the user to ensure it is in line with the authorised version on the database.

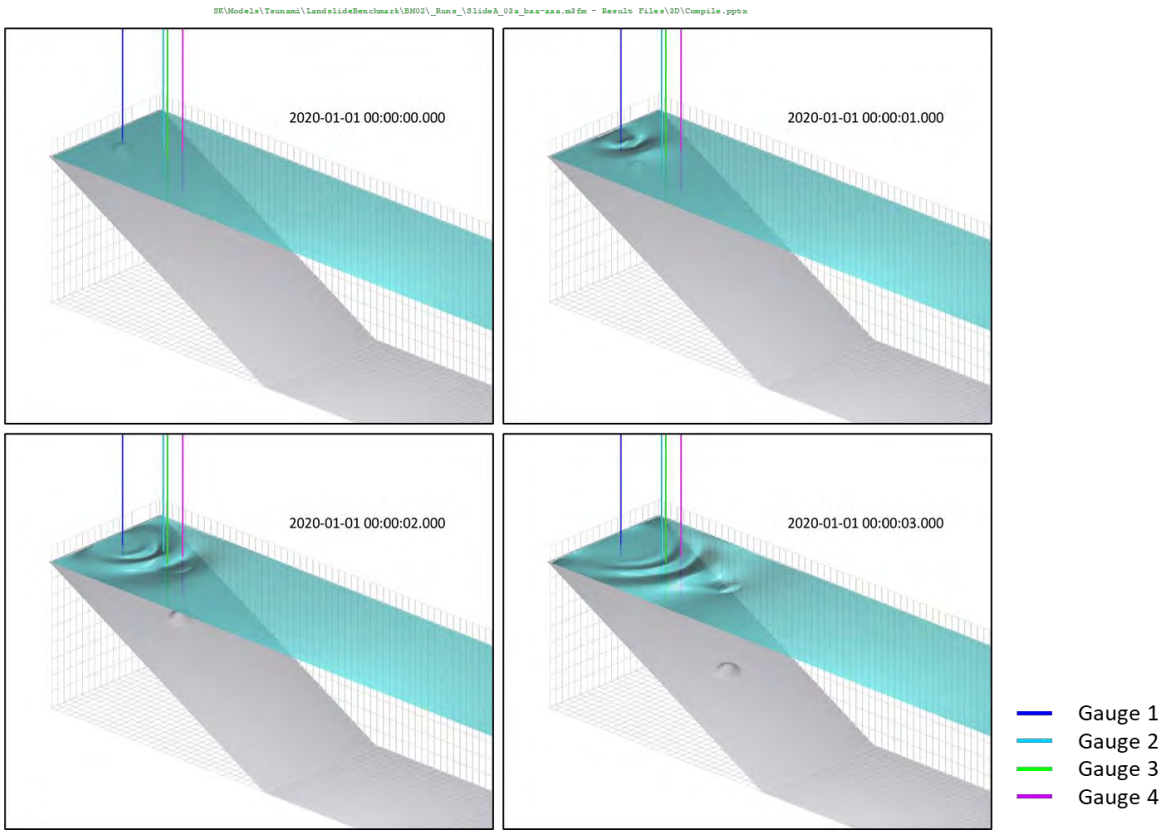


Figure 5.9.92: Snapshots in Time Showing the Propagation of the Slide-generated Waves. Note the Plots Have a Vertical Exaggeration Factor of ×2.

CONTROLLED DISCLOSURE

When downloaded from the EDS database, this document is uncontrolled and the responsibility rests with the user to ensure it is in line with the authorised version on the database.

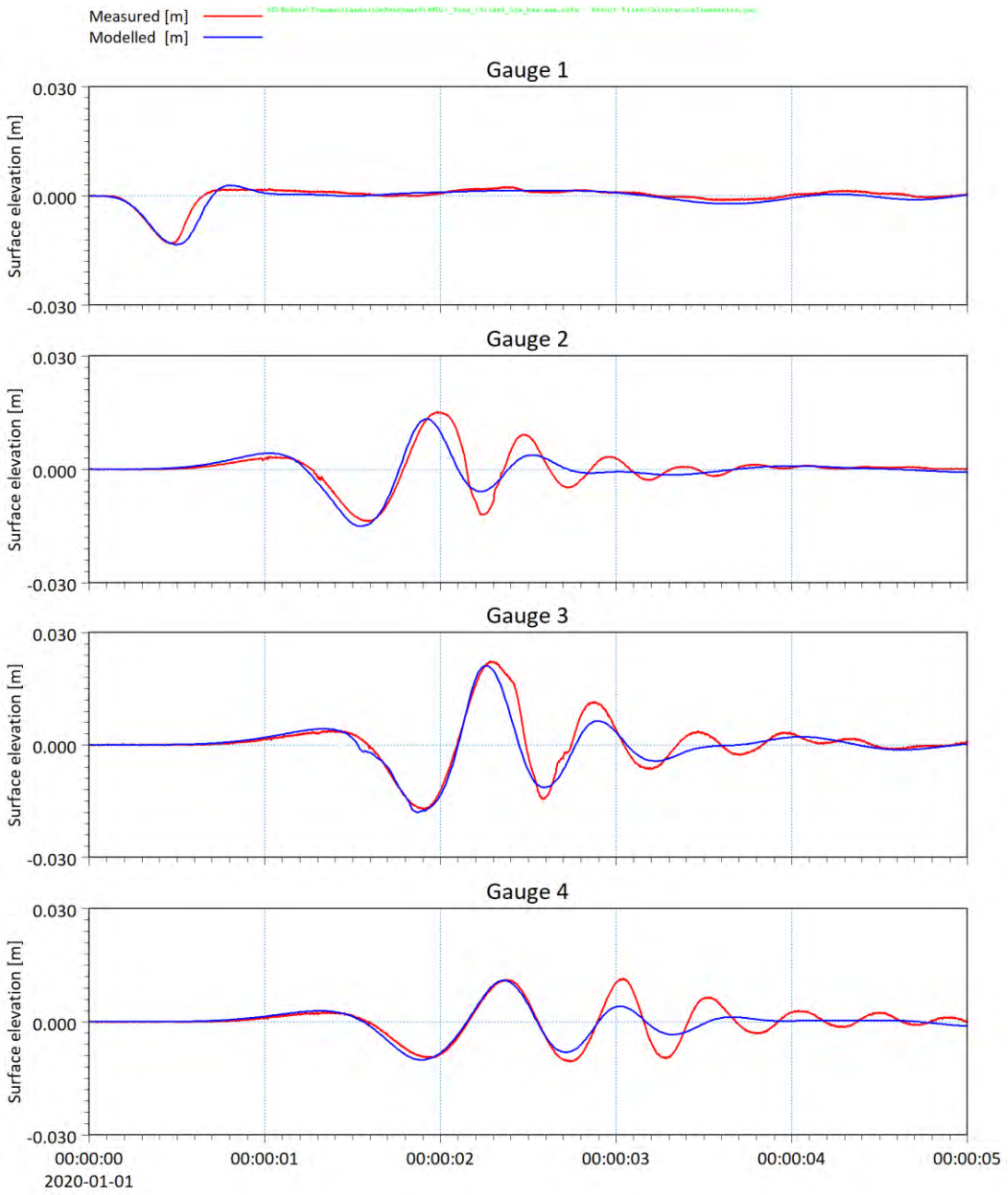


Figure 5.9.93: Time-series Comparison of Measured and Modelled Water Surface Elevation at the Four Wave Gauges.

CONTROLLED DISCLOSURE

When downloaded from the EDS database, this document is uncontrolled and the responsibility rests with the user to ensure it is in line with the authorised version on the database.

Table 5.9.40: Comparison of Measured and Modelled Amplitudes.

Wave Gauge	Maximum Amplitude			Minimum Amplitude		
	Measured (mm)	Modelled (mm)	Difference[(a)] (%)	Measured (mm)	Modelled (mm)	Difference[(a)] (%)
1	2.5	2.9	15.8%	-13.1	-13.3	1.5%
2	15.1	13.3	12.0%	-13.6	-15.1	9.2%
3	22.1	21.1	5.4%	-17.1	-18.1	5.7%
4	11.5	10.*	4.5%	-10.4	-10.1	4.7%
Average			**9.4%**			**5.2%**

Notes:

(a) $Relative\ difference = \left|\frac{Measured - Modelled}{Measured}\right|$

The biggest relative difference is observed at the maximum amplitude from Wave Gauge 1 (located above the centroid of the SMF at its starting position) due to the comparison of relatively small amplitudes. In contrast, the minimum amplitude at Wave Gauge 1 showed excellent accuracy (1.5% relative difference). The average relative difference for all four gauges was 9.4% for the maximum amplitude and 5.2% for the minimum amplitude. Although there are no acceptability criteria for these benchmarks, the average difference in amplitudes was below 10% (2011 NTHMP Model Benchmarking Workshop passing criteria) and would have ranked 3rd when compared to the results of the original 13 workshop participants.

Forcing terms

For seismic sources, the vertical displacement of the seabed was estimated using the double-couple method of Okada (1985). This widely used method assumes a homogeneous isotropic elastic earth's crust, and calculates the vertical displacement based on the following set of source parameters:

- Location (latitude and longitude of the mid-point of the upper border of the fault plane);
- Depth (distance from the earth's crust to the upper border of the fault plane);
- Fault dimensions (length, width and slip (or dislocation));
- Fault orientation (dip, strike, and slip (or rake) angles).

The seismic moment (M_0, units of N m) is defined as $M_0 = \mu LWD$, where μ is the rigidity or shear modulus given in units of Pa, and L, W and D are the length, width and slip of the fault measured in units of m. The moment magnitude (**M**) is calculated as $M = \frac{2}{3}\log_{10} M_0 - 10.7$, where M_0, is the seismic moment given in units of dyne cm (= 10^{-7} N m).

CONTROLLED DISCLOSURE

When downloaded from the EDS database, this document is uncontrolled and the responsibility rests with the user to ensure it is in line with the authorised version on the database.

The vertical displacement of the seabed is assumed to generate a corresponding instantaneous displacement of the water surface which is used as the initial water water surface elevation in the model. The results for each sub-fault or unit source are calculated separately and the resulting displacements added. It is also possible to simulate a propagating rupture by including a time lag between the seabed displacement of each sub-fault.

For landslide sources, a numerical routine was developed to define the dynamic changes in seabed level arising from a landslide. The submarine landslide was simulated as a semi-gaussian body moving down a slope. The equation describing the landslide motion follows Enet & Grilli (2007), where the centroid of the semi-gaussian shape motion was modelled as a body sliding down a slope. The rigid body is subject to external forces due to gravity, added mass, hydrodynamic drag and shear stress. The detailed equations are available in the DTHA Report (PRDW, 2022a).

The equations only consider a cross-section of the slope and a straight trajectory of the slide on the horizontal plane. The trajectory and shape dimensions are converted to a space and time varying bathymetry adjustment which is coupled to the hydrodynamic model. ***Figure 5.9.94*** illustrates the process of the kinematics implementation and coupling to the hydrodynamic model.

CONTROLLED DISCLOSURE

When downloaded from the EDS database, this document is uncontrolled and the responsibility rests with the user to ensure it is in line with the authorised version on the database.

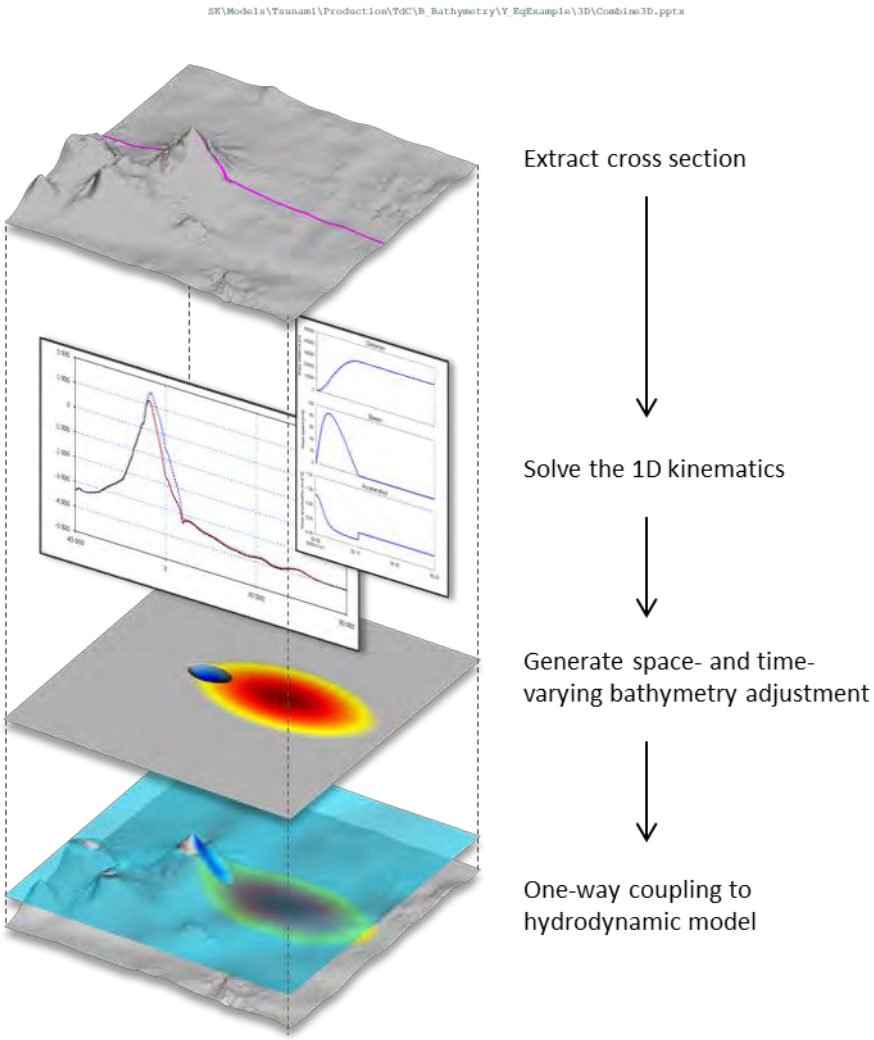


Figure 5.9.94: Process of the Kinematics Implementation and Coupling to the Hydrodynamic Model.

In modelling applications, the dimensions of a typical landslide are commonly approximated by half an ellipsoid. For numerical viability the semi-ellipsoid shape is approximated by a semi-gaussian shape. The slide's shape is able to deform, while conserving volume, by changing in width, length and thickness at a rate proportional to the slide's distance travelled with a prescribed maximum deformation limit.

Generic model settings

- The generic bathymetry and topography dataset described in ***Subsection 5.9.8*** was used in all models.
- For the regional models, spherical coordinate systems were used. For the local inundation model a projected coordinate system was used.

CONTROLLED DISCLOSURE

When downloaded from the EDS database, this document is uncontrolled and the responsibility rests with the user to ensure it is in line with the authorised version on the database.

- All regional models were run at a water level of 0 m msl without any external forcings (e.g., tides, wind) with the exception of Coriolis forcing.

5.9.12.6 Screening of Tsunami Sources

This section provides a summary of the preliminary screening process followed to identify which potential sources pose a hazard at the Duynefontyn site, and which sources can be screened out. The process which includes preliminary source characterisation and modelling is described in detail Sections 4 to 7 of the DTHA Report (PRDW, 2022a). The refined source characterisation and modelling are described in ***Subsections 5.9.12.7*** to ***5.9.12.12***.

Earthquakes, volcanos and submarine slumps/slides

A preliminary source characterisation model was developed for use in screening of possible tsunami sources that could potentially lead to consequential flooding of the Duynefontyn site. Based on a review of historical tsunamis in South Africa, previous Duynefontyn site characterisation reports and data (e.g., bathymetry and selected seismic profile data), and recent pertinent literature and lessons from the occurrence of tsunamis worldwide the following potential tsunamigenic sources were evaluated:

- Far-field earthquake (teleseismic subduction-zone) sources. These included sources from the Makran (**M** 9.1), Sumatra (**M** 9.4), and Scotia (**M** 9.1) subduction zones.
- Far-field volcanogenic (edifice or flank-collapse) sources. These included 83 km^3 flank collapses from the Canary Islands, Cape Verde Islands, Ascension Island, Tristan da Cunha Island, Marion Island, Reunion Island, and the Comoros Archipelago.
- Near-field fault sources. These included three potential fault sources in Table Bay of **M** 6.8.
- Submarine slumps/slides directly adjacent to site and on the continental slope. These included six submarine canyon slides with volumes ranging between 1.5 km^3 and 6.3 km^3, and four open slope slides with volumes of 33.5 km^3.

Subaerial landslides

Potential hazard from local terrestrial (subaerial) landslides was considered but not characterised due to the geological conditions near the site not being conducive to these events.

CONTROLLED DISCLOSURE

When downloaded from the EDS database, this document is uncontrolled and the responsibility rests with the user to ensure it is in line with the authorised version on the database.

Meteorites

Meteoroids capable of generating hazardous tsunamis, approximately 200 m diameter according to some studies, impact the Earth approximately every 100 000 years (Bland & Artemieva, 2006). This indicates that a tsunamigenic impact event in the south-eastern Atlantic would be much less frequent than every 100 000 years, i.e., the exceedance probability is less than 10^{-5} y^{-1}. Through the end of 2017, US National Aeronautics and Space Administration (NASA) calculated that they had identified over 50% of Near-Earth Objects (NEO) that are greater than 160 m diameter and all greater than 1 km in diameter (NSTC, 2018). For tracked NEO, impact can be predicted up to several years in advance. For previously unidentified NEO greater than 40 m NASA estimates NEO will be identified a few days or more before potential impact allowing for some mitigation and preparedness. Based on industry seismic data and desktop assessment, the hypotheses that the bathymetric depression on the outer shelf and the imbricated boulders on the Atlantic Seaboard are evidence of historical meteorite impact tsunamis are not supported.

Based on the above discussion, meteorite impact tsunamis cannot be screened out at the 10^{-8} y^{-1} exceedance probability. A previous hazard assessment for the site (Eskom, 2015) concluded the frequency of an impact generated tsunami exceeding 8 m would be approximately 2×10^{-5} y^{-1}. This frequency was based on meteor size at the top of the Earth's atmosphere. When the effects of the Earth's atmosphere on meteor size is accounted for, the frequency could be as low as approximately 7.7×10^{-7} y^{-1}. Although there are many factors which mitigate the risk (e.g., no currently identified asteroids are predicted to have any consequences in the next 100 years, impact from NEOs can be predicted up to several years in advance for tracked NEOs and a few days or more in advance for previously unidentified NEOs, and ongoing development is expected to greatly increase NEO identification capability), it is recommended that further investigation is carried out to quantify this and update previous assessments.

Preliminary source propagation modelling

The generation and propagation of the preliminary earthquake, volcano and submarine slide sources were simulated using the numerical models described in ***Subsection 5.9.12.5***. Full details of the model setup, tsunami generation and propagation for each source type are given in the DTHA Report (PRDW, 2022a).

The spatial resolution of the large-scale meshes used in the propagation runs was not refined to a resolution required to simulate penetration of tsunamis into the KNPS basin or to simulate wave run-up at the site. This was modelled only for the refined sources using the tsunami inundation

CONTROLLED DISCLOSURE

When downloaded from the EDS database, this document is uncontrolled and the responsibility rests with the user to ensure it is in line with the authorised version on the database.

model described in ***Subsection 5.9.12.11***. The bathymetry was truncated at -10 m msl along the coastline (i.e., all depths deeper than -10 m msl were set to -10 m msl) for all the tsunami propagation models, to produce consistent and comparable results (i.e., maximum and minimum water surface elevations) at the site across the different model meshes. From each model the maximum and minimum water surface elevations were extracted anywhere along the coastline at the site, defined for this purpose as the region between Melkbospunt and Matroospunt (see ***Figure 5.9.4***), extending from the coastline approximately to the -15 m msl depth contour to account for drying and flooding due to tsunami drawdown. A summary of the maximum and minimum water surface elevations at the site from all preliminary sources is presented in ***Figure 5.9.95***.

CONTROLLED DISCLOSURE

When downloaded from the EDS database, this document is uncontrolled and the responsibility rests with the user to ensure it is in line with the authorised version on the database.

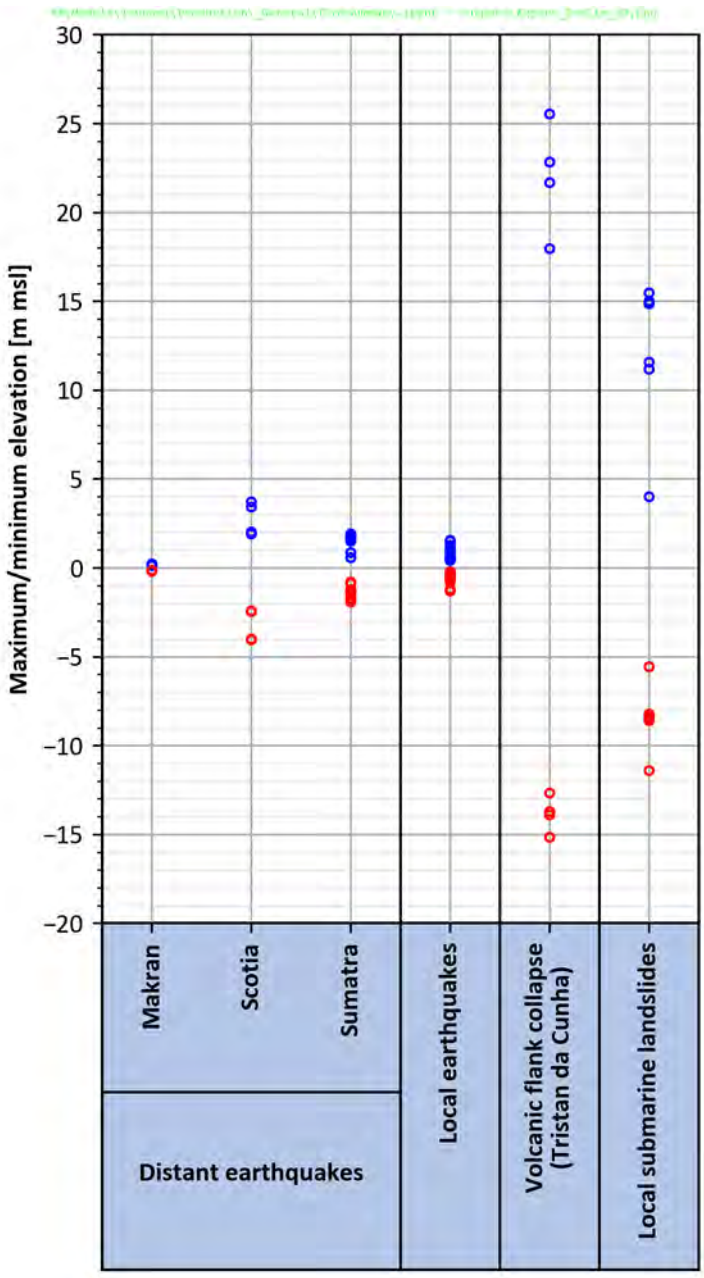


Figure 5.9.95: Maximum and Minimum Water Surface Elevations Along the Coastline at the Site Collated from All the Propagation Sensitivity Runs.

Based on the results of the tsunami propagation models for the preliminary sources, the Makran and Sumatra subduction zones and the local earthquakes were screened out from further analysis as they are enveloped by the Scotia subduction zone and are at least one order of magnitude smaller than the volcanic flank collapse sources. The following sources were screened in:

CONTROLLED DISCLOSURE

When downloaded from the EDS database, this document is uncontrolled and the responsibility rests with the user to ensure it is in line with the authorised version on the database.

- Subduction zone interface earthquakes on the Scotia subduction zone;
- Volcanic flank collapse landslides from Ascension, Tristan da Cunha and Marion Islands; and
- Local submarine landslides.

The source characterisation, model setup and results for these sources are presented in ***Subsections 5.9.12.7*** to ***5.9.12.9***.

5.9.12.7 Distant Earthquakes

Source characterisation

The tsunami source models for this study were modified from the global source model of the US National Oceanic and Atmospheric Administration's (NOAA) National Center for Tsunami Research. These sources were developed as part of a global tsunami forecast model. This source model divides subduction zones into 100 km by 50 km unit sources such that 1 m of slip on a unit source would represent a **M** 7.5 earthquake. These unit sources can be combined to generate longer and wider earthquake sources with variation in slip on different unit sources.

NOAA unit input source parameters were modified for the Scotia subduction source to have a consistent 5 km depth for the top of the upper unit source for the length of the subduction zone. This modification was made to be consistent with the Makran and Sumatra (Sunda-Java) sources. The Scotia subduction zone is one of the least studied subduction zones and the variation in the top depth in the NOAA model was assessed to not be defensible with the current scientific understanding. This uncertainty was accommodated by allowing the top of the fault plane to vary between 0 and 5 km depth to test the sensitivity of the model. Scotia sources were also modified to close a gap between the upper and lower sources.

Recent studies show that during large subduction interface earthquake events, zones of higher slip, called asperities, occur. For all subduction zone interface sources included in this study, the effect of zones of higher slip were tested. The maximum slip in the asperity was based on analogy to other great subduction events (i.e., areas with 20 m or more of slip during the 2004 Sumatra earthquake and regions with 40 m of slip or more during the 2011 Tohoku earthquake). Other model parameters were taken from established global values. The shear modulus (μ), or rigidity parameter, was based on the value used for other studies of tsunami generation from subduction interface earthquakes. All sources were modelled as pure thrust events.

The refined Scotia source parameters are given in ***Table 5.9.41***.

CONTROLLED DISCLOSURE

When downloaded from the EDS database, this document is uncontrolled and the responsibility rests with the user to ensure it is in line with the authorised version on the database.

Table 5.9.41: Unit Sources Used in the Refined Source Model SCO3 for the Scotia Subduction Zone (PRDW, 2022a).

Name[a]	Latitude	Longitude	Depth[b]	Strike	Dip	Slip[c]
	(degrees)	(degrees)	(km)	(degrees)	(degrees)	(m)
1ss5a	-55.91648	-26.40767	13.68	123.1	28.5	12
1ss5b	-55.54527	-25.9784	5	123.1	10	12
1ss6a	-56.41177	-25.51568	12.9	145.6	23.3	30
1ss6b	-56.16068	-24.85523	5	145.6	9.1	30
1ss7a	-57.09076	-24.94116	11.61	162.9	21.2	30
1ss7b	-56.95968	-24.15804	5	162.9	7.6	30
1ss8a	-57.85546	-24.72381	12.3	178.2	20.3	12
1ss8b	-57.84127	-23.88798	5	178.2	8.4	12
1ss9a	-58.61062	-24.91631	12.22	195.4	25.8	12
1ss9b	-58.72827	-24.0904	5	195.4	8.3	12
1ss10a	-59.30636	-25.5318	14.03	212.5	32.8	12
1ss10b	-59.54356	-24.79764	5	212.5	10.4	12
1ss11a	-59.93963	-26.54402	14.8	224.2	33.7	12
1ss11b	-60.24704	-25.90895	5	224.2	11.3	12
Total magnitude (**M**) for a rigidity of μ = 40 GPa.						**9.1**

Notes:
(a) Each unit source is 100 km (length) by 50 km (width), and a rake angle of 90 degrees is used (pure thrust).
(b) The depth of the top of the subduction zone was allowed to range from 0 to 5 km.
(c) The 30 m asperity was allowed to move laterally along the subduction zone to test effects of its location on simulated wave heights in South Africa.

Model setup

Figure 5.9.96 presents the Scotia model domain and bathymetry. A depth-dependent mesh refinement was used to maintain a resolution of approximately 50 points per wavelength for areas deeper than 250 m along the main propagation path towards the site, based on mesh sensitivity tests described in the DTHA Report (PRDW, 2022a). Further depth-dependent refinement down to a depth of 50 m was applied along the southern coastline of South Africa. This resulted in a total number of 5.7 million mesh elements with resolutions varying between 3.6 km and 400 m for a characteristic wave period of 15 minutes.

CONTROLLED DISCLOSURE

When downloaded from the EDS database, this document is uncontrolled and the responsibility rests with the user to ensure it is in line with the authorised version on the database.

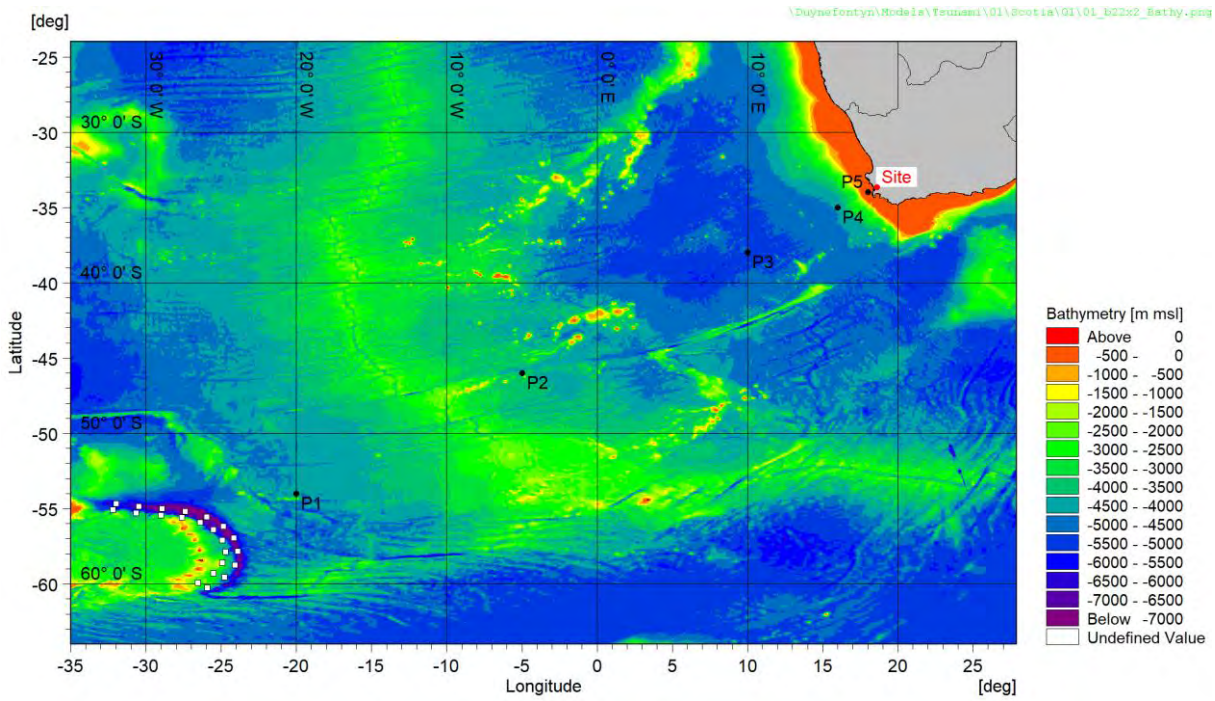


Figure 5.9.96: Scotia Model Domain and Bathymetry.

Flather boundary conditions were applied along the open ocean boundaries to absorb the tsunami as it propagates out of the domain. Bed resistance was modelled using a Manning's M of 32 $m^{1/3}/s$ and no horizontal eddy viscosity was included. The model was run for a duration of 24 hours.

Vertical displacements were generated for each of the earthquake sources as described in ***Subsection 5.9.12.5***, using the source parameters presented in ***Table 5.9.41***. The displacements were applied as initial water surface elevations in the model. The simulations included several positions of the 30 m asperity to test the sensitivity of the tsunami propagation to directionality of the source. Fault depths at both ends of the given range were also tested.

Results

Example results are shown in ***Figure 5.9.97*** which presents the maximum water surface elevation for the default asperity location for the shallow fault (0 km depth, SCO3c1). A summary of the maximum and minimum water surface elevations along the coastline at the site is presented in ***Subsection 5.9.12.10***.

CONTROLLED DISCLOSURE

When downloaded from the EDS database, this document is uncontrolled and the responsibility rests with the user to ensure it is in line with the authorised version on the database.

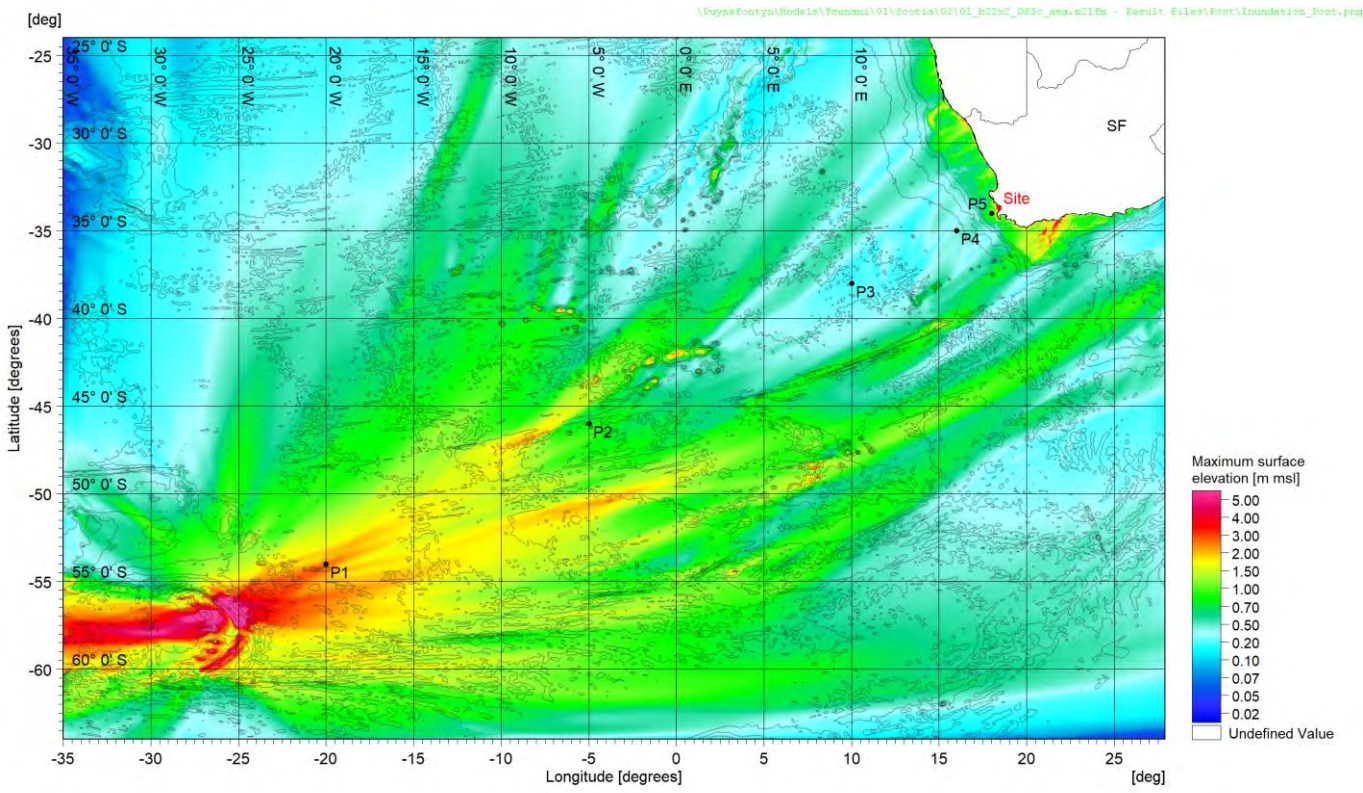


Figure 5.9.97: Maximum Water Surface Elevation for the SCO3c1 Scenario (Default Asperity Location, 0 km Depth). Isolines Show the Bathymetry Contours at 1 000 m Intervals.

5.9.12.8 Volcanic Flank Collapse

Source characterisation

Flank collapse events have been identified as the volcanogenic sources with the most tsunamigenic potential. Three volcanic flank collapse sources were included after the screening process:

- Ascension Island;
- Tristan da Cunha; and
- Marion Island.

The maximum credible event for all scenarios is expected to be approximately 80 km^3, similar in size to the well-studied maximum credible events in the Canary Islands based on analysis of offshore turbidite records and modelling studies. The Canary Islands landslides were used as an analogue for the other islands which are not as well studied. A generic 82.9 km^3 failure having a length of 16 km, width of 9 km, and thickness of 1.1 km has been prescribed for all the scenarios. The source parameters are given in ***Table 5.9.42***.

CONTROLLED DISCLOSURE

When downloaded from the EDS database, this document is uncontrolled and the responsibility rests with the user to ensure it is in line with the authorised version on the database.

Table 5.9.42: Refined Volcanogenic Flank Collapse Sources (PRDW, 2022a).

Location	Latitude	Longitude	Length[(a)]	Width[(b)]	Thickness	Volume[(c)]	Relative Density[(d)]	Heading
	(degrees)	(degrees)	(km)	(km)	(km)	(km^3)	(-)	(degrees)
Tristan da Cunha	-37.1001	-12.2054	16.0	9.0	1.1	82.9	1.96	91.4[(e)]
Marion Island (southern)	-46.8872	37.5871	16.0	9.0	1.1	82.9	1.96	301.5[(e)]
Marion Island (northern)	-46.8779	37.6422	16.0	9.0	1.1	82.9	1.96	324.6
Ascension Island	-7.9851	-14.3039	16.0	9.0	1.1	82.9	1.96	145.0[(e)]

Notes:
(a) Ellipsoidal length of landslide is measured down the slope.
(b) Ellipsoidal width of landslide is measured across the slope.
(c) Volume of semi-ellipsoid is π/6 × length × width × thickness.
(d) Ratio of wet bulk density (2 006 kg/m^3) to sea water density (1 025 kg/m^3).
(e) Final headings as used in numerical models. For Ascension Island the final heading was determined from sensitivity tests.

Three deposit geometries have been proposed based on analogues from Reunion, Tristan da Cunha and Cape Verde Islands. Marion and Ascension Island have no site-specific data and were therefore assumed to have the same deposit geometry as Tristan da Cunha Island. The three options for the refined volcanogenic deposit geometries are listed in ***Table 5.9.43***.

Table 5.9.43: Refined Volcanogenic Deposit Geometries.

Deposit Geometry	Length[(a)]	Width[(a)]	Thickness	Volume[(b)]	Runout Distance[(c)]
	(km)	(km)	(km)	(km^3)	(km)
D_1	71.0	37.2	0.06	82.9	35.5
D_2	60.0	52.8	0.05	82.9	30.0
D_3	38.4	59.0	0.07	82.9	19.2

Notes:
(a) Ellipsoidal dimensions.
(b) Volume of semi-ellipsoid is π/6 × length × width × thickness.
(c) Horizontal distance, centroid to centroid.

Model setup

Figure 5.9.98 presents Tristan da Cunha model domain and bathymetry. The computational mesh comprised triangular and quadrangular elements with resolutions ranging between 1 750 m in deep water (< -2 000 m msl) to 250 m in shallow water (> -250 m msl), such that a resolution of 24 points per wavelength was maintained for a characteristic wave period of approximately 10 minutes (first wave). The vertical mesh comprised three

CONTROLLED DISCLOSURE

When downloaded from the EDS database, this document is uncontrolled and the responsibility rests with the user to ensure it is in line with the authorised version on the database.

sigma layers with equal layer thicknesses. The same approach was followed for the Marion Island and Ascension Island sources.

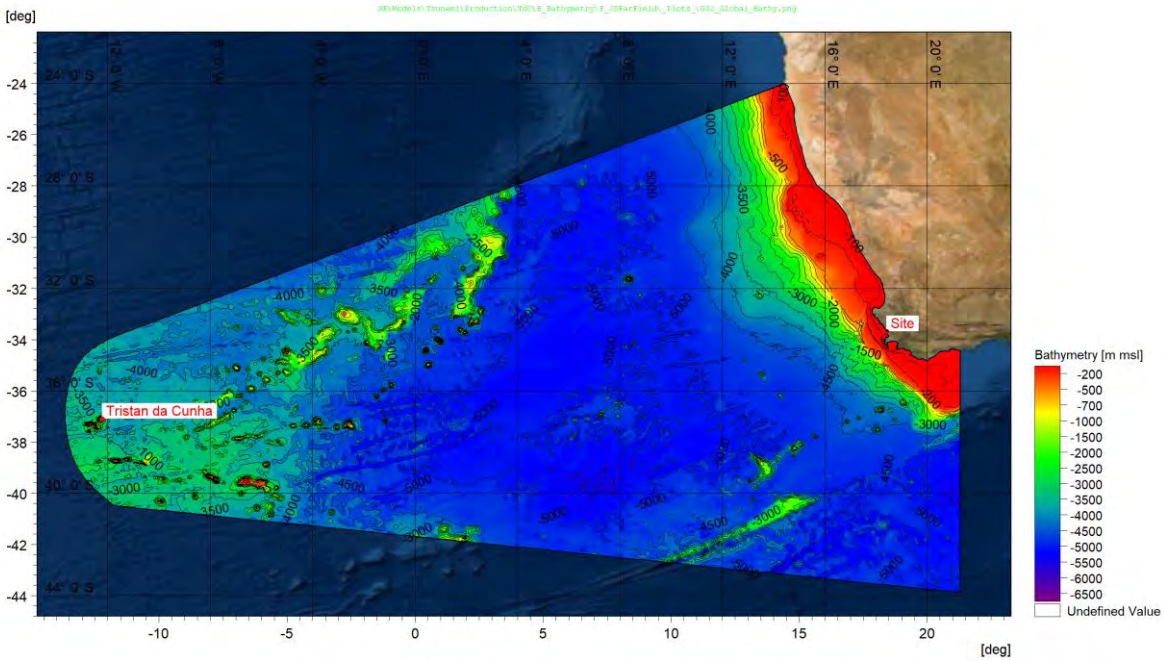


Figure 5.9.98: Tristan da Cunha Model Domain and Bathymetry.

The kinematics equations for the landslide motion described in ***Subsection 5.9.12.5*** were set up to fit the source descriptions from ***Table 5.9.42***. A bathymetry cross-section (***Figure 5.9.99***) was extracted from the generic bathymetry dataset (***Subsection 5.9.8***) to solve the kinematics.

With a prescribed deposit for each source the approach was to adjust the basal Coulomb friction (ψ) to achieve the correct runout distance. By default, all landslides were modelled as deforming landslides to match the final deposit geometries from ***Table 5.9.43***. The three deposit geometries, D_1 to D_3, varied from a long and narrow deposit with a longer runout distance, to a short and wide deposit with a shorter runout distance. The deformation was assumed to occur over the distance from the source centroid to the runout distance at a rate proportional to the slide distance.

The hydrodynamic drag coefficient, $C_d = 0.36$, was based on values used by Enet & Grilli (2007) for a similar shape. Sensitivity testing on this parameter within a range of realistic values showed little influence on the kinematics and nearshore water surface elevations. The added mass coefficient was conservatively assumed zero ($C_m = 0$).

CONTROLLED DISCLOSURE

When downloaded from the EDS database, this document is uncontrolled and the responsibility rests with the user to ensure it is in line with the authorised version on the database.

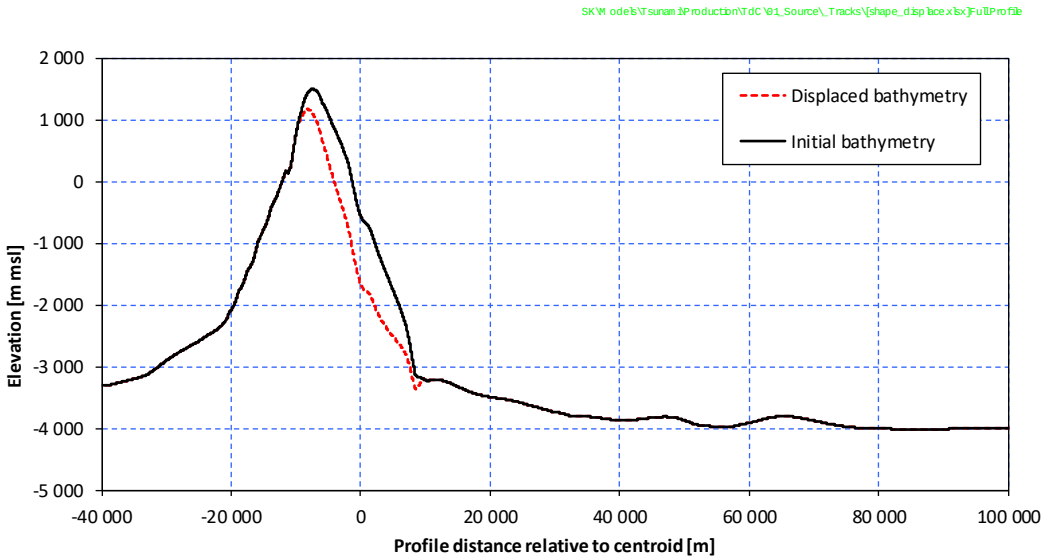


Figure 5.9.99: Cross-section of Tristan da Cunha and the Initial Landslide Geometry. Note the Vertical and Horizontal Axes are Not to Scale.

The outputs of the kinematics were coupled to the hydrodynamic model as a moving seabed. The horizontal and vertical eddy viscosities were computed using the k-ε turbulence closure scheme. The bed friction was set to zero. A 50 km-wide sponge layer was applied along the open model boundaries to absorb outgoing waves.

The Tristan da Cunha sources were run for a duration of 6 h, while the Marion Island and Ascension Island sources were run for 8 h and 8h30 min, respectively, due to the longer arrival times of these tsunamis. All three deposit geometries were modelled for the Tristan da Cunha and Ascension Island sources. For Marion Island, since the source geometries are identical to the other islands, it was assumed that the sensitivity of water surface elevations to the deposit geometries would be analogous to that of Tristan da Cunha. A failure on the southern site with a deposit geometry D_1 (i.e., expected worst case nearshore elevations) was therefore initially modelled to assess if further modelling was required. The results showed that the maximum and minimum water surface elevations were much smaller than that of Tristan da Cunha. The alternative deposit geometry scenarios and northern source location were therefore excluded from the modelling.

Results

Example results for the Tristan da Cunha D_1 scenario are shown below. ***Figure 5.9.100*** presents snapshots of instantaneous water surface elevation. ***Figure 5.9.101*** presents a detailed view of the maximum and instantaneous water surface elevation at the site along with a time-series of water surface elevation in front of the KNPS and at the location of maximum water surface elevation. A summary of the maximum and minimum water

When downloaded from the EDS database, this document is uncontrolled and the responsibility rests with the user to ensure it is in line with the authorised version on the database.

surface elevations along the coastline at the site is presented in ***Subsection 5.9.12.10***.

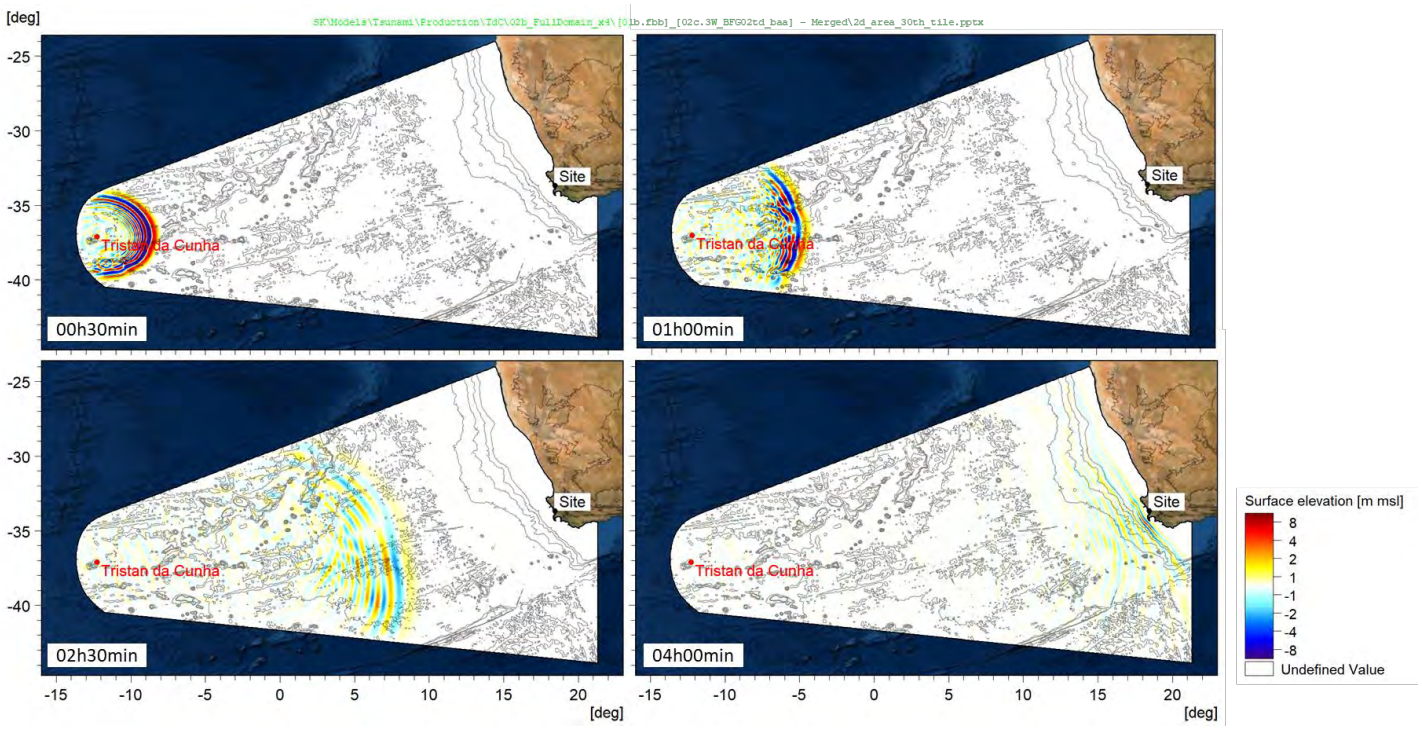


Figure 5.9.100: Tristan da Cunha D_1 Scenario. Snapshots of Instantaneous Water Surface Elevation. Isolines Show the Bathymetry Contours at 1 000 m Intervals.

CONTROLLED DISCLOSURE

When downloaded from the EDS database, this document is uncontrolled and the responsibility rests with the user to ensure it is in line with the authorised version on the database.

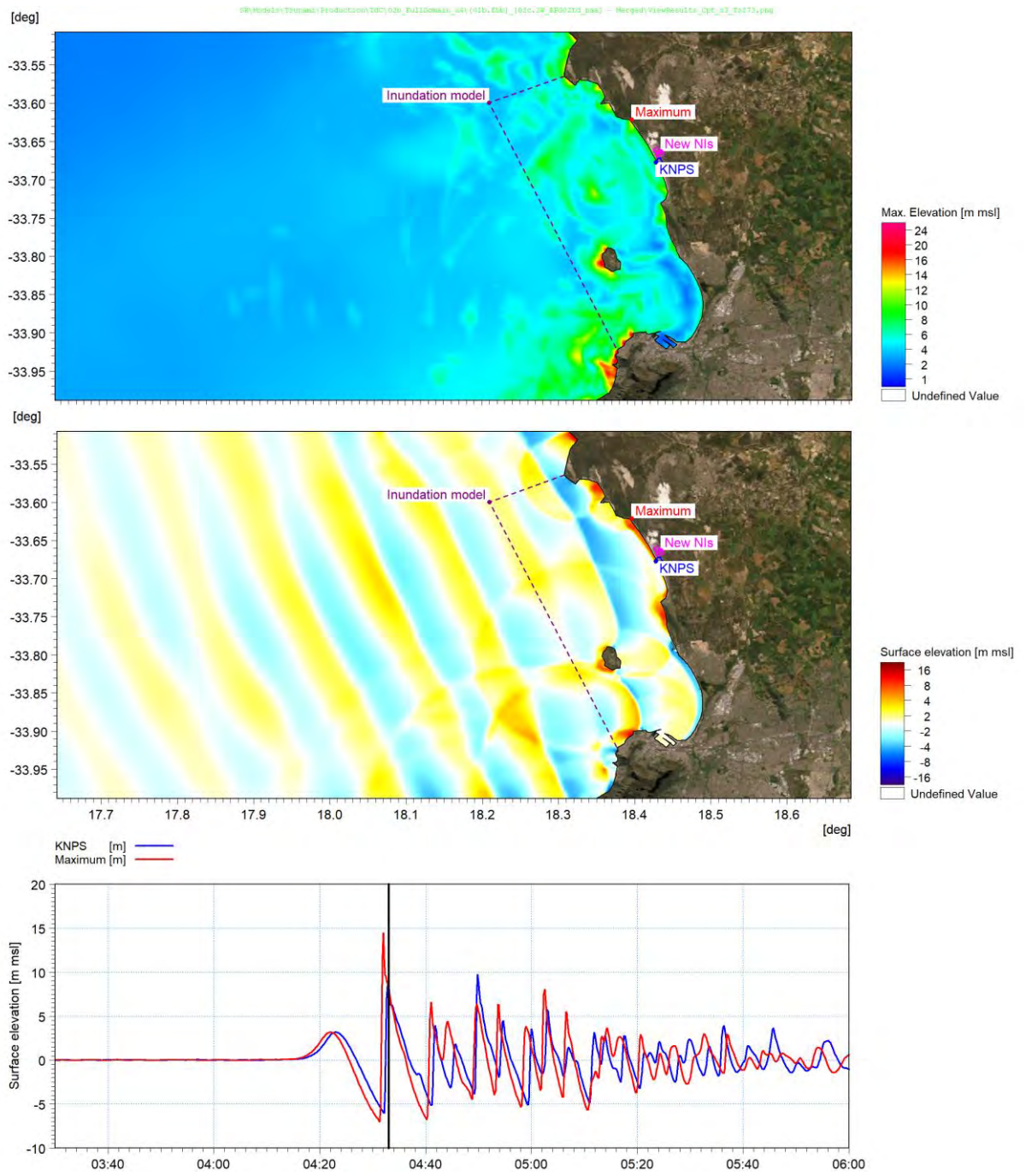


Figure 5.9.101: Tristan da Cunha D_1: Maximum Water Surface Elevation (Top), Snapshot of Instantaneous Water Surface Elevation (Middle), Time-series of Water Surface Elevation at KNPS and at the Location of Maximum Nearshore Water Surface Elevation (Bottom).

CONTROLLED DISCLOSURE

When downloaded from the EDS database, this document is uncontrolled and the responsibility rests with the user to ensure it is in line with the authorised version on the database.

5.9.12.9 Local Submarine Landslides

Source characterisation

Dingle (1980) and Dingle et al. (1987) refer to a large area of mass wasting as the Cape Town Slump. However, more recent, higher resolution Anadarko Petroleum Corporation multibeam bathymetric data does not show evidence for mass wasting at the scale of the Cape Town Slump. Sources identified in this study are characterised as slides rather than slumps based recent studies such as Palan (2017) which do not show evidence for large scale slumps.

The outer continental shelf and slope are dissected by a number of submarine canyons, the northernmost and largest being shelf-indenting Cape Canyon. This dissection limits the width of potential slides that could initiate in the upper slope region south of the Cape Canyon. Two general types of landslide sources that could pose a hazard to the Duynefontyn site were considered in the analysis:

- Submarine canyon failures (LSL1–LSL6); and
- Open slope failures (LSL7–LSL16, including LSL11a)

The canyon failures are more limited in width relative to the open-slope failures. Based on the sizes of apparent headscarps as imaged in hillshaded bathymetry maps a generic maximum single event slope canyon failure was defined with dimensions 8 km wide, 15 km long, and volumes varying between 3.1 km^3 and 5 km^3 depending on the thickness of the sediment. The size of LSL6, which is more tightly constrained by the head region of a hooked canyon, is modelled as a 4 km long, 7 km wide, with a 1.2 km^3 volume.

There are fewer constraints on the dimensions of the open-slope failures (LSL7 – LSL16). The estimated width of the maximum failures is based on the lengths of anomalous features observed in the bathymetry on the slope that have been suggested as possible incipient landslide scarps and the general width of what appear to be some of the larger areas of slumping as inferred from interpretation of bathymetry data. Based on these observations, a generic maximum single event open-slope failure was defined with dimensions 14 km wide, 20 km long, and volumes varying between 7.3 km^3 and 11.7 km^3 depending on the thickness of the sediment.

The source parameters are summarised in ***Table 5.9.44***.

CONTROLLED DISCLOSURE

When downloaded from the EDS database, this document is uncontrolled and the responsibility rests with the user to ensure it is in line with the authorised version on the database.

Table 5.9.44: Refined Local Submarine Landslide Sources (PRDW, 2022a).

Source	Latitude	Longitude	Depth at Centroid	Length[(a)]	Width[(b)]	Thickness	Volume[(c)]	Relative Density	Heading[(d)]
	(degrees)	(degrees)	(m msl)	(km)	(km)	(km)	(km^3)	(-)	(degrees)
LSL1	-33.722	17.010	-1 673	15.0	8.0	0.050	3.1	1.65	220
LSL2	-33.931	17.315	-1 119	15.0	8.0	0.080	5.0	1.65	232
LSL3	-34.113	17.443	-1 488	15.0	8.0	0.080	5.0	1.65	239
LSL4	-34.337	17.388	-2 034	15.0	8.0	0.080	5.0	1.65	270
LSL5	-34.483	17.613	-1 597	15.0	8.0	0.080	5.0	1.65	210
LSL6[(e)]	-33.793	17.359	-910	4.0	7.0	0.080	1.2	1.65	233
LSL7	-33.574	16.639	-2 000	20.0	14.0	0.050	7.3	1.65	243
LSL8	-33.506	16.990	-978	20.0	14.0	0.050	7.3	1.65	199
LSL9	-34.707	17.968	-856	20.0	14.0	0.080	11.7	1.65	218
LSL10	-34.248	17.520	-891	20.0	14.0	0.080	11.7	1.65	247
LSL11	-33.106	16.675	-1 128	20.0	14.0	0.050	7.3	1.65	256
LSL11a	-33.229	16.975	-581	20.0	14.0	0.050	7.3	1.65	249
LSL12	-33.356	16.654	-1 470	20.0	14.0	0.050	7.3	1.65	221
LSL13	-33.533	17.185	-754	20.0	14.0	0.050	7.3	1.65	242
LSL14	-34.558	17.815	-813	20.0	14.0	0.080	11.7	1.65	192
LSL15	-34.858	18.300	-483	20.0	14.0	0.080	11.7	1.65	197
LSL16	-35.412	18.743	-766	20.0	14.0	0.080	11.7	1.65	248

Notes:

(a) Ellipsoidal length of landslide is measured down the slope.
(b) Ellipsoidal width of landslide is measured across the slope.
(c) Volume of semi-ellipsoid is π/6 × length × width × thickness.
(d) Headings are based on a straight path from the source centroid to where the steepest path crosses the -2 500 m msl contour.
(e) Can be rigid or deforming.

A wide range of values were considered for the expected runout distances, ranging from a minimal runout, with the top of the slide mass proximal to the centroid location of the initial failure, to a maximum distance that correlates to a break in the slope at a water depth of -2 500 m msl – where there is an apparent break in slope (flattening) that might result in a decrease in slide velocity. Final dimensions of the deposits were based on the widths of the canyons that the landslides would be flowing through. Based on maintaining a deposit thickness of 0.02 km, three alternatives of landslide deposit length and width were determined for each initial landslide volume.

As per the volcanic deposits, the slide deposit geometry preserves the source volume, and cases named D_1 to D_3 for each source become increasingly longer and narrower. Full details are available in the DTHA Report (PRDW, 2022a).

CONTROLLED DISCLOSURE

When downloaded from the EDS database, this document is uncontrolled and the responsibility rests with the user to ensure it is in line with the authorised version on the database.

Model setup

Figure 5.9.102 presents the domain and bathymetry used in the refined model. The mesh comprised triangular elements with a depth-varying resolution ranging between 1 750 m in deep water (< -2 000 m msl) to 350 m in shallow water (> -250 m msl), such that a resolution of 24 points per wavelength was maintained for a characteristic wave period of approximately 14 minutes (first wave). The vertical mesh comprised three sigma layers with equal layer thicknesses.

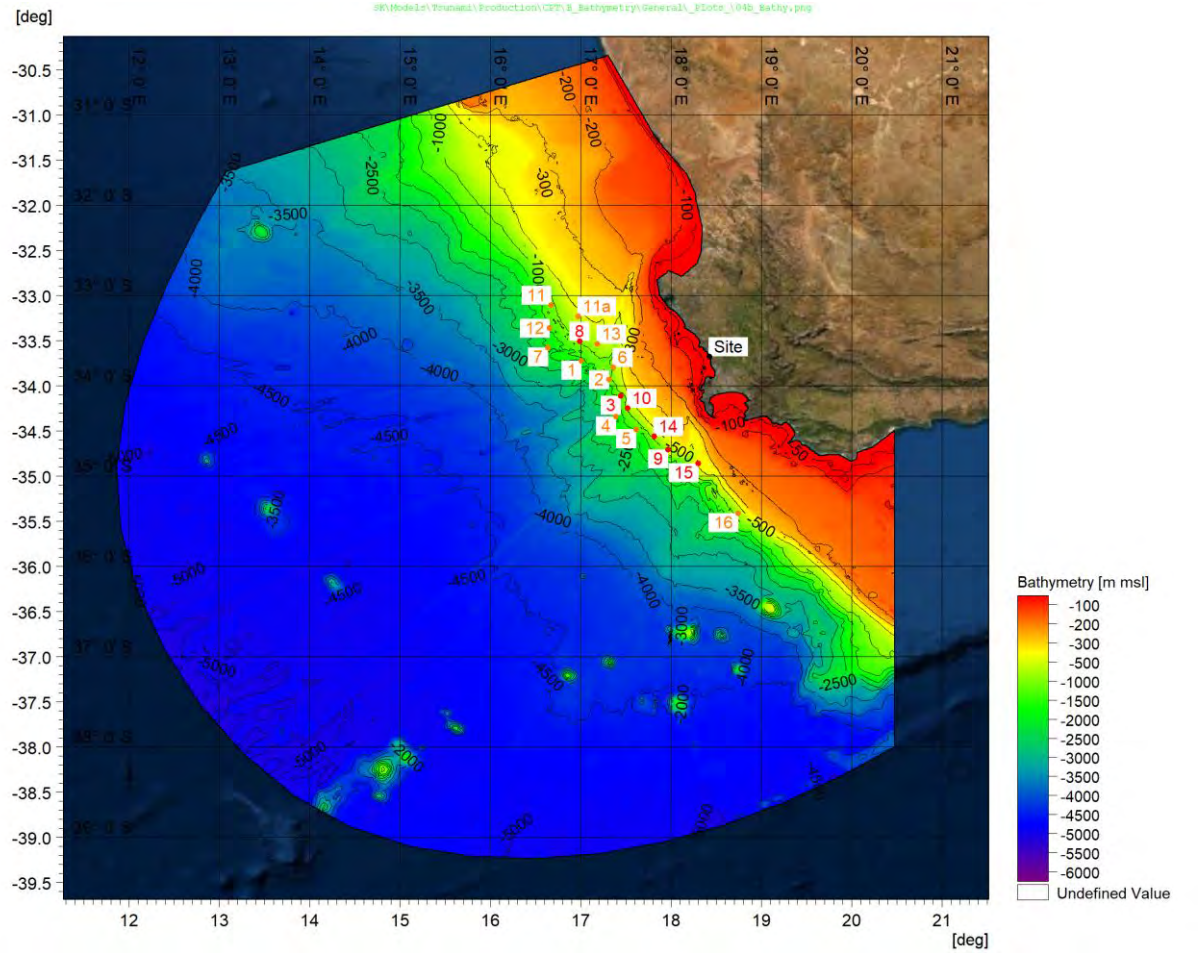


Figure 5.9.102: Bathymetry Used for the Local Submarine Landslide Models. The Source Centroids of the Landslides are Shown in Red for the Six Local Submarine Landslides Which Resulted in the Largest Water Surface Elevations at the Site and Orange for the Rest.

The kinematics equations for the landslide motion described in ***Subsection 5.9.12.5*** were set up to fit the source descriptions from ***Table 5.9.44***. The kinematics were calculated from the cross-sections following the curved path of the steepest slope. Since the results of the kinematics are projected onto a straight trajectory, a single heading was

CONTROLLED DISCLOSURE

When downloaded from the EDS database, this document is uncontrolled and the responsibility rests with the user to ensure it is in line with the authorised version on the database.

calculated for each landslide from the source centroid to where the steepest path crosses the -2 500 m msl contour.

The modelling approach was to let the landslides accelerate freely towards the -2 500 m msl contour where the slope flattens, before gradually decelerating to a stop. For this approach the friction was conservatively set to zero ($\psi = 0$), which made it possible to model all the sources with consistent assumptions. The same assumptions and coefficients from the volcanic flank collapse models were applied to the hydrodynamic drag coefficient and added mass coefficient.

By default, all sources were modelled as deforming landslides. The deformation was assumed to occur over the distance from the source centroid to the -2 500 m msl contour at a rate proportional to the distance travelled. The second runout option where the top of the deposit starts at the centroid of the initial landslide was not considered for the modelling as the shorter runout distance is expected to be less conservative.

All seventeen sources were initially modelled with the D_1 deposit geometry as initial tests showed the largest water surface elevations occurred with this geometry. The top five sources each with the highest maximum water surface elevations and the lowest minimum water surface elevations at the site were screened in for further runs with the alternative deposit geometries (D_2 and D_3).

Results

Figure 5.9.103 presents snapshots of instantaneous water surface elevation for the LSL9 D_1 deposit geometry. A detailed view of the maximum and instantaneous water surface elevation at the site is shown in ***Figure 5.9.104*** along with a time-series of water surface elevation in front of the KNPS and at the location of maximum water surface elevation. A summary of the maximum and minimum water surface elevations along the coastline at the site is presented in ***Subsection 5.9.12.10***.

CONTROLLED DISCLOSURE

When downloaded from the EDS database, this document is uncontrolled and the responsibility rests with the user to ensure it is in line with the authorised version on the database.

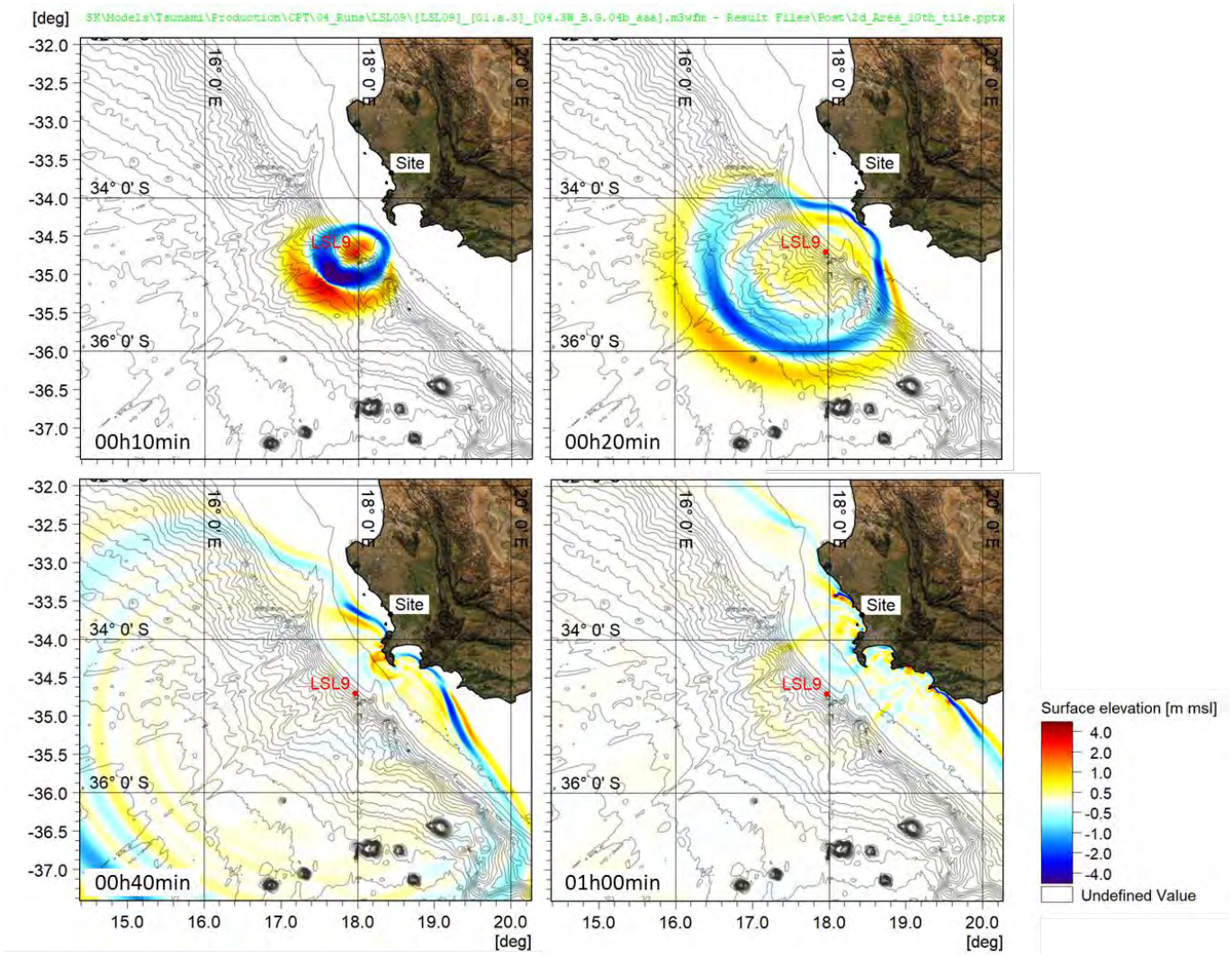


Figure 5.9.103: LSL9 D_1 scenario. Snapshots of Instantaneous Water Surface Elevation. Isolines Show the Bathymetry Contours at 200 m Intervals.

CONTROLLED DISCLOSURE

When downloaded from the EDS database, this document is uncontrolled and the responsibility rests with the user to ensure it is in line with the authorised version on the database.

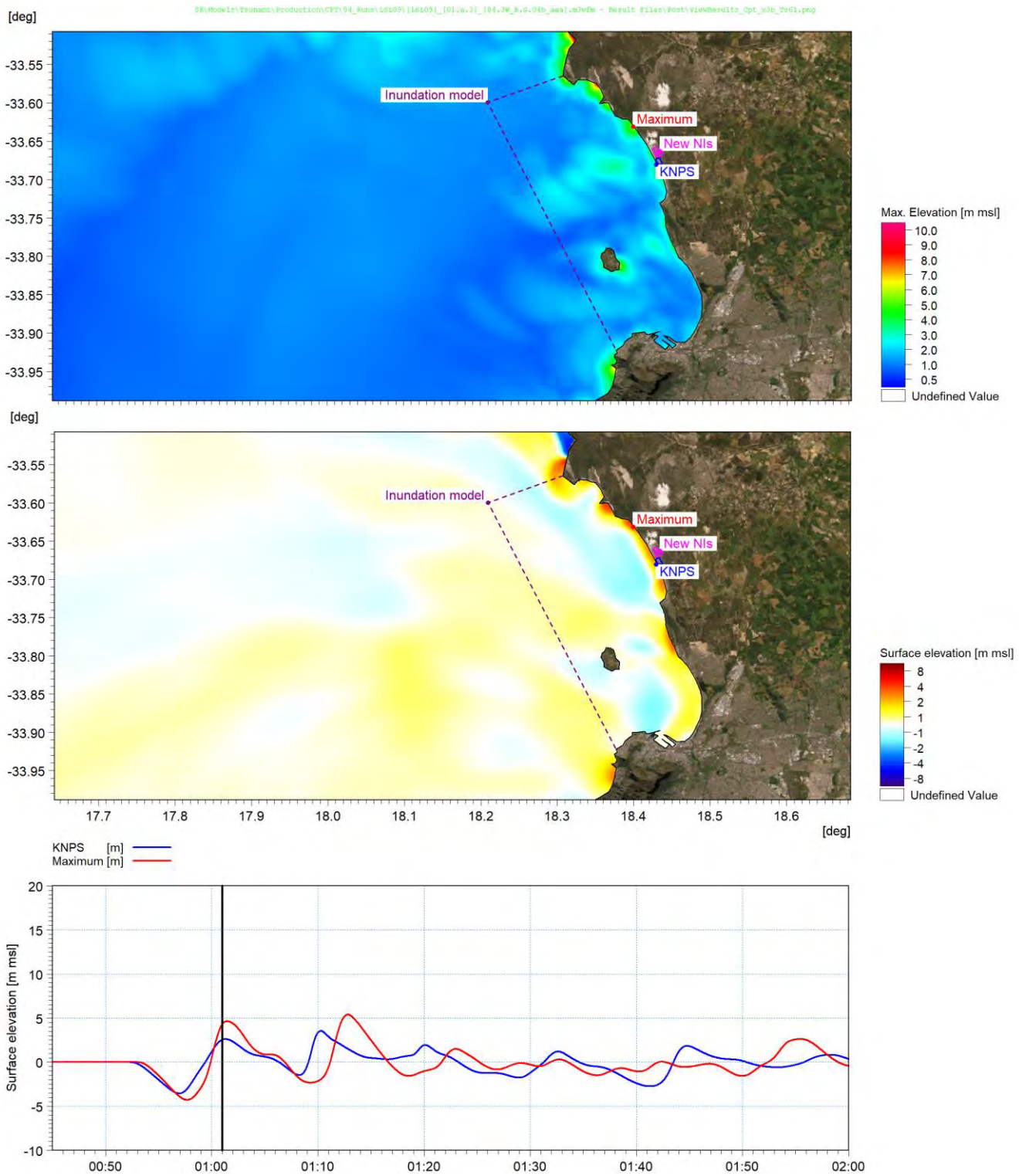


Figure 5.9.104: LSL9 D_1 scenario. Maximum Water Surface Elevation (Top), Snapshot of Instantaneous Water Surface Elevation (Middle), Time-series of Water Surface Elevation at KNPS and at the Location of Maximum Nearshore Water Surface Elevation.

CONTROLLED DISCLOSURE

When downloaded from the EDS database, this document is uncontrolled and the responsibility rests with the user to ensure it is in line with the authorised version on the database.

5.9.12.10 Regional Model Results

A summary of the maximum and minimum water surface elevations along the coastline at the site from all screened in sources is presented in ***Figure 5.9.105***.

Since long waves (including meteo-tsunamis) can produce similar wave patterns and associated run-up and drawdown to geological tsunamis, i.e., a sequence of wave trains with a wave period of 10 to 20 min, the extreme positive and negative long wave amplitudes were included in ***Figure 5.9.105*** to allow comparison to the geological tsunami results. The long wave results used were the positive (95th percentile) and negative (5th percentile) 10^{-8} y^{-1} exceedance probability long wave amplitudes, refer to ***Subsection 5.9.9.3*** and ***Table 5.9.14***.

Figure 5.9.105 shows that the minimum and maximum water surface elevations from the long waves are less than those from any of the geological tsunamis, i.e., distant earthquakes, volcanic flank collapse and local submarine landslides. The long waves (including meteo-tsunamis) are thus enveloped by the other tsunami types and are not analysed further.

CONTROLLED DISCLOSURE

When downloaded from the EDS database, this document is uncontrolled and the responsibility rests with the user to ensure it is in line with the authorised version on the database.

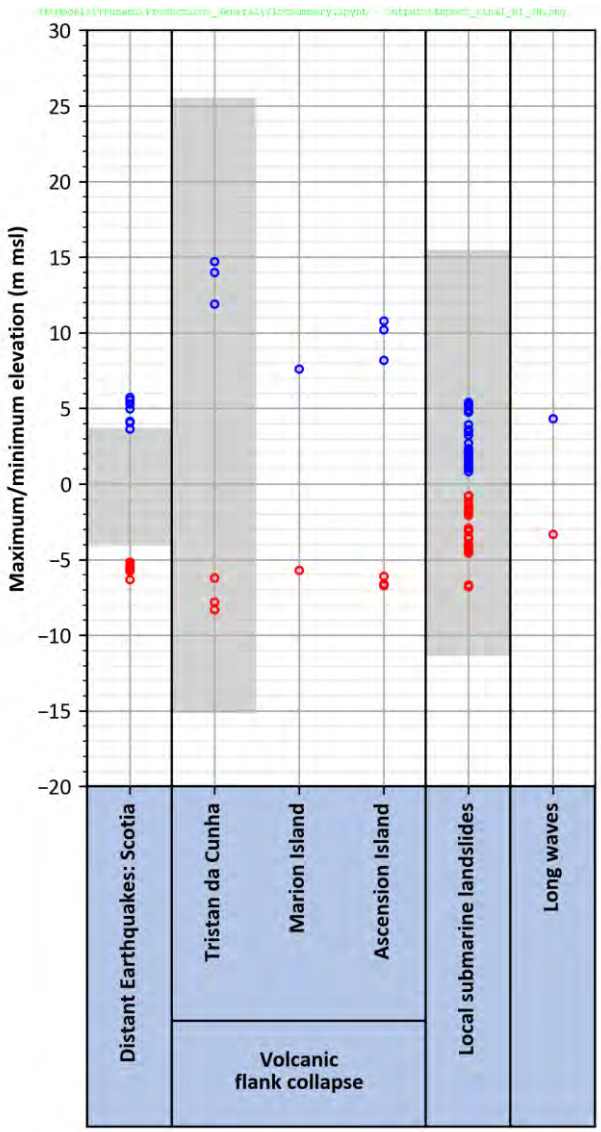


Figure 5.9.105: Maximum and Minimum Water Surface Elevations Along the Coastline at the Site Collated from All the Refined Runs. The Shaded Grey Bars Show the Range of Minimum and Maximum Values from the Sensitivity Runs. For Reference, the 10^{-8} y^{-1} Exceedance Probability Long Waves Are Also Shown.

5.9.12.11 Tsunami Inundation Model

Model setup

Detailed modelling of tsunami wave inundation at the site was carried out to determine the PMT defined by the maximum vertical run-up level, maximum horizontal inundation distance, minimum vertical drawdown and the maximum current velocities at KNPS and at the new NIs.

CONTROLLED DISCLOSURE

When downloaded from the EDS database, this document is uncontrolled and the responsibility rests with the user to ensure it is in line with the authorised version on the database.

The model mesh and bathymetry are presented in ***Figure 5.9.106*** and ***Figure 5.9.107***. The model domain extended approximately 15 km offshore to a depth of approximately -70 m msl. The mesh resolution varied between approximately 200 m at the offshore boundary to 5 m at KNPS to resolve the flow around the structures on the nuclear terrace. A resolution of approximately 10 m was used along the coastline opposite the new NIs to resolve flow around and over the dunes.

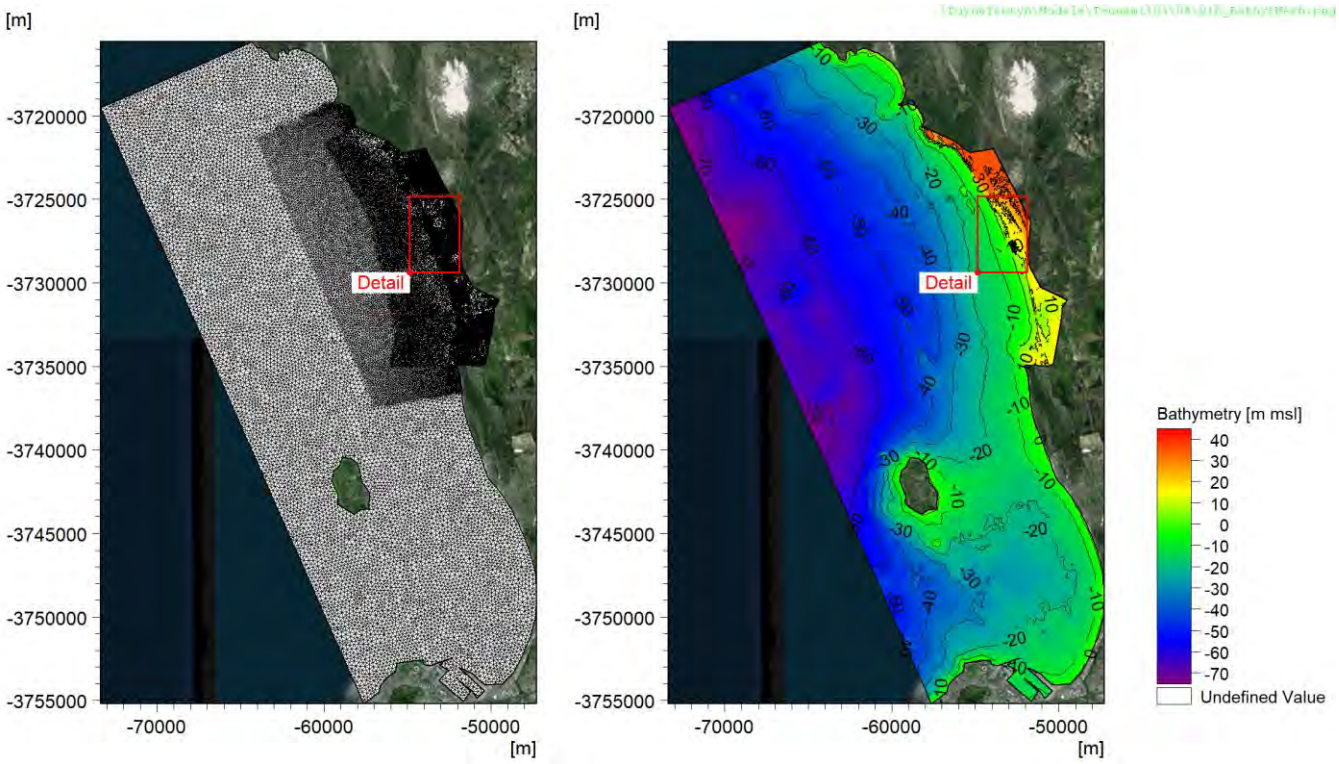


Figure 5.9.106: Tsunami Inundation Model Mesh and Bathymetry.

CONTROLLED DISCLOSURE

When downloaded from the EDS database, this document is uncontrolled and the responsibility rests with the user to ensure it is in line with the authorised version on the database.

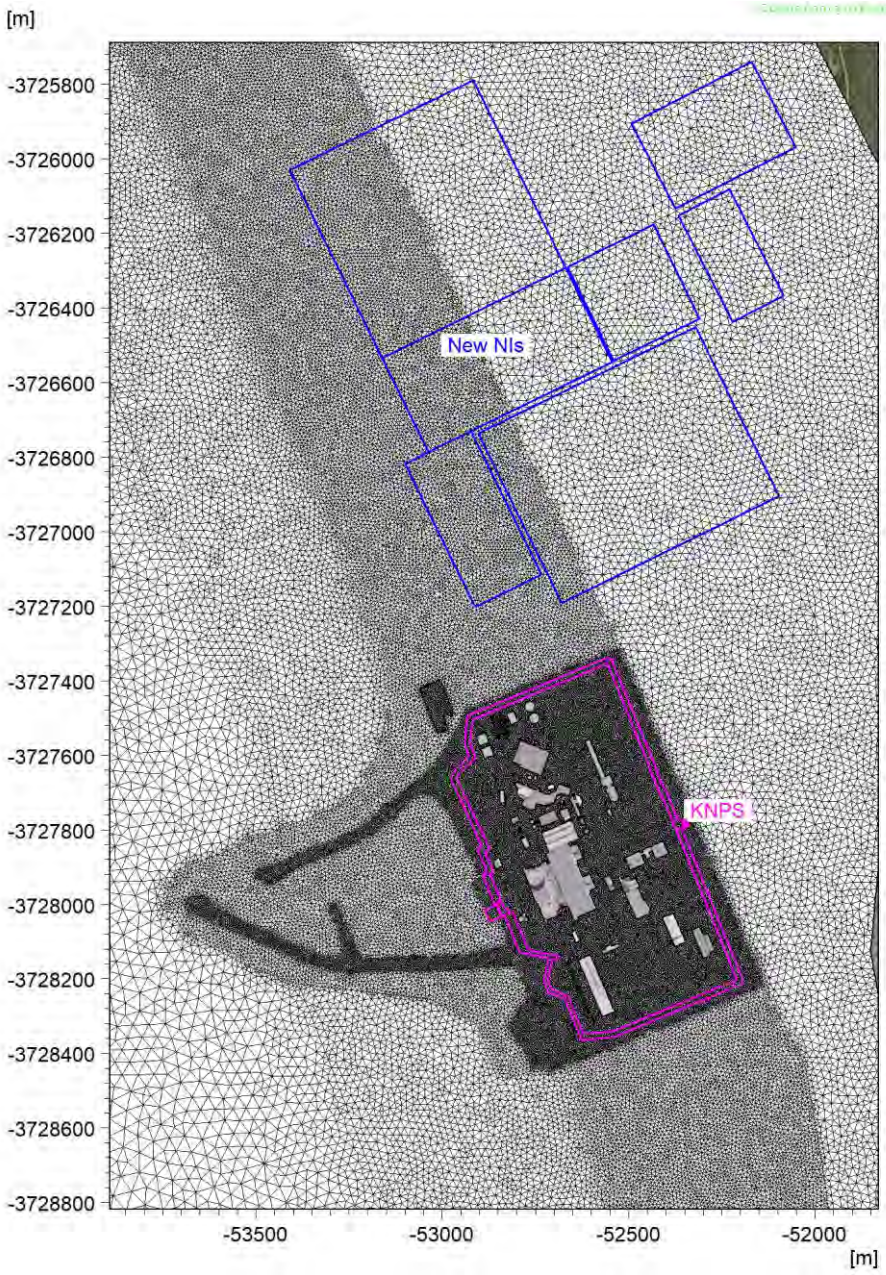


Figure 5.9.107: Detail of Tsunami Inundation Model Mesh.

Three base bathymetries were applied for the three years modelled (2021, 2064 and 2130). For 2021 the existing bathymetry was used. For 2064 and 2130, the coastline position was adjusted to account for climate change and long-term trends as described in ***Subsection 5.9.10***. Adjustments of the bathymetry for tsunami-induced erosion were also made to the dune ridges north and south of KNPS and to the intake basin entrance as described in ***Subsection 5.9.16.2***.

CONTROLLED DISCLOSURE

When downloaded from the EDS database, this document is uncontrolled and the responsibility rests with the user to ensure it is in line with the authorised version on the database.

Flather boundary conditions were specified along the offshore boundaries of the model. For each modelled tsunami, the time- and space-varying water levels and velocities were extracted directly from the regional models described in ***Subsection 5.9.12.7*** to ***5.9.12.9***.

Eddy viscosity was modelled using the Smagorinsky formulation. For each surface type in the model domain the corresponding Manning roughness was estimated from literature as described in detail in the DTHA Report (PRDW, 2022a). The applied roughness parameters are given in ***Table 5.9.37***.

Cases modelled

33 tsunami sources were modelled, comprising the following:

- Distant earthquakes: 8 sources from the Scotia subduction zone.
- Volcanic Flank Collapse: 7 sources:
    - Tristan da Cunha (deposit geometries D_1, D_2 and D_3)
    - Marion Island (deposit geometry D_1)
    - Ascension Island (deposit geometries D_1, D_2 and D_3)
- Local submarine landslides: 18 sources:
    - The sources resulting in the top five maximum and minimum water surface elevations were selected: LSL3, 8, 9, 10, 14, and 15. For each case, all three deposit geometries were modelled (D_1, D_2 and D_3).

Each tsunami source was modelled at high and low antecedent water levels, conservative for the maximum run-up and inundation, and the minimum drawdown, respectively. The levels were defined by the 10^{-1} y^{-1} exceedance probability 95th percentile maximum still water level (comprising tide + SLR + positive storm surge, refer ***Table 5.9.12***) and the 10^{-1} y^{-1} exceedance probability 5th percentile minimum still water level (comprising tide + negative storm surge, refer ***Table 5.9.13***) for each of the three dates (2021, 2064, 2130). The 10^{-1} y^{-1} exceedance still water level was selected as a conservative non-tidal water level component, given that tsunamigenic sources are uncorrelated to meteorological storm events which cause storm surge.

Results

To illustrate the model outputs and post-processing, selected figures are shown below for the Tristan da Cunha D_1 volcanic flank collapse scenario, modelled at the 2021 high antecedent water level.

CONTROLLED DISCLOSURE

When downloaded from the EDS database, this document is uncontrolled and the responsibility rests with the user to ensure it is in line with the authorised version on the database.

Figure 5.9.108 shows the inundation from the second wave crest. This wave resulted in the largest water depths on the southern side of KNPS for this scenario. At the time of the snapshot, water is seen overtop the intake basin breakwaters, and to have flowed onto the nuclear terrace.

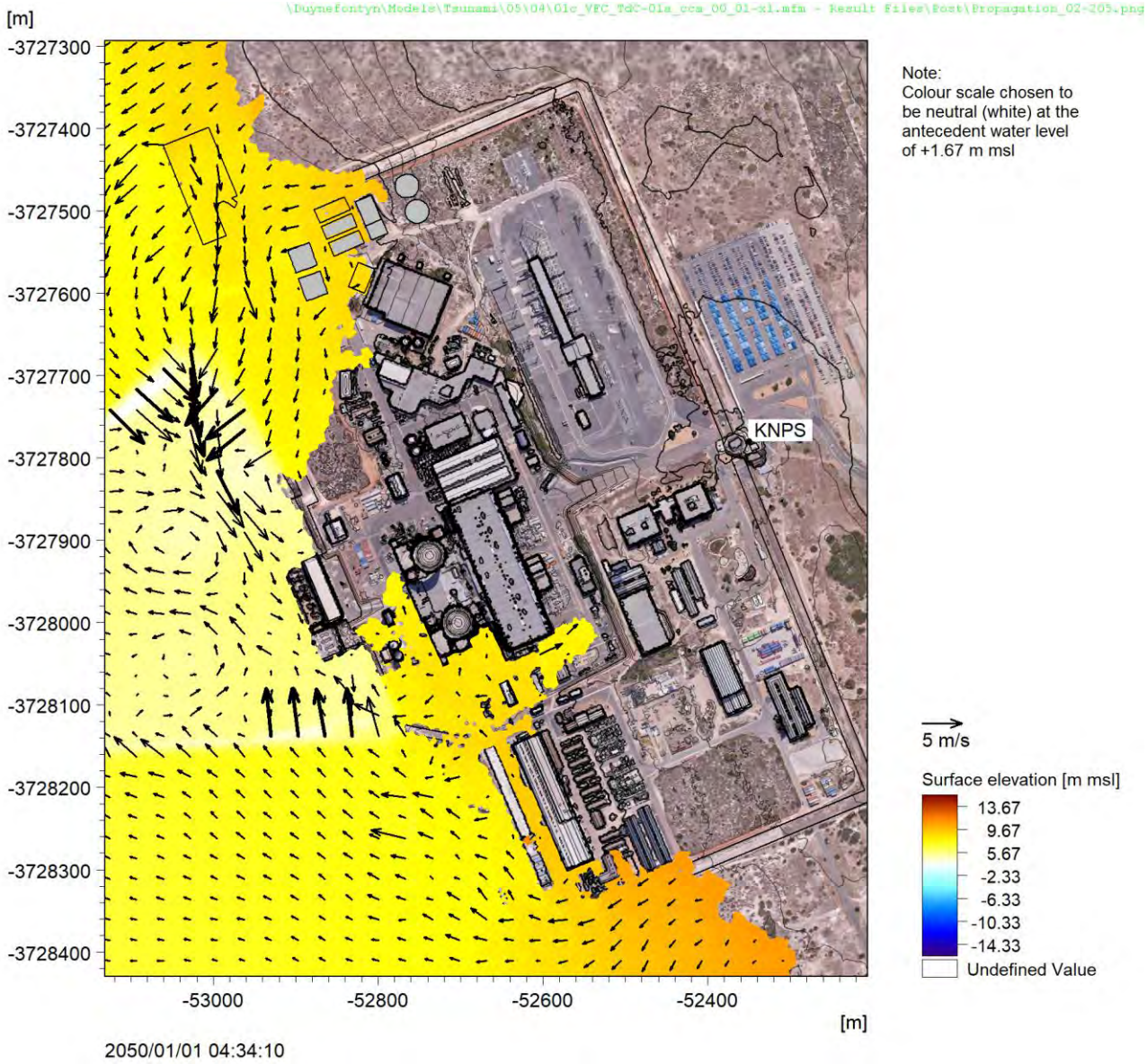


Figure 5.9.108: Instantaneous Water Surface Elevation (Colours) and Currents (Vectors) for the Tristan da Cunha D_1 Volcanic Flank Collapse Tsunami at the 2021 High Antecedent Water Level, Showing Inundation from the Second Wave Crest. Thick Vectors Show Current Speeds Exceeding 6 m/s.

The following key results were extracted from the model outputs for each case:

CONTROLLED DISCLOSURE

When downloaded from the EDS database, this document is uncontrolled and the responsibility rests with the user to ensure it is in line with the authorised version on the database.

- The maximum water depth and maximum current speed over the simulation.
- The maximum horizontal inundation distance that the water reached, measured perpendicularly inland from a predefined baseline (see ***Figure 5.9.85***). Separate domains were used for KNPS and the new NIs. For KNPS, the baseline was chosen to run parallel to the terrace and seaward of the intakes. At the new NIs, the baseline was chosen to approximately correspond to the present-day +2 m msl contour. The baselines and domains are illustrated in ***Figure 5.9.109*** and ***Figure 5.9.110*** for KNPS and the new NIs, respectively.
- The maximum vertical run-up level, defined as the highest ground or building level that was flooded (see ***Figure 5.9.85***). Depending on the topography this point may or may not coincide with the maximum inundation. The same domains as for the horizontal inundation were used.
- The minimum drawdown level at the KNPS cooling water intake pumps, and at the -20 m and -30 m msl depths opposite the new NIs.

Figure 5.9.109 presents a detailed view of KNPS showing the maximum water depth over the entire simulation. The figure highlights the location of the greatest horizontal inundation distance from the baseline (black dotted line) and the location with the highest level that was flooded. It is noted that the two locations differ, i.e., the highest level that was flooded in this scenario is the roof of the building directly landward of the outfall channel (+11.82 m msl), while the greatest horizontal inundation distance was at the landward limit of the nuclear terrace (382 m from the baseline).

CONTROLLED DISCLOSURE

When downloaded from the EDS database, this document is uncontrolled and the responsibility rests with the user to ensure it is in line with the authorised version on the database.

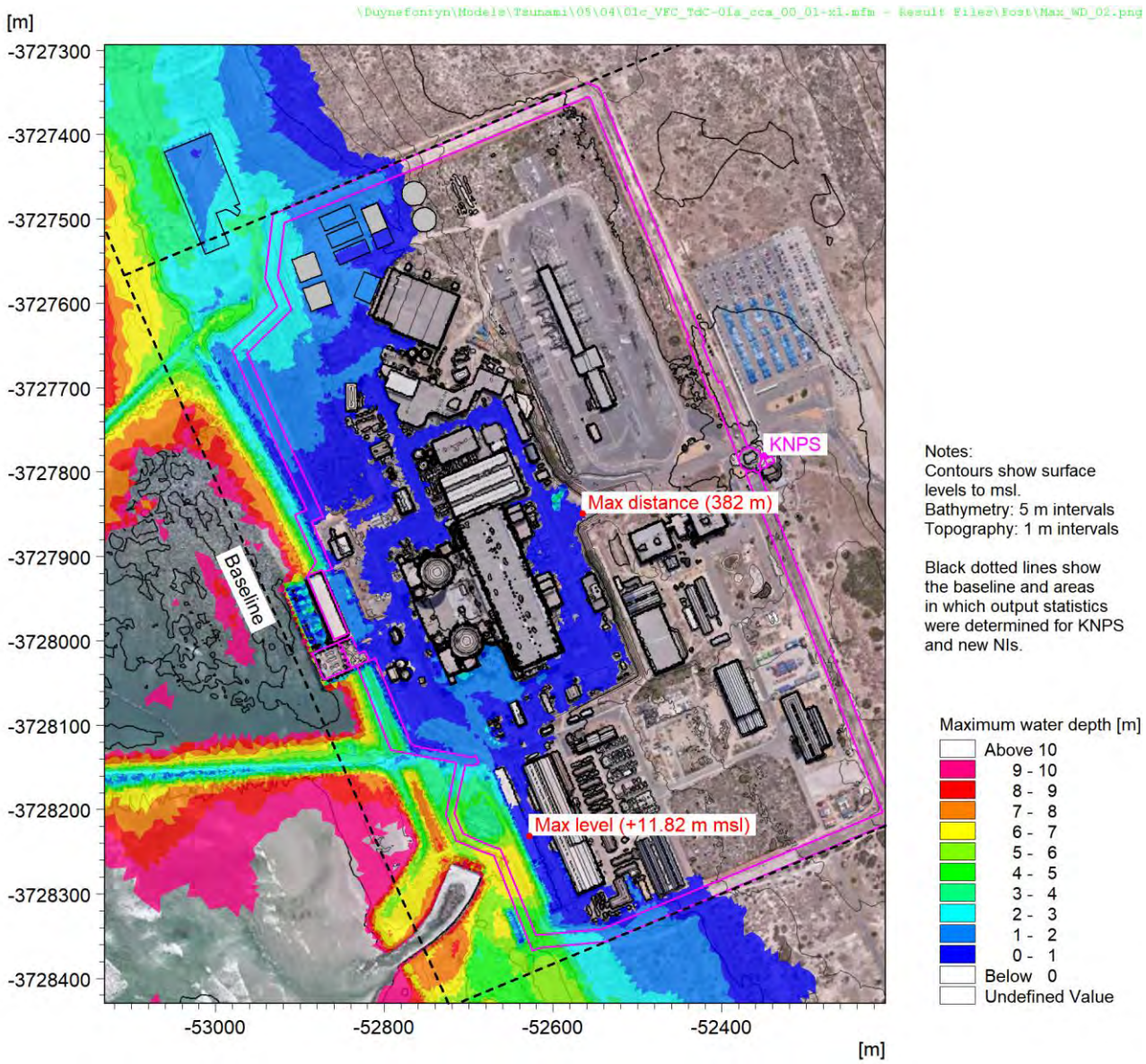


Figure 5.9.109: Maximum Water Depth at KNPS for the Tristan da Cunha D_1 Volcanic Flank Collapse Tsunami at the 2021 High Antecedent Water Level.

Figure 5.9.110 presents a similar figure for the new NIs. The areas of greatest horizontal inundation distance are the dune valleys. In this case, the maximum distance overlaps with the estimated position of the new NIs.

CONTROLLED DISCLOSURE

When downloaded from the EDS database, this document is uncontrolled and the responsibility rests with the user to ensure it is in line with the authorised version on the database.

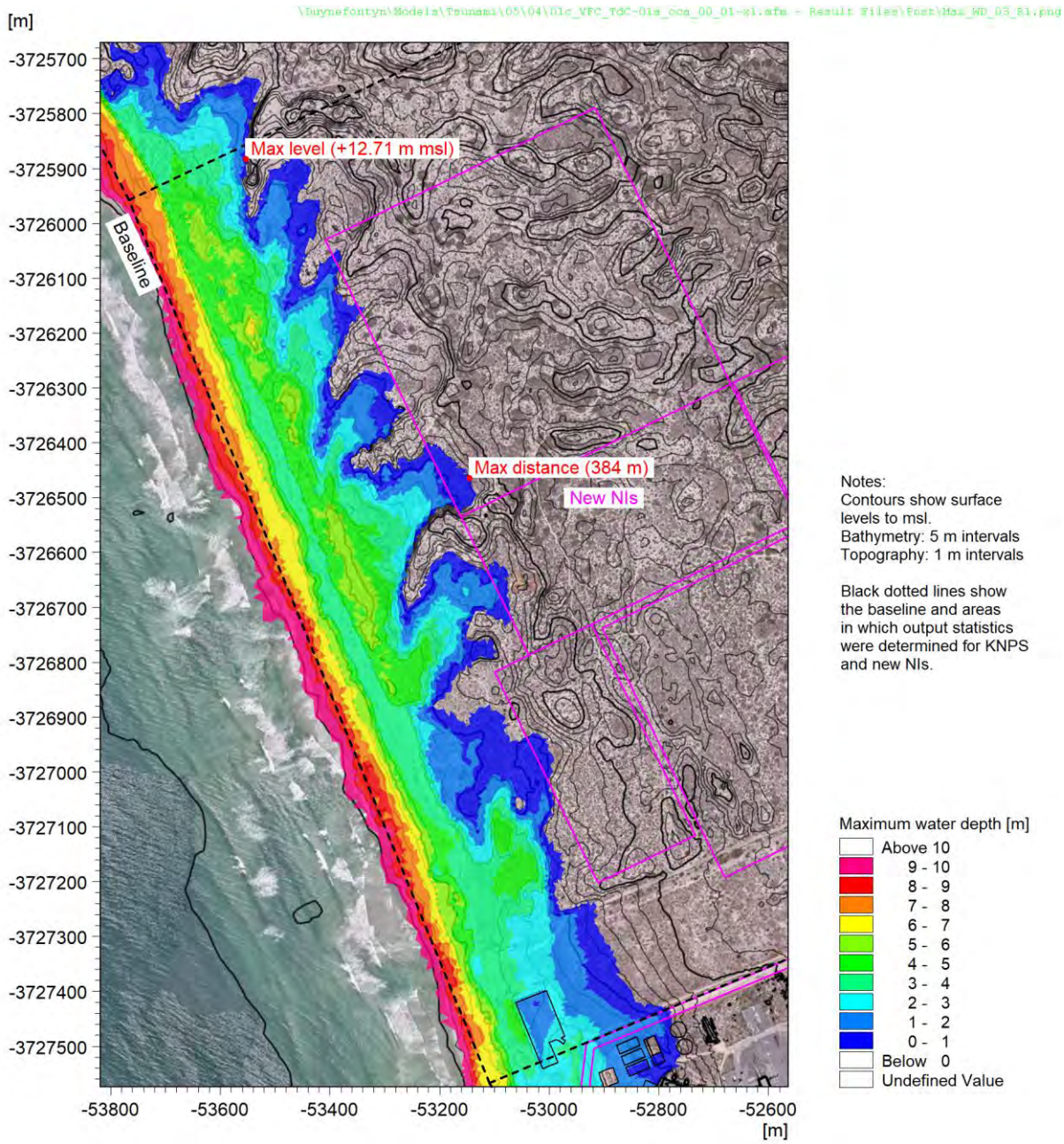


Figure 5.9.110: Maximum Water Depth at the New NIs for the Tristan da Cunha D_1 Volcanic Flank Collapse Tsunami at the 2021 High Antecedent Water Level.

5.9.12.12 Tsunami Results

A complete set of results, including spatial plots of the maximum water depth and maximum current speeds from each source type are presented in the DTHA Report (PRDW, 2022a), together with run-up, inundation and drawdown statistics for each individual source modelled.

CONTROLLED DISCLOSURE

When downloaded from the EDS database, this document is uncontrolled and the responsibility rests with the user to ensure it is in line with the authorised version on the database.

A set of figures showing the maximum water depth and current speeds at KNPS (2021 and 2064) and at the new NIs (2021, 2064, 2130) for the PMT are included in ***Appendix B***. The tsunami flooding results are summarised in ***Table 5.9.45***, while the extreme low water levels due to tsunamis are summarised in ***Table 5.9.46***.

Table 5.9.45: Flooding Due to Tsunamis.

Source Type	KNPS				New NIs					
	Max Vertical Run-up Level		Max Horizontal Inundation Distance		Max Vertical Run-up Level			Max Horizontal Inundation Distance		
	(m msl)		(m from Baseline[a])		(m msl)			(m from Baseline[b])		
	2021	2064	2021	2064	2021	2064	2130	2021	2064	2130
Distant earthquakes	6.05	6.81	137	162	6.67	7.22	8.95	80	169	333
Volcanic flank collapse	11.82	13.95	382	399	12.71	13.93	15.82	384	399	553
Local submarine landslides	6.80	7.04	143	175	6.80	8.19	10.08	123	184	333
Probable Maximum Tsunami (PMT)	11.82	13.95	382	399	12.71	13.93	15.82	384	399	553

Notes:
(a) At KNPS the baseline is parallel to the terrace and seaward of the intakes.
(b) At the new NIs the baseline corresponds to the present-day +2 m msl contour.

Table 5.9.46: Extreme Low Water Levels due to Tsunamis.

Source Type	KNPS		New NIs								
	Minimum vertical drawdown level at pumps		Minimum vertical drawdown level at pumps[a]			Minimum vertical drawdown at -20 m msl			Minimum vertical drawdown at -30 m msl		
	(m msl)		(m msl)			(m msl)			(m msl)		
	2021	2064	2021	2064	2130	2021	2064	2130	2021	2064	2130
Distant earthquakes	-2.26	-2.26	-2.26	-2.26	-2.23	-4.96	-5.04	-5.19	-3.90	-3.87	-3.81
Volcanic flank collapse	-1.83	-1.81	-1.83	-1.81	-1.77	-7.18	-7.16	-7.18	-6.64	-6.65	-6.51
Local submarine landslides	-2.12	-2.12	-2.12	-2.12	-2.14	-5.35	-5.36	-5.40	-4.69	-4.70	-4.73
Probable Maximum Tsunami (PMT)	-2.26	-2.26	-2.26	-2.26	-2.23	-7.18	-7.16	-7.18	-6.64	-6.65	-6.51

Notes:
(a) Assuming a basin intake with similar geometry to KNPS.

The warning time for these tsunami events is related to the travel time of the tsunami wave from the source to the site. The modelled travel times for each of the three source types are as follows:

- Distant earthquakes (Scotia subduction zone): 6 h
- Volcanic flank collapse (Tristan da Cunha): 4 h

CONTROLLED DISCLOSURE

When downloaded from the EDS database, this document is uncontrolled and the responsibility rests with the user to ensure it is in line with the authorised version on the database.

- Local submarine landslides (located in water depths between 500 and 1500 m on the shelf break offshore of the site): 40 min.

The duration that the tsunami wave impacts the site ranges from more than 1 day for distant earthquakes to a few hours for local submarine landslides, although in all cases the maximum run-up and minimum drawdown are associated with a small number of large waves in the wave train.

These results are compared to the equivalent storm results (see ***Subsection 5.9.11***) to determine the extreme flooding from the sea (see ***Subsection 5.9.13***) and the extreme low water levels at the cooling water intakes (see ***Subsection 5.9.14***).

5.9.13 Flooding from the Sea

Flooding from the sea can occur due to:

- Storm wave run-up combined with sea level rise, high tides, positive storm surge, wave set-up and basin seiche, as described in ***Subsection 5.9.11***; and
- Tsunami run-up combined with sea level rise, high tides and positive storm surge, as described in ***Subsection 5.9.12***.

The flooding results are summarised in ***Table 5.9.47*** and plotted in ***Figure 5.9.111*** to ***Figure 5.9.114***. Since the PMT does not have an associated exceedance probability, these results are plotted as horizontal lines in the figures.

CONTROLLED DISCLOSURE

When downloaded from the EDS database, this document is uncontrolled and the responsibility rests with the user to ensure it is in line with the authorised version on the database.

Table 5.9.47: Flooding from the Sea.

Source of Flooding	Exceedance Probability	KNPS				New NIs					
		Max Vertical Run-up Level		Max Horizontal Inundation Distance		Max Vertical Run-up Level			Max Horizontal Inundation Distance		
	(y^{-1})	(m msl)		(m from Baseline[a])		(m msl)			(m from Baseline[b])		
		2021	2064	2021	2064	2021	2064	2130	2021	2064	2130
Storm Waves	10^{-2}	6.55	6.53	104	127	6.38	6.66	9.38	79	160	328
Storm Waves	10^{-4}	7.85	7.67	145	186	8.97	9.87	12.41	125	210	345
Storm Waves	10^{-5}	8.69	8.33	156	222	9.10	10.35	13.36	177	257	365
Storm Waves	10^{-6}	9.54	9.00	168	258	9.23	10.83	14.31	229	305	385
Storm Waves	10^{-7}	10.13	10.41	207	321	10.11	12.03	15.52	259	321	406
Storm Waves	10^{-8}	10.72	11.83	246	383	10.98	13.24	16.73	288	336	427
Tsunami: Distant earthquakes	(c)	6.05	6.81	137	162	6.67	7.22	8.95	80	169	333
Tsunami: Volcanic flank collapse	(c)	11.82	13.95	382	399	12.71	13.93	15.82	384	399	553
Tsunami: Local submarine landslides	(c)	6.80	7.04	143	175	6.80	8.19	10.08	123	184	333
Probable Maximum Tsunami (PMT)	(d)	11.82	13.95	382	399	12.71	13.93	15.82	384	399	553

Notes:
(a) At KNPS the baseline is parallel to the terrace and seaward of the intakes.
(b) At the new NIs the baseline corresponds to the present-day +2 m msl contour.
(c) Maximum for each tsunami source type.
(d) Maximum for all tsunami source types.

CONTROLLED DISCLOSURE

When downloaded from the EDS database, this document is uncontrolled and the responsibility rests with the user to ensure it is in line with the authorised version on the database.

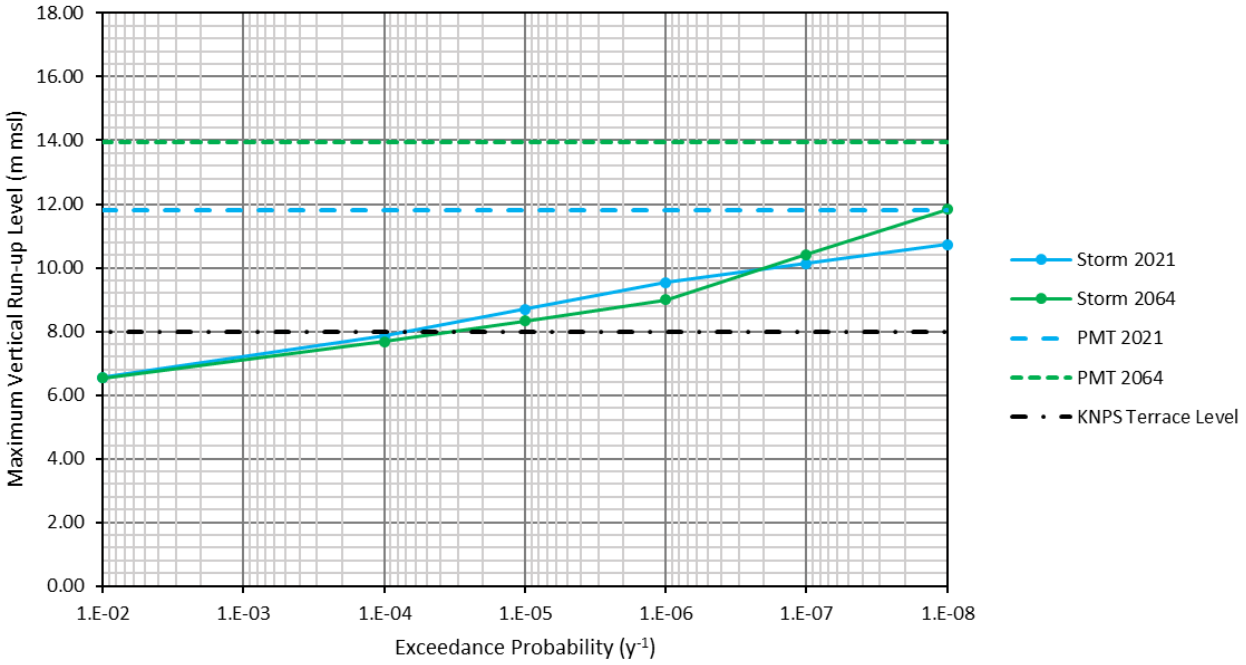


Figure 5.9.111: Vertical Run-up Levels at KNPS.

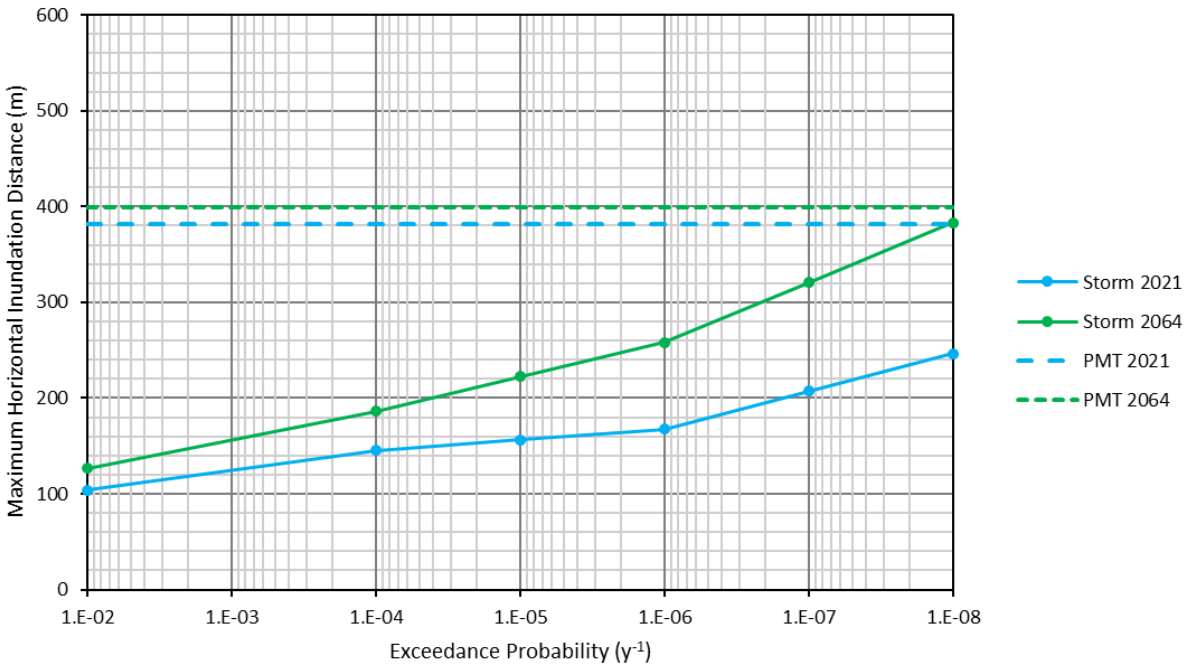


Figure 5.9.112: Horizontal Inundation Distance at KNPS.

CONTROLLED DISCLOSURE

When downloaded from the EDS database, this document is uncontrolled and the responsibility rests with the user to ensure it is in line with the authorised version on the database.

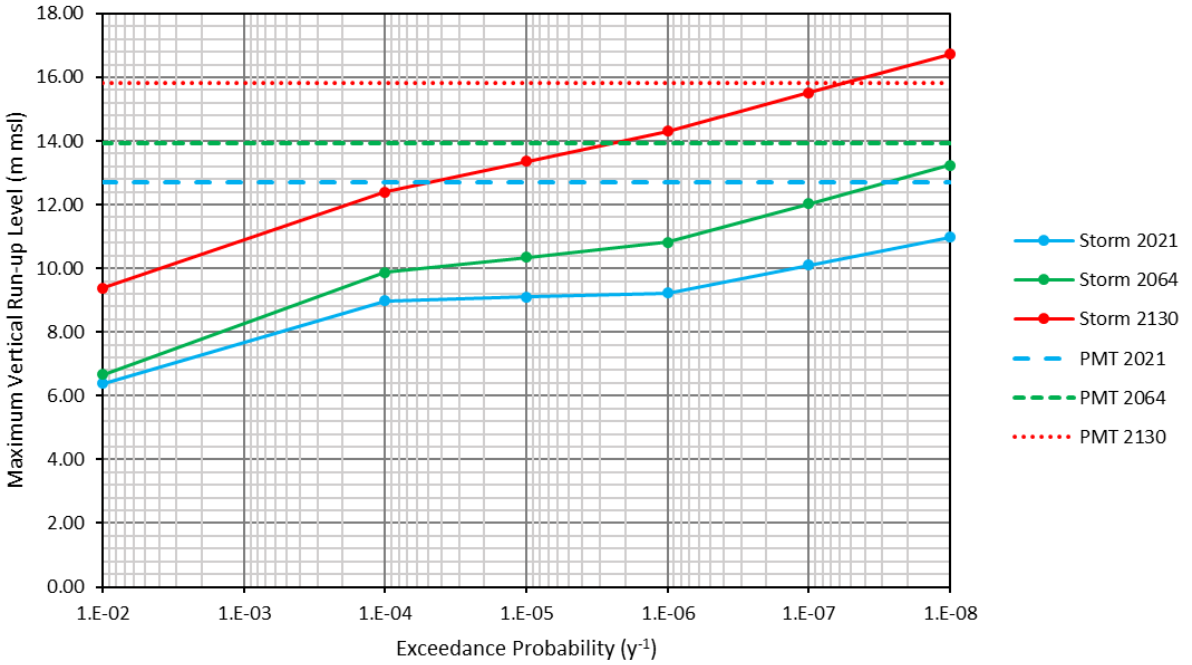


Figure 5.9.113: Vertical Run-up Levels at new NIs.

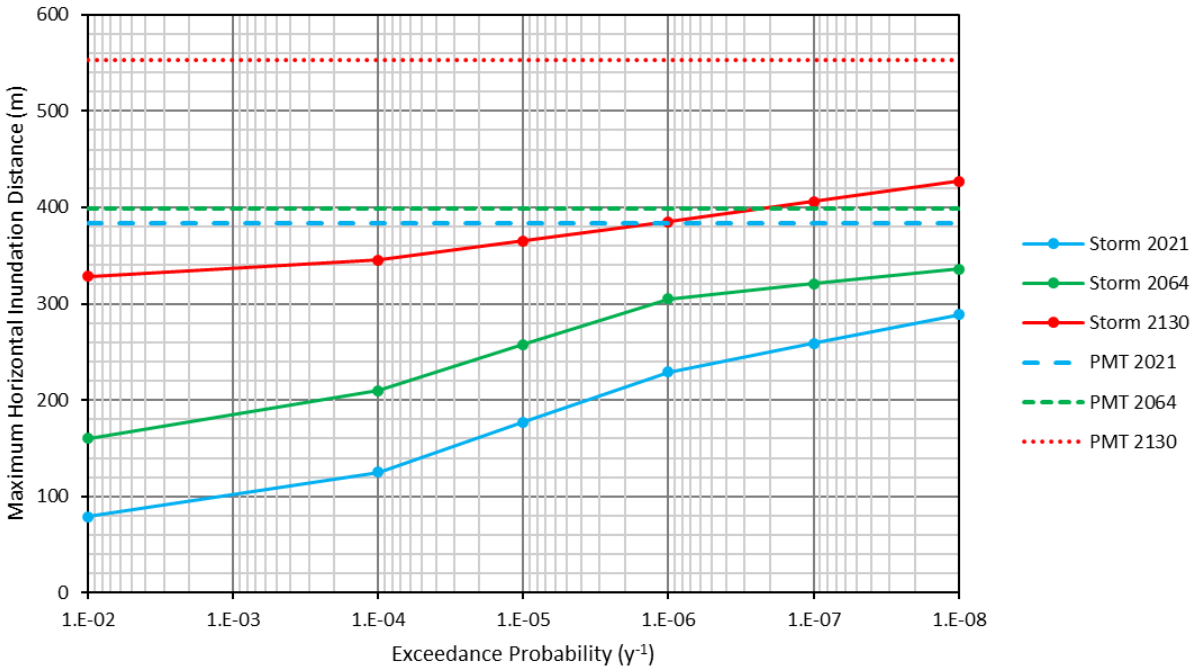


Figure 5.9.114: Horizontal Inundation Distance at new NIs.

CONTROLLED DISCLOSURE

When downloaded from the EDS database, this document is uncontrolled and the responsibility rests with the user to ensure it is in line with the authorised version on the database.

The results presented above show the following:

- The flooding hazard generally increases over time due to climate change and long-term coastline erosion. The only exceptions are the run-up levels at KNPS for the larger exceedance probabilities which are lower in 2064 compared to 2021, which is due to accretion of the coastline south of KNPS (see ***Subsection 5.9.10.6***).
- At KNPS, the PMT run-up and inundation are governed by the volcanic flank collapse tsunamis which result in extensive flooding of the KNPS nuclear terrace level located at approximately +8 m msl. No other tsunamigenic sources, including distant earthquakes and local submarine landslide sources, result in run-up above the KNPS nuclear terrace level, even including climate change to 2064.
- The run-up due to storm waves reaches +8 m msl at exceedance probabilities between 10^{-4} y^{-1} and 10^{-6} y^{-1}, however these locations are north and south of the nuclear terrace. Only at 10^{-8} y^{-1} does the wave run-up flood the terrace adjacent to the reactor buildings. Refer to the figures in Appendices A and B for the spatial extent of the inundation.
- The predicted flooding at KNPS will require further assessment, e.g., through further analysis of the probability of these events occurring in the remaining 42 y until the end of decommissioning (assumed in 2064), by analysing the impact of the predicted flood water depths and currents on the SSCs, and consideration of protective structures such as wave walls.
- The PPE for the new NIs states that the terrace height must be such that the terrace is elevated above design basis flooding hazards. These results show the maximum flood level is +16.7 m msl, due to an extreme 10^{-8} y^{-1} wave storm in 2130. The maximum horizontal inundation is 553 m due to the PMT in 2130. Due to the topography the location of the maximum horizontal inundation seldom coincides with the location of the maximum vertical run-up, as can be seen in the figures in Appendices A and B.
- The inundation extends into the estimated position of the new NIs for the PMT in all years. For wave storms the inundation does not reach the position of the new NIs in 2021 and 2064, however in 2130 the position of the new NIs is reached for exceedances of 10^{-2} y^{-1} and lower. Refer to the figures in Appendices A and B for the spatial extent of the inundation.
- For the new NIs the SSCs will need to be placed above these maximum flood levels and landward of the maximum inundation, or alternatively protective structures such as revetments and wave walls will need to be placed in front of the SSCs.

CONTROLLED DISCLOSURE

When downloaded from the EDS database, this document is uncontrolled and the responsibility rests with the user to ensure it is in line with the authorised version on the database.

- Note that these flooding values are based on the SLR corresponding to the RCP8.5 upper end of likely range (0.44 m in 2064 and 1.80 m in 2130), rather than the maximum plausible SLR (0.79 m in 2064 and 3.26 m in 2130). This additional 0.35 m in the case of KNPS and 1.5 m in the case of the new NIs should be considered during the SAR and engineering design phase, either as safety buffer or as part of an adaptive design strategy.
- Another possible mechanism for flooding from the sea is a seiche generated in the intake basin by an earthquake, which is distinct from a tsunami. This would require an earthquake that has sufficient magnitude, duration and seismic energy at the required frequencies to excite one of the natural resonance modes of the intake basin. For the existing KNPS intake basin these modes have frequencies of 85 s (0.0118 Hz), 114 s (0.0088 Hz), 170 s (0.0059 Hz) and 17 mins (0.00098 Hz) (refer to ***Subsection 5.9.11.4***). The amplitude of the seiche generated inside the intake basin will be limited by the wave energy lost through the entrance of the intake basin and by overtopping over the breakwaters, which have minimum crest levels of +4.5 m msl on the northern breakwater and +4.9 m msl on the southern breakwater. These crest levels indicate that the maximum vertical level of an earthquake-induced seiche will be enveloped by the vertical run-up levels in ***Table 5.9.47***, i.e., lower than +6.05 m msl.

5.9.14 Extreme Low Water Levels

Extreme low water levels at the cooling water intakes can occur due to:

- Storm wave drawdown combined with low tides, negative storm surge and basin seiche, as described in ***Subsection 5.9.11***; and
- Tsunami drawdown combined with low tides and negative storm surge, as described in ***Subsection 5.9.12***.

The extreme low water levels at the KNPS cooling water intake pumps inside the intake basin, and at the -20 m and -30 m msl depths opposite the new NIs, corresponding to possible tunnel intake locations, are shown in ***Table 5.9.48*** and plotted in ***Figure 5.9.115*** to ***Figure 5.9.118***. Since the PMT does not have an associated exceedance probability, these results are plotted as horizontal lines in the figures.

CONTROLLED DISCLOSURE

When downloaded from the EDS database, this document is uncontrolled and the responsibility rests with the user to ensure it is in line with the authorised version on the database.

Table 5.9.48: Extreme Low Water Levels.

Source of Drawdown	Exceedance Probability	KNPS		New NIs								
		Minimum vertical drawdown level at pumps		Minimum vertical drawdown level at pumps[(a)]			Minimum vertical drawdown at -20 m msl			Minimum vertical drawdown at -30 m msl		
	(y^{-1})	(m msl)		(m msl)			(m msl)			(m msl)		
		2021	2064	2021	2064	2130	2021	2064	2130	2021	2064	2130
Storm Waves	10^{-2}	-1.10	-1.11	-1.10	-1.11	-1.13	-3.55	-3.47	-3.47	-4.87	-4.79	-5.27
Storm Waves	10^{-4}	-1.42	-1.39	-1.42	-1.39	-1.45	-3.66	-3.81	-3.85	-5.39	-5.44	-5.55
Storm Waves	10^{-5}	-1.53	-1.54	-1.53	-1.54	-1.62	-3.74	-3.86	-3.93	-5.76	-6.04	-6.17
Storm Waves	10^{-6}	-1.64	-1.69	-1.64	-1.69	-1.80	-3.83	-3.90	-4.01	-6.14	-6.64	-6.79
Storm Waves	10^{-7}	-1.79	-1.83	-1.79	-1.83	-1.95	-3.94	-4.00	-4.03	-6.41	-6.61	-6.80
Storm Waves	10^{-8}	-1.94	-1.97	-1.94	-1.97	-2.09	-4.04	-4.10	-4.05	-6.68	-6.58	-6.82
Tsunami: Distant earthquakes	(b)	-2.26	-2.26	-2.26	-2.26	-2.23	-4.96	-5.04	-5.19	-3.90	-3.87	-3.81
Tsunami: Volcanic flank collapse	(b)	-1.83	-1.81	-1.83	-1.81	-1.77	-7.18	-7.16	-7.18	-6.64	-6.65	-6.51
Tsunami: Local submarine landslides	(b)	-2.12	-2.12	-2.12	-2.12	-2.14	-5.35	-5.36	-5.40	-4.69	-4.70	-4.73
Probable Maximum Tsunami (PMT)	(c)	-2.26	-2.26	-2.26	-2.26	-2.23	-7.18	-7.16	-7.18	-6.64	-6.65	-6.51

Notes:
(b) Assuming a basin intake with similar geometry to KNPS.
(c) Minimum level for each tsunami source type.
(d) Minimum level for all tsunami source types.

CONTROLLED DISCLOSURE

When downloaded from the EDS database, this document is uncontrolled and the responsibility rests with the user to ensure it is in line with the authorised version on the database.

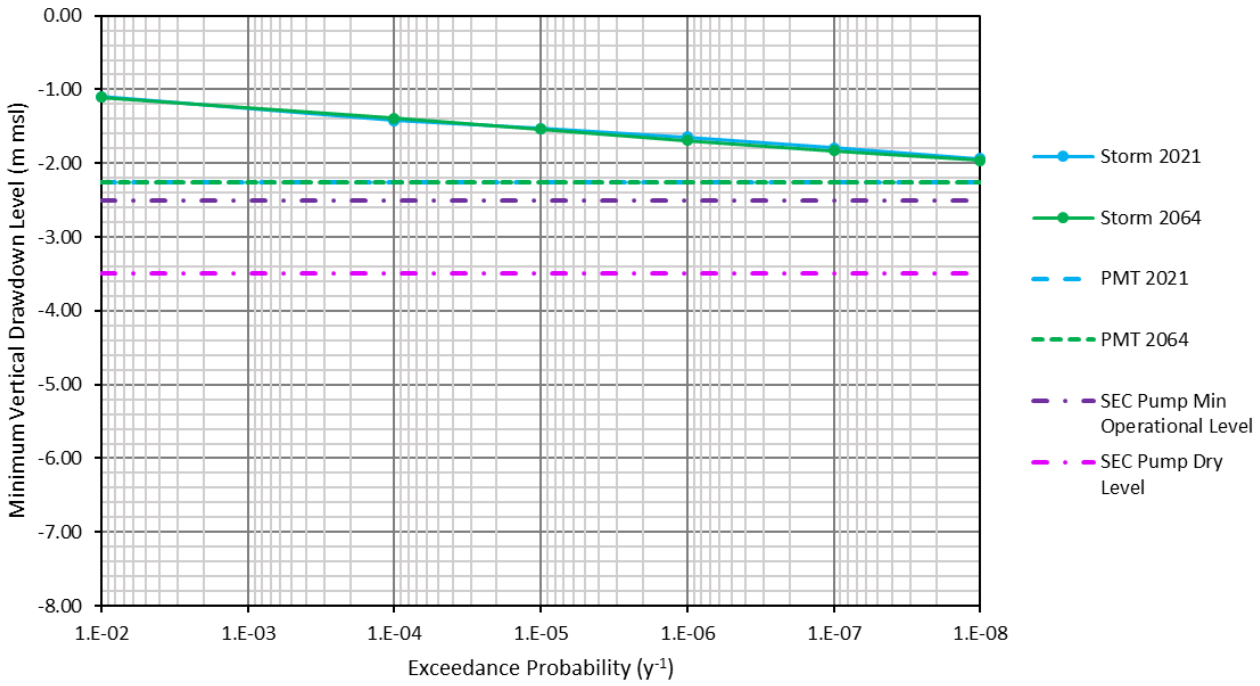


Figure 5.9.115: Extreme Low Water Levels at KNPS Pump Intakes.

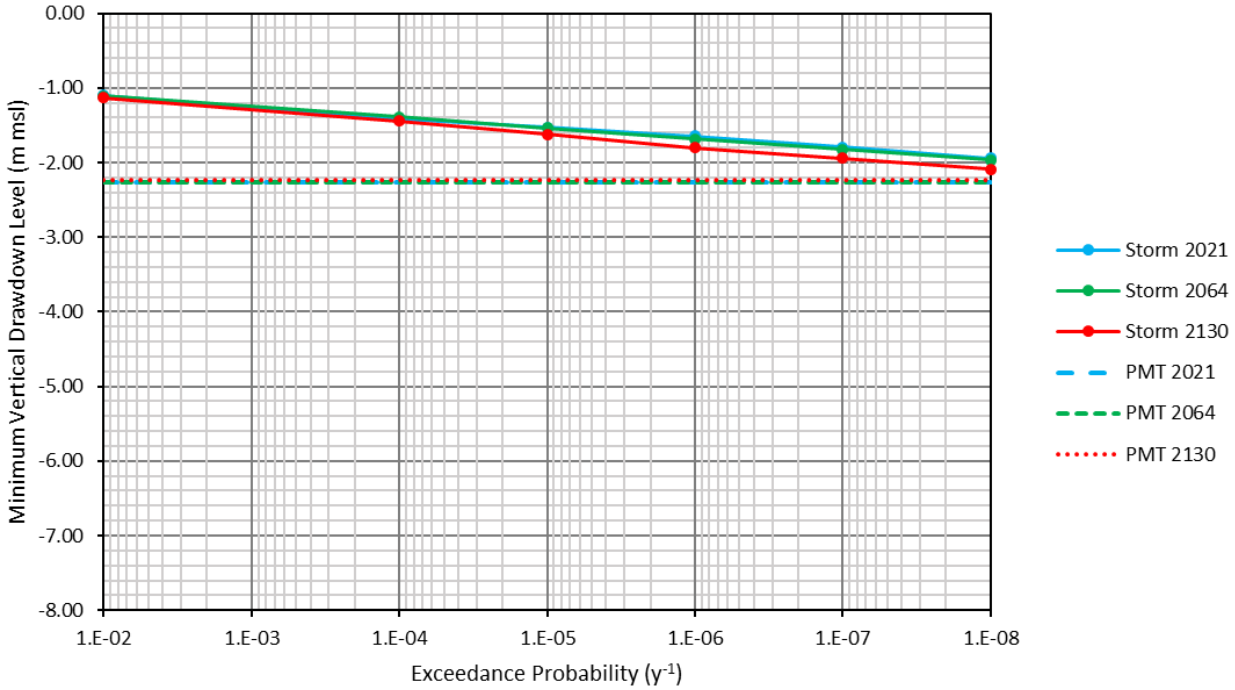


Figure 5.9.116: Extreme Low Water Levels at New Nls Pump Intakes (Assuming a Basin Intake with Similar Geometry to KNPS).

CONTROLLED DISCLOSURE

When downloaded from the EDS database, this document is uncontrolled and the responsibility rests with the user to ensure it is in line with the authorised version on the database.

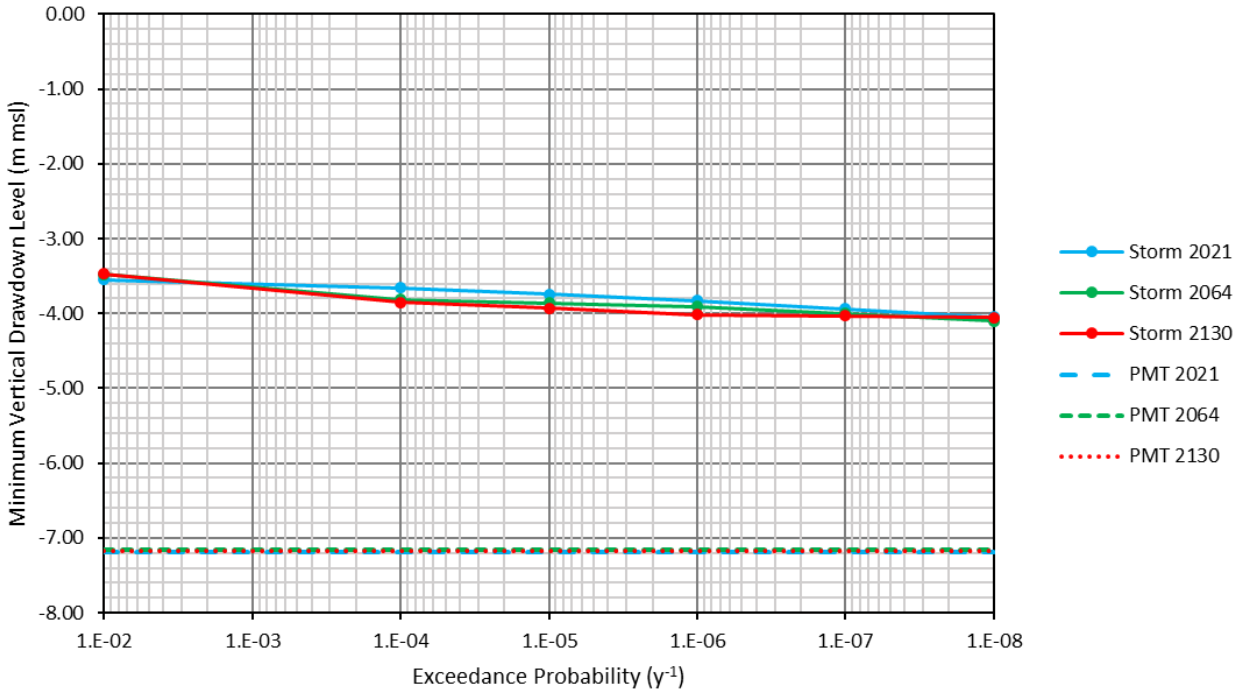


Figure 5.9.117: Extreme Low Water Levels at a Depth of -20 m msl Opposite the new NIs (Possible Tunnel Intake Location).

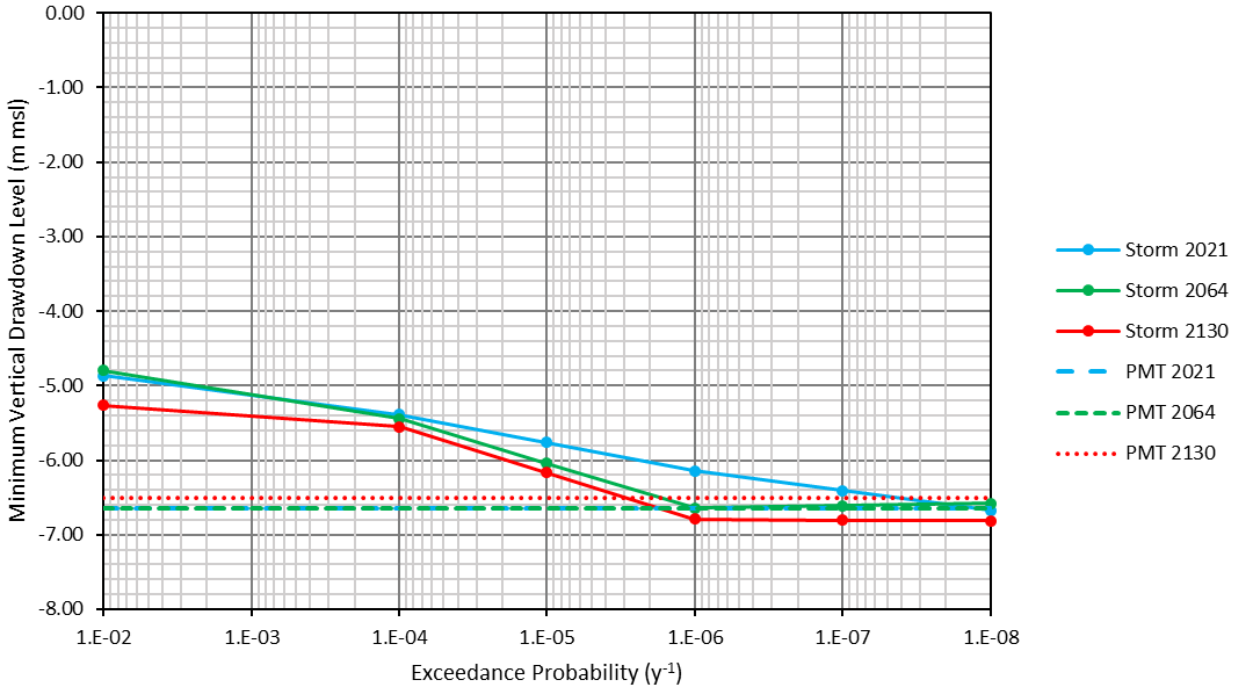


Figure 5.9.118: Extreme Low Water Levels at a Depth of -30 m msl Opposite the new NIs (Possible Tunnel Intake Location).

CONTROLLED DISCLOSURE

When downloaded from the EDS database, this document is uncontrolled and the responsibility rests with the user to ensure it is in line with the authorised version on the database.

The results presented above show the following:

- The extreme low water levels do not change significantly over time, since sea level rise has conservatively been excluded, and because the coastline erosion has little impact on these low water levels.
- The minimum water levels in the KNPS intake basin are limited by the sand levels in the entrance to the basin which prevent the levels from dropping significantly.
- The PMT results in lower levels at -20 m msl compared to -30 m msl, which is due to wave shoaling and reflection.
- The storms result in lower levels at -30 m msl compared to -20 m msl, which is due to less wave breaking and less wave set-up.
- For the existing KNPS basin, the Essential Service Water System (SEC) pumphouse is designed to accommodate a minimum short duration water level of -2.5 m msl under normal operating conditions. If the sea level drops below -3.5 m msl no water would reach the pumps (Eskom, 2006). At KNPS, the results show that the lowest water level is -2.3 m msl, which is driven by the PMT. The KNPS pumps will thus continue to operate for all events assessed.
- If a basin intake with similar geometry to KNPS is selected for the new NIs, then the results show that the intake should accommodate a minimum water level of -2.3 m msl.
- If a tunnel intake in a depth of -20 m msl is selected for the new NIs, then the results show that the intake should accommodate a minimum water level of -7.2 m msl, which is driven by the PMT.
- If a tunnel intake in a depth of -30 m msl is selected for the new NIs, then the results show that the intake should accommodate a minimum water level of -6.8 m msl, which is driven by the 10^{-8} y^{-1} storm event.

5.9.15 Thermal Plume Dispersion

5.9.15.1 Introduction

It is proposed that the new NIs will be cooled using a once-through seawater cooling system. Four different conceptual layouts for the seawater cooling intake and outfall system have been developed and thermal plume dispersion modelling has been performed to demonstrate the technical feasibility of the site regarding the following PPE parameters for the new NIs (see ***Table 5.9.3***):

- The range of water temperatures at the intake is -0.5°C to 30°C.

CONTROLLED DISCLOSURE

When downloaded from the EDS database, this document is uncontrolled and the responsibility rests with the user to ensure it is in line with the authorised version on the database.

- The intake and the outfall configuration should not result in a net rise in the cooling water temperature. The maximum increase in the temperature (ΔT) of the recirculated water should be less than 1.5°C.

The potential impact of the thermal discharges from the new NIs on the KNPS seawater cooling system is also assessed for the following:

- For the existing KNPS a shut-down of the reactor will be necessary if the intake temperature exceeds 23°C (Eskom, 2006).

5.9.15.2 Discharge Characteristics

The following discharge scenarios are defined from ***Chapter 3*** (Overview of Planned Activities at the Site):

- KNPS with steam generator replacement (SGR) and thermal power uprate (TPU) projects to generate 2108 MWe;
- KNPS + new NIs (new power station to generate 2500 MWe);
- KNPS + new NIs (new power station to generate 4000 MWe).

The cooling water discharge characteristics for KNPS are based on the combined discharges from the Circulating Water System (CRF) and the Essential Service Water System (SEC) using mean flow rates under normal operation. The discharge characteristics are given in ***Table 5.9.49***. The temperature increase (ΔT) between the intake and the outfall is provided.

Table 5.9.49: Discharge characteristics for KNPS including SGR and TPU.

Parameter	Unit	Value
CRF discharge	m^3/s	91.1
CRF ΔT	°C	11.7
SEC discharge	m^3/s	1.4
SEC ΔT	°C	12
Combined discharge	m^3/s	92.5
Combined ΔT	°C	11.7

The cooling water discharge characteristics for the new NIs are given in ***Table 5.9.50***. The discharge rates were calculated using the PPE cooling water flow rate of 76 m^3/s per 1650 MWe.

CONTROLLED DISCLOSURE

When downloaded from the EDS database, this document is uncontrolled and the responsibility rests with the user to ensure it is in line with the authorised version on the database.

Table 5.9.50: Discharge Characteristics for New NIs

Parameter	Unit	2500 MWe	4500 MWe
Discharge	m^3/s	115.2	184.2
ΔT	°C	12	12

5.9.15.3 Engineering Concepts for Intake and Outfall Structures

No engineering feasibility studies were performed for the SSR and these conceptual layouts thus serve only to demonstrate the technical feasibility of the layouts in terms of thermal plume dispersion, recirculation and sediment transport.

Layout 0: Existing KNPS

Layout 0 comprises the existing KNPS, including the existing intake basin and channel outfall discharging into the surf-zone. The layout is shown in ***Figure 5.9.119***.

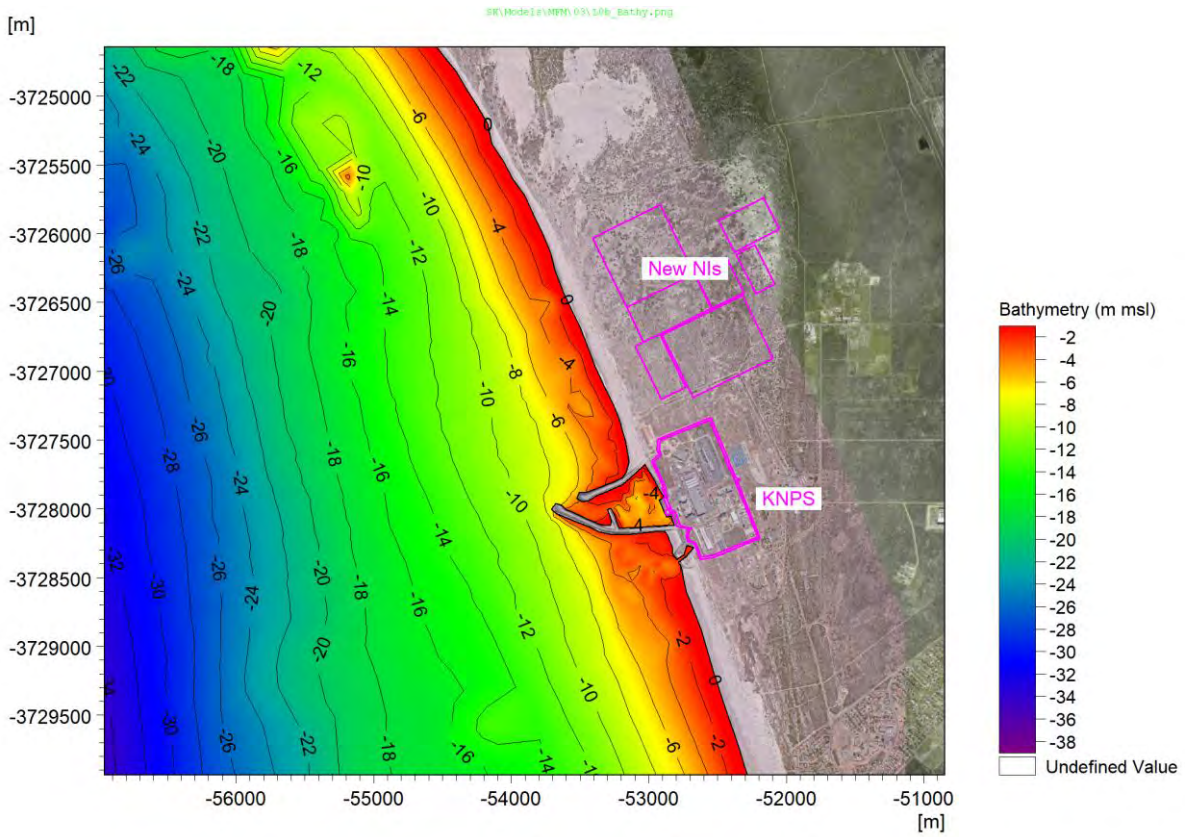


Figure 5.9.119: Layout 0: Existing KNPS Intake Basin and Outfall Channel.

CONTROLLED DISCLOSURE

When downloaded from the EDS database, this document is uncontrolled and the responsibility rests with the user to ensure it is in line with the authorised version on the database.

The south breakwater of the intake basin extends to a depth of approximately -7 m msl and is longer than the north breakwater to reduce recirculation effects. The intake openings for the CRF pumphouse are located between levels of -1.5 and -6.0 m msl (top and bottom of the opening). The intake openings for the SEC pumphouse are located between -3.7 and -5.2 m msl (top and bottom of the opening).

The 150 m long outfall channel contains a bend to direct the flow offshore. The channel discharges at an invert level of -2 m msl with a width of approximately 19.5 m, resulting in a discharge velocity of approximately 1.6 to 3.3 m/s for water levels corresponding to the 90th percentile high tide and the 10th percentile low tide, respectively.

Layouts 1 to 4 are various proposed options for intake and outfall structure layouts for the new NIs. In all cases the existing KNPS intake and outfall is included.

Layout 1: Short tunnel intakes and outfalls

Layout 1 considers offshore tunnel intakes and outfalls for the new NIs as shown by the schematic diagram in ***Figure 5.9.120***.

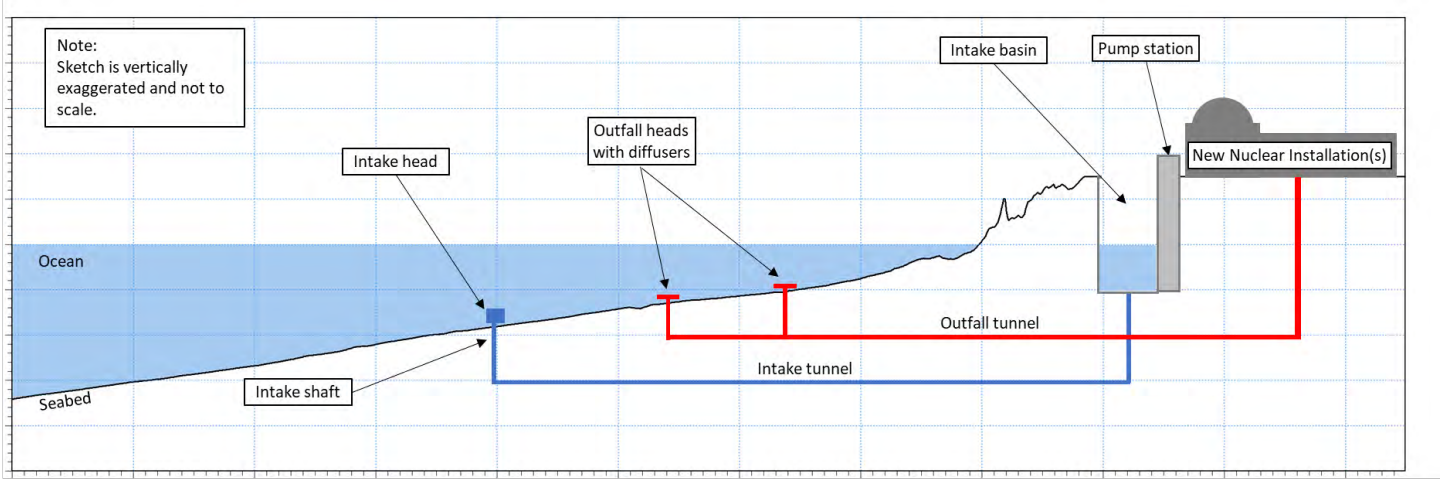


Figure 5.9.120: Schematic Diagram Showing the Main Components for an Offshore Tunnel Intake and Outfall Configuration.

Figure 5.9.120 illustrates a generic cross-section identifying the main components of this configuration as follows:

- Seawater is pumped from an intake basin located on land to deliver cooling water to the new NIs. The basin will be adequately sized to ensure low current speeds and sedimentation of sand during normal operation of the nuclear installation(s). In the extreme case of a loss of

When downloaded from the EDS database, this document is uncontrolled and the responsibility rests with the user to ensure it is in line with the authorised version on the database.

the ultimate heat sink (if applicable in the case of the adopted technology), the intake basin will need to have sufficient volume for the cooling of safety related systems of the new NIs.

- An intake tunnel connects the landside intake basin to the sea. Water is abstracted via an intake head located approximately 4 m above the seabed to prevent the drawing in of large quantities of sediment (assessed in ***Subsection 5.9.16.3***).
- The heated cooling water is pumped offshore via an outfall tunnel to two outfall heads spaced 500 m apart to reduce plume interactions. Each outfall head comprises a rosette diffuser with six ports spaced at 60° angles, discharging horizontally at a height of 2 m above the seabed.
- The tunnel diameters are designed to maintain a tunnel flow velocity of 2.5 to 3.0 m/s to avoid sedimentation.

A plan view of Layout 1 is presented in ***Figure 5.9.121***. Details of the intake and outfall configurations for the 2500 MWe and 4000 MWe new NIs are given in ***Table 5.9.51***.

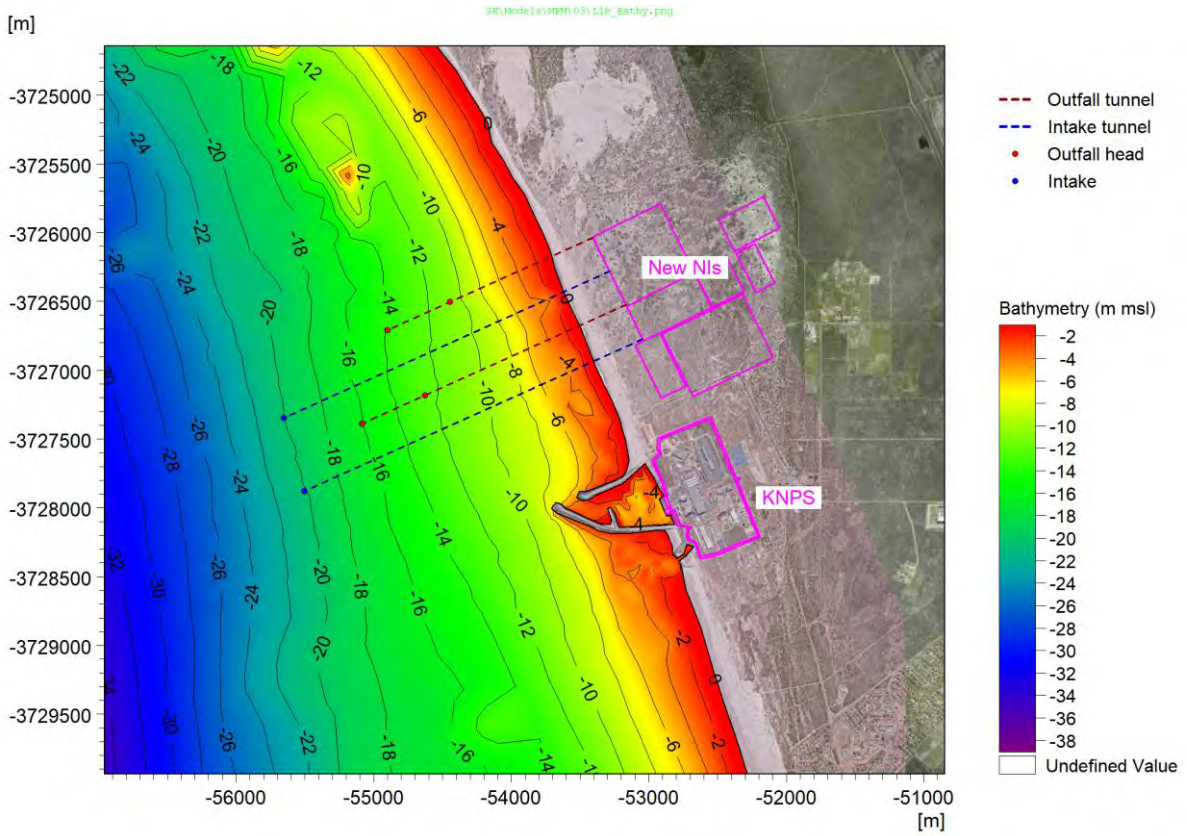


Figure 5.9.121: Layout 1: Short Tunnel Intakes and Outfalls (4000 MWe). For 2500 MWe the Southern Intake and Outfall Tunnels Are Excluded.

CONTROLLED DISCLOSURE

When downloaded from the EDS database, this document is uncontrolled and the responsibility rests with the user to ensure it is in line with the authorised version on the database.

Table 5.9.51: Layout 1 Intake and Outfall Configurations.

Parameter	Unit	2500 MWe	4000 MWe
Discharge	m^3/s	115.2	184.2
Number of intake/outfall tunnels	No.	1	2
Discharge per tunnel	m^3/s	115.2	92.1
Tunnel diameter	m	7.0	6.3
Tunnel velocity	m/s	3.0	3.0
Intake tunnel length from coastline	km	2.3	North: 2.3 South: 2.4
Depth at intake head	m msl	-20.1	North: -20.1 South: -20.1
Intake height above seabed	m	4	4
Outfall tunnel length from coastline	km	1.3	North: 1.3 South: 1.8
Depth at outfall head	m msl	-11.0 and -13.8	North: -11.0 and -13.8 South: -12.4 and -16.1
Outfall heads per tunnel	No.	2	2
Ports per outfall head	No.	6	6
Port discharge	m^3/s	9.6	7.7
Port diameter	m	1.8	1.6
Port velocity, discharging horizontally	m/s	3.8	3.8
Port height above seabed	m	2	2

The inshore outfall head of the northern tunnel is located at a depth of -11 m msl to extend the outfall beyond the surf zone. The inshore head of the southern outfall is located mid-way between the inshore and offshore outfall heads of the northern tunnel (measured parallel to the depth contours) to reduce plume interactions. The intake heads are located 500 m offshore from the most offshore outfall head to reduce recirculation, noting that the intake and buoyant plume are also separated vertically.

Layout 2: Long tunnel intakes and outfalls

Layout 2 considers the same offshore tunnel intake and outfall concept as Layout 1, but with longer tunnels into deeper water. A plan view of Layout 2 is presented in ***Figure 5.9.122***, with details of the intake and outfall configurations given in ***Table 5.9.52***.

CONTROLLED DISCLOSURE

When downloaded from the EDS database, this document is uncontrolled and the responsibility rests with the user to ensure it is in line with the authorised version on the database.

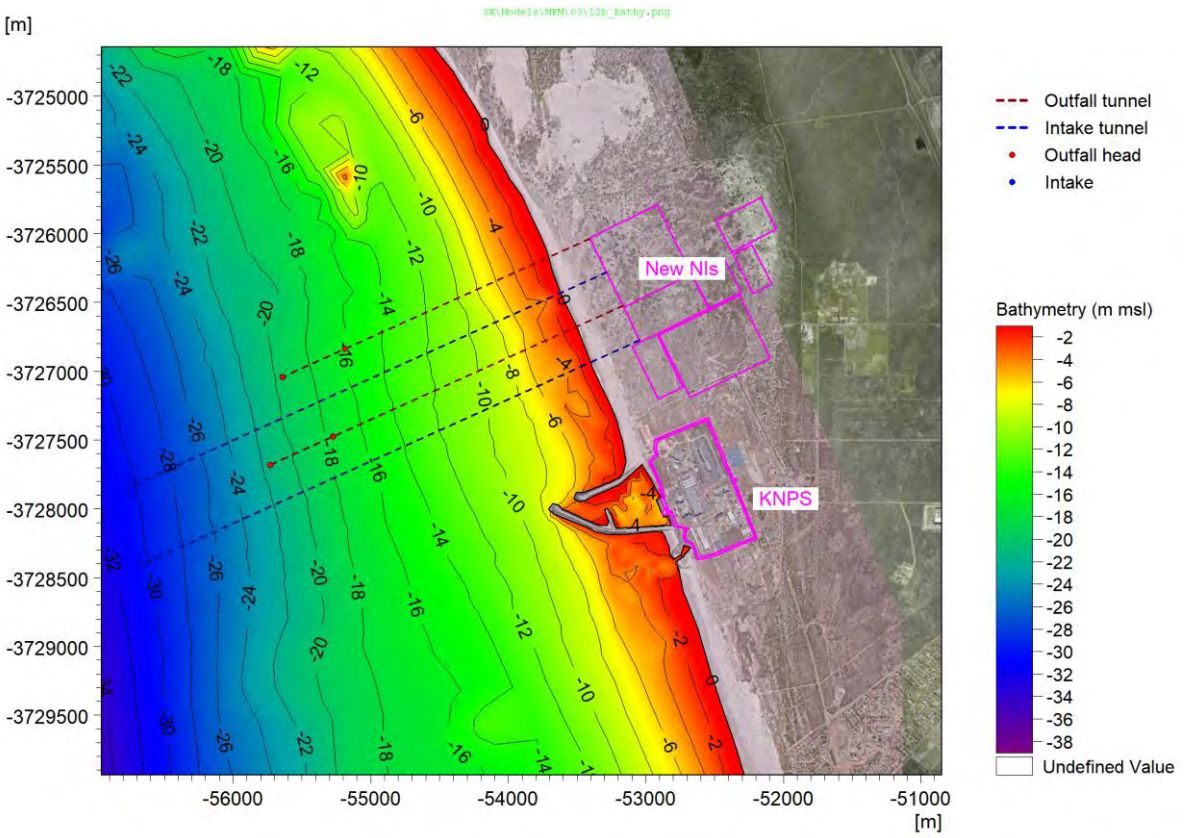


Figure 5.9.122: Layout 2: Long Tunnel Intakes and Outfalls (4000 MWe). For 2500 MWe the Southern Intake and Outfall Tunnels Are Excluded.

CONTROLLED DISCLOSURE

When downloaded from the EDS database, this document is uncontrolled and the responsibility rests with the user to ensure it is in line with the authorised version on the database.

Table 5.9.52: Layout 2 Intake and Outfall Configurations.

Parameter	Unit	2500 MWe	4000 MWe
Discharge	m^3/s	115.2	184.2
Number of intake/outfall tunnels	No.	1	2
Discharge per tunnel	m^3/s	115.2	92.1
Tunnel diameter	m	7.0	6.3
Tunnel velocity	m/s	3.0	3.0
Intake tunnel length from coastline	km	3.5	North: 3.5 South: 3.6
Depth at intake head	m msl	-30.3	North: -30.3 South: -30.5
Intake height above seabed	m	4	4
Outfall tunnel length from coastline	km	2.1	North: 2.1 South: 2.5
Depth at outfall head	m msl	-16.0 and -19.6	North: -16.0 and -19.6 South: -17.6 and -21.4
Outfall heads per tunnel	No.	2	2
Ports per outfall head	No.	6	6
Port discharge	m^3/s	9.6	7.7
Port diameter	m	1.8	1.6
Port velocity, discharging horizontally	m/s	3.8	3.8
Port height above seabed	m	2	2

The inshore outfall head of the northern tunnel is located at a depth of -16 m msl. The inshore head of the southern outfall is located mid-way between the inshore and offshore outfall heads of the northern tunnel (measured parallel to the depth contours) to reduce plume interactions. The intake heads are located 1000 m offshore of the most offshore outfall head to reduce recirculation, noting that the intake and buoyant plume are also separated vertically.

Layout 3: Basin intake and tunnel outfalls

Layout 3 considers the same offshore tunnel outfalls as for Layout 2 but utilises a similar intake basin to KNPS. A plan view of Layout 3 is presented in ***Figure 5.9.123***, with details of the outfall configurations given in ***Table 5.9.53***.

CONTROLLED DISCLOSURE

When downloaded from the EDS database, this document is uncontrolled and the responsibility rests with the user to ensure it is in line with the authorised version on the database.

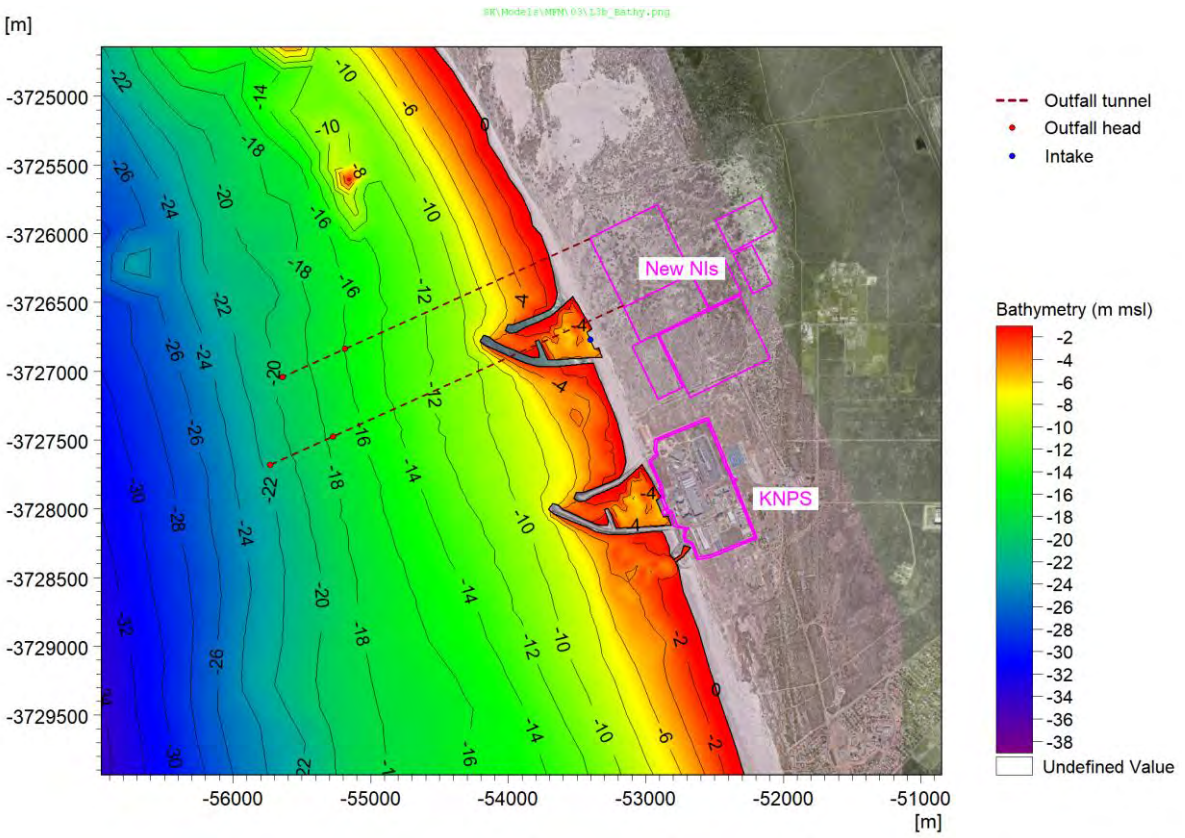


Figure 5.9.123: Layout 3: Basin Intake and Tunnel Outfalls (4000 MWe). For 2500 MWe the Southern Outfall Tunnel Is Excluded.

CONTROLLED DISCLOSURE

When downloaded from the EDS database, this document is uncontrolled and the responsibility rests with the user to ensure it is in line with the authorised version on the database.

Table 5.9.53: Layout 3 Outfall Configuration.

Parameter	Unit	2500 MWe	4000 MWe
Discharge	m^3/s	115.2	184.2
Number of outfall tunnels	No.	1	2
Discharge per tunnel	m^3/s	115.2	92.1
Tunnel diameter	m	7.0	6.3
Tunnel velocity	m/s	3.0	3.0
Outfall tunnel length from coastline	km	2.1	North: 2.1 South: 2.5
Depth at outfall head	m msl	-16.0 and -19.6	North: -16.0 and -19.6 South: -17.6 and -21.4
Outfall heads per tunnel	No.	2	2
Ports per outfall head	No.	6	6
Port discharge	m^3/s	9.6	7.7
Port diameter	m	1.8	1.6
Port velocity, discharging horizontally	m/s	3.8	3.8
Port height above seabed	m	2	2

The orientation of the intake basin was chosen to reduce recirculation from KNPS. Thus, the southern breakwater extends to approximately -7 m msl and is longer than the northern breakwater. The bathymetry at the basin entrance and inside the basin was modified to be the same as the existing KNPS intake basin.

Layout 4: Basin intake and rubble-mound outfall structure

Layout 4 utilises a similar intake basin to KNPS and an emerged rubble-mound outfall structure. A plan view of Layout 4 is presented in ***Figure 5.9.124***.

CONTROLLED DISCLOSURE

When downloaded from the EDS database, this document is uncontrolled and the responsibility rests with the user to ensure it is in line with the authorised version on the database.

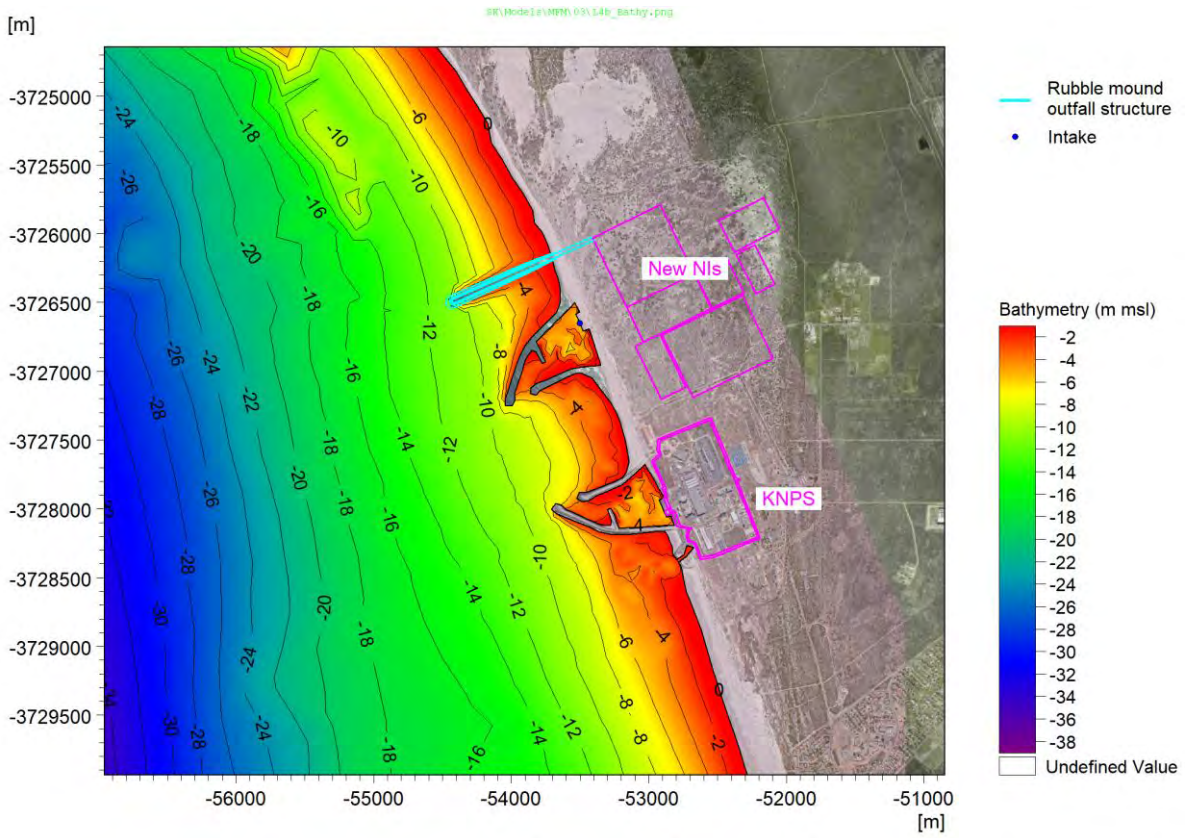


Figure 5.9.124: Layout 4: Basin intake and rubble-mound outfall structure.

The intake basin is a mirror image of the KNPS intake basin to reduce recirculation from the new NIs outfall. At the basin entrance and inside the basin the bathymetry was modified to be the same as the existing KNPS intake basin.

The outfall structure is conceptualised as an emerged rubble-mound structure which houses rectangular concrete outfall pipes within the structure core. The structure extends to a depth of -11 m msl to extend the outfall beyond the surf zone, based on both environmental and dispersion considerations. At the head of the structure a concrete caisson facilitates the discharge through two rectangular openings, discharging horizontally at 4.5 m above the seabed. Details of the outfall configuration are given in ***Table 5.9.54***.

CONTROLLED DISCLOSURE

When downloaded from the EDS database, this document is uncontrolled and the responsibility rests with the user to ensure it is in line with the authorised version on the database.

Table 5.9.54: Layout 4 Outfall Configuration.

Parameter	Unit	2500 MWe	4000 MWe
Discharge	m^3/s	115.2	184.2
Number of pipes in rubble mound structure	No.	1	2
Discharge per pipe	m^3/s	115.2	92.1
Pipe height	m	5	5
Pipe width	m	7	6
Pipe velocity	m/s	3.3	3.1
Length of outfall structure from coastline	km	0.8	0.8
Depth at outfall head	m msl	-11	-11
Total area of exit openings	m^2	27	45
Outfall exit velocity, discharging horizontally	m/s	4.3	4.1
Discharge height of outfall above seabed	m	4.5	4.5

5.9.15.4 Damage to Cooling Water Intake and Outfall Structures

In the case of offshore intake or outfall structures, the structures need to be positioned in a depth where extreme wave conditions will have no damaging impact on the structure or any of its components which might jeopardise the intake or discharge of cooling water. In the case of nearshore basin or channel type structures armoured with rock or concrete armour units, the structure should be designed for a 'no-damage' criterion, defined as less than 5% damage.

The extreme still water level and wave conditions at the site are provided in ***Table 5.9.12*** and ***Table 5.9.25***, respectively. These environmental conditions along with the design considerations given above will need to be accounted for in the design development of the cooling water supply system.

5.9.15.5 Dispersion Modelling

Model description

The MIKE 3 Flow Model Flexible Mesh was used for the thermal plume dispersion modelling. The details of the physical processes and numerical implementation are provided in the model documentation (see ***Table 5.9.7***), while details of the model setup, sensitivity testing, and V&V are provided in the DTHA V&V Report (PRDW, 2021).

CONTROLLED DISCLOSURE

When downloaded from the EDS database, this document is uncontrolled and the responsibility rests with the user to ensure it is in line with the authorised version on the database.

The model is based on the numerical solution of the three-dimensional incompressible Reynolds averaged Navier-Stokes equations invoking the assumptions of Boussinesq and of hydrostatic pressure. The model consists of the continuity, momentum, temperature, salinity and density equations and is closed by a k-ε vertical turbulence closure scheme. Horizontal eddy viscosity is modelled with the Smagorinsky formulation.

The time integration of the shallow water equations and the transport equations is performed using a semi-implicit scheme, where the horizontal terms are treated explicitly and the vertical terms are treated implicitly. In the vertical direction a structured mesh, based on a sigma-coordinate transformation is used, while the geometrical flexibility of the unstructured flexible mesh comprising triangles or quadrangles is utilised in the horizontal plane.

The model includes the following physical phenomena:

- Currents due to tides;
- Currents due to wind stress on the water surface;
- Currents due to density gradients;
- Currents due to waves; the second order stresses due to breaking of short period waves are included using the radiation stresses computed in the Spectral Wave model;
- Coriolis forcing;
- Bottom friction;
- Flooding and drying;
- Sources and sinks including dynamic near and far-field coupling; and
- Heat exchange.

An important feature of the model is a dynamic coupling of a near-field jet model and the 3D far-field hydrodynamic model. The near-field solution based on the integral jet model equations by Jirka (2004). Entrainment into the jet is using Distributed Entrainment Sink Approach by Choi and Lee (2007). At the end of the near-field the diluted discharge is released into far-field model as a source, as shown in ***Figure 5.9.125***.

CONTROLLED DISCLOSURE

When downloaded from the EDS database, this document is uncontrolled and the responsibility rests with the user to ensure it is in line with the authorised version on the database.

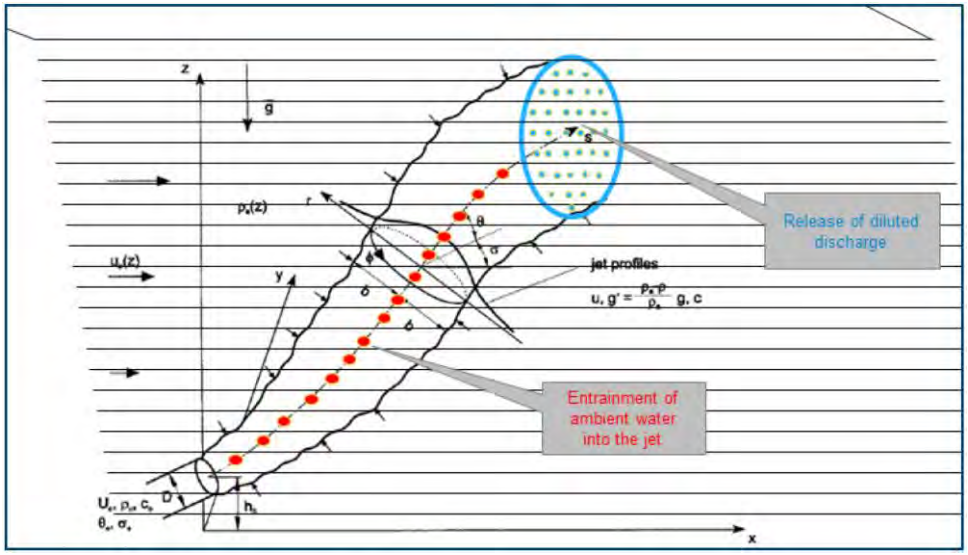


Figure 5.9.125: Dynamic Coupling of Near-Field and Far-Field Models: Entrainment Sinks Along the Plume Trajectory and Distributed Sources at the Release Location.

Model setup

The model domain and bathymetry are shown in ***Figure 5.9.126***. A unique mesh was set up for each of the five layouts modelled. The meshes comprise triangles with a resolution varying between approximately 3 500 m at the offshore boundary to approximately 35 m at the site of interest. For Layouts 1 to 4 structured triangles with a resolution of 75 m was used around the outfalls. The vertical mesh comprises eight sigma layers with equal thicknesses. ***Figure 5.9.127*** shows an example detail view of the mesh used for Layout 1. Mesh plots for the other four layouts are provided in ***Appendix C***.

CONTROLLED DISCLOSURE

When downloaded from the EDS database, this document is uncontrolled and the responsibility rests with the user to ensure it is in line with the authorised version on the database.

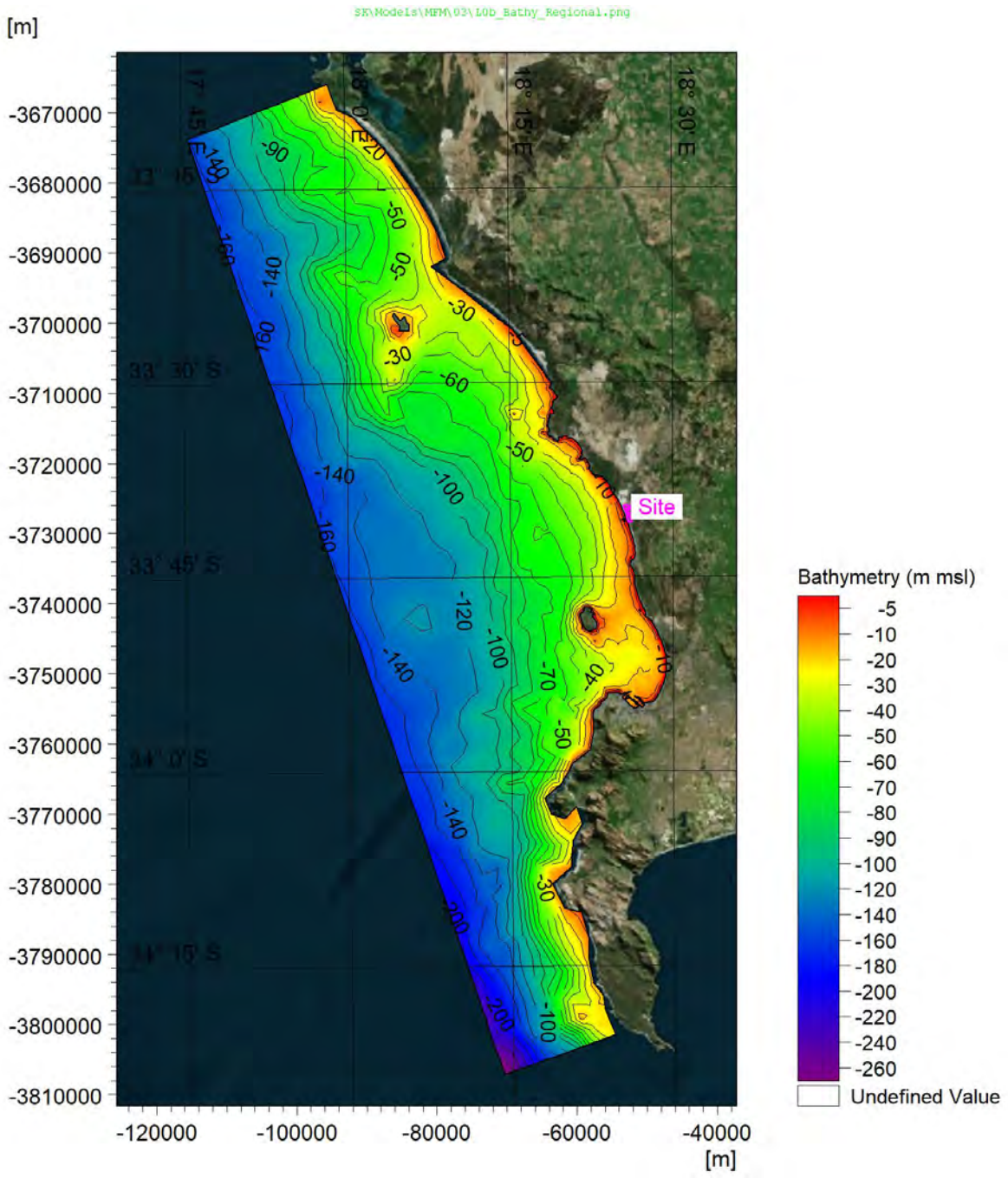


Figure 5.9.126: Model Domain and Bathymetry.

CONTROLLED DISCLOSURE

When downloaded from the EDS database, this document is uncontrolled and the responsibility rests with the user to ensure it is in line with the authorised version on the database.

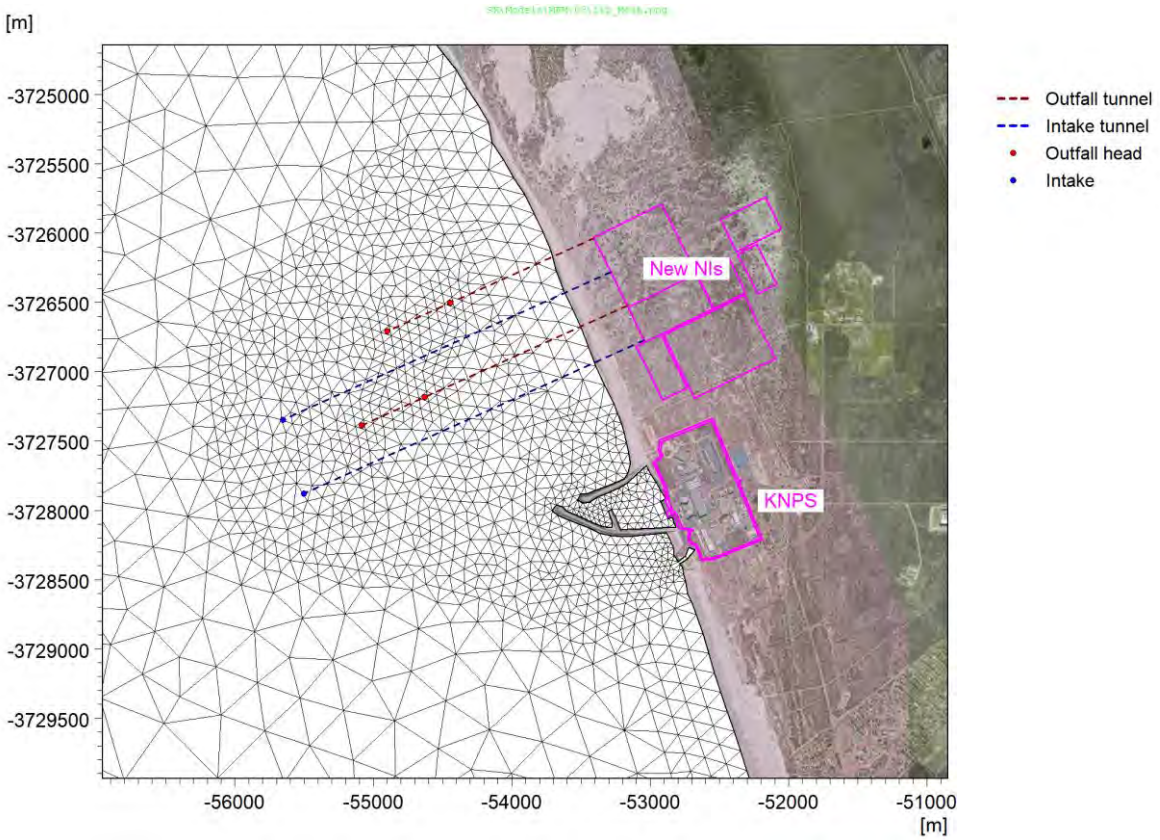


Figure 5.9.127: Detail of Model Mesh Used for Layout 1.

The following boundary conditions and forcings were applied in the model:

- Non-tidal water levels, ocean currents and seawater temperature were extracted from the 3D HYbrid Coordinate Ocean Model (HYCOM) global ocean circulation model and applied along the offshore boundaries (HYCOM, 2020).
- Predicted tides and currents were available from the DTU10 global tide model (DTU, 2010) and were applied along the offshore boundaries in addition to the non-tidal water levels and currents.
- Heat exchange between the water and the atmosphere was included in the model. The heat exchange includes the physical processes of latent heat, sensible heat, short wave radiation and long wave radiation.
- Weather data measured at the Koeberg meteorological station (see ***Section 5.8*** (Meteorology)) included wind and air temperature data at 10 m above ground level. The hourly average wind speed was applied over the model domain with a wind friction coefficient C_d of 0.002425. The air temperature was used to model the heat exchange between the water and the atmosphere.

CONTROLLED DISCLOSURE

When downloaded from the EDS database, this document is uncontrolled and the responsibility rests with the user to ensure it is in line with the authorised version on the database.

- Space and time varying humidity and cloud cover data was extracted from the European Centre for Medium-Range Weather Forecasts (EMCWF) ERA5 global atmospheric model for use in the heat exchange model (ECMWF, 2020).
- Wave-driven currents were included using a coupled spectral wave model based on the calibrated parameters presented in ***Subsection 5.9.9.8***. The wave model was run in the directionally decoupled parametric, quasi-stationary formulation.

The vertical eddy viscosity was computed using the k-ε vertical turbulence closure scheme, while the vertical eddy dispersion was set to 0.1 times the vertical eddy viscosity. This scaling factor was applied to compensate for additional vertical mixing caused by the use of only 8 vertical layers and the associated smoothing of the vertical density gradients.

The intake and outfall for KNPS was modelled using an intake connected to a simple discharge source in the outfall channel. The near-field jet model was used to model the discharges for Layouts 1 to 4 using the intake and outfall configurations as detailed in ***Subsection 5.9.15.3***. The jet calculations were performed at 30-minute intervals. In all cases the discharge is dynamically coupled to the intake so that the discharge temperature is the intake temperature plus ΔT.

Model calibration

The hydrodynamic model was calibrated against current and temperature measurements available at Site A and B, C1, D and E (the measurement programme and the site locations are detailed in ***Subsection 5.9.6.1***).

The model was run for a full year between 1 January and 31 December 2009, which allowed the calibration to be performed against the data collected during this period. The calibration model was run using the mesh and discharge configuration of Layout 0 with the KNPS output of 2108 MWe.

The modelled currents were compared to the measurements near-seabed and near-surface currents at Site A (-10 m msl) and Site B (-29 m msl). ***Figure 5.9.128*** and ***Figure 5.9.129*** present time-series comparisons of modelled and measured current speed and direction at Site A and B respectively. Current rose comparisons for Site A and B follow in ***Figure 5.9.130*** and ***Figure 5.9.131***. Percentile comparisons of current speeds for both sites are shown in ***Figure 5.9.132***. Note the roses and percentiles only include the timesteps where the modelled and measured data overlap.

CONTROLLED DISCLOSURE

When downloaded from the EDS database, this document is uncontrolled and the responsibility rests with the user to ensure it is in line with the authorised version on the database.

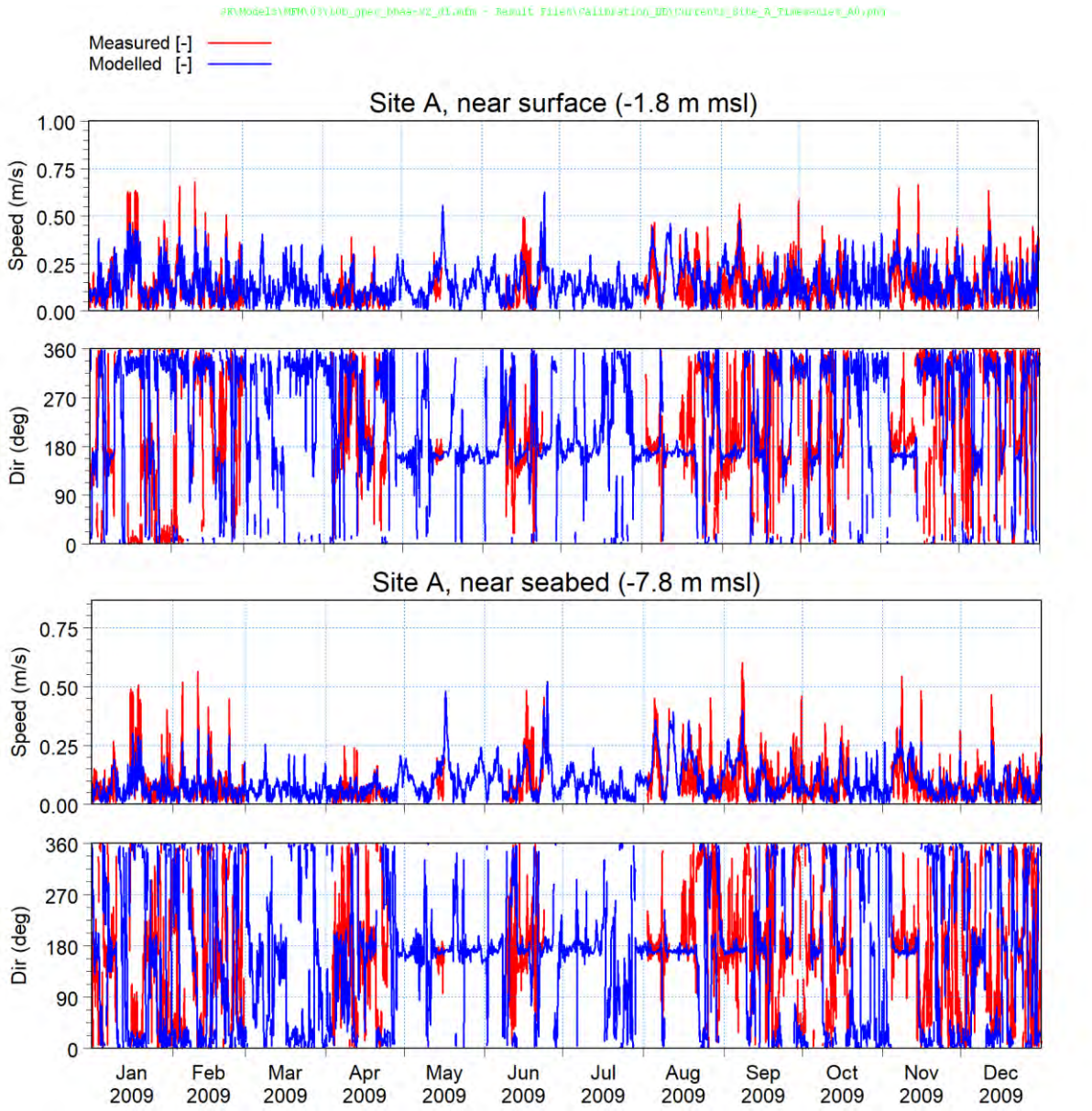


Figure 5.9.128: Time-Series Comparison of Modelled and Measured Current Speed and Direction at Site A (Depth -10 m msl).

CONTROLLED DISCLOSURE

When downloaded from the EDS database, this document is uncontrolled and the responsibility rests with the user to ensure it is in line with the authorised version on the database.

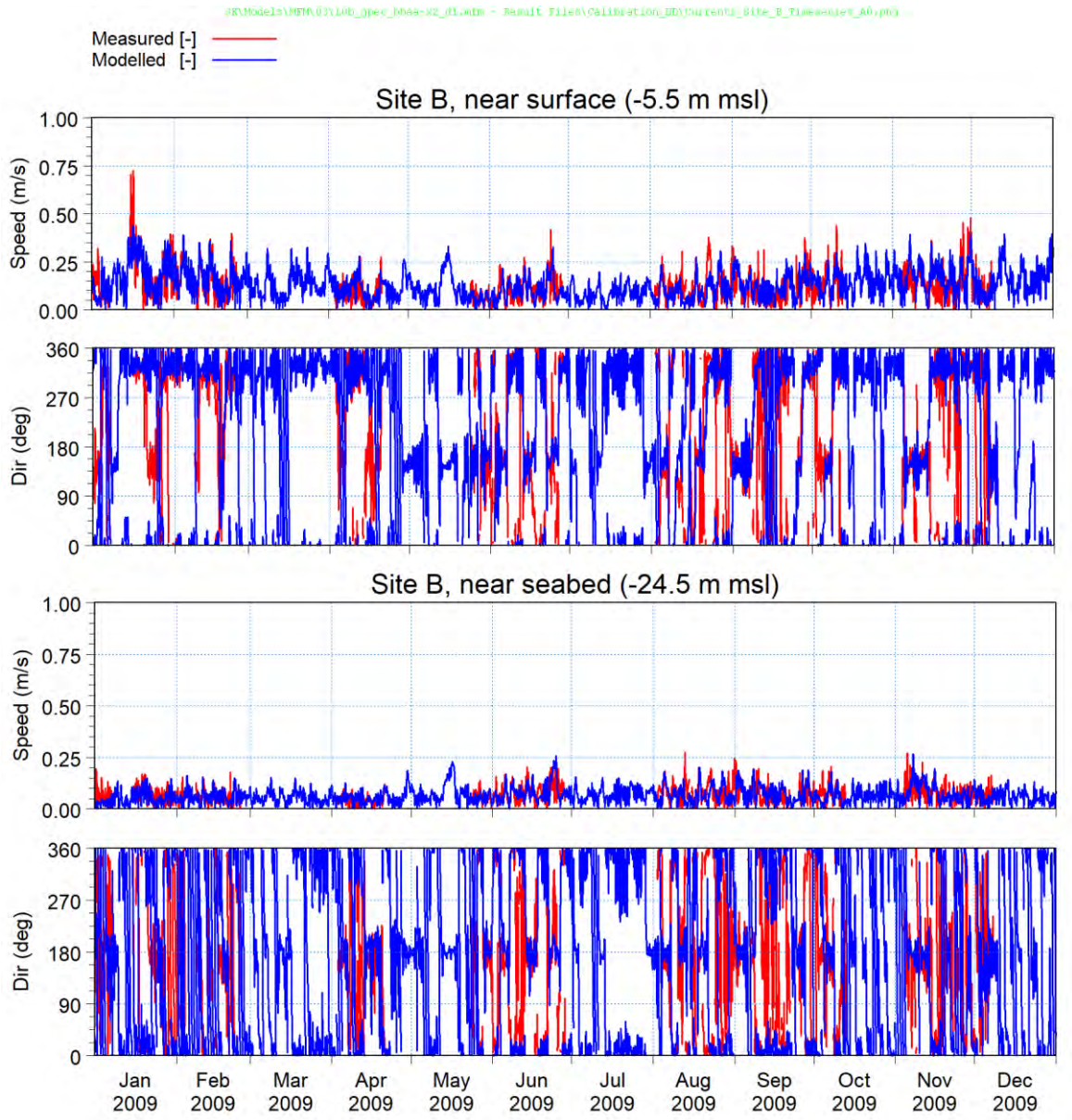


Figure 5.9.129: Time-Series Comparison of Modelled and Measured Current Speed and Direction at Site B (Depth -29 m msl).

CONTROLLED DISCLOSURE

When downloaded from the EDS database, this document is uncontrolled and the responsibility rests with the user to ensure it is in line with the authorised version on the database.

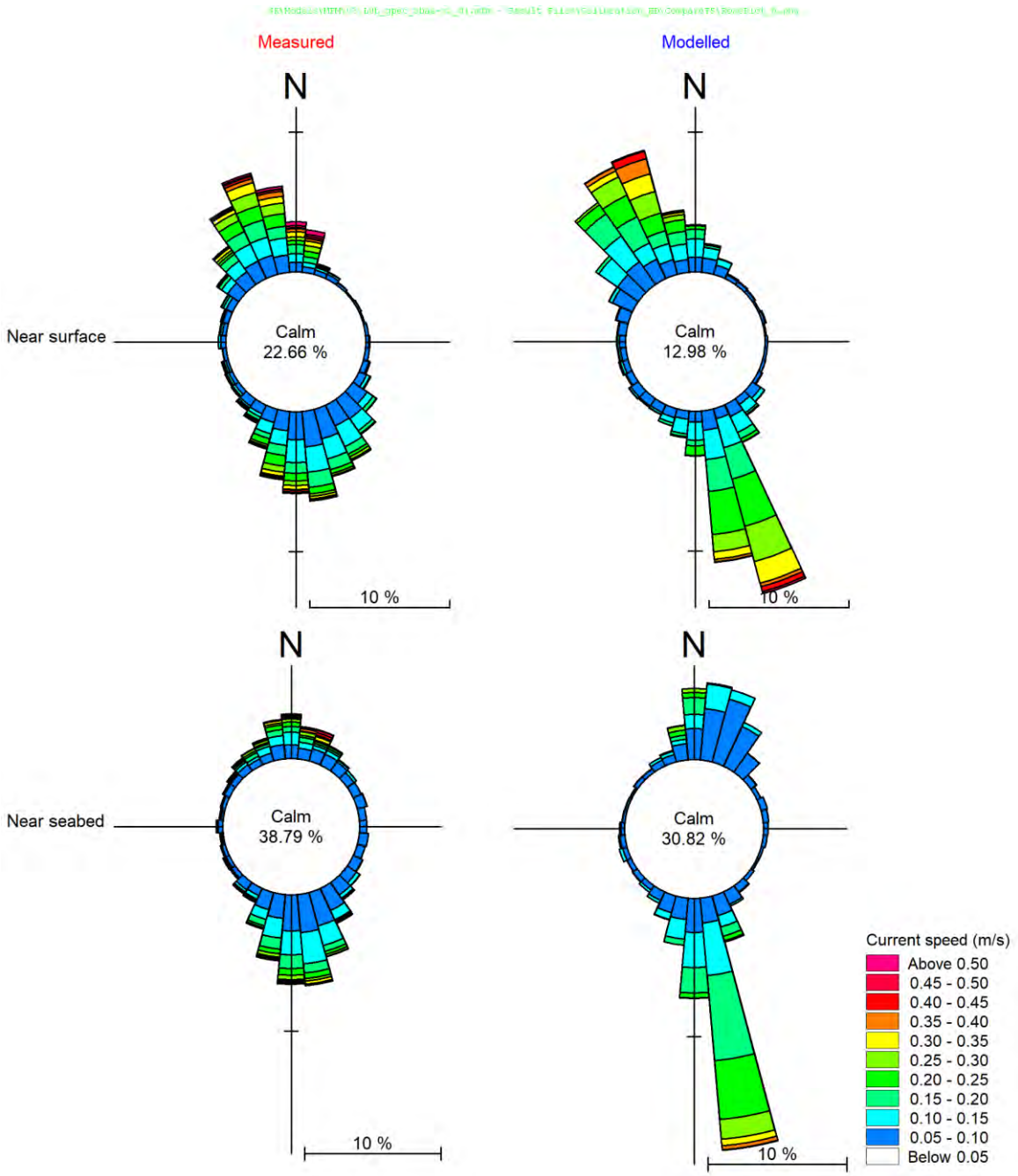


Figure 5.9.130: Current Rose Comparison of Modelled and Measured Currents at Site A (1 January 2009 to 31 December 2009).

CONTROLLED DISCLOSURE

When downloaded from the EDS database, this document is uncontrolled and the responsibility rests with the user to ensure it is in line with the authorised version on the database.

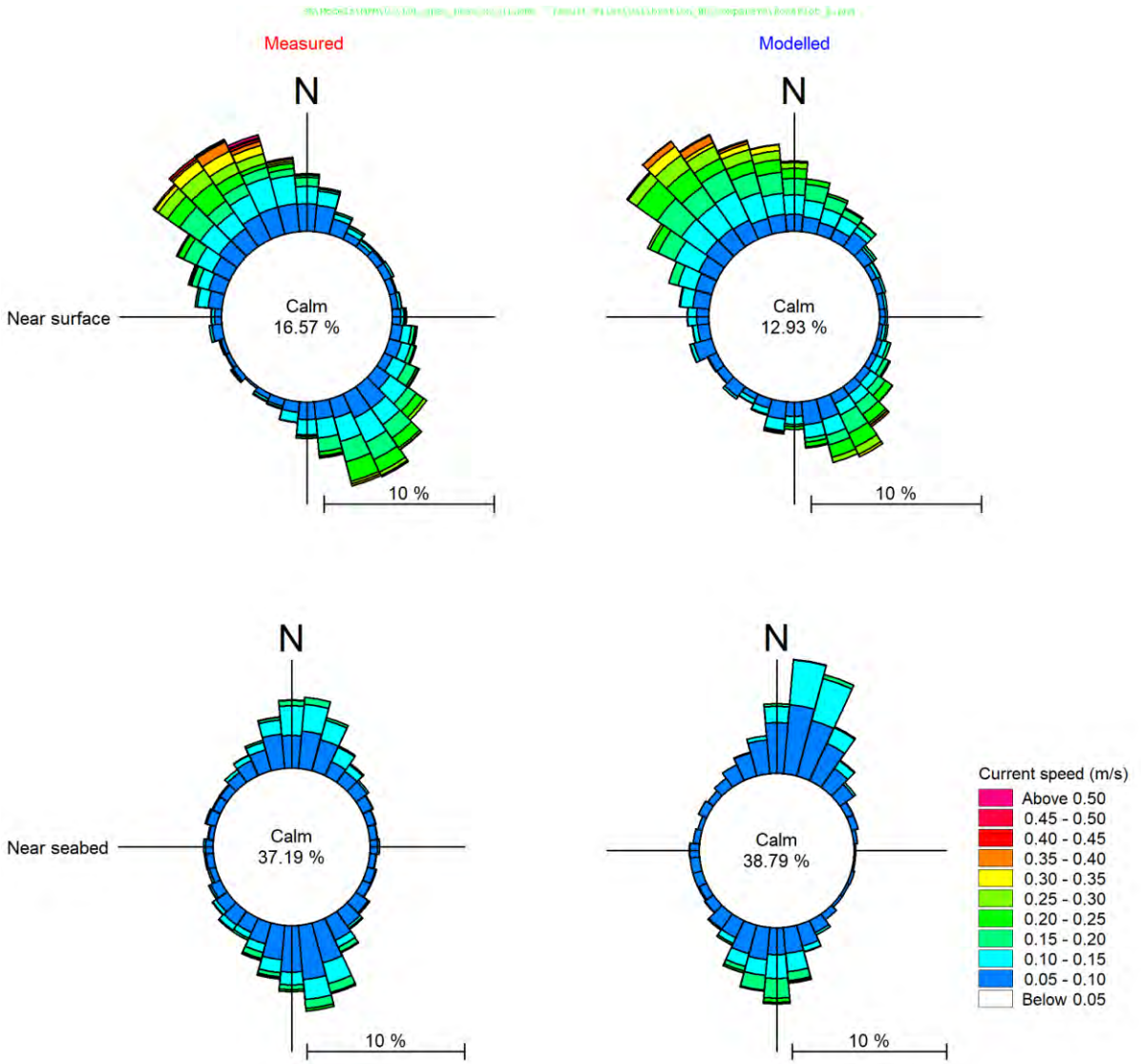


Figure 5.9.131: Current Rose Comparison of Modelled and Measured Currents at Site B (1 January 2009 to 31 December 2009).

CONTROLLED DISCLOSURE

When downloaded from the EDS database, this document is uncontrolled and the responsibility rests with the user to ensure it is in line with the authorised version on the database.

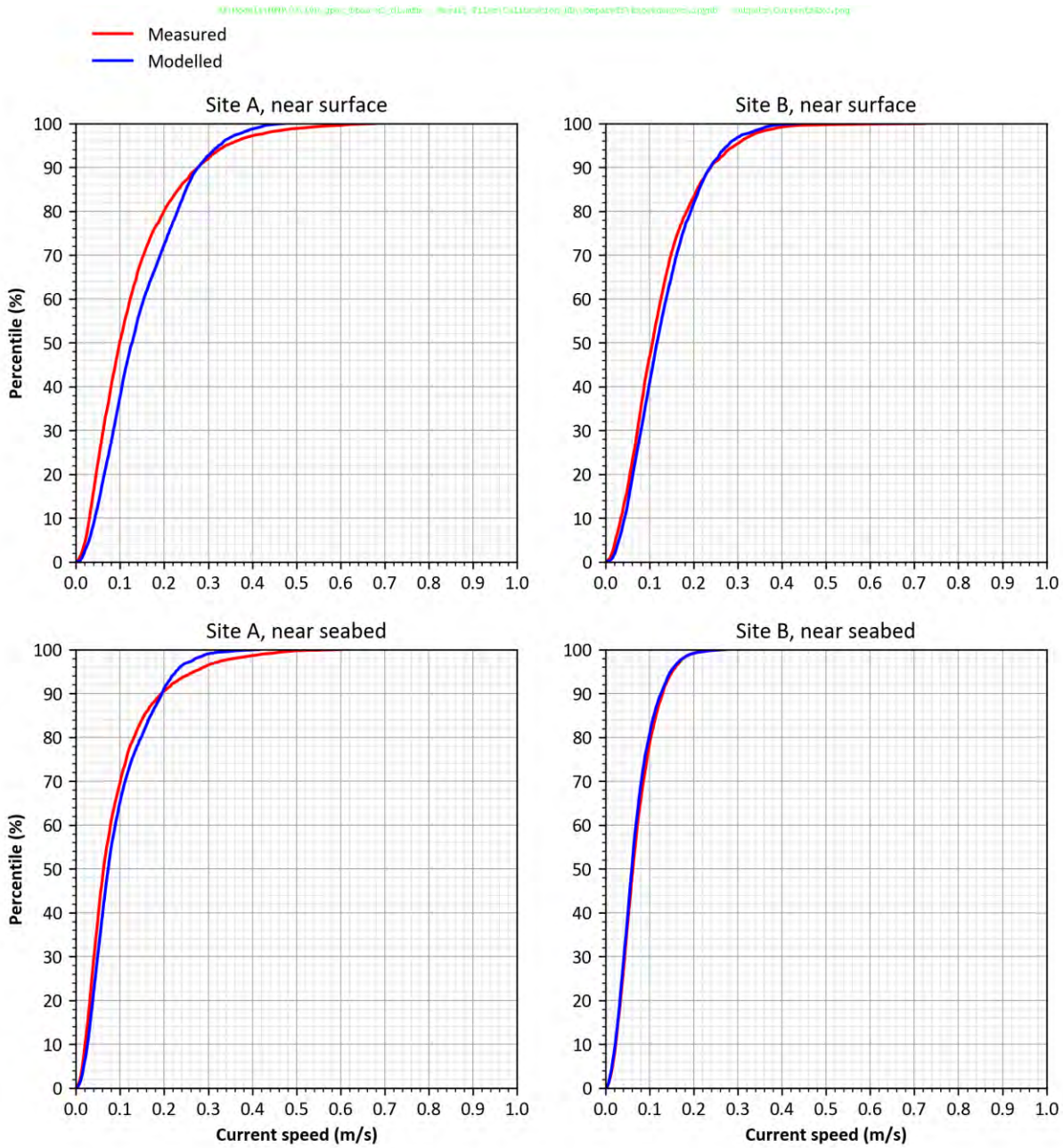


Figure 5.9.132: Percentile Comparisons of Modelled and Measured Current Speeds at Site A and B (1 January 2009 to 31 December 2009).

The percentile comparison plots use the times-series data at the particular site over the year and show the percentiles for these data from 0 to 100%. This allows a comparison of the distribution of the data magnitudes between model and the measurements.

The model tends to slightly overpredict the operational currents at Site A, but underpredicts some of the more extreme current speeds. The directions correlate well at both depths. The current speeds at Site B are resolved

CONTROLLED DISCLOSURE

When downloaded from the EDS database, this document is uncontrolled and the responsibility rests with the user to ensure it is in line with the authorised version on the database.

more accurately but some of the extreme events are still underpredicted. The near-surface directions show an excellent comparison, while the modelled near-seabed currents are slightly more rotated clockwise.

The modelled temperatures were compared to seabed measurements at Site C1 (-3 m msl), A (-10 msl) and B (-29 m msl). Site D (-27 m msl) and E (-50 m msl) are presented but were excluded from the calibration due to the short overlap of data.

Figure 5.9.133 presents a time-series comparison of modelled and measured near-seabed seawater temperatures at Site C1, A, B, D and E. Percentile comparisons of modelled and measured seawater temperatures at Site C1, A, and B are shown in ***Figure 5.9.134***. Also shown are temperature differences between the three sites. Considering the range of depths (-3 m msl to -29 m msl) the temperature differences serve as a proxy to temperature stratification in the water column.

CONTROLLED DISCLOSURE

When downloaded from the EDS database, this document is uncontrolled and the responsibility rests with the user to ensure it is in line with the authorised version on the database.

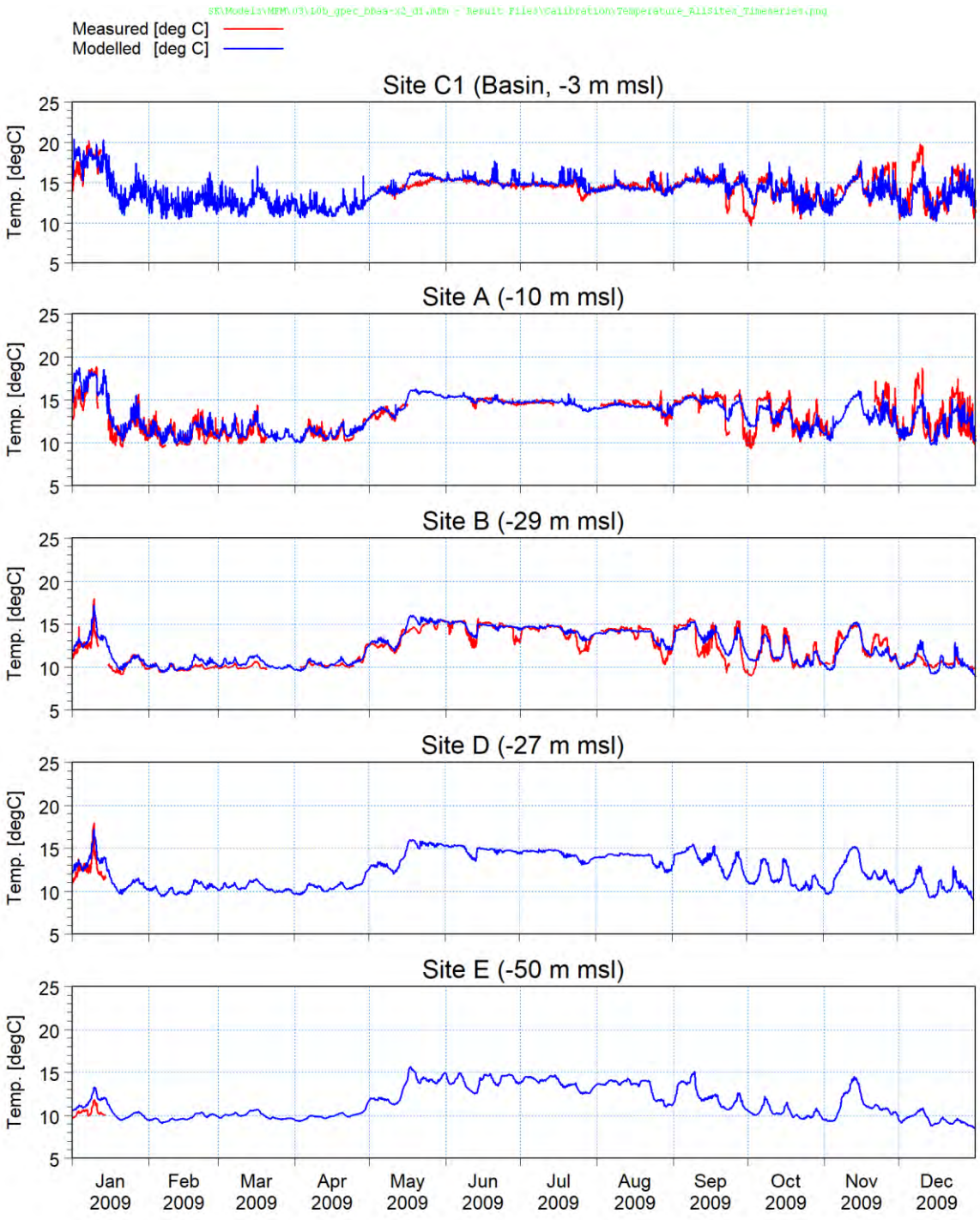


Figure 5.9.133: Time-Series Comparison of Modelled and Measured Near-Seabed Seawater Temperatures at Site C1, A, B, D and E.

CONTROLLED DISCLOSURE

When downloaded from the EDS database, this document is uncontrolled and the responsibility rests with the user to ensure it is in line with the authorised version on the database.

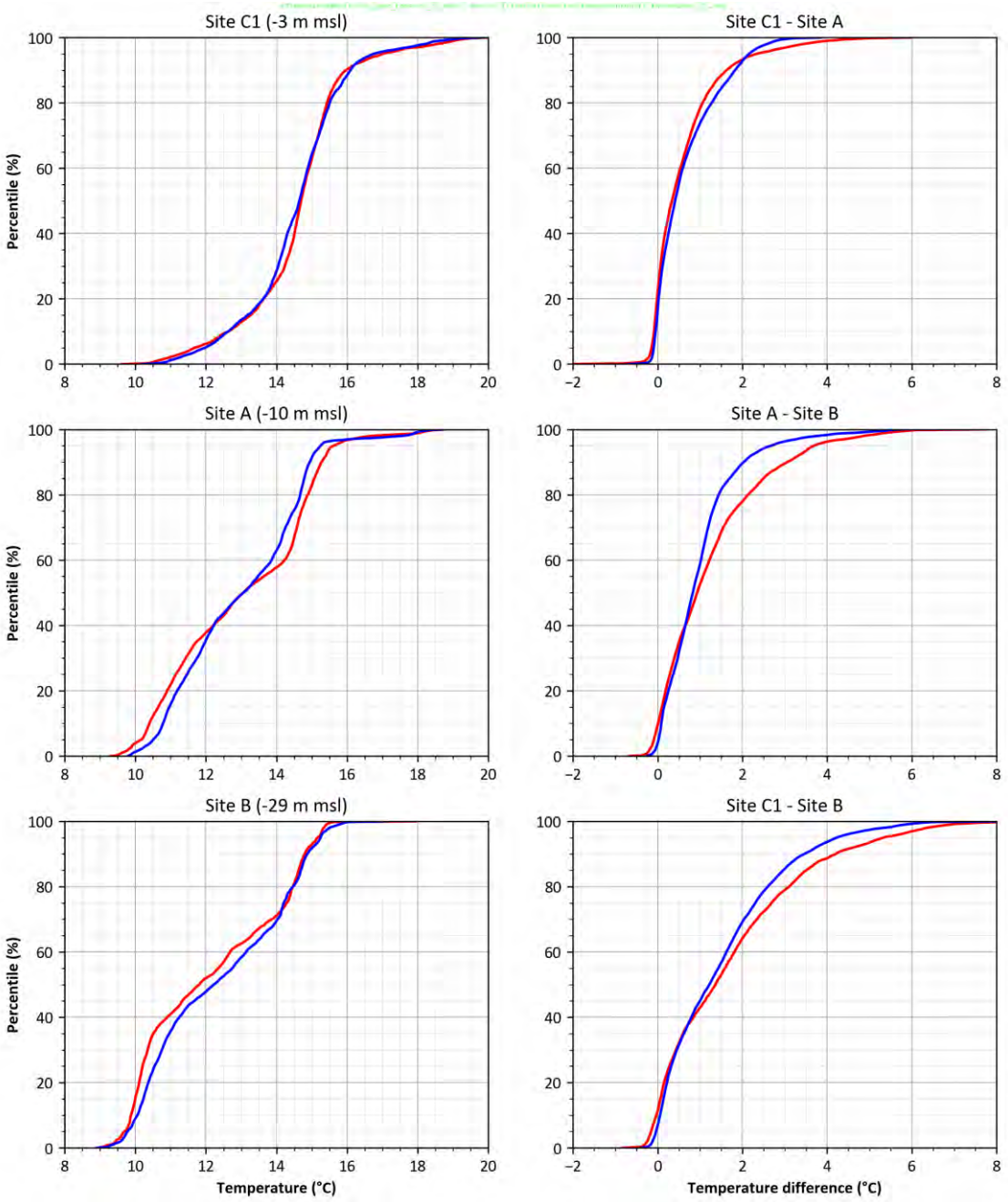


Figure 5.9.134: Percentile Comparisons of Modelled and Measured Seawater Temperatures at Site C1, A, and B, and Temperature Differences Between the Sites (right).

From the time-series and distributions it can be observed that the model is able to predict the mean trend in seawater temperatures and a number of the upwelling and heating events, but tends to underpredict the full range of some of the dynamic events. The temperature distributions show an excellent agreement at Site C1 but towards deeper water (Site B) the temperatures are slightly overpredicted. As a result the model tends to

When downloaded from the EDS database, this document is uncontrolled and the responsibility rests with the user to ensure it is in line with the authorised version on the database.

underpredict the stratification, mostly between Site A and Site B, but overall the modelled and measured stratifications show a good comparison.

Scenarios modelled

The five intake and outfall structure layouts as discussed in ***Subsection 5.9.15.3*** were modelled:

- Layout 0: Existing KNPS intake basin and outfall channel;
- Layout 1: Short tunnel intakes and outfalls;
- Layout 2: Long tunnel intakes and outfalls;
- Layout 3: Basin intake and tunnel outfalls;
- Layout 4: Basin intake and rubble-mound outfall structure.

Layout 0 included a single scenario for a power output of 2108 MWe from the KNPS, while Layouts 1 to 4 each included two scenarios of 2500 MWe and 4 000 MWe for the new NIs in addition to the KNPS power output, thus totalling nine cases.

In addition, each layout included a baseline scenario without thermal discharges which were used to quantify the change in temperature (ΔT) due to the thermal discharge.

Each scenario was run for a full calendar year to account for the effect of seasonal variations of waves, wind, currents, and temperature on the thermal plume dispersion. The year of 2009 was selected for modelling since it was covered by all the datasets required as model input and by those necessary for the proper calibration of the model. Furthermore, the highest seawater temperatures recorded in the KNPS intake basin (Site C1, ***Figure 5.9.21***) occurred in January 2009, thereby making this a conservative year to assess the impact of temperature releases.

Results

The primary model output parameter is the seawater temperature in each horizontal and vertical element of the computational mesh at 1-hour intervals for the full simulated year. These results were used to calculate the change in temperature (ΔT) for the discharge case compared to the baseline case without any thermal discharge, in each element at 1-hr interval. The 99th percentile ΔT's, which are presented in the contour plots below, will be exceeded 1% of the time and are thus close to the maximum ΔT's.

Figure 5.9.135 and ***Figure 5.9.136*** present examples of instantaneous seawater temperature and currents at the surface for Layout 1 and Layout 4

When downloaded from the EDS database, this document is uncontrolled and the responsibility rests with the user to ensure it is in line with the authorised version on the database.

respectively. ***Figure 5.9.137*** shows the 99th percentile ΔT at surface (top) and seabed (bottom) for Layout 1.

CONTROLLED DISCLOSURE

When downloaded from the EDS database, this document is uncontrolled and the responsibility rests with the user to ensure it is in line with the authorised version on the database.

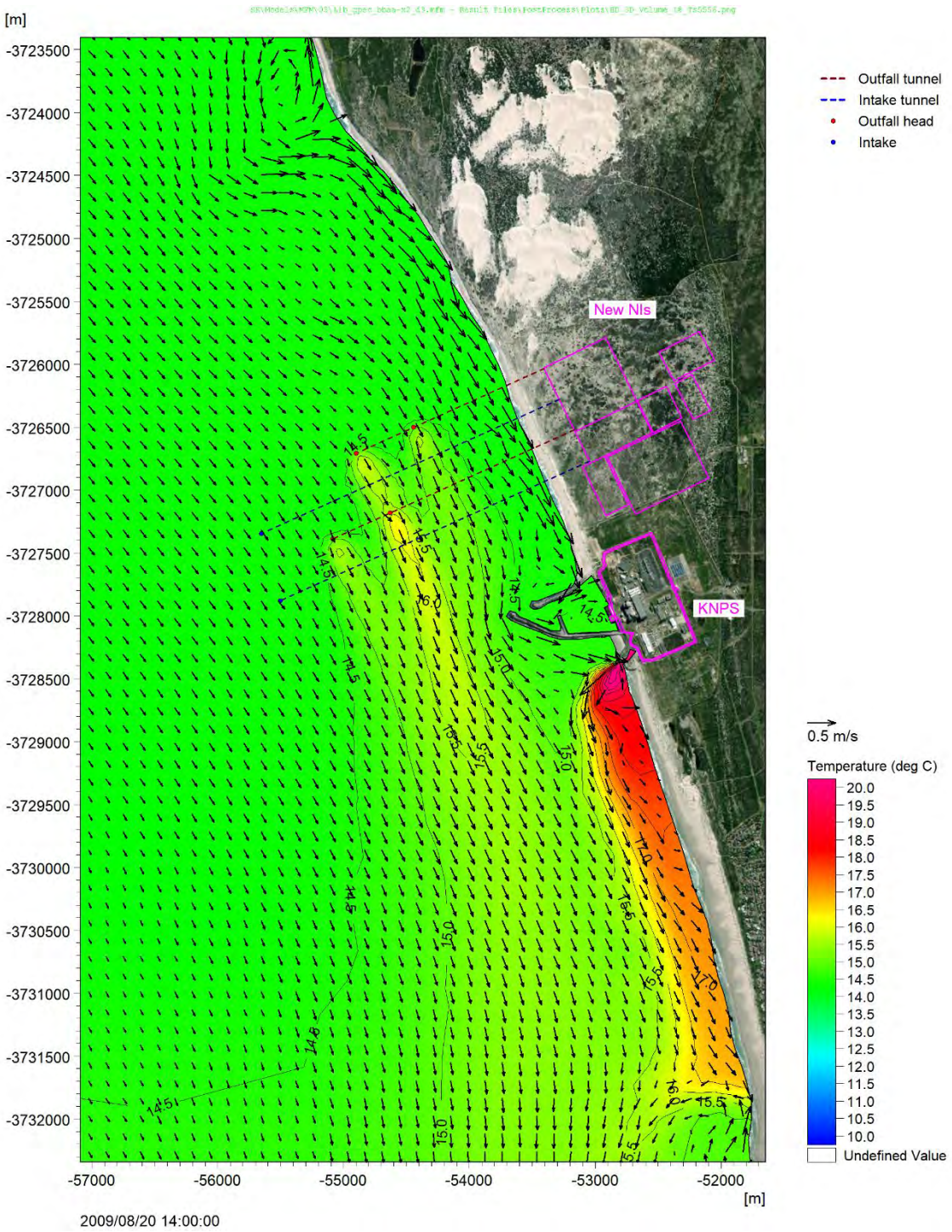


Figure 5.9.135: KNPS + new Nls (4000 MWe) Layout 1: Example of Instantaneous Seawater Temperature and Currents at Surface.

CONTROLLED DISCLOSURE

When downloaded from the EDS database, this document is uncontrolled and the responsibility rests with the user to ensure it is in line with the authorised version on the database.

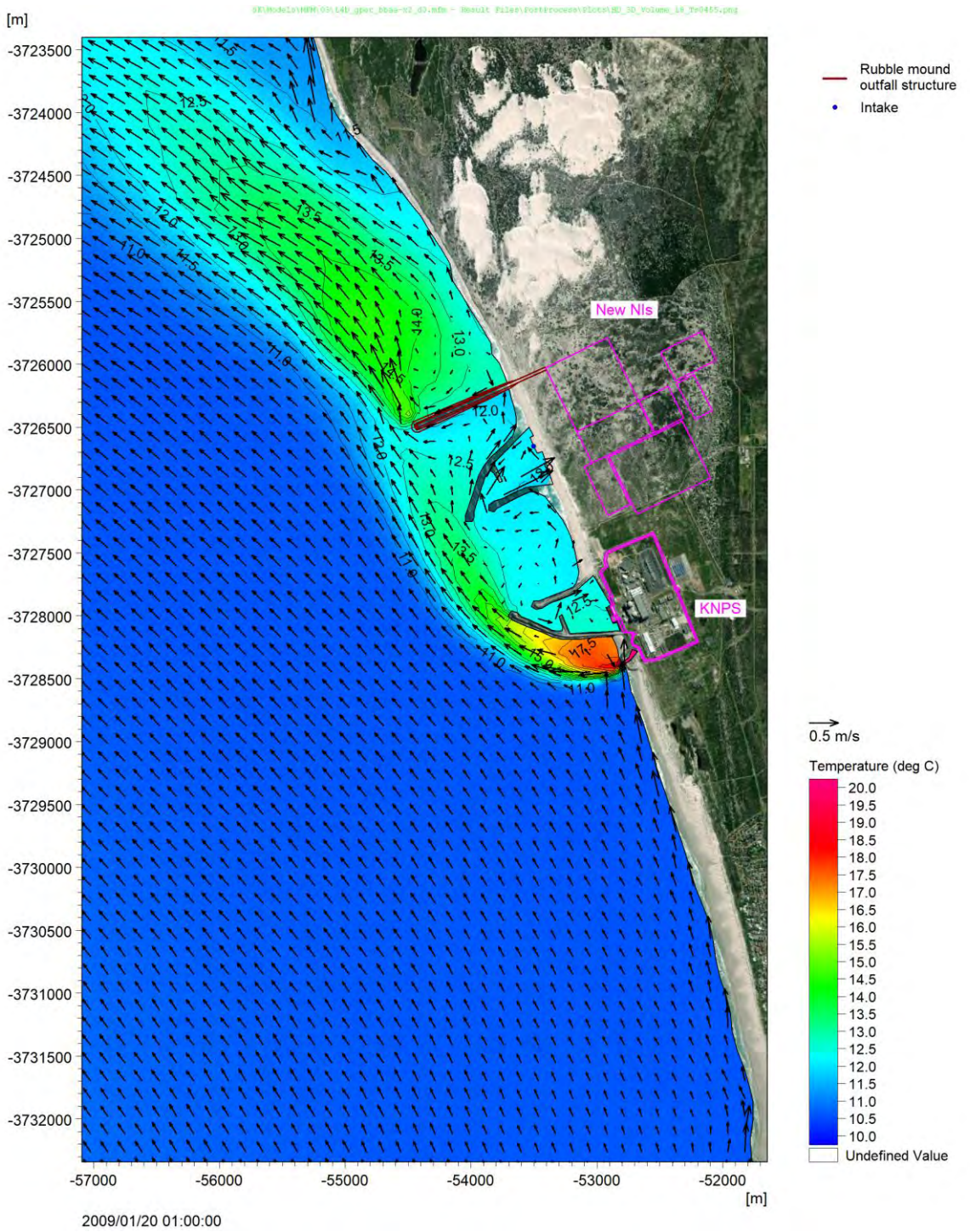


Figure 5.9.136: KNPS + new Nls (4000 MWe) Layout 4: Example of Instantaneous Seawater Temperature and Currents at Surface.

CONTROLLED DISCLOSURE

When downloaded from the EDS database, this document is uncontrolled and the responsibility rests with the user to ensure it is in line with the authorised version on the database.

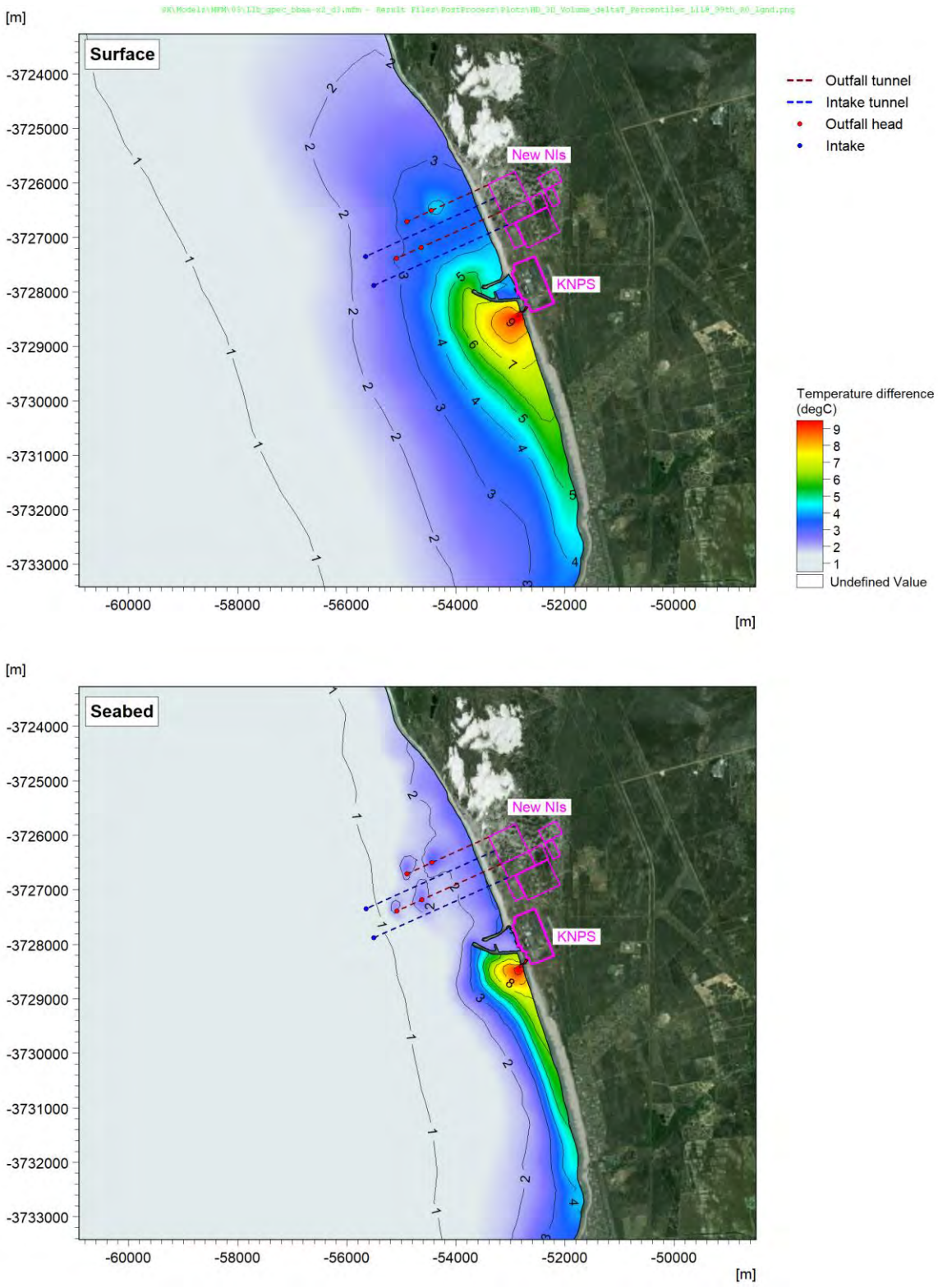


Figure 5.9.137: KNPS + new NIs (4000 MWe) Layout 1: 99th Percentile ΔT at Surface (top) and Seabed (bottom).

CONTROLLED DISCLOSURE

When downloaded from the EDS database, this document is uncontrolled and the responsibility rests with the user to ensure it is in line with the authorised version on the database.

Figure 5.9.137 shows that due to buoyancy the highest ΔT's tend to be near the water surface, although in some cases the plume may be trapped below the surface resulting in a higher ΔT lower in the water column. The 99th percentile ΔT has been calculated for each of the eight vertical layers in the model and at each horizontal element the layer with the highest ΔT has been selected. These are referred to as the 99th percentile ΔT at worst water depth and are shown in ***Figure 5.9.138*** to ***Figure 5.9.142***. These results are for the 4000 MWe power station, whilst the results for the 2500 MWe power station are provided in ***Appendix C***.

CONTROLLED DISCLOSURE

When downloaded from the EDS database, this document is uncontrolled and the responsibility rests with the user to ensure it is in line with the authorised version on the database.

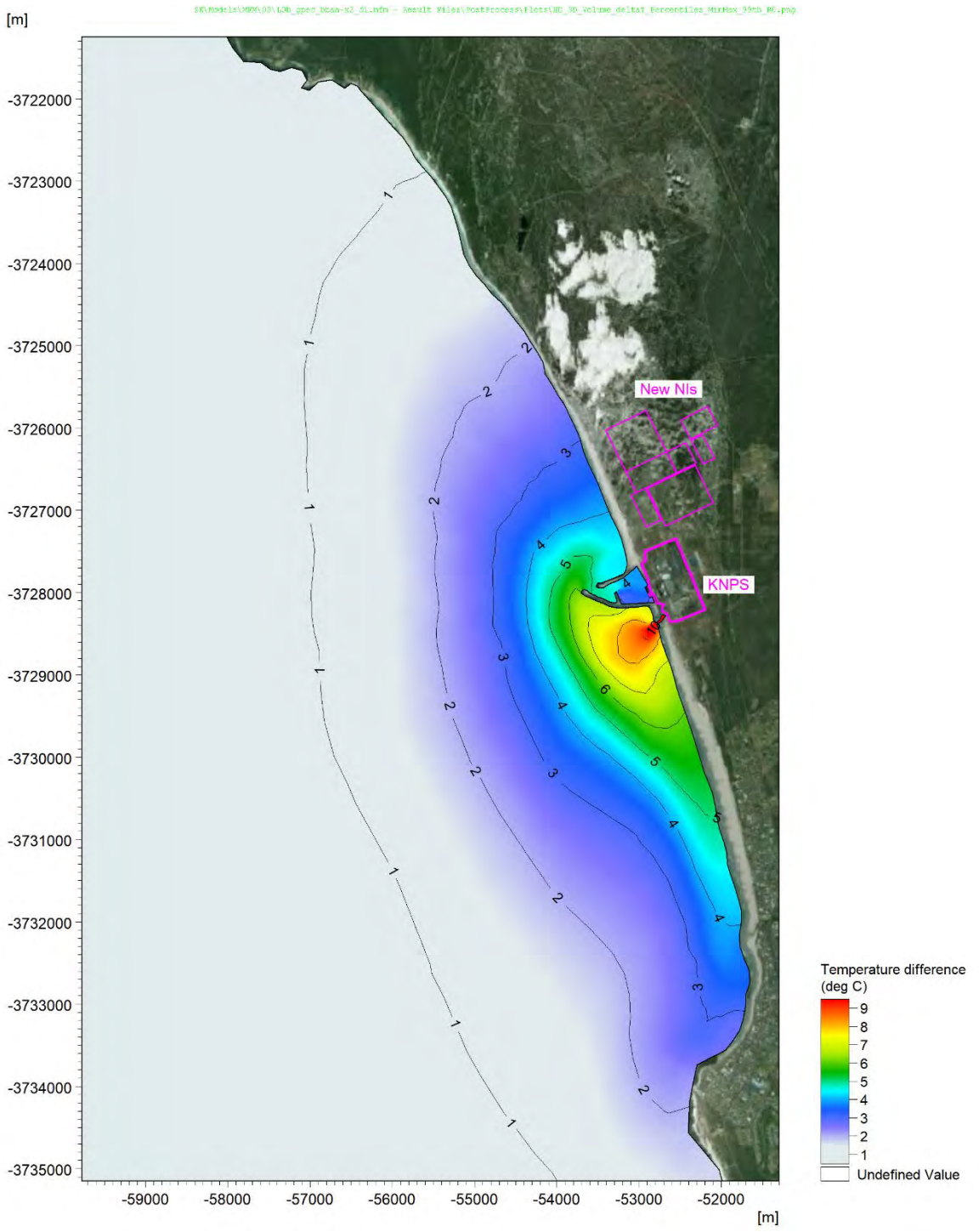


Figure 5.9.138: KNPS (2108 MWe): 99th Percentile ΔT at Worst Water Depth.

CONTROLLED DISCLOSURE

When downloaded from the EDS database, this document is uncontrolled and the responsibility rests with the user to ensure it is in line with the authorised version on the database.

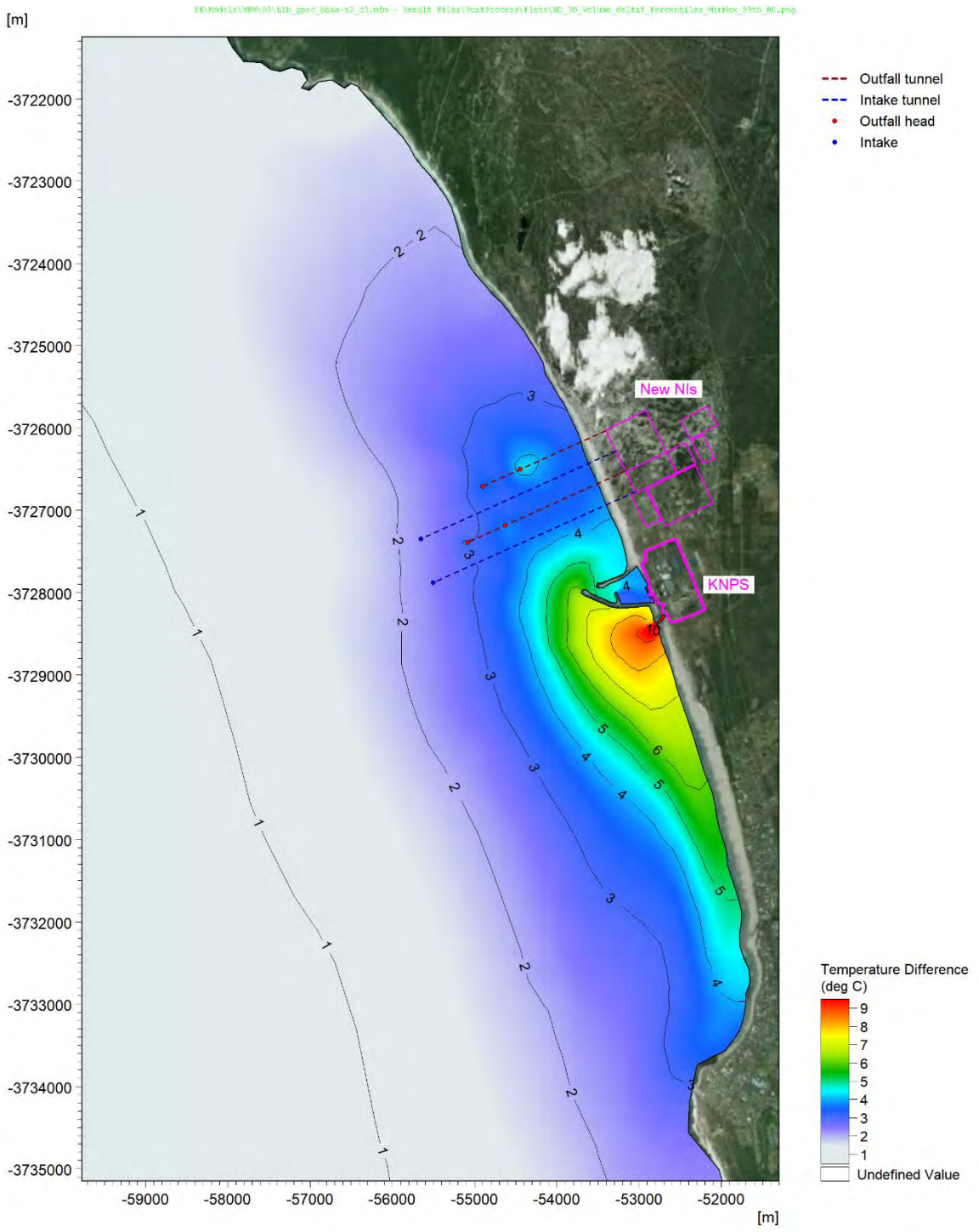


Figure 5.9.139: KNPS + new Nls (4000 MWe) Layout 1: 99th Percentile ΔT at Worst Water Depth.

CONTROLLED DISCLOSURE

When downloaded from the EDS database, this document is uncontrolled and the responsibility rests with the user to ensure it is in line with the authorised version on the database.

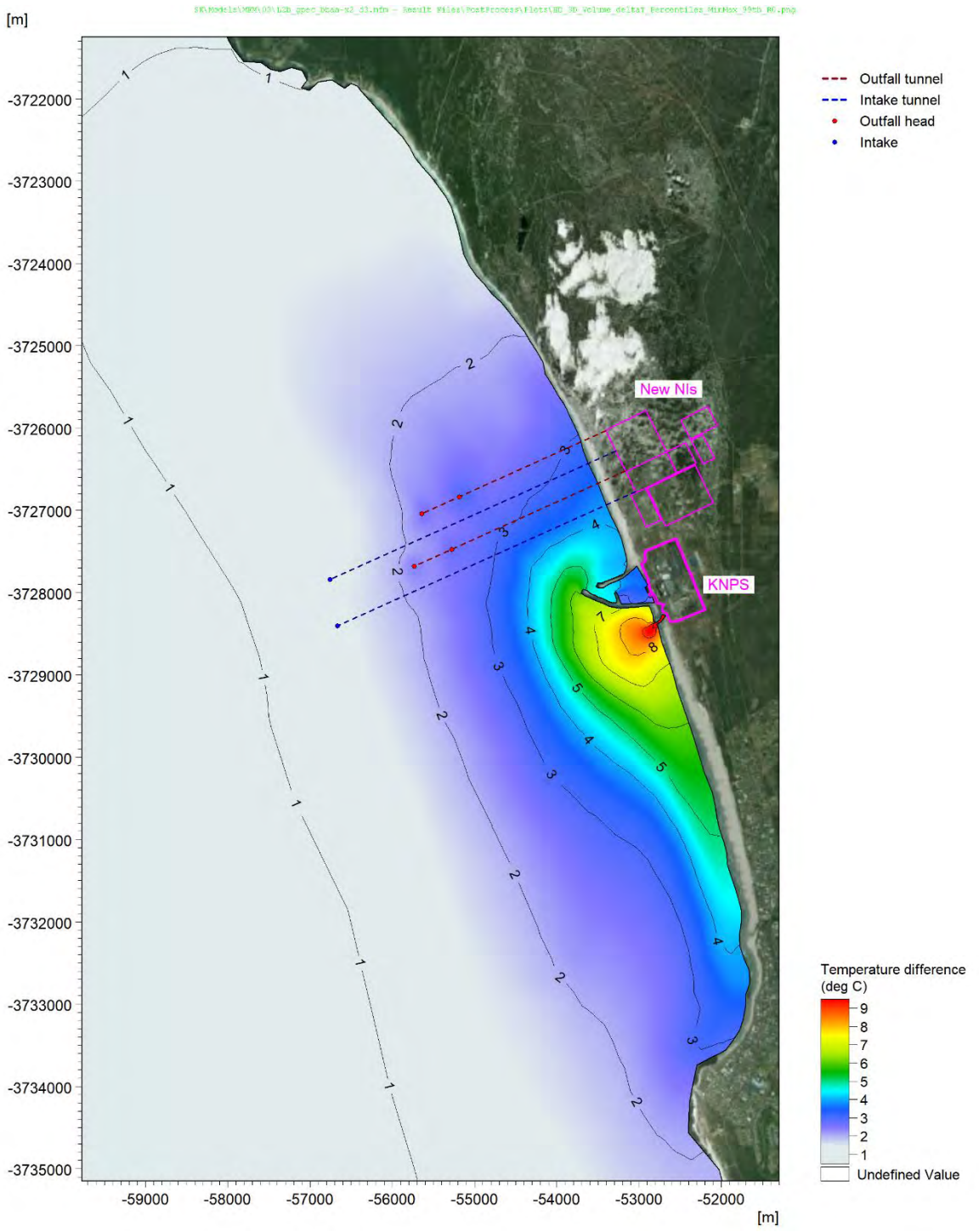


Figure 5.9.140: KNPS + new NIs (4000 MWe) Layout 2: 99th Percentile ΔT at Worst Water Depth.

CONTROLLED DISCLOSURE

When downloaded from the EDS database, this document is uncontrolled and the responsibility rests with the user to ensure it is in line with the authorised version on the database.

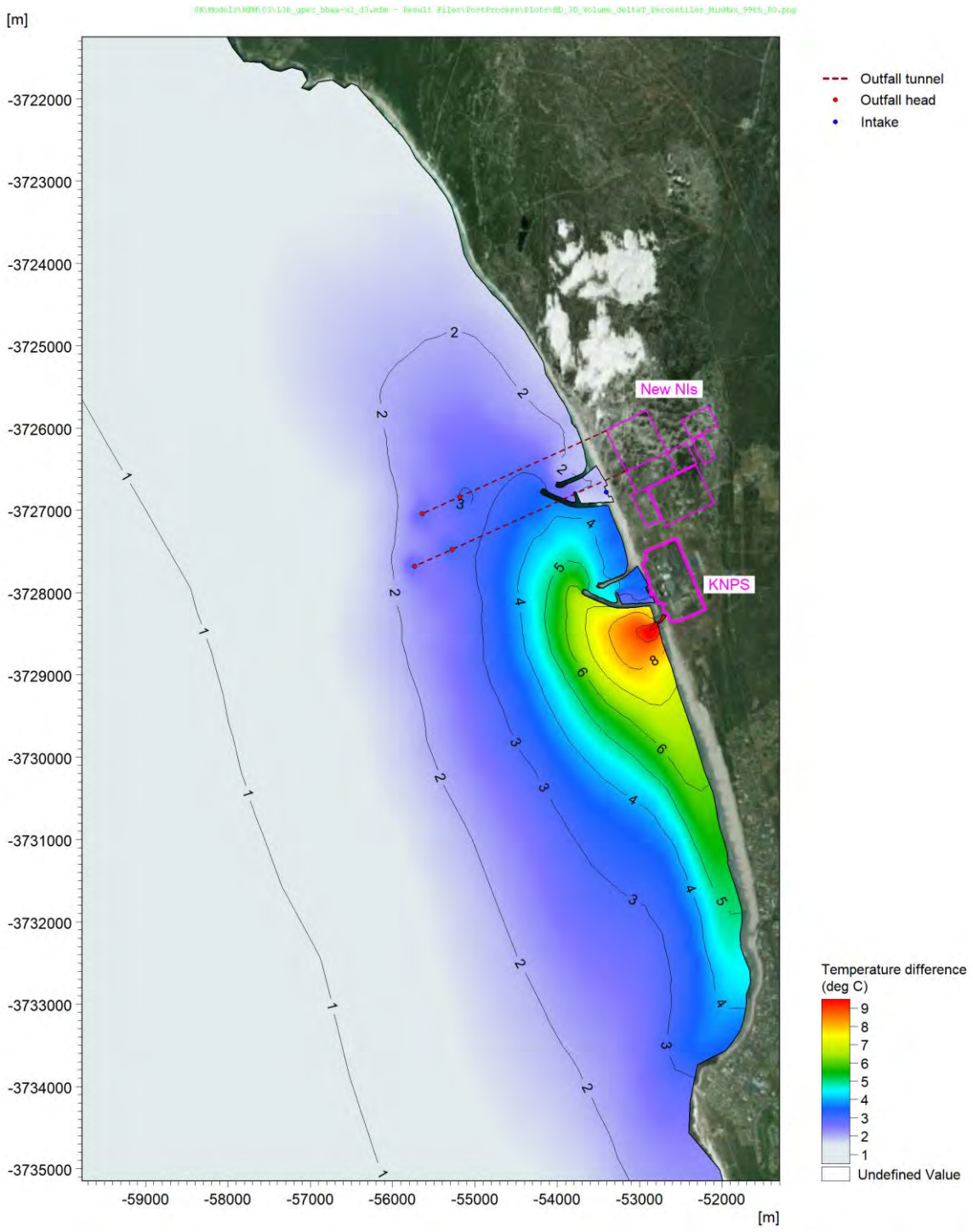


Figure 5.9.141: KNPS + new Nls (4000 MWe) Layout 3: 99th Percentile ΔT at Worst Water Depth.

CONTROLLED DISCLOSURE

When downloaded from the EDS database, this document is uncontrolled and the responsibility rests with the user to ensure it is in line with the authorised version on the database.

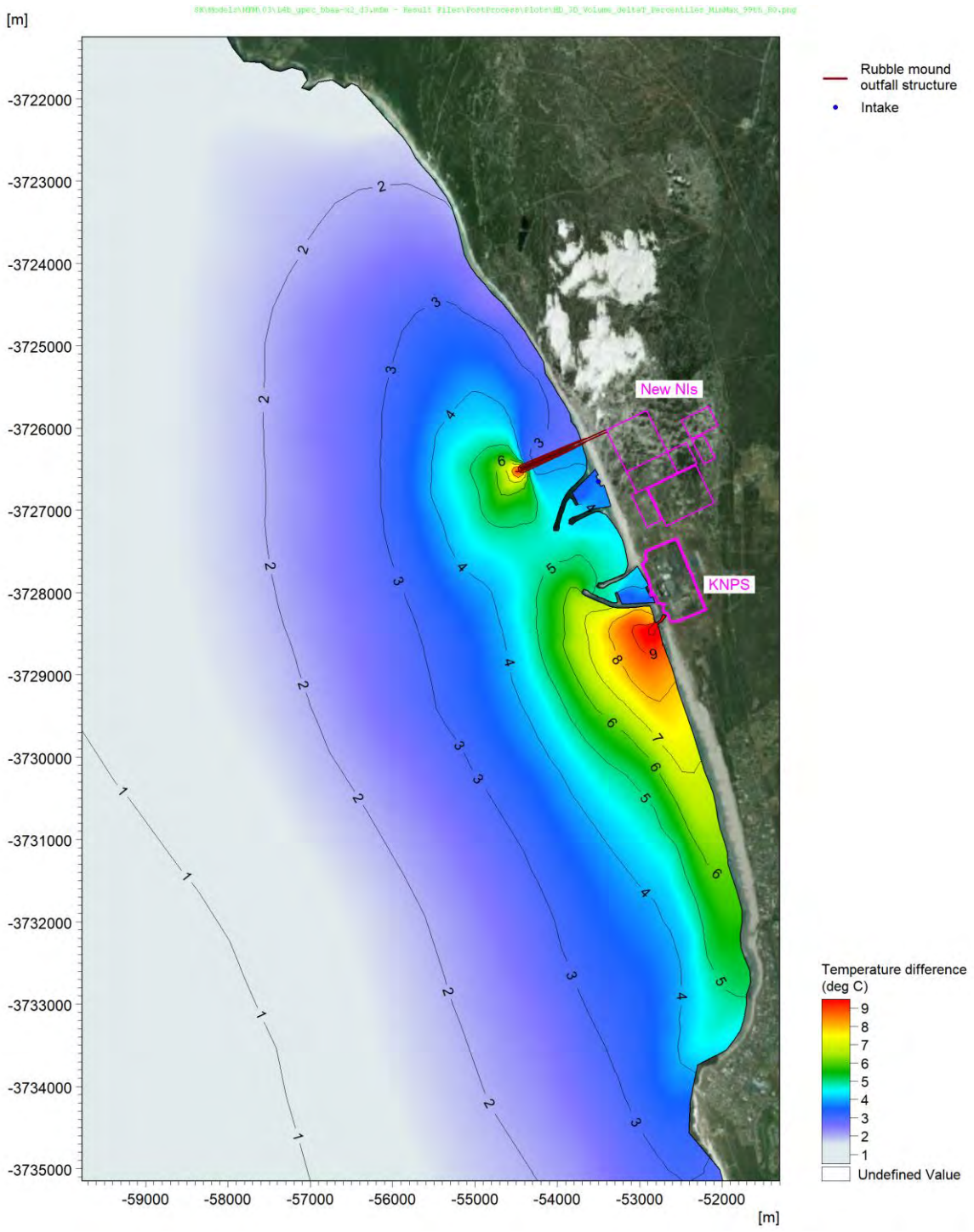


Figure 5.9.142: KNPS + new NIs (4000 MWe) Layout 4: 99th Percentile ΔT at Worst Water Depth.

These results show the following:

- The KNPS surf-zone outfall results in significantly higher temperatures relative to the layouts presented for the new NIs.

CONTROLLED DISCLOSURE

When downloaded from the EDS database, this document is uncontrolled and the responsibility rests with the user to ensure it is in line with the authorised version on the database.

- The tunnel outfalls generally disperse the heat better, with Layout 2 (long tunnel intakes and outfalls) showing the lowest temperatures, due to the deeper mixing depth, entrainment of colder bottom water and reduced recirculation.
- Layout 4 (basin intake and rubble-mound outfall structure) was the least effective due to the concentrated jet in shallower water combined with increased recirculation between the KNPS and new NI basins.

5.9.15.6 Thermal Recirculation

The PPE for the new NIs specifies that the maximum ΔT of the re-circulated water should be less than 1.5°C (see ***Table 5.9.3***). The maximum ΔT of the re-circulated water at the KNPS is not specified.

The recirculation of temperature from the discharge back to the intake is equal to the modelled ΔT at the location and depth of the intake. In ***Figure 5.9.143*** these recirculation ΔT's at the KNPS intake and at the new NIs intake are presented as percentiles for the nine modelled cases. ***Table 5.9.55*** summarises these results for the 50th, 95th and 99th percentiles. For layouts with dual intakes the maximum ΔT percentile of the two is shown.

CONTROLLED DISCLOSURE

When downloaded from the EDS database, this document is uncontrolled and the responsibility rests with the user to ensure it is in line with the authorised version on the database.

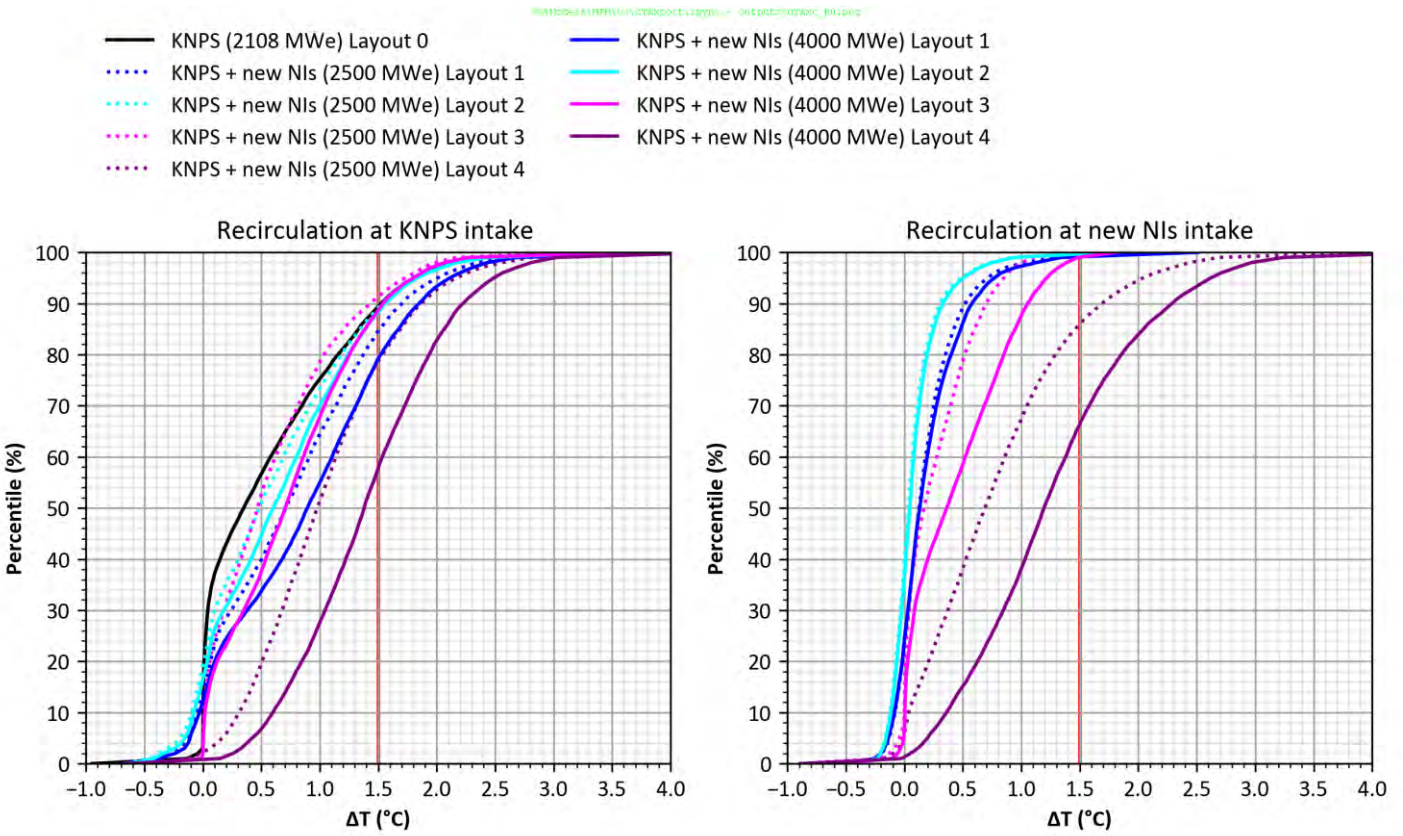


Figure 5.9.143: Recirculation at KNPS Intake and New NIs Intake for the Nine Modelled Cases.

Table 5.9.55: Recirculation at KNPS Intake and New NIs Intake.

Case	ΔT at KNPS Intake (°C)			ΔT at new NIs Intake (°C)		
	50th Percentile	95th Percentile	99th Percentile	50th Percentile	95th Percentile	99th Percentile
KNPS (2108 MWe)	0.35	1.80	2.40	-	-	-
KNPS + new NIs (2500 MWe) Layout 1	0.71	2.01	2.57	0.13	0.71	1.33
KNPS + new NIs (2500 MWe) Layout 2	0.48	1.79	2.41	0.03	0.48	0.92
KNPS + new NIs (2500 MWe) Layout 3	0.47	1.73	2.17	0.17	0.85	1.10
KNPS + new NIs (2500 MWe) Layout 4	0.98	2.17	2.81	0.69	2.04	2.69
KNPS + new NIs (4000 MWe) Layout 1	0.89	2.11	2.69	0.08	0.70	1.17
KNPS + new NIs (4000 MWe) Layout 2	0.60	1.83	2.44	0.05	0.50	0.94
KNPS + new NIs (4000 MWe) Layout 3	0.70	1.80	2.27	0.36	1.22	1.48
KNPS + new NIs (4000 MWe) Layout 4	1.38	2.49	3.02	1.19	2.62	3.24

The results above show the following regarding recirculation:

CONTROLLED DISCLOSURE

When downloaded from the EDS database, this document is uncontrolled and the responsibility rests with the user to ensure it is in line with the authorised version on the database.

- The 99th percentile ΔT at the existing KNPS intake is 2.4°C.
- The new NIs generally increase the ΔT at the existing KNPS intake, with Layout 4 resulting in the largest increase (+0.6°C for the 99th percentile), while Layout 3 had the least impact.
- At the new NIs intake, Layouts 1 to 3 meet the ΔT of 1.5°C for the 99th percentile. Layout 4 has a 99th percentile ΔT of 2.7 and 3.2°C for power outputs of 2500 and 4000 MWe, respectively.

5.9.15.7 Extreme Seawater Temperatures at Intakes

The PPE also specifies a maximum cooling water intake temperature for the new NIs of 30°C (see ***Table 5.9.3***). For the existing KNPS a shut-down of the reactor will be necessary if the intake temperature exceeds 23°C (Eskom, 2006).

The maximum seawater temperature at the cooling water intakes will depend on:

- The intake and outfall layout, the power output and resultant ΔT due to recirculation from the outfall to the intake, as determined from the thermal plume dispersion modelling (***Table 5.9.55***);
- The extreme maximum background seawater temperature at the intake location and climate change, as determined from the EVA of the site measurements, noting that these temperatures already include the ΔT from the KNPS thermal plume (***Table 5.9.19***).

The additional ΔT contributed by the NIs was estimated by calculating the difference in absolute temperature distributions at the intakes between the KNPS thermal plume and the KNPS + new NIs thermal plume. From these ΔT distributions the maximum value above the 90th percentile have been added to the extreme maximum background seawater temperatures. The results have been presented as the best estimate return period in years to exceed 23°C at the KNPS intake and the best estimate annual probability to exceed 30°C at the new NIs intake, as shown in ***Table 5.9.56*** below.

CONTROLLED DISCLOSURE

When downloaded from the EDS database, this document is uncontrolled and the responsibility rests with the user to ensure it is in line with the authorised version on the database.

Table 5.9.56: Extreme Maximum Seawater Temperatures at the Intakes (Including Recirculation).

Case	Best Estimate Return Period to Exceed 23°C at KNPS Intake[(a)] (y)			Best Estimate Probability to Exceed 30°C at New NIs Intake (y^{-1})		
	2021	2044	2064	2021	2064	2130
KNPS (2108 MWe) Layout 0	98	56	35	-	-	-
KNPS + new NIs (2500 MWe) Layout 1	56	32	20	1.0E-05	2.8E-05	1.3E-04
KNPS + new NIs (2500 MWe) Layout 2	71	40	25	3.4E-06	9.1E-06	4.1E-05
KNPS + new NIs (2500 MWe) Layout 3	73	42	26	8.5E-06	2.3E-05	1.0E-04
KNPS + new NIs (2500 MWe) Layout 4	51	29	18	1.5E-05	4.0E-05	1.8E-04
KNPS + new NIs (4000 MWe) Layout 1	44	25	15	1.1E-05	2.8E-05	1.3E-04
KNPS + new NIs (4000 MWe) Layout 2	65	37	23	3.6E-06	9.6E-06	4.4E-05
KNPS + new NIs (4000 MWe) Layout 3	61	35	21	8.5E-06	2.3E-05	1.0E-04
KNPS + new NIs (4000 MWe) Layout 4	29	17	10	3.1E-05	8.2E-05	3.8E-04

Note:
(a) Expressed as the return period for convenience, where return period = 1/exceedance probability.

These results show the following regarding maximum intake temperatures:

- For KNPS the maximum specified intake temperature is 23°C. Without the new NIs, the best estimate return period to exceed 23°C is 98 y for the year 2021 and 35 y for the year 2064.
- In all cases the addition of the new NIs reduces the return period (increased exceedance probability) to exceed 23°C at the KNPS intake. Layout 4 with a 4000 MWe power station has the largest impact on the KNPS, with the 23°C threshold reducing to a 29 y return period for the year 2021 and a 10 y return period for the year 2064. Layout 4 will thus increase the probability of a shut-down of the KNPS reactor due to high seawater temperatures.
- At the new NIs intakes, the higher maximum specified intake temperature of 30°C, combined with lower recirculation ΔT's results in significantly lower exceedance probabilities of between 3.4×10^{-6} and 3.8×10^{-4} y^{-1}, with the latter for Layout 4 with the 4000 MWe power station in 2130. These exceedance probabilities indicate that the intake seawater temperatures will need to be considered in the design of the cooling system for the new NIs.

CONTROLLED DISCLOSURE

When downloaded from the EDS database, this document is uncontrolled and the responsibility rests with the user to ensure it is in line with the authorised version on the database.

5.9.16 Sediment Transport

5.9.16.1 Sedimentation and Scour Due to Storms

Sediment transport modelling

Sediment transport modelling was carried out to assess the sedimentation in the KNPS intake basin entrance and scour around coastal structures during extreme storm events.

The modelling was carried out using the MIKE 21 Sand Transport model. The details of the physical processes and numerical implementation are provided in the model documentation (see ***Table 5.9.7***), while details of the model setup, sensitivity testing, and V&V are provided in the V&V Report (PRDW, 2022b).

The Sand Transport model calculates the transport of non-cohesive sediment (grain size > 0.063 mm) based on the combination of flow conditions from the hydrodynamic module (see description in ***Subsection 5.9.12.5***) and wave conditions from the spectral wave module (see description in ***Subsection 5.9.9.8***). For the case of combined waves and currents, sediment transport rates are derived by linear interpolation in a sediment transport lookup table. The values in the table are calculated by the quasi three-dimensional sediment transport model (STPQ3D). The STPQ3D model calculates the instantaneous and time-averaged hydrodynamics and sediment transport in two horizontal directions. As the model calculates the bed load and the suspended load separately, the values in the sediment transport table are the total load.

The morphological development can be included by updating the bathymetry for every time step with the net sedimentation in each cell, which is based on the divergence of the sediment transport field and the porosity of the seabed. In order to reduce computer time, the morphological development can be sped up by multiplying the sedimentation by a speed-up factor. A varying sand layer thickness can be specified as the start condition for the simulation. This option is used when simulating sand transport in areas with rock bed present (i.e., cases with non-erodible bed and limited sand supply). It is possible to include the effect of slope failure on the morphological update of the bathymetry. The slope failure mechanism will come into effect if the local bed slope becomes steeper than a specified angle of repose.

The model computational mesh and bathymetry are presented in ***Figure 5.9.144***.

CONTROLLED DISCLOSURE

When downloaded from the EDS database, this document is uncontrolled and the responsibility rests with the user to ensure it is in line with the authorised version on the database.

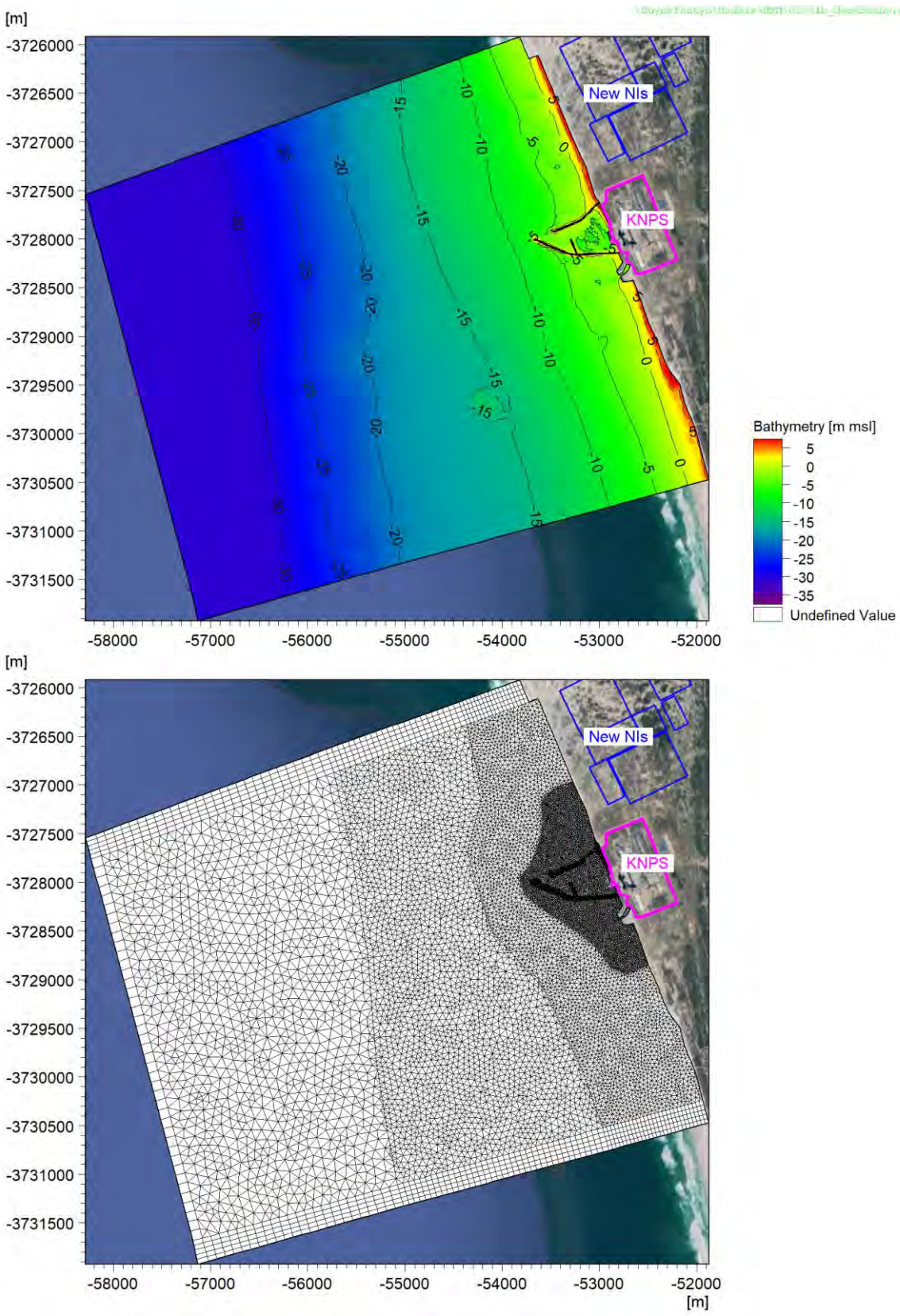


Figure 5.9.144: Storm Sedimentation and Scour Model Bathymetry and Mesh.

CONTROLLED DISCLOSURE

When downloaded from the EDS database, this document is uncontrolled and the responsibility rests with the user to ensure it is in line with the authorised version on the database.

The model bathymetry is derived from the generic dataset described in ***Subsection 5.9.8***. The computational mesh extends approximately 5 km offshore KNPS to beyond the -31 m msl depth contour and approximately 2.5 km north and south of KNPS. The mesh comprises quadrangular and triangular mesh elements with resolutions varying between 100 m at the offshore boundary to 8 m on the breakwater slopes. The bathymetry was truncated at -31 m msl (i.e., all depths deeper than -31 m msl were set to -31 m msl) to align with the specified wave boundary conditions defined at Point 1 (location shown in ***Figure 5.9.33***).

The spectral wave model was run in the quasi-stationary, parametric formulation with no additional wind generation. Wave parameters were applied along the offshore model boundary, with lateral boundaries along the north and south boundaries. Bottom friction was modelled using a constant Nikuradse roughness of 0.02 m, in alignment with the calibrated wave model described in ***Subsection 5.9.9.8***. Water levels were obtained through a direct coupling with the hydrodynamic model.

Time-varying water levels were applied along all three boundaries of the 2D hydrodynamic model. Wave-driven currents and water levels were modelled using wave radiation stresses obtained through a direct coupling with the wave model. Bed resistance was modelled using a Chezy number of 50 $m^{1/2}/s$, except on the slopes of rubble-mound structures where a Chezy number of 20 $m^{1/2}/s$ was used to account for the additional roughness. Wind-driven currents were not included. Horizontal eddy viscosity was modelled using the Smagorinsky formulation. The KNPS cooling water circulation was included in the model through a coupled source-sink pair to account for its effect on the hydrodynamics in the intake basin.

A median sediment grain diameter of D_{50} = 0.25 mm and a grading coefficient of $(D_{84}/D_{16})^{1/2}$ = 1.4 were used based on the available sediment data described in ***Subsection 5.9.8***. A space-varying initial bed thickness was used to specify a non-erodible bed on the rubble-mound structures of the intake basin, within the outfall channel, and at offshore rocky reefs. Morphological updating of the bed was included to account for the effects of changes in the bed level on the hydrodynamics. Slope failure was included in the model by specifying an angle of repose of 5.7 degrees, corresponding to a 1:10 slope. Slopes up to 1:5 were allowed within the intake basin based on the bathymetry data.

Cases modelled

Only the 2021 (present-day) date was modelled. The sedimentation and scour in 2064 are not expected to be significantly different for the following reasons:

CONTROLLED DISCLOSURE

When downloaded from the EDS database, this document is uncontrolled and the responsibility rests with the user to ensure it is in line with the authorised version on the database.

- Although the climate change to 2064 will result in higher water levels, the depth at the entrance to the intake basin is generally in equilibrium with the long-term water level and cooling water intake flow rate (PRDW, 2005). For higher water levels due to sea level rise, the bed levels in the intake basin are therefore expected to rise in concert, and thus the initial water depth is not expected to be significantly different to the present-day conditions.
- Outside the basin sea level rise may induce deeper water depths at the breakwater roundheads, resulting in larger waves in depth-limited storm conditions. However, deeper water depths are also expected to result in lower current speeds as longshore currents accelerate past the intake basin entrance.
- Due to the receding coastline north of KNPS (see ***Subsection 5.9.10.6***), in 2064 the intake basin entrance will be located further from the coastline where the highest littoral drift occurs.

The following storm cases were modelled:

- The 10^{-2}, 10^{-4}, 10^{-6}, and 10^{-8} y^{-1} exceedance probabilities.
- For each exceedance probability, the best estimate H_{m0}, T_p and DSD at Point 1 in -31 m msl were modelled (see ***Table 5.9.25***). Considering the sensitivity of sediment transport to wave direction, the 5th, 50th and 95th percentiles of the distribution of MWD for wave heights exceeding the 1 y^{-1} exceedance probability were modelled (see ***Figure 5.9.44***).
- For each exceedance probability, the cases considered the co-occurrence of the storm peak with an extreme maximum or minimum still water level, as defined in ***Table 5.9.12*** and ***Table 5.9.13***.
- The joint exceedance probability between the waves and storm surge was accounted for as described in ***Subsection 5.9.9.9***. For each joint probability both combinations of storm surge and wave height were modelled, and the most conservative result was selected.
    - For the maximum still water level case, the dominant variable was combined with a factor 10 higher exceedance probability of the second variable, and vice versa.
    - For the minimum still water level case, the dominant variable was combined with a 1 y^{-1} exceedance probability for the second variable, and vice versa.
- Initial sensitivity tests indicated low KNPS cooling water intake flow rates to be conservative. Therefore, a conservatively low flow rate of 1.4 m^3/s was modelled, which corresponds to only the SEC running at normal operation (see ***Table 5.9.49***).

CONTROLLED DISCLOSURE

When downloaded from the EDS database, this document is uncontrolled and the responsibility rests with the user to ensure it is in line with the authorised version on the database.

- The total number of cases is: 1 date x 4 exceedance probabilities x 3 wave directions x 2 water levels x 2 joint probability combinations = 48 cases.
- The wave height time-series for each storm event has a triangular shape with a duration of 4.1 days, as described in ***Subsection 5.9.10.5***.

Results

Example model results are shown in ***Figure 5.9.145*** for the 10^{-2} y^{-1} storm, 50th percentile wave direction, high water level, and dominant waves. The figure shows instantaneous plots of the waves, currents, and sediment transport at the peak of the storm.

Figure 5.9.146, ***Figure 5.9.147***, and ***Figure 5.9.148*** show the maximum scour at any time during the storm over all cases corresponding to three of the exceedances and wave directions modelled. ***Figure 5.9.149*** presents the maximum bed level reached at any time during the storm over all cases corresponding to one of the exceedances and wave directions modelled.

CONTROLLED DISCLOSURE

When downloaded from the EDS database, this document is uncontrolled and the responsibility rests with the user to ensure it is in line with the authorised version on the database.

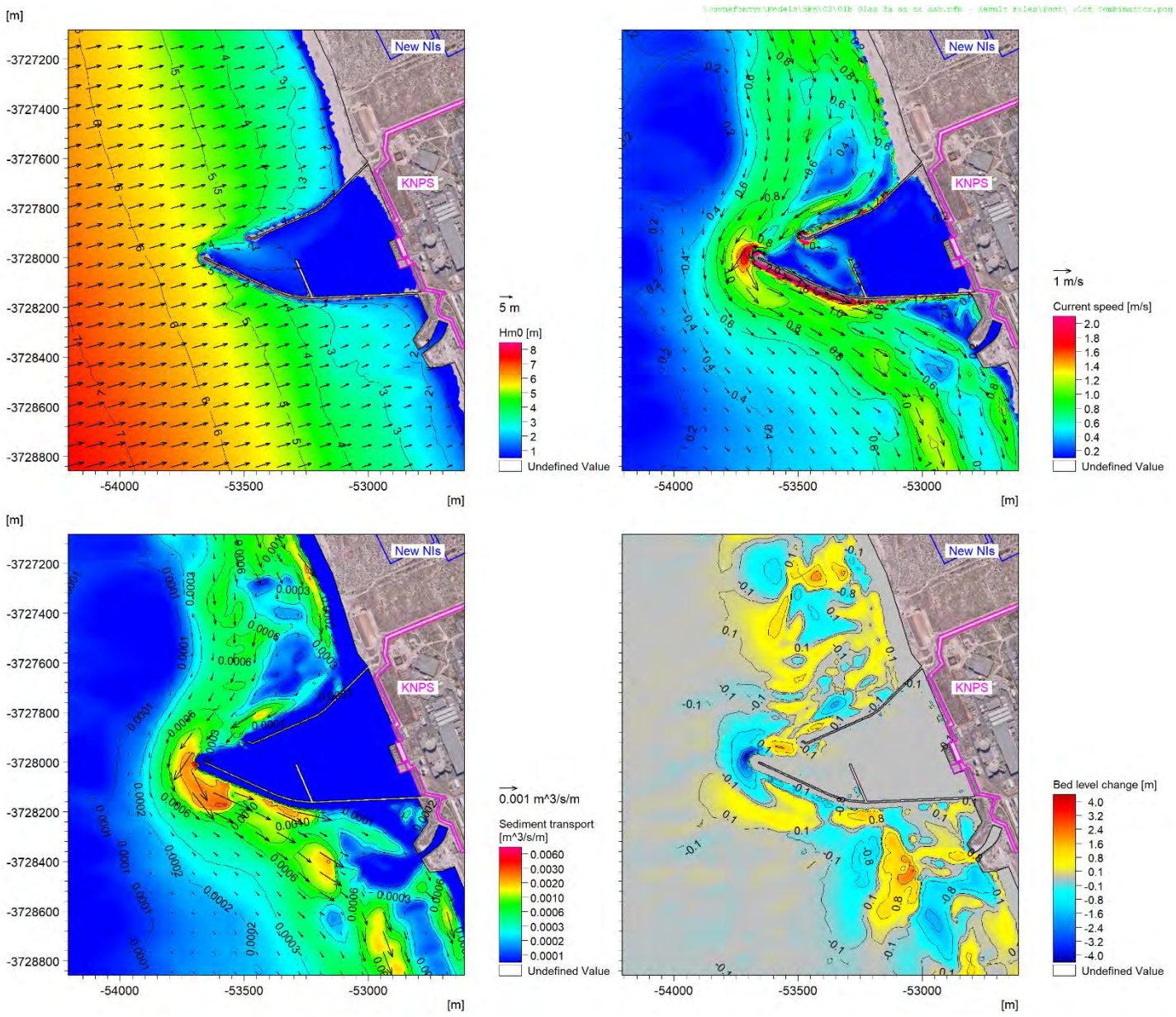


Figure 5.9.145: Example Results of 10^{-2} y^{-1} Storm, 50th Percentile Wave Direction, High Water Level, with Waves Dominant, Showing Instantaneous Waves (Top Left), Currents (Top Right) and Sediment Transport (Bottom Left) at the Peak of the Storm, and Bed Level Change at the End of the Storm (Bottom Right).

CONTROLLED DISCLOSURE

When downloaded from the EDS database, this document is uncontrolled and the responsibility rests with the user to ensure it is in line with the authorised version on the database.



Figure 5.9.146: Maximum Scour Depth: 10^{-2} y^{-1} Storm, 50th Percentile Wave Direction.

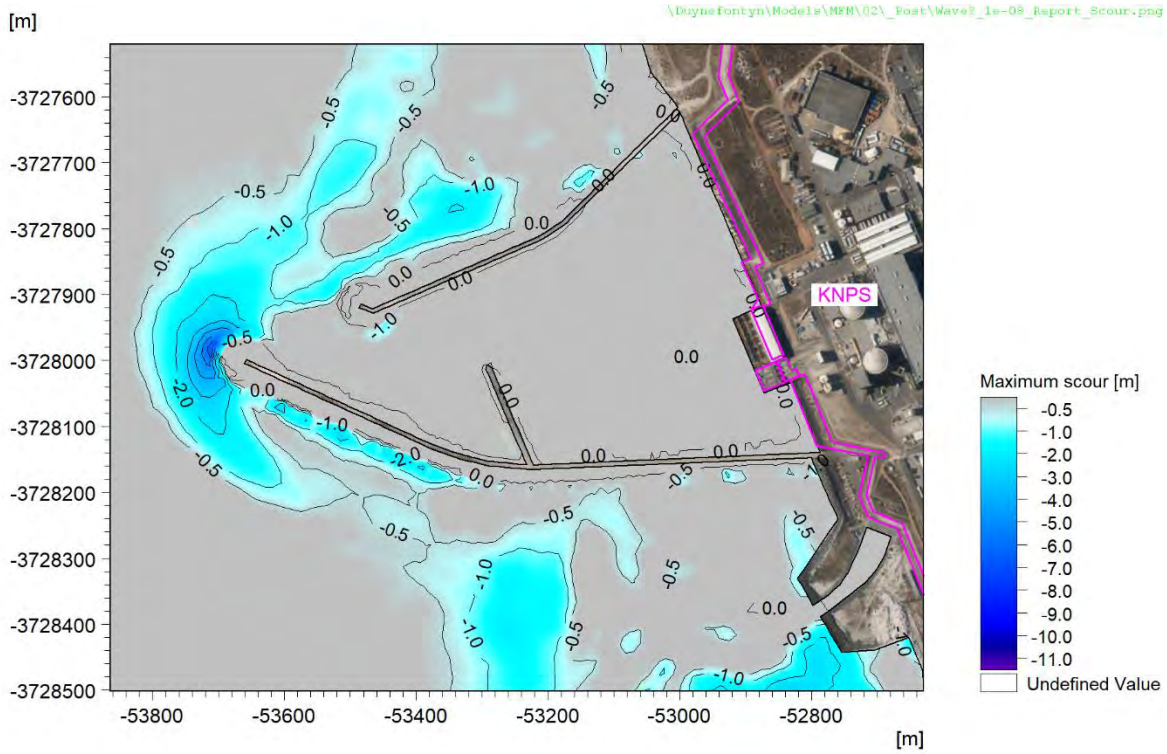


Figure 5.9.147: Maximum Scour Depth: 10^{-8} y^{-1} Storm, 50th Percentile Wave Direction.

CONTROLLED DISCLOSURE

When downloaded from the EDS database, this document is uncontrolled and the responsibility rests with the user to ensure it is in line with the authorised version on the database.



Figure 5.9.148: Maximum Scour Depth: 10^{-8} y^{-1} Storm, 5th Percentile Wave Direction.

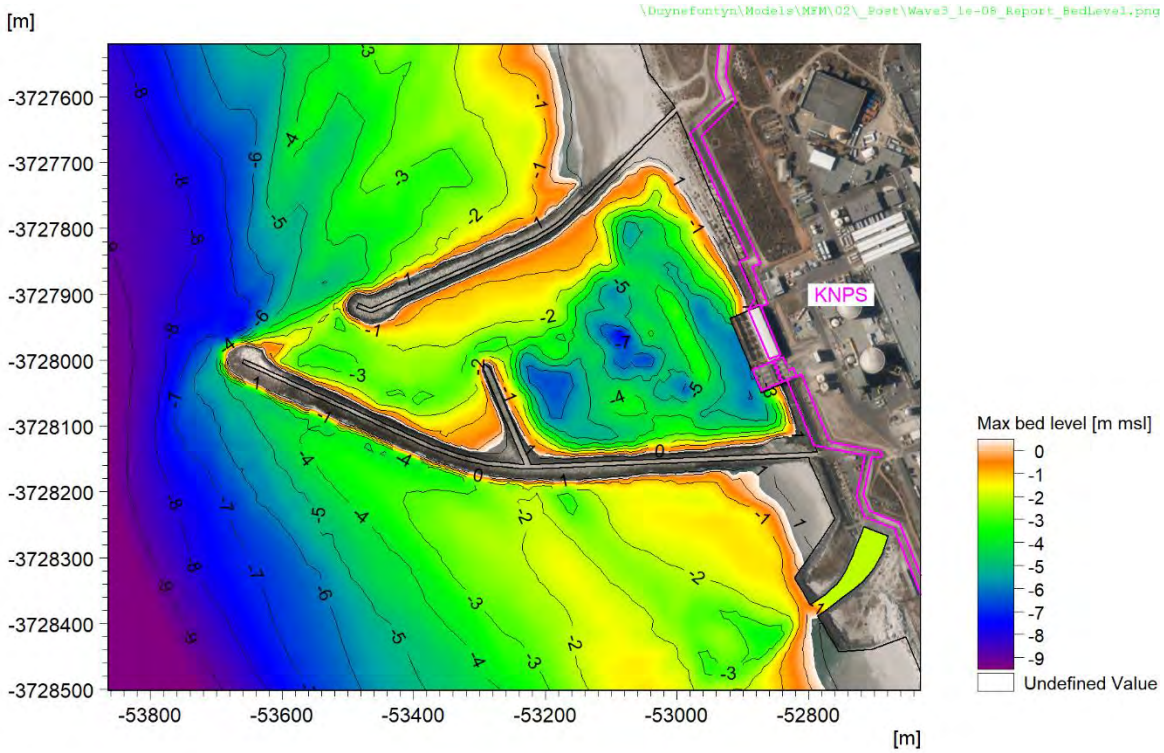


Figure 5.9.149: Maximum Bed Level: 10^{-8} y^{-1} Storm, 95th Percentile Wave Direction.

CONTROLLED DISCLOSURE

When downloaded from the EDS database, this document is uncontrolled and the responsibility rests with the user to ensure it is in line with the authorised version on the database.

The maximum scour depth below the seabed and maximum bed level in the intake basin entrance (measured as the shallowest point along the deepest flow path between the intakes and the sea) for each exceedance probability and wave direction are given in ***Table 5.9.57***.

Table 5.9.57: Sedimentation and Scour at the KNPS Intake Basin due to Storms.

Exceedance Probability	Uncertainty[a]	Maximum Bed Level in Intake Basin Entrance[b]	Maximum Scour Adjacent to Structures[c]
y^{-1}		(m msl)	(m)
10^{-2}	5th	-2.7	-5.0
	50th	-2.7	-6.1
	95th	-2.7	-9.1
10^{-4}	5th	-2.7	-5.4
	50th	-2.7	-6.4
	95th	-2.4	-10.4
10^{-5}	5th	-2.7	-5.5
	50th	-2.7	-6.8
	95th	-2.3	-10.6
10^{-6}	5th	-2.7	-5.6
	50th	-2.7	-7.3
	95th	-2.2	-10.9
10^{-7}	5th	-2.7	-5.7
	50th	-2.6	-7.5
	95th	-2.1	-11.2
10^{-8}	5th	-2.7	-5.7
	50th	-2.5	-7.8
	95th	-1.9	-11.6

Notes:

(a) In this case uncertainty refers to the distribution of MWD for waves exceeding the 1 y^{-1} exceedance probability H_{m0}.

(b) Measured as the shallowest point along the deepest flow path between the intakes and the sea. The initial maximum bed level was -2.68 m msl.

(c) Defined as the depth below the existing seabed. For the 5th percentile wave direction cases, the maximum scour occurred along the southern breakwater trunk (see ***Figure 5.9.148***). For the other cases, the maximum scour occurred at the southern breakwater roundhead (see ***Figure 5.9.147***).

The modelled initial bed level at the roundhead is approximately 2.5 m above the level during construction, based on comparison of the best available bathymetry listed in ***Subsection 5.9.8*** with design drawings (PRDW, 2005). The effective scour depth below the toe level is therefore approximately 2.5 m shallower than shown in ***Table 5.9.57***. The constructed toe of the breakwater roundhead has a horizontal width of 7.4 m. Design guidelines recommend a toe width of three times the expected vertical scour. Thus, the toe is theoretically able to accommodate

CONTROLLED DISCLOSURE

When downloaded from the EDS database, this document is uncontrolled and the responsibility rests with the user to ensure it is in line with the authorised version on the database.

2.5 m of scour below the toe level, i.e., a modelled scour depth of -5.0 m below the existing seabed level. This is exceeded below the 10^{-2} y^{-1} storm (50^{th} percentile wave direction) which predicts a scour depth of -6.1 m. Mitigating factors include that design guidelines typically contain an element of conservatism and that the cross-section includes a 6 m wide dolos toe, which would be able to accommodate some settlement without affecting units higher up the slope. These results indicate that the KNPS breakwater may be vulnerable to scour during extreme storm events and this requires further investigation.

These results show the following:

- Under extreme storm conditions scour exceeding -5 m is predicted at the roundhead and along the outside of the southern trunk of the KNPS breakwater. The effect of this on the stability of the breakwater requires additional investigation. The design of any similar coastal structures for the new NIs should account for scour due to storms as shown in ***Table 5.9.57***.
- Under extreme storm conditions sedimentation results in a maximum bed level in the KNPS intake basin entrance of -1.94 m msl (95^{th} percentile) and -2.53 m msl (50^{th} percentile). The minimum still water levels below this level occur for the best estimate exceedance probabilities lower than 10^{-7} y^{-1} (see ***Table 5.9.13***). This shows that storm-induced sedimentation is not predicted to close off the intake basin and seawater will be able to enter the intake basin. Regular maintenance dredging is however required to remove the annual sedimentation in the KNPS intake basin of approximately 132 000 m^3/y, which may increase after extreme storm events.
- These results would also apply should an intake basin with the same geometry be selected for the new NIs. The annual maintenance dredging would however increase with increasing intake seawater flow rate.

5.9.16.2 Sedimentation and Scour Due to Tsunamis

Sediment transport modelling

Modelling of the sediment transport during an extreme tsunami event was carried out to assess the following:

- Sedimentation in the KNPS intake basin;
- Scour against coastal structures;
- Erosion of the intake basin entrance, which would reduce attenuation of the propagation of tsunami waves into the intake basin; and

When downloaded from the EDS database, this document is uncontrolled and the responsibility rests with the user to ensure it is in line with the authorised version on the database.

- Erosion of the primary dune crest along the coastline north and south of KNPS, which provides some protection against flooding from the sea.

The MIKE 21 Sand Transport model described in ***Subsection 5.9.16.1*** was used for the sediment transport modelling. The model was coupled to the 2D hydrodynamic detailed tsunami inundation model described in ***Subsection 5.9.12.11***.

For the case of pure currents, sediment transport rates are calculated continuously throughout the simulation based on sediment transport formulae derived from empirical and deterministic principles. The sediment transport modelling is divided into bed load and suspended load due to their different nature. The bed load, which mainly is controlled by the bed shear stress, reacts instantaneously with the flow. In modelling terms this is referred to as an equilibrium transport description. The suspended load is characterised by a phase-lag required for the transport to adapt to the flow which is termed a non-equilibrium transport description. In the model it is possible to use either an equilibrium transport approach where the total load (bed load plus suspended load) reacts instantaneously with the flow, or a non-equilibrium transport approach where the bed loads reacts instantaneously and the suspended load includes lag effects.

The non-equilibrium transport approach was used with the formulations of van Rijn used to calculate the bed load (van Rijn, 1984a) and suspended load (van Rijn, 1984b) separately. A constant median sediment grain diameter of D_{50} = 0.20 mm, with a relative density of 2.65 and a porosity of 0.4 was applied over the model domain. Bed resistance in the sand transport model was included using a constant Chezy number of 40 $m^{1/2}/s$, representative of the typical total roughness for a sandy bottom. Morphological updating of the bed was included to account for the effects of changes in the bed level on the hydrodynamics. A space-varying initial bed thickness was used to specify a non-erodible bed at offshore rocky reefs, on the rubble-mound structures of the intake basin, within the outfall channel, and on paved surfaces on the KNPS nuclear terrace. Slope failure due to local scouring of the seabed was not included.

Cases modelled

The Tristan da Cunha D_1 tsunami scenario was modelled at the high antecedent water level (see example run-up and inundation in ***Figure 5.9.108*** to ***Figure 5.9.110***). Although this scenario was found to be the PMT in most cases, this does not imply that the modelled bed changes for this scenario are the PMT erosion or sedimentation. However, these results provide an indication of the potential for tsunami-induced erosion or sedimentation to pose a hazard to KNPS or the new NIs.

CONTROLLED DISCLOSURE

When downloaded from the EDS database, this document is uncontrolled and the responsibility rests with the user to ensure it is in line with the authorised version on the database.

The simulation was run for a duration of 2 hours during which the largest tsunami waves reach the site.

Results

Figure 5.9.150 presents detailed views at the KNPS intake basin of the bed level at the start and end of the simulation, the integrated net transport (total load), and the bed level change at the end of the simulation. ***Figure 5.9.151*** and ***Figure 5.9.152*** present the maximum bed level and maximum scour depth over the simulation, respectively.

CONTROLLED DISCLOSURE

When downloaded from the EDS database, this document is uncontrolled and the responsibility rests with the user to ensure it is in line with the authorised version on the database.

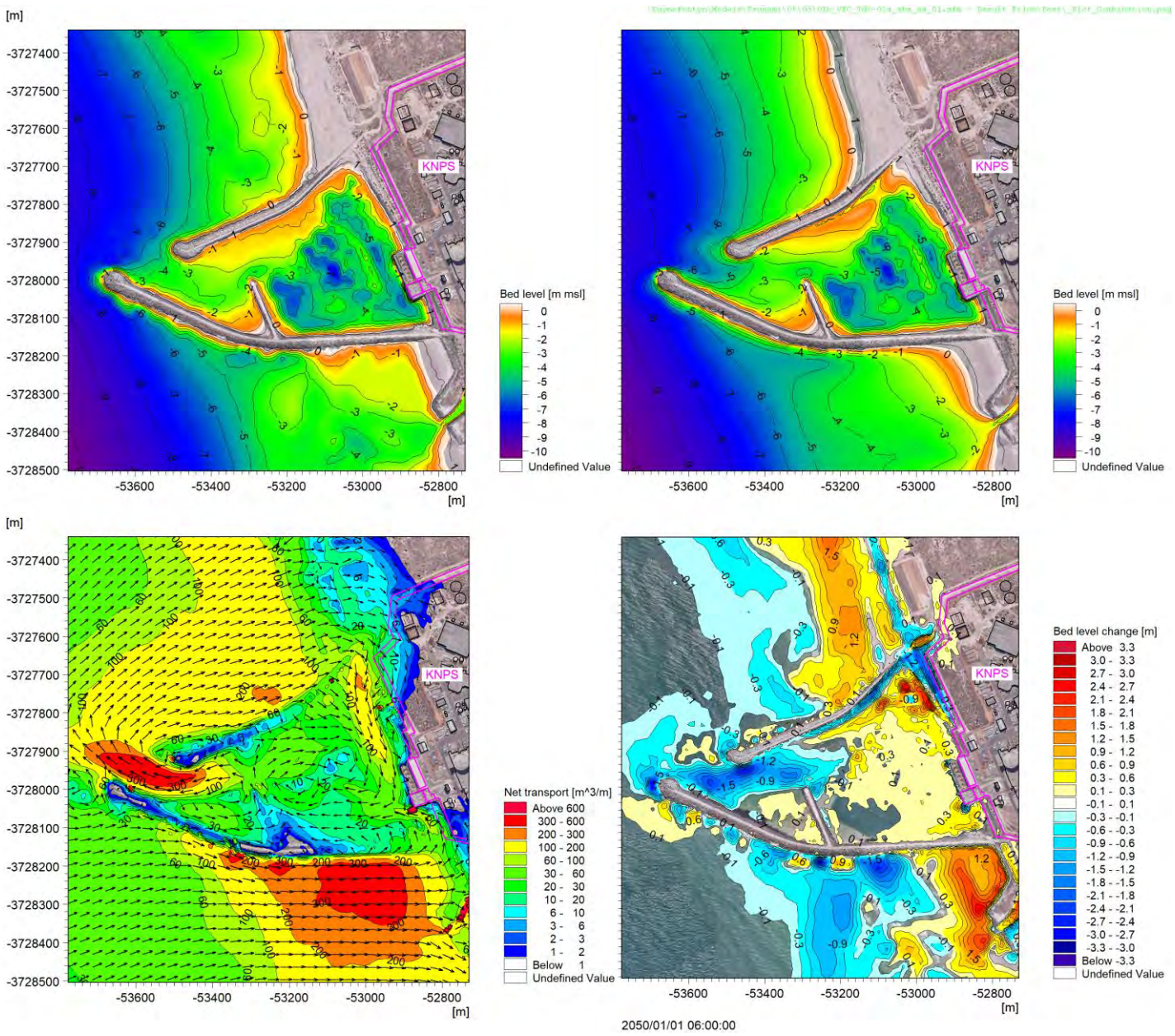


Figure 5.9.150: Bed Level at the Start (Top Left) and End (Top Right) of the Simulation, Integrated Net Transport (Bottom Left), and Bed Level Change at the End of the Simulation (Bottom Right).

CONTROLLED DISCLOSURE

When downloaded from the EDS database, this document is uncontrolled and the responsibility rests with the user to ensure it is in line with the authorised version on the database.

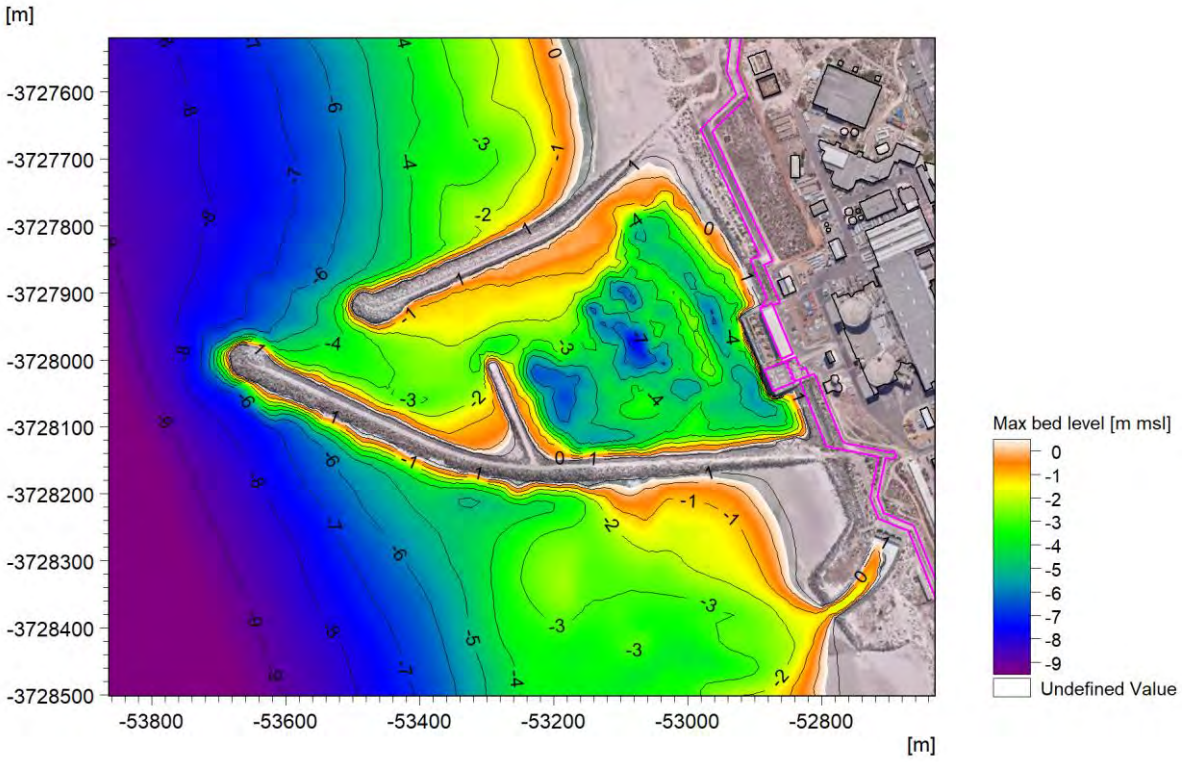


Figure 5.9.151: Maximum Bed Level During the Simulation.

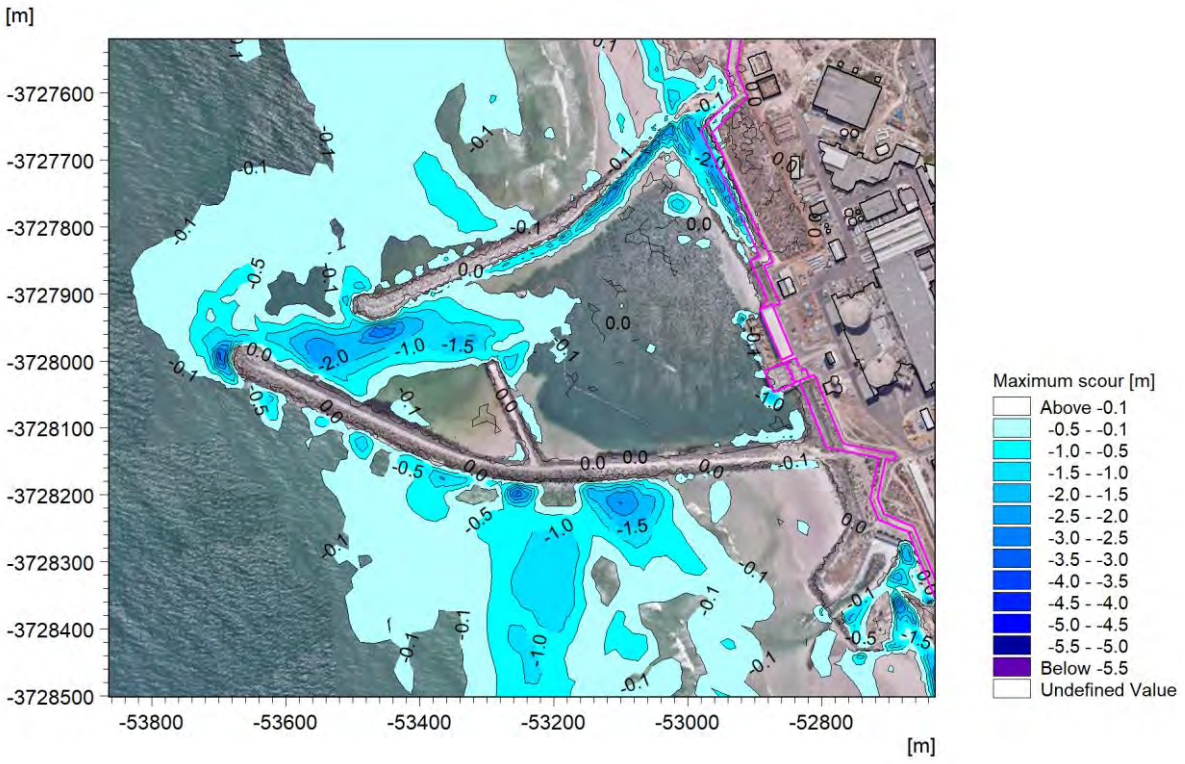


Figure 5.9.152: Maximum Scour Depth During the Simulation.

CONTROLLED DISCLOSURE

When downloaded from the EDS database, this document is uncontrolled and the responsibility rests with the user to ensure it is in line with the authorised version on the database.

During tsunami drawdown sand is eroded from the intake basin entrance and deposited outside the basin. Sedimentation in the inner basin occurs mainly due to sediment transport over the root of the northern and southern breakwaters, and is generally less than 0.3 m deep, except in the northern corner where sand is eroded from the beach and deposited into deeper water as the tsunami waves overtop the breakwater.

Table 5.9.58 summarises the sedimentation and scour at the KNPS intake basin.

Table 5.9.58: Sedimentation and Scour at the KNPS Intake Basin due to Tsunamis.

Exceedance Probability	Maximum Bed Level in Intake Basin Entrance[(a)]	Maximum Scour Adjacent to Structures[(b)]
y^{-1}	(m msl)	(m)
N/A	-2.68	-3.5

Notes:
(a) Measured as the shallowest point along the deepest flow path between the intakes and the sea.
(b) Defined as the depth below the existing seabed. The maximum scour occurred in the lee of the northern breakwater roundhead.

The modelled initial bed level at the northern breakwater where the maximum scour occurs is approximately -1.1 m msl, which is 3.9 m above the level during construction of -5 m msl (PRDW, 2005). The scour of -3.5 m therefore does not undermine the structure toe.

These results show the following:

- For the modelled tsunami, scour of -3.5 m is predicted in the lee of the northern breakwater roundhead, which does not undermine the structure toe.
- Less than 0.3 m of tsunami-induced sedimentation is predicted in front of the CRF and SEC pumphouses.
- The existing KNPS intake basin is not closed off by sedimentation during the modelled extreme tsunami event.

The erosion in the basin entrance at the end of the simulation was conservatively applied as a depth correction to the detailed tsunami inundation model (for all cases modelled) to account for the associated reduction in wave attenuation (see ***Subsection 5.9.12.11***).

Figure 5.9.153 presents profiles extracted along the dune ridges north and south of KNPS (ridges identified in ***Figure 5.9.5***), also showing the dune

CONTROLLED DISCLOSURE

When downloaded from the EDS database, this document is uncontrolled and the responsibility rests with the user to ensure it is in line with the authorised version on the database.

crest levels following erosion during the modelled tsunami. The figure shows the levels after the second wave crest (the first wave crest did not overtop the dunes) and the levels at the end of the simulation.

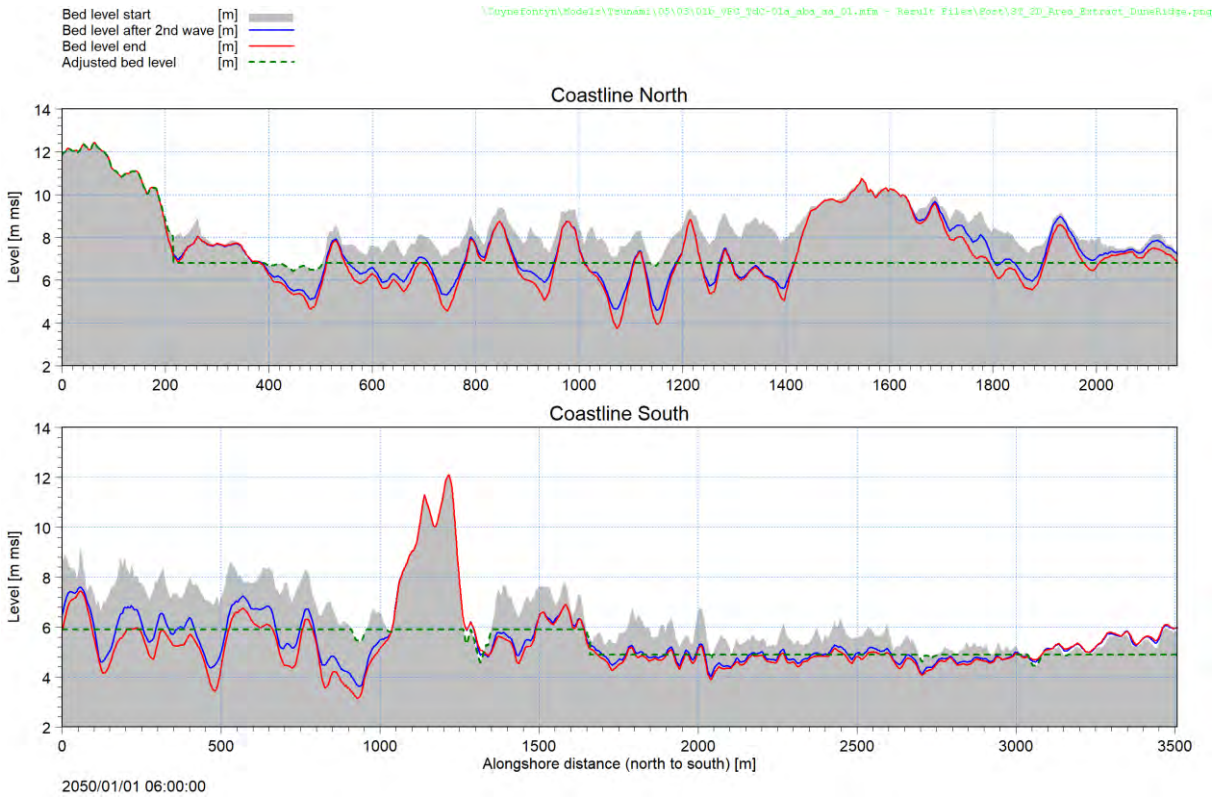


Figure 5.9.153: Tsunami Erosion of the Dune Ridges North and South of KNPS During the Tristan da Cunha D_1 Volcanic Flank Collapse Tsunami for 2021 and a High Antecedent Water Level.

Based on these results, the dune ridges were schematically truncated to the average level after the first wave, as indicated by the green dotted line in the figure. Further details are available in the DTHA Report (PRDW, 2022a).

5.9.16.3 Suspended Sand at Intakes

Introduction

For Layouts 1 and 2 the proposed seawater intake is a tunnel extending to approximately -20 and -30 m msl water depth respectively, with the intake opening positioned 3 to 5 m above the seabed (see ***Subsection 5.9.15.3***). One of the design parameters will be the volume of sand drawn into the intake which will have to be removed from the proposed landside intake basin. Modelling was performed to estimate the volume of sand drawn into the intakes.

CONTROLLED DISCLOSURE

When downloaded from the EDS database, this document is uncontrolled and the responsibility rests with the user to ensure it is in line with the authorised version on the database.

Model description

The MIKE Littoral Processes model was applied to model the suspended sand concentrations. The details of the physical processes and numerical implementation are provided in the model documentation (see ***Table 5.9.7***), while details of the model setup, sensitivity testing, and V&V are provided in the V&V Report (PRDW, 2022b).

The model solves the vertical diffusion equation on an intrawave period grid to provide a detailed description of the suspended sand concentration both vertically and over the wave period. The model accounts for waves and currents at arbitrary angles, breaking waves, Stokes 5th order wave theory, ripple-covered bed and graded bed material. The sediment is divided into 30 size fractions based on a log-normal grading curve characterized by the median grain diameter D_{50} and the sediment grading defined by $(D_{84}/D_{16})^{0.5}$.

The model output is the time-averaged vertical profile of suspended sand concentration. The model only simulates non-cohesive sand with grain sizes greater than 0.063 mm.

Cases modelled

The sediment properties were based on the measured seabed samples closest to the proposed intakes (see ***Subsection 5.9.8***), resulting in D_{50} = 0.13 mm and a sediment grading of 1.2.

Layouts 1 and 2 were modelled with the proposed seawater intakes in -20 and -30 m msl water depth, respectively. For each layout both power station outputs of 2500 and 4000 MWe with associated intake flow rates of 115.2 and 184.2 m^3/s were modelled.

Each layout was modelled for normal operational conditions and for four extreme storm events with exceedance probabilities of 10^{-2}, 10^{-4}, 10^{-6} and 10^{-8} y^{-1}, as described below:

- The operational conditions were based on 6.2 years of hourly-averaged depth-averaged currents measured at Site B (see ***Subsection 5.9.9.4***) and the wave parameters measured at the same location (see ***Subsection 5.9.9.8***). These conditions were applied at the -30 m msl depth.
- Operational currents and waves at -20 m msl depth were obtained by scaling the measurements at -30 m msl depth based on linear regressions between model results at these two depths. The currents were scaled based on one year of hydrodynamic model results (see ***Subsection 5.9.15.5***). The waves were scaled based on ten years of spectral wave model results (see ***Subsection 5.9.9.8***). The operational

When downloaded from the EDS database, this document is uncontrolled and the responsibility rests with the user to ensure it is in line with the authorised version on the database.

model was run for the full 6.2 years of data with a constant water level of ML.

- For the extreme storm events the joint exceedance probability between waves and currents was accounted for as described in ***Subsection 5.9.9.9***, where for example the 10^{-4} y^{-1} dominant wave is combined with the 10^{-3} y^{-1} current.
- The extreme currents in -30 m msl were based on an extreme value analysis of the measured currents at Site B, as presented in ***Subsection 5.9.9.4***. The same scaling as applied for the operational currents was applied to obtain the extreme currents in -20 m msl.
- The extreme dominant waves and water levels applied were extracted from the results of the coupled hydrodynamic and spectral wave model used for the extreme sedimentation and scour modelling (***Subsection 5.9.16.1***). Each storm event has a triangular shape with a duration of 4.1 days, as described in ***Subsection 5.9.10.5***.

Results

Figure 5.9.154 shows an example of the modelled vertical profile of suspended sand in depths of -20 and -30 m msl at the peak of the 10^{-8} y^{-1} storm. The results show the reduction in sand concentrations with increasing distance from the seabed, as well as higher concentrations for the shallower -20 m msl depth due to increased wave breaking and orbital velocities on the seabed.

CONTROLLED DISCLOSURE

When downloaded from the EDS database, this document is uncontrolled and the responsibility rests with the user to ensure it is in line with the authorised version on the database.

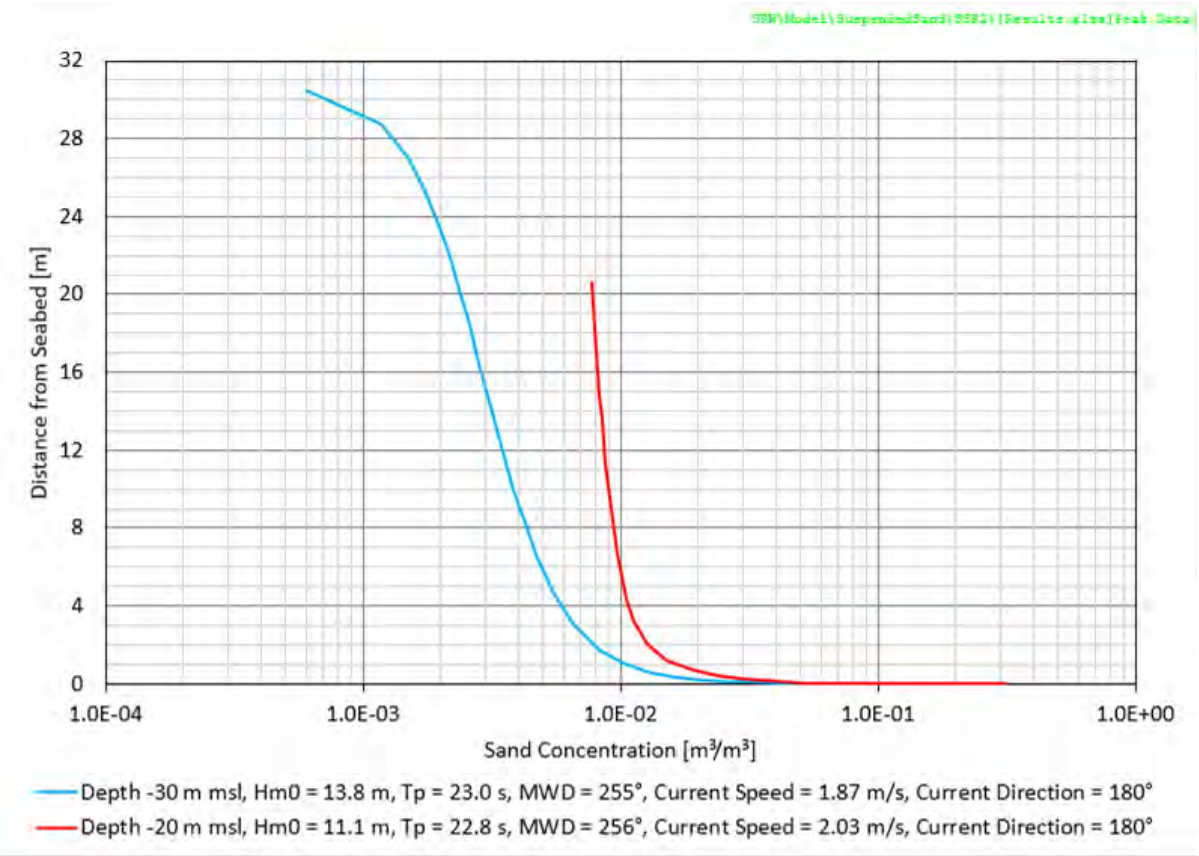


Figure 5.9.154: Example of Modelled Vertical Profile of Suspended Sand in Depths of -20 and -30 m msl at the Peak of the 10^{-8} y^{-1} Storm.

The sand volume drawn into the cooling water intake tunnels for the 2500 and 4000 MWe power stations are provided in ***Table 5.9.59*** and ***Table 5.9.60***, respectively. Results are provided at the level of the intake openings 3 m and 5 m above the seabed, as well as 1 m above seabed. The latter accounts for the possible enhancement of sediment concentration around the intake shafts, or sand wave-induced build-up around the intake. However, it is sediment scour that is more likely around the intake structure which makes the results at 1 m above the seabed conservative.

The volumes are calculated as the suspended sand concentration at the given distance above seabed multiplied by the intake flow rate, integrated over the duration of the event, and then converted to bulk sand volume assuming a porosity of 0.4.

CONTROLLED DISCLOSURE

When downloaded from the EDS database, this document is uncontrolled and the responsibility rests with the user to ensure it is in line with the authorised version on the database.

Table 5.9.59: Sand Volume Drawn into Cooling Water Intake Tunnels for 2 500 MWe Power Station.

Exceedance Probability (y^{-1})	Case	Units	Layout 1 (Intake at -20 m msl)			Layout 2 (Intake at -30 m msl)		
			1 m above bed	3 m above bed	5 m above bed	1 m above bed	3 m above bed	5 m above bed
-	Operational Conditions	m^3/y	1 400	280	150	380	140	80
10^{-2}	Storm event	m^3/event	6 300	2 600	1 600	2 100	710	460
10^{-4}	Storm event	m^3/event	55 000	36 000	30 000	17 000	7 100	5 000
10^{-5}	Storm event	m^3/event	91 000	62 000	53 000	32 000	15 000	11 000
10^{-6}	Storm event	m^3/event	150 000	110 000	92 000	60 000	30 000	23 000
10^{-7}	Storm event	m^3/event	220 000	160 000	140 000	110 000	57 000	45 000
10^{-8}	Storm event	m^3/event	330 000	240 000	210 000	180 000	110 000	88 000

Table 5.9.60: Sand Volume Drawn into Cooling Water Intake Tunnels for 4 000 MWe Power Station.

Exceedance Probability (y^{-1})	Case	Units	Layout 1 (Intake at -20 m msl)			Layout 2 (Intake at -30 m msl)		
			1 m above bed	3 m above bed	5 m" above bed	1 m above bed	3 m above bed	5 m above bed
-	Operational Conditions	m^3/y	2 200	450	230	610	220	130
10^{-2}	Storm event	m^3/event	10 000	4 200	2 600	3 400	1 100	740
10^{-4}	Storm event	m^3/event	88 000	58 000	48 000	27 000	11 000	8 000
10^{-5}	Storm event	m^3/event	150 000	99 000	84 000	51 000	23 000	17 000
10^{-6}	Storm event	m^3/event	240 000	170 000	150 000	96 000	48 000	36 000
10^{-7}	Storm event	m^3/event	360 000	260 000	220 000	170 000	91 000	71 000
10^{-8}	Storm event	m^3/event	530 000	380 000	340 000	290 000	170 000	140 000

These results show the following:

- For operational conditions the volume of sand drawn into the tunnel intakes which will have to be removed from the proposed landside intake basins is less than 2 200 m^3/y. This is significantly less than the average maintenance dredging volume of the existing KNPS intake basin of approximately 132 000 m^3/y.
- A maintenance dredging programme will be required to prevent excessive sedimentation in the basin and to keep a sufficient buffer for storm events.

CONTROLLED DISCLOSURE

When downloaded from the EDS database, this document is uncontrolled and the responsibility rests with the user to ensure it is in line with the authorised version on the database.

- For extreme storm events the sand volume increases significantly and the 10^{-6} storm event results in similar sand volumes over the 4.1-day event as the annual maintenance dredging at KNPS. The intake basin will need to be designed to accommodate these sediment volumes without blocking the pumps.
- The shallower intake in -20 m msl depth results in a threefold increase in sand volumes compared to the intake in -30 m msl. This increase will need to be considered in the detailed engineering and costing of the intakes.

5.9.17 Blockage of Intakes and Biofouling

In the case of an offshore intake structure, cooling water is taken from greater depths (>15 m) compared with a basin intake. This significantly reduces the risk of blockage of the intake structure. A 'velocity cap' should be placed over the vertical terminal of the offshore intake tunnel/pipe. This converts vertical flow into horizontal flow at the intake entrance in order to reduce fish entrainment. Chlorine or other biocides should be used to keep the cooling system free of marine growth.

In case of a nearshore intake structure (basin or channel type structure), the pumphouse should be designed to limit the possibility of blockage of the intakes by drawing water at a sufficiently low level to limit risk of blockage by flotsam, fuel oil and marine flora and fauna. Suitable coarse and fine screens should be provided to prevent a sudden complete blockage. The layout and position of the basin should be designed to reduce the siltation rate of the basin and the depth of the basin should be maintained by maintenance dredging.

A study by the World Association of Nuclear Operators (WANO) (EPRI, 2008) found that in the period 2004 to 2006, there were 44 occurrences of blockages at nuclear installations. Of the 44 events, 37 of these were attributed to aquatic life, including algae, seaweed and other grasses, mussels, jellyfish, crustaceans (shrimps and crabs) and fish. The remaining blockage events were caused by depositions of sand and silt and ingress of crude oil. The risk from oil spills is addressed in ***Section 5.7*** (Nearby Transportation, Industrial and Military Facilities).

The marine ecology specialist study conducted for the environmental impact assessment for the proposed site (Eskom, 2008) indicated that the species listed in ***Table 5.9.61*** were found at the site.

CONTROLLED DISCLOSURE

When downloaded from the EDS database, this document is uncontrolled and the responsibility rests with the user to ensure it is in line with the authorised version on the database.

Table 5.9.61: Marine Species Found at the Site.

Zones	Species
Intertidal Zone	Isopods, amphipods, polychaete worms, white sand mussels, mussels, barnacle, whelk, limpet and algae
Benthic Environment	Sea urchin, gastropods, abalone, west coast rock lobster, polychaete worms, burrowing anemones and small crustaceans
Open Water	Southern harder, catshark, South African fur seal, phytoplankton, zooplankton, dusky dolphin, common dolphin, southern right and humpback whales

A study by the Electric Power Research Institute (EPRI, 2021) culminated in the development of a best management practices manual for preventing cooling water intake blockages. The report identifies current best practices and technology fixes for effectively addressing debris-related intake blockage events worldwide. It provides background and context of debris events at cooling water intake structures, successful and unsuccessful mitigation approaches, up-to-date procedural and best practice guidance, state-of-technology information, and detailed site audits of various power plants around the world, including KNPS. KNPS has experienced multiple jellyfish ingress events since 1997, as well as ingress of fish and Spoon Worm, as shown in ***Table 5.9.62***. These events had operational impacts such as screen failures, pump trips, and reductions in plant power output. The plant has been able to manage the production risk linked to jellyfish invasions, although there have been at least four instances over the last two decades when plant power reductions were required to deal with the events.

Table 5.9.62: Summary of Major Debris Events at KNPS Since 1997 (EPRI, 2021).

Date	Debris	Description
1997-02-12	Jellyfish	A significant inflow of jellyfish caused two trash recovery baskets to overflow, and a third was damaged, causing the recirculation of the jellyfish in the pumping station. No plant load reduction was required.
1999-05-20	Jellyfish	The inflow of jellyfish caused the activation of alarms due to the pressure loss on the level of the filter drums on the two units and high-speed activation on two drums. No plant load reduction was required.
1999-06-20	Jellyfish	A significant inflow of jellyfish resulted in cavitation of the main cooling water circulating pump. Unit electrical output was decreased to 60% on both units; Unit 2 was then shut down following a failure of the device for rotating the drum screen 2 CRF 002 TF.
2005-05-08	Jellyfish	A significant inflow of jellyfish, estimated to be at a rate of 32 tons per hour, caused tripping of a main seawater circulating water pump (1 CRF 003 PO). The event started on May 8 and continued for 12 days. As a result of the event, the power output was reduced to between 60% and 70% during this period.

CONTROLLED DISCLOSURE

When downloaded from the EDS database, this document is uncontrolled and the responsibility rests with the user to ensure it is in line with the authorised version on the database.

Date	Debris	Description
2008-07-28	Jellyfish	On July 28, 2008, a jellyfish migration into the plant intake basin was reported. The number of jellyfish was small, and, therefore, the event did not have any significant impact on plant power production operations (that is, the plant remained at full-power operation).
2016-04-23	Jellyfish	On April 23, 2016, Unit 1 reduced load to 70% power due to significant jellyfish ingress. The drum screen, 1 CFI 002 TF, was stationary, and the drive motor was running uncoupled. The coupling had disengaged on torque overload. At around 08h00, 1 CRF 002 PO tripped on low suction pit level. The on-duty mechanical maintenance team was called to remove the coupling cover to inspect the coupling. Jellyfish fouling of the drum screen was evident, although excessive foaming made it difficult to clearly observe the extent of the fouling.
2020-03	Fish	This event was marked with a sudden ingress of fish (suspected to be anchovies) although some jellyfish and kelp were also found in the trash baskets. The event significance was characterized by latent shortcomings of plant equipment designed to deal with the event rather than the event initiator itself. Although the observed amount of debris was within the motor's design capacity, an incorrect (lower) torque setpoint on the coupling caused the coupling to disengage. Although the remaining train was able to maintain sufficient vacuum in the main condenser to maintain the reduced electrical load, fouling of the related heat exchanger train for secondary cooling systems resulted in temperature increases, which further necessitated a complete reduction of unit output to the national transmission grid. Review of the processes and practices identified that improvements were required in the guidance available in maintenance procedures for the torque settings, as well as adjustment and renewal of drum screen components.
2022-01-19	Spoon Worm	This event occurred after publication of (EPRI, 2021). Information describing the event below is from the Marine Ingress Feedback Report (Eskom, 2022b). An unusual event was declared due to ingress of marine organisms (worm-like creatures) into the cooling water intake basin. The marine ecologist that reviewed photos of the worms advised that they were likely to have been Echiurus echiurus, a species of spoon worm (Echiura). There were high swells with long periods on the day. Echuirans are mostly infaunal animals (common in soft sediments), occupying burrows in the seabed, either in the lower intertidal zone or the shallow subtidal zone. The large waves and strong currents experienced during this period may have forced the worms out of their underwater burrows and washed them ashore and into the KNPS cooling water intake basin. It is very difficult to predict whether a recurrence of an event of this nature is likely or not. Adverse environmental conditions, and the associated impact on the marine life present at that time is to a large extent unpredictable. *Author comment:* The KNPS procedure for dealing with marine ingress was implemented and successfully mitigated affects to the nuclear cooling system. There is nothing to suggest that a more severe

When downloaded from the EDS database, this document is uncontrolled and the responsibility rests with the user to ensure it is in line with the authorised version on the database.

Date	Debris	Description
		ingress may be expected in the future and that the KNPS procedures nor the SSC and procedures of a new NI will not be able to manage such an event.

The EPRI study concludes that there is no single solution to preventing intake blockages, and the best practice will be determined by site-specific factors, such as the type and extent of debris present, screening equipment in use, and forecasting ability at the facility. Five main categories for tackling the problem of blockages are identified (EPRI, 2021), viz:

- Routine maintenance of equipment increases its reliability when called into action during a major clogging event.
- Standard operating procedures (SOPs) provide explicit instructions to station team members on how intake event response tasks are to be implemented and should be tailored to the intake, the equipment, and the types of debris typically encountered.
- Event response teams can be used to implement the SOPs when certain events are forecasted or triggered.
- Having a debris management plan documents the actions to take prior to and/or during a debris event.
- An early warning or event forecasting system can contribute to effective management of power plant operation, reduce plant downtime, minimise damage to plant equipment, and improve safety.

The recommendations put forward by WANO and the EPRI best management practices manual will form an important and valuable input to the new NIs intake design and prevention of cooling water intake blockages through the plant life.

Biofouling has been measured at the site between February 2008 and July 2010. Asbestos plates, approximately 20 cm x 20 cm were deployed at specific depths for time periods of approximately three, six and twelve months. These plates were periodically removed, photographed and the thickness of marine growth measured.

Initially the plates were moored 3 m and 8 m below the water surface in 10 m water depth. The plates were later mounted directly on the two ADCP frames at Sites A and B (see ***Figure 5.9.1***) in depths of -10 m msl and -29 m msl, respectively. These plates were mounted approximately 0.5 m above the sea floor. Photographs of the plates after removal are shown in ***Figure 5.9.155***. The biofouling results are summarised in ***Table 5.9.63***.

CONTROLLED DISCLOSURE

When downloaded from the EDS database, this document is uncontrolled and the responsibility rests with the user to ensure it is in line with the authorised version on the database.



Figure 5.9.155: Biofouling after 6 Months at 8 m Depth (Left) and After 14 Months in 10 m Depth (Right).

Table 5.9.63: Summary of Measured Biofouling Thickness.

Duration	Date Deployed	Date Retrieved	Depth Below Surface	Average Biofouling Thickness	Average Rate of Growth
			(m)	(mm)	(mm/month)
6 Months	2008/05/01	2008/10/18	3	16.0	2.7
			8	17.5	2.9
6 Months	2009/05/22	2009/11/20	10	7.0	1.2
			29	4.5	0.8
14 Months	2009/05/22	2010/07/24	10	70.0	5.0

Based on the above results, the biofouling growth rate ranges from 1 to 5 mm/month. The growth rates increase after the initiation of the “bacterial film” whereby smaller fauna and flora attach on to the surface of foreign objects, thus making the surface more amenable to the growth/habitation of larger fauna. Chlorine produced by means of electrolysis is used to keep the cooling water system at the KNPS free of marine growth, although marine growth at the pumphouse intakes has previously been a maintenance problem owing to deficiencies in the chlorination system (Eskom, 2006).

Based on the KNPS and worldwide experience (EPRI, 2021) it can be concluded that the new NIs intakes could be designed to cope with the species identified in ***Table 5.9.61*** and to minimise the risk of complete blockage of the intake.

5.9.18 Uncertainties and Future Work

The estimation of the influence of climate change has been based on the most reliable scientific information available at the time that this study was undertaken, but must be continually reassessed as new data and research

CONTROLLED DISCLOSURE

When downloaded from the EDS database, this document is uncontrolled and the responsibility rests with the user to ensure it is in line with the authorised version on the database.

results become available (at least every five years). This shall include the IPCC 6th Assessment Report (AR6) which has recently been published in draft format. The SSR would only need to be updated should one of the relevant climate change parameters change significantly.

In line with Eskom's external hazards requirements (Eskom, 2011) and the NNR defined risk categories (NNR, 2014), the external hazards have been quantified for the following exceedance probabilities: 10^{-2}, 10^{-4}, 10^{-5}, 10^{-6}, 10^{-7} and 10^{-8} y^{-1}. This has been done by performing extreme value analysis on datasets which have a maximum duration of 42 y. Recent IAEA guidance is that hazards cannot be estimated with sufficient accuracy for return periods more than three to four times the length of the sample period (IAEA, 2011). This implies that return periods longer than approximately 168 y or equivalently exceedance probabilities less than $6x10^{-3}$ y^{-1}need to be interpreted with caution. In the case of datasets with shorter durations the accuracy will reduce proportionally.

The conceptual seawater cooling intakes and outfalls which have been developed and modelled for the SSR will need to be refined in the future based on an engineering feasibility study. Marine geotechnical surveys and additional numerical modelling will be required as part of future engineering design studies of the intake and outfall structures.

Based on available information, meteorite impact tsunamis cannot be screened out at the 10^{-8} y^{-1} exceedance probability. Although there are many factors which mitigate the risk (e.g., no currently identified asteroids are predicted to have any consequences in the next 100 years, impact from NEOs can be predicted up to several years in advance for tracked NEOs and a few days or more in advance for previously unidentified NEOs, and ongoing development is expected to greatly increase NEO identification capability), it is recommended that further investigation is carried out to quantify this and update previous assessments.

The tsunami sources due to local earthquakes should be reviewed once the results of the Duynefontyn Probabilistic Seismic Hazard Analysis (PSHA) study currently being undertaken by CGS are available.

5.9.19 Monitoring Programme

A comprehensive oceanographic data collection programme has been implemented at the site and is described in ***Subsection 5.9.6.1***.

The present-day monitoring programme comprises the following:

- water level and seawater temperature measurements at Site C inside the KNPS intake basin in a depth of -3 m msl;

CONTROLLED DISCLOSURE

When downloaded from the EDS database, this document is uncontrolled and the responsibility rests with the user to ensure it is in line with the authorised version on the database.

- wave, current and seawater temperature measurements at Site B in a depth of -29 m msl;
- seawater temperature measurements at Site A in a depth of -10 m msl;
- annual beach profile surveys at the 21 locations.

It is recommended that the present-day monitoring programme be continued to extend the duration of the datasets and to capture any extreme events that occur. The monitoring programme should be reviewed and updated every two years, e.g., with regard to the number, position and frequency of measurements.

5.9.20 Management System

A quality assurance programme was established to control the effectiveness of the execution of the coastal engineering and oceanography investigations, and the formulation of conclusions on the site acceptability. This conforms to the overall management system for the SSR as outlined in ***Chapter 10***.

The classification of the services and resultant quality management are described in Eskom's Technical Requirement Specification (Eskom, 2021). The classification of the products and processes related to the updating of the oceanography and coastal engineering section excluding the Tsunami Hazard Analyses determines that the quality management system of the organisation responsible for this service must comply with the Safety Level 2 requirements of RD-0034 (NNR, 2008). This requires implementation and maintenance of an effective, documented quality and safety management system as required by the Eskom specification for Quality and Safety Management Requirements for Nuclear Suppliers Level 2 (Eskom, 2018).

The classification of the products and processes related to the updating of the Tsunami Hazard Analyses determines that the quality management system of the organisation responsible for this service must comply with the Safety Level 1 requirements of RD-0034 (NNR, 2008). This requires implementation and maintenance of an effective, documented quality and safety management system as required by the Eskom specification for Quality and Safety Management Requirements for Nuclear Suppliers Level 1 (Eskom, 2017).

The detailed supporting information about this evaluation of the site and the results achieved is available and contains sufficient data to support key decisions taken, the choice of methodologies and models selected and applied, and the conclusions made. It provides the back-up for the data presented in ***Section 5.9***. A clear audit trail is provided to illustrate the conclusions reached. The data and information presented in ***Section 5.9*** forms the foundation for the peer review process of the SSR.

CONTROLLED DISCLOSURE

When downloaded from the EDS database, this document is uncontrolled and the responsibility rests with the user to ensure it is in line with the authorised version on the database.

Prior to site work commencing, the following documents were compiled:

- Method statement;
- Project quality plan;
- Risk assessment;
- Health safety and environmental management plan.

Table 5.9.64 lists the activities carried out by the author, links of this ***Section 5.9*** to other SSR sections and chapters, and quality control requirements.

CONTROLLED DISCLOSURE

When downloaded from the EDS database, this document is uncontrolled and the responsibility rests with the user to ensure it is in line with the authorised version on the database.

Table 5.9.64: Summary of Activities, Links and Quality Requirements.

Activity	Links		Quality Requirements
	Inputs	Outputs	
All	***Section 3*** (Overview of Planned Activities): Plant Parameter Envelope (PPE)		
Climate change	***Section 5.8*** (Meteorology): Operational and extreme wind speeds including climate change. Extreme high and low atmospheric pressure including climate change.	***Section 5.8*** (Meteorology): Climate change alignment.	Based on best available climate science.
		Sections 5.10 (Hydrology and Hydraulics) and ***5.11*** (Geohydrology). Sea level rise.	Based on best available climate science.
Tsunamis		***Chapter 6*** (External Events). Tsunami run-up, rundown and velocity.	RD-0034 Level 1.
Hydrodynamic modelling	***Section 5.8*** (Meteorology): Wind speed and direction measurements at the site.		Calibrated instrumentation
	Section 5.13 (Geology): Bathymetry, side scan and marine geology within 8 km radius of the site.		Calibrated instrumentation
		Section 5.2 (Monitoring): Description of monitoring programme.	Calibrated instrumentation
		Chapter 6 (Evaluation of External Events): Waves, erosion and sedimentation.	RD-0034 Level 2.
Flooding		***Sections 5.10*** (Hydrology and Hydraulics) and ***5.11*** (Geohydrology): Extreme seawater levels.	RD-0034 Level 2.
		Chapter 6 (Evaluation of External Events): Climate change, tides, seiche, storm surge, wave run-up, maximum flooding sea level, minimum low sea level.	RD-0034 Level 2.
Thermal plume modelling	***Sections 5.3*** (Ecology): Biofouling.	***Section 5.6*** (Adjacent Sea Use): Thermal plume dispersion results.	RD-0034 Level 2.
		Chapter 6 (Evaluation of External Events): Extreme seawater cooling temperature.	RD-0034 Level 2.
		Chapter 7 (PIPE): Thermal plume dilution factors.	RD-0034 Level 2.

CONTROLLED DISCLOSURE

When downloaded from the EDS database, this document is uncontrolled and the responsibility rests with the user to ensure it is in line with the authorised version on the database.

The establishment of oceanography and coastal engineering site parameters and evaluations does not lend itself to direct verification by inspections or tests that can be precisely defined and controlled. Peer review of these evaluations is therefore essential, by suitably qualified and experienced persons who are independent from those who performed the work.

Specific quality assurance/control requirements applicable to the oceanography section are:

- calibration of monitoring instruments and quality control of the data from the monitoring programme;
- correct use of the numerical models, i.e., model selection, model setup and interpretation of model results.

Detailed records of the work carried are kept by the author, i.e., calculations performed and data bases established. These include:

- oceanographic data from the monitoring programme;
- setup and calibration of numerical models;
- model V&V as per the requirements contained in NSIP02761 (Eskom, 2020a) and RG-0016 (NNR, 2016b);
- post-processing of numerical model results.

Electronic records are stored in a secure central repository with regular off-site back-up procedures and subject to Eskom's approval.

The regulatory compliance matrix for ***Section 5.9*** is shown in ***Table 5.9.65***.

CONTROLLED DISCLOSURE

When downloaded from the EDS database, this document is uncontrolled and the responsibility rests with the user to ensure it is in line with the authorised version on the database.

Table 5.9.65: Regulatory Compliance Matrix.

Act/ Regulation	Section/ Regulation	Requirements/Issue	Addressed in Sub-Section
R.927: Regulations on Licensing of Sites for New Nuclear Installations (Department of Energy, 2011)	Regulation 4(5)	Natural phenomena and potential man-made hazards must be appropriately accounted for in the design of the new nuclear installation(s)	5.9.9, 5.9.10, 5.9.11, 5.9.12, 5.9.13, 5.9.14, 5.9.15, 5.9.16, 5.9.17
	Regulation 5(3)	The characteristics of the site relevant to the design assessment, risk and dose calculations, including inter alia: (a) external events; (b) meteorological data; (f) projections of the above data commensurate with the design life of the nuclear installation(s)".	5.9.7, 5.9.8, 5.9.9. 5.9.10, 5.9.11, 5.9.12, 5.9.13, 5.9.14, 5.9.15, 5.9.16, 5.9.17
RG-0011: Interim Guidance on the Siting of Nuclear Facilities (NNR, 2016a);	Section 6.1(1)	In the evaluation of the suitability of a site for a nuclear facility, the following aspects should be considered: a) Effects of external events occurring in the region of the particular site (natural or human induced);	5.9.9, 5.9.10, 5.9.11, 5.9.12, 5.9.13, 5.9.14, 5.9.15, 5.9.16, 5.9.17
	Section 6.1(4)	Site characteristics that may affect the safety of the nuclear facility should be investigated and assessed.	5.9.7, 5.9.8, 5.9.9. 5.9.10, 5.9.11, 5.9.12, 5.9.13, 5.9.14, 5.9.15, 5.9.16, 5.9.17
	Section 6.1(5)	A quality management programme should be established to control the effectiveness of the execution of the site investigations and assessments and engineering activities performed in the different stages of the site evaluation process, covering all activities that may influence safety or the derivation of parameters for the design basis.	5.9.20
	Section 6.6.3(2)	The Site Safety Report should characterise all the factors relevant to the site, including natural and human-induced external events.	5.9.7, 5.9.8, 5.9.9. 5.9.10, 5.9.11, 5.9.12, 5.9.13, 5.9.14, 5.9.15, 5.9.16, 5.9.17
	Section 6.6.3(3)	The Site Safety Report should include the necessary external events data in support of the safety assessment for a given facility.	5.9.7, 5.9.8, 5.9.9. 5.9.10, 5.9.11, 5.9.12, 5.9.13, 5.9.14, 5.9.15, 5.9.16, 5.9.17
	Section 7.1(2)	Proposed sites should be adequately investigated with respect to all the characteristics that could affect safety in relation to natural and human-induced events.	5.9.9, 5.9.10, 5.9.11, 5.9.12, 5.9.13, 5.9.14, 5.9.15, 5.9.16, 5.9.17

CONTROLLED DISCLOSURE

When downloaded from the EDS database, this document is uncontrolled and the responsibility rests with the user to ensure it is in line with the authorised version on the database.

Act/ Regulation	Section/ Regulation	Requirements/Issue	Addressed in Sub-Section
	Section 7.1(3)	The hazards associated with external events, which are to be considered in the design of the nuclear facility, must be determined. For an external event (or a combination of events), the parameters and the values of those parameters used to characterise the hazards must be chosen so that they can be used readily in the design of the nuclear facility.	5.9.9.9, 5.9.10.6, 5.9.13, 5.9.14, 5.9.15.7
	Section 7.1(5)	Prehistorical, historical and instrumental information and records, as applicable, of the occurrences and severity of those important natural phenomena or human-induced situations/activities should be collected for the region and carefully analysed for reliability, accuracy and completeness.	5.9.6.1, 5.9.12.4
	Section 7.1(6)	Appropriate methodologies should be adopted for establishing the hazards from important external phenomena.	5.9.6
	Section 7.1(7)	The methodologies used should be the current and state of the art, and should be justified as being compatible with the characteristics of the region.	5.9.6
	Section 7.1(8)	Preferential consideration should be given to applicable probabilistic methodologies.	5.9.6
	Section 7.1(9)	It should be noted that probabilistic hazard curves are generally required to conduct external event PSAs.	5.9.6
	Section 7.1(10)	The size of the region, to which a method for establishing the hazards associated with major external phenomena is to be applied, should be large enough to include all the features and areas that could be of significance in the determination of the natural and human-induced phenomena under consideration and for the characteristics of the event.	5.9.8
	Section 7.1(11)	All natural events that have a probability of occurrence of more than the minimum safety goal defined in PP-0014 (i.e. about 10^{-7} per year) should be considered. Natural phenomena, which may exist or can occur in the region of a proposed site, should be identified and classified as per their impact on plant safety. Design bases should be derived for each credible event and credible combination of events by adopting appropriate methodologies.	5.9.6, 5.9.9.9, 5.9.10.6, 5.9.13, 5.9.14, 5.9.15.7
	Section 7.1(15)	The evaluation of site characteristics to determine design basis parameters should include considerations for exceedance of design basis and/or design extension conditions.	5.9.6.2
	Section 7.1(16)	The evaluation of site characteristics to determine design basis parameters should take into account changes of hazards (both natural and human induced) with regards to the design life of the facility.	5.9.7
	Section 7.2.2(1)	Meteorological events/parameters to be considered for evaluation of design bases include: …, storm surge, cooling water temperature, …	5.9.9.2, 5.9.9.5
	Section 7.2.3(2)	Coastal sites should be assessed for: high tides, cyclones/storm surge, wind-induced waves, precipitation, tsunami-generated waves, etc. Appropriate combinations of these phenomena should also be considered.	5.9.9.1, 5.9.9.2, 5.9.9.8, 5.9.12, 5.9.9.9

CONTROLLED DISCLOSURE

When downloaded from the EDS database, this document is uncontrolled and the responsibility rests with the user to ensure it is in line with the authorised version on the database.

Act/ Regulation	Section/ Regulation	Requirements/Issue	Addressed in Sub-Section
	Section 7.2.3(3)	The design basis should take into account the highest water level reached at the site during the above events. Other associated parameters like the duration of flood, flow conditions, warning time for flood and the height and period of waves, if relevant, should also be estimated.	5.9.11, 5.9.12, 5.9.13
	Section 7.2.3(4)	Suitable meteorological, hydrological and topographical data, including data on relevant bodies of water, should be collected. Uncertainty and data inadequacy, if any, should be taken into consideration when deriving the design basis value of the flood water level. The design basis' highest water level at the site should be arrived at by using appropriate flood routing models.	5.9.6.1, 5.9.8, 5.9.11, 5.9.13
	Section 7.2.3(9)	The potential for seiches in enclosed bodies of water should be examined for inland sites located close to such bodies of water.	5.9.11, 5.9.13, 5.9.14
	Section 7.2.3(10)	Coastal sites should be examined for potential flooding caused by a surge due to cyclones, wind-induced waves as well as tsunami waves.	5.9.9.2, 5.9.9.8, 5.9.11, 5.9.12, 5.9.13
	Section 7.2.3(11)	Wave run-up should also be considered taking into account any amplification due to the coastal configuration adjacent to the site.	5.9.11
	Section 7.2.3(12)	Bathymetry and topography data of the coastal region should be collected and utilised.	5.9.6.1, 5.9.8
	Section 7.2.3(13)	The region should be evaluated to determine the potential for tsunamis that could affect the safety of nuclear facilities on the site. The hazards associated with tsunamis should include potential drawdown and run-up as well as hydrodynamic forces, if applicable.	5.9.12
	Section 7.2.3(14)	Design basis earthquake should be arrived at with data of earthquakes resulting from a tsunami wave landing at the site using appropriate hydrological and numerical models.	5.9.12
	Section 7.2.3(15)	The frequency of occurrence, magnitude and height of regional tsunamis should be estimated. On the basis of the available data for the region, prehistorical and historical, and comparison with similar regions that have been well studied, all potential tsunamigenic sources and their maximum potential should be identified and used in determining the possible hazards associated with tsunamis. Appropriate models should be used in the evaluation and should take into account any amplification due to the coastal configuration adjacent to the site.	5.9.12
	Section 7.2.4(12)	For coastal sites, the potential for shore instability due to erosion or sedimentation should be investigated.	5.9.10
	Section 7.2.4(14)	The potential for the loss of ultimate heat sink of a nuclear facility should be analysed. If the potential exists, the site should be considered unsuitable unless a reliable and practical engineering solution is available.	5.9.14, 5.9.15.7, 5.9.16, 5.9.17
	Section 8.4.3(1)(a)	The general shore and bottom configuration in the region, and unique features of the shoreline in the vicinity of the discharge. Data on bathymetry out to a distance of several kilometres, and data on the amount and character (transport, deposition and resuspension) of sediments in the shallow shelf waters.	5.9.8, 5.9.9.7

CONTROLLED DISCLOSURE

When downloaded from the EDS database, this document is uncontrolled and the responsibility rests with the user to ensure it is in line with the authorised version on the database.

Act/ Regulation	Section/ Regulation	Requirements/Issue	Addressed in Sub-Section
	Section 8.4.3(1)(b)	Speeds, temperatures and directions of any near shore currents that could affect the dispersion of discharged radioactive material. Measurements should be made at appropriate depths and distances, depending on the bottom profile and the location of the point of discharge.	5.9.9.4
	Section 8.4.3(1)(c)	The duration of stagnation and characteristics of current reversals.	5.9.9.4
	Section 8.4.3(1)(d)	The thermal stratification of water layers and its variation with time, including the position of the thermocline and its seasonal changes.	5.9.9.5
	Section 8.6.3(1)(b)	Hydrological, physical, physicochemical and biological characteristics governing the transport, diffusion and retention of radioactive materials.	5.9.8, 5.9.9.4, 5.9.9.5
	Section 10.4(11)	Physical protection systems that are exposed to anticipated weather and environmental conditions or probable maximum flood conditions should be identified and considered in determining any challenges or impediments to designs.	5.9.13
	Section 10.4(12)	Changes to the topography of the site caused by low water conditions should be considered for determining if resulting conditions would present challenges or impediments to the design of engineered and administrative security controls.	5.9.10, 5.9.14
	Section 11.1(1)	The site characteristics relevant to the nuclear facility that are considered in the safety requirements and that are pertinent to licensing and safe operation should be monitored for the period of applicability of the NSL, or until the NL is superseded by the construction licence.	5.9.6.1
	Section 11.1(4)	The data obtained should be used as a baseline in future investigations.	5.9.6.1

5.9.21 Conclusions

5.9.21.1 Climate Change

The effect of climate change on all relevant oceanographic and coastal engineering parameters has been included. The primary guidance is taken from the latest publications from the Intergovernmental Panel for Climate Change (IPCC), along with peer-reviewed journal articles where IPCC projections are outdated or unavailable. For each parameter the baseline date was taken as the middle of the period of available data at the site. Projections derived from literature were converted relative to the baseline date for each parameter. The effect of climate change was evaluated over both the operating life and the decommissioning period of the existing KNPS and the proposed new NIs at the site. ***Table 5.9.66*** shows the climate change values applied.

CONTROLLED DISCLOSURE

When downloaded from the EDS database, this document is uncontrolled and the responsibility rests with the user to ensure it is in line with the authorised version on the database.

Note that the assessment of coastline stability and flooding from the sea are based on the sea level rise (SLR) corresponding to the RCP8.5 upper end of likely range (0.44 m in 2064 and 1.80 m in 2130), rather than the maximum plausible SLR (0.79 m in 2064 and 3.26 m in 2130). This additional 0.35 m in the case of KNPS and 1.5 m in the case of the new NIs should be considered during the SAR and engineering design phase, either as safety buffer or as part of an adaptive design strategy.

The estimation of the influence of climate change has been based on the most reliable scientific information available at the time that this study was undertaken, but must be continually reassessed as new data and research results become available (at least every five years). This shall include the IPCC 6th Assessment Report (AR6) which has recently been published in draft format. The SSR would only need to be updated should one of the relevant climate change parameters change significantly.

Table 5.9.66: Climate Change Applied for Each Oceanographic Parameter and Date.

Parameter	Description	Scenario	Units	Baseline date	2021	2044	2064	2110	2130
Sea level rise	Regional mean sea level rise	RCP8.5 Upper end of likely range	m	2019	0.01	0.20	0.44	1.36	1.80
		Maximum plausible	m	2019	0.02	0.36	0.79	2.46	3.26
Seawater temperature	Near-surface	RCP8.5, no uncertainty ranges available	°C	2012	0.2	0.7	1.2	2.3	2.7
Wind speed	Annual average	RCP8.5, mean estimate	%	1993.5	1.4%	3.0%	4.5%	8.7%	11.0%
	Annual maximum		%	1993.5	0.5%	1.2%	1.7%	3.3%	4.2%
Atmospheric pressure	Extreme low pressure	RCP8.5, mean estimate	%	1993.5	-0.01%	-0.03%	-0.05%	-0.09%	-0.12%
	Extreme high pressure		%	1993.5	0%	0%	0%	0%	0%
Storm surge	Extreme positive	RCP8.5, mean estimate	%	1993.5	1.0%	2.3%	3.4%	6.8%	8.6%
	Extreme negative		%	1993.5	1.0%	2.3%	3.4%	6.8%	8.6%
Meteo-tsunami	Positive	RCP8.5, mean estimate	%	2013	0.3%	1.6%	2.7%	6.0%	7.9%
	Negative		%	2013	0.3%	1.6%	2.7%	6.0%	7.9%
Wave height	Extreme in deep water offshore	RCP8.5, no uncertainty ranges available	%	2000	0.8%	1.7%	2.5%	4.2%	5.0%
	Mean in deep water offshore		%	2004.5	0.0%	0.0%	0.0%	0.0%	0.0%
Wave period	Extreme in deep water offshore	RCP8.5, no uncertainty ranges available	%	2000	0.4%	0.8%	1.2%	2.1%	2.5%
	Mean in deep water offshore		%	2004.5	0.0%	0.0%	0.0%	0.0%	0.0%
Wave direction	Extreme in deep water offshore	RCP8.5, no uncertainty ranges available	Degrees, positive clockwise	Not available					
	Mean in deep water offshore			2004.5	-0.7	-1.8	-2.7	-4.8	-5.7
Current speed	Extreme depth-averaged wind-driven current	RCP8.5, mean estimate	%	2015	0.1%	0.8%	1.3%	2.9%	3.8%

CONTROLLED DISCLOSURE

When downloaded from the EDS database, this document is uncontrolled and the responsibility rests with the user to ensure it is in line with the authorised version on the database.

5.9.21.2 Nearshore Waves

The best estimate extreme nearshore wave climate at a depth of -31 m msl in front of the site is provided in ***Table 5.9.67***. H_{m0} is the significant wave height (the mean of the highest one-third of waves), T_p is the peak wave direction, MWD is the mean wave direction and DSD is the directional standard deviation (a measure of the directional spreading).

Table 5.9.67: Extreme Wave Parameters at a Depth of -31 m msl in Front of the Site.

Exceedance Probability	H_{m0}			T_p			MWD	DSD
(y^{-1})	(m)			(s)			(°)	(°)
	2021	2064	2130	2021	2064	2130	All	All
10^{-2}	9.6	9.7	10.0	16.7	16.8	17.0	250	21.9
10^{-4}	12.8	13.0	13.3	19.3	19.4	19.7	250	21.9
10^{-5}	14.3	14.6	14.9	20.4	20.6	20.9	250	21.9
10^{-6}	15.9	16.1	16.5	21.5	21.7	22.0	250	21.9
10^{-7}	17.4	17.7	18.1	22.5	22.7	23.0	250	21.9
10^{-8}	18.9	19.2	19.7	23.5	23.7	24.0	250	21.9

These results indicate a rough wave climate that will need to be accounted for in the design of all coastal structures at the site during the SAR and engineering design phases, e.g., intake structures, outfall structures and revetments.

5.9.21.3 Coastline Erosion

The best estimate coastline stability at the site has been assessed including long-term coastline trends, sea level rise, wave rotation and cross-shore storm erosion. ***Table 5.9.68*** summarises the maximum horizontal coastline erosion adjacent to the KNPS and in front of the new NIs.

CONTROLLED DISCLOSURE

When downloaded from the EDS database, this document is uncontrolled and the responsibility rests with the user to ensure it is in line with the authorised version on the database.

Table 5.9.68: Maximum Coastline Erosion Adjacent to KNPS and in Front of New NIs.

Exceedance Probability	Total Coastline Erosion[(a)] Adjacent to KNPS		Total Coastline Erosion[(a)] in Front of New NIs		
(y^{-1})	(m from Baseline[(b)])		(m from Baseline[(c)])		
	2021	2064	2021	2064	2130
10^{-2}	-59	-145	-96	-178	-346
10^{-4}	-74	-159	-96	-178	-346
10^{-5}	-80	-167	-107	-180	-350
10^{-6}	-87	-175	-143	-182	-354
10^{-7}	-181	-182	-143	-185	-356
10^{-8}	-286	-306	-157	-195	-358

Note:
(a) Defined as the most landward extent where any erosion occurs.
(b) At KNPS the baseline is parallel to the terrace and seaward of the intakes.
(c) At the new NIs the baseline corresponds to the present-day +2 m msl contour.

- These results show significant erosion of the coastline, which increases over time due to long-term coastline trends, sea level rise and larger waves.
- Further engineering studies should be undertaken to ensure that the breakwater and outfall structures at KNPS can withstand the predicted erosion over the operating life of the plant.
- The predicted erosion does not reach the estimated position of the new NIs for 2021 and 2064. For 2130 the southern section the new NIs are eroded for all exceedance probabilities modelled. It will thus be necessary to move the position of the new NIs landward, or to design appropriate coastal protection such as revetments.
- Note that the assessment of coastline stability is based on the sea level rise (SLR) corresponding to the RCP8.5 upper end of likely range (0.44 m in 2064 and 1.80 m in 2130), rather than the maximum plausible SLR (0.79 m in 2064 and 3.26 m in 2130). This additional 0.35 m in the case of KNPS and 1.5 m in the case of the new NIs should be considered during the SAR and engineering design phase, either as safety buffer or as part of an adaptive design strategy.

5.9.21.4 Flooding from the Sea

Flooding from the sea was assessed due to:

- Storm wave run-up combined with sea level rise, high tides, positive storm surge, wave set-up and basin seiche; and
- Tsunami run-up combined with sea level rise, high tides and positive storm surge.

CONTROLLED DISCLOSURE

When downloaded from the EDS database, this document is uncontrolled and the responsibility rests with the user to ensure it is in line with the authorised version on the database.

The best estimate results are presented in ***Table 5.9.69***.

Table 5.9.69: Flooding from the Sea.

Source of Flooding	Exceedance Probability	KNPS				New NIs					
		Max Vertical Run-up Level		Max Horizontal Inundation Distance		Max Vertical Run-up Level			Max Horizontal Inundation Distance		
	(y^{-1})	(m msl)		(m from Baseline[(a)])		(m msl)			(m from Baseline[(b)])		
		2021	2064	2021	2064	2021	2064	2130	2021	2064	2130
Storm Waves	10^{-2}	6.55	6.53	104	127	6.38	6.66	9.38	79	160	328
Storm Waves	10^{-4}	7.85	7.67	145	186	8.97	9.87	12.41	125	210	345
Storm Waves	10^{-5}	8.69	8.33	156	222	9.10	10.35	13.36	177	257	365
Storm Waves	10^{-6}	9.54	9.00	168	258	9.23	10.83	14.31	229	305	385
Storm Waves	10^{-7}	10.13	10.41	207	321	10.11	12.03	15.52	259	321	406
Storm Waves	10^{-8}	10.72	11.83	246	383	10.98	13.24	16.73	288	336	427
Tsunami: Distant earthquakes	(c)	6.05	6.81	137	162	6.67	7.22	8.95	80	169	333
Tsunami: Volcanic flank collapse	(c)	11.82	13.95	382	399	12.71	13.93	15.82	384	399	553
Tsunami: Local submarine landslides	(c)	6.80	7.04	143	175	6.80	8.19	10.08	123	184	333
Probable Maximum Tsunami (PMT)	(d)	11.82	13.95	382	399	12.71	13.93	15.82	384	399	553

Notes:
(a) At KNPS the baseline is parallel to the terrace and seaward of the intakes.
(b) At the new NIs the baseline corresponds to the present-day +2 m msl contour.
(c) Maximum for each tsunami source type.
(d) Maximum for all tsunami source types.

- At KNPS, the PMT run-up and inundation are governed by the volcanic flank collapse tsunamis which result in extensive flooding of the KNPS nuclear terrace level located at approximately +8 m msl. No other tsunamigenic sources, including distant earthquakes and local submarine landslide sources, result in run-up above the KNPS nuclear terrace level, even including climate change to 2064.
- The run-up at the KNPS due to storm waves reaches +8 m msl at exceedance probabilities between 10^{-4} y^{-1} and 10^{-6} y^{-1}, however these locations are north and south of the nuclear terrace. Only at 10^{-8} y^{-1} does the wave run-up flood the terrace adjacent to the reactor buildings.
- The predicted flooding at KNPS will require further assessment, i.e., through further analysis of the probability of these events occurring in the remaining 42 y until the end of decommissioning (assumed in 2064), by analysing the impact of the predicted flood water depths and currents on the SSCs, and consideration of protective structures such as wave walls.

CONTROLLED DISCLOSURE

When downloaded from the EDS database, this document is uncontrolled and the responsibility rests with the user to ensure it is in line with the authorised version on the database.

- The PPE for the new NIs states that the terrace height must be such that the terrace is elevated above design basis flooding hazards. These results show the maximum flood level is +16.7 m msl, due to an extreme 10^{-8} y^{-1} wave storm in 2130. The maximum horizontal inundation is 553 m due to the PMT in 2130. The inundation extends into the estimated position of the new NIs for the PMT in all years.
- For wave storms the inundation does not reach the position of the new NIs in 2021 and 2064, however in 2130 the position of the new NIs is reached for exceedances of 10^{-2} y^{-1} and lower.
- For the new NIs the SSCs will need to be placed above these maximum flood levels and landward of the maximum inundation, or alternatively protective structures such as revetments and wave walls will need to be placed in front of the SSCs.
- Note that the assessment of flooding for both storms and tsunamis is based on the sea level rise (SLR) corresponding to the RCP8.5 upper end of likely range (0.44 m in 2064 and 1.80 m in 2130), rather than the maximum plausible SLR (0.79 m in 2064 and 3.26 m in 2130). This additional 0.35 m in the case of KNPS and 1.5 m in the case of the new NIs should be considered during the SAR and engineering design phase, either as safety buffer or as part of an adaptive design strategy.

5.9.21.5 Extreme Low Water Levels

Extreme low water levels at the cooling water intakes can occur due to:

- Storm wave drawdown combined with low tides, negative storm surge and basin seiche; or
- Tsunami drawdown combined with low tides and negative storm surge.

The best estimate extreme low water levels at the KNPS cooling water intake pumps inside the intake basin, and at the -20 m and -30 m msl depths opposite the new NIs, corresponding to possible tunnel intake locations, are presented in ***Table 5.9.70***.

CONTROLLED DISCLOSURE

When downloaded from the EDS database, this document is uncontrolled and the responsibility rests with the user to ensure it is in line with the authorised version on the database.

Table 5.9.70: Extreme Low Water Levels.

Source of Drawdown	Exceedance Probability	KNPS		New NIs								
		Minimum vertical drawdown level at pumps		Minimum vertical drawdown level at pumps[(a)]			Minimum vertical drawdown at -20 m msl			Minimum vertical drawdown at -30 m msl		
	(y^{-1})	(m msl)		(m msl)			(m msl)			(m msl)		
		2021	2064	2021	2064	2130	2021	2064	2130	2021	2064	2130
Storm Waves	10^{-2}	-1.10	-1.11	-1.10	-1.11	-1.13	-3.55	-3.47	-3.47	-4.87	-4.79	-5.27
Storm Waves	10^{-4}	-1.42	-1.39	-1.42	-1.39	-1.45	-3.66	-3.81	-3.85	-5.39	-5.44	-5.55
Storm Waves	10^{-5}	-1.53	-1.54	-1.53	-1.54	-1.62	-3.74	-3.86	-3.93	-5.76	-6.04	-6.17
Storm Waves	10^{-6}	-1.64	-1.69	-1.64	-1.69	-1.80	-3.83	-3.90	-4.01	-6.14	-6.64	-6.79
Storm Waves	10^{-7}	-1.79	-1.83	-1.79	-1.83	-1.95	-1.79	-3.94	-4.00	-4.03	-6.41	-6.61
Storm Waves	10^{-8}	-1.94	-1.97	-1.94	-1.97	-2.09	-4.04	-4.10	-4.05	-6.68	-6.58	-6.82
Tsunami: Distant earthquakes	(b)	-2.26	-2.26	-2.26	-2.26	-2.23	-4.96	-5.04	-5.19	-3.90	-3.87	-3.81
Tsunami: Volcanic flank collapse	(b)	-1.83	-1.81	-1.83	-1.81	-1.77	-7.18	-7.16	-7.18	-6.64	-6.65	-6.51
Tsunami: Local submarine landslides	(b)	-2.12	-2.12	-2.12	-2.12	-2.14	-5.35	-5.36	-5.40	-4.69	-4.70	-4.73
Probable Maximum Tsunami (PMT)	(c)	-2.26	-2.26	-2.26	-2.26	-2.23	-7.18	-7.16	-7.18	-6.64	-6.65	-6.51

Notes:
(a) Assuming a basin intake with similar geometry to KNPS.
(b) Minimum level for each tsunami source type.
(c) Minimum level for all tsunami source types.

- For the existing KNPS basin, the Essential Service Water System (SEC) pumphouse is designed to accommodate a minimum short duration water level of -2.5 m msl under normal operating conditions. If the sea level drops below -3.5 m msl no water would reach the pumps. At KNPS, the results show that the lowest water level is -2.3 m msl, which is driven by the PMT. The KNPS pumps will thus continue to operate for all events assessed.
- If a basin intake with similar geometry to KNPS is selected for the new NIs, then the intake should accommodate a minimum water level of -2.3 m msl.
- If a tunnel intake in a depth of -20 m msl is selected for the new NIs, then the intake should accommodate a minimum water level of -7.2 m msl, which is driven by the PMT.
- If a tunnel intake in a depth of -30 m msl is selected for the new NIs, then the intake should accommodate a minimum water level of -6.8 m msl, which is driven by the 10^{-8} y^{-1} storm event.

CONTROLLED DISCLOSURE

When downloaded from the EDS database, this document is uncontrolled and the responsibility rests with the user to ensure it is in line with the authorised version on the database.

5.9.21.6 Thermal Plume Dispersion and Recirculation

It is proposed that the new NIs will be cooled using a once-through seawater cooling system. Four different conceptual layouts for the seawater cooling intake and outfall system have been developed and thermal plume dispersion modelling has been performed to demonstrate the technical feasibility of the site:

- Layout 0: Existing KNPS intake basin and outfall channel;
- Layout 1: Short tunnel intakes and outfalls;
- Layout 2: Long tunnel intakes and outfalls;
- Layout 3: Basin intake and tunnel outfalls;
- Layout 4: Basin intake and rubble-mound outfall structure.

The PPE for the new NIs specifies that the maximum ΔT of the re-circulated cooling water between the discharge and the intake should be less than 1.5°C. The maximum ΔT of the re-circulated water at the KNPS is not specified.

The modelled recirculation ΔT's at the KNPS intake and at the new NIs intake are presented in ***Table 5.9.71***.

Table 5.9.71: Recirculation at KNPS Intake and New NIs Intake.

Case	ΔT at KNPS Intake (°C)			ΔT at new NIs Intake (°C)		
	50th Percentile	95th Percentile	99th Percentile	50th Percentile	95th Percentile	99th Percentile
KNPS (2108 MWe)	0.35	1.80	2.40	-	-	-
KNPS + new NIs (2500 MWe) Layout 1	0.71	2.01	2.57	0.13	0.71	1.33
KNPS + new NIs (2500 MWe) Layout 2	0.48	1.79	2.41	0.03	0.48	0.92
KNPS + new NIs (2500 MWe) Layout 3	0.47	1.73	2.17	0.17	0.85	1.10
KNPS + new NIs (2500 MWe) Layout 4	0.98	2.17	2.81	0.69	2.04	2.69
KNPS + new NIs (4000 MWe) Layout 1	0.89	2.11	2.69	0.08	0.70	1.17
KNPS + new NIs (4000 MWe) Layout 2	0.60	1.83	2.44	0.05	0.50	0.94
KNPS + new NIs (4000 MWe) Layout 3	0.70	1.80	2.27	0.36	1.22	1.48
KNPS + new NIs (4000 MWe) Layout 4	1.38	2.49	3.02	1.19	2.62	3.24

- The results show that the 99th percentile ΔT at the existing KNPS intake is 2.4°C. The new NIs generally increase the ΔT at the existing KNPS intake, with Layout 4 resulting in the largest increase (+0.6°C for the 99th percentile), while Layout 3 had the least impact.

CONTROLLED DISCLOSURE

When downloaded from the EDS database, this document is uncontrolled and the responsibility rests with the user to ensure it is in line with the authorised version on the database.

- At the new NIs intake, Layouts 1 to 3 meet the ΔT of 1.5°C for the 99th percentile. Layout 4 has a 99th percentile ΔT of 2.7 and 3.2°C for power outputs of 2500 and 4000 MWe, respectively.

5.9.21.7 Extreme Seawater Temperatures

The PPE also specifies a maximum cooling water intake temperature for the new NIs of 30°C. For the existing KNPS a shut-down of the reactor will be necessary if the intake temperature exceeds 23°C. The maximum seawater temperature at the cooling water intakes will depend on:

- The intake and outfall layout, the power output and resultant ΔT due to recirculation from the outfall to the intake; and
- The extreme maximum background seawater temperature at the intake location and climate change.

The best estimate return period in years to exceed 23°C at the KNPS intake and the best estimate annual probability to exceed 30°C at the new NIs intake are presented in ***Table 5.9.72***.

Table 5.9.72: Extreme Maximum Seawater Temperatures at the Intakes (Including Recirculation).

Case	Best Estimate Return Period to Exceed 23°C at KNPS Intake[(a)]			Best Estimate Probability to Exceed 30°C at New NIs Intake		
	(y)			(y^{-1})		
	2021	2044	2064	2021	2064	2130
KNPS (2108 MWe) Layout 0	98	56	35	-	-	-
KNPS + new NIs (2500 MWe) Layout 1	56	32	20	1.0E-05	2.8E-05	1.3E-04
KNPS + new NIs (2500 MWe) Layout 2	71	40	25	3.4E-06	9.1E-06	4.1E-05
KNPS + new NIs (2500 MWe) Layout 3	73	42	26	8.5E-06	2.3E-05	1.0E-04
KNPS + new NIs (2500 MWe) Layout 4	51	29	18	1.5E-05	4.0E-05	1.8E-04
KNPS + new NIs (4000 MWe) Layout 1	44	25	15	1.1E-05	2.8E-05	1.3E-04
KNPS + new NIs (4000 MWe) Layout 2	65	37	23	3.6E-06	9.6E-06	4.4E-05
KNPS + new NIs (4000 MWe) Layout 3	61	35	21	8.5E-06	2.3E-05	1.0E-04
KNPS + new NIs (4000 MWe) Layout 4	29	17	10	3.1E-05	8.2E-05	3.8E-04

Note:
(a) Expressed as the return period for convenience, where return period = 1/exceedance probability

- Without the new NIs, the best estimate return period to exceed 23°C at the KNPS intake is 98 y for the year 2021 and 35 y for the year 2064.
- In all cases the addition of the new NIs reduces the return period to exceed 23°C at the KNPS intake. Layout 4 with a 4000 MWe power station has the largest impact on the KNPS, with the 23°C threshold reducing to a 29 y return period for the year 2021 and a 10 y return

When downloaded from the EDS database, this document is uncontrolled and the responsibility rests with the user to ensure it is in line with the authorised version on the database.

period for the year 2064. Layout 4 will thus increase the probability of a shut-down of the KNPS reactor due to high seawater temperatures.

- At the new NIs intakes, the higher maximum specified intake temperature of 30°C, combined with lower recirculation ΔT's results in significantly lower exceedance probabilities of between 3.4×10^{-6} and 3.8×10^{-4} y^{-1}, with the latter for Layout 4 with the 4000 MWe power station in 2130. These exceedance probabilities indicate that the intake seawater temperatures will need to be considered in the design of the cooling system for the new NIs.

5.9.21.8 Sedimentation and Scour

Sediment transport modelling was carried out to assess the sedimentation in the KNPS intake basin entrance and scour around coastal structures during extreme storm and tsunami events.

The best estimate maximum scour depth below the seabed and maximum bed level in the intake basin is presented in ***Table 5.9.73***.

Table 5.9.73: Sedimentation and Scour at the KNPS Intake Basin due to Storms.

Source	Exceedance Probability	Maximum Bed Level in Intake Basin Entrance[(a)]	Maximum Scour Adjacent to Structures[(b)]
	y^{-1}	(m msl)	(m)
Storm waves	10^{-2}	-2.7	-6.1
Storm waves	10^{-4}	-2.7	-6.4
Storm waves	10^{-5}	-2.7	-6.8
Storm waves	10^{-6}	-2.7	-7.3
Storm waves	10^{-7}	-2.6	-7.5
Storm waves	10^{-4}	-2.5	-7.8
Tsunami	Not applicable	-2.7	-3.5

Notes:
(a) Measured as the shallowest point along the deepest flow path between the intakes and the sea. The initial maximum bed level was -2.68 m msl.
(b) Defined as the depth below the existing seabed.

- Under extreme storm conditions scour exceeding -5 m is predicted at the roundhead and along the outside of the southern trunk of the KNPS breakwater. The effect of this on the stability of the breakwater requires additional investigation. The design of any similar coastal structures for the new NIs should account for similar levels of scour.
- Storm-induced sedimentation is not predicted to close off the intake basin and seawater will be able to enter the intake basin.

CONTROLLED DISCLOSURE

When downloaded from the EDS database, this document is uncontrolled and the responsibility rests with the user to ensure it is in line with the authorised version on the database.

- Regular maintenance dredging is however required to remove the annual sedimentation in the KNPS intake basin of approximately 132 000 m^3/y, which may increase after extreme storm events.
- Less than 0.3 m of tsunami-induced sedimentation is predicted in front of the KNPS pumphouses and the intake basin is not closed off by sedimentation during the modelled extreme tsunami event.
- These results would also apply should an intake basin with the same geometry be selected for the new NIs. The annual maintenance dredging would however increase with increasing intake seawater flow rate.

For Layouts 1 and 2 the proposed seawater intake is a tunnel extending to approximately -20 and -30 m msl water depth respectively, with the intake opening positioned 3 to 5 m above the seabed. Modelling was performed to estimate the volume of sand drawn into the intakes which will have to be removed from the proposed landside intake basin. The results presented in ***Table 5.9.74*** are conservatively based on the suspended sediment concentrations 1 m above seabed.

Table 5.9.74: Sand Volume Drawn into Cooling Water Intake Tunnels.

Exceedance Probability (y^{-1})	Case	Units	2500 MWe		4000 MWe	
			Layout 1 (Intake at -20 m msl)	Layout 2 (Intake at -30 m msl)	Layout 1 (Intake at -20 m msl)	Layout 2 (Intake at -30 m msl)
-	Operational Conditions	m^3/y	1 400	380	2 200	610
10^{-2}	Storm event	m^3/event	6 300	2 100	10 000	3 400
10^{-4}	Storm event	m^3/event	55 000	17 000	88 000	27 000
10^{-5}	Storm event	m^3/event	91 000	32 000	150 000	51 000
10^{-6}	Storm event	m^3/event	150 000	60 000	240 000	96 000
10^{-7}	Storm event	m^3/event	220 000	110 000	360 000	170 000
10^{-8}	Storm event	m^3/event	330 000	180 000	530 000	290 000

- For operational conditions the volume of sand drawn into the tunnel intakes which will have to be removed from the proposed landside intake basins is less than 2 200 m^3/y. This is significantly less than the average maintenance dredging volume of the existing KNPS intake basin of approximately 132 000 m^3/y.
- A maintenance dredging programme will be required to prevent excessive sedimentation in the basin and to keep a sufficient buffer for storm events.
- For extreme storm events the sand volume increases significantly and the 10^{-6} storm event results in similar sand volumes over the 4.1-day

CONTROLLED DISCLOSURE

When downloaded from the EDS database, this document is uncontrolled and the responsibility rests with the user to ensure it is in line with the authorised version on the database.

storm event as the annual maintenance dredging at KNPS. The intake basin will need to accommodate these sediment volumes without blocking the pumps.

- The shallower intake in -20 m msl depth results in a threefold increase in sand volumes compared to the intake in -30 m msl. This increase will need to be considered in the detailed engineering and costing of the intakes.

5.9.21.9 Blockage of Intakes and Biofouling

Based on the KNPS and worldwide experience and it can be concluded that the new NIs intakes could be designed to cope with the marine species found at the site and to minimise the risk of complete blockage of the intake.

Chlorine or other biocides should be used to keep the cooling system free of marine growth.

The recommendations put forward by WANO and the EPRI best management practices manual will form an important and valuable input to the new NIs intake design and prevention of cooling water intake blockages through the plant life.

CONTROLLED DISCLOSURE

When downloaded from the EDS database, this document is uncontrolled and the responsibility rests with the user to ensure it is in line with the authorised version on the database.

5.9.22 References

Airshed, 2021. *Proposed Methodology for Including Climate Change Forecasts into the Duyntefontyn Site Safety Report. Ref No 21SRK01. Rev0 Draft3.,* Midrand: Airshed Planning Professionals (Pty) Ltd.

Bland, P. A. & Artemieva, N. A., 2006. The rate of small impacts on Earth. *Meteorics & Planetary Science,* 4(41), pp. 607-631.

Bruun, P., 1962. Sea Level Rise as a Cause of Shore Erosion. *J. Waterways Harbors Div,* 88(1), pp. 117-132.

CGS, 2006. *Marine Operational Survey Report. Eskio Site Surveys, South Africa. Koeberg. Volume 2. Report no. 2006-0347,* Bellville, South Africa: Council for Geoscience.

CGS, 2008. *Potential Sources of Tsunami along the South African Coast. CGS Report Number: 2008-0220,* Bellville: Council for Geoscience.

CGS, 2022. *Tsunami Source Characterisation for the Duynefontyn Site, South Africa. Report number 2021-0067 (Rev. 5). 2022/03/24,* Pretoria: Council for Geoscience.

CoCT, 2015. *City of Cape Town Open Data Portal. Digital model (10m Grid) depicting the elevation of the geographical surface (Bare Earth Model) of the Cape Town municipal area..* [Online]
Available at:
https://web1.capetown.gov.za/web1/opendataportal/DatasetDetail?DatasetName=Digital%20elevation%20model

Cowell, P. J., Roy, P. & Jones, R., 1992. Shoreface translation model: computer simulation of coastal-sand-body response to sea level rise. *Mathematics and Computers in Simulation,* 33(5-6), p. 603–608.

D'Anna, M. et al., 2021. Reinterpreting the Bruun Rule in the Context of Equilibrium Shoreline Models. *Journal of Marine Science and Engineering,* 9(974).

Department of Energy, 2011. *R.927: The Regulations on Licencing of Sites for New Nuclear Installations. Government Gazette No. 34735,* Pretoria: Department of Energy.

DHI, 2021a. *Extreme Value Analysis, User Guide. DHI A/S, Hørsholm, Denmark.* [Online]
Available at:
https://manuals.mikepoweredbydhi.help//2021/General/EVA_UserGuide.pdf

CONTROLLED DISCLOSURE

When downloaded from the EDS database, this document is uncontrolled and the responsibility rests with the user to ensure it is in line with the authorised version on the database.

DHI, 2021b. *Extreme Value Analysis, Technical Reference and Documentation. DHI A/S, Hørsholm, Denmark.* [Online]
Available at:
https://manuals.mikepoweredbydhi.help//2021/General/EVA_SciDoc.pdf

DHI, 2021c. *MIKE 21 Spectral Waves FM, User Guide. DHI A/S, Hørsholm, Denmark.* [Online]
Available at:
https://manuals.mikepoweredbydhi.help//2021/Coast_and_Sea/MIKE21SW.pdf

DHI, 2021d. *MIKE 21 Spectral Waves FM, Scientific Documentation. DHI A/S, Hørsholm, Denmark.* [Online]
Available at:
https://manuals.mikepoweredbydhi.help//2021/Coast_and_Sea/M21SW_Scientific_Doc.pdf

DHI, 2021e. *Littoral Processes FM, User Guide. DHI A/S, Hørsholm, Denmark.* [Online]
Available at:
https://manuals.mikepoweredbydhi.help//2021/Coast_and_Sea/MIKE_FM_LP.pdf

DHI, 2021f. *Littoral Processes FM, Scientific Documentation. DHI A/S, Hørsholm, Denmark.* [Online]
Available at:
https://manuals.mikepoweredbydhi.help//2021/Coast_and_Sea/LittoralProcessesFM_ScientificDoc.pdf

DHI, 2021g. *MIKE 3 Wave Model FM, User Guide. DHI A/S, Hørsholm, Denmark.* [Online]
Available at:
https://manuals.mikepoweredbydhi.help//2021/Coast_and_Sea/MIKE_FM_Wave.pdf

DHI, 2021h. *MIKE 3 Wave Model FM, Scientific Documentation. DHI A/S, Hørsholm, Denmark.* [Online]
Available at:
https://manuals.mikepoweredbydhi.help//2021/Coast_and_Sea/MIKE_3_Wave_FM_Scientific_Doc.pdf

DHI, 2021i. *MIKE 21 Flow Model FM, User Guide. DHI A/S, Hørsholm, Denmark.* [Online]
Available at:
https://manuals.mikepoweredbydhi.help//2021/Coast_and_Sea/MIKE_FM_HD_2D.pdf

CONTROLLED DISCLOSURE

When downloaded from the EDS database, this document is uncontrolled and the responsibility rests with the user to ensure it is in line with the authorised version on the database.

DHI, 2021j. *MIKE 21 Flow Model FM, Scientific Documentation. DHI A/S, Hørsholm, Denmark.* [Online]
Available at:
https://manuals.mikepoweredbydhi.help//2021/Coast_and_Sea/MIKE_21_Flow_FM_Scientific_Doc.pdf

DHI, 2021k. *MIKE 3 Flow Model FM, User Guide. DHI A/S, Hørsholm, Denmark.* [Online]
Available at:
https://manuals.mikepoweredbydhi.help//2021/Coast_and_Sea/MIKE_FM_HD_3D.pdf

DHI, 2021l. *MIKE 3 Flow Model FM, Scientific Documentation. DHI A/S, Hørsholm, Denmark.* [Online]
Available at:
https://manuals.mikepoweredbydhi.help//2021/Coast_and_Sea/MIKE_3_Flow_FM_Scientific_Doc.pdf

DHI, 2021m. *MIKE 21 Flow Model FM Sand Transport Module, User Guide. DHI A/S, Hørsholm, Denmark.* [Online]
Available at:
https://manuals.mikepoweredbydhi.help//2021/Coast_and_Sea/MIKE_FM_ST_2D.pdf

DHI, 2021n. *MIKE 21 Flow Model FM Sand Transport Module, Scientific Documentation. DHI A/S, Hørsholm, Denmark.* [Online]
Available at:
https://manuals.mikepoweredbydhi.help//2021/Coast_and_Sea/MIKE_FM_ST_Scientific_Doc.pdf

DHI, 2021q. *MIKE C-MAP Electronic Charts Database. DHI A/S, Hørsholm, Denmark,* Hørsholm, Denmark: DHI A/S.

Dingle, R. V., 1980. Large allochthonous sediment masses and their role in the construction of the continental slope and rise off southwestern Africa.. *Marine Geology,* Issue 37, pp. 333-354.

Dingle, R. v. et al., 1987. Deep-sea sedimentary environments around southern Africa (South-East Atlantic and South-West Indian Oceans). *Annals of the South African Museam,* Issue 98, pp. 1-27.

DTU, 2010. *Improvement in global ocean tide model in shallow water regions,* Copenhagen, Denmark: Technical University of Denmark.

ECMWF, 2020. *European Centre for Medium-Range Weather Forecasts: ERA5.* [Online]
Available at:

CONTROLLED DISCLOSURE

When downloaded from the EDS database, this document is uncontrolled and the responsibility rests with the user to ensure it is in line with the authorised version on the database.

https://confluence.ecmwf.int/display/CKB/ERA5+data+documentation [Accessed October 2020].

Enet, F. & Grilli, S., 2007. Experimental Study of Tsunami Generation by Three-Dimensional Rigid Underwater Landslides. *Journal of Waterway. Port, Coastal and Ocean Engineering,* 133(6), pp. 442-454.

Enet, F., Grilli, S. & Watts, P., 2003. Laboratory Experiments for Tsunamis Generated by Underwater Landslides: Comparison with Numerical Modeling. *Proceedings of The Thirteenth International Offshore and Polar Engineering Conference*.

EPRI, 2008. *Best Management Practices for Preventing Cooling Water Intake Blockage. 1016319,* Palo Alto, California: Electric Power Research Institute.

EPRI, 2021. *Best Management Practices Manual for Preventing Cooling Water Intake Blockages. 3002019660,* Palo Alto, California: Electric Power Research Institute.

Eskom, 2006. *Koeberg Site Safety Report. Chapter 6, Oceanography and Cooling Supply. Rev 3,* Johannesburg: Eskom.

Eskom, 2008. *Environmental Impact Assessment for the Proposed Nuclear Power Station ('Nuclear-1') and Associated Infrastructure - Marine Ecology Study,* Johannesburg: Eskom.

Eskom, 2011. *External Hazards Requirements for New Nuclear Installations. Unique Identifier 238-1503. Rev 1,* Johannesburg: Eskom.

Eskom, 2015. *External Events Review Initiative: Extra-Terrestrial Hazard Report. EERT-13-001-RPT Revision 1.,* Cape Town: Eskom.

Eskom, 2017. *Quality and Safety Management Requirements for Nuclear Suppliers Level 1. Unique Identifier: 238-101. Rev 1.,* Johannesburg: Eskom.

Eskom, 2018. *Quality and Safety Management Requirements for Nuclear Suppliers Level 2. Unique Identifier: 238-102. Rev 1,* Johannesburg: Eskom.

Eskom, 2020a. *Specification for Validation and Verification Tasks for Simulation Models used in Nuclear Siting. Unique Identifier: NSIP02761. Rev 1,* Johannesburg: Eskom.

CONTROLLED DISCLOSURE

When downloaded from the EDS database, this document is uncontrolled and the responsibility rests with the user to ensure it is in line with the authorised version on the database.

Eskom, 2020b. *NSIP03800: Safety Justification for the Duynefontyn Tsunami Hazard Analysis. Revision 1.,* Johannesburg: Eskom Nuclear Engineering.

Eskom, 2020c. *Koeberg Nuclear Power Station: Existing Services and Contours. Construction Drawing. Doc No. KBA0003B081000. Doc 136278,* Johannesburg: Eskom.

Eskom, 2021. *Revision and Update of the Site Safety Report for Duynefontyn. Technical Requirement Specification, Unique Identifier: NSIP 03273. Rev 3,* Johannesburg: Eskom.

Eskom, 2022a. *Plant Parameter Envelope. Document Identifier: NSIP03179. Rev 2,* Johannesburg: Eskom.

Eskom, 2022b. *Koeberg Nuclear Power Station: KORC Feedback, Marine Ingress into Intake Basin, Jana Uys, 7 February 2022,* Cape Town: Eskom.

Fugro, 2007. *Survey Report for the Koeberg Site Extension. Eskom Site Surveys South Africa. Report No. NZ647za-01-RPT-02-01,* Cape Town, South Africa: Fugro Survey Africa (Pty) Ltd.

GEBCO Compilation Group, 2020. *General Bathymetric Charts of the Oceans. 2020 Grid. doi:10.5285/a29c5465-b138-234d-e053-6c86abc040b9.* s.l.:s.n.

Hands, E., 1983. *The Great Lakes as a Test Model for Profile Responses to Sea-Level Changes.* s.l.:CRC Press.

HYCOM, 2020. *Hybrid Coordinate Ocean Model.* [Online]
Available at:
https://tds.hycom.org/thredds/catalogs/GLBy0.08/expt_93.0.html
[Accessed 2020].

IAEA, 2004. *Safety Standards Series, NS-G-1.9. Design of the Reactor Coolant System and Associated Systems in Nuclear Power Plants,* Vienna: International Atomic Energy Agency.

IAEA, 2011. *Safety Standards Series. SSG-18. Meteorological and Hydrological Hazards in Site Evaluation for Nuclear Installations,* Vienna: International Atomic Energy Agency.

IAEA, 2012. *Report on Protection against Extreme Earthquakes and Tsunamis in the Light of the Accident at the Fukushima Daiichi Nuclear Power Plant, International Experts Meeting, 4–7 September 2012.,* Vienna.: International Atomic Energy Agency.

CONTROLLED DISCLOSURE

When downloaded from the EDS database, this document is uncontrolled and the responsibility rests with the user to ensure it is in line with the authorised version on the database.

IPCC, In press. *Climate Change 2021: The Physical Science Basis. Contribution of Working Group I to the Sixth Assessment Report of the Intergovermental Panel on Climate Change.,* s.l.: Cambridge University Press.

McCarrol, R. et al., 2021. A rules-based shoreface translation and sediment budgeting tool for estimating coastal change: ShoreTrans. *Marine Geology,* Volume 435.

Meucci, A. et al., 2020. Projected 21st century changes in extreme wind-wave events.. *Science Advances,* Issue 6, pp. 1-9.

Morim, J., Hemer, M. & Wang, X. L., 2019. Robustness and uncertainties in global multivariate wind-wave climate projections.. *Nature Climate Change,* Issue 9, pp. 711-718.

Morim, J. et al., 2020. A global ensemble of ocean wave climate projections from CMIP5-driven models. *Scientific Data,* Volume 7.

NCEP, 2021. *WAVEWATCH III® Hindcast and Reanalysis Archives.* [Online]
Available at: https://polar.ncep.noaa.gov/waves/hindcasts/
[Accessed 2021].

NNR, 2008. *RD-0034: Quality and Safety Management Requirements for Nuclear Installations. Rev 0.,* Centurion: National Nuclear Regulator.

NNR, 2014. *PP-0014: Position Paper on Consideration of External Events for New Nuclear Installations. Rev. 0.,* Centurion: National Nuclear Regulator.

NNR, 2016a. *RG-0011: Interim Guidance on the Siting of Nuclear Facilities,* Centurion: National Nuclear Regulator.

NNR, 2016b. *RG-0016: Guidance on the Verification and Validation of Evaluation and Calculation Models used in Safety and Design Analyses. Rev 0.,* Centurion: National Nuclear Regulator.

NRC, 1976. *Regulatory Guide 1.102. Flood Protection for Nuclear Power Plants.,* Washington DC: US Nuclear Regulatory Commission.

NRC, 1977. *Regulatory Guide 1.59. Design Basis Floods for Nuclear Power Plants. Rev. 2. (errata published in 1980).,* Washington DC: US Nuclear Regulatory Commission.

CONTROLLED DISCLOSURE

When downloaded from the EDS database, this document is uncontrolled and the responsibility rests with the user to ensure it is in line with the authorised version on the database.

NRC, 1978. *Regulatory Guide 1.70, Standard Format and Content of Safety Analysis Reports for Nuclear Power Plants. Rev. 3,* Washington DC: US Nuclear Regulatory Commission.

NRC, 2007a. *Combined License Applications for Nuclear Power Plants. Regulatory Guide 1.206,* Washington DC: US Nuclear Regulatory Commission.

NRC, 2007b. *Standards Review Plan. NUREG-0800, Part 2.4.5, Probable Maximum Surge and Seiche Flooding,* Washington DC: US Nuclear Regulatory Commission.

NRC, 2007c. *NUREG-0800. Part 2.4.6. Probable Maximum Tsunami Hazards,* Washington DC: US Nuclear Regulatory Commission.

NRC, 2007d. *Standards Review Plan. NUREG-0800, Part 2.4.11. Low Water Considerations,* Washington DC: US Nuclear Regulatory Commission.

NRC, 2009. *Tsunami Hazard Assessment at Nuclear Power Plant Sites in the United States of America. Final Report. NUREG/CR-6966,* Richland, WA: United States Nuclear Regulatory Commission.

NRC, 2011. *Design-Basis Flood Estimation for Site Characterization at Nuclear Power Plants in the United States of America. NUREG/CR-7046 (PNNL-20091),* Washington DC: US Nuclear Regulatory Commission.

NRC, 2015. *Regulation 1.27. Ultimate Heat Sink for Nuclear Power Plants. Rev. 3,* Washington DC: US Nuclear Regulatory Commission.

NRC, 2016. *Tsunami Hazard Assessment: Best Modeling Practices and State-of-the-Art Technology. NUREG/CR-7223,* Washington DC: US Nuclear Regulatory Commission.

NSTC, 2018. *National Near-Earth Object Preparedness Strategy and Action Plan,* s.l.: National Science and Technology Council.

Okada, Y., 1985. Surface deformation due to shear and tensile faults ina half-space.. *Bulletin of the Seismological Society of America.,* 75(4), pp. 1135-1154.

Okal, E. A., Visser, J. N. J. & de Beer, C. H., 2014. The Dwarskersbos, South Africa local tsunami of August 27, 1969: fiel d survey and simulation as a meteorological event.. *Natural Hazards,* Issue 74, pp. 254-268.

Oppenheimer, M. et al., 2019. Sea Level Rise and Implications for Low-Lying Islands, Coasts and Communities. In: A. Abe-Ouchi, K. Gupta & J.

CONTROLLED DISCLOSURE

When downloaded from the EDS database, this document is uncontrolled and the responsibility rests with the user to ensure it is in line with the authorised version on the database.

Pereira, eds. *IPCC Special Report on the Ocean and Cryosphere in a Changing Climate.* s.l.:IPCC, pp. 321-446.

Palan, K. J., 2017. *Submarine canyon evolution of the Southwest Cape continental margin (Masters' dissertation).,* s.l.: s.n.

Petroliagkis, T. I., Voukouvalas, E., Disperati, J. & Bildot, J., 2016. *Joint Probabilities of Storm Surge, Significant Wave Height and River Discharge Components of Coastal Flooding Events. EUR 27824 EN. doi:10.2788/677778,* Italy: European Union.

PRDW, 2005. *Koeberg Nuclear Power Station, Cooling Water Intake Basin and Outfall Structure, Design Base Document, Report No. 201/96/7 Rev.02,* Cape Town: Prestedge Retief Dresner Wijnberg (Pty) Ltd..

PRDW, 2021. *Duynefontyn Tsunami Hazard Analysis (DTHA): V&V Report. Report S2052-QP-QM-023-R0,* Cape Town: PRDW.

PRDW, 2022a. *Duynefontyn Tsunami Hazard Analysis (DTHA). Report S2052-07-RP-CE-001-R4,* Cape Town: PRDW.

PRDW, 2022b. *Duynefontyn SSR Ch 5.9: V&V Report. S2052-QP-QM-022-R2,* Cape Town: PRDW.

PRDW, 2022c. *Dunefontyn SSR Ch 5.9: 4 Yrs Oceanographic Monitoring Data, S2052-02-RP-CE-005-R0,* Cape Town: PRDW.

PRDW, 2022d. *Palaeotsunami Field Study Report. S2052-07-RP-CE-004-R0.,* Cape Town: PRDW (Pty) Ltd..

Ranasinghe, R., Callaghan, D. & Stive, M., 2011. Estimating Coastal Recession due to Sea Level Rise: Beyond the Bruun Rule. *Climatic Change.*

Ranasinghe, R. & Stive, M. J. F., 2009. Rising Seas and Retreating Coastlines. *Climatic Change,* Volume 97, p. 465–468.

Shand, T. et al., 2013. A Review of Shoreline Response Models to Changes in Sea Level. *Coasts and Ports Australasian Conference.*

SRK, 2021. *Duynefontein Areas: Final Survey Report,* Cape Town, South Africa: SRK Consulting.

Tritan Survey, 2007. *Koeberg Outside And Inner Basin,* s.l.: s.n.

Tritan Survey, 2021. *Technical Survey Report. Report No. TS1085.0,* Cape Town, South Africa: Tritan Survey (Pty) Ltd.

CONTROLLED DISCLOSURE

When downloaded from the EDS database, this document is uncontrolled and the responsibility rests with the user to ensure it is in line with the authorised version on the database.

USACE, 1989. *SBEACH: Numerical Model for Simulating Storm-Induced Beach Change. Report 1: Empirical Foundation and Model Development. Technical Report CERC-89-9,* Vicksburg, Mississippi, USA: US Army Corps of Engineers.

USACE, 1990. *SBEACH: Numerical Model for Simulating Storm-Induced Beach Change. Report 2: Numerical Formulation and Model Tests. Technical Report CERC-89-9,* Vicksburg, Mississippi, USA: US Army Corps of Engineers.

USACE, 1996b. *SBEACH: Numerical Model for Simulating Storm-Induced Beach Change. Report 4: Cross-Shore Transport Under Random Waves and Model Validation with SUPERTANK and FIeld Data. Technical Report CERC-89-9,* Vicksburg, Mississippi, USA: US Army Corps of Engineers.

USACE, 1996. *SBEACH-32 Interface User's Manual,* s.l.: US Army Corps of Engineers.

USACE, 2002. *Coastal Engineering Manual: Part IV Chapter 3 - Coastal Morphodynamics,* Washington DC, USA: US Army Corps of Engineers.

Van Gent, M. et al., 2008. Large-scale dune erosion tests to study the influence of wave periods. *Coastal Engineering,* Volume 55, pp. 1041-1051.

van Rijn, L. C., 1984a. Sediment Transport, Part I: Bed Load Transport. *Journal of Hydraulic Engineering,* 110(10), pp. 1431-1456.

van Rijn, L. C., 1984b. Sediment Transport, Part II: Suspended Load Transport. *Journal of Hydraulic Engineering,* 110(11), pp. 1613-1641.

Wijnberg, A. R., 1993. *Design Sea Levels for Southern Africa: A Probabilistic Approach. PhD Dissertation,* Cape Town: University of Cape Town.

CONTROLLED DISCLOSURE

When downloaded from the EDS database, this document is uncontrolled and the responsibility rests with the user to ensure it is in line with the authorised version on the database.

APPENDIX A: STORM WAVE RUN-UP RESULTS

CONTROLLED DISCLOSURE

When downloaded from the EDS database, this document is uncontrolled and the responsibility rests with the user to ensure it is in line with the authorised version on the database.

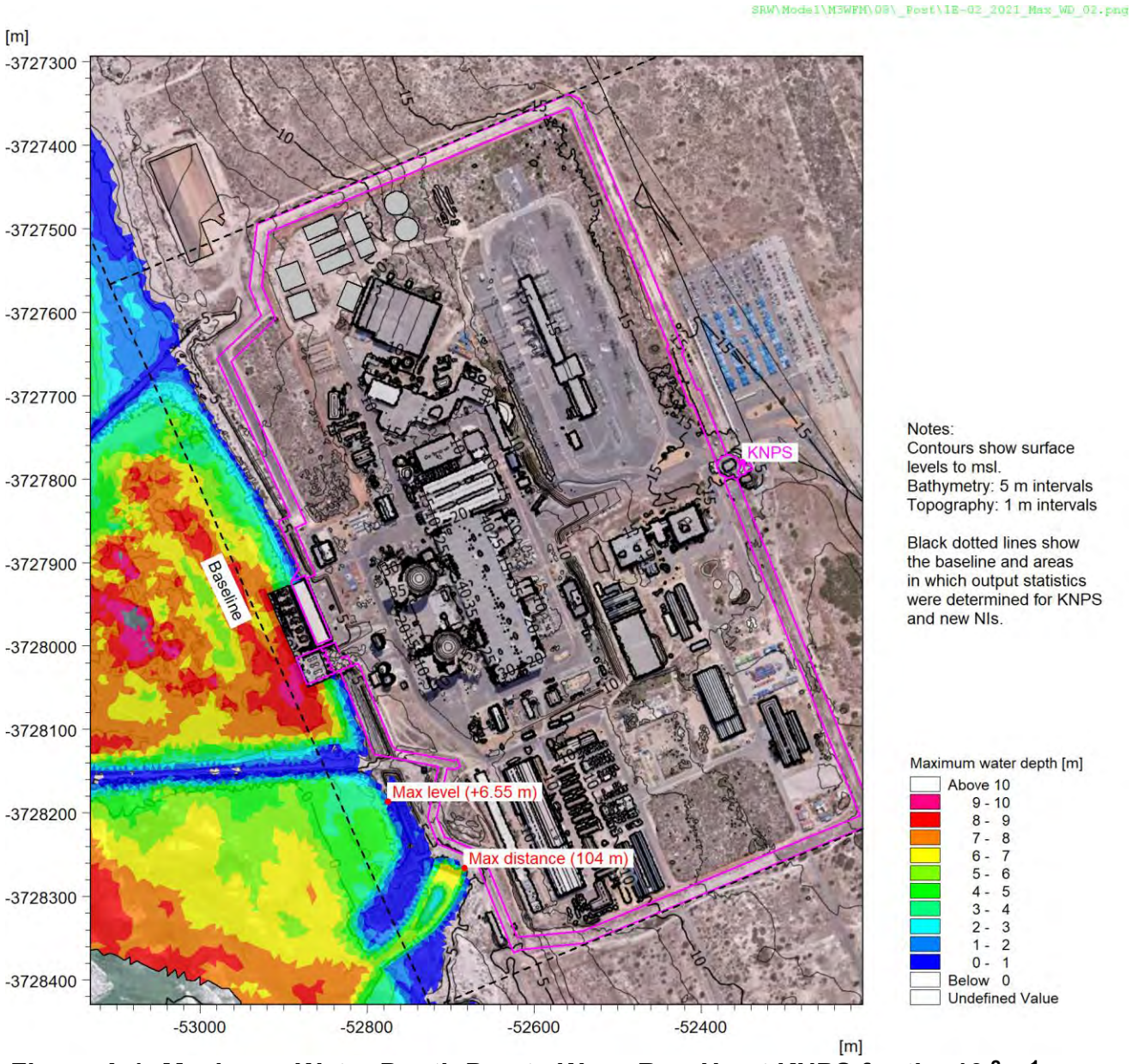


Figure A.1: Maximum Water Depth Due to Wave Run-Up at KNPS for the 10^{-2} y^{-1} Storm in 2021.

CONTROLLED DISCLOSURE

When downloaded from the EDS database, this document is uncontrolled and the responsibility rests with the user to ensure it is in line with the authorised version on the database.

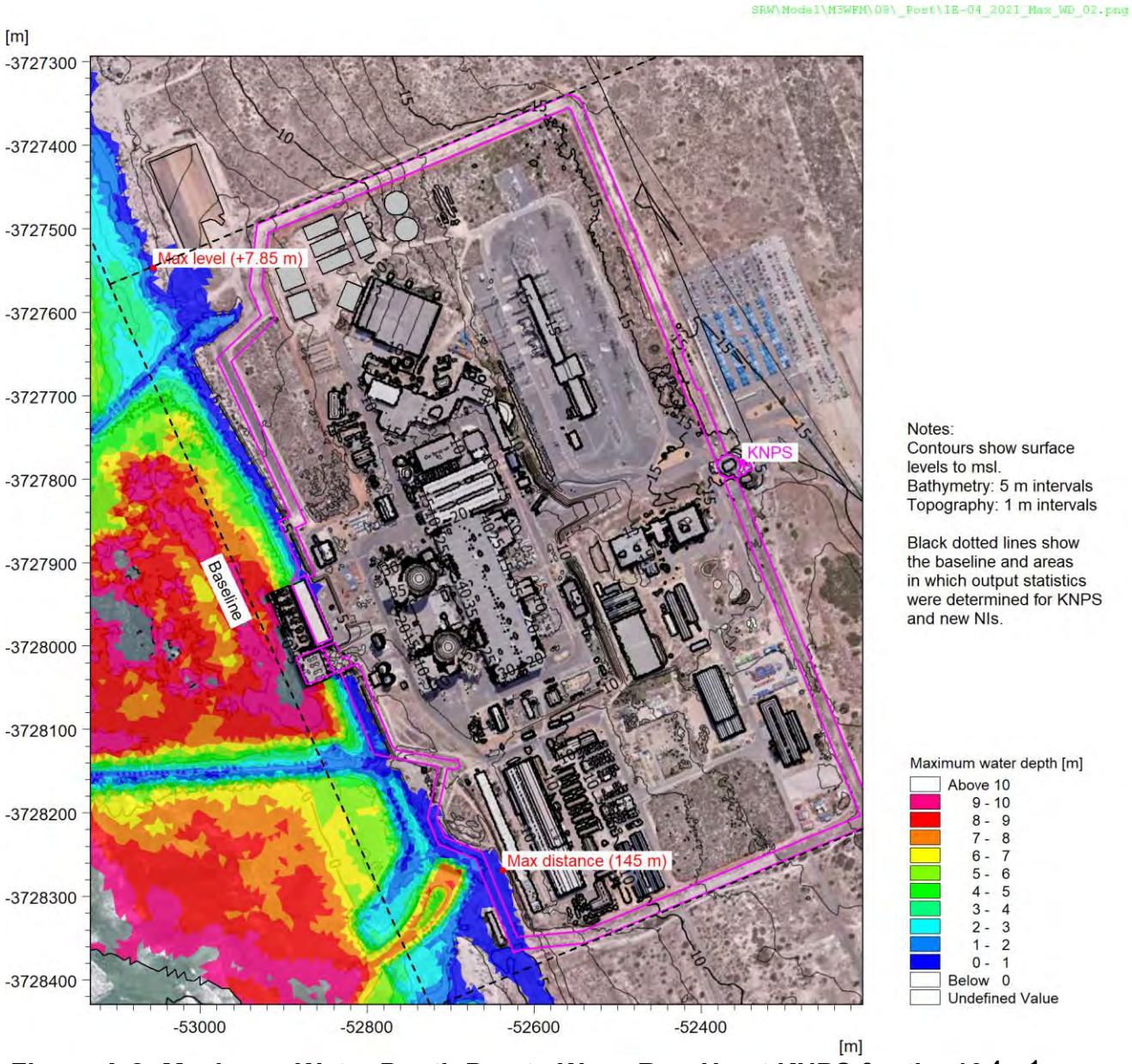


Figure A.2: Maximum Water Depth Due to Wave Run-Up at KNPS for the 10^{-4} y^{-1} Storm in 2021.

CONTROLLED DISCLOSURE

When downloaded from the EDS database, this document is uncontrolled and the responsibility rests with the user to ensure it is in line with the authorised version on the database.

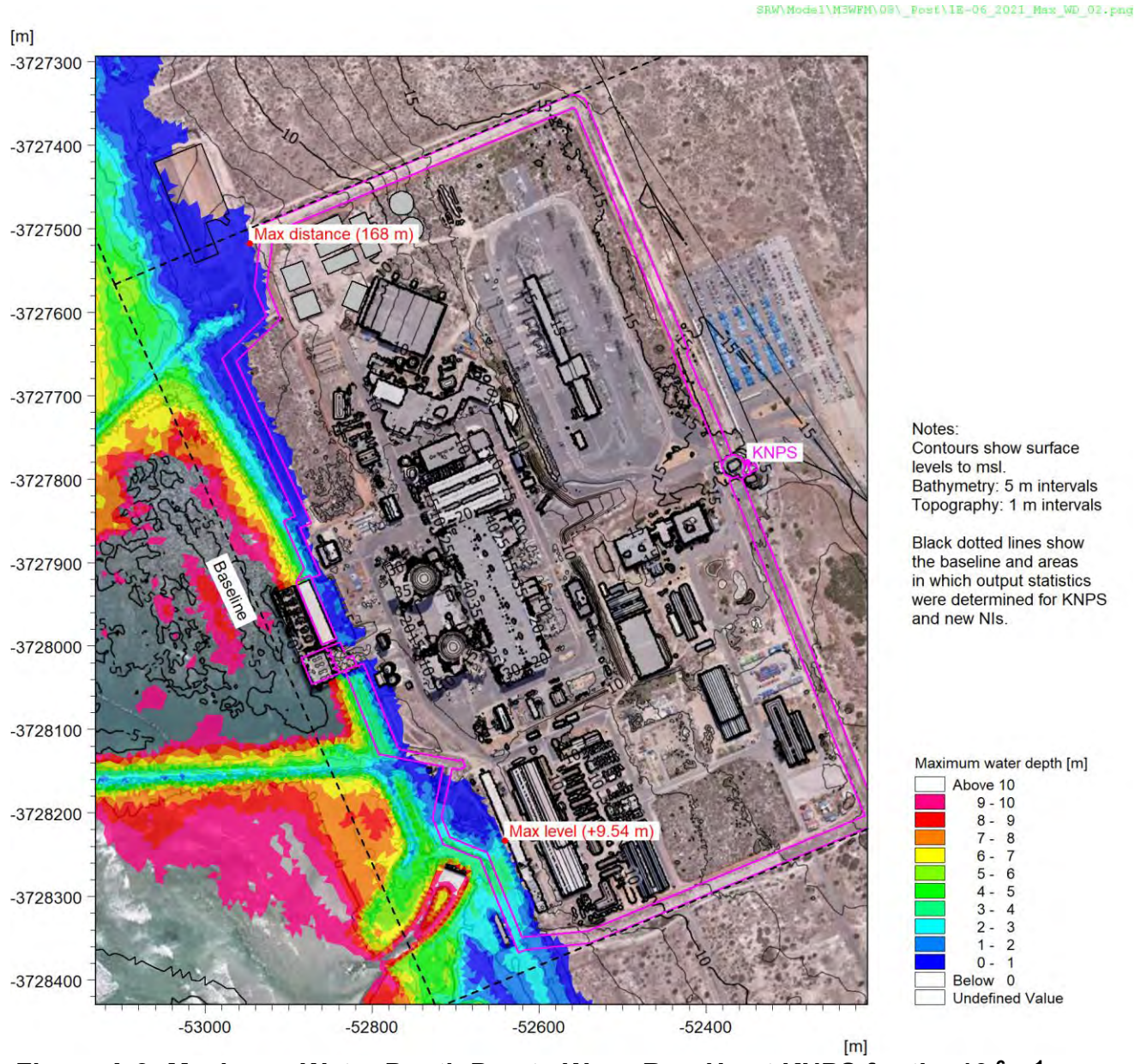


Figure A.3: Maximum Water Depth Due to Wave Run-Up at KNPS for the 10^{-6} y^{-1} Storm in 2021.

CONTROLLED DISCLOSURE

When downloaded from the EDS database, this document is uncontrolled and the responsibility rests with the user to ensure it is in line with the authorised version on the database.

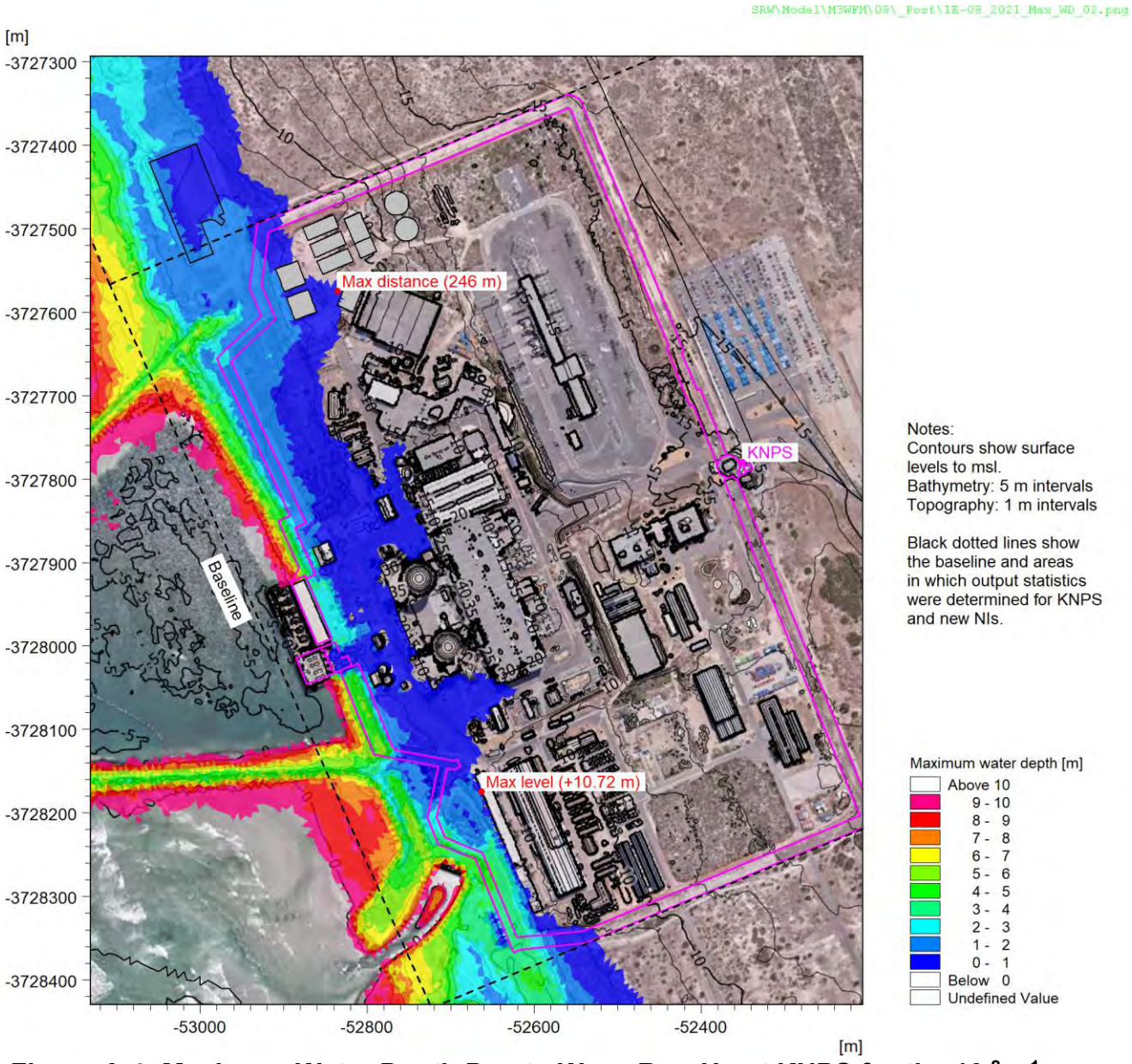


Figure A.4: Maximum Water Depth Due to Wave Run-Up at KNPS for the 10^{-8} y^{-1} Storm in 2021.

CONTROLLED DISCLOSURE

When downloaded from the EDS database, this document is uncontrolled and the responsibility rests with the user to ensure it is in line with the authorised version on the database.

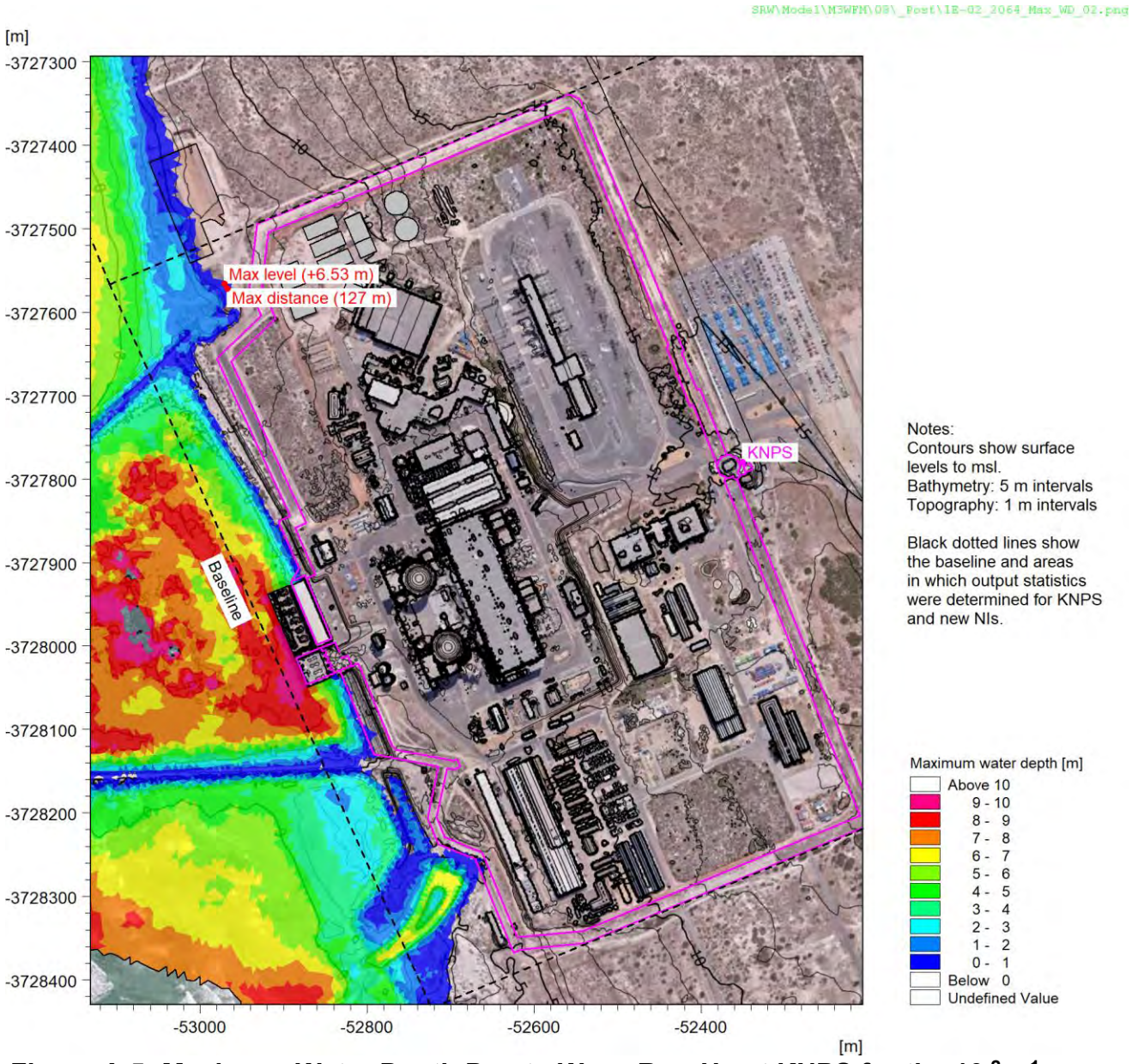


Figure A.5: Maximum Water Depth Due to Wave Run-Up at KNPS for the 10^{-2} y^{-1} Storm in 2064.

CONTROLLED DISCLOSURE

When downloaded from the EDS database, this document is uncontrolled and the responsibility rests with the user to ensure it is in line with the authorised version on the database.

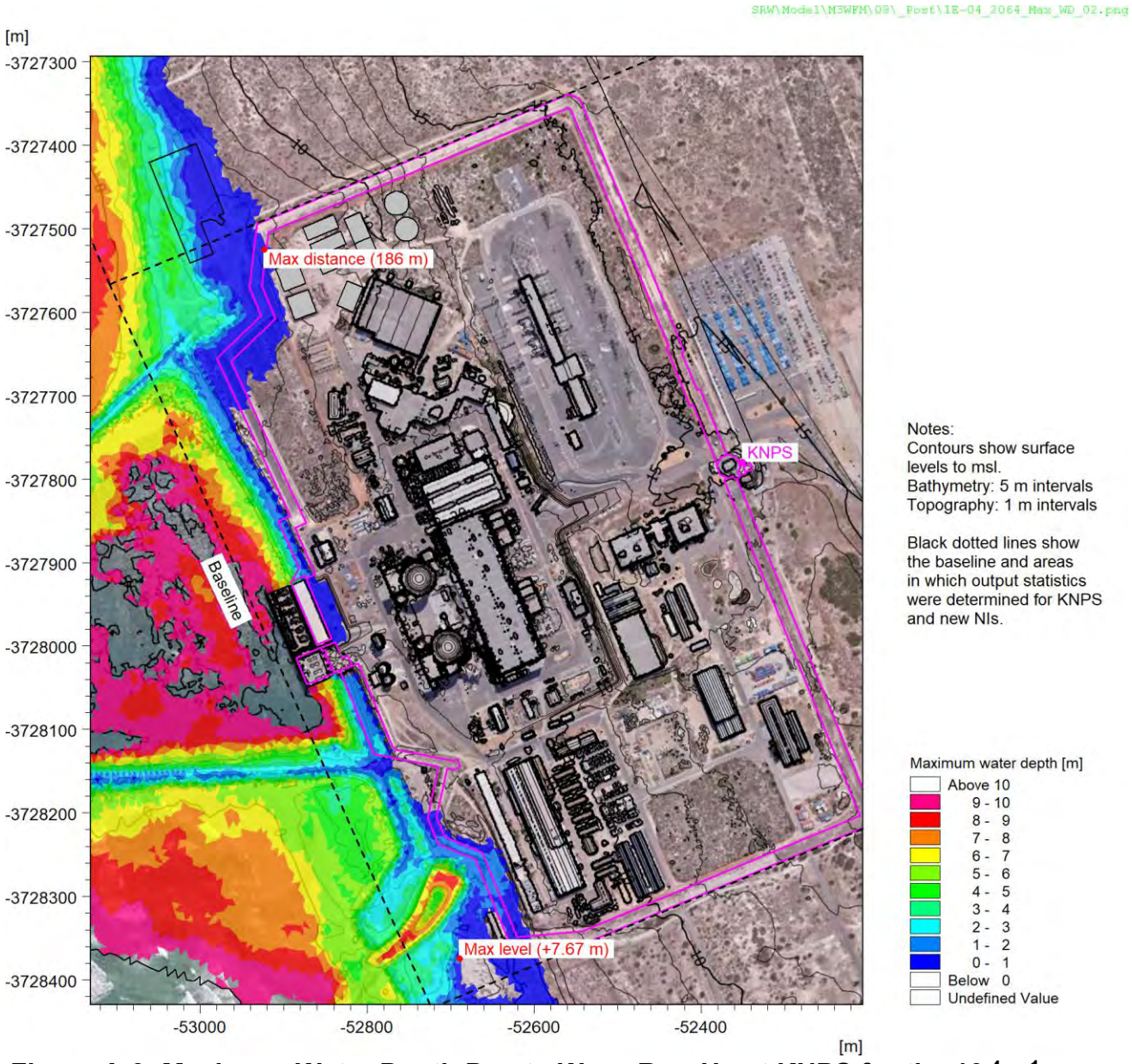


Figure A.6: Maximum Water Depth Due to Wave Run-Up at KNPS for the 10^{-4} y^{-1} Storm in 2064.

CONTROLLED DISCLOSURE

When downloaded from the EDS database, this document is uncontrolled and the responsibility rests with the user to ensure it is in line with the authorised version on the database.

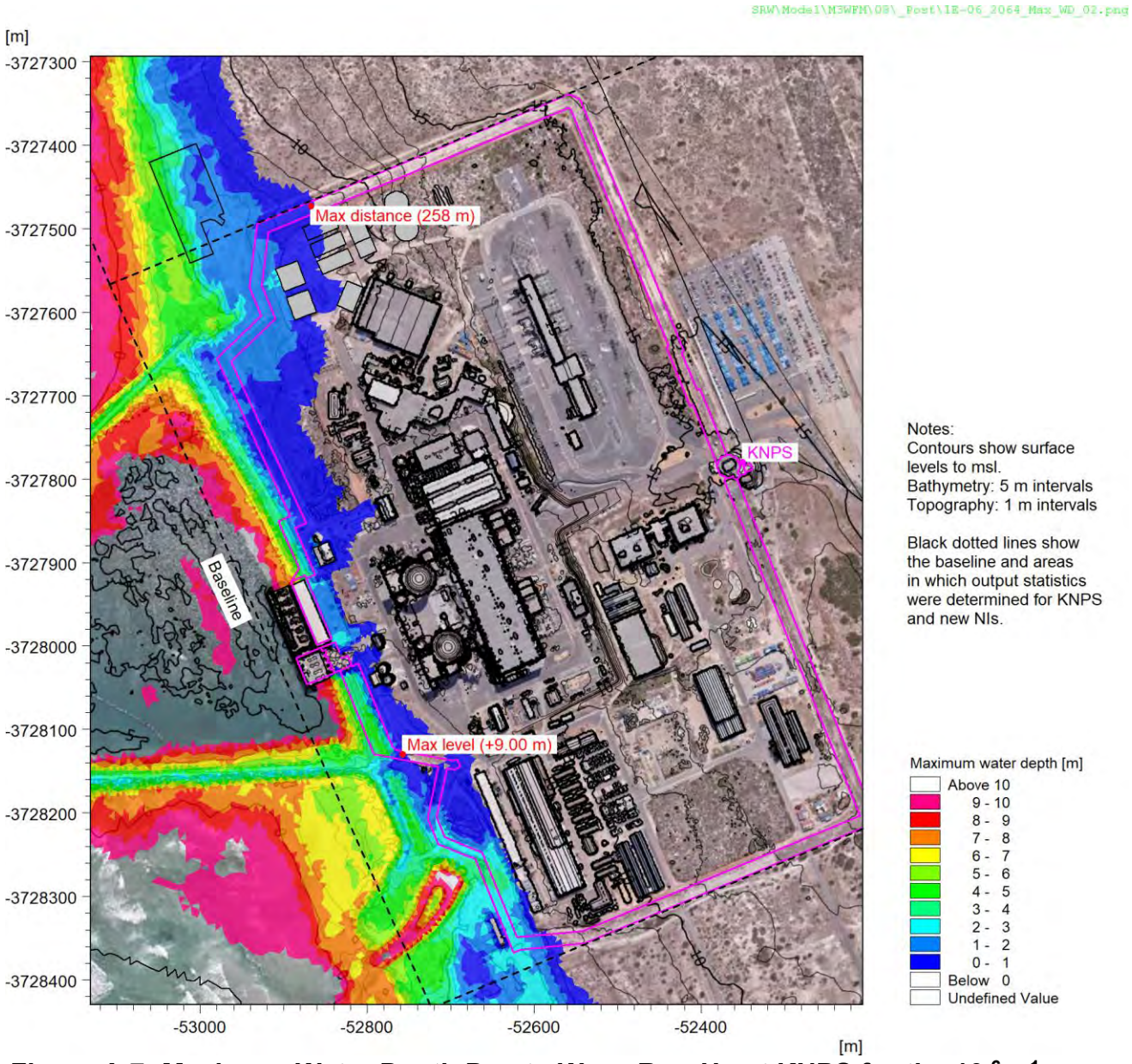


Figure A.7: Maximum Water Depth Due to Wave Run-Up at KNPS for the 10^{-6} y^{-1} Storm in 2064.

CONTROLLED DISCLOSURE

When downloaded from the EDS database, this document is uncontrolled and the responsibility rests with the user to ensure it is in line with the authorised version on the database.

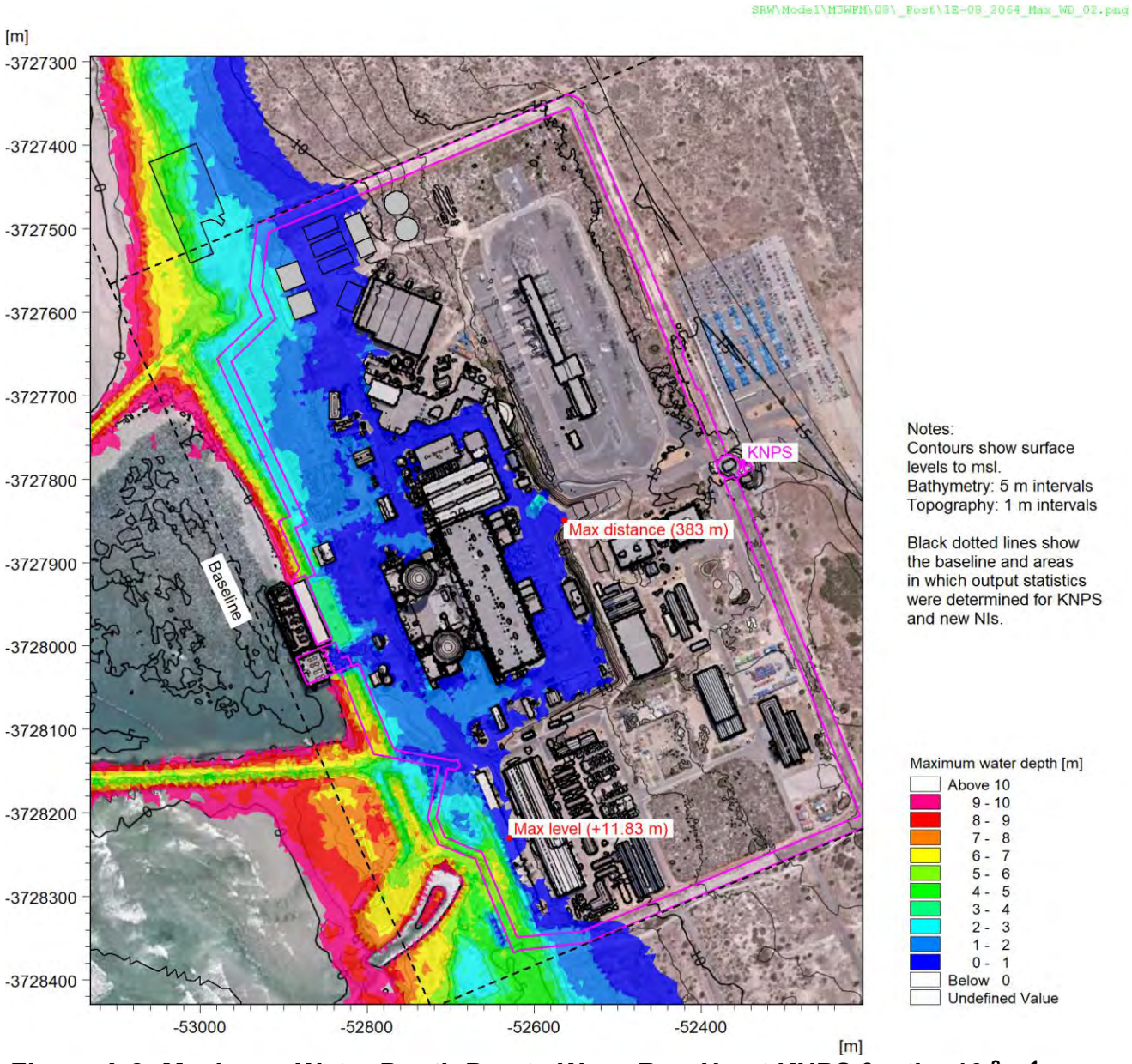


Figure A.8: Maximum Water Depth Due to Wave Run-Up at KNPS for the 10^{-8} y^{-1} Storm in 2064.

CONTROLLED DISCLOSURE

When downloaded from the EDS database, this document is uncontrolled and the responsibility rests with the user to ensure it is in line with the authorised version on the database.

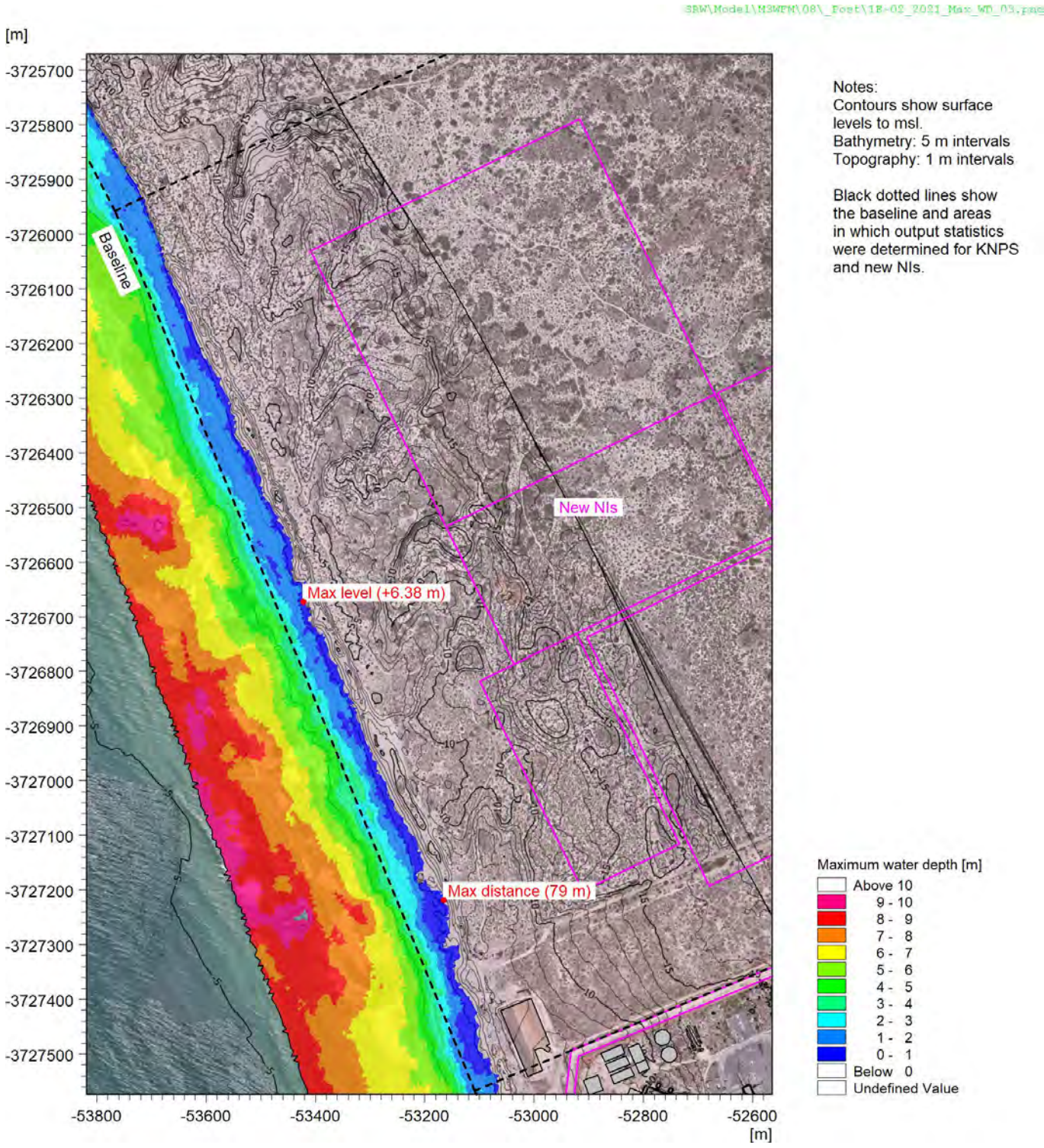


Figure A.9: Maximum Water Depth Due to Wave Run-Up at the New NIs for the 10^{-2} y^{-1} Storm in 2021.

CONTROLLED DISCLOSURE

When downloaded from the EDS database, this document is uncontrolled and the responsibility rests with the user to ensure it is in line with the authorised version on the database.

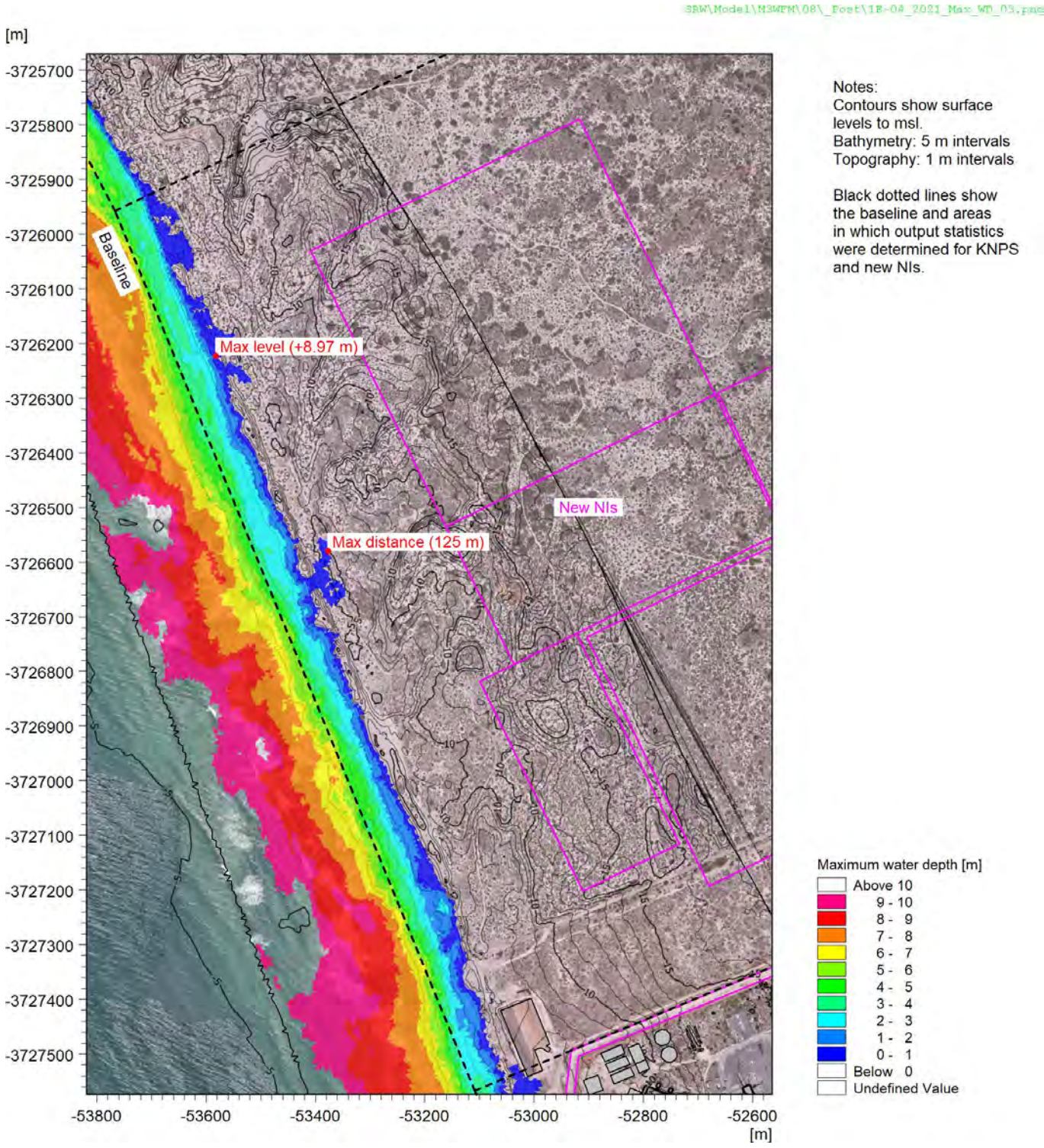


Figure A.10: Maximum Water Depth Due to Wave Run-Up at the New NIs for the 10^{-4} y^{-1} Storm in 2021.

CONTROLLED DISCLOSURE

When downloaded from the EDS database, this document is uncontrolled and the responsibility rests with the user to ensure it is in line with the authorised version on the database.

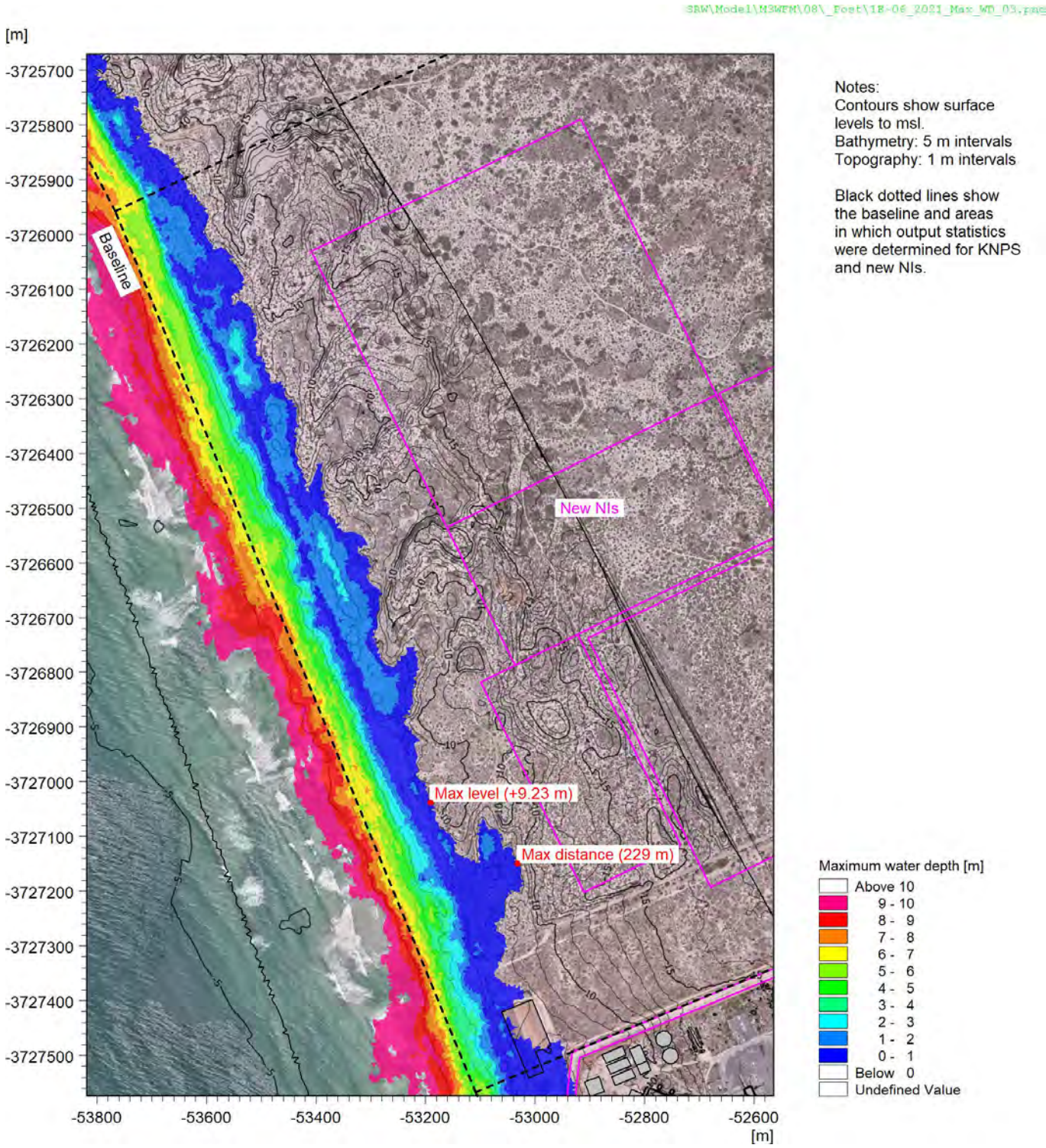


Figure A.11: Maximum Water Depth Due to Wave Run-Up at the New NIs for the 10^{-6} y^{-1} Storm in 2021.

CONTROLLED DISCLOSURE

When downloaded from the EDS database, this document is uncontrolled and the responsibility rests with the user to ensure it is in line with the authorised version on the database.

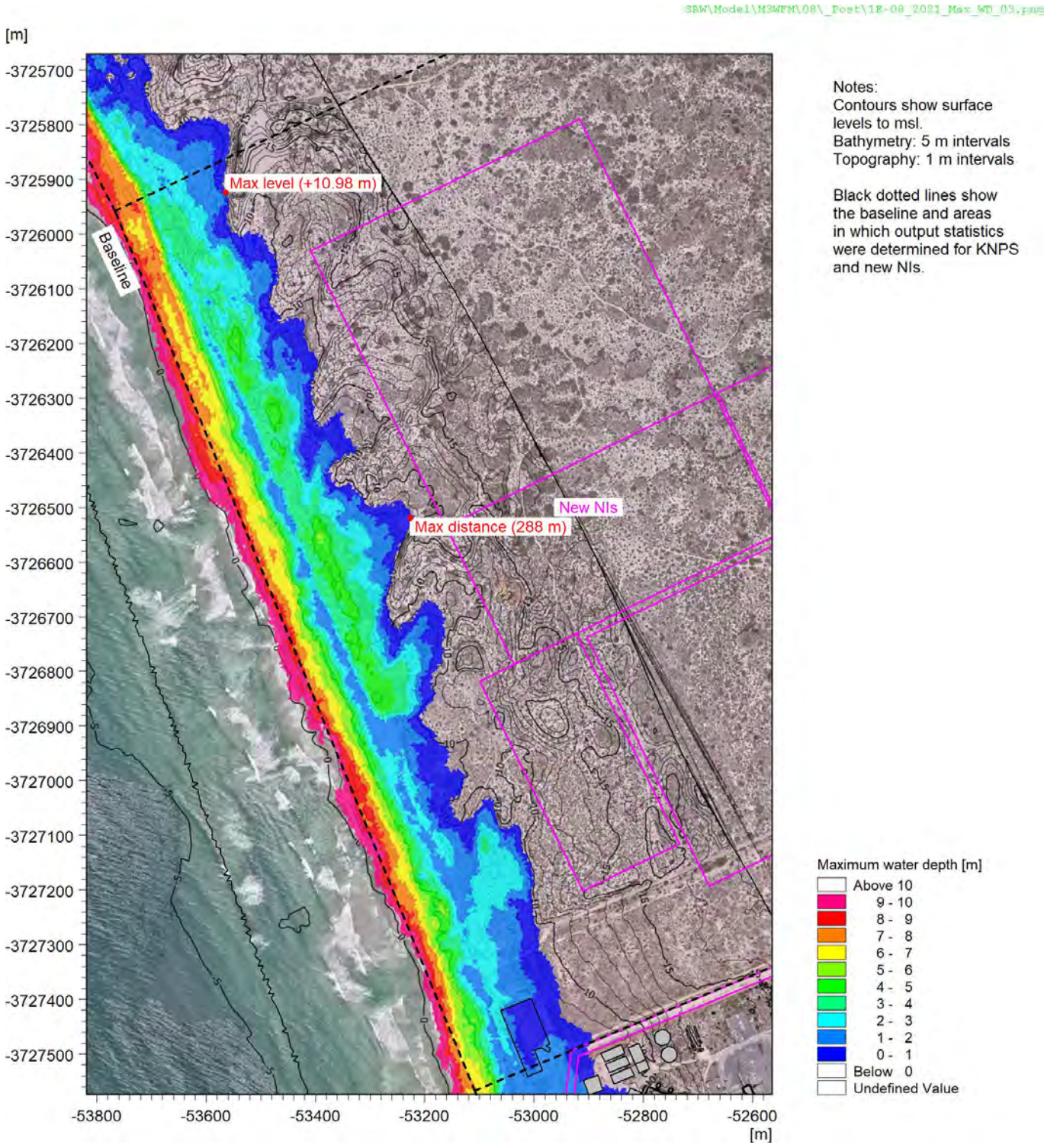


Figure A.12: Maximum Water Depth Due to Wave Run-Up at the New NIs for the 10^{-8} y^{-1} Storm in 2021.

CONTROLLED DISCLOSURE

When downloaded from the EDS database, this document is uncontrolled and the responsibility rests with the user to ensure it is in line with the authorised version on the database.

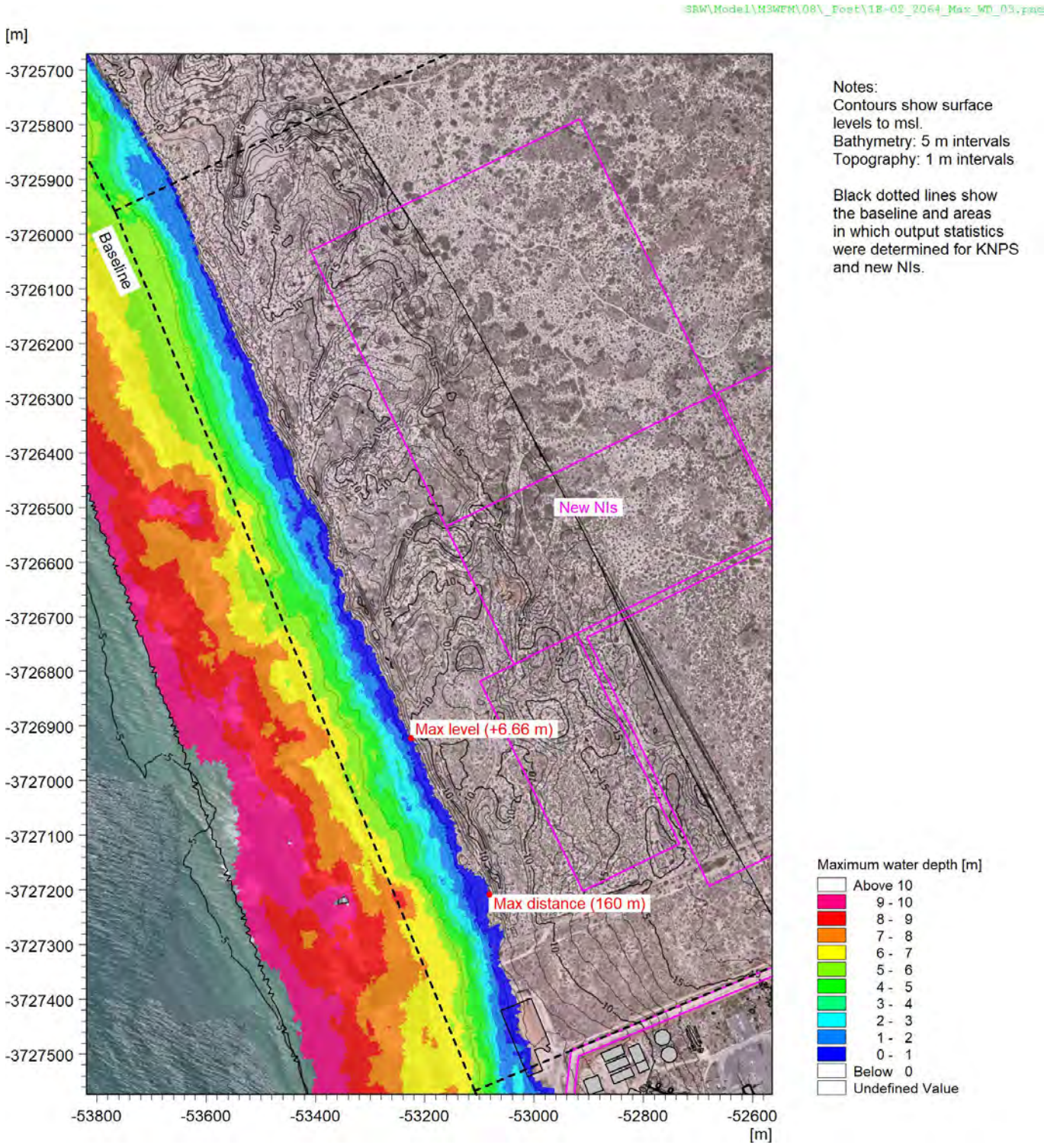


Figure A.13: Maximum Water Depth Due to Wave Run-Up at the New NIs for the 10^{-2} y^{-1} Storm in 2064.

CONTROLLED DISCLOSURE

When downloaded from the EDS database, this document is uncontrolled and the responsibility rests with the user to ensure it is in line with the authorised version on the database.

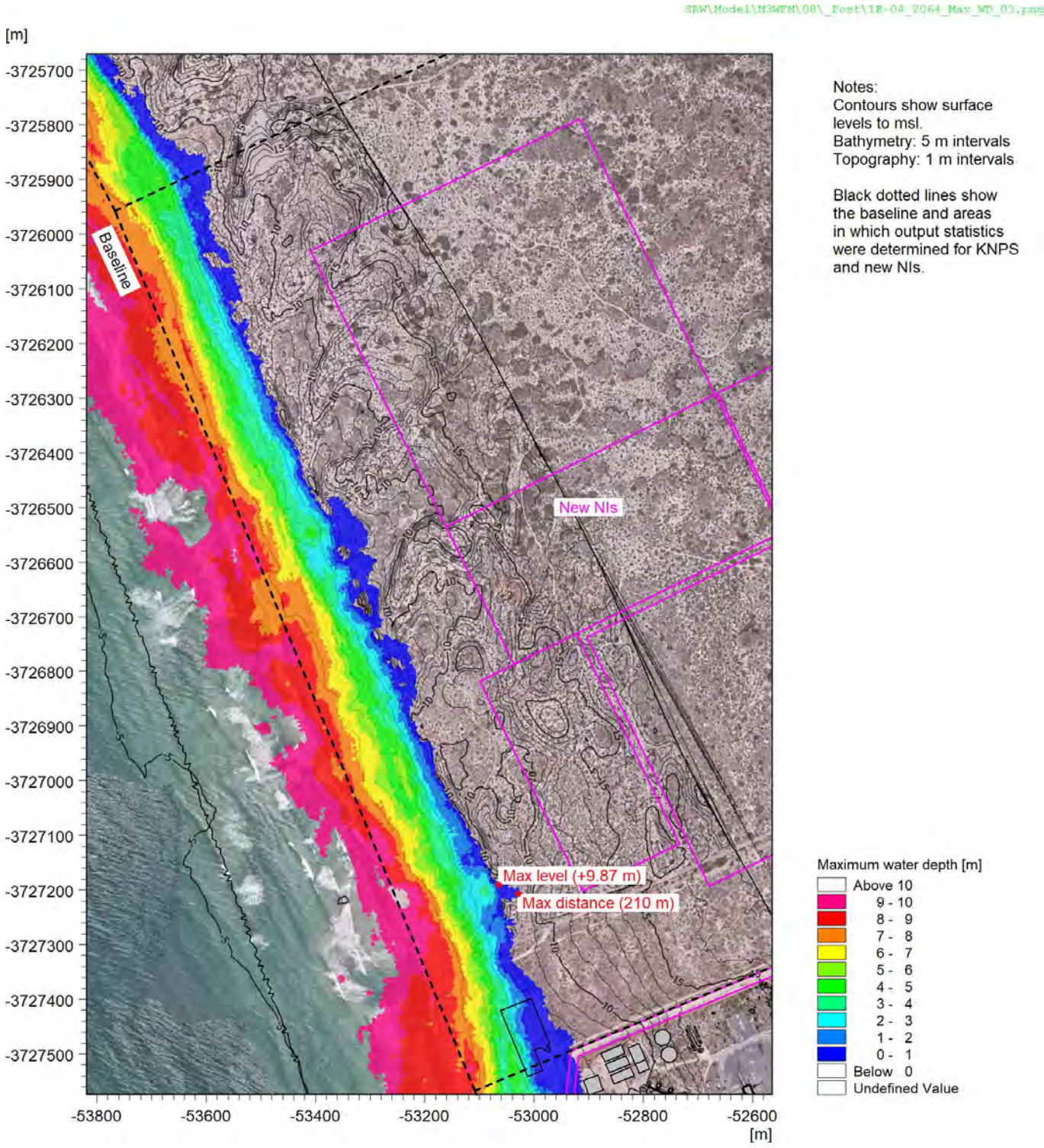


Figure A.14: Maximum Water Depth Due to Wave Run-Up at the New NIs for the 10^{-4} y^{-1} Storm in 2064.

CONTROLLED DISCLOSURE

When downloaded from the EDS database, this document is uncontrolled and the responsibility rests with the user to ensure it is in line with the authorised version on the database.

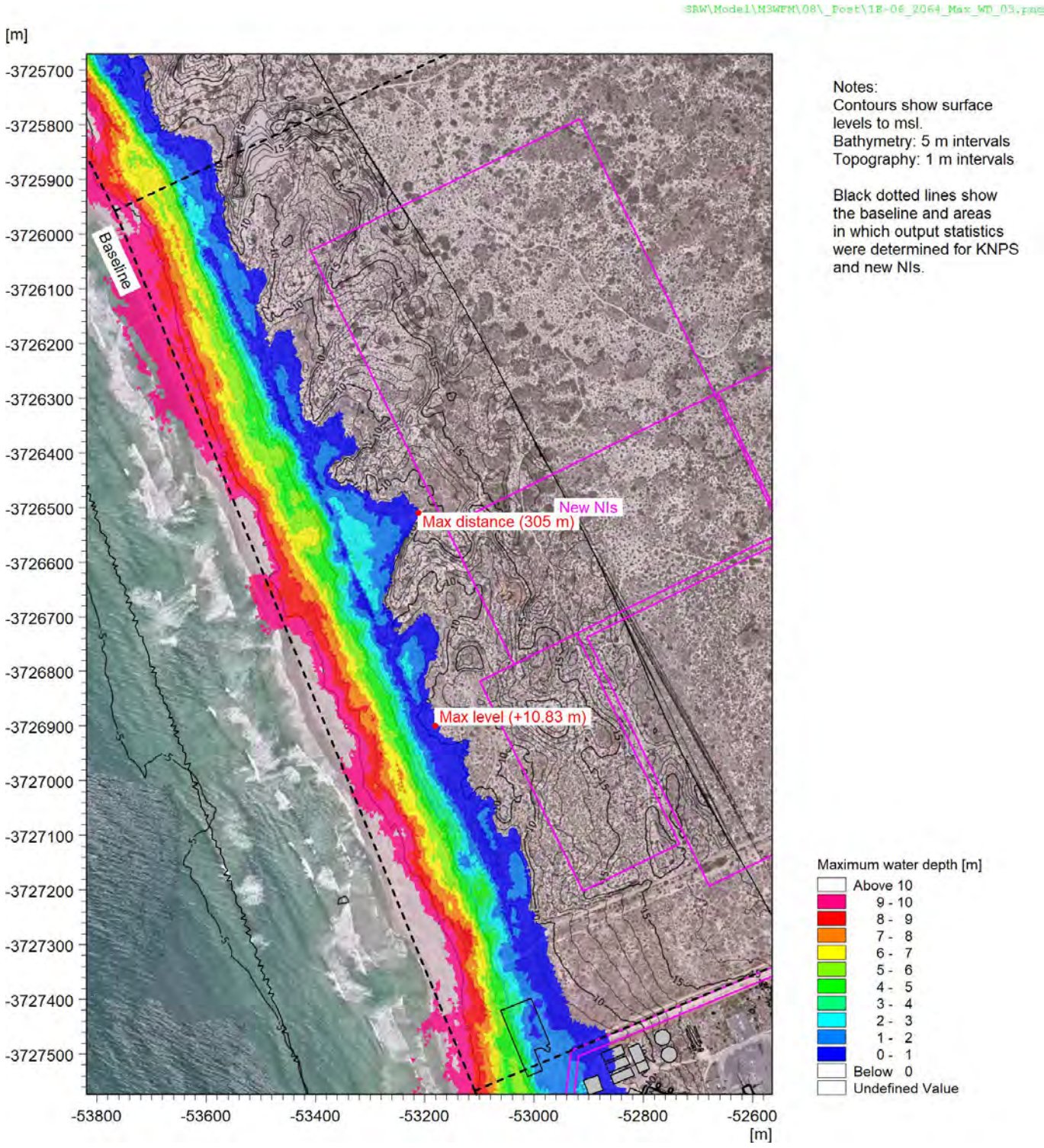


Figure A.15: Maximum Water Depth Due to Wave Run-Up at the New NIs for the 10^{-6} y^{-1} Storm in 2064.

CONTROLLED DISCLOSURE

When downloaded from the EDS database, this document is uncontrolled and the responsibility rests with the user to ensure it is in line with the authorised version on the database.

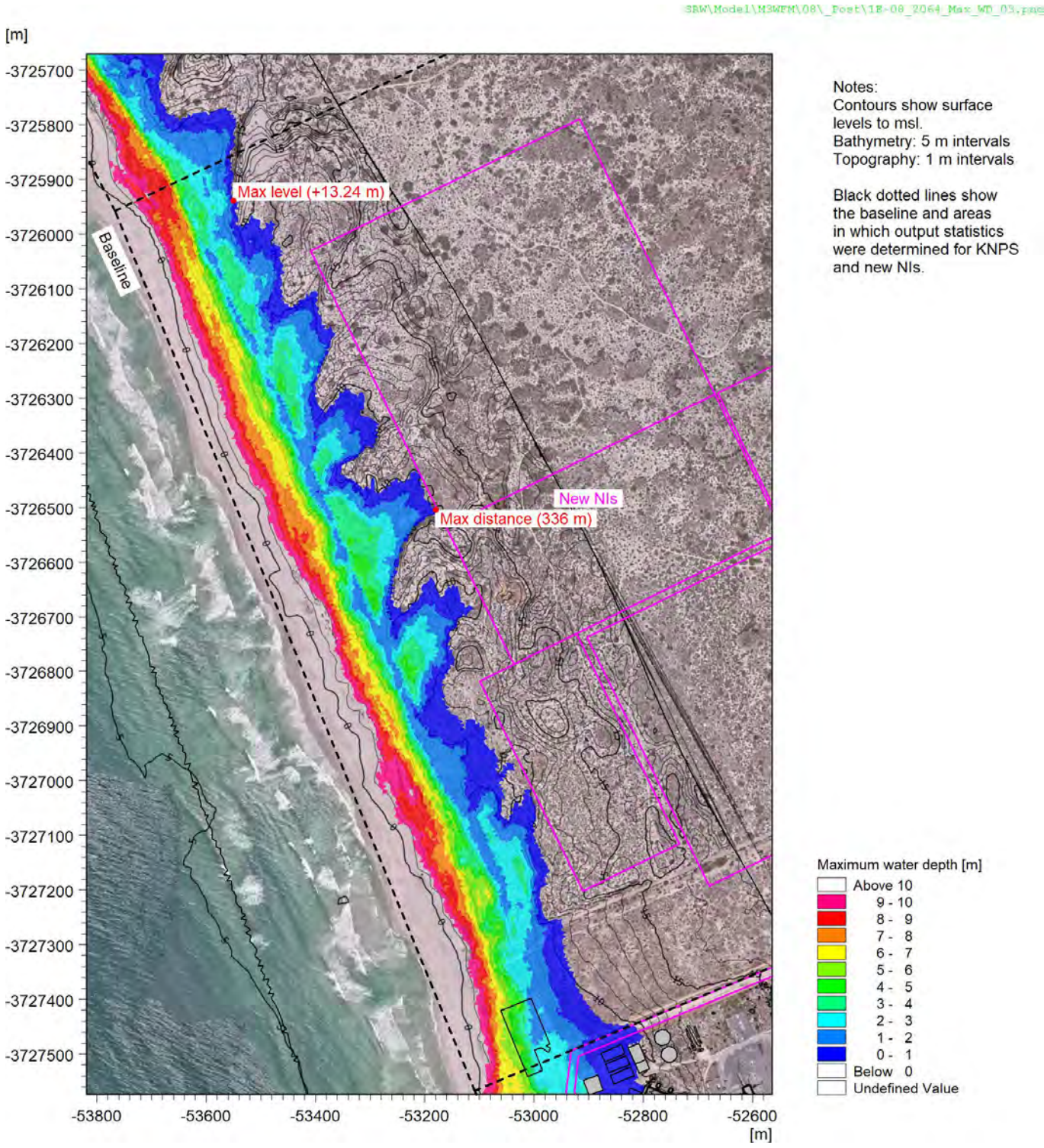


Figure A.16: Maximum Water Depth Due to Wave Run-Up at the New NIs for the 10^{-8} y^{-1} Storm in 2064.

CONTROLLED DISCLOSURE

When downloaded from the EDS database, this document is uncontrolled and the responsibility rests with the user to ensure it is in line with the authorised version on the database.

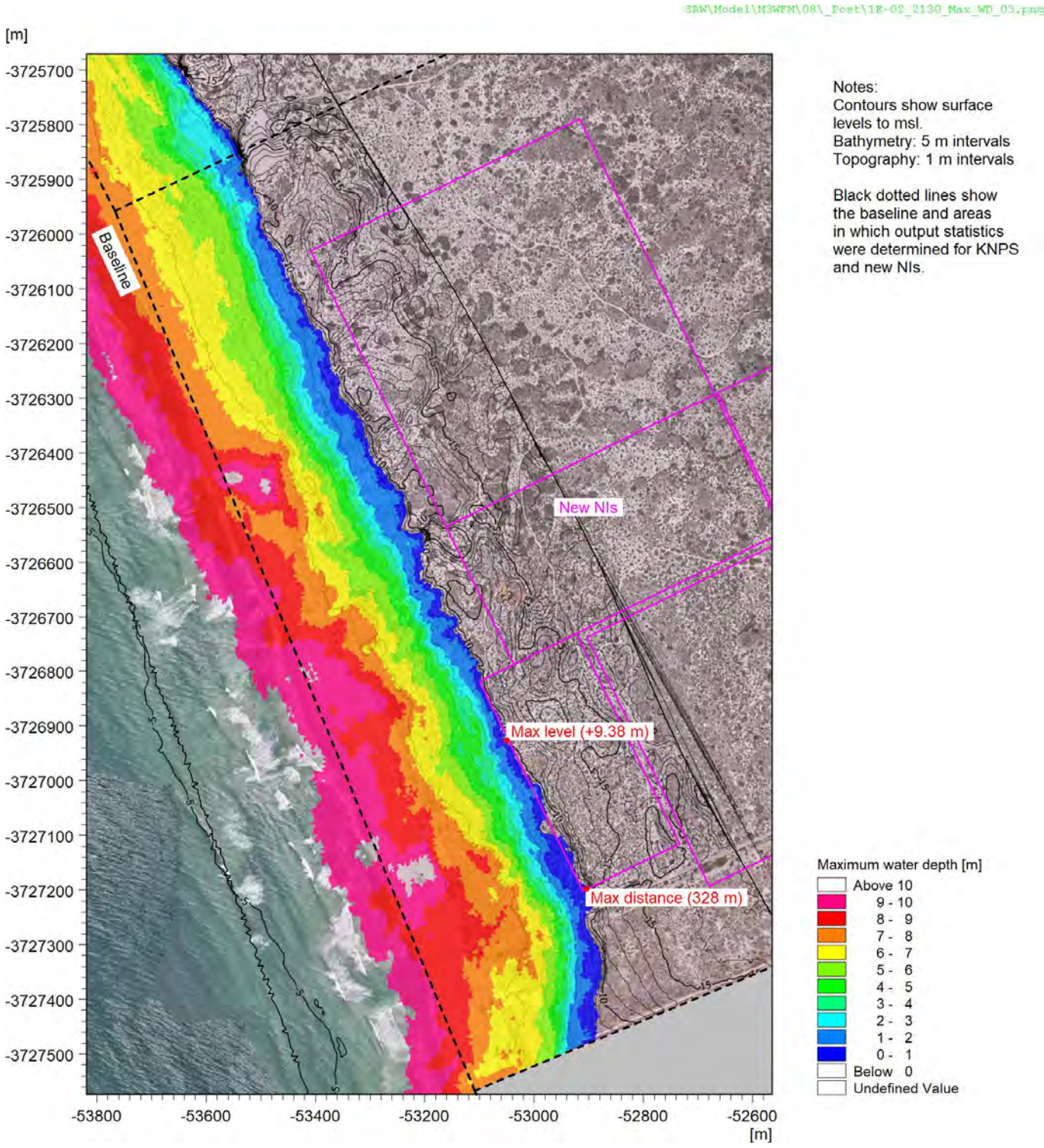


Figure A.17: Maximum Water Depth Due to Wave Run-Up at the New NIs for the 10^{-2} y^{-1} Storm in 2130.

CONTROLLED DISCLOSURE

When downloaded from the EDS database, this document is uncontrolled and the responsibility rests with the user to ensure it is in line with the authorised version on the database.

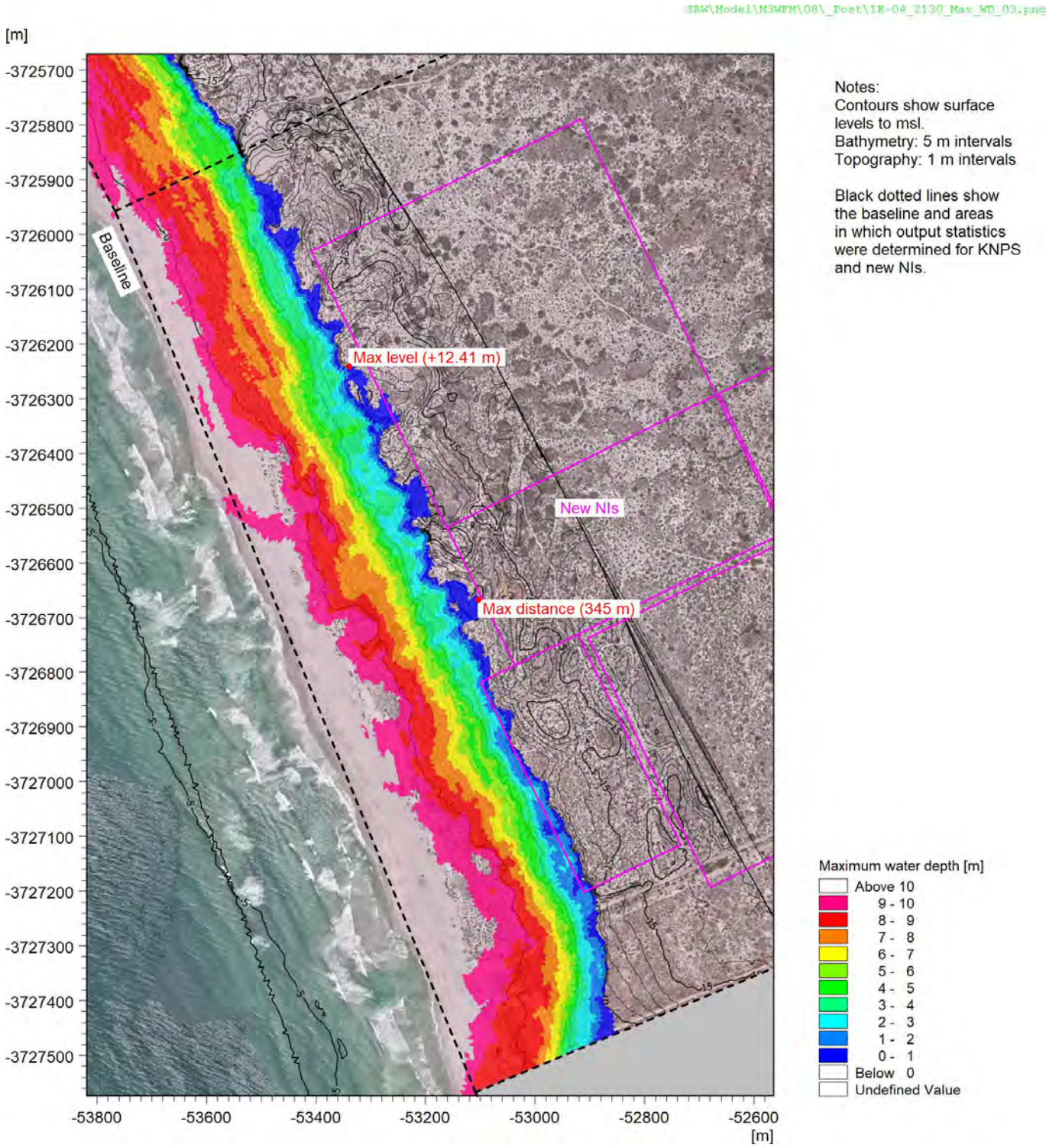


Figure A.18: Maximum Water Depth Due to Wave Run-Up at the New NIs for the 10^{-4} y^{-1} Storm in 2130.

CONTROLLED DISCLOSURE

When downloaded from the EDS database, this document is uncontrolled and the responsibility rests with the user to ensure it is in line with the authorised version on the database.

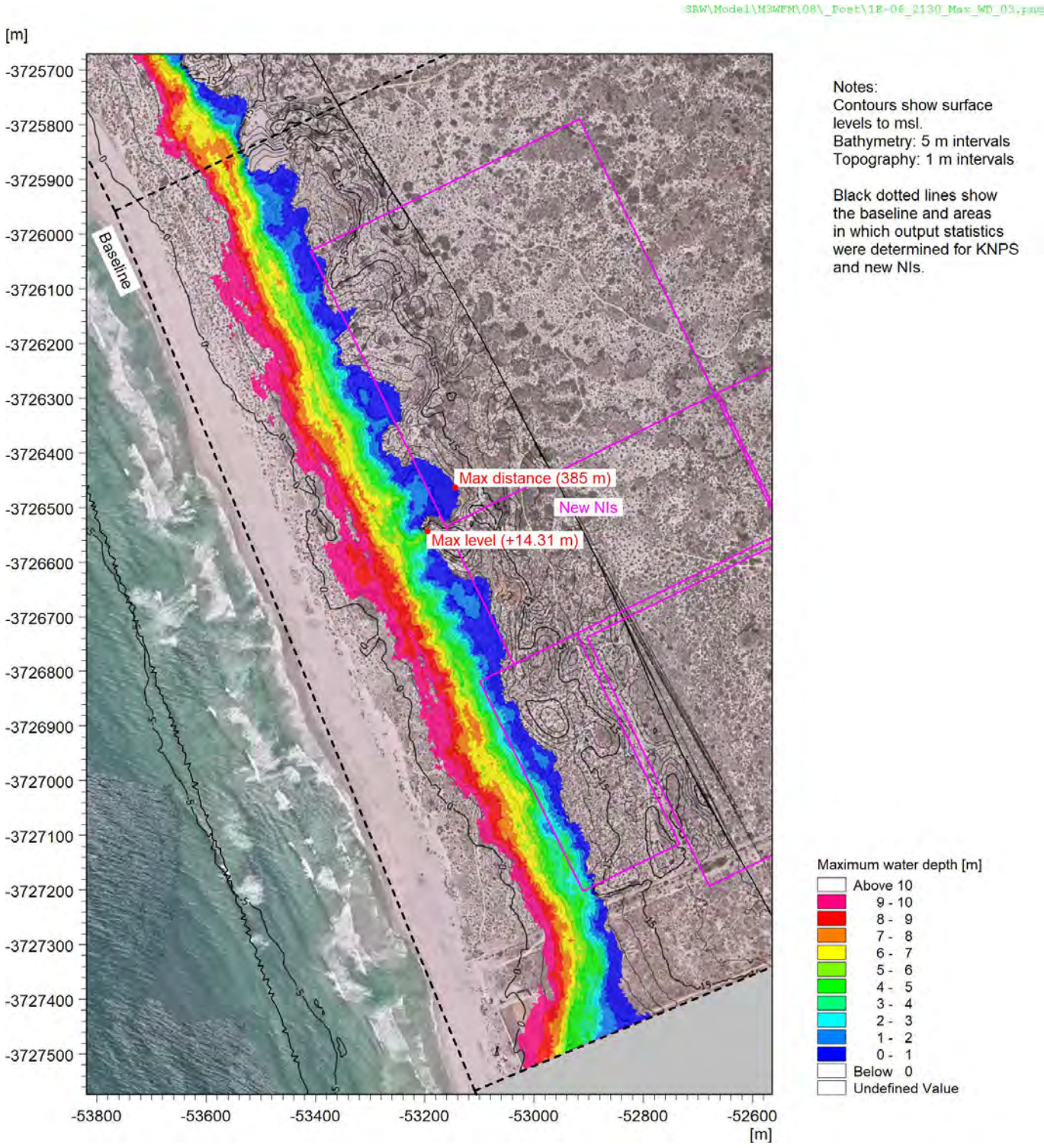


Figure A.19: Maximum Water Depth Due to Wave Run-Up at the New NIs for the 10^{-6} y^{-1} Storm in 2130.

CONTROLLED DISCLOSURE

When downloaded from the EDS database, this document is uncontrolled and the responsibility rests with the user to ensure it is in line with the authorised version on the database.

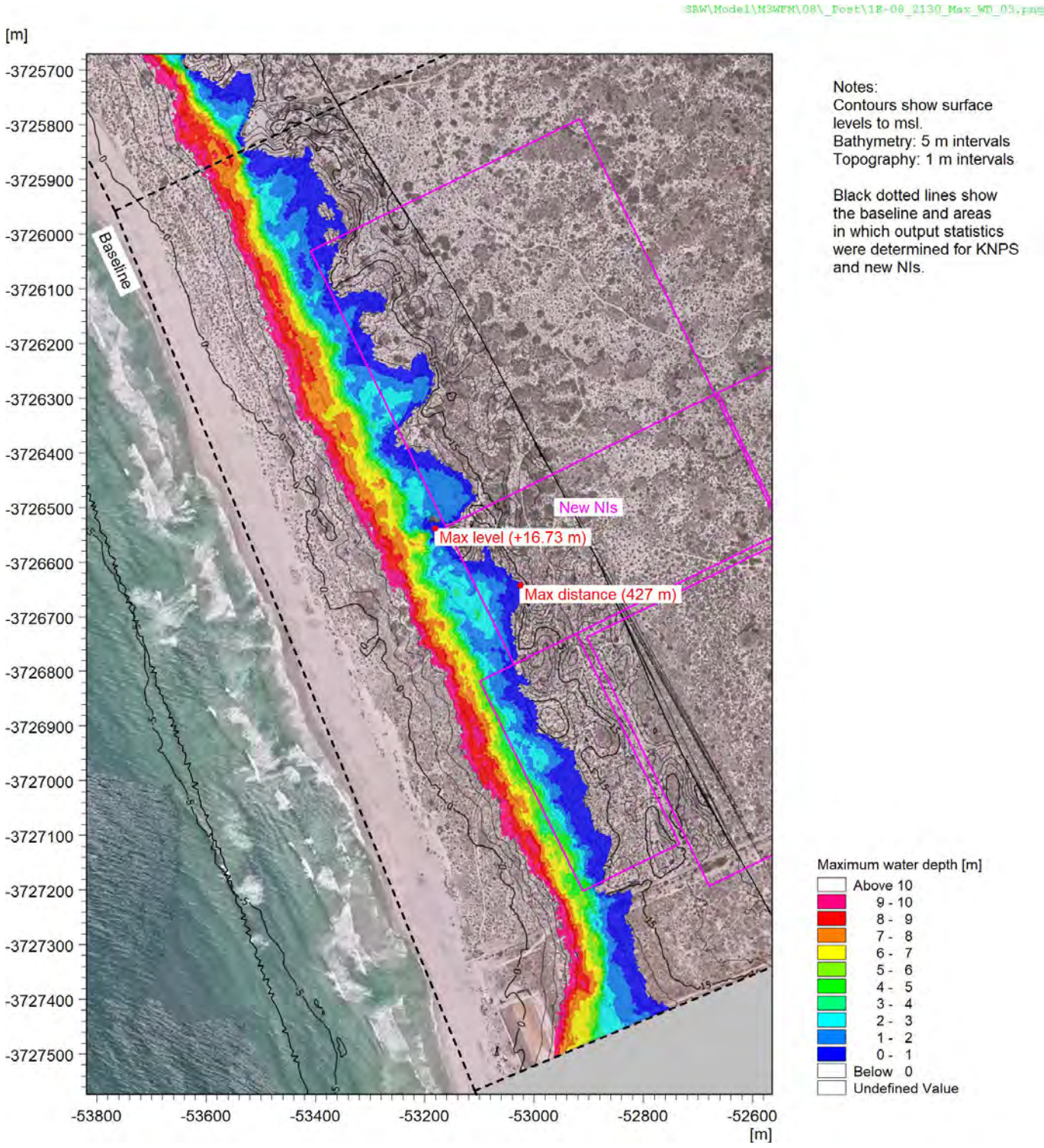


Figure A.20: Maximum Water Depth Due to Wave Run-Up at the New NIs for the 10^{-8} y^{-1} Storm in 2130.

CONTROLLED DISCLOSURE

When downloaded from the EDS database, this document is uncontrolled and the responsibility rests with the user to ensure it is in line with the authorised version on the database.

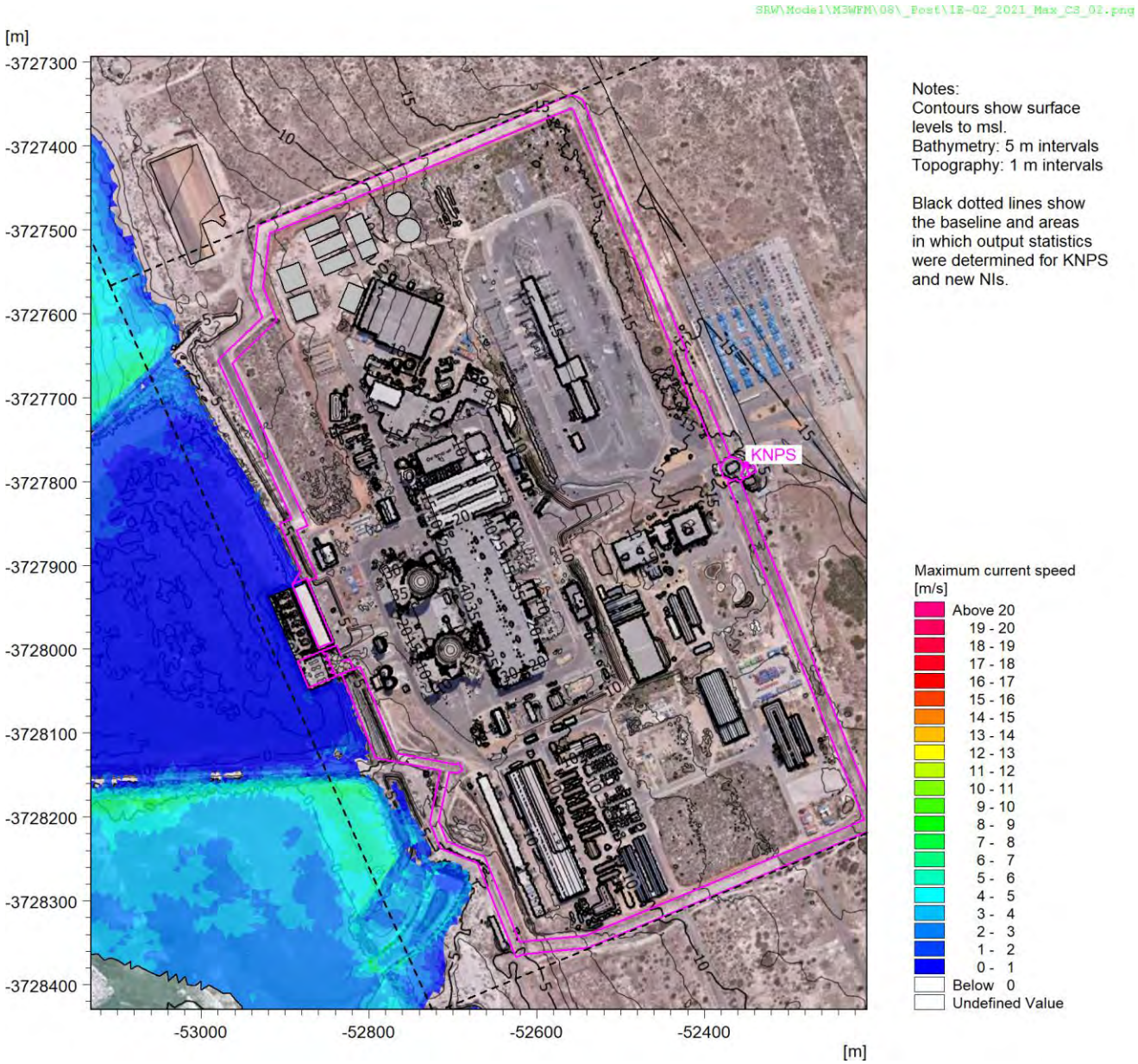


Figure A.21: Maximum Depth-Averaged Current Speed Due to Wave Run-Up at KNPS for the 10^{-2} y^{-1} Storm in 2021.

CONTROLLED DISCLOSURE

When downloaded from the EDS database, this document is uncontrolled and the responsibility rests with the user to ensure it is in line with the authorised version on the database.

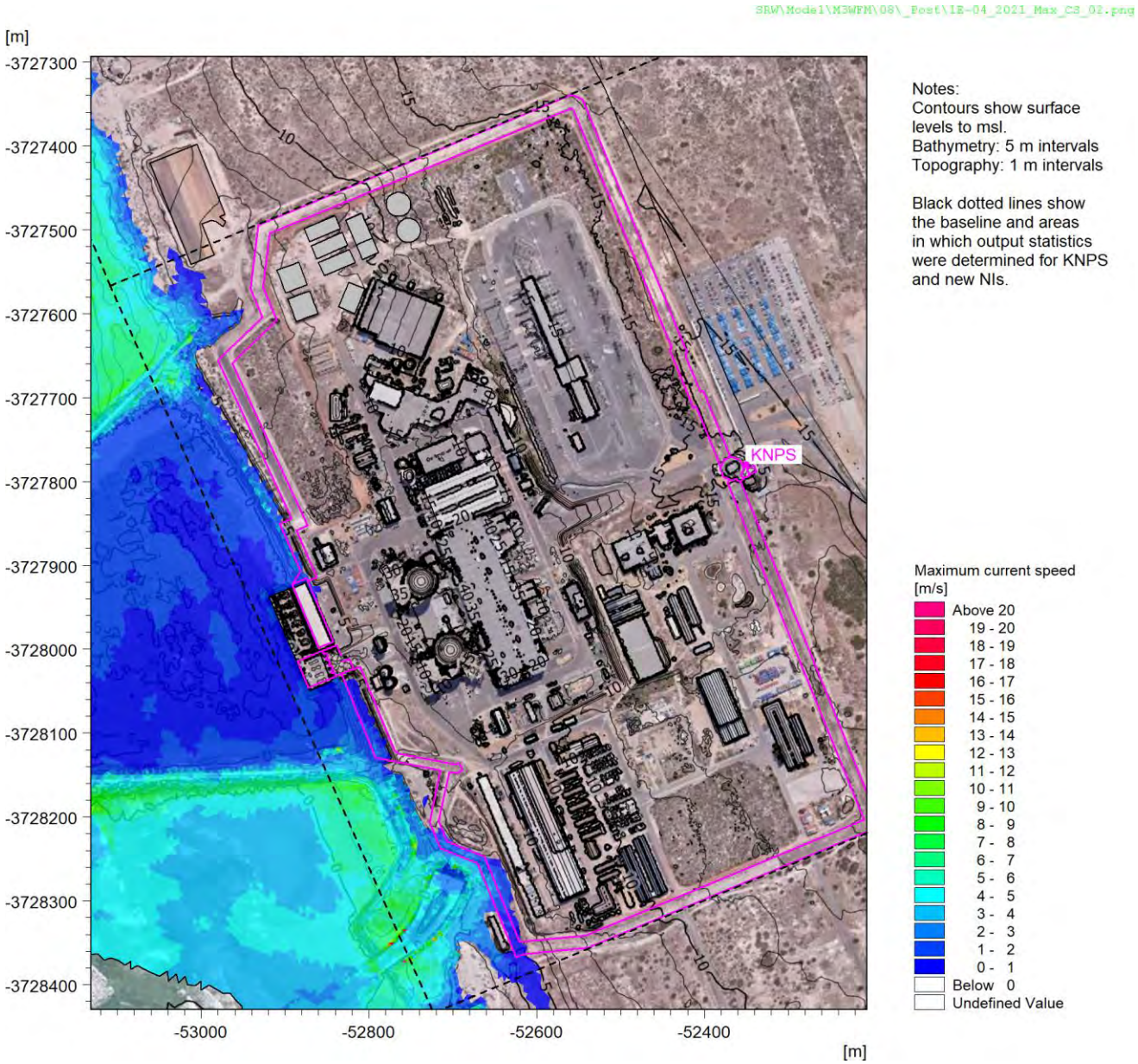


Figure A.22: Maximum Depth-Averaged Current Speed Due to Wave Run-Up at KNPS for the 10^{-4} y^{-1} Storm in 2021.

CONTROLLED DISCLOSURE

When downloaded from the EDS database, this document is uncontrolled and the responsibility rests with the user to ensure it is in line with the authorised version on the database.

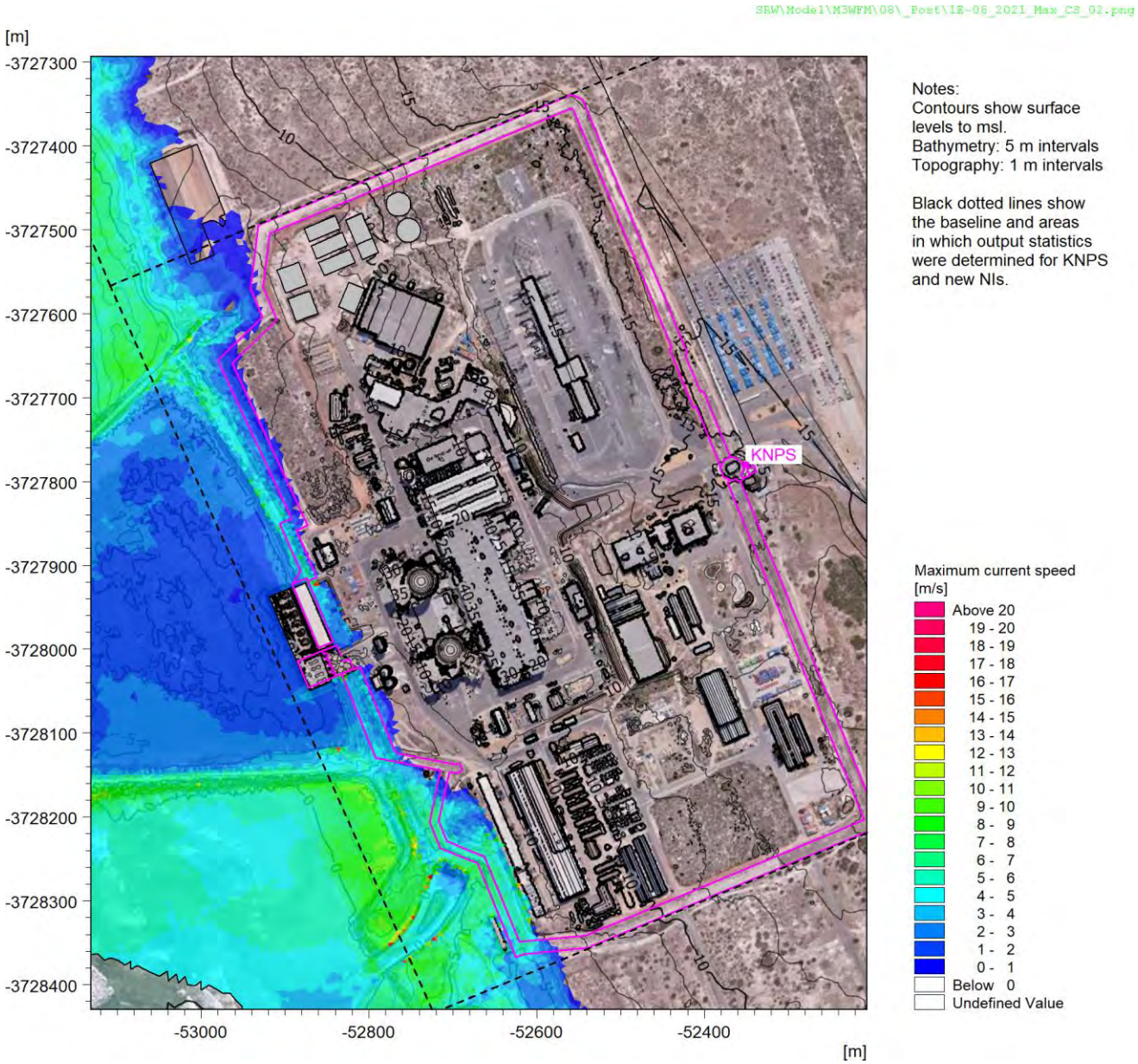


Figure A.23: Maximum Depth-Averaged Current Speed Due to Wave Run-Up at KNPS for the 10^{-6} y^{-1} Storm in 2021.

CONTROLLED DISCLOSURE

When downloaded from the EDS database, this document is uncontrolled and the responsibility rests with the user to ensure it is in line with the authorised version on the database.

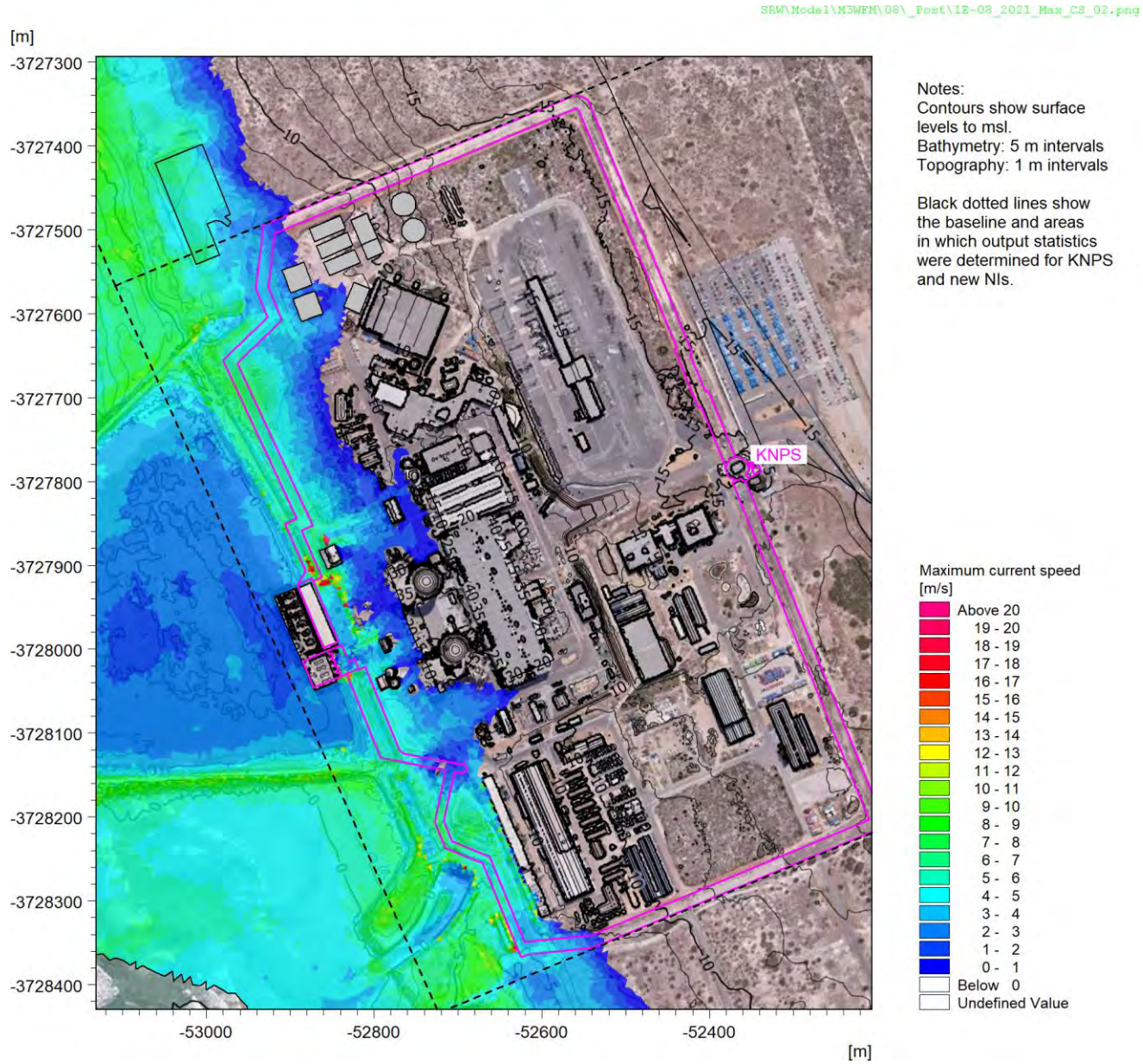


Figure A.24: Maximum Depth-Averaged Current Speed Due to Wave Run-Up at KNPS for the 10^{-8} y^{-1} Storm in 2021.

CONTROLLED DISCLOSURE

When downloaded from the EDS database, this document is uncontrolled and the responsibility rests with the user to ensure it is in line with the authorised version on the database.

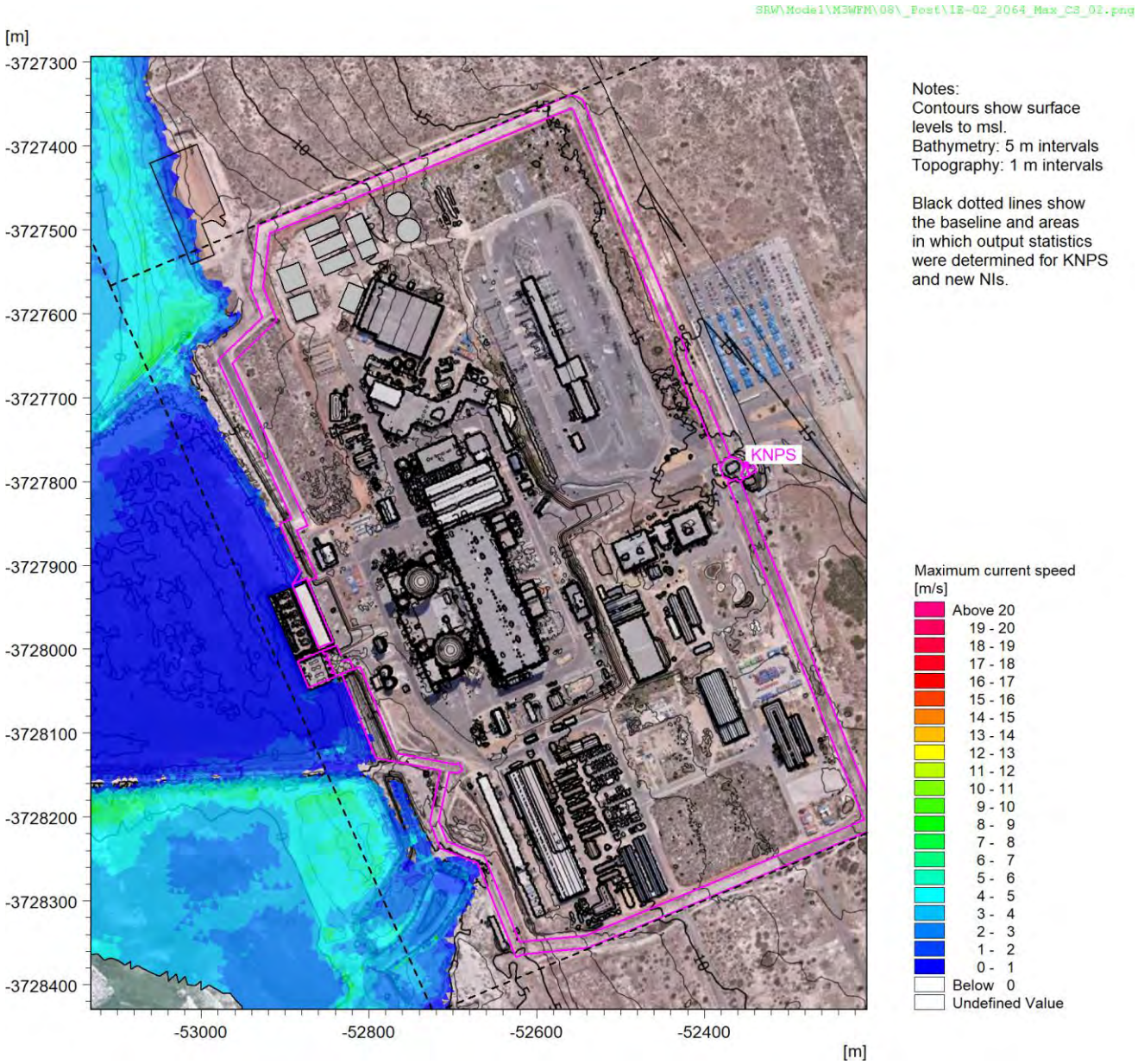


Figure A.25: Maximum Depth-Averaged Current Speed Due to Wave Run-Up at KNPS for the 10^{-2} y^{-1} Storm in 2064.

CONTROLLED DISCLOSURE

When downloaded from the EDS database, this document is uncontrolled and the responsibility rests with the user to ensure it is in line with the authorised version on the database.

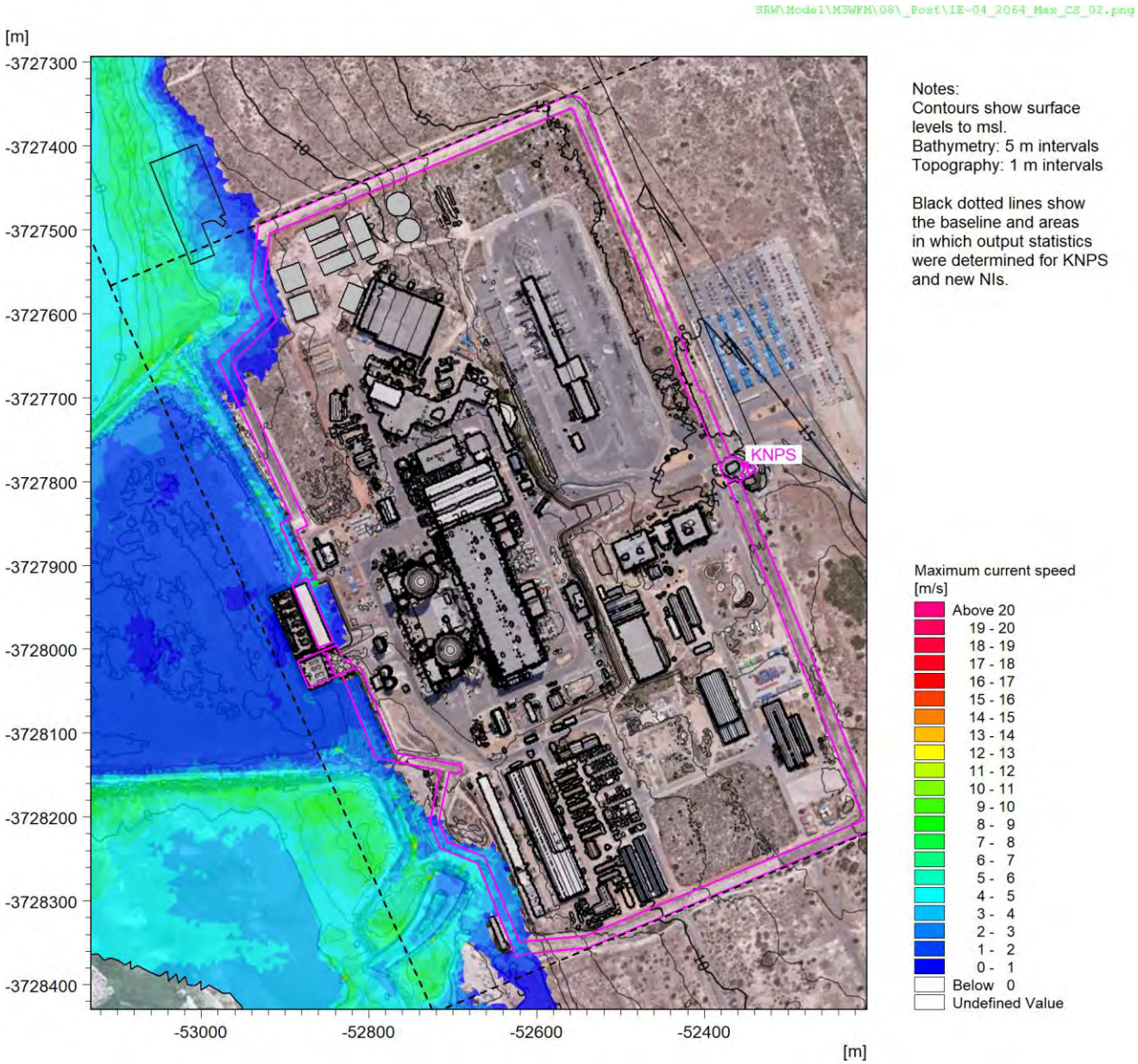


Figure A.26: Maximum Depth-Averaged Current Speed Due to Wave Run-Up at KNPS for the 10^{-4} y^{-1} Storm in 2064.

CONTROLLED DISCLOSURE

When downloaded from the EDS database, this document is uncontrolled and the responsibility rests with the user to ensure it is in line with the authorised version on the database.

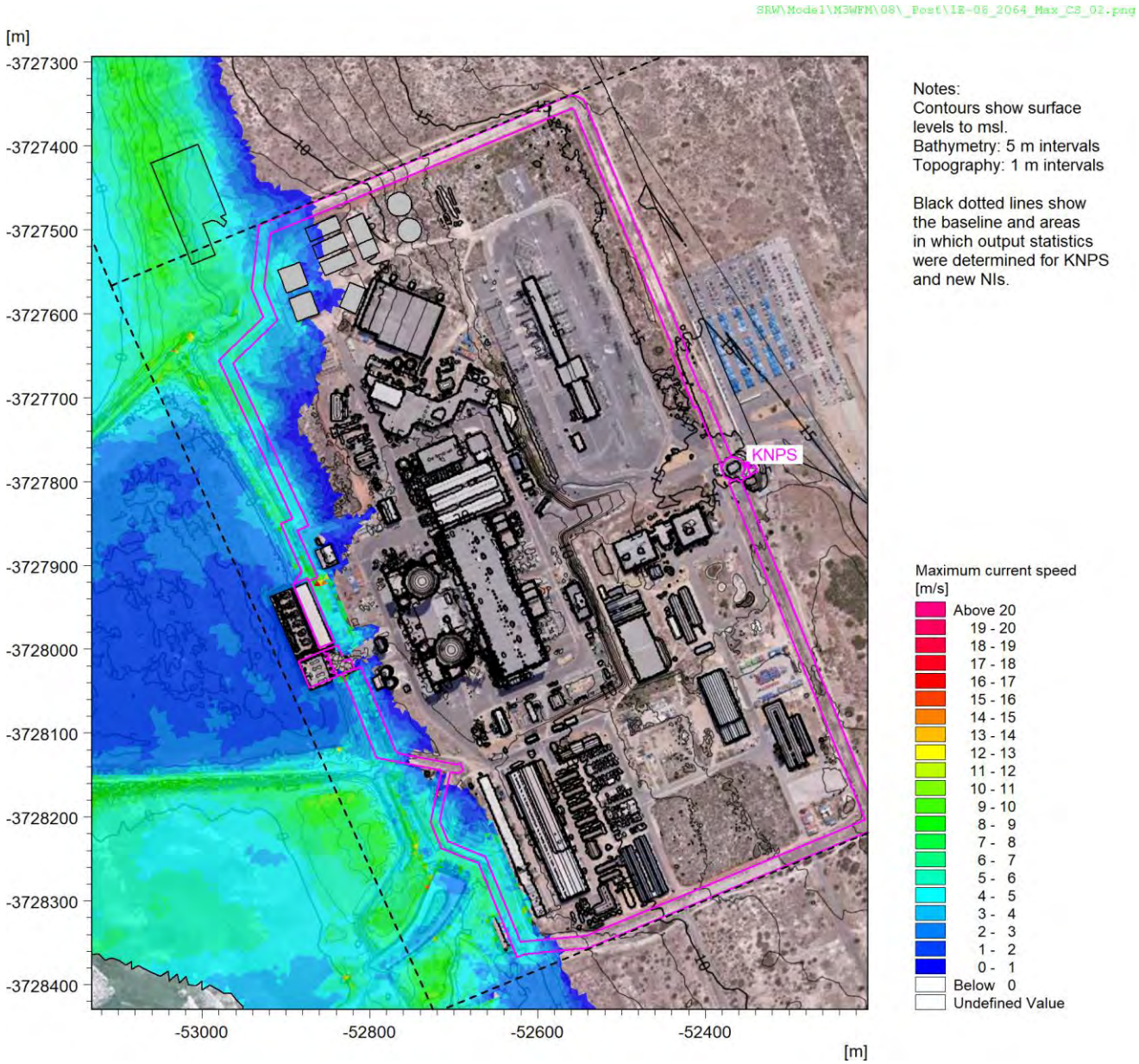


Figure A.27: Maximum Depth-Averaged Current Speed Due to Wave Run-Up at KNPS for the 10^{-6} y^{-1} Storm in 2064.

CONTROLLED DISCLOSURE

When downloaded from the EDS database, this document is uncontrolled and the responsibility rests with the user to ensure it is in line with the authorised version on the database.

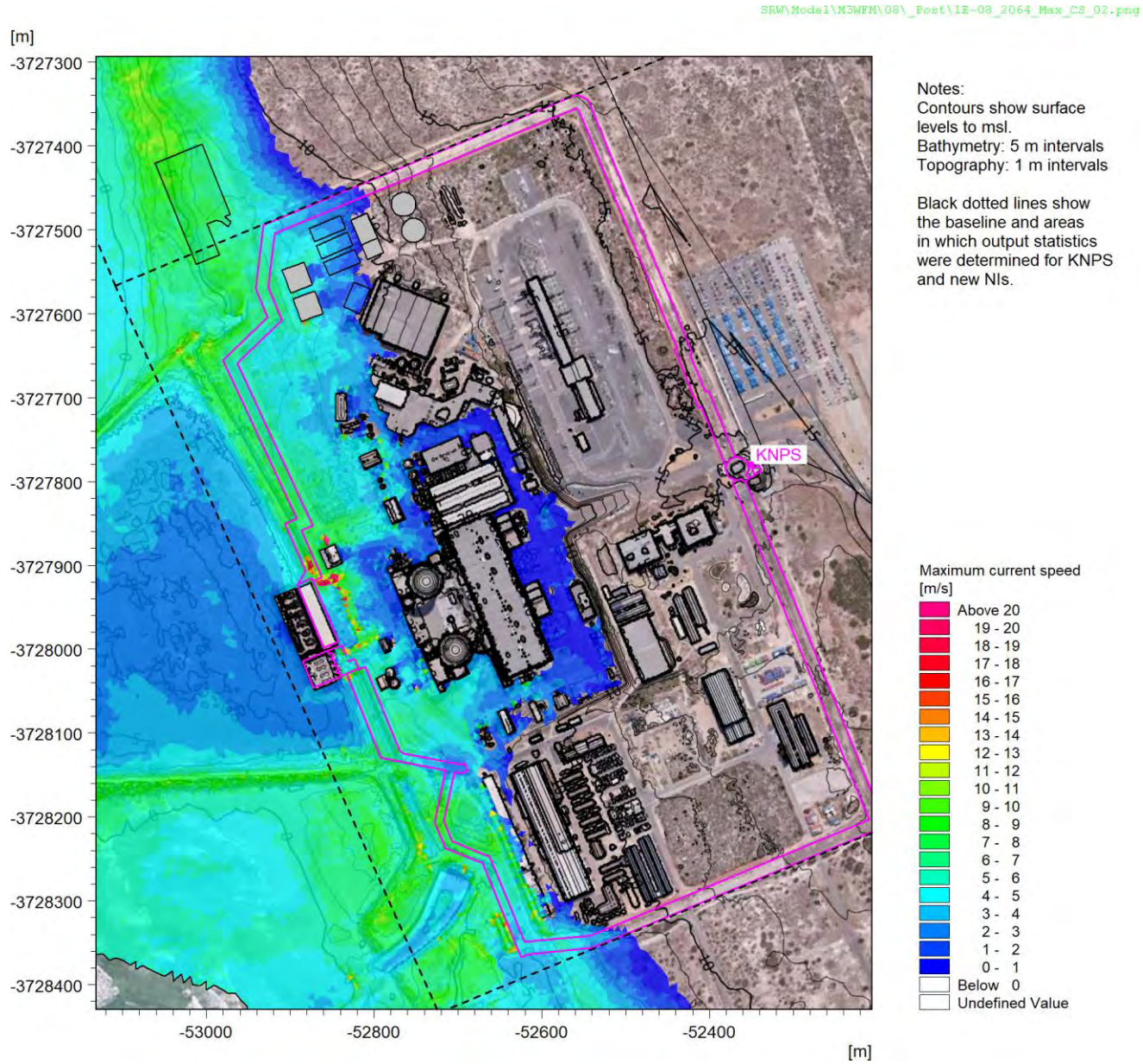


Figure A.28: Maximum Depth-Averaged Current Speed Due to Wave Run-Up at KNPS for the 10^{-8} y^{-1} Storm in 2064.

CONTROLLED DISCLOSURE

When downloaded from the EDS database, this document is uncontrolled and the responsibility rests with the user to ensure it is in line with the authorised version on the database.

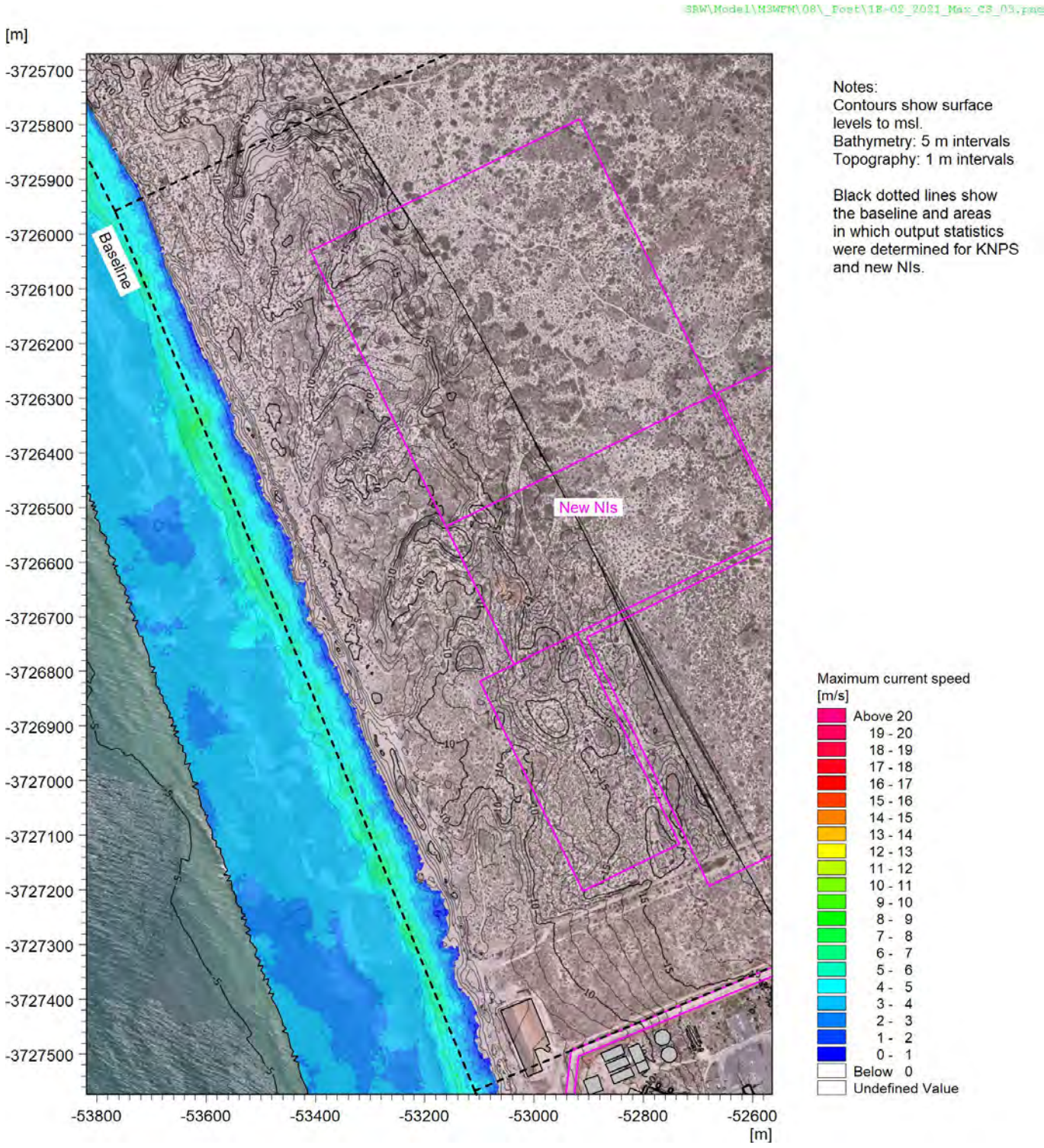


Figure A.29: Maximum Depth-Averaged Current Speed Due to Wave Run-Up at the New NIs for the 10^{-2} y^{-1} Storm in 2021.

CONTROLLED DISCLOSURE

When downloaded from the EDS database, this document is uncontrolled and the responsibility rests with the user to ensure it is in line with the authorised version on the database.

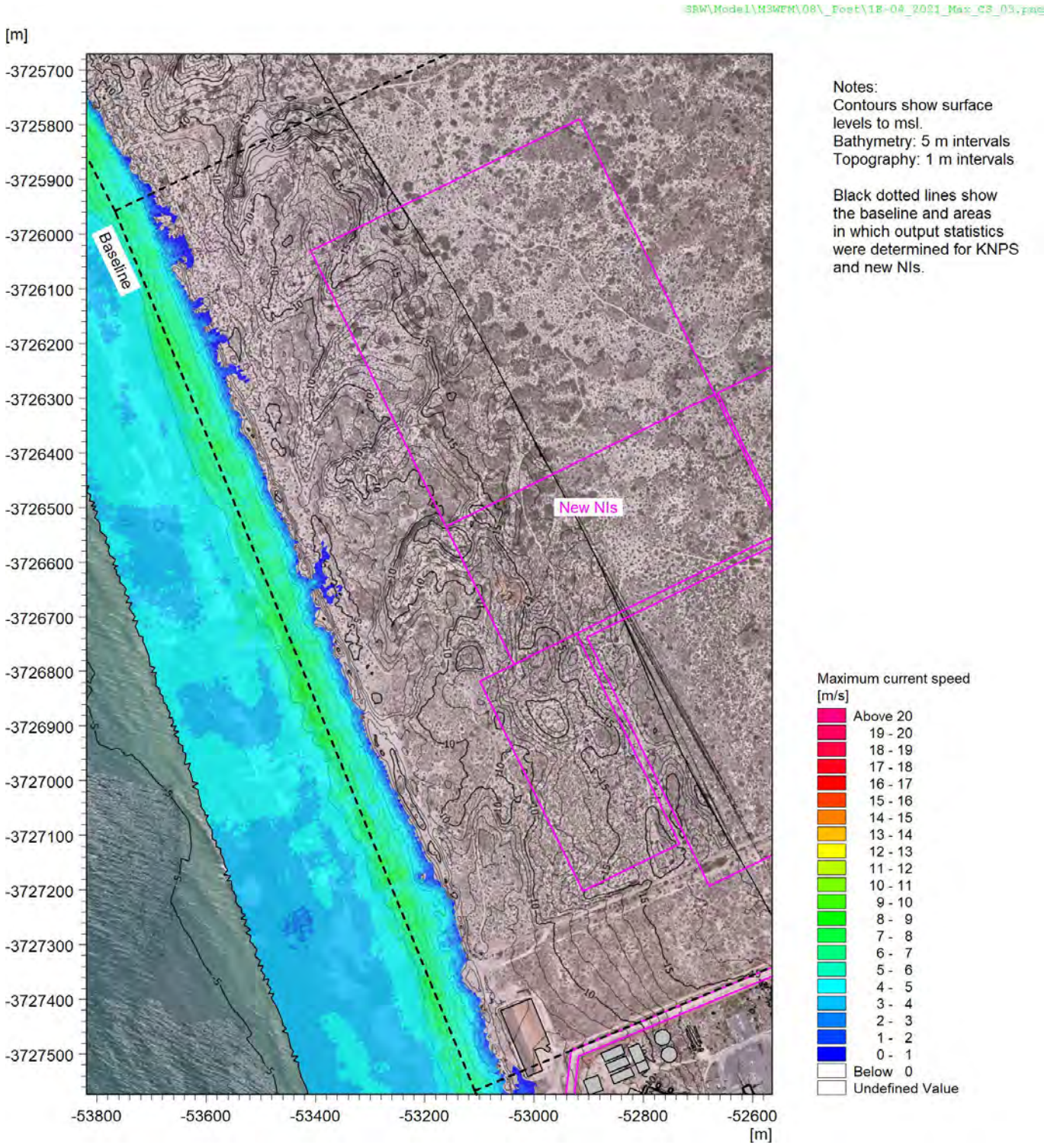


Figure A.30: Maximum Depth-Averaged Current Speed Due to Wave Run-Up at the New NIs for the 10^{-4} y^{-1} Storm in 2021.

CONTROLLED DISCLOSURE

When downloaded from the EDS database, this document is uncontrolled and the responsibility rests with the user to ensure it is in line with the authorised version on the database.

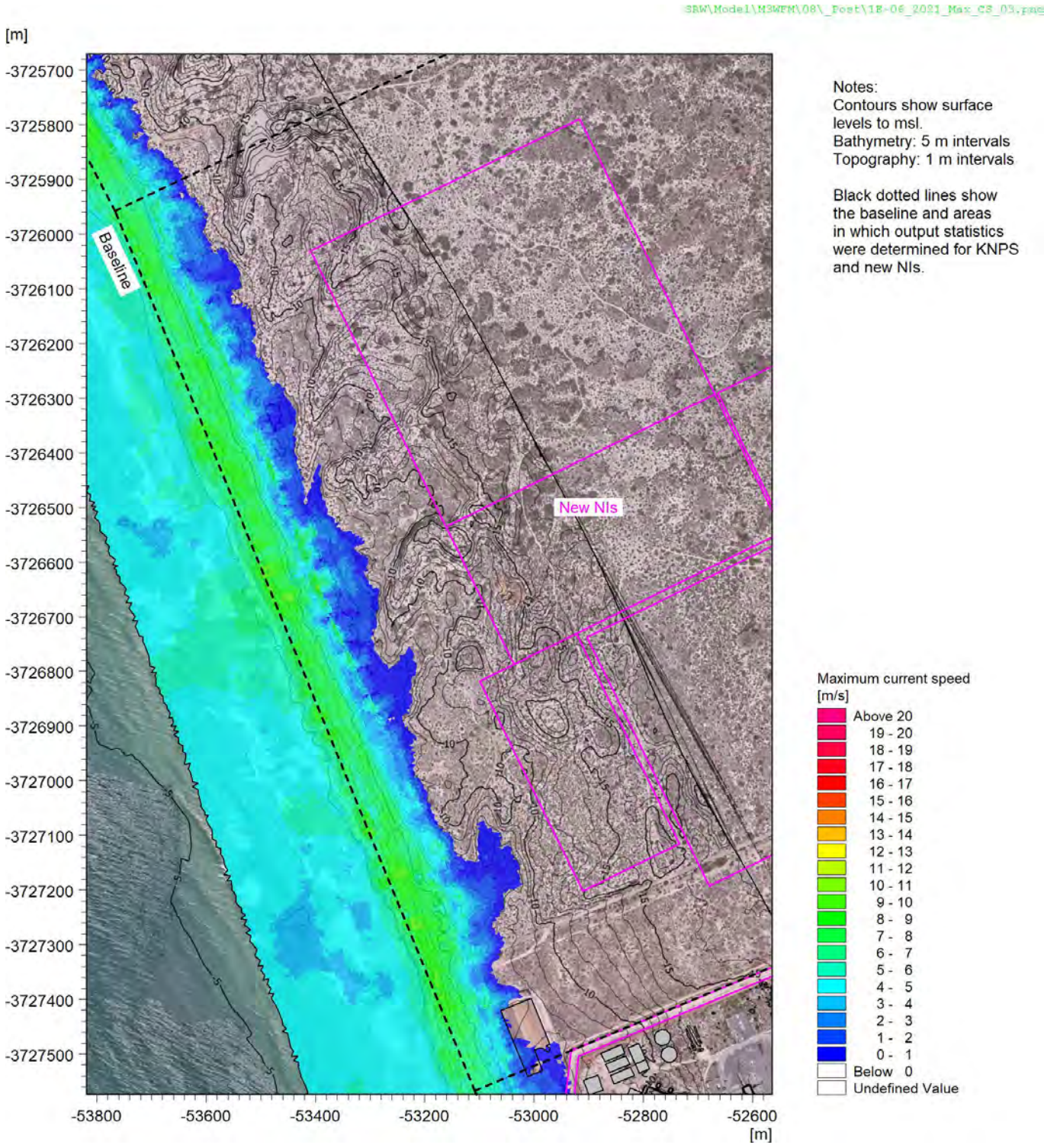


Figure A.31: Maximum Depth-Averaged Current Speed Due to Wave Run-Up at the New NIs for the 10^{-6} y^{-1} Storm in 2021.

CONTROLLED DISCLOSURE

When downloaded from the EDS database, this document is uncontrolled and the responsibility rests with the user to ensure it is in line with the authorised version on the database.

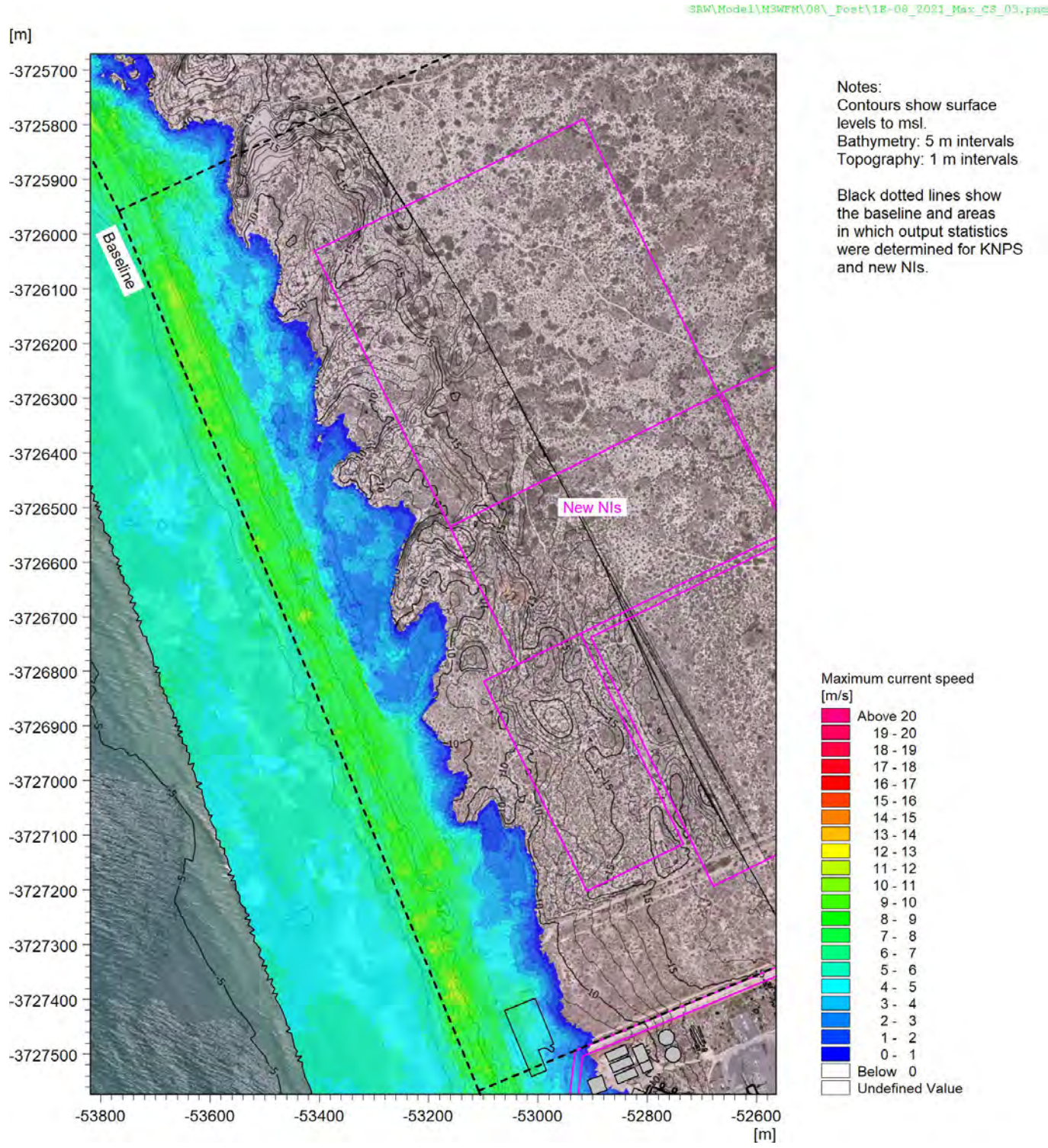


Figure A.32: Maximum Depth-Averaged Current Speed Due to Wave Run-Up at the New NIs for the 10^{-8} y^{-1} Storm in 2021.

CONTROLLED DISCLOSURE

When downloaded from the EDS database, this document is uncontrolled and the responsibility rests with the user to ensure it is in line with the authorised version on the database.

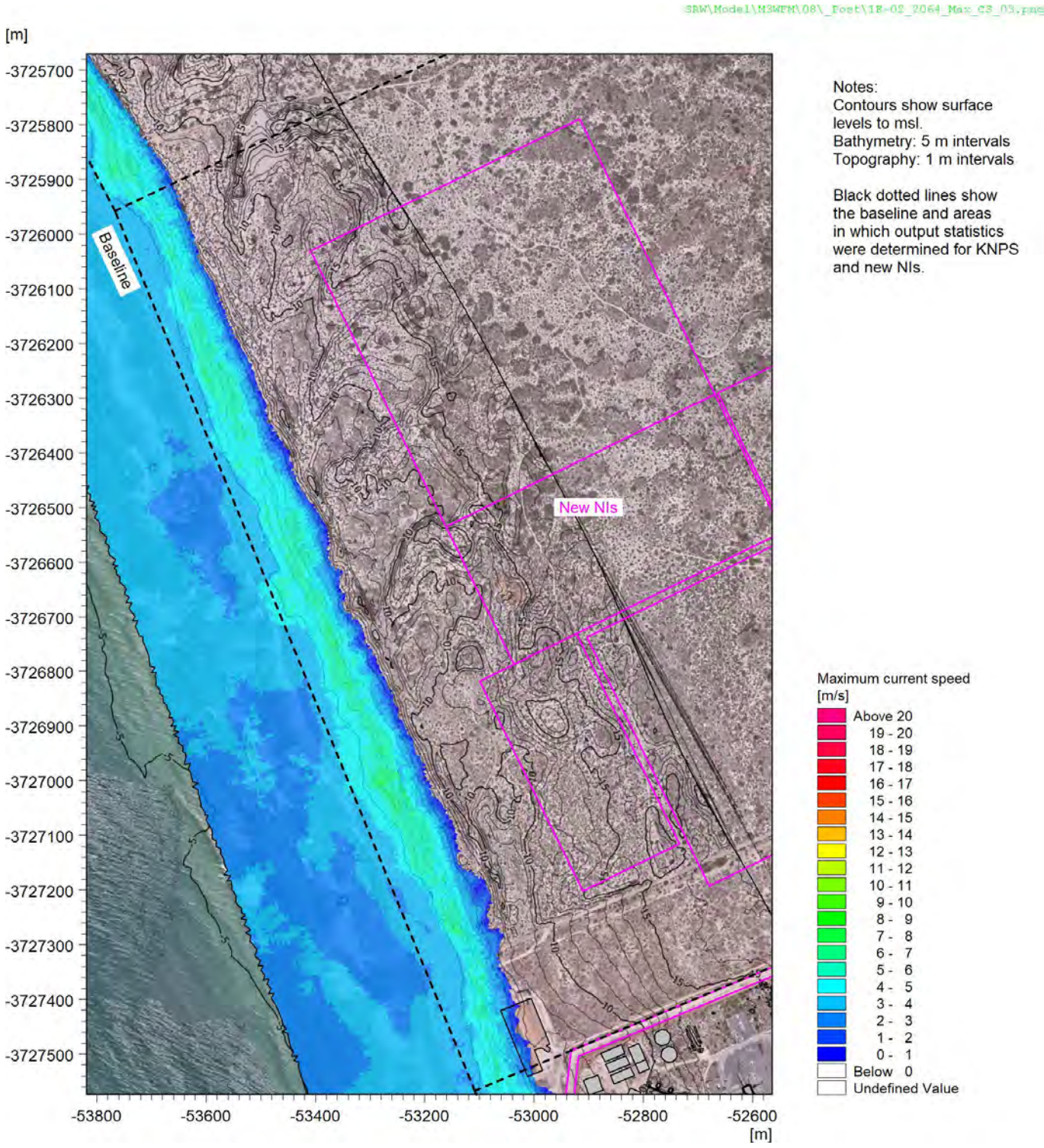


Figure A.33: Maximum Depth-Averaged Current Speed Due to Wave Run-Up at the New NIs for the 10^{-2} y^{-1} Storm in 2064.

CONTROLLED DISCLOSURE

When downloaded from the EDS database, this document is uncontrolled and the responsibility rests with the user to ensure it is in line with the authorised version on the database.

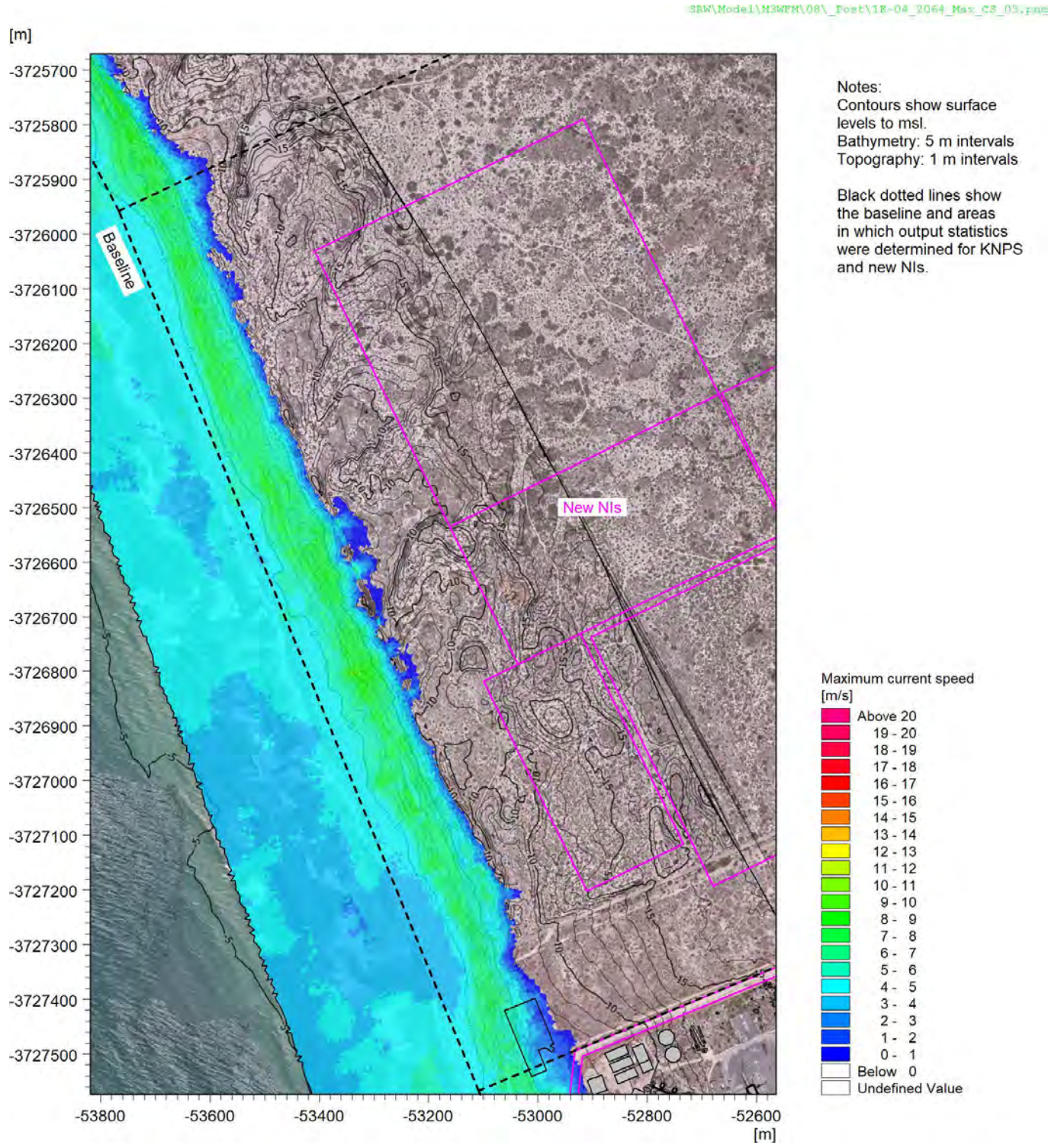


Figure A.34: Maximum Depth-Averaged Current Speed Due to Wave Run-Up at the New NIs for the 10^{-4} y^{-1} Storm in 2064.

CONTROLLED DISCLOSURE

When downloaded from the EDS database, this document is uncontrolled and the responsibility rests with the user to ensure it is in line with the authorised version on the database.

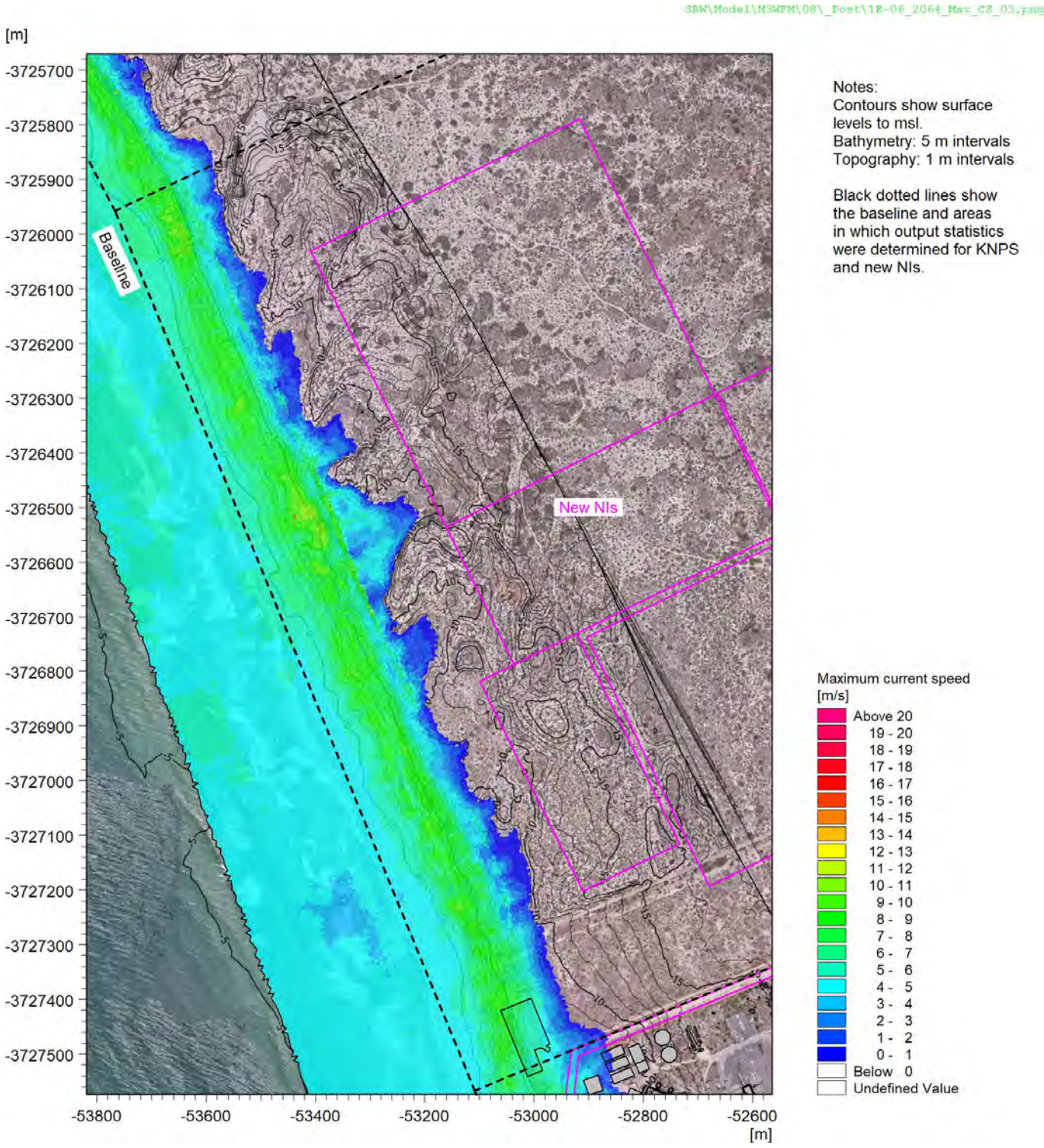


Figure A.35: Maximum Depth-Averaged Current Speed Due to Wave Run-Up at the New NIs for the 10^{-6} y^{-1} Storm in 2064.

CONTROLLED DISCLOSURE

When downloaded from the EDS database, this document is uncontrolled and the responsibility rests with the user to ensure it is in line with the authorised version on the database.

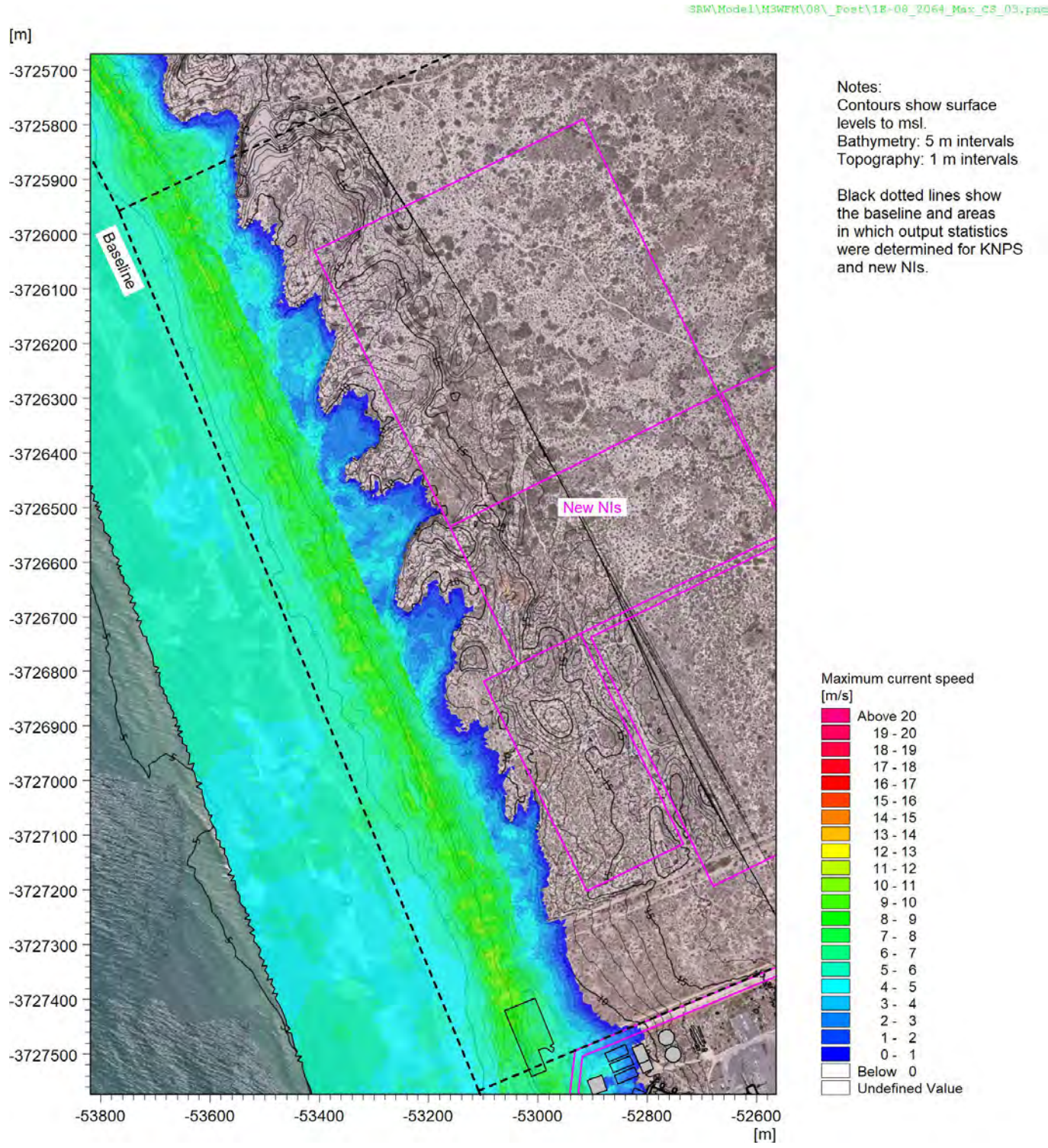


Figure A.36: Maximum Depth-Averaged Current Speed Due to Wave Run-Up at the New NIs for the 10^{-8} y^{-1} Storm in 2064.

CONTROLLED DISCLOSURE

When downloaded from the EDS database, this document is uncontrolled and the responsibility rests with the user to ensure it is in line with the authorised version on the database.

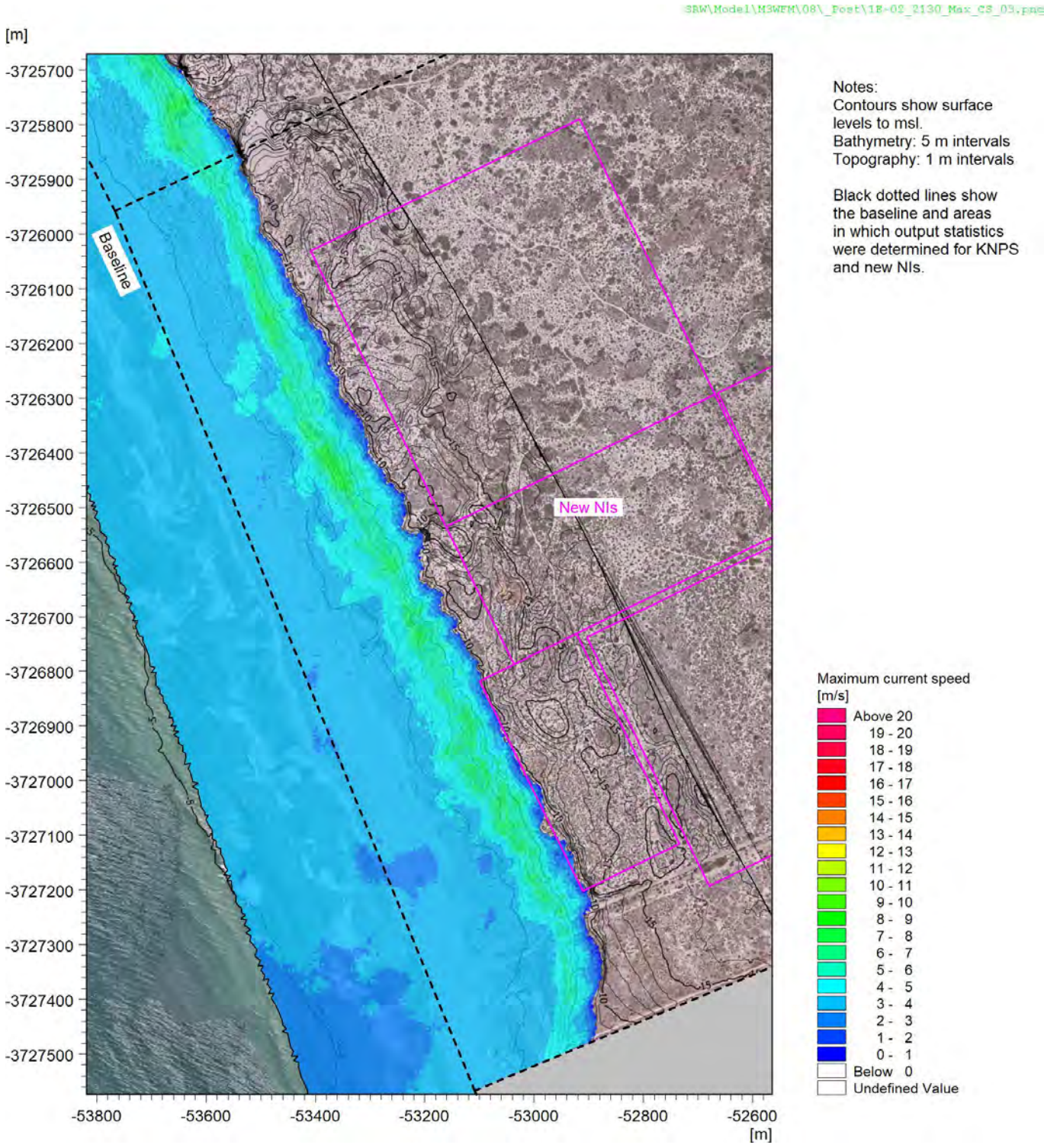


Figure A.37: Maximum Depth-Averaged Current Speed Due to Wave Run-Up at the New NIs for the 10^{-2} y^{-1} Storm in 2130.

CONTROLLED DISCLOSURE

When downloaded from the EDS database, this document is uncontrolled and the responsibility rests with the user to ensure it is in line with the authorised version on the database.

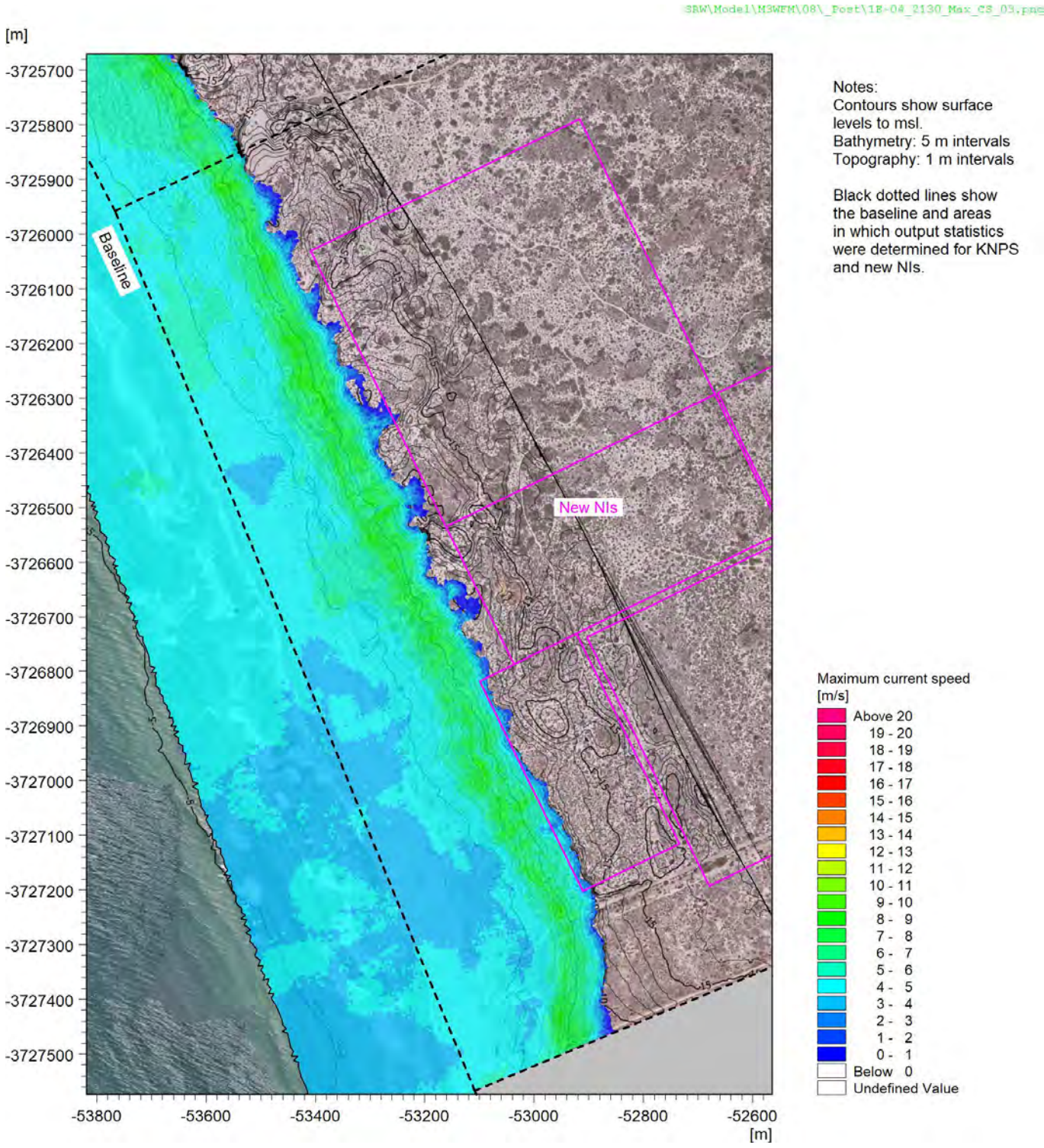


Figure A.38: Maximum Depth-Averaged Current Speed Due to Wave Run-Up at the New NIs for the 10^{-4} y^{-1} Storm in 2130.

CONTROLLED DISCLOSURE

When downloaded from the EDS database, this document is uncontrolled and the responsibility rests with the user to ensure it is in line with the authorised version on the database.

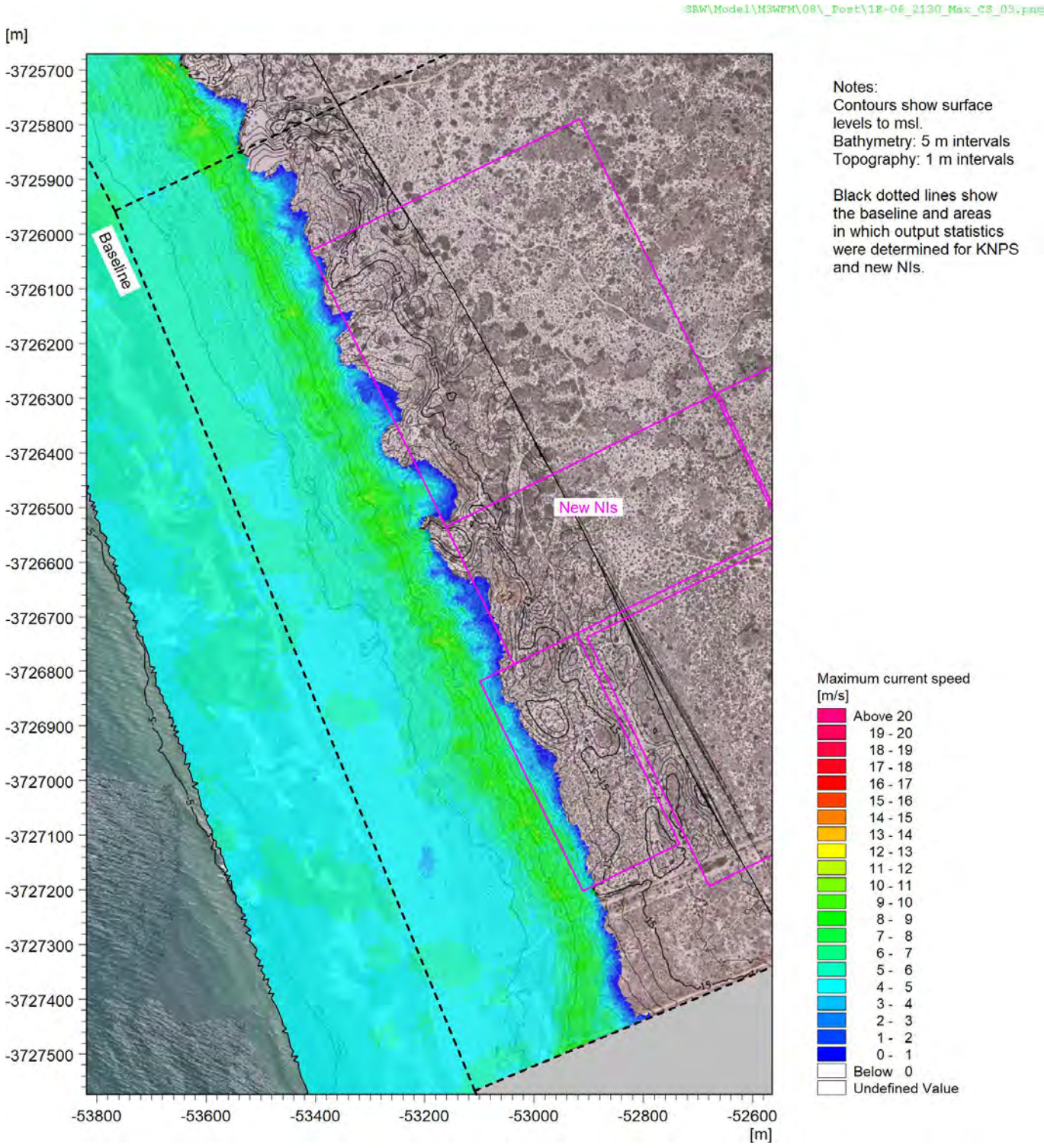


Figure A.39: Maximum Depth-Averaged Current Speed Due to Wave Run-Up at the New NIs for the 10^{-6} y^{-1} Storm in 2130.

CONTROLLED DISCLOSURE

When downloaded from the EDS database, this document is uncontrolled and the responsibility rests with the user to ensure it is in line with the authorised version on the database.

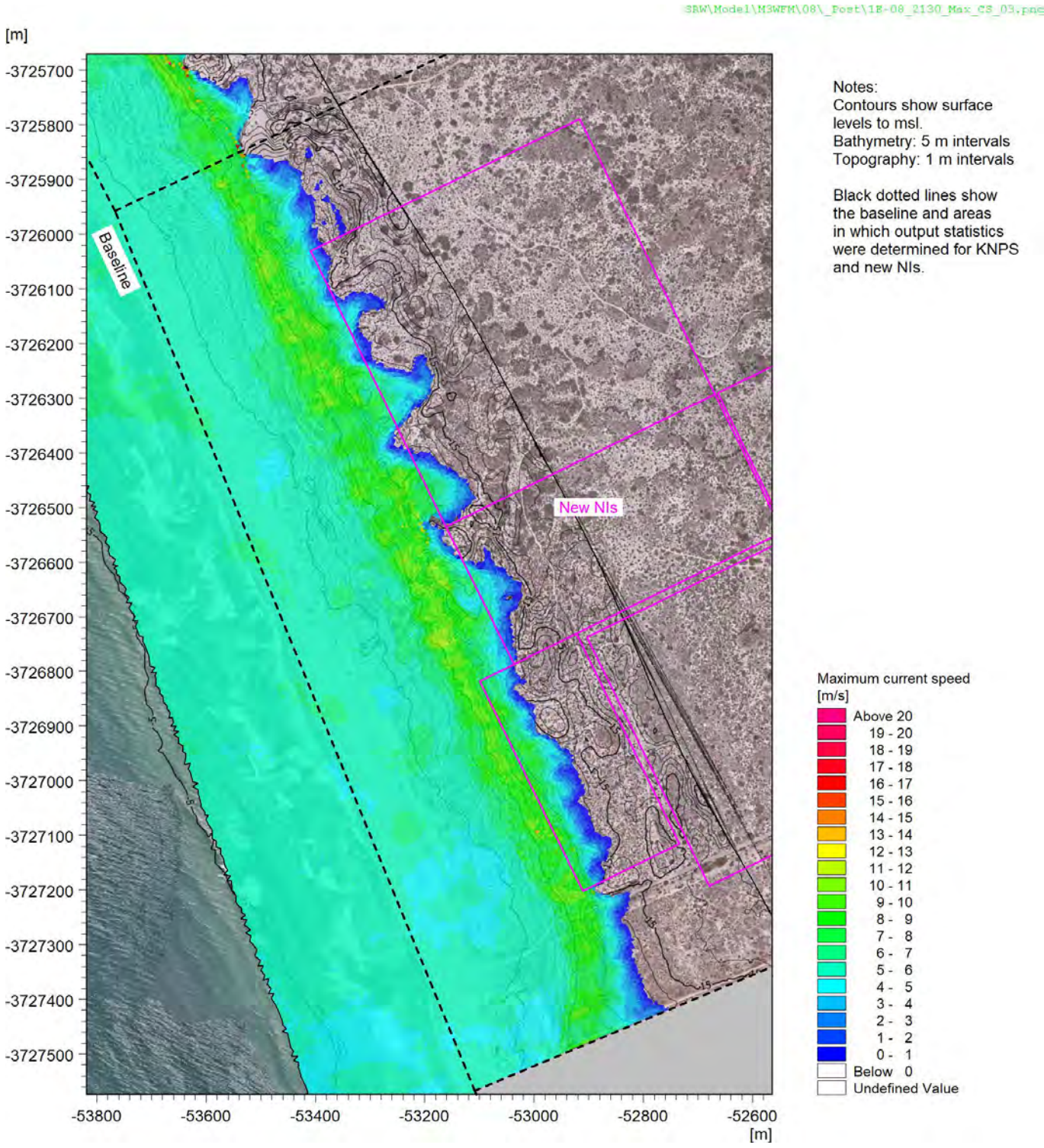


Figure A.40: Maximum Depth-Averaged Current Speed Due to Wave Run-Up at the New NIs for the 10^{-8} y^{-1} Storm in 2130.

CONTROLLED DISCLOSURE

When downloaded from the EDS database, this document is uncontrolled and the responsibility rests with the user to ensure it is in line with the authorised version on the database.

APPENDIX B: TSUNAMI RESULTS

CONTROLLED DISCLOSURE

When downloaded from the EDS database, this document is uncontrolled and the responsibility rests with the user to ensure it is in line with the authorised version on the database.

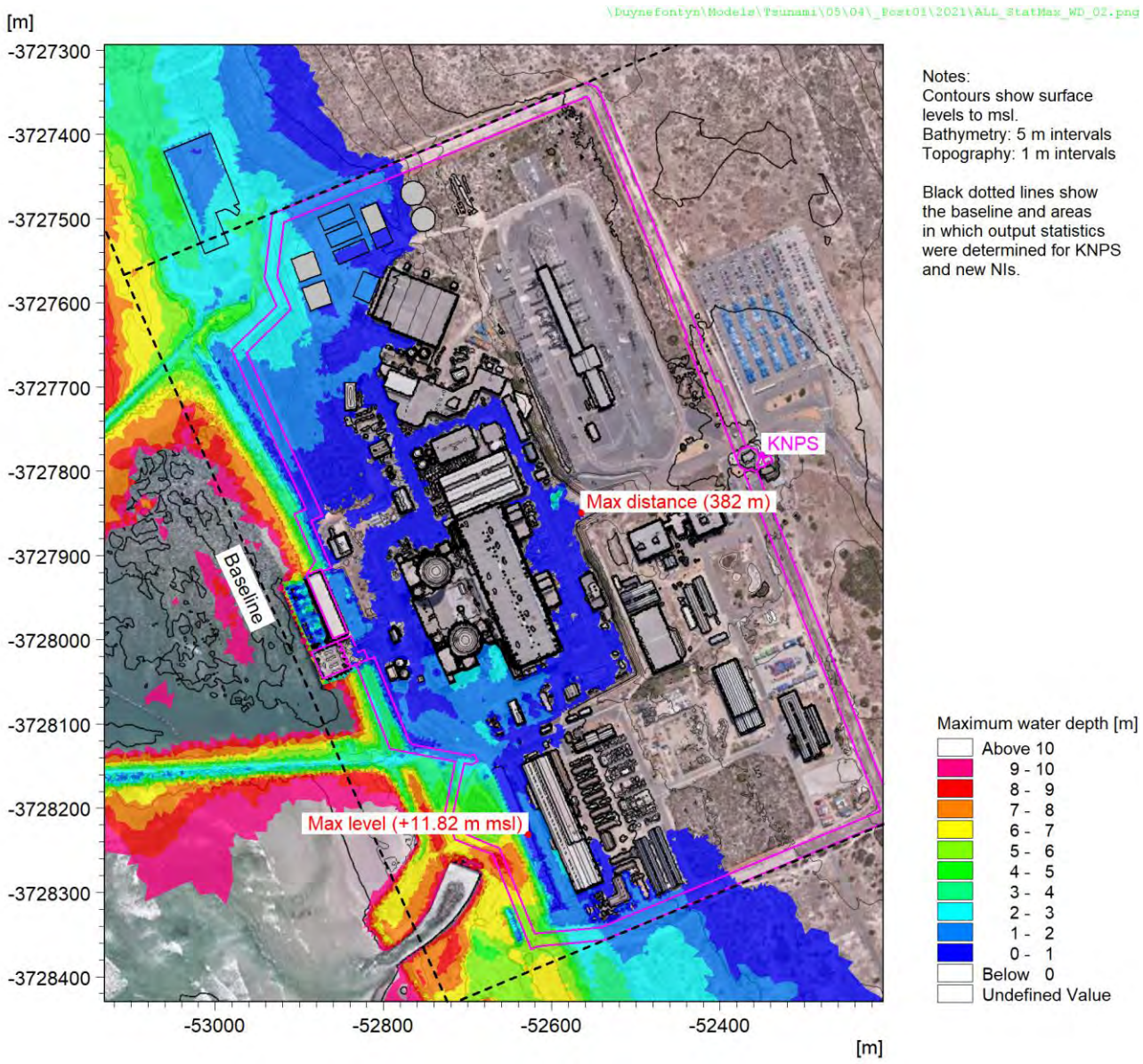


Figure B.1: Maximum Water Depth Due to the PMT at KNPS in 2021.

CONTROLLED DISCLOSURE

When downloaded from the EDS database, this document is uncontrolled and the responsibility rests with the user to ensure it is in line with the authorised version on the database.

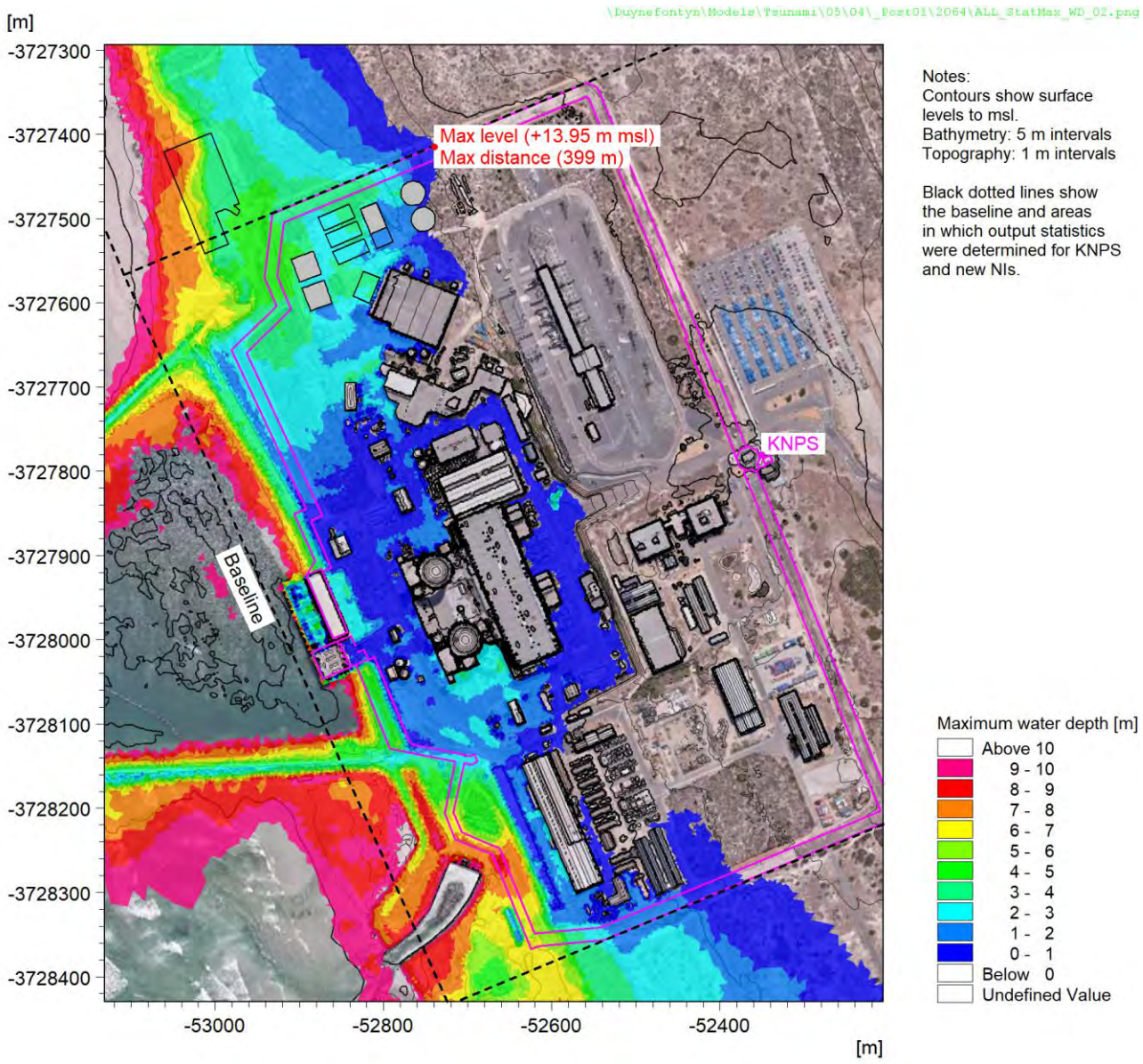


Figure B.2: Maximum Water Depth Due to the PMT at KNPS in 2064.

CONTROLLED DISCLOSURE

When downloaded from the EDS database, this document is uncontrolled and the responsibility rests with the user to ensure it is in line with the authorised version on the database.

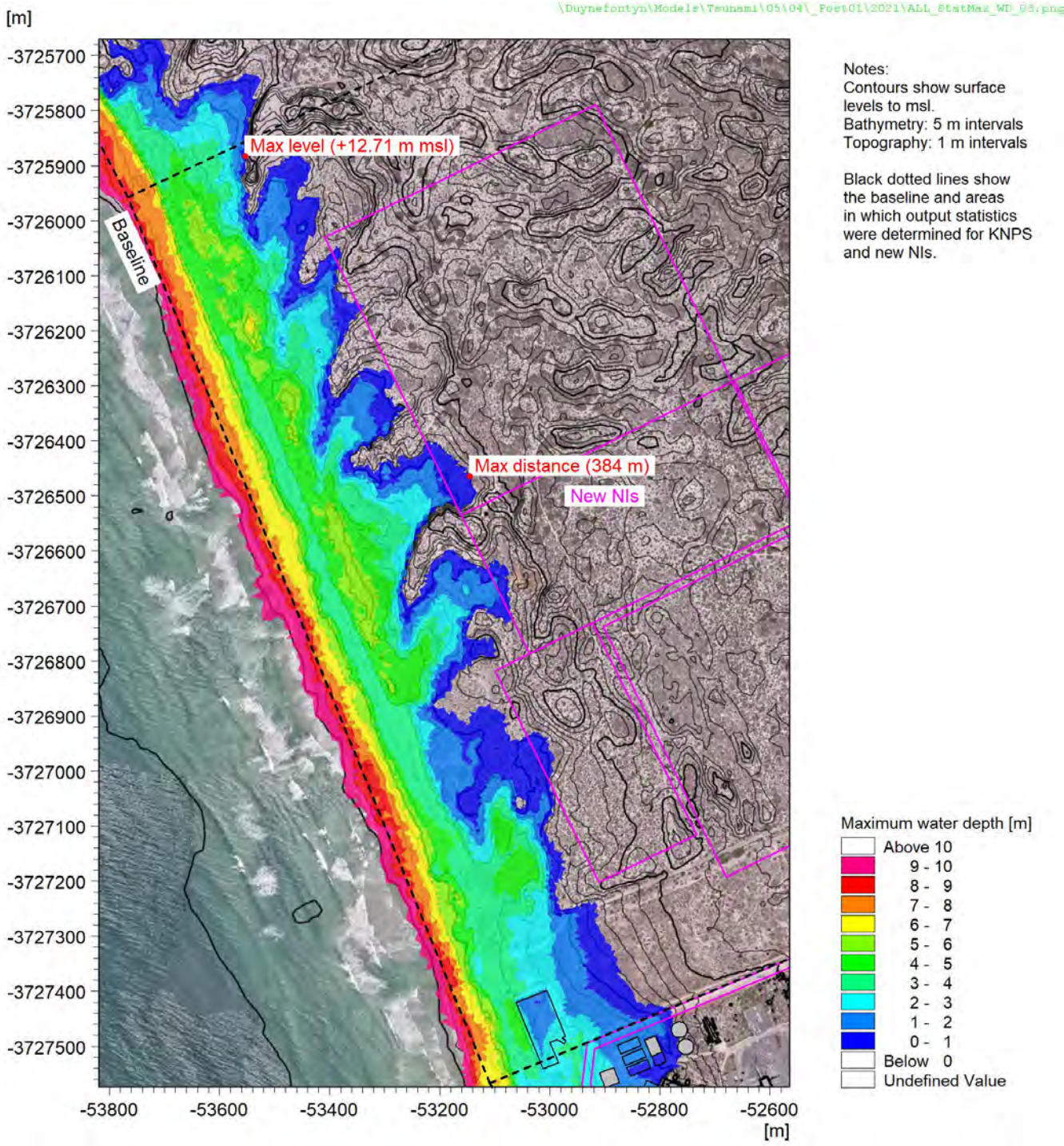


Figure B.3: Maximum Water Depth Due to the PMT at the New NIs in 2021.

CONTROLLED DISCLOSURE

When downloaded from the EDS database, this document is uncontrolled and the responsibility rests with the user to ensure it is in line with the authorised version on the database.

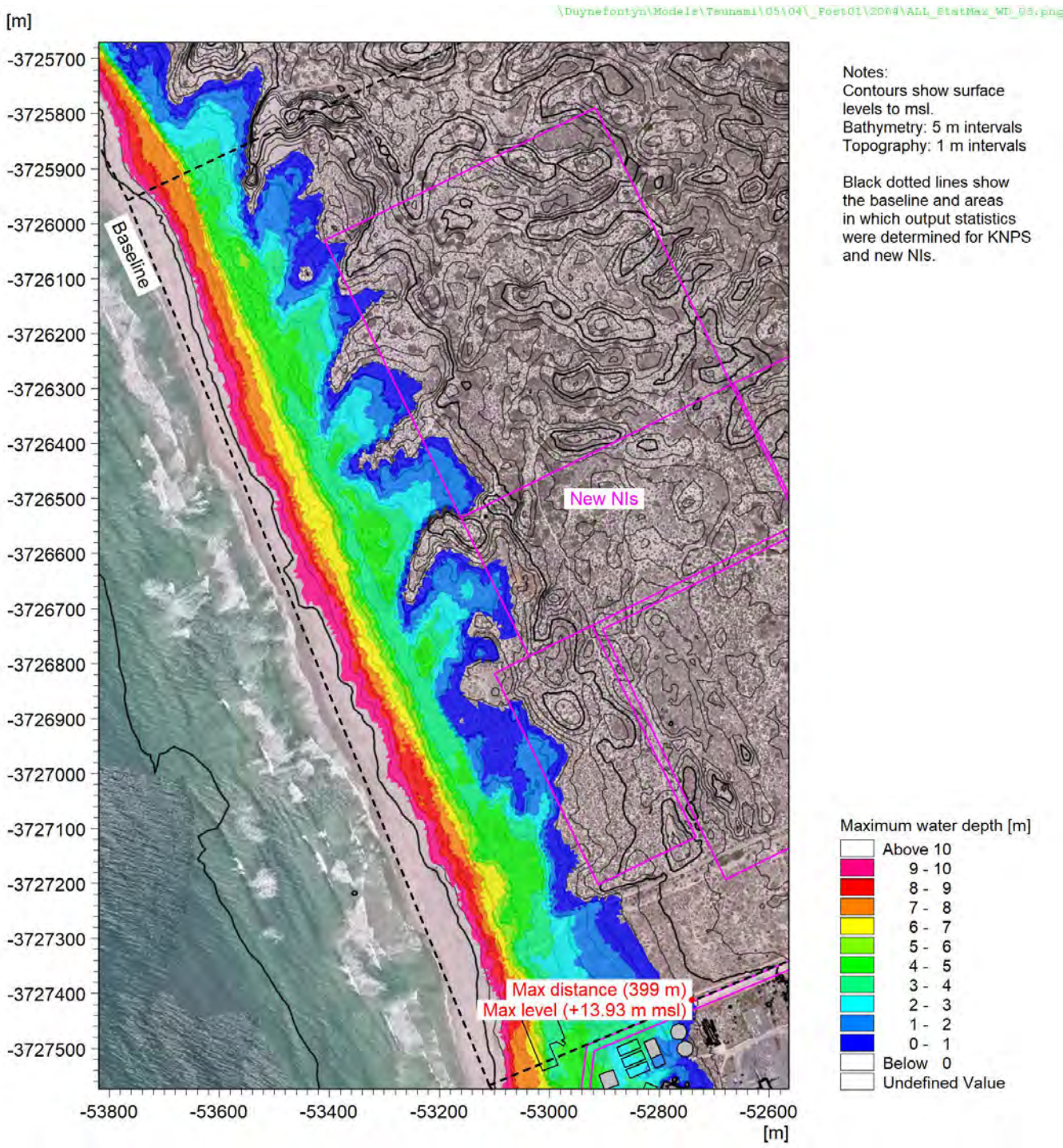


Figure B.4: Maximum Water Depth Due to the PMT at the New NIs in 2064.

CONTROLLED DISCLOSURE

When downloaded from the EDS database, this document is uncontrolled and the responsibility rests with the user to ensure it is in line with the authorised version on the database.

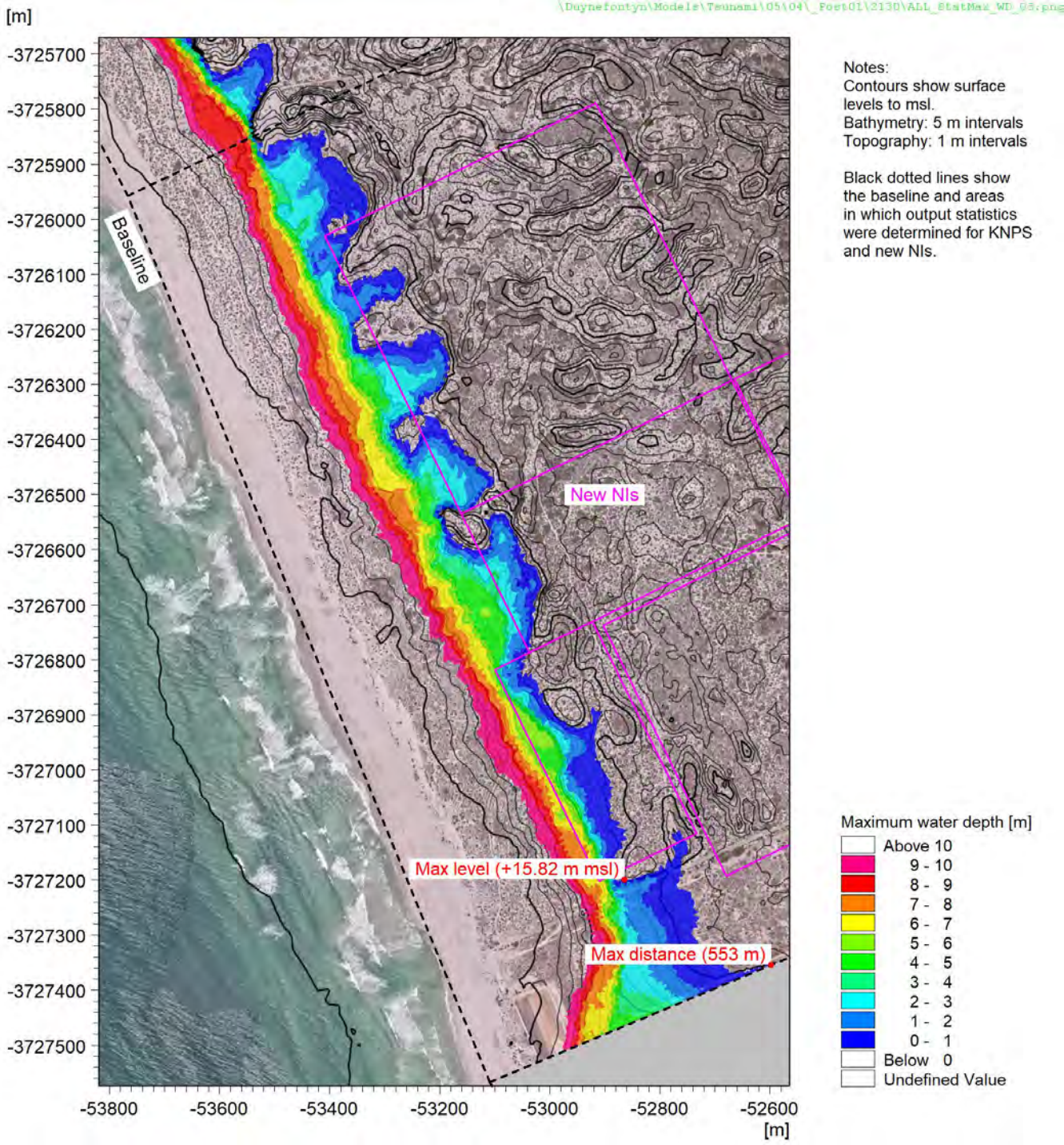


Figure B.5: Maximum Water Depth Due to the PMT at the New NIs in 2130.

CONTROLLED DISCLOSURE

When downloaded from the EDS database, this document is uncontrolled and the responsibility rests with the user to ensure it is in line with the authorised version on the database.

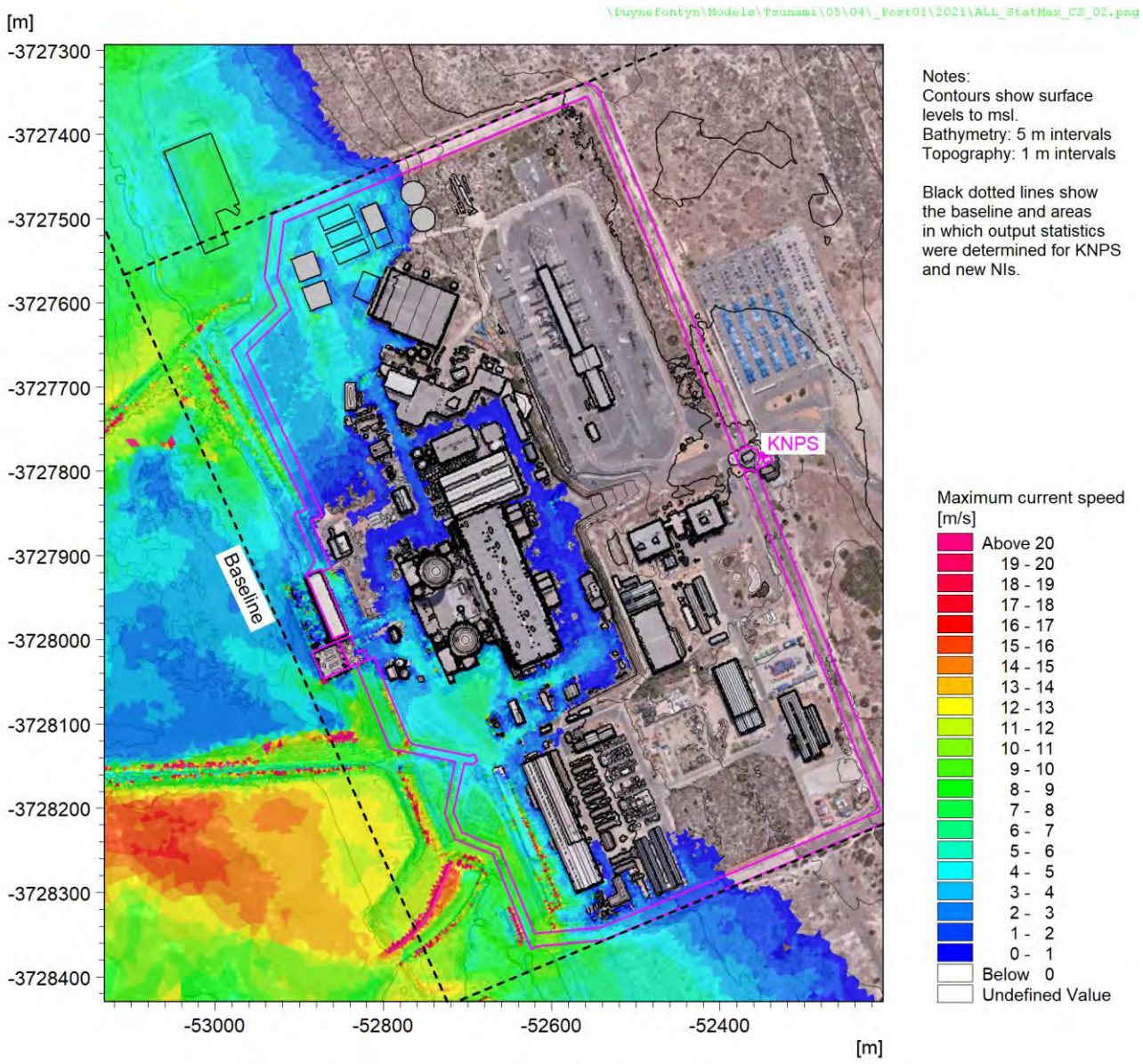


Figure B.6: Maximum Current Speed Due to the PMT at KNPS in 2021.

CONTROLLED DISCLOSURE

When downloaded from the EDS database, this document is uncontrolled and the responsibility rests with the user to ensure it is in line with the authorised version on the database.

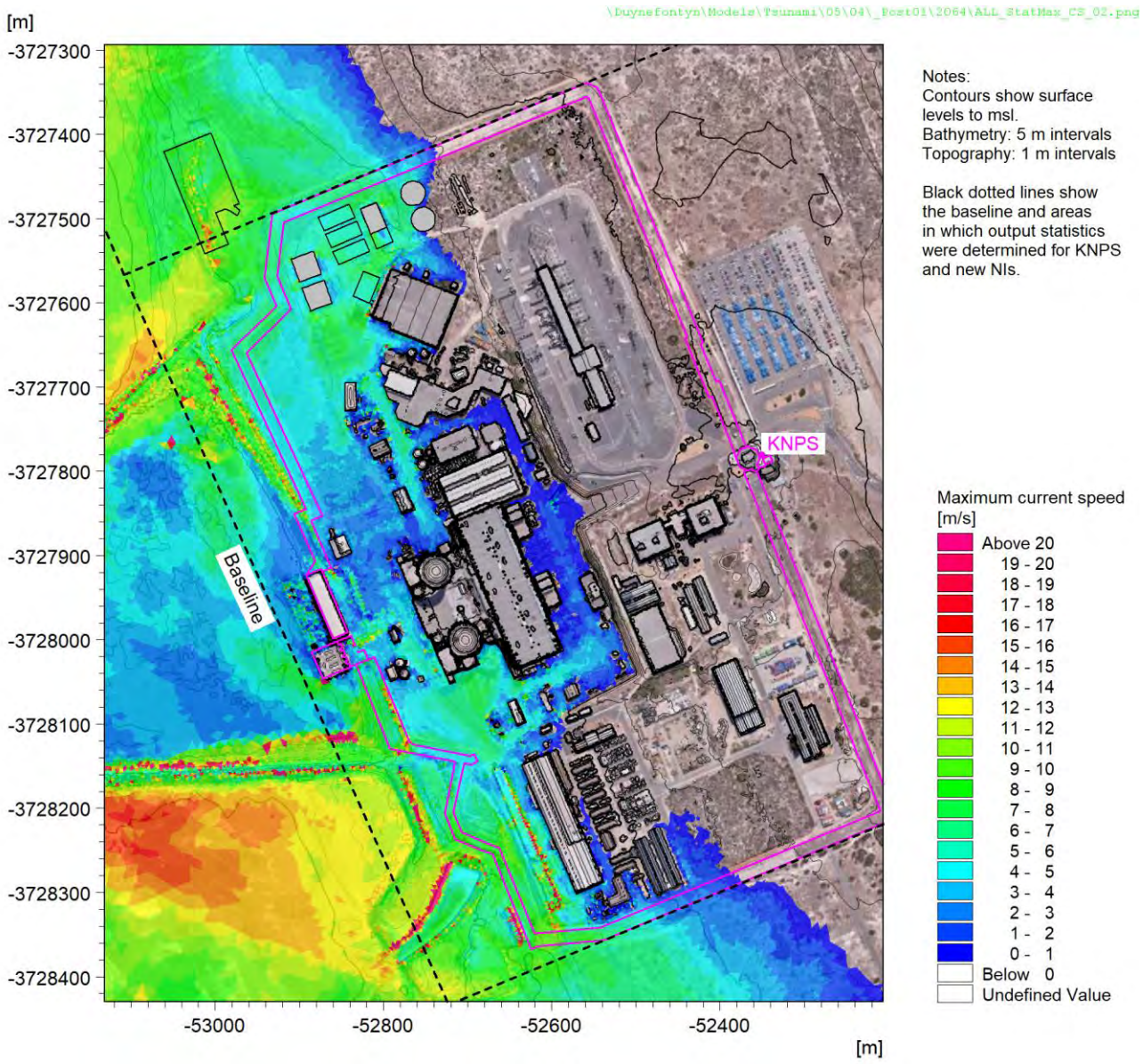


Figure B.7: Maximum Current Speed Due to the PMT at KNPS in 2064.

CONTROLLED DISCLOSURE

When downloaded from the EDS database, this document is uncontrolled and the responsibility rests with the user to ensure it is in line with the authorised version on the database.

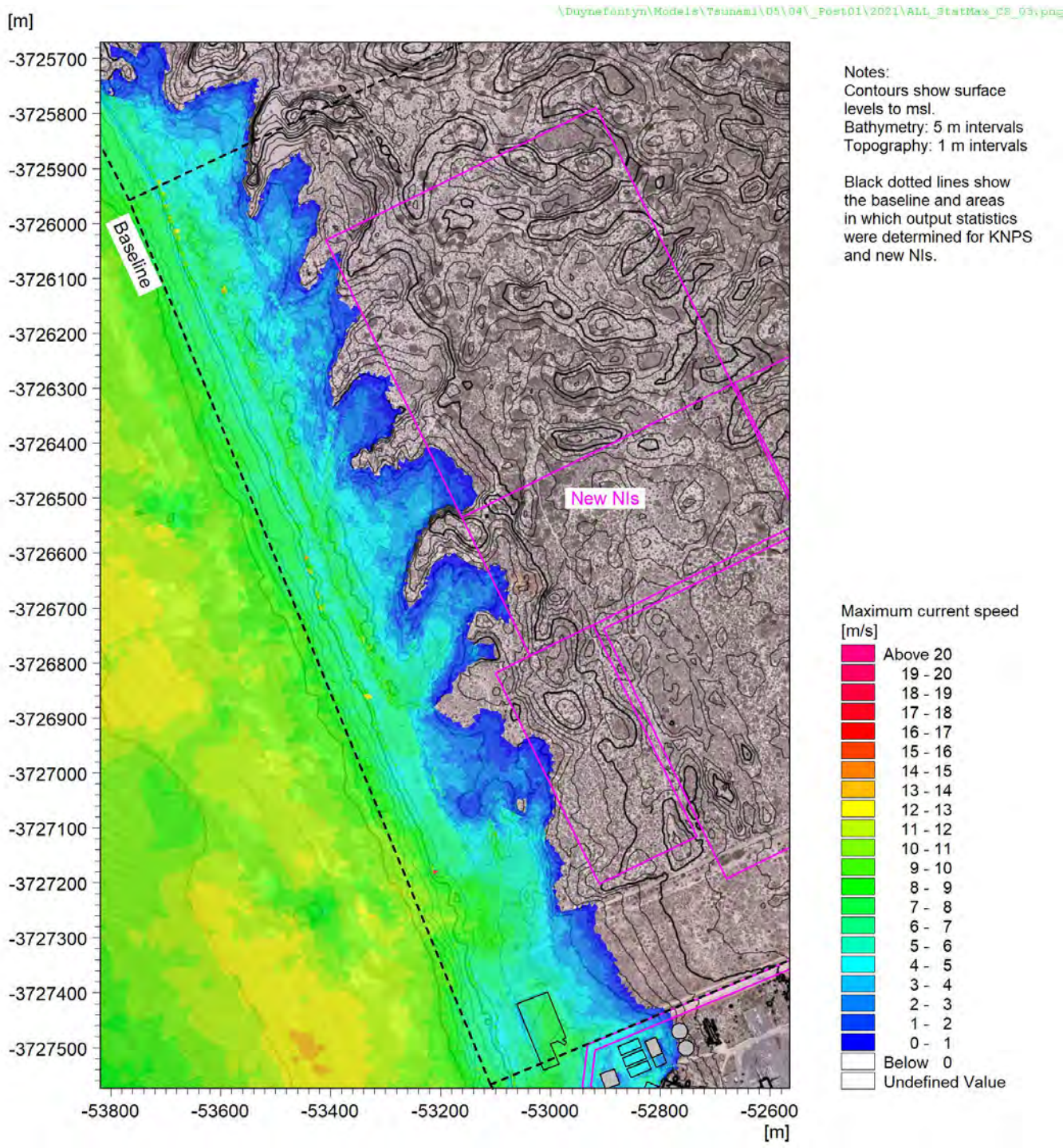


Figure B.8: Maximum Current Speed Due to the PMT at the New NIs in 2021.

CONTROLLED DISCLOSURE

When downloaded from the EDS database, this document is uncontrolled and the responsibility rests with the user to ensure it is in line with the authorised version on the database.

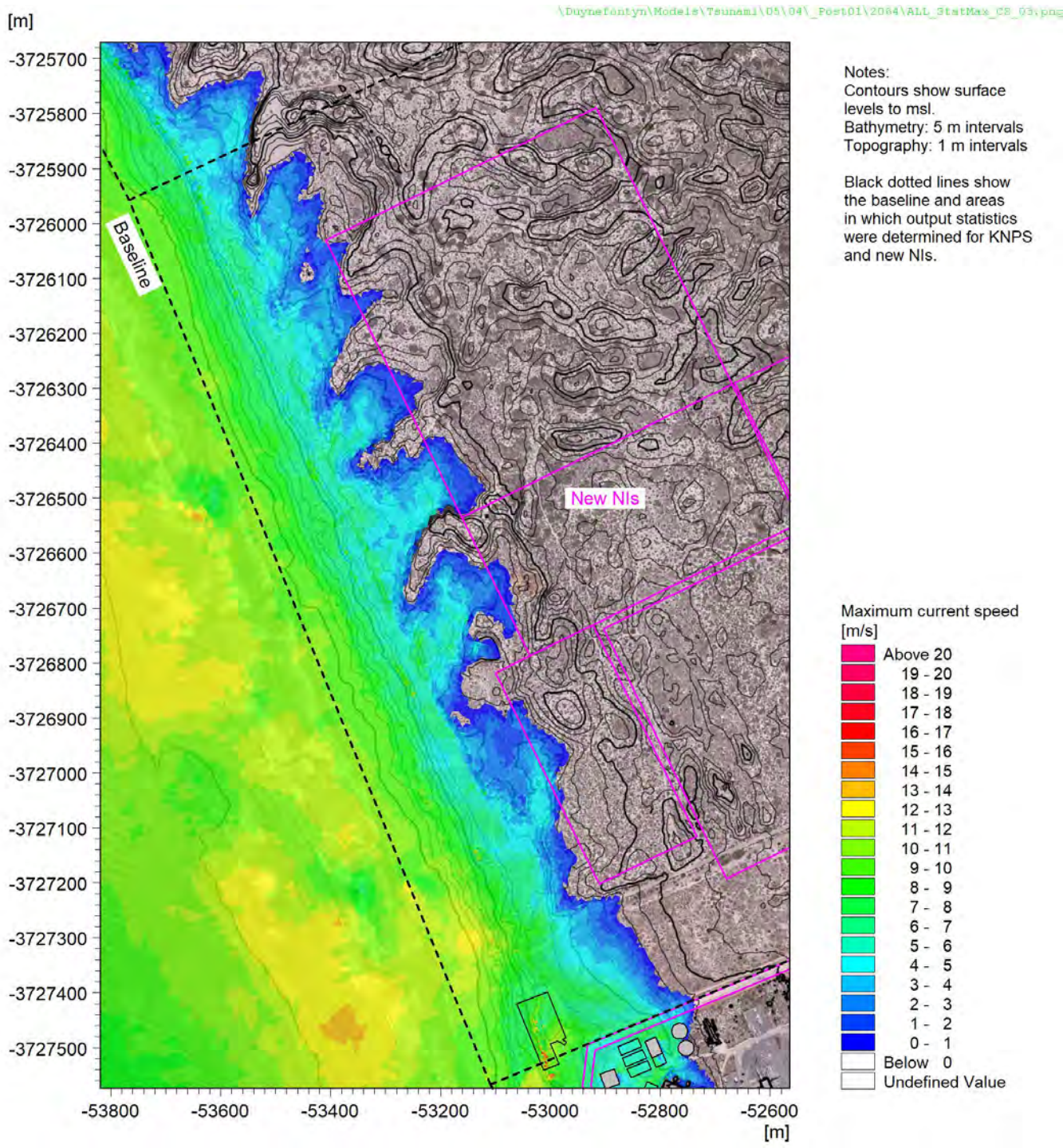


Figure B.9: Maximum Current Speed Due to the PMT at the New NIs in 2064.

CONTROLLED DISCLOSURE

When downloaded from the EDS database, this document is uncontrolled and the responsibility rests with the user to ensure it is in line with the authorised version on the database.

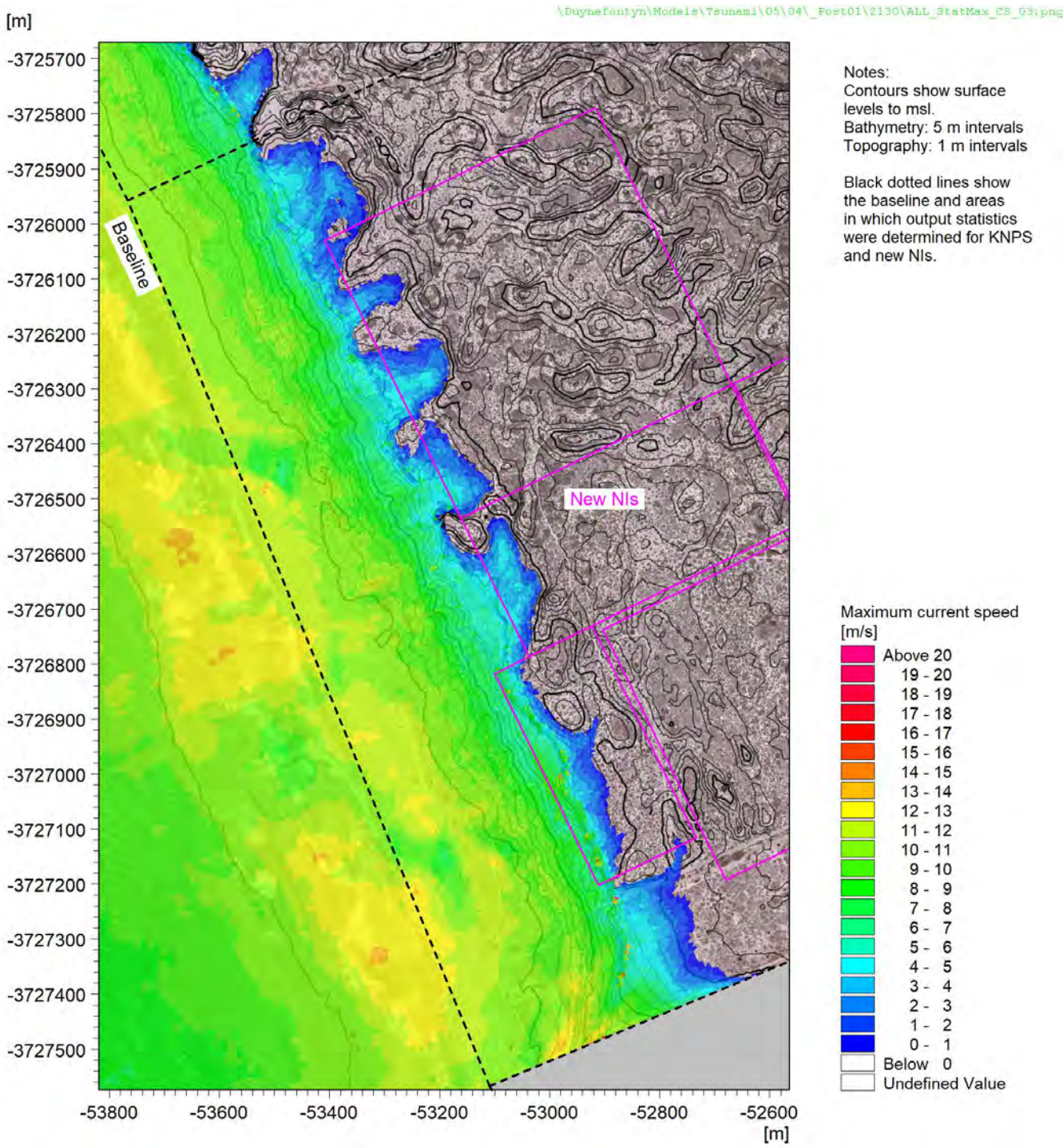


Figure B.10: Maximum Current Speed Due to the PMT at the New NIs in 2130.

CONTROLLED DISCLOSURE

When downloaded from the EDS database, this document is uncontrolled and the responsibility rests with the user to ensure it is in line with the authorised version on the database.

APPENDIX C: THERMAL PLUME DISPERSION FIGURES

CONTROLLED DISCLOSURE

When downloaded from the EDS database, this document is uncontrolled and the responsibility rests with the user to ensure it is in line with the authorised version on the database.

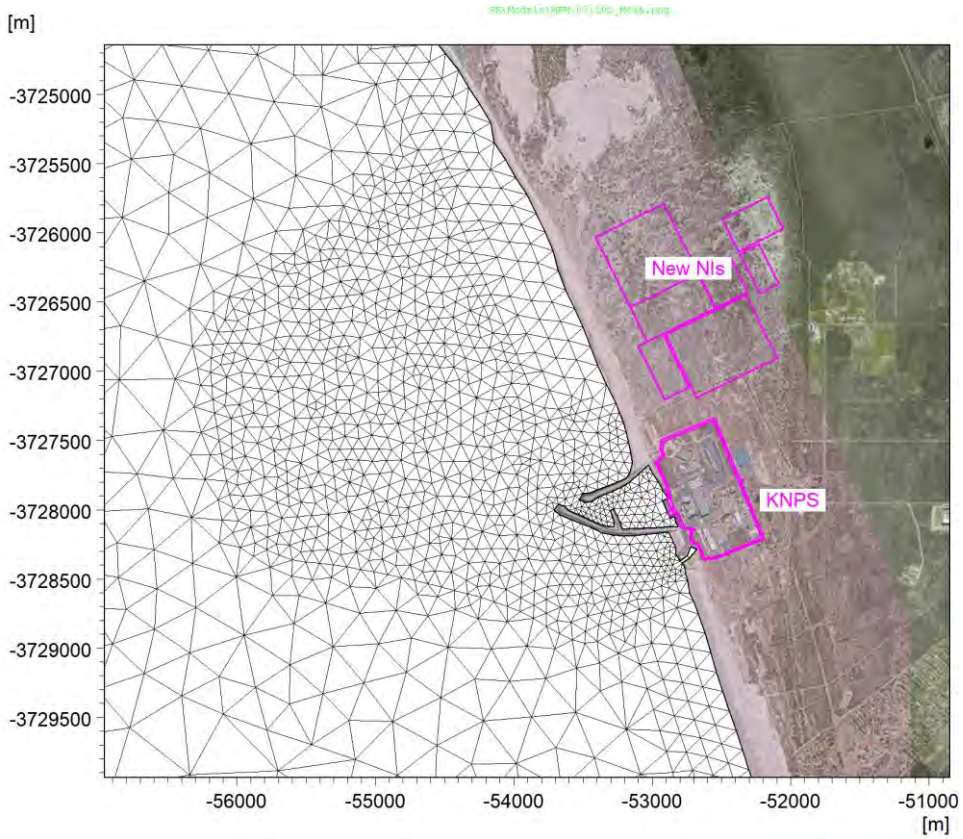


Figure C.1: Detail of Model Mesh Used for Layout 0.

CONTROLLED DISCLOSURE

When downloaded from the EDS database, this document is uncontrolled and the responsibility rests with the user to ensure it is in line with the authorised version on the database.

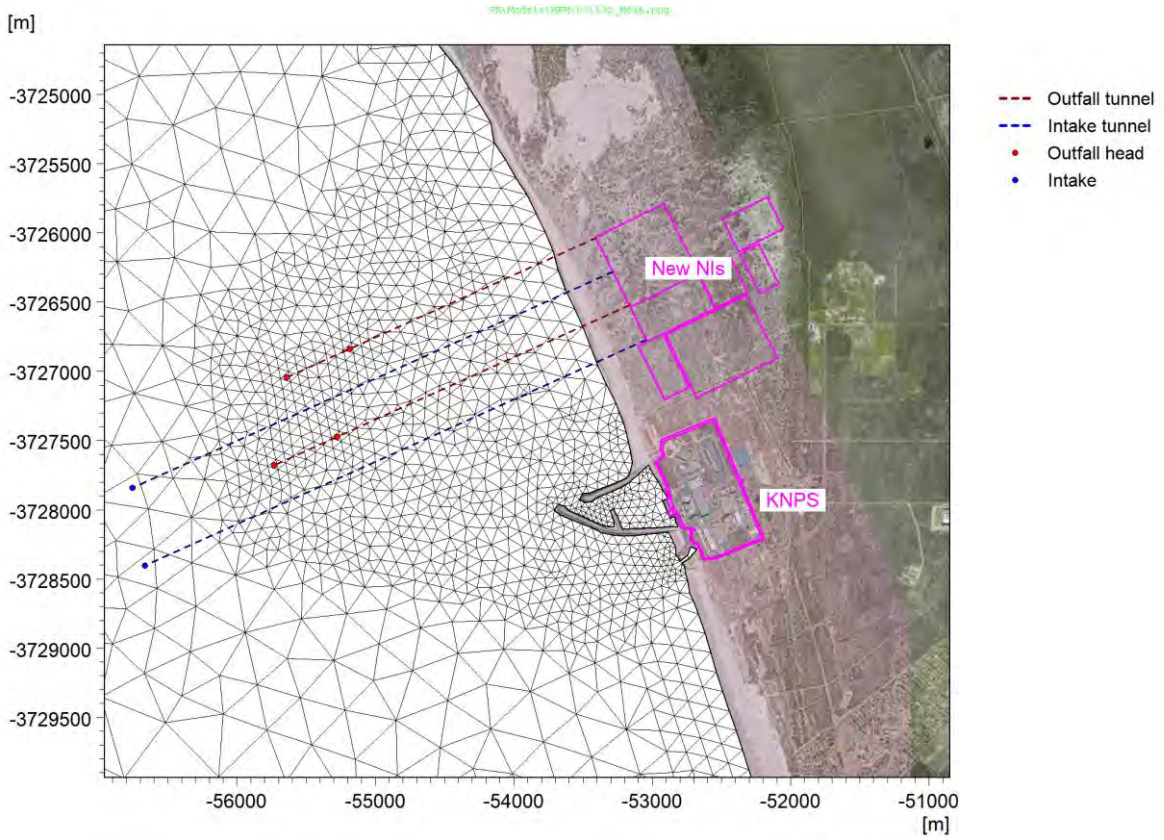


Figure C.2: Detail of Model Mesh Used for Layout 2.

CONTROLLED DISCLOSURE

When downloaded from the EDS database, this document is uncontrolled and the responsibility rests with the user to ensure it is in line with the authorised version on the database.

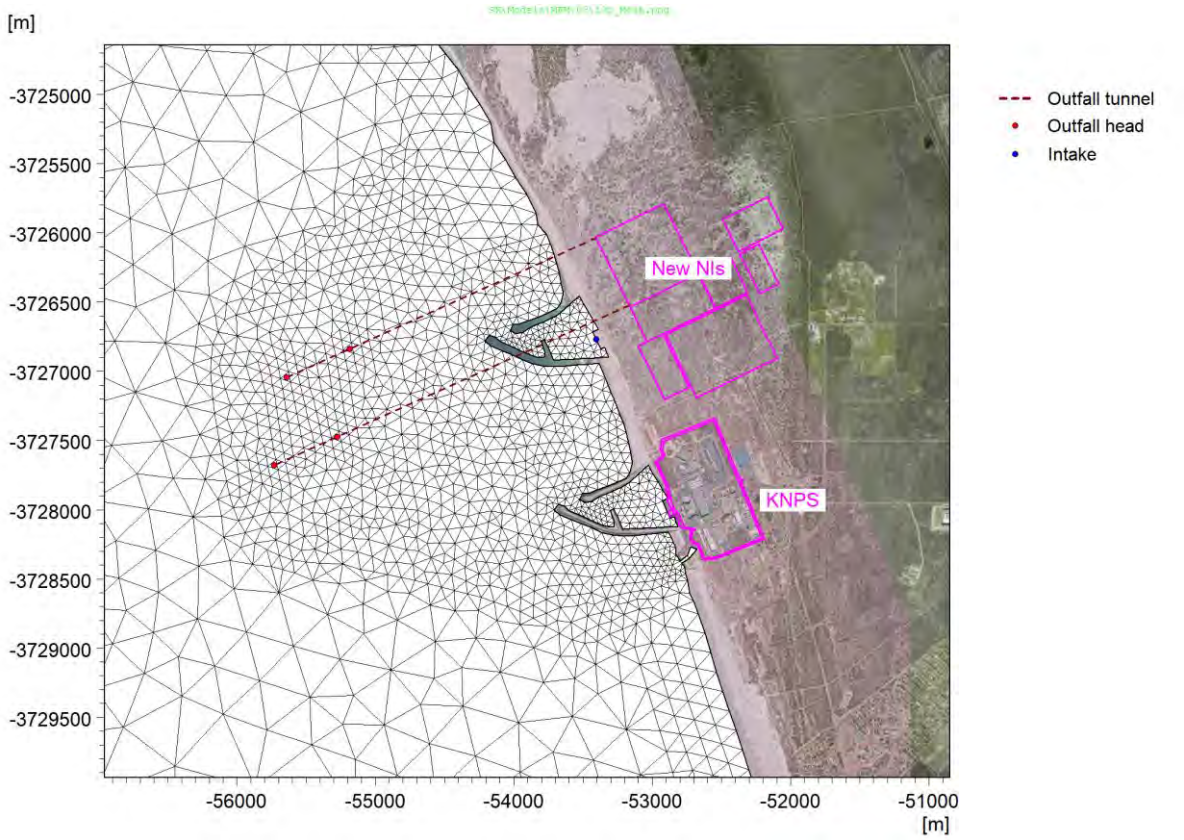


Figure C.3: Detail of Model Mesh Used for Layout 3.

CONTROLLED DISCLOSURE

When downloaded from the EDS database, this document is uncontrolled and the responsibility rests with the user to ensure it is in line with the authorised version on the database.

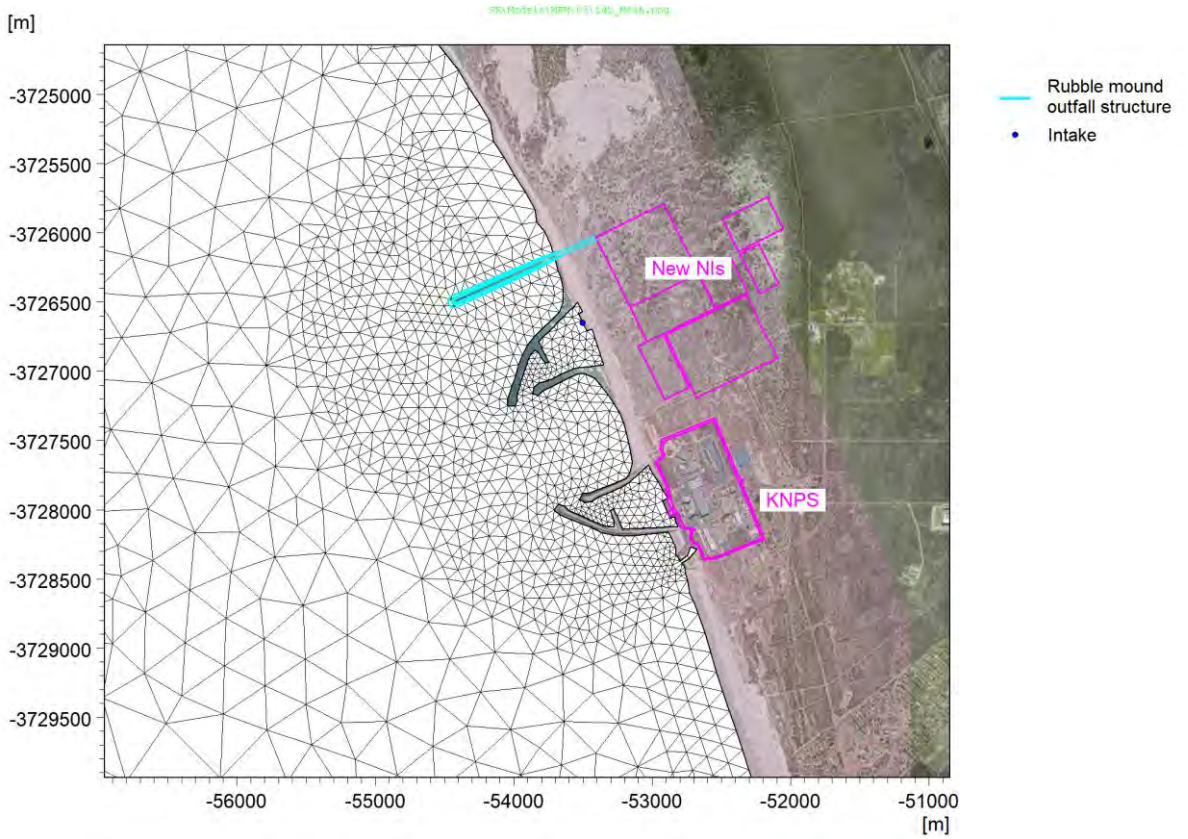


Figure C.4: Detail of Model Mesh Used for Layout 4.

CONTROLLED DISCLOSURE

When downloaded from the EDS database, this document is uncontrolled and the responsibility rests with the user to ensure it is in line with the authorised version on the database.

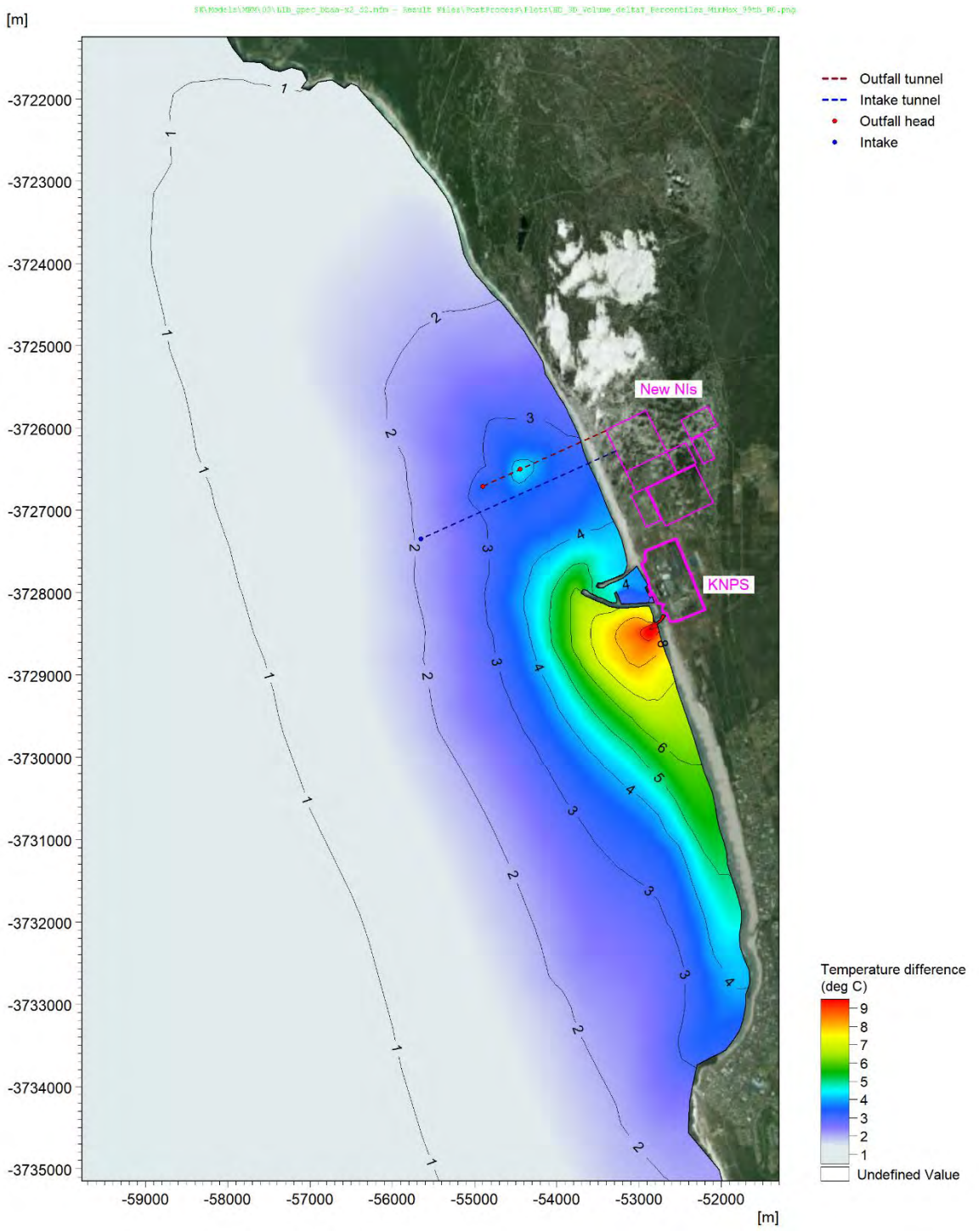


Figure C.5: KNPS + new Nls (2500 MWe) Layout 1: 99th Percentile ΔT at Worst Water Depth.

CONTROLLED DISCLOSURE

When downloaded from the EDS database, this document is uncontrolled and the responsibility rests with the user to ensure it is in line with the authorised version on the database.

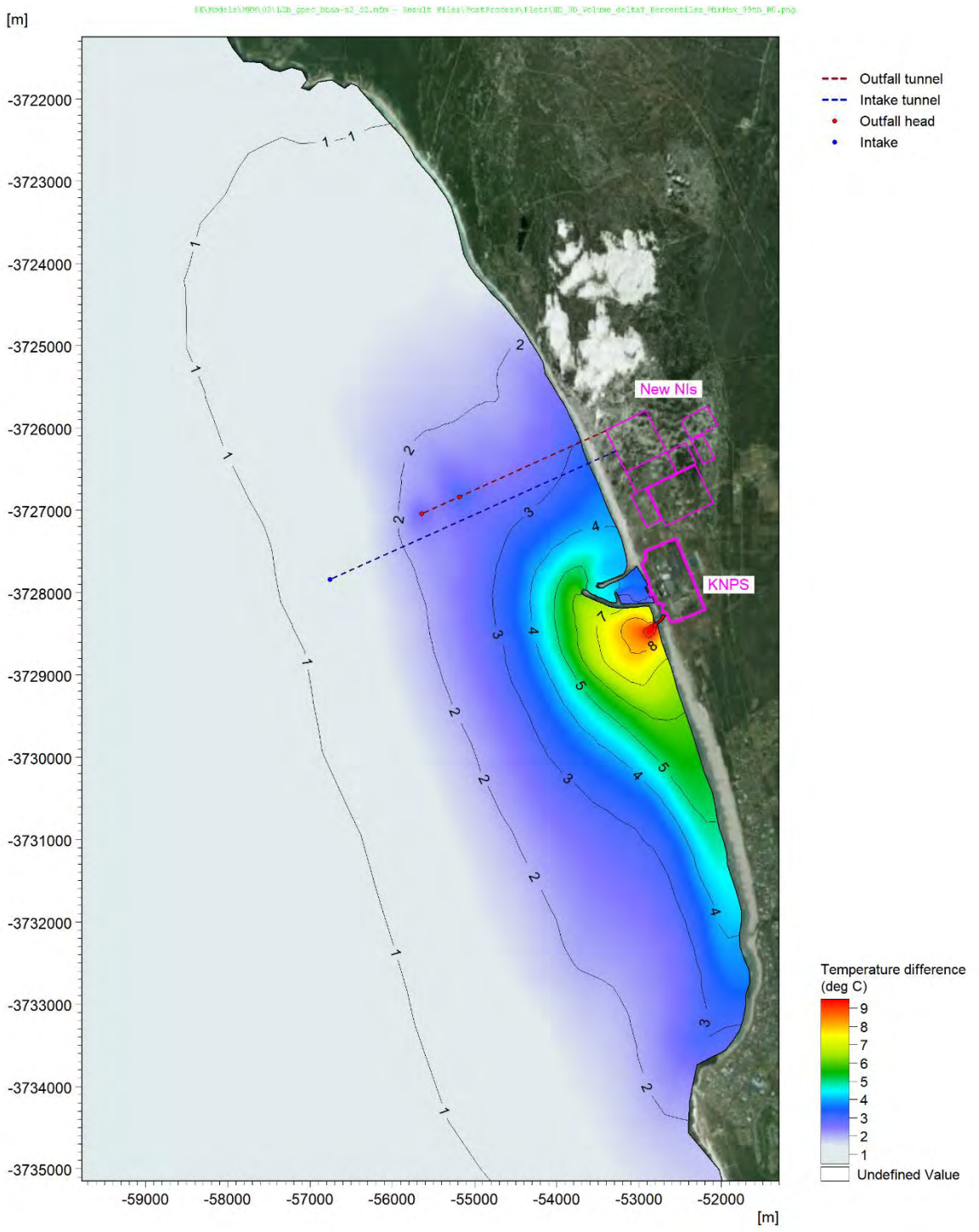


Figure C.6: KNPS + new NIs (2500 MWe) Layout 2: 99th Percentile ΔT at Worst Water Depth.

CONTROLLED DISCLOSURE

When downloaded from the EDS database, this document is uncontrolled and the responsibility rests with the user to ensure it is in line with the authorised version on the database.

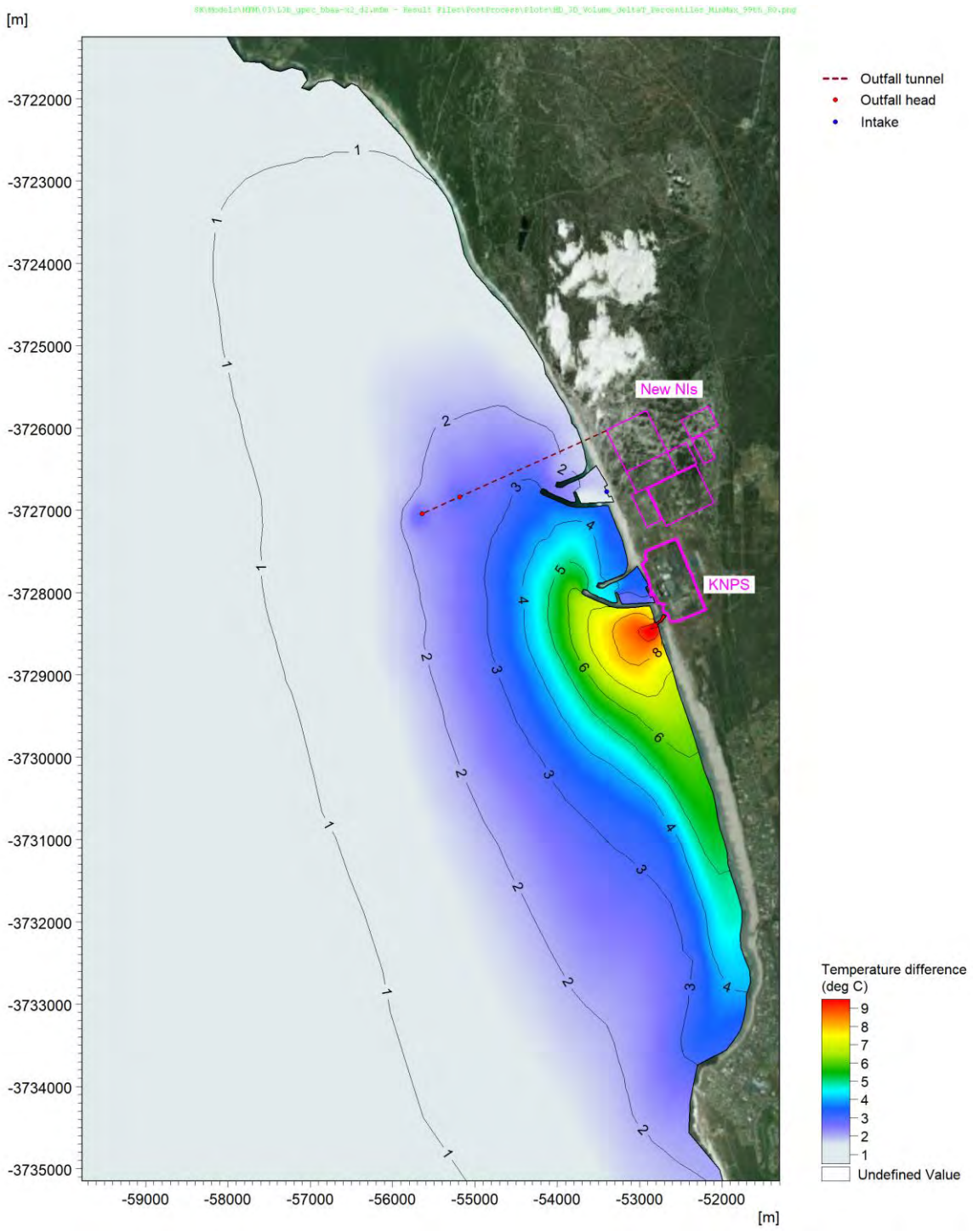


Figure C.7: KNPS + new NIs (2500 MWe) Layout 3: 99th Percentile ΔT at Worst Water Depth.

CONTROLLED DISCLOSURE

When downloaded from the EDS database, this document is uncontrolled and the responsibility rests with the user to ensure it is in line with the authorised version on the database.

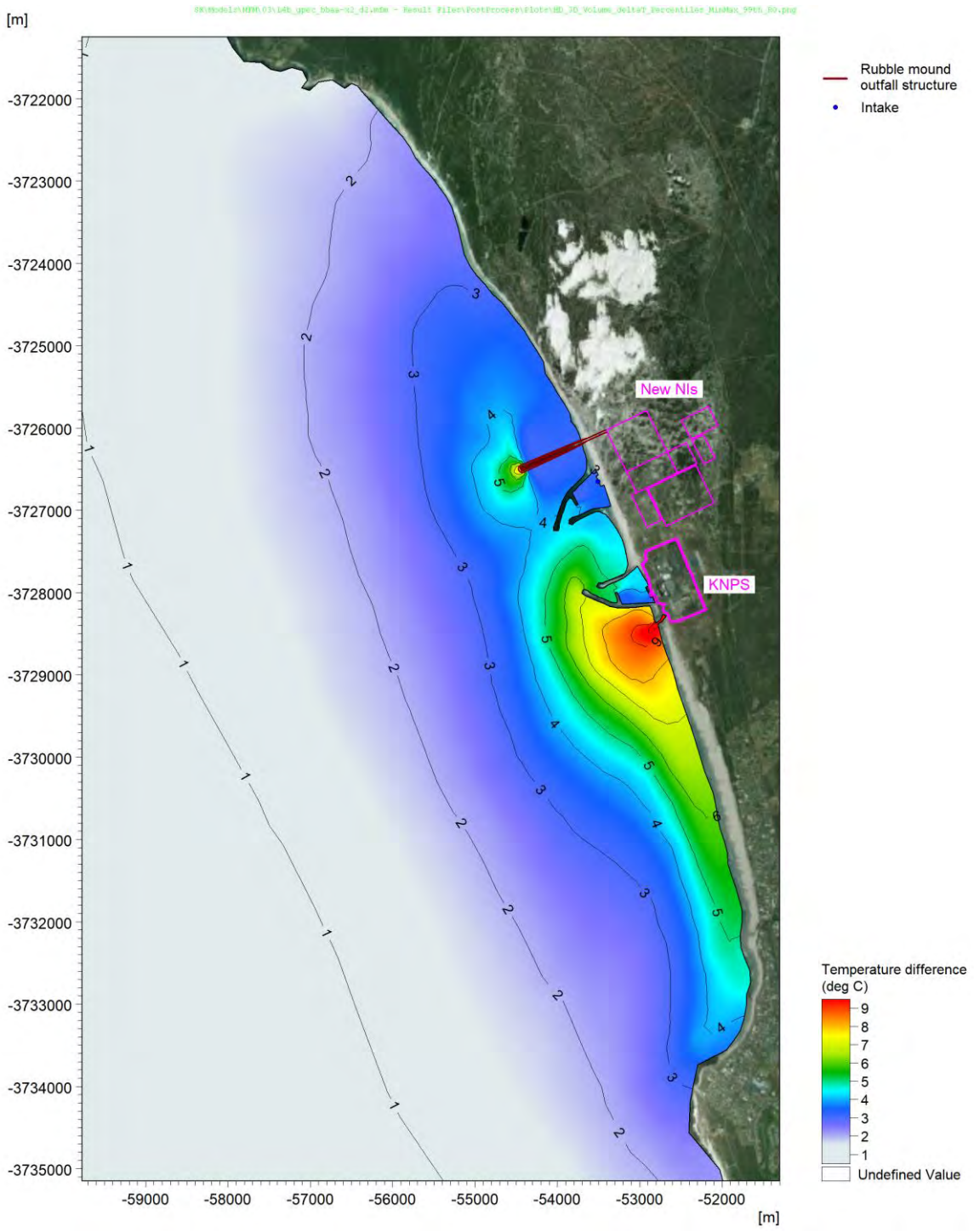


Figure C.8: KNPS + new NIs (2500 MWe) Layout 4: 99th Percentile ΔT at Worst Water Depth.

CONTROLLED DISCLOSURE

When downloaded from the EDS database, this document is uncontrolled and the responsibility rests with the user to ensure it is in line with the authorised version on the database.